SCCWRP #0265

FINAL REPORT

SEPTEMBER 1992

MODIFICATION AND VERIFICATION OF SEDIMENT DEPOSITION MODELS

SOUTHERN CALIFORNIA COASTAL WATER RESEARCH PROJECT AUTHORITY

646 W. PACIFIC COAST HIGHWAY, LONG BEACH, CALIFORNIA 90806 U.S.A.

MODIFICATION AND VERIFICATION OF SEDIMENT DEPOSITION MODELS

FINAL REPORT

TAREAH HENDRICKS
AND
ROBERT EGANHOUSE

SOUTHERN CALIFORNIA COASTAL WATER RESEARCH PROJECT
646 W. PACIFIC COAST HIGHWAY
LONG BEACH, CA 90806

SEPTEMBER 19, 1992

Table of Contents

EXECUTIVE SUMMARY

FIELD STUDIES

In general, the bulk properties of the four effluents from Hyperion (City of Los Angeles), Joint Water Pollution Control Plan (Los Angeles County), County Sanitation Districts of Orange County, and Point Loma Treatment Plant (City of San Diego) were quite similar. Total suspended solids (TSS) concentrations ranged from 50-120 mg l^{-1}. Point Loma effluent had the highest levels probably because of the lower level of treatment (advanced primary only) compared with the others. For the three effluents used by the modeling studies (Point Loma, Orange County, and Los Angeles County), TOC concentrations were about 32% and TN concentrations were about 4%.

The bulk properties of the effluents were similar to those measured a decade ago. By contrast, the stable carbon isotopic compositions of the effluent particles are less depleted in ^{13}C compared with ratios for samples collected in 1979. The nitrogen isotope ratio has not changed during this period. Stable carbon isotopes are no longer useful as indicators of the degree of sewage contamination in offshore sediments.

There were no consistent differences in the trace metal composition of the three effluents used in the studies. However, JWPCP effluent particles generally had higher concentrations of all metals. The majority of the trace metal burden in contemporary effluents was present in the dissolved, as opposed to the particulate, phase. This is a significant change since the early 1970s when the metals were predominantly associated with particles; this change is presumably due to improved treatment and source control.

Molecular markers (linear alkylbenzenes orLABs, coprostanol, and epicoprostanol) were found in all effluents; JWPCP effluent had the highest concentrations. The particulate concentration of LABs in the JWPCP effluent has decreased since 1979 (i.e., mg ΣLAB dry g^{-1} of effluent) as a result of either source control measures and/or a decline in industrial production rates.

Effluent particle degradation studies performed to determine the rate(s) of particle decomposition during initial sedimentation were not successful principally due to the difficulty of maintaining adequate concentrations of oxygen in the incubation vessels and a satisfactory mass balance of particles. The rate of degradation of effluent particles appeared to depend on the experimental conditions (e.g. oxygen content, geometry of the apparatus, amount of particles) as well as the characteristics of the effluent.

Off White Point, the particles collected in sediment traps were derived from relatively unaltered effluent discharged from the outfall within days to weeks of their trapping, and resuspended sediments deposited as far back as 25 yr or more. Evidence for the effluent source included unaltered LABs (the abundance of which tended to increase with elevation of the traps above the sea floor), low nitrogen isotope ratios, low Pb/Cd ratios, high Ni/Cd ratios, and high fecal sterol concentrations. Contributions of resuspended (historically-deposited) sediments were demonstrated by the presence of the tetrapropylene-based alkybenzenes whose production in the U.S. ended in the mid-1960s. Based on stable isotopic composition, 45-100% of the nitrogen in sediment trap particles, and 75-100% of the nitrogen in surface sediments, was derived from the effluent.

The results for the Orange County and Point Loma discharge sites were generally similar to those obtained off White Point. The LABs in the sediment trap particles and surface sediments off Point Loma and Orange County were more degraded, and ΣLAB concentrations (normalized to organic carbon) were much less, than the White Point samples. Point Loma values were less than Orange County values. Either the effluent particles discharged from the Point Loma and Orange County outfalls underwent more rapid decomposition during initial sedimentation, or a higher proportion of the particles were derived from resuspension of older (historically-deposited) sediments than off White Point.

It appears that effluent characteristics and/or treatment may be important factors controlling the rate of deposition of wastewater particles on the coastal shelf. For sediment trap particles collected off Orange County, 31-46% of the nitrogen came from effluent (based on $\delta^{15}N$measurements). The corresponding values for sediment trap particles collected off Point Loma were 10-20%. For sediments collected off Orange County,

67% of the nitrogen came from effluent. The corresponding values for sediments collected off Point Loma were 20-30%.

SEDIMENT MODELS

The two sediment simulation models, DECAL and SED2D, were identified as the most promising models for simulating the fate of municipal wastewater particles discharged from ocean outfalls at a workshop sponsored by the U.S. Environmental Protection Agency. The purpose of this study was to correct deficiencies in these models identified during the workshop and then assess the ability of the models to predict the characteristics of the sediments at three sites of municipal wastewater discharge off southern California.

The revised models were used to simulate sediment characteristics at three outfall sites (Point Loma, Huntington Beach, and White Point), and to test the sensitivity of model predictions to changes in the input data. The representations of processes that affect the fates of particles were compared between the models. Although both models incorporate roughly the same processes, the mathematical representations of these processes were generally quite different.

The model predictions were sensitive to some of the input values, including 1) effective thickness of the wastefield for particle aggregation, 2) concentration of cohesive natural particles entrained into the plume during initial dilution, 3) rate of decay of natural and effluent particles in the water column and in the sediments, and 4) rate of accumulation of natural particles in the absence of discharge. The appropriate values for these parameters were unknown and the predicted fluxes of suspended solids to the ocean floor varied over two orders of magnitude.

The concentration of organic material in the sediments predicted by DECAL ranged from 3.5 to 21 times higher than the observed values, while the predicted values for SED2D ranged from 0.5 to 42 times higher than observed values. Simulations with "best guess" values for the input parameters predicted concentrations of organic material higher than observed values. The primary exception was the organic content of sediments off White Point predicted with SED2D. Parameter values that resulted in predictions comparable to observations near the outfall generally underestimated the concentration of organic material at greater distances from the discharge.

DECAL was also used to make predictions of the concentration of lead and cadmium in the sediments. The predicted concentrations of lead ranged from 1.3 to 12 times greater than the observed concentrations. The predicted concentrations of cadmium ranged from 0.3 to 7.6 times greater than the observed concentrations.

The simulations point out the need to refine some of the process representations in both models (e.g., particle aggregation in absence of homogeneous distributions associated with strong mixing) and the need to obtain better estimates for some of the input parameters (e.g., decay rates, accumulation rate of natural particles in the absence of discharge, composition of natural particles).

I. BACKGROUND

I.A. FIELD SITES

The first deepwater ocean outfalls in southern California were designed and constructed in the early and middle 1900s. From the engineers' viewpoint, the principle objective of these outfall systems was to achieve maximum dilution of the effluent and to prevent, as much as possible, resurfacing of the wastewater plume and exposure of beaches to waste debris and attendant pathogenic microorganisms. During the 1950s and early 1960s, little thought was given to the fate and effects of the toxic substances that were discharged to the ocean because virtually no information existed on the types and amounts of contaminants that were present in the effluents; it was presumed that high dilutions and swift currents would prevent their accumulation in the coastal ecosystem. This assumption was shown to be incorrect during the late 1960s and early 1970s when it was discovered that the outfalls were serving as conduits for massive amounts of pollutants to the nearby shelf off Palos Verdes (Carry and Redner 1970; SCCWRP 1973) and that accumulations had already developed (Klein and Goldberg 1970; MacGregor 1974).

Growing awareness about the potential effects of some of these contaminants (e.g. DDT; Keith *et al.* 1970) led to the formation in 1969 of the Southern California Coastal Water Research Project (SCCWRP), an organization whose mission was to better understand the effects of Man's activities (including waste discharge) on the coastal ecosystem off southern California. Within a few years scientists at SCCWRP and other organizations began to conduct surveys of the distribution of heavy metals and trace organic contaminants in sediments, organisms and waters near the outfall systems (Galloway 1979; McDermott *et al.* 1974; MacGregor 1976; among others). Because of the massive contamination of the shelf off Palos Verdes, this site was the focus of the majority of the offshore work, and the Palos Verdes Shelf is probably the most intensively studied portion of the continental shelf in the world today. The other major outfalls, with the possible exception of those off the Hyperion treatment plant, (e.g. Orange County, Point Loma) have generally received less attention, and the databases for these sites are proportionately smaller.

Two general types of studies have been carried out at White Point in attempts to understand the fate of wastewater effluent particles: computer simulations and field studies. Many of the computer simulations have been developed by T. Hendricks (see references in following subsection) and others (e.g. Morel *et al.* 1975; Koh *et al.* 1982) and have formed the basis for the present investigation. The field studies have tended to rely on comparing inventories of the mass of waste-related contaminants or markers accumulated in shelf sediments with information on the mass emissions of same from the outfall system (Eganhouse and Kaplan 1988; Galloway 1979; Kettenring 1981; Myers 1974; Sweeney *et al.* 1980). These various investigations have given rise to two competing hypotheses: 1) that only a small fraction (1-10%) of the particle-associated contaminants are deposited on the shelf and 2) that most of the effluent particles have been deposited in the sediments but that associated constituents (trace metals, organic matter) are remobilized subsequent to initial deposition (during resuspension events). The purpose of the present study is not to differentiate between these alternate hypotheses. Instead, the objective of this project is to improve the representation of important sedimentation processes in two existing models and compare the results of the revised models with field-collected data.

Over the last two decades improved source control and waste treatment procedures have resulted in dramatic reductions in the emissions of solids from all of the outfall systems (SCCWRP 1991b). These reductions are reflected in the vertical distribution of effluent-related contaminants in sediments off Palos Verdes (Eganhouse and Kaplan 1988; Logan *et al.* 1989; Stull *et al.* 1986). Thus, it seems reasonable to expect that models could be developed to simulate and even predict the changes in deposition rates as a function of changing effluent emission rates. The models examined in this report attempt to predict the deposition rates of effluent particles on the shelf at three outfall sites off southern California. Geochemical data to be presented provide a means of comparing the field measurements with the model predictions.

I.B. Simulation Models

This study focuses on the two numerical simulation models *DECAL* and *SED2D*. These models were identified as the most promising of the initial attempts to simulate the sedimentation and accumulation of particles from municipal wastewater outfalls at a workshop sponsored by the Environmental Protection Agency (EPA, Newport, OR; 1987).

The *DECAL* model was developed by Dr. Kevin Farley of Clemson University; the *SED2D* model, by Dr. Tareah Hendricks of the Southern California Coastal Water Research Project (SCCWRP).

A large number of complex processes determine the fate of both natural and effluent particles in the ocean (see Figure 1.1). Only a subset of this group are represented in the two simulation models. These include:

1. The initial dilution process (to determine the initial concentration of effluent particles in the wastefield).

2. The concentration, flux, or production rate of natural particles in the water column.

3. The aggregation of particles into larger, faster settling particles.

4. The settling of these particles while being transported by the ocean currents.

5. Decay of organic material in the water column and in the sediments.

6. Mobilization and demobilization of trace constituents on the particles (*DECAL*).

7. Resuspension (*DECAL* and *SED2D*), transport, and redeposition (*SED2D*) of sediment particles.

8. Accumulation rates and concentration of organic material (*DECAL* and *SED2D*) and trace constituents (*DECAL*) in the sediments.

Although the two models have similar goals and generally incorporate representations of the same processes, the approaches used for the simulations are substantially different.

I.B.1. DECAL Overview

I.B.1.a. Two Layer Ocean. Only a brief overview of the *DECAL* model will be presented here (see Farley 1990 for more details). The primary feature of the model is the assumption that physical-chemical aggregation processes control the settling of suspended particles from the water column. Estimates of the flux rates of the settling particles are calculated using the results of numerical simulation studies of aggregation processes reported by Farley and Morel(1986).

A number of simplifying assumptions were required in order to carry out these latter simulations (Lawler *et al.* 1980; Farley and Morel 1986):

1. particle aggregation is only the result of collisions produced by Brownian motion, fluid shear, and differential settling between two particles;

2. particles before an after each aggregation are spherical;

3. particles approach one another on rectilinear paths, the path of one particle not being affected by the presence of another;

4. no force acts on the particles until they come into physical contact, after which they eventually will adhere;

5. the adherence of particles, with formation of an aggregate, is only dependent upon a collision efficiency, the magnitude of the collision efficiency is constant and independent of the particle size or mechanism of coagulation;

6. the water column is divided into vertically homogeneous layers, thus vertical mixing of the water within each layer is fast relative to sedimentation, and

7. aggregate breakup does not occur.

With these assumptions, they found that the change in concentration of suspended solids in a layer of homogeneously mixed water due to the settling of aggregate particles could be represented by the equation:

$$\frac{dC}{dt} = -B_{ds}C^{2.3} - B_{sh}C^{1.9} - B_{b}C^{1.3} \qquad (1.1)$$

where:

C = concentration of suspended solids (wet weight)

B_{ds} = proportionality factor (differential settling)
B_{sh} = proportionality factor (current shear)
B_b = proportionality factor (Brownian motion)

Each term in the equation represents one of the three aggregation processes. The corresponding proportionality factors (B_{ds}, B_{sh}, and B_b) depend on the collision efficiency, shear, particle and fluid density, floc porosity, and other environmental factors. These relationships are enumerated in various references (Farley and Morel 1986; Tetra Tech 1987; Castro 1990; and Farley and Castro 1990). The flux of settling aggregate particles out of the bottom of the column is:

$$J_s = h_w \frac{\partial C}{\partial t} \tag{1.2}$$

The original version of *DECAL* divides the water column into two well mixed layers (Figure 1.2a)--an upper layer of ambient water, and an underlying wastefield layer. The bottom of the latter coincides with the ocean bottom. This partitioning may occur in the presence of a pycnocline if there is strong vertical mixing within each layer, or if the ambient water available for mixing during the initial dilution of the wastewater is restricted.

A detailed description of this two-layer version is contained in Tetra Tech (1987). In the discussion, they note that the aggregation associated with Brownian motion will generally be negligible compared with that associated with shear or differential settling unless suspended solids concentrations are less than about 0.1 mg l^{-1}. To simplify the calculations within *DECAL*, the aggregation term associated with Brownian motion is dropped, and the two terms associated with differential settling and shear are consolidated into a single composite term. With these approximations, the change in concentration of suspended solids out of a layer due to aggregate particle settling is proportional to the square of the particle concentration (Tetra Tech 1987):

$$\frac{dC}{dt} = -BC^2 \tag{1.3}$$

and:

$$B = f^{1.3} B_{ds} C^{0.3_{avg}} + f^{0.9} B_{sh} C^{-0.1_{avg}} \tag{1.4}$$

$$f = 1 + \frac{e}{(1-e)} \frac{\rho_f}{\rho_p} \tag{1.5}$$

The factor f converts the concentration C from dry weight to wet weight, where p_p = particle density, p_f = fluid density, and e = floc porosity.

The concentration of suspended particles in the water column is computed in an Eulerian (fixed) reference frame. In that coordinate system, the rate of change of suspended solids concentration in the wastefield is:

$$\begin{aligned} J_s &= h \frac{\partial C}{\partial t} + TRANSPORT\ FLUXES \\ &= J_n - h(BC^2 - k_d C) \end{aligned} \tag{1.6}$$

where:

Trans. Fluxes = mass transport associated with nontidal advection
J_s = source flux of particles
= $J_n + J_e$
J_n = natural particle flux (e.g. phytoplankton productivity)
J_e = effluent particle flux (e.g. outfall discharge)
k_d = decomposition coefficient of organic particles
B = approximate aggregation coefficient (equation 1.4)

The flux of natural particles into the wastefield, J_n, is assumed to be associated with the sedimentation of natural particles from the overlying layer associated with phytoplankton production. Productivity occurring within the wastefield is not included in the simulation.

A mass balance equation analogous to equation 1.6 is used to compute the concentration of suspended solids in the upper layer. In this upper layer, the production rate of phytoplankton mass replaces the source term, J_n, in equation 1.6 (Tetra Tech 1987):

$$\frac{dC_u}{dt} = 2.5\frac{P_{total}}{h_u} - k_{du} - BC_u^2 \qquad (1.7)$$

where:

C_u = suspended solids concentration in the upper layer
h_u = thickness of the upper layer
k_{du} = decomposition coefficient for organic material
P_{total} = phytoplankton productivity

The factor of 2.5 converts carbon mass to dry mass. This equation is solved to yield the steady-state concentration of natural suspended solids. The flux rate of natural particles, J_n, into the wastefield layer is then obtained by substituting this concentration into the simplified aggregation flux equation (equation 1.6):

$$J_n = \frac{k_{du}^2 h_u}{10B}\left[1 - \left(1 + \frac{10B}{k_{du}^2 h_u}P_{total}\right)^{0.5}\right]^2 \qquad (1.8)$$

In order to solve equation 1.2 for the wastefield layer, it is necessary to specify the initial concentration of suspended solids in the wastefield. There are two sources of these particles: (a) the discharged effluent and, (b) natural particles entrained during the initial dilution process. *DECAL* assumes that the concentration of natural particles is negligible compared with the post-dilution concentration of effluent particles.

A mass balance approach is used to estimate the concentration of effluent particles in the wastefield at the completion of the initial dilution process. In this method, an "extended source" is created. The size of this source depends on the length of the diffuser, the average characteristics of one, or more, components of the tidal currents, and the orientation of the diffuser relative to these flows. The extended source is used in combination with the thickness of the wastefield, the strength and direction of a net flow, the volumetric discharge rate of effluent, and the concentration of suspended solids in the effluent, to compute the initial concentration in the wastefield. The process is described in more detail in Tetra Tech (1987).

After initial dilution is complete, the suspended solids within the wastefield are transported by a net current of constant magnitude and direction. Slow variations (subtidal frequency) in the actual currents are approximated by using multiple, weighted, net flows with different strengths and directions of flow. No horizontal dispersion processes (other than associated with the set of varying net flows) are represented in the simulation.

Equation 1.2 reflects changes in both the natural and effluent particles as they are carried away from the outfall area by the net flows. These include the loss of mass and particle size due to the decay of labile material, increases in particle size due to inter-particle aggregation, and the loss of aggregated particles from the wastefield due to settling. It is assumed that the particles consist entirely of labile organic material that is subject to degradation by microbial activity. A first-order rate (loss flux proportional to concentration) is used to describe this degradation.

A mass balance equation is used to compute the accumulation of natural and wastewater particles in the sediments (Tetra Tech 1987):

$$h_s \frac{dC_s}{dt} = J_s - k_r C_s \tag{1.9}$$

The source term in this equation, J_s, is equal to the rate of loss of particles from the wastefield layer due to settling. The parameter K_r is used to represent the combined effects of resuspension, decomposition and burial.

Equation 1.9 is readily solved for the case of a constant sedimentation rate (J_s) and decay rate (k_r):

$$C_s = \frac{J_s}{k_r} + \left[C_s^o - \frac{J_s}{k_r} \right] \exp^{-\left(\frac{k_r}{h_s}\right)t} \tag{1.10}$$

Here the parameter h_s/k_r represents the "characteristic response time" T_R, of the sediments. For long elapsed times, i.e. $t/T_R >> 1$, the concentration of organic material in the sediments approaches the steady-state value:

$$C_s(x,y) = \frac{J_s(x,y)}{k_r} \tag{1.11}$$

DECAL also estimates the concentration and accumulation of a trace constituent in the sediments. The approach is an extension of the method used in computing the concentration and accumulation of organic material. The trace constituent analog to the mass balance equation for the wastefield is (Tetra Tech 1987):

$$\frac{\partial C_t}{\partial t} + TRANSPORT\ FLUXES = J_{te} - BC^2\gamma \tag{1.12}$$

where:

C_t = total concentration of a trace chemical in the water column
J_t = source mass flux of the trace chemical (e.g. discharge)
τ = particulate concentration of the trace chemical

Here BC^2 is the deposition rate for the chemical due to the sedimentation of trace constituent bearing suspended solids. The mass concentration of the trace constituent on the particles is related to the total trace constituent concentration, C_t, by the relationship (Tetra Tech 1987):

$$C_t = \gamma C + C_{dis} \tag{1.13}$$

where:

C_{dis} = dissolved chemical concentration

In this equation, C_t and C_{dis} are in $\mu g\ l^{-1}$; γ is in $mg\ g^{-1}$; and C_s is in $mg\ l^{-1}$. If it is assumed that mobilization-demobilization reactions are rapid compared with the sedimentation times, the partitioning of the trace constituent between the particulates and the dissolved component will be at equilibrium. In that case, by definition:

$$\gamma = 10^{-6} K_p C_{dis} \tag{1.14}$$

The mass balance, equation 1.12, can then be written:

$$\frac{\partial C_t}{\partial t} + TRANSPORT\ FLUXES = J_t - \frac{10^{-6} B k_p C^2 C_t}{1 + 10^{-6} k_p C} \tag{1.15}$$

The flux of trace constituent to the sediments is given by:

$$J_t = B h_w C^2 \gamma \tag{1.16}$$

where h_w is the thickness of the wastefield (lower) layer. Equations 1.14, 1.15 and 1.16 can be combined to yield:

$$J_t = B h_w C^2 \frac{10^{-6} k_p C}{1 + 10^{-6} k_p C} \tag{1.17}$$

DECAL numerically computes the daily-averaged deposition rates at a fixed location by using this trace constituent equation in a Lagrangian coordinate system (moving with a segment of the water column), and then transforming to the fixed (Eulerian) system (Tetra Tech 1987).

The sediment trace constituent analog to equation 1.9 is:

$$h_s \frac{dC_{ts}}{dt} = J_t - k_{rt} C_{ts} \tag{1.18}$$

where:

C_{ts} = accumulation of trace chemical in the surface sediment
J_s = daily averaged deposition rate
k_{rt} = apparent interfacial removal rate of the trace chemical

The parameter k_{rt} is the apparent interfacial removal rate. It represents the combined effects of resuspension, burial, desorption/dissolution, and chemical transformations. Equations for the time-dependent and steady-state concentrations of the trace constituent in the sediments analogous to equations 1.10 and 1.11 are readily obtained by substituting k_{rt} for k_r.

I.B.1.b. Extension to a Three-Layer Ocean. In general, a two-layer representation of the water column will not be a good representation of ocean discharges into stratified waters. Figure 1.3 shows the vertical distribution of ammonia in the water column for a period of about 40 hr as the wastefield moves away from the Point Loma (City of San Diego, CA) ocean outfall. A subsurface wastefield is formed because of the density stratification of the water column. Although the centroid of the ammonia mass moves up and down in the water column (due to internal tides and waves), there is no indication of strong mixing at the wastefield or deeper depths. Although no pycnocline is present in this region, vertical mixing is suppressed by residual density stratification of the water column.

Figures 1.4a,b,c,d shows the distribution of salinity, temperature, density, and transmissivity at four locations near the Hyperion 5-mile ocean outfall (City of Los Angeles). Depressions in the salinity, transmissivity, dissolved oxygen, and temperature at three of the stations (HR001, HR007, and 050) indicate presence of the wastefield from this outfall. These stations lie 2-4 km away from the diffuser. Again, a three-layer nature to the water column is evident (consisting of a wastefield surrounded by overlying and underlying layers of ambient water). The fourth station (HR011, 10 km from the diffuser) shows no evidence that wastefield constituents are present.

The sedimentation flux equations developed for the two-layer *DECAL* model are insufficient to predict the sedimentation of particles in a three-layer water column (Figure 1.2b) since the settling speed(s) of the particles leaving the wastefield are unknown. The intervention of the bottom layer between the wastefield and the ocean bottom will introduce a lag between the time a particle leaves the wastefield and when it reaches the sediments. If the ocean current is unidirectional and of constant magnitude, and the loss of organic mass due to decay during the lag period can be neglected, the depositional pattern for the three-layer case will be identical to that predicted for a two-layer water column. The location of the pattern will, however, be shifted downstream from the outfall by the distance, X_{offset}:

$$X_{offset} = t_s v_s = h_s \left(\frac{v_x}{v_s} \right) \tag{1.19}$$

where h_s is the distance from the bottom of the wastefield to the ocean bottom, v_x is the current speed, and v_s is the settling speed.

If the decay of organic material during the lag interval, t_s, cannot be neglected, the difference between the sedimentation fluxes to the bottom for the two cases will increase with increasing distance from the discharge. In order to assess the spatial offset in the depositional pattern, the significance of decay of organic material, or predict the depositional pattern for more complex flows, it is necessary to determine the settling speeds of the particles leaving the wastefield.

We subcontracted Dr. Kevin Farley to carry out simulations of particle aggregation dynamics for a three-layer water column. Of particular interest was the settling speeds of the particles and the extent of additional aggregation within the underlying layer. This subcontract contributed to a graduate student study by Mr. Palo Castro under the direction of Dr. Farley. Ultimately, his work culminated in a Masters degree from Clemson University. This work is reported in his thesis, entitled "Modeling Deposition of Particles and Particle-Bound Contaminants in Stratified Waters" (Castro 1990). The thesis investigation was carried out for a wastefield thickness of 1 m. Dr. Farley subsequently carried out analogous simulations for a wastefield thickness of 10 m. The results from that study, and an example application to ocean discharges, is reported in "Effects of Stratification on the Deposition of Organic Material near Marine Sewage Outfalls" (Farley and Castro 1990).

The reader is referred to these reports for a detailed discussion of the particle aggregation dynamics simulation studies, as well as a general review of aggregation dynamics. This report presents only an overview.

These new studies began by dividing the original wastefield layer into four new layers. The uppermost layer represented the wastefield; the other three, the underlying layer(s) of water. At the beginning of the simulation (t=0), the particles are restricted to the wastefield layer. With the passage of time, the particles aggregate and settle out of this layer and into the underlying layers. Therefore the concentration of particles in the wastefield layer decreases, while the concentrations in the lower layers begin to increase. The purpose of using multiple underlying layers was to examine the extent of particle aggregation within this portion of the water column.

The initial distribution of the particles was assumed to be uniform, by volume, between particle diameters of 0.06-1.5 um. For computational simplicity and accuracy, the size classes used in the simulation were selected so that particle volumes double between each class (corresponding to a 26% increase in particle diameter). The change in particle number in each size class during a discrete interval of time was calculated from an equation of the form (Castro 1990):

$$\frac{dn_k}{dt} = \frac{1}{2}\sum_{i+j=k} \alpha(i,j)\beta(i,j)n_i n_j - n_k\sum_{i=1}^{j} \alpha(i,k)\beta(i,k)n_i \pm \frac{W_{sk}}{h}n_k \qquad (1.20)$$

where:

n_k = number of particles in the k_{th} size class
$\alpha(i,j)$ = collision efficiency between i_{th} and j_{th} size class particles
$\beta(i,j)$ = collision frequency between i_{th} and j_{th} size class particles
W_{sk} = settling speed of particles in the k_{th} size class
h = layer thickness

Euler's method was used to integrate the set of equations. Restrictive conditions were placed on the magnitude of the stepping interval to minimize the computation errors.

In the old and new versions of *DECAL*, particle settling speed for each size class, W_{sk}, was estimated using Stoke's law. The friction force on a spherical particle at low Reynolds number is:

$$F_k = 3\pi\eta d_k W_{sk} \qquad (1.21)$$

where:

F_k = friction force on the particle
d_k = particle diameter
n = viscosity of the fluid

At equilibrium, this friction force is balanced by a (negative) buoyancy force on the particle:

$$B_k = g(\rho_p - \rho_w)V_k \qquad (1.22)$$

where:

B_k = buoyancy force on a particle in the kth size class
V_k = volume of the particle in the kth size class
p_p = density of the particles (dry mass)
p_w = density of the water
g = gravitational acceleration

The particle settling speed is thus:

$$W_{sk} = \left(\frac{g}{\eta}\right)(\rho_p - \rho_w) V_k^{2/3} \tag{1.23}$$

Since the particle density is held constant during the simulation, the settling speed is also proportional to the two-thirds power of particle mass. Castro (1990) notes that this simple relationship is no longer valid when the aggregate particle size increases lead to particle settling speed that result Reynolds numbers in excess of about one (Schlichting 1960).

From a microscopic point of view, it is the concentration of particle mass in each layer, and the fluxes of particle mass into and out of each layer, that are of interest. During any particular interval in time, the flux of particle mass, $J_{m,m+1}$, out of one layer, m, into the layer below, $m+1$, is the sum of the individual fluxes associated with each size class. Similarly, the mass concentration of particles, C_m, in the m_{th} layer is the sum of the particle masses in each size class within that layer.

The simulation studies indicated only minor particle aggregation took place within the lower three layers. Hence the sedimentation of particles through this region could be obtained by neglecting any additional aggregation, and the underlying three layers could be represented by a single layer. It was also found that only a small number of size classes were present at any given time within each layer. Therefore an average settling speed could be used to describe the combined effects of each size class on the sedimentation of particle mass.

Outputs from the simulation included the flux rate of aggregate particles out of the upper (wastefield) layer, and the average settling speed of those particles. The flux equations derived from the two sets of simulations (1 m wastefield thickness-Castro 1990; 10 m thickness, Farley and Castro 1990) are:

$$J_w(1) = 0.16\,C^{2.31} + 0.174\,C^{1.34} \tag{1.24a}$$

$$J_w(10) = 2.7\,C^{2.3} + 0.37\,C^{1.3} \tag{1.24b}$$

These equations were felt to be valid for suspended solids concentrations up to about 10 mg l^{-1} (Farley and Castro 1990). The first term in each equation is the rate of loss of particle mass associated with aggregation due to differential settling; the second term, the loss associated with Brownian motion. Fluid shears of 0.0 and 0.1 s^{-1} were used in the simulations. These levels were felt to be representative of the subpycnocline ocean environment (Farley 1990b). At these low levels of turbulence, aggregation associated with shear was found to be negligible.

In the original aggregation simulation studies, the dependence of each term in the flux rate equation on the thickness of the layer could be represented as a power function of the form h_w^m. Applying this relationship to equations 1.23 and 1.24 results in the general flux equation:

$$J_w(h_w, C) = 0.016\,h_w^{1.23} C^{2.3} + 0.174\,h_w^{0.33} C^{1.3} \tag{1.25}$$

Since there is no difference between aggregation in the wastefield layer in this study and the wastefield layer in the previous study (Farley and Morel 1986), the flux equation deduced from this study should be the same as in the earlier study. The exponents for the dependence of the flux on the wastefield thickness (1.23, 0.33) are slightly smaller than deduced from the previous study (1.32, 0.40). These differences were attributed to the improved computational accuracy of the new simulations (Farley 1990a).

The two equations deduced for the average aggregate particle settling speeds are:

$$W_s(1) = 0.0001(2.57\,C^{1.78} + 2.19\,C^{0.36}) \quad (1.26a)$$

$$W_s(10) = 0.001(14.0\,C^{1.78} + 0.40\,C^{0.36}) \quad (1.26b)$$

We assumed that these settling speed relationships also have a power-law dependence on the thickness of the wastefield. Generalizing equation 1.26 to the case of an arbitrary wastefield thickness, h_w, yields:

$$W_s(h_w, C) = 0.0001\left(2.57\,h_w^{1.74}C^{1.78} + 0.022\,h_w^{0.46}\,C^{0.36}\right) \quad (1.27)$$

The new (three-layer) version of *DECAL* uses the equivalent of equation 1.24b to compute the production rate of aggregate suspended solids, and equation 1.26b to calculate the average particle settling speed. Since the settling speeds in *DECAL* are computed on the basis of a 10 m thick wastefield, it is important to scale the two *DECAL* settling speed parameters by the factors:

$$Q(h_w) = Q(h_w{=}10)\left(\frac{h_w}{10}\right)^{1.74} \quad (1.28)$$

$$Q(h_w) = Q(h_w{=}10)\left(\frac{h_w}{10}\right)^{0.46} \quad (1.29)$$

where:

$Q_{ds}(h_w)$ = settling speed factor for differential settling (thickness h_w)
$Q_{br}(h_w)$ = settling speed factor for brownian motion (thickness h_w)
h_w = wastefield thickness in meters

I.B.2. SED2D Overview

I.B.2.a. Modular Approach. The *DECAL* program represents an "all in one" approach. All the simulation processes are contained within a single model, and a sediment prediction is obtained from a single simulation run. In contrast, *SED2D* refers to a collection of subprograms, or modules. These modules are independent programs, but with file structures that allow the output from various modules to be used as the input for other modules. The subprograms currently incorporated into *SED2D* simulations are:

TSLINE	(Initial dilution)
DPA,DPS	(Particle settling)
PRX,PRY,PCOMB	(1-D transport probabilities)
DPA2DPY	(1-D depositional probability)
PXY,PXYCMB2,SEDF2D	(2-D depositional probabilities)
TRANS,DISPER,ACCUM,SEDR	(Sediment resuspension and deposition)
PXYACC	(Sediment accumulation and concentration)
XTRACT	(Extract data along transects)
PRB2GT, DPY2GT	(Convert probability data files to ASCII)

Figure 1.5a is the flow diagram for this set of submodels.

I.B.2.b. Simulation Approach. The set of submodels incorporated into *SED2D* is based on a conceptual approach that divides a column of the ocean into eight layers (Figure 1.5b). These layers can be consolidated into three groups. The first group consists of the upper three layers. These layers are identical to those in the *DECAL* model: (1) a surface layer of water overlying the wastefield layer, (2) the wastefield layer and, (3) the layer of ambient water underlying the wastefield. Ocean currents within these layers are assumed to have only small gradients along a vertical axis--except possibly between the upper layer and the two lower layers when a thermocline is present. The sub-models TSLINE, DPA, DPS, PRX, PRY, PCOMB, DPA2DPY, PXY, and PXYCMB2 are used to simulate processes that occur within these three layers.

The next two layers (4, 5) comprise the next grouping. This group consists of a near-bottom layer of water and a thin layer of particles on the surface of the sediments ("surficial sediments"). These two layers are used to simulate particle resuspension, transport, and deposition. The layer of water has a characteristic thickness of a few meters. Particles resuspended from the bottom are largely confined to this layer and are transported by the near bottom currents. The currents within this layer differ in some respects from those in the overlying portion of the water column due to frictional effects with the bottom (and possibly other processes).

The thin layer of particles on the surface of the sediments is used in this model as a conceptualization of the processes leading to our sediment trap observations. Fluxes into near bottom sediment traps (in 55-60m of water) are roughly one to two orders of magnitude greater than estimates of the net accumulation rate of particulate mass in the sediments (e.g., 1000-5000 mg cm^{-2} yr^{-1} versus 9-60 mg cm^{-2} yr^{-1}). In this conceptual model, the disparity in fluxes is attributed to the differences between resuspension and deposition fluxes between the sediments and the sediment traps. The accumulation flux, F_a, (neglecting the effects of decay) is equal to the difference between the depositional flux F_d and the resuspension flux, F_r:

$$F_a = F_d - F_r \tag{1.30}$$

If the sediment traps provide an accurate estimate of the rate of deposition of settling particles (either from the overlying water column, or resuspended from the sediments), then the depositional flux, F_d, measured by the traps is equal to the depositional flux to the surface of the sediments. On the other hand, the resuspension flux, F_r, is essentially zero for particulates that have settled into the traps, but not for particles that have settled on the surface of the sediments. If the resuspension flux for the particles in the surficial sediments is comparable with the deposition rate, F_d, the rate of accumulation of particles in the sediments will be much smaller than the deposition rate.

If this is a valid interpretation and resuspension occurs frequently, the mass and thickness of the particles in the surficial sediments will be small. For example, if there are two resuspensions per day (e.g. associated with the combination the net ocean current and the peak tidal flow), the mass of particles in the surface layer will be on the order of 1.5 to 7 mg cm^{-2}. Assuming a density (dry mass per wet cubic centimeter) for this material of 0.1 gm cm^{-3}, the thickness of the material will be on the order of 0.15 to 0.7 mm. These numbers should not be taken too literally--they are only order of magnitude estimates of the "average" thickness. However, they are an indicator of the potential difficulties associated with observing and sampling particles in this layer. The processes of sediment resuspension, transport, deposition, and transfer into the surface layer of sediments are simulated by the submodels TRANS, DISPER, ACCUM, and SEDR.

The bottom three layers constitute the third group. The uppermost of these layers represents the region in which the decay of organic material is taking place (i.e. the "decay" layer). We estimate that the effective thickness of this layer is on the order of 0.13 to 0.33 cm (assuming a decay layer density of 0.2 to 0.5 gm cm^{-3} and a decay flux of 120 mg cm^{-2} yr^{-1}). This is about an order of magnitude greater than the thickness of the surficial sediments. The decay layer should be considered a sublayer within the surface sediment layer (layer 8). The latter is used to represent the region of the sediments that are mixed by biological and physical processes. In the *SED2D* conceptual model, it is assumed that material is homogeneously mixed within this layer. Typical thicknesses for this layer range from less than a millimeter (anoxic basins) to on the order of 10-20 cm (aerobic

sediments populated by "conveyor belt" feeders or subject to strong mixing by waves and swell). In the model, this region is referred to as the "surface sediment" layer.

Below this layer, mixing and decay are assumed to be negligible. We refer to this layer (with an indefinite lower boundary) as the "deep sediments". If wastewater discharge related materials are evident, it may be appropriate to divide this layer into two layers, separated by the "discharge horizon" marking the boundary between the presence and absence of this material. The submodel PXYACC is used to compute the accumulation flux of particle mass in the sediments and the concentration of organic material in the surface sediments.

In the *SED2D* simulation discussions, the term "accumulation flux" is used to represent the rate of increase of particle mass (in mg cm^{-2} yr^{-1}) in the sediments relative to some fixed point in the deep sediments. If the density of the particles (dry mass per wet cm^3) in the deep sediments is known, dividing the accumulation flux by this density yields the rate of growth in the thickness of the sediments.

I.B.2.c. Subprogram Overview. In the following sections, we present a more detailed description of the individual submodels used in the *SED2D* simulations.

I.B.2.c.i. *Initial Sedimentation*.
TSLINE. TSLINE is a numerical simulation model of initial dilution based on the physical model studies reported by Roberts *et al.* (1989a, 1989b, 1989c), which were conducted for the following conditions:

1. a buoyant line source diffuser
2. constant density gradient in the ambient water column
3. uniform current speed and direction

TSLINE computes time-series of various characteristics of the initial dilution process using simultaneous measurements of the ocean currents and the thermal stratification of the water column. One calculation is made for each observation in the time-series. The calculation proceeds in the following manner:

> A near-bottom temperature gradient in the water column is computed from the temperature difference between the lowermost pair of thermistors (e.g. in a string of thermistors) and their vertical separation. This gradient is used to compute the temperature at the depth of the diffuser port. The density of the water at the level of the diffuser port and at the depth of the upper of the two thermistors is computed from these two temperatures. CTD data is used to obtain an empirical relationship between density and temperature if salinity gradients contribute to the density gradient. This density gradient is combined with the current velocity in the entrainment region (measured at the same time as the temperature measurements) to compute the height-of-rise of the wastewater to the level of minimum dilution.
>
> The water depth at the level of minimum dilution is computed by subtracting this height-of-rise from the depth of the diffuser port. Next, this wastefield depth is compared with the depth of the upper thermistor (of the pair) used in computing the temperature gradient. If the wastefield depth lies at, or below, the thermistor depth, the remaining characteristics of the wastefield are computed and the collection of stored as records in a set of computer files. The initial dilution calculation then proceeds to the next set of observations.
>
> For a typical distribution of thermistors in the water column, the predicted wastefield depth will virtually always lie above the depth of the upper thermistor (of this initial pair). In that case, the next higher thermistor in the string is used for a new trial simulation. A new density gradient, computed from the temperature recorded at this thermistor and the temperature at the diffuser port, is used to compute a new estimate of the height-of-rise of the wastefield. The resulting wastefield depth is again compared with the thermistor depth to see if the wastefield is trapped below the level of the thermistor. If so, the remaining characteristics are

computed and stored, as previously described. If not, the calculation proceeds in an iterative fashion until the thermistor lies above the wastefield.

On occasion, the gradient associated with the temperature recorded by a thermistor at a depth of D_i will result in a wastefield that is predicted to lie above the depth of the thermistor--but using the temperature information from the next higher thermistor (depth D_{i+1}) results in a predicted wastefield that lies not only below this thermistor (depth D_{i+1}), but also below the depth of the lower thermistor (depth D_i). This situation is the result of a strong increase in the thermal (and density) stratification of the water column between the thermistor(s) and the diffuser port, so that a constant gradient is a poor approximation to the actual density distribution. In this case, we note that the wastefield must lie between the depths of the two thermistors (i.e. $D_{i+1} < D_m < D_i$, D_m = depth at minimum dilution in the wastefield). The estimated depth is obtained by interpolating between the two thermistor depths, using the predicted depths based on the two temperature gradients (current, previous iteration) as weighting factors.

The angle between the direction of flow and the alignment of the diffuser affects the magnitude of the initial dilution and the height-of-rise. Therefore separate simulations are generally carried out for each leg of a multi-leg diffuser.

The time-series output generated by the model includes:

1. The heights-of-rise to the level of minimum dilution (within the wastefield) and the top of the wastefield.
2. The thickness of the wastefield.
3. The dilution at the level of minimum dilution and the average dilution.
4. The temperature of the ambient water at the top of the wastefield and at the level of minimum dilution.

The output also includes a printed summary of the average and rms values, and distributional information for a number of characteristics of the process. These include:

1. The depth to the top, level of minimum dilution, and the bottom of the wastefield.
2. The thickness of the wastefield.
3. The average temperature gradient (and effective temperature gradient including salinity effects).
4. The average and rms minimum and average dilutions.
5. The average and rms values of the average concentration of wastewater in the wastefield.

The predicted wastefield depths (and thicknesses) were used in both the *DECAL* and *SED2D* simulations. The rms average concentrations (relative to a unit effluent concentration) were used, in combination with the actual effluent concentration, to compute the initial concentration of effluent suspended solids in the wastefield in the *SED2D* simulations. In subsequent discussions, unless otherwise stated, when we refer to "initial dilution", or "average initial dilution" in regard to the *SED2D* simulations, we mean the dilutions based on the change in concentration during the (simulated) initial dilution process.

DPA. DPA simulates the movement of effluent and natural particles from the wastefield to the ocean bottom. Particles can be divided into three components: (1) inorganic, (2) organic, but refractory and, (3) labile organic material. By "organic-refractory", we mean the component of the organic material that is associated with a sufficiently slow decay rate so that loss due to decay is negligible over the time-scales that characterize the sedimentation of particles from the wastefield to the ocean bottom (within the simulation area). This material may, however, be degradable over the time-scales that characterize the residence times of particles in the surface layer of the sediments.

The simulation of this sedimentation is based on the aggregation kinetics expressed by equations 1.25 and 1.27, a first-order decay rate for organic-labile material, and Stoke's Law for the settling speed. In the simulation, a column of water is tracked as it moves along with the ocean currents (i.e., in a Lagrangian reference frame) and the sedimentation to the bottom of the column is computed. The output consists of the mass flux of particles to the bottom as a function of elapsed time. This mass flux is stored as a time-series and is later integrated into spatial depositions with the submodel DPA2DPY.

The calculation is carried out in the following manner:

The water column is divided into two layers--the wastefield and an underlying region of water. Aggregation is assumed to be limited to the wastefield layer. The initial conditions for the simulation are:

1. The concentrations of effluent and natural suspended solids and their inorganic, organic-refractory, and organic-labile fractions.

2. The flux of natural particles into the wastefield (settling from an overlying layer) and their composition.

3. The decay rate for the organic-labile fraction of the effluent and natural particles.

4. The initial thickness of the wastefield.

5. The rate of decrease in the thickness of the wastefield (e.g. associated with "gravitational collapse--e.g. Wu 1969).

6. The settling height (i.e. the distance from the bottom of the wastefield to the ocean bottom).

The concentration of suspended solids in the wastefield, flux of particles through the bottom of the wastefield, movements of particles settling through the underlying layer, loss of organic material, change in settling speeds, and the flux to the ocean bottom are computed for discrete intervals of time.

The mass of aggregate particle mass settling out of the wastefield over a time interval, dT, is computed by an approximate integration of equation 1.25. Rewriting this equation:

$$\frac{dC}{dt} = -B_{ds}C^{2.3} - B_{br}C^{1.3} \qquad (1.31)$$

$$\frac{dC}{dt} \approx -C(bC + a) \qquad (1.32)$$

where:

$$b = B_{ds}C_{beg}^{0.3}$$

$$a = B_{br}C_{beg}^{0.3}$$

and C_{beg} is the concentration at time t=0, then integrating:

$$\int_{C_o}^{C(t)} \frac{dC}{C\cdot(a + bC)} \approx -\int_0^{\Delta t} dt \qquad (1.33)$$

yields:

$$C(t) = C_o \frac{a}{(a + bC)e^{a\cdot\Delta t} - bC_o} \qquad (1.34)$$

The settling velocity of the mass associated with this change in concentration is assumed to be the average of the aggregate particle settling speeds at the beginning and the end of the interval. At the end of the interval, the position of the mass in the water column is assumed to be equal to the product of the average settling speed and the average settling time (i.e. one-half the simulated time interval). The composition of the particles in the group is set equal to the composition of the particles in the wastefield at the beginning of the interval.

The next step is to compute the compositions and positions of all the particles in the groups that previously settled out of the wastefield. First the loss of natural and effluent labile material due to decay is computed. The average settling speed of the particles in the group is reduced to reflect this loss of mass, using Stoke's law. The distance the group of particles has settled during the interval is computed by multiplying the average settling speed by the simulated time interval, and the new position in the water column is updated by adding this additional settling to the previous depth of the particles. The final step is to compare this depth with the depth to the ocean bottom to see if the group of particles has been deposited during this time step. If so, the component masses (natural/effluent; inorganic/organic-refractory/organic-labile) of this group are added to the masses associated with other groups deposited during the time step. Each deposited group is also removed from the inventory of particle groups still settling in the water column. The total component masses deposited during this interval are stored as a new record in a file containing the history of deposition to the bottom from this column of water.

Next the component masses (or concentrations) of the particles remaining in the water column are updated. The concentrations of natural and effluent labile material are reduced to reflect the loss due to decay.

The final step is to adjust the component masses of the effluent and natural particles for the loss of material due to aggregate particle settling from the wastefield. Then the natural particle component masses are increased to reflect the sedimentation of natural particles into the wastefield from the overlying water column.

This set of calculations continues in an iterative fashion until the desired duration of the simulation has been reached. The output consists of time-series of the depositional fluxes of each of the six components of the wastefield suspended solids (natural: inorganic, labile, organic-refractory; effluent: inorganic, labile, organic-refractory).

DPS. DPS provides the same function as DPA, but for noncohesive effluent particles that do not aggregate with each other, or with natural particles. Since the effluent and natural particles do not aggregate, their depositional fluxes can be computed independently (e.g. the natural fluxes can be estimated from the historical rate of accumulation of sediments in the absence of the discharge).

The DPS submodel uses measurements of the mass distribution of effluent particle settling speeds. This distribution can be determined from laboratory-based measurements with a settling column, or other means. The first step in a DPS simulation is to present this data in a log-log plot of the cumulative mass fraction of particles with a settling speed $v_s > v_r$ versus a reference settling speed, v_r. This mass distribution of particle settling speeds is approximated by a set of straight line segments (see Figure 1.6). Within each segment, the cumulative mass fraction can be represented by an equation of the form:

$$F_c\,(v_s \geq v_r) = \frac{a}{v_r{}^b} \tag{1.35}$$

where:

F_c = cumulative mass fraction
a,b = parameters

The parameters "a" and "b" describing each line segment are one element of the input into DPS. The settling depth, duration of the simulation, and output interval are the other elements. The deposition calculation proceeds as follows:

The settling speed required to reach the ocean bottom is calculated for each cell in cross-shore transect:

$$v_{s,i} = \frac{h_L}{t_i} \tag{1.36}$$

where:

$v_{s,i}$ = settling speed corresponding to i^{th} interval
h_L = thickness of the lower layer (settling distance)
t_i = elapsed time after the i_{th} interval

Using the current and previous values of the settling speed, the fraction of the combined inorganic, organic-refractory, and organic-labile particle mass that has been deposited between the i-1^{th} and the i^{th} interval is calculated:

$$\begin{aligned} F_i^d(ir) &= f_i(ir) - f_{i-1}(ir) \\ F_i^d(ol) &= f_i(ol) - f_{i-1}(ol) \end{aligned} \tag{1.37}$$

where:

F^D_i(ir,ol) = mass fraction deposited between the ith and i-1th interval
f_i(ir,ol) = cumulative mass fraction at t = $i \cdot$ t
f_{i-1}(ir,ol) = cumulative mass fraction at t = $(i\text{-}1) \cdot$ t

Here f_i is computed from the appropriate straight line segment used to represent the cumulative mass distribution, and (ir,ol) refer to the inorganic plus the organic-refractory, and the organic-labile fractions of the total mass respectively. The cumulative mass fractions f_i(ir)

and $f_i(ol)$ are obtained from the total mass cumulative mass fraction f_i by the relationships:

$$f_\epsilon^d(ir) = f_i \cdot (q_{inorgic} + q_{organic-ref}) \quad (1.38a)$$

$$f_i^d(ol) = f_i \cdot q_{organic-labile} \cdot e^{-k_d t_i} \quad (1.38b)$$

This calculation is repeated for increasing elapsed time, $i \cdot t$, until the desired total simulation time is reached.

The output file from DPS consists of a time-series records analogous to those produced by DPA. However, since the deposition of natural particles is not computed, the output only describes the depositional fluxes of the three components of the effluent particles.

Application of Depositional History to Simulation Grid. The set of *SED2D* submodels simulate the deposition and accumulation of particles within a rectangular grid of cells (Figure 1.7). There are 32 cells in both the "longshore" and "cross-shore" directions, but the dimensions of the cells can vary between the two axes. The longshore axis of the grid is generally taken to be parallel with the principal major axis of variation of the subtidal component of the ocean currents at the depth of the wastefield. This direction usually corresponds to the "longshore" movement of the currents. Positive longshore values (or cell number) increase to the right when facing offshore. The cross-shore axis is perpendicular to the longshore axis, with positive values in the offshore direction. Distances are measured relative to the "bottom-left" corner of the grid. The location of the discharge point can be anywhere within the grid, and the inshore boundary of the grid does not need to coincide with the coastline.

The depth of the water can vary within the grid in the cross-shore direction, but all cells in the same longshore row have the same depth. Water depths are specified for each (longshore) cell boundary across the cross-shore transect; the average of the two boundary values is used to represent the average cell depth.

Both DPA and DPS compute a depositional time-series for each cell along this transect. Each time series represents the depositional history in each cell--assuming that the wastefield (and the associated column of settling particles) exists in each cell in the transect. This depositional history can be represented by the variable $P_d(i,j,k)$, where $P_d(i,j,k)$ represents the mass of the k^{th} component of the suspended solids deposited during the i^{th} time interval, in the j^{th} cross-shore cell. The deposition is set equal to zero in cells whose depth is less than the depth to the bottom of the wastefield. A later submodel (PXYCMB2) uses an approximate method to estimate the deposition in the region where only part of the wastefield is present (i.e. the water depth lies between the upper and lower bounds of the wastefield).

PRY. The next step is to estimate the probability that the wastefield (and column of settling particles) is present in each cross-shore cell. This probability is a function of the elapsed time since discharge and is estimated with the submodel PRY. This probability can be expressed by the variable, $P_y(j|i)$, where the index "*i*" refers to the i^{th} (simulated) elapsed time since discharge, and the index "*j*" to the j^{th} cross-shore cell.

The probability is computed by assuming that the *true* statistical distribution of wastewater in the cross-shore direction can be adequately represented by the statistical distribution obtained from the transport calculated using a "progressive vector diagram" type calculation ("PVD"). In this method, each observation of the currents is represented by an arrow (vector) whose length is proportional to the speed of the current at the time of the sampling. The orientation of the arrow is along the direction of the flow. The head of this arrow is used as the origin for the next arrow (i.e. corresponding to the next observation in the time-series of current velocities). The projection of this motion on the cross-shore axis yields the cross-shore position as a function of elapsed time; the projection on the longshore axis, the longshore movement.

This computational technique implicitly assumes that the currents everywhere in the simulation area are identical to those measured at the current meter mooring. Measurements of currents in southern California coastal waters indicate that this assumption is justified for longshore movements along reasonably "straight" coastlines. Coherency length-scales for these motions are on the order of 15 to 30 km (Hendricks 1978; Winant 1983). The situation is substantially different for cross-shore motions, where the coherency length-scales are much shorter (a few kilometers, or less for horizontal separations; less than 20m vertically for stratified waters--e.g. Hendricks 1990). Therefore the computational technique becomes suspect. However, limited comparisons of the cross-shore movements of drogues with the cross-shore motions predicted from simultaneously collected current meter data suggest that the range of displacements and the time-scales of the two motions are similar--even if the actual motion of drogues is not well predicted from the current meter data (Hendricks 1982). This similarity suggests that the *statistical* properties predicted from current meter data may be representative of the range of cross-shore motions even if deterministic calculations are not possible.

The cross-shore position of a column of wastewater, y_i (discharged at y=0 at time t=0), after an elapsed time $t_i = i \cdot t$, is:

$$y_I = \sum_{j=1}^{I} v_j^y \cdot \Delta t \tag{1.39}$$

The result consists of a sequence of cross-shore positions:

$$Y = [y_0, y_1, y_2, \cdots, y_N] \tag{1.40}$$

where $y_o = 0$.

The probability that the column of wastewater is located in cell j after an elapsed time (following discharge) equal to one simulated time interval, t, is estimated by counting all the differences between adjacent pairs of positions in this sequence that fall within the boundaries of the j^{th} longshore cell. Similarly, the probability that the column of wastewater is located in cell j, after an elapsed time equal to i simulated time steps, $t = i$ t, is:

$$P_y(k|j) = \frac{1}{N-j} \sum_{I=j}^{N} \delta((y_I - y_{j-I}) - y_k) \tag{1.41}$$

where:

$\delta(y-y_j) = 1$ if $y_j - \frac{1}{2}\Delta y < y \leq y_i + \frac{1}{2}\Delta y$
$= 0$ otherwise
y = cross-shore length of a simulation cell

As in the case of the output from DPA and DPS, the output from this subprogram consists of a sequence of records. Again, each record corresponds to a fixed value of the elapsed time, and contains 32 fields, with each field listing the probability that the water column lies within the boundaries of the corresponding cell at that elapsed time.

So far, this computational scheme ignores the presence of the coastal boundary. No effort has been made to restrict the movements from entering water that is shallower than the top of the wastefield (or even inshore of the coast). In order to prevent transport of wastewater into these areas, we consider the cell boundary that has a water depth closest to the depth of the bottom of the wastefield as a barrier to onshore transport of the

wastefield. The occupation probabilities for the cells inshore of this barrier are "reflected" across the barrier and added to the cell probabilities on the offshore side of the barrier. Thus the probability for the first cell inshore of the boundary is added to that for the first cell offshore of the boundary; the probability for the second inshore cell is added to that for the second cell offshore, etc. The probabilities for all the cells inshore of the boundary are then set equal to zero. This approach is analogous to the "virtual source" approach used in computing diffusional transport in the presence of a barrier.

PCOMB. Current meter data is frequently available for an extended period of time. It may not be possible, however, to directly use this data in the subprogram PRY. There are two possible difficulties: 1) the data set may consist of a series of deployments separated by short periods when data was not collected, or 2) the number of observations may exceed 2048 (the array storage provided in PRY). One way to get around this problem is to compute the cross-shore probability distributions for each deployment period. Then, with PCOMB, the output files are weighted by the number of observations and combined into a single file representing the long-term average cross-shore, time-dependent probability. PCOMB can be used in a similar fashion for the longshore transport.

DPA2DPY. At this stage in the simulation, we have a description of the deposition of wastefield particles on the bottom for each cross-shore cell--assuming that the wastefield (and column of settling particles) is present, and the probability that the wastefield is actually present. Both of these are expressed as a function of the elapsed time since a segment of the wastefield and associated column of settling particles moved away from the outfall diffuser. The program DPA2DPY estimates the actual deposition in each cross-shore cell by simply combining the two probabilities (depositional, positional). The combined probability of deposition to the bottom in the cell j at the elapsed time i is:

$$P_{dy}(j \mid i) = P_{dpa}(j \mid i) \cdot P_{y}(j \mid i) \qquad (1.42)$$

where:

$P_{dy}(j|i)$ = probability of deposition in cell j at time i
$P_{dpa}(j|i)$ = prob. of deposition in cell j at time i (column of settling particles present)
$P_{y}(j|i)$ = probability that the column of settling particles is at cell j at time i

Implicit in this equation is the assumption that the probability of deposition on the bottom in cell j at time i is independent of the prior history of movements of the column. The output from DPA2DPY is a file containing this time-history of the estimated "actual" deposition in each cell at each elapsed time i.

PRX. Although we now have an estimate of the time-dependent deposition of wastefield particles in a cross-shore transect of cells, we do not know the longshore location of this transect as a function of time. The subprogram PRX estimates the probability that this transect of cells will be at some longshore position (identified by the longshore cell index k) as a function of elapsed time. The computational scheme used to compute this probability is identical to that used to compute the cross-shore transport--up to, but not including, the effects of a coastal boundary.

Although the computational algorithm is the same as in PRY, the theoretical basis is somewhat different. As noted previously, the coherence length-scales for longshore transport are comparable with, or exceed, the longshore dimension of a typical simulation grid. Limited observations indicate that the longshore movements of drogues are predicted reasonably well from current meter data collected by the same time. Thus the longshore movements of a segment of the wastefield (and the column of particles settling from that segment) are often adequately predicted by current measurements from a single mooring (one should be cautious however, in regions of complex bathymetry). As a result, the statistical distribution of longshore transport can be predicted from the current meter data and we do not need to assume the equivalency of the predicted and actual distributions.

PXY. We now have a statistical estimate of the time-dependent deposition of particles into each cell in a cross-shore transect, and a time-dependent statistical estimate of the longshore location of this transect. The program PXY estimates the depositional distribution (probability) of wastefield particles into the two-dimensional grid of cells by combining these two conditional probabilities. The deposition into a specific cell (longshore index k, cross-shore index j) over the entire period simulated by the previous submodels is the sum (over elapsed time) of the product of the longshore positional probability that the transect of cross-shore cells lies over the longshore cell k, by the depositional probability for the cross-shore cell j (within the transect):

$$P_{xy}(k,j) = \sum_{i=1}^{N} P_x(k|i) \cdot P_{dy}(j|i) \tag{1.43}$$

where N is the total number of simulation time-steps.

These values represent the total depositional probability, expressed in terms of a unit mass of suspended solids in the (DPA or DPS) simulation column. For example, if the depositional probability of effluent particle total suspended solids into cell (k,j) is 0.01, one percent of all the effluent-related suspended solids discharged from the outfall will be deposited in that cell.

PXYCMB2. PXYCMB2 provides a number of functions. One of these is to estimate the deposition that occurs inshore of the reflective boundary (see PRY discussion). This deposition is assumed to occur in cells that have water depths that range between the top and bottom of the wastefield. In the case of aggregating particles (DPA simulations), the sedimentation in these water depths is controlled by the flux of particles out of the wastefield since the wastefield is now in contact with the bottom (i.e. the situation is equivalent to the 2-layer version of *DECAL*). We assume that the aggregation flux is dominated by differential settling. In that case, the rate varies with the thickness of the wastefield raised to the 1.23 power (equation 1.25). The thickness of the wastefield in this inshore region is equal to the difference between the depth of the water in the cell and the depth to the top of the wastefield. No deposition is permitted if the water depth is less than the depth to the top of the wastefield. The deposition in each cross-shore cell with water depths between the top and bottom of the wastefield is approximated by the equation:

$$F_d(j) = F_d(j_r)\left(\frac{d_c - d_t}{h_w}\right)^{1.23} \tag{1.44}$$

where:

d_t = depth to top of the wastefield
d_c = water depth in the cell j
h_t = wastefield thickness
$F_d(j)$ = depositional flux into cell j
$F_d(j_r)$ = depositional flux immediately offshore of the reflective boundary (cell j_r)

If the simulation is for noncohesive particles (i.e. a DPS simulation), an analogous weighting is used, but the exponent is changed from 1.23 to 1.00. This weighting reflects the reduced mass of suspended solids contained in the thinner wastefield.

PXYCMB2 also allows one to weight and combine multiple PXY files. Most ocean outfalls terminate in an extended, multi-port diffuser (instead of a point discharge) whose length often exceeds the dimensions of the simulation cells. Multiple discharge points are often used in *SED2D* simulations to approximate the effects of an extended source. The two-dimensional depositional patterns (from PXY) associated with each of these discharge points can be combined at this point to produce a single depositional file representing the extended

source. If two outfalls are present in the simulation area, PXYCMB2 can be used in an analogous manner to combine the depositional flux patterns (an alternative method is provided by the subprogram PXYADD).

PXYCMB2 provides two types of output. One form generates the two-dimensional deposition probabilities (i.e., PXY-type files); the other form outputs the depositional fluxes in mg cm^{-2} yr^{-1}. These latter are computed from the equation:

$$F_m(k,j) = F_d(k,j)\left(\frac{0.001 M_e}{A}\right) \qquad (1.45)$$

where:

F_m = deposition rate in mg cm^{-2} yr^{-1}
F_d = deposition probability
M_e = annual suspended solids mass emissions in metric-tons per year
A = area of a simulation cell (km^2)
0.001 = conversion factor from km^2 to cm^2 and mt to mg

The final capability provided by PXYCMB2 is the ability to combine component depositional probabilities (or flux rates) into a single depositional probability (or flux). For example, decay in the sediments may involve both the "organic-labile" and "organic-refractory" material. Therefore, it may be appropriate to combine these two components into a single new component (e.g. "organic material"). Similarly, if natural and effluent organic material have the same decay rate in the sediments, these two categories can also be combined into a new category (e.g. "total"). These steps can reduce the time required to carry out the subsequent simulation steps (and associated number of files) by a factor of three.

PXYADD. The submodel PXYADD provides an alternative method of simulating the effects of multiple discharges (either from multiple outfalls, or from an extended diffuser). The procedure is to use a single two-dimensional flux (or probability) file from PXYCMB2 (or PXY) as a template. A second discharge can be simulated by shifting this pattern relative to the grid of cells and combining this new pattern with the original pattern. The process implicitly assumes that the discharge from the second location has characteristics that are identical to those of the first source. Therefore it may be inappropriate to use PXYADD to simulate discharges that have significantly different discharge depths or diffuser configurations (however, different initial suspended solids concentrations can be approximated by applying a suitable weighting to the "strengths" of the two sources). The advantage of using PXYADD is that it can appreciably reduce the effort and time required for a simulation.

I.B.2.c.ii. *Sediment Resuspension*. The submodels described so far simulate processes in the upper three layers of the simulation. The next phase of the simulation estimates the resuspension, transport, deposition, and "accumulation" of these particles after they reach the bottom. Note that in the discussion of resuspension processes, we use a somewhat different meaning for the term "accumulation" than used in the other discussions. In the present context, it refers to the transfer of particles from the surficial sediment layer into the surface layer of the sediments (Figure 1.5b). This use of the term accumulation came about as a result of the computational approach used in the models (discussed with reference to the ACCUM submodel).

All the processes that give rise to sediment resuspension, and their relative importance and dependence on environmental conditions, are not known at the present time. The *SED2D* suite of submodels that simulate this aspect of the particle fates should be regarded as providing an indication of the potential importance of these processes, rather than accurate estimates. The inclusion of some estimate of this potential into the simulation process is motivated by the observed disparity between the flux of particles into near-bottom sediment traps and the net accumulation flux of particles in the adjacent sediments.

Simulation Approach. These processes are simulated in four phases. First the transport of particles during an individual resuspension event is estimated by the submodel TRANS. Next the dispersion of particles after a single resuspension event is calculated for a point source of resuspended particles. This distribution is calculated by the subprogram DISPER. An ensemble of single resuspension events, using the transport data generated by TRANS, is used to calculate this distribution. The next step is to estimate the dispersion and final accumulation (after a large number of resuspensions) of a unit mass of particles that were originally in a single cell. This calculation is carried out by the submodel ACCUM and typically represents the single most time consuming step in a simulation. Next, the accumulation distribution produced by ACCUM is applied to each cell in the simulation grid using the submodel SEDR. In this calculation, the mass (flux) of particles "available" for resuspension is weighted by the mass (flux) of particles that are deposited to that cell from the overlying water column. (i.e. the deposition generated by PXY or PXYCMB2). The output from SEDR consists of the accumulation (flux) of particles into the surface layer of sediments after the effects of resuspension.

TRANS. A variety of physical and biological processes can lead to the resuspension of sediment particles. In our simplified approach, only the resuspension associated with stress on the bottom by the near-bottom currents is simulated. The combined effects of waves (or swell) and ocean currents can significantly alter the stress on the bottom (Grant and Madsen 1979, 1986), compared with the stress associated solely with the currents, but these effects are not included in the simplified representation incorporated into TRANS. Bioresuspension processes are also not included.

In this simplified representation, it is assumed that resuspension commences when the near bottom ocean current speed exceeds some threshold resuspension speed, v_r. The resuspended particles are deposited when the current speed falls below some threshold deposition speed, v_d. TRANS generates a sequence of estimates of the transport vector for individual resuspension-redeposition events of this type. The transport is computed using a PVD-type calculation. Output from TRANS consists of a set of records, with each record listing the terminal (x,y) coordinates of the PVD, relative to the point that resuspension commenced (0,0).

DISPER. DISPER uses the set of transport vectors from TRANS (including from multiple data sets) to generate the probability, P_r, of the transport of resuspended particles from a single location (x=0,y=0) to each cell (k,j) in an array of longshore and cross-shore cells (Figure 1.8). The array, or grid of cells, differs from the primary simulation grid in that: (a) its dimensions are 63 x 63 cells and, (b) the origin of the coordinate system is in the center of the grid (cell 32,32). Resuspension begins with a unit mass of cells at the center of the grid. The probability that a resuspension event terminates in cell (k,j) (i.e. deposition occurs in this cell) is computed using the equation:

$$P_d(k,j) = \frac{1}{N} \sum_{i=1}^{N} \delta(\vec{x}_i - \vec{x}_{cell}(k,j)) \qquad (1.46)$$

where:

$$\delta(x_i - x_{k,j}) = 1 \quad \text{if } x_i \in x_{cell}\ (k,j)$$
$$= 0 \quad \text{otherwise}$$

x_i corresponds to the ith transport vector calculated by TRANS, $x_{cell}(k,j)$ refers to the set of (x,y) values associated with cell(k,j). The output from DISPER is a file containing the probabilities of deposition in each of the grid cells after a single resuspension event originating at the center of the grid.

ACCUM. ACCUM estimates the "accumulation" rate of particles in the surface layer of the sediments. It is assumed that there is some probability, f_a, that a particle in the surficial sediments is transferred from the surficial layer to the underlying surface layer. After this transfer, it is assumed that the particle will no longer be available for chronic resuspension. This is equivalent to assuming that the average particle settling from the overlying water column undergoes n_r ($=1/f_a$) resuspensions before it becomes part of the surface layer sediments.

This conceptual model is used to compute the accumulation distribution of particles within the resuspension grid. At the beginning, all the particles are confined to the center cell. The calculation proceeds in the following manner:

Four resuspension simulation grids are used (Figure 1.9). One of these ("source grid") contains information on the mass of particles available for resuspension in each cell at the beginning of a resuspension event. The next grid is the "transfer grid" that was generated by TRANS and DISPER simulations. At the beginning of the simulation, a unit mass is placed in the center cell (i.e., 32,32). All the other cells start out without any particle mass. The third grid ("deposition grid") contains the mass of particles transferred from the source grid to each of the deposition grid cells following a resuspension event. The last grid ("accumulation grid") contains the mass of particles that are transferred from the deposition grid to the surface layer of the sediments and "accumulate" there. It contains statistical information on the transfer of mass from one cell in the source grid to cells in the deposition grid during a single resuspension event.

The center cell starts with a unit mass of particles in the surficial sediments. Before the first resuspension event, a mass equal to the accumulation fraction, f_a, is transferred from the surficial sediments in this cell to the surface layer of the center cell (i.e. into the center cell of grid 3). The mass remaining for resuspension in the center grid of the center cell is reduced to $1-f_a$. Thus the initial conditions for the first resuspension event are:

Grid 1 (Source grid):
- Cell (*32,32*): $f_{avail} = 1\ (1 - f_a)$
- All other cells: $f_{avail} = 0$

Grid 2 (Transfer grid):
- Cell transfer probabilities (calculated previously with DISPER).

Grid 3 (Deposition grid):
- All cells: $f_{depo} = 0$

Grid 4 (Accumulation grid):
- Cell (*32,32*): $f_{accum} = f_a$
- All other cells: $f_{accum} = 0$

The first resuspension event is computed by superimposing the transfer grid (grid 2) over the source grid (grid 1) with a 1:1 correspondence between the cells (i.e. the two grids are congruent). The mass of particles in a cell(k,j) in the deposition grid at the end of the first resuspension event is equal to the probability in the corresponding cell (i.e. k,j) in the transfer grid (grid 2) multiplied by the mass in the center source grid just before resuspension (i.e. $1-f_a$):

$$P_2(k,j) = P_1(32,32) \cdot P_2(k,j) \tag{1.47}$$

where:

$P_1(k,j)$ refers to the source grid (= $1-f_a$ for the first resuspension)
$P_2(k,j)$ refers to the transfer grid
$P_3(k,j)$ refers to the deposition grid

At the end of this resuspension event, a fraction (= f_a) of the mass in each of the deposition grid cells is transferred into the corresponding cell of the accumulation grid:

$$\begin{aligned} P_3(k,j) &= f_a P_2(k,j) \qquad [for\ (k,j) \neq 32,32] \\ P_3(k,j) &= f_a(1 + P_2(k,j)) \qquad [for\ (k,j) = 32,32] \end{aligned} \tag{1.48}$$

The mass remaining in each cell of the deposition grid is then reduced to reflect this loss. Next the remaining mass in each deposition cell is transferred to the corresponding cell in the source grid and then the mass of the deposition grid cell is reset to zero. At the end of this first resuspension, the mass available for a second resuspension in each of the source grid cells is:

$$P_{1,2}(k,j) = (1 - f_a) \cdot P_4(k,j) \tag{1.49}$$

where $P_{1,2}$ refers to the mass available in source grid (1) for the second (2) resuspension event.

In general, after this first resuspension a number of cells in the source grid will contain particles for the second resuspension event. The effects of a second resuspension are computed in a manner analogous to that used for the first resuspension event. However, the transfer grid is now positioned over each cell in the source grid and the transfer to each cell in the deposition grid is computed. The transport to deposition grid cell (k,j) from source grid cell (k',j') after i resuspension events is:

$$P_{3,i+1}(k,j) = (1 - f_a) \cdot P_{2,i}(k',j') \cdot P_{1,1}(k'-k+32, j'-j+32) \tag{1.50}$$

As before, after each resuspension event the mass of particles in each deposition grid cell is multiplied by f_a and the result added to the corresponding cell in the accumulation grid.

The number of source cells can grow roughly as $(N_d)_m$, where N_d is the number of cells in the transfer grid with a non-zero value, and m is the number of resuspension events. Therefore the amount of computation time required to compute a resuspension event can increase geometrically with the number of events. Ultimately, each of the cells in the source grid can contain mass available for the next resuspension event. At that point, the number of transfers that must be computed for each resuspension event is 3959 x N_d. If $N_d = 30$, the number of transfers for a single resuspension event will total almost 120,000. If the accumulation fraction, f_a, is 0.01 (i.e. the average particle undergoes 100 resuspensions), up to 12 million transfers could be required to determine the state of suspended solids in the surficial sediment layer and in the surface sediment layer after 100 resuspensions. At that time, 1/e (i.e. 37%) of the original unit mass of particles will still reside in the surficial sediments. Obviously a simulation of the transfer of particle mass into the surface layer of sediments may require extensive computation times.

A number of factors can help to limit this computation time. The two most important of these factors are: (1) resuspended particle mass is transported out of the grid and lost from the inventory and, (2) the effects of particle resuspension become less important as the number of resuspensions increases. These two factors limit the number of resuspension events that must be calculated--particularly if some error is acceptable in the predicted accumulation rates on the fringe of the area affected by deposition of wastefield particles.

The ACCUM resuspension simulations are repeated until one of a number of conditions are met. Usually these are: (a) the mass of material remaining available for resuspension within the entire ACCUM grid is less than some reference value or, (b) the mass deposited during the last resuspension event is less than some

reference percentage of the mass deposited during the previous time step. At that point, the simulation ceases and the mass of particles in the accumulation grid cells are transferred to a file (63 x 63 matrix). At the present time, any effects of the decomposition of organic material during this sequence of resuspensions are neglected.

SEDR. So far the resuspension effects have been computed for a single source cell. SEDR combines this information with the initial deposition pattern (i.e. the pattern generated with the set of submodels DPA(DPS)->PXYCMB2. The output from *SED2D* is the transfer rate of wastefield particles into the surface layer of the sediments in the primary simulation grid.

The calculational procedure is identical to that used for a single resuspension event in the ACCUM simulations. However, in the SEDR simulations, the output matrix from ACCUM replaces the transfer matrix from DISPER (it can be regarded as the transfer matrix from a single source cell of virgin surficial sediments directly into the surface layer of the sediments). The source grid (grid 1) is replaced the primary simulation grid (32 x 32 cells) generated by PXYCMB2, so that the source grid now contains the flux rate of wastewater particles settling from the water column. The deposition grid (grid 2) is truncated to 32 x 32 cells and will contain the flux of wastefield particles transferred into the surface layer of sediments in the primary simulation grid. The old transfer grid (grid 4), which contained the transfer values generated by disper, is replaced by the transfer probabilities values generated by the ACCUM calculation.

Only one transfer ("resuspension event" calculation) is required for this simulation since all the surficial sediment material is transferred to the surface layer of the sediments in a single step. The output consists of a file containing the flux rates into the surface sediments of the primary simulation grid (32 x 32). The format is identical to file structure generated by PXY and PYXCMB2. An example of a typical distribution is shown in Figure 1.10.

I.B.2.c.iii. *Sediment Processes*. Once particles are transferred into the permanent sediments, they can be mixed with other sediment material (e.g. through bioturbation) accompanied by additional decay of organic material. Ultimately they may be transferred into the deeper sediments, and where mixing processes may be weak and decay rates very slow. PXYACC estimates the effects of sediment mixing and decay within the surface layer of the sediments. The input flux of wastefield particle mass (natural + effluent) into this layer is contained in the file generated by SEDR (or PXYCMB2 in the absence of resuspension). To this flux must be added the flux of natural particles that occurs in the absence of the wastefield sedimentation. This includes sedimentation from the water column and from coastal erosion. These fluxes have not been included in the simulations up to this point. Losses from the surface layer include the decomposition of organic material and the transfer of material (burial) into the underlying layer. Note the surface layer moves upward with the transfer of particle mass into the underlying "deep" layer of sediments, reflecting the build-up of sediments.

The concentration of organic material in the upper layer is determined by the mass balance equation:

$$\frac{d}{dt}(C \cdot M_B) = C_i \cdot F_i - C \cdot (F + F_d) \qquad (1.51)$$

where:

C = organic concentration in the upper layer (fraction of mass)
C_i = organic concentration in the input flux of material
F = output flux of total mass into the underlying layer (deep sediments)
F_i = input flux of total mass
F_d = decay flux of organic material
$= k_d M_d = k_d \epsilon M_d$ (where: $0 \leq \epsilon \leq 1$)
k_d = decay rate of organic material in the upper layer
M_b = mass (/unit area) in the upper (mixed) layer
M_d = mass (/unit area) in which decay occurs

The output flux, F, is determined by the mass balance equation:

$$F_o = F_i - F_d \cdot C \tag{1.52}$$

If the concentration and flux rate of material into the upper layer are constant, equation 1.52 can be substituted into equation 1.51, and the latter integrated to yield the concentration of organic matter in the upper layer as a function of the elapsed time, t, since the commencement of the discharge:

$$\frac{2\gamma \cdot C(t) + \beta + \sqrt{q}}{2\gamma \cdot C(t) + \beta - \sqrt{q}} = \frac{2\gamma \cdot C_n + \beta + \sqrt{q}}{2\gamma \cdot C_n + \beta - \sqrt{q}} \cdot e^{-\sqrt{q}t} \tag{1.53}$$

where:

C_n = organic concentration in the upper layer at t=0

and:

$$\begin{aligned} \alpha &= 1/t_i \\ \gamma &= 1/t_d \\ \beta &= -(\alpha + \gamma) \\ q &= \alpha^2 + 2(2C_i - 1)\cdot\alpha\gamma + \gamma^2 \end{aligned} \tag{1.54}$$

where:

$t_i = (F_i/M_b)^{-1}$
$t_d = (F_d/M_d)^{-1}$

These parameters have the dimensions of time, and can be regarded as two characteristic response times of the surface sediments to changes in the flux or composition of the particles into them. We define the first parameter, t_i, as the "input" response time. It is the time required to input a mass of particles into the surface layer that is equal to the surface layer mass in the absence of decay. After this time, 1/e (i.e. 37%) of the original particles are still in the surface layer, and the remainder have been transferred (buried) in the deep sediments. The second parameter, t_d, is the "decay" response time. It is the time required to reduce a mass of organic material equal to the total mass in the surface layer to 1/e of that value. This decay response time is analogous to the response time of the surface sediments in *DECAL* (see equation 1.10), although it is expressed in terms of a mass and mass flux, instead of a decay rate per unit thickness and a thickness. However, in this scenario, the actual decay flux has a maximum value equal to the decay flux, F_d (i.e. if the organic fraction = 1). In the *DECAL* simulation, the flux of decaying material is unbounded (i.e. it increases with the accumulation of organic mass in the surface sediments). This difference can produce significant differences between the *DECAL* and *SED2D* predicted concentration of organic material in the surface layer if the input fluxes are significantly higher than the decay flux. The combined response time is:

$$t_\lambda = \frac{1}{\sqrt{q}} \tag{1.55}$$

Figure 1.11a shows how this response time for the surface layer depends on the ratio of these two response times, assuming that the concentration of organic material in the flux of material into the layer is 0.65. If the flux of total particle mass into the sediments is much greater than the decay flux (far right hand area of Figure 1.11a), then the actual response time is equal to the input response time, t_i. On the other hand, if the ratio is much less than one, then the actual response time becomes equal to the decay response time, t_d. For ratios

between about 0.03 and 5, the actual response time is in transition between these two values. When the input flux and decay flux are equal, the actual response time becomes equal to:

$$t_A = 2\sqrt{C_1}\cdot t_1 \tag{1.56}$$

For long times, i.e. $1/t << q$, the concentration of organic material in the upper layer, and the mass flux of material into the lower layer, approach their steady-state values:

$$C\left(t>\frac{1}{\sqrt{q}}\right) \rightarrow \frac{1}{2}\left[\left(\frac{t_d}{t_1}\right)^2 + (4\,C_1 - 1)\left(\frac{t_d}{t_1}\right) + 2\right] \tag{1.57}$$

Figure 1.11b illustrates how this steady-state concentration changes with the input flux-decay flux ratio. At high values, there is very little decay and the concentration is nearly the same as in the particles entering the surface layer (0.65). At low values of this ratio, the concentration is nearly proportional to this ratio. At a ratio of one, the steady-state concentration falls to about 0.40.

The time-dependent rate of mass transfer out of the upper layer into the lower layer can be solved by substituting the results of equation 1.53 into equation 1.52. Figure 1.11c shows the ratio of the steady-state accumulation flux to the flux of particles into the surface layer as a function of this ratio. At high ($F_i/F_d>10$) values, the accumulation flux is nearly equal to the input flux. At low values (<0.10), the accumulation flux becomes equal to the flux of inorganic material in the particles entering the surface layer (i.e. nearly all the organic material is lost to decay). At a ratio of one, the accumulation flux is about 60% of the input flux.

PXYACC presently computes these steady-state values for each of the cells in the 32 x 32 simulation grid based on:

1. The accumulation flux and composition of wastefield particles into the upper layer of permanent sediments (SEDR output);

2. The accumulation flux and composition of natural particles (from sources other than the wastefield) (user specified);

3. The decay flux of organic material in the upper layer.

The output from PXYACC consists of two files containing information on the organic content and the net accumulation rate of particle mass in the primary simulation grid of cells. This is the final simulation output from the *SED2D* suite of models.

I.B.2.d. Utility Programs.

XTRACT. XTRACT extracts a row or column of data from the matrix produced by PXY, PXYCMB2, SEDR, or PXYACC and writes a new file containing this information in ASCII format. This file can be used examine the distribution along a specified longshore or cross-shore transect. In particular, the output file can be used with commercial plotting programs to graphically present this data.

PRB2GT, DPY2GT. These programs provide a similar function for the output files from DPA (or DPS) and PRX (or PRY, PCOMB, and DPA2DPY). They convert these binary files into ASCII arrays that can be used to create surface or contour plots with commercial plotting programs.

II. METHODS

II.A. FIELD STUDIES

II.A.1. Sampling Design and Rationale

II.A.1.a. Effluent. Figure 2.1 shows matrices of the effluent sampling/analysis schedule as planned and as carried out in this project. The purpose of collecting and analyzing these samples was to establish the concentration of total organic carbon (TOC), total nitrogen (TN), Cd and Pb, potential marker compounds (linear alkylbenzenes, coprostanol, multielement scan) and the stable isotopic composition ($\delta^{13}C$, $\delta^{15}N$) of particulate matter in final effluent from four waste treatment plants. Owing to budgetary constraints, we did not plan to carry out more than bimonthly collections of effluent from three of the four plants (i.e. Orange County Sanitation District-OCSD, City of San Diego, Point Loma Treatment Plant-PLTP, City of Los Angeles-Hyperion). Moreover, Hyperion sampling was not a state-funded component of the present study, but was added by SCCWRP to enhance the value of the effluent data set. Although samples were collected from the Hyperion Treatment Plan as described in Figure 2.1, analyses (except for TSS and the 11/89 TOC and TN analyses) were not completed during this study. In the case of the JWPCP (Joint Water Pollution Control Plant, Los Angeles County Sanitation Districts) effluent, a 13 month (monthly) sampling program was undertaken in order to develop a more extensive database that could be compared with historical data (Eganhouse and Kaplan 1982a, 1982b; Eganhouse *et al.* 1983a; Eganhouse and Gossett 1991).

Total suspended solids measurements were performed on all effluent samples as a matter of course (i.e. all samples were filtered). Total organic carbon, total nitrogen, Pb and Cd measurements, on the other hand, were primarily made in support of the model verification effort (i.e. to obtain starting concentrations of these constituents on effluent particles). Consequently, these analyses were performed only for the contracted samples (bimonthly for JWPCP, OCSD and PLTP). Stable isotope ratios of organic carbon and nitrogen were determined on only two samples per plant during the 12 month period. These data were collected to determine if isotopic composition could be used to differentiate effluent organic matter from natural marine organic matter as has been suggested previously (cf. Eganhouse and Kaplan 1988; Myers 1974; Burnett and Schaeffer 1980). The isotopic data were expected to provide useful ancillary information but not be directly utilized in the course of modeling. In much the same way, the ICP-MS (inductively coupled plasma-mass spectrometry) multielement scan was envisioned as an opportunity to evaluate whether unique elemental signatures existed for any of the effluents (e.g. Olmez *et al.* 1991). Consequently, only two samples per discharge were submitted for the 13 element scan. Finally, the marker compounds (linear alkylbenzenes-LABs and coprostanol, epicoprostanol) were determined in two samples per discharge to establish concentrations and compositions. These data are directly comparable with those found in sediment trap particles and sediments collected at each site. Additionally, the determination of these compounds in a limited number of effluent samples was expected to offer a direct comparison with historical data (Eganhouse and Kaplan 1988; Eganhouse *et al.* 1988; Eganhouse *et al.* 1983a; *inter alia*) and provide valuable information concerning the character of the effluent particles prior to sedimentation and early diagenetic transformation. The linear alkylbenzenes give information on the amount and age of sewage-derived particles (SCCWRP 1991a), whereas coprostanol is primarily an indicator of mammalian fecal matter. Although the sampling program was planned so that all "extended" analyses (markers, ICP-MS, stable isotopes) would be carried out on the same samples, this was not possible. Thus, the marker analyses were performed on effluent samples collected in the months of January and July, whereas the ICP-MS and stable isotope analyses were performed on samples collected in July, September, and November of 1990.

II.A.1.b. Sediment Traps. Sediment traps were deployed over a 12 month period at each of the three outfall sites. Traps were positioned at elevations of 0.5, 2.0 and 5.0 m above the sea floor in order to collect sinking particulate matter over defined periods of time, thereby permitting fluxes to be estimated. These data were used in the modeling as input to the ACCUM module of the of the *SED2D* model. Although collections were made each month, the traps were frequently lost (26% of the moorings). Moreover, budgetary constraints limited the number of samples that could be analyzed, particularly for the extended list of constituents (markers, 13 metals, and stable isotopes).

Figure 2.2 provides matrices describing the planned sediment trap retrieval schedule and the actual recovery/analysis schedule. Whenever possible total mass, TOC, TN, Pb, and Cd were determined on samples

collected on every alternate month. In cases where mooring losses prevented us from maintaining the bimonthly collections, traps recovered successfully in other months were substituted. These measurements provide estimates of the flux of dry solids, particulate organic carbon, particulate nitrogen and particulate Pb and Cd to the near-bottom traps. Ultimately, these data were used for comparison with the results obtained during model simulations (cf. DISCUSSION: IV. Comparison of Model Predictions with Observed Sediments). Samples collected in intervening periods (when analyses were not scheduled) were archived for possible later use. The multielement scan, stable isotope and marker compound measurements were performed on a subset of the samples (two times per site during the 12 month period). As before, these data were intended to provide additional information on the origins (e.g., fresh effluent, resuspended sediments, planktonic debris) and dynamics of the particles collected in traps near the sea floor at three outfall sites. Decisions concerning the numbers of samples to be analyzed were guided by budgetary constraints.

II.A.1.c. Sediments. The modeling described in this report attempts to predict the concentrations of particulate organic carbon and trace metals (Pb and Cd) in sediments near three outfall systems. The sediment collections carried out in the course of the project were designed to provide material for purposes of model verification. The number of sediment samples collected per site was constrained by budgetary considerations. We collected a maximum of 15 surface (0-2 cm) sediment samples per site at two of the sites (Orange County, Point Loma) to provide some measure of coverage in both longshore and cross-shelf directions. Intersecting transects forming a "tee" were developed based on ten stations in the longshore direction (direction along which subsurface currents principally flow) and five stations in the cross-shelf direction (perpendicular). The spacing of the stations and their distance from the outfall termini were determined at each site using data from annual reports prepared by the Orange County and San Diego Sanitation Districts' ocean monitoring programs. The stations were, thus, concentrated within a limited zone near the outfalls where the largest gradients in sediment contamination were expected to occur (cf. Figures 2.3 and 2.4). Total organic carbon and total nitrogen concentrations were determined in all fifteen samples from each site. In the case of Pb and Cd, however, a subset of 10 stations per site was selected as dictated by the contract.

Sediment coring was intended to provide information on the accumulation of organic matter and Pb and Cd in sediments impacted by the outfalls. Because of uncertainties about the contemporary sedimentation on the Palos Verdes shelf (Kolpack 1987; section IV.C. of this report), sampling efforts were confined to the Orange County and Pt. Loma outfall sites. Two locations were selected at each of these sites for purposes of obtaining sediment from the impacted zone and at a location that was relatively unimpacted. Figures 2.3 and 2.4 show the targeted locations at each of the two outfall sites. Selection of the coring sites was based on the results of our analyses of surface sediments for TOC and TN. Attempts to collect cores off Orange County were unsuccessful, and sampling efforts at this site were ultimately abandoned after repeated failures at the targeted (and several alternate) locations. For purposes of model verification, the Point Loma cores were sectioned into 2 cm intervals, and each section was analyzed for water content, TOC, TN, Pb and Cd. The upper section (0-2 cm) of each of the two San Diego cores was also analyzed for stable isotopic composition, the ICP-MS multielement scan and the marker compounds. Once again, these analyses were carried out to improve our understanding of the origins of surficial sediments and the possible fate of effluent particles. They were not made in direct support of or to provide input data to the sedimentation models.

II.A.1.d. Effluent Decomposition Experiments. In the original incarnation of this project, a vital piece of information for the modeling effort was determined to be the kinetics of effluent decomposition. As will be discussed later, we undertook a series of experiments to estimate decomposition kinetics both in the field and in the laboratory. These efforts were largely unsuccessful because of difficulties associated with simulating the behavior of fine effluent particles under controlled conditions. Ultimately, experimentation had to be abandoned. The results of some of these experiments are described in later sections of this report (RESULTS and DISCUSSION). Rather than elaborate on the design and rationale of each experiment here, this information is presented in the RESULTS section along with the experimental data.

II.A.2. Sampling Methods

II.A.2.a. Effluent. Twenty-four hour, flow-proportioned composite samples of final effluent were collected at each of the three waste treatment plants (JWPCP, OCSD and PLTP). Table 2.1 lists the dates on which

sampling was performed. (This table lists more dates than were originally planned [cf. Figure 2.1 and Table 2.1]. Some of the "unplanned" samples were collected because of opportunities afforded by ongoing effluent degradation experiments.) After manually mixing the sample, treatment plant personnel poured aliquots of effluent into two containers: 1) a four liter amber glass bottle previously kilned (540°C for 4 hr) and sealed with a teflon-lined lid (trace organics, TSS) and 2) a 2000 ml polyethelyene bottle previously cleaned in 6% HNO_3 (Pb, Cd, TOC, TN, stable isotopes, and ICP-MS multielement scan). These samples were picked up by SCCWRP personnel within 12 hr of collection and transported to the laboratory on ice. Upon arrival, the samples were allowed to come to ambient temperatures. They were then immediately filtered and processed as described below (cf. Chemical Analyses section).

II.A.2.b. Navigation. Sampling station locations were obtained with LORAN-C (long range navigation). After arriving on station, coordinates and depth were recorded when the grab sampler was on the bottom and/or the sediment trap moorings were deployed. Prior to sediment trap retrieval, positions were rechecked and recorded.

II.A.2.c. Sediment Traps. The sediment traps used in this study were designed to collect sinking particles without incurring contamination from the trap itself (Figure 2.5). The trap, constructed of PVC and polyethylene, is simple to break down and has the same geometry as those used previously by SCCWRP in other studies in the Southern California Bight (SCCWRP 1987; Hendricks 1987). The aspect ratio of the trap (i.e. height/diameter) is 2.28.

The new trap consists of two compartments, the lower one containing a glass centrifuge bottle with a teflon-lined silicone rubber seal through which a glass funnel is positioned. Contact between funnel and collection bottle is maintained by a spring loaded in the bottom section beneath the bottle. The funnel is stabilized by a silicone rubber o-ring sandwiched between the coupling and the ground glass rim of the funnel bowl. When the traps are retrieved, water in the lower section of the trap automatically drains through three holes in the bottom. After the trap is removed from the mooring, water is manually drained from the upper section of the trap by removing a plug in the coupling. The sediment trap can then be disassembled, the sampling bottle + funnel is removed and the funnel is raised slowly to permit water within the funnel bowl to drain *via* a small hole in the glass stem. The funnel is removed, and a cap containing a teflon-lined lid is used to replace the funnel seal. The bottle is stored on ice until return to the laboratory.

Sediment traps were deployed at three positions in the water column (0.5, 2.0 and 5.0 m above the sea floor) at one location per site (White Point, Orange County, Point Loma; Figures 2.3, 2.4, and 2.6). The locations were in 60 m of water within 1 km downcurrent from each of the outfalls (JWPCP, OCSD, PLTP). The moorings consisted of a 110 kg weight to which a ¼ in polypropylene line was attached. The sediment traps were secured to the line with a tie wrap around the coupling and electrical tape near the ends of the upper and bottom sections. Traps were maintained in an upright position by a 7 in plastic float with 7 lbs of buoyancy positioned 1 m above the upper trap. Just before the traps were lowered below the water surface, a piece of solvent-rinsed heavy duty aluminum foil (used to cap the open end of the trap), was removed. The traps were not poisoned.

The sediment traps were retrieved approximately a month after deployment (16-36 d, mean = 31 d; Table 2.2) depending upon the availability of ship and staff time. The mooring was located visually by a surface float attached to the line. The ship was brought on station and a CTD cast was performed. The mooring was then raised. During this process, the line was manually stripped of fouling organisms except for the last few meters of line above the float. Once the traps were aboard, the electrical tape and tie wraps that secured the traps to the line were removed. The sediment traps were then transferred to a rack on the deck. After all three traps had been recovered, the water in the upper section of each trap was removed, and the traps were broken down as described above. The appearance of the sediments (e.g. odor, texture, color, presence of organisms) was noted on tracking sheets by the field crew. Care was taken to prevent the loss of particles during handling.

II.A.2.d. Sediments. Sediment samples were collected by two methods: Van Veen grab and gravity coring. Grab samples were collected at fifteen locations each off Orange County and Pt. Loma (cf. Figures 2.3 and 2.4 for locations, Table 2.3 for coordinates, water depths, and dates). Coring was attempted at two locations at each of

these sites. However, intact sediment cores were not successfully recovered off Orange County. After repeated attempts at several alternate locations, coring at the Orange County site was abandoned. Consequently, data presented in this report are for the two cores (SD A-5, SD A-16) collected off Pt. Loma.

The operation of the modified 0.1 m^2 Van Veen grab sampler and the subsampling procedures used for collection of surface sediments for chemical analysis are described in Stubbs *et al.* (1987). Briefly, upon retrieval of the grab sampler the surface of the sediments was inspected to assure that a relatively undisturbed sample had been obtained. If so, subsamples were immediately taken using a 50 cm^3 syringe (whose tip had been removed) by pushing the barrel of the syringe vertically into the sediments approximately 4-5 cm while holding the plunger stationary so as to maintain the sediment surface against the face of the plunger. After removing the syringe, excess (sub-bottom) sediments were discarded by pushing on the plunger and scraping off the sediments with a stainless steel spatula. Only the upper 2 cm of the sediment column (as measured with calibration marks on the side of the syringe) were then extruded into each of two containers. One container (for trace organics, TOC, TN and stable isotope analyses) was a precombusted (540°C for 4 hr) glass jar. After the jar had been filled to approximately two-thirds of its capacity, it was sealed with a teflon-lined lid and placed on ice. Samples were also collected in pre-cleaned plastic jars (trace metals). Upon return to the laboratory, all samples were placed in freezers where they were maintained at -20°C until analyses could be performed. The syringe was cleaned with fresh seawater between stations.

The gravity corer used in this project is described in detail by Bascom *et al.* (1982) and is shown in Figure 2.7. The corer was designed to collect sediments with minimum disruption of the surficial layers (from the bow wave) and stratigraphy. The large bore (12.5 cm) and reduced wall thickness of the corer (liner + barrel = <1.6 mm) also helps reduce the effects of compaction (Garrison *et al.* 1981). This corer is not as effective as a box core at collecting and preserving the easily resuspended surficial layers of sediment (1-2 mm thick). However, if deployed properly it will provide a reasonably well preserved stratigraphic record and is capable of penetrating to greater depths than a box corer (ca. 1 m versus 50 cm) in soft sediments.

Upon retrieval, the corer is placed on a rubber pad and disassembled. Water overlying the surface sediments is carefully removed with a teflon hose, and the core barrel is raised, thus, releasing the sediments contained within a thin-walled (0.25 mm) acetate liner. Sediments are held in place at the bottom by a thin stainless steel core catcher. The core liner is secured with electrical tape, and the sediment core is placed upright in a freezer. Once frozen solid, the cores were archived in a freezer at -20°C until sectioning could be carried out.

Sectioning involved cutting of the frozen core, pre-hardened by liquid nitrogen, into 2 cm vertical intervals using a carborundum steel cutoff wheel. The sectioning was carried out with the aid of personnel from the Los Angeles County Sanitation Districts. Each section was placed on a clean teflon sheet, the outer 1-2 cm (radially) was removed with a stainless steel spatula and each section was transferred to a pre-cleaned glass container sealed with a teflon-lined lid. The teflon sheet and implements were cleaned with re-distilled water between core sections to minimize cross contamination. The sections were then stored at -20°C until analyses could be performed.

II.A.3. Chemical Analyses

II.A.3.a. Effluent Pretreatment. Effluent samples were filtered in preparation for total suspended solids (TSS), stable isotope ($\delta^{13}C$, $\delta^{15}N$), TOC, TN, trace organic, and trace metal analyses (Figure 2.8).

Effluent in the *glass* sample bottle was homogenized by vigorous shaking. Approximately 90-100 ml was transferred with a graduated cylinder in increments of 25 ml (with shaking between transfers) into an all-glass filtration assembly on which a precombusted (4 hr at 425°C), preweighed 47 mm Whatman GF/C glass fiber filter had been positioned. Filters were always handled with solvent rinsed, stainless steel forceps and vacuum was provided by a jet aspirator. Once the filtration was complete, the bowl was rinsed with redistilled water, and the filter was transferred to a previously kilned glass petri dish. The petri dish was placed inside of a vacuum dessicator where it was allowed to dry for at least 2 d at room temperature. The volume of effluent that was filtered was measured with the graduated cylinder used to transfer effluent to the filtration assembly. The concentration of total suspended solids was then determined by reweighing the dry filter on a Cahn 31

microbalance. The same procedure was employed when filtering effluent samples for TOC, TN and stable isotope analyses. In these cases, however, the effluent was removed from the *polyethylene* bottle, and the resultant filters were archived in vacuum dessicators until gravimetric analysis and carbonate removal could be performed.

Effluent particles were treated for carbonate removal prior to TOC, TN and stable isotope analyses. The method that we used is a modification of the acid vapor technique described by Hedges and Stern (1984). The dry filters containing the effluent particles were transferred in petri dishes to an all-glass dessicator (without dessicant) in which a beaker of concentrated HCl (50 ml) had been placed. The filters were allowed to rest within the dessicator for a period of 18 hr. The filters were then placed in an oven at 60°C for 4-6 hr to drive off excess HCl and water. Afterwards, they were covered with the petri dish lids and maintained in a vacuum dessicator (with dessicant) until analyses could be performed. The glass fiber filters containing carbonate-free effluent particles were loaded into tin combustion boats (Carlo Erba) just prior to the TOC, TN analysis.

Following the filtration of effluent for determination of total suspended solids, filtrations were carried out for the trace organic analyses. The *glass* bottle was shaken again, and five successive aliquots (ca. 100 ml each) were filtered in an all-glass assembly using pre-combusted 47 mm Whatman GF/C glass fiber filters. The filters were removed after each aliquot using stainless steel tongs. Each filter was immediately placed at the bottom of a pre-extracted cellulose thimble (sonicated sequentially in methanol and dichloromethane for 30 min each) positioned inside a Soxhlet extraction apparatus. The first filter was amended with small volumes (40-200 μl) of recovery surrogate solutions containing PAH, PCBs, androstanol and linear alkylbenzenes (Table 2.4). This was followed by the addition of 40 ml of a 9:1 dichloromethane/methanol mixture (to wet filter and start extraction). The condenser was replaced atop the Soxhlet extractor after each filter transfer. The volume of effluent filtered was determined with a graduated cylinder. This measurement was made prior to transferring sample to the filtration assembly. Details of the extraction procedure are provided below.

The effluent filtrations for trace metal analysis (*polyethylene* bottle) were performed in an all-glass assembly using a pre-weighed 47 mm 0.4 μm Nuclepore filter. Typical filtration volumes were 20-30 ml. For purposes of the Cd and Pb analyses, only one filtration or, at most, duplicate filtrations were performed. However, in the case of the samples to be used for multielement scans by ICP-MS, five successive filtrations were carried out. These (ICP-MS) filters were later digested together, and the sample weights obtained for each filter were combined to compute metal concentrations (see below). Once the filtration was complete, the bowl was rinsed with redistilled water. The moist filter was then placed inside of a vacuum dessicator for >2 d after which it was reweighed on a Cahn 31 microbalance.

II.A.3.b. Sediment Pretreatment. Frozen sediments were allowed to warm to room temperature and were manually homogenized using a clean glass rod. Aliquots (10-35 g) of wet sediment were then transferred to a pre-weighed solvent-rinsed aluminum pan. The wet sediments were placed in an oven at 60°C overnight after which they were removed, and the pan + sediments were reweighed. The weight difference was used to compute the water content. Subsamples of the oven-dried sediments were placed into pre-combusted, acid-rinsed (6% HNO_3) glass vials for later analysis (TOC, TN, $\delta^{13}C$, $\delta^{15}N$ and trace metals).

For purposes of the TOC, TN and stable isotope analyses, inorganic carbon was removed from the sediments. In the case of the TOC and TN analyses, small aliquots of homogenized sediment (20-30 mg) were weighed into pre-cleaned, pre-tared silver boats (Carlo Erba; Milan, Italy) using a Cahn 31 microbalance. The boats were placed inside of a teflon rack which was then introduced to the vapor phase acidification dessicator as described above (18 hr exposure). The carbonate-free sediments were dried at 60°C for 2 hr, after which the silver boats were sealed and packed inside of tin combustion boats (Carlo Erba) for TOC and TN analysis. Sediments were decarbonated for stable isotope analyses by exposing small quantities of dried sediment(100-200 mg) in glass vials to HCl vapors in a vacuum dessicator. Drying was performed as described above, and the dry carbonate-free sediments were submitted for analysis to the subcontractor (Global Geochemistry Corporation).

II.A.3.c. Sediment trap particles Pretreatment. Upon return from the field, the pre-weighed sediment trap centrifuge bottles were inspected to determine if the suspended particle concentration in the overlying water

was high enough to warrant centrifugation. If not (i.e., if it was visibly clear), the supernatant was siphoned off using a Pasteur pipet connected to a jet aspirator. Macrofauna (e.g. amphipods, shrimp, etc.) were carefully removed. If the supernatant was turbid, the bottle was centrifuged prior to siphoning. Following removal of excess water, the bottles were placed in a freezer (-20°C) until they could be processed further.

Later, the frozen sediment trap samples were allowed to thaw at room temperature, and the bottles were reweighed. The particles were then mixed with a glass rod, and an aliquot corresponding to approximately one-third of the sample was removed for determination of water content, TOC, TN, stable isotopes, and trace metals. This aliquot was placed in a precombusted, acid-soaked (and rinsed) glass jar. The sediments were dried at 60°C overnight after which the jar was reweighed (for determination of water content). The sediments were then manually homogenized with an agate mortar and pestle. The homogenized sediments were stored in the same glass vial. Portions of dried sediment were taken for TOC, TN, and stable isotope analysis. Carbonate removal was performed in the same fashion as described for sediment samples.

II.A.3.d. Elemental analysis. Elemental analyses (TOC, TN) were carried out on effluent, sediments and sediment trap particles sealed within combustion boats as described above. The analyses were conducted by high temperature (flash) combustion using a Carlo Erba EA1108 elemental analyzer. Data were acquired and reprocessed with a Carlo Erba EAGER 100 data system which utilizes an IBM-compatible microcomputer. The instrument was calibrated with acetanilide daily at a rate of 3-4 times per batch. The maximum number of samples that can be run under these conditions is 46. The precision of the sediment and sediment trap analyses for TOC and TN are estimated at <2% and <5%, respectively, based on replicate determinations of carbonate-free sediments (Table 2.5). The precision of the effluent particle analyses is estimated at <5% based on replicate analyses of JWPCP final effluent filtered from a single 24 hr composite and measurements made on JWPCP primary sludge (Table 2.5). Analysis of pure acetanilide showed that the instrument yielded results within 0.5, 0.5 and 3.3% of the actual amounts of carbon, nitrogen and hydrogen, respectively. Analysis of National Research Council of Canada standard reference sediments, PACS-1, for total carbon yielded results that agreed with the certified value to within 5.7% (Table 2.5). All concentrations presented here are relative to total sediment weight (i.e., including carbonate carbon).

II.A.3.e. Stable isotopes. Effluent, sediments, and sediment trap particles were analyzed for stable carbon and nitrogen isotopes by Global Geochemistry Corporation (Canoga Park, CA). Carbonate-free effluent particles were supplied on glass fiber filters (25 mm Whatman GF/C) as described above; sediments and sediment trap particles were provided as carbonate-free powders. In addition, one pre-combusted glass fiber filter, processed in the same manner as effluent (using glass re-distilled water in place of effluent during filtration), was submitted as a blank. Organic carbon and nitrogen in the samples were converted to gases (CO_2, N_2) by high temperature combustion in evacuated quartz tubes. The methodology represents a modification of procedures described by Minagawa *et al.* (1984). The samples were loaded into a 6 mm id quartz tube placed inside of a 9 mm id quartz tube, packed with cupric oxide, copper granules and silver foil. The 9 mm quartz tube was evacuated and sealed after which it was heated at 850°C for 2 hr. This was followed by an 18 hr cooling period. The tubes were then cracked onto a vacuum line, and the combustion gases (CO_2, N_2) were separated cryogenically and collected in glass tubes. The isotopic ratios of carbon ($^{13}C/^{12}C$) and nitrogen ($^{15}N/^{14}N$) were determined on a Nuclide 3-60 RMS isotope ratio mass spectrometer. The data presented here are given in the conventional "del" notation; the isotopic composition of the sample is related to appropriate standard reference materials (N-air; C-$CaCO_3$ from the Pee Dee Belemnite formation) as follows:

$$\delta^{13}C\,(^{o}/_{oo}) = \frac{[^{13}C/^{12}C]_{sample} - [^{13}C/^{12}C]_{std}}{[^{13}C/^{12}C]_{std}} \times 1000$$

The precision of the method for both elements is approximately $\pm 0.1^{o}/_{oo}$. Duplicate analyses of NBS-22, a reference material for carbon, yielded values of -29.84 and $-29.75^{o}/_{oo}$ *vs.* the certified value of $-29.8^{o}/_{oo}$.

II.A.3.f. Trace metals. Effluent, sediments and sediment trap particles were analyzed for trace metals by West Coast Analytical Service, Inc. (WCAS; Santa Fe Springs, CA). Originally, SCCWRP intended to carry out all of

the Pb and Cd determinations, whereas WCAS was to perform the multielement scans by ICP/MS. However, in the middle of this study, SCCWRP lost its ability to perform trace metal measurements. After some discussion with the project officer, we decided to sub-contract the trace metal work to a local contract laboratory (WCAS). Prior to submitting samples for analysis, we carried out a limited intercomparison with WCAS using two standard reference materials from the Canadian National Research Council (NRC) (Table 2.6).

These reference materials are estuarine sediments collected from the Gulf of St. Lawrence (MESS-1) and Esquimalt Harbor in British Columbia (PACS-1). The data provided by the Canadian NRC are based on total dissolution of the sediment. This contrasts with procedures employed by SCCWRP and WCAS which rely upon acid digestion using HNO_3 and HCl or HNO_3 alone. In such digestions, silicate minerals are not dissolved and some fraction of certain metals, trapped within the crystal lattice, is not extracted. The difference in digestion procedures employed by the NRC and SCCWRP/WCAS probably accounts for the sometimes higher concentrations reported by the NRC.

Variations in technique notwithstanding, the data produced by SCCWRP and the WCAS generally show acceptable agreement. The only obvious differences are for Cr and possibly Cd. WCAS obtained higher concentrations for Cr for both of the reference materials. Given the fact that the concentrations obtained by the NRC for Cr exceed those of WCAS and SCCWRP to a greater extent than for any other metal, the discrepancy between the SCCWRP and WCAS measurements may reflect some difference in extraction efficiency during the digestion step. The only other apparent discrepancy is for the Cd results obtained with the PACS-1 reference material. It is difficult to explain why agreement was found for MESS-1 and not for PACS-1 in the case of Cd.

Effluent particles collected on Nuclepore filters were delivered to WCAS along with sediments and sediment trap particles in March and April of 1991. The filters were soaked in 20 ml of a 25% HNO_3 solution for 24 hr. An internal standard solution containing Sc, In and Tb was added, and the volume of the sample was brought to 100 ml with redistilled water. The solution was then filtered *via* a syringe using a 0.8 μm cellulose acetate filter.

In the case of the sediment and sediment trap samples, 0.5 grams of dry powder were placed inside a glass test tube and digested in 2 ml of concentrated HNO_3 for 2 hr at 120°C. The digest was cooled to room temperature, the internal standard solution was added (see above) and the volume was brought to 100 ml with redistilled water. The diluted digest was then filtered through a 0.8 μm cellulose acetate filter as described above.

Diluted digests were analyzed on a VG Plasma Quad inductively coupled plasma-mass spectrometer (Model PQ2 Turbo Plus). The mass spectrometer was operated in full scan mode (2-250 amu) with quantitation ions selected to minimize interference. Limits of detection for these analyses are provided in Table 2.7. Precision is estimated at 10-15%. Analysis of SRM 1646 (estuarine sediment) on 3/19/91 yielded the following results: Cd-0.4 $\mu g\ g^{-1}$, Pb-26.4 $\mu g\ g^{-1}$. The NIST certified value for Cd is 0.36 $\mu g\ g^{-1}$ and Pb is 28.2 $\mu g\ g^{-1}$.

II.A.3.g. Trace organics.

II.A.3.g.i. *Extraction*. Glass fiber filters bearing effluent particles were placed inside a Soxhlet extraction apparatus. A 250 ml boiling flask was charged with 200 ml of 9:1 dichloromethane/methanol plus a few pre-cleaned teflon chips (to prevent bumping). The condensers were cooled by a recirculating cooling bath (temp=10°C) that uses a 1:1 mix of water and antifreeze. Once the condensers were cool, the solvent mixture was heated (with mantles) to reflux at a rate of three cycles per hour. Extraction was performed for 48 hr after which the flasks were cooled, and the excess solvent in the extraction chamber was siphoned into the boiling flask. The extract was transferred into a 250 ml separatory funnel equipped with a teflon stopcock and previously charged with 60 ml of pre-extracted (three times with dichloromethane) water and a scoop of pre-combusted sodium sulfate. The mixture was shaken vigorously for one minute, and once the phases had separated, the (bottom) dichloromethane layer was drained into a clean boiling flask. The flask was sealed with a glass stopper and stored in the dark.

Sediment trap bottles stored in the freezer at -20°C were reweighed and allowed to warm up to ambient temperatures. The sediments were mixed with a glass rod and an aliquot of wet sediment (2-36 g) was transferred to a pre-cleaned cellulose Soxhlet thimble. The centrifuge bottle was then reweighed to determine the sample weight (by difference). After the thimble was placed inside the Soxhlet extractor, the sediments were amended with a small volume of recovery surrogate solution (Table 2.4) and 25 ml of methanol. The Soxhlet apparatus was closed, a 250 ml boiling flask containing 175 ml methanol (and a few teflon boiling chips) was attached and the condensers were cooled. The sediments were extracted overnight (ca. 18 hr) at a reflux rate of three cycles per hour. The mantles were then removed, and once the flasks had cooled, excess methanol was siphoned *via* the sidearm from the extraction chamber into the receiving flask. The methanol was transferred to a 500 ml separatory funnel for back extraction with 150 ml of water and 50 ml of dichloromethane. After the phases had separated, the dichloromethane layer was drained into a clean boiling flask. This (back) extraction procedure was repeated twice more using 50 ml of dichloromethane each time. Meanwhile, a fresh boiling flask charged with 200 ml of dichloromethane and a few teflon boiling chips was attached to the Soxhlet apparatus. As before, this extraction was carried out overnight at a reflux rate of three cycles per hour. The next day, the solvent was drained as described above and combined with the dichloromethane back extract. The flask was then sealed with a glass stopper and stored in the dark. Surface sediment samples were extracted using this same procedure.

II.A.3.g.ii. *Water and sulfur removal, fractionation*. All extracts were concentrated to a small volume (ca. 1-3 ml) by rotary evaporation at <30°C. Water was removed by adding excess precombusted anhydrous sodium sulfate to the flask and allowing the extract to sit overnight. Sulfur was removed at the same time by adding activated copper granules. The next day, the extract was transferred quantitatively to a clean one dram borosilicate vial, and the volume was adjusted by evaporation under a stream of dry, organic-free nitrogen gas. The total volume was measured by comparison with a calibrated vial. At this point, the concentration of total extractable organics (TEO) could be made.

Small aliquots of extract (3-4 μl) were transferred to a clean aluminum dish placed on one weighing pan of a Cahn Model 31 microbalance. The extract was allowed to dry for three minutes, and the weight of the residue was measured. Replicate measurements (at least three) were made on each extract such that the coefficient of variation was less than 15%. The total mass of extractable matter was computed using the mean of these measurements and the total volume of extract. Dividing this mass by the sample weight (or volume) yielded the TEO concentration. If the mass of TEO was less than 25 mg, all of the sample was fractionated as described below. Otherwise, an aliquot of about 25 mg was transferred to a separate vial. The extract to be fractionated was evaporated under a stream of nitrogen gas and taken up in 250 μl of dry hexane.

Extracts were separated into three fractions by adsorption chromatography using a 1:2 alumina/silica gel column (each deactivated 3% with water). The fractionation procedure is a modification of that described in Eganhouse *et al.* (1989). The three fractions correspond to: 1) aliphatic hydrocarbons (F1), 2) aromatic hydrocarbons (F2-including PAH, LABs, and PCBs) and 3) polar compounds (F3-including the fecal sterols). The F1 fraction is eluted with 15 ml hexane, the F2 with an additional 5 ml hexane + 30 ml 30% dichloromethane in hexane and the F3 with 30 ml of methanol. Generally the F1 fraction was discarded. The F2 fraction was collected in a pear-shaped 50 ml flask and concentrated by rotary evaporation. It was then transferred to a half-dram vial and stored in a freezer until analyses could be performed. The F3 fraction was evaporated to just dryness (rotovap) and taken up in dichloromethane. It was then transferred to a vial and stored in the freezer.

II.A.3.g.iii. *Instrumental analysis*. The F2 fractions containing the linear alkylbenzenes were concentrated to small volumes (20-100 μl), and an aliquot of the internal standard solution (Table 2.4) was added to the vial. These final fractions were analyzed on a Hewlett-Packard 5970B benchtop GC/MS. Splitless injections were made onto a 30 m capillary column (0.25 mm id, 0.25 μm film thickness) coated with DB-5 (J&W; Folsom, CA). The column was directly interfaced to the ion source of a quadrupole mass spectrometer (HP5970B). Analyses were performed in the full scan, electron impact mode (electron energy 70 eV) with scanning from 50-550 amu at one second intervals. Instrument calibration was performed with a secondary standard comprised of a synthetic mixture of secondary phenylalkanes to which had been added the internal quantitation and recovery

surrogate standards (Eganhouse *et al.* 1983a, 1983b). Table 2.8 provides the chromatographic conditions, whereas Table 2.9 indicates the ions used for purposes of quantitation and the internal standard compounds that were employed for quantitation of specific linear alkylbenzenes.

The GC/MS was controlled by, and data were acquired with, an HP 59970B Workstation. Recoveries were determined for each of five 1-phenylalkanes in effluent, sediment, and sediment trap samples (cf. Table 2.4). Recoveries of the LAB surrogates for effluent samples were variable and sometimes low. The amounts of surrogates spiked into sediment and sediment trap samples were too small to be reliably detected (due to problems of background interference with the quantitation ions for these compounds). Recovery correction was, thus, warranted for the effluent samples but was impossible for the sediment and sediment trap samples. Recovery correction was made using the surrogate having one less alkyl carbon than the corresponding linear alkylbenzene (e.g. 1-phenyldecane was used for the phenylundecanes). This was done because the physical properties of the 1-phenylalkanes are most similar to the secondary phenylalkanes having one more carbon atom in the alkyl chain (Sherblom and Eganhouse 1988). Precision of the LAB analyses was estimated at 10-15% (Eganhouse *et al.* 1988).

Fecal sterol analyses were performed on a Varian 4600 high resolution gas chromatograph equipped with a cool on-column capillary injector (Model 1095) and a flame ionization detector. F3 fractions were concentrated to volumes expected to yield satisfactory signals based on previous studies (ca. 100-3500 μl). A small portion of the F3 fraction (ca. 20-40 μl) was then combined with an aliquot of the internal standard solution containing 5α(H)-cholestane (20 μl; cf. Table 2.4) inside of a 100 μl conical micro reaction vial. The solvent was evaporated under a stream of dry nitrogen, and 20 μl of BSTFA (N,O-bis(trimethylsilyl)trifluoroacetamide; Pierce Chemical Co.; Rockford, IL) was added. The vial was sealed with a cap containing a teflon-faced silicone rubber liner, and the contents were heated in a heater block at 70°C for 20 min. The vial was allowed to cool to room temperature after which excess BSTFA was evaporated under a stream of dry nitrogen gas. The derivatized sterols were immediately taken up in a small volume (20 μl) of dry 8:2 hexane/dichloromethane and injected onto the capillary column. The chromatographic conditions are given in Table 2.8. Data were acquired using a PE Nelson 2700 Turbochrom chromatography data system (v. 3.1) equipped with an IBM-compatible microcomputer and a PE Nelson 900 series A/D interface. The signal was sampled at a rate of 2 Hz, and data were reprocessed with quantitation by the internal standard method. The amounts of recovery surrogate (androstanol) added to the sediment and sediment trap samples was inadequate. Consequently, we have no estimates of recovery for these samples, and no recovery correction was possible. Recoveries obtained for the effluent samples were variable, ranging from 40 to >80%. Sterol concentrations reported for effluent samples have, therefore, been corrected for recovery.

II.A.3.g.iv. *Quality Control/Quality Assurance.*

Chemicals. Solvents (methanol, dichloromethane, hexane; Burdick and Jackson distilled-in-glass grade) were used without further purification. Water used for back extractions was extracted three times with dichloromethane (1:10 DCM/water) and stored in a precombusted amber bottle. Copper granules were activated in a chromatography column by passing pre-extracted 6N HCl over them at a rate of ca. 2-4 ml min^{-1} followed by rinsing with methanol and dichloromethane. Activated copper was then stored in a reagent bottle under dichloromethane until use. Anhydrous sodium sulfate was muffled at 540°C for 4 hr and maintained in a jar sealed with a teflon lined lid inside of a vacuum dessicator. Nuclepore filters were used without further purification, whereas glass fiber filters were muffled at 425°C for 4 hr. The latter were stored within glass jars sealed with teflon-lined lids until use. Adsorbents used for column chromatography were cleaned by successive sonications in methanol and dichloromethane followed by air drying. Details of the adsorbent preparation are given in Eganhouse *et al.* (1989). Sterols (androstanol, coprostanol, epicoprostanol; >98% purity) and 5α(H)-cholestane (99% purity) were purchased from Steraloids, Inc. and Aldrich Chemical, respectively. These compounds were used without further purification. Standard solutions made up in either hexane or dichloromethane were stored in sealed ampules at -4°C until just prior to instrumental analysis. Details of the preparation methods can be found in Eganhouse *et al.* (1987). Acetanailide (for calibration of the elemental analyzer) was used as provided by Carlo Erba.

Labware cleaning. Plastic implements (except teflon) were scrupulously avoided. All glassware was muffled at 540°C for 4 hr in a large kiln. After the kiln had cooled, the glassware was transferred to the laboratory where it was covered with aluminum foil. Prior to using glassware, surfaces expected to contact the sample were rinsed with dichloromethane. Metal implements (including glass and stainless steel syringes) were either sonicated in dichloromethane and air dried or rinsed with solvent assiduously prior to use.

Blanks. For the trace organic analyses, blanks consisting of glass redistilled water (effluent) or precleaned cellulose Soxhlet thimbles (sediments, sediment trap particles) were processed along with samples at a rate of approximately one per 7-10 samples. The blanks used in the trace organic analyses were amended with recovery surrogate solutions in the same manner as described above for samples. For TOC, TN, stable isotope and trace metal analyses of effluent, blanks were processed at a rate of at least two per eight samples. WCAS processed their own in-house blanks, but we supplied them two blank filters for ICP-MS analysis. Similarly, Global Geochemistry was provided a blank (precombusted) filter for the stable isotope analyses.

Instrumental analysis. TOC, TN and trace organic analyses were performed at SCCWRP as described earlier. For the analysis of effluent particles and sediments for TOC and TN, standard calibrations were performed daily.

LAB measurements were carried out on an HP5790B GC/MS. The data were acquired on an HP57990B Workstation. Peak identities were determined by relative retention times established by calibration runs performed daily. The data were reviewed for inconsistencies, and if necessary, questionable peak identifications were evaluated by comparing the full mass spectrum of the target peak with that of the pure compound. The integrated areas of the quantitation ions for all peaks were used to compute the concentrations of individual LABs. In cases where surrogate recoveries exceeded 100%, the mass spectra were examined to determine peak purity.

Sterol measurements were performed by high resolution gas chromatography of the trimethylsilyl (TMS) ethers formed by reaction of the hydroxy-functional F3 fraction components with BSTFA (N,O-bis(trimethylsilyl)trifluoroacetamide). A calibration standard consisting of androstanol, cholestane, and the fecal sterols (coprostanol, epicoprostanol) was run at the beginning of each day. Before proceeding with samples, the calibration run was inspected to determine whether relative response factors of the sterol-TMS ethers (relative to cholestane) were within 5% of the average values established in prior analyses. In addition, the chromatograms were examined for the presence of extraneous peaks resulting from incomplete derivatization and/or hydrolysis. If evidence of these problems was found, no samples were run until acceptable results were obtained with the calibration standard. Sample chromatograms were likewise inspected for such effects and the presence of ghost peaks, which occasionally arise from relatively involatile constituents of the F3 fractions. Samples whose chromatograms had interfering ghost peaks were re-analyzed to insure proper quantitation.

II.B. Simulations

II.B.1. DECAL

The input information required for to carry out a simulation with the three-layer version of *DECAL* can be divided into the following categories:

1. Effluent
2. Simulation area
3. Water column
4. Diffuser
5. Currents
6. Simulation Parameters

Individual data requirements, and values used in the simulations for the three test sites are discussed in the following sections.

II.B.1.a. Effluent. The effluent characteristics required to carry out a simulation are:

1. Discharge flow rate ($m^3 s^{-1}$)
2. Effluent suspended solids concentration ($mg l^{-1}$)
3. Trace contaminant concentration ($\mu g l^{-1}$)

II.B.1.a.i. *Background*. *DECAL* (and *SED2D*) are formulated to estimate the accumulation of particulates in the sediments for constant discharge conditions. However, the volume of effluent discharged daily, and constituent concentrations in the effluent (suspended solids and contaminants) have changed significantly over the years at each of the simulation sites. These changes introduce significant difficulties into the simulation process. *DECAL* and *SED2D* treat the sediments as a homogeneously mixed upper layer. This mixing introduces a buffering effect on the composition of the surface layer to changes in the flux and composition of particles entering the layer. This lag can be described in terms of a "characteristic response time" (eqn 1.10, *DECAL* and eqn 1.55, *SED2D*) that provides a measure of the time between when these changes occur in the discharge and when they fully manifest themselves in the surface sediments. To further complicate matters, these characteristic times may also change with changes in the discharge. For example, they depend on the magnitude of the sedimentation flux, the mixing depth (or mass), and the decomposition rate of organic material. The latter, in turn can vary with the composition and flux of particles from the water column, through their effects on the abundance and composition of the benthic biota and the chemical composition of the near-bottom and interstitial waters. Thus it is difficult, *a priori*, to select individual values for the discharge rate and the composition of the effluent during periods of change.

II.B.1.a.i. *Temporal variations in effluent characteristics*. Figure 2.9 shows the annual average values of the volumetric discharge rate of effluent from the outfalls at the three sites. The flow at the Los Angeles County outfall site changed relatively little during the period from 1975 to 1989. On the other hand, discharges from the Orange County and San Diego outfalls nearly doubled during the same period.

The latter variations are relatively small, however, when compared with changes in the concentration of suspended solids and trace constituents at all three sites. Figure 2.10 shows the concentration of suspended solids for this same period. By 1988 the suspended solids concentrations in the effluents had diminished to between 25% (Los Angeles County) and 45% (San Diego) of their peak values. Figure 2.11 shows the mass emissions of suspended solids from each of the outfalls during the same period and also shows significant declines. This indicates that any increase in mass emissions resulting from the increased discharge rates at the Orange County and San Diego outfalls were more than offset by the declining suspended solids concentrations. Most of these reductions resulted from changes in the treatment process and increased source control.

Because of the buffering action of the surface layer of the sediments, and the changes in outfall characteristics, it is necessary to choose some representative (but constant) values for the flow and the suspended solids emissions for each of the outfall sites. The predicted characteristics of the upper layer of sediments will be compared with samples collected in 1990 at the San Diego and Orange County sites. Therefore the values of the input parameters should represent a weighted average of the effluent characteristics for some period preceding 1990. In the case of the Los Angeles County simulations, the comparisons will be made using samples collected in 1981 and the effluent parameters should be selected for that time.

Let us assume that at the steady-state concentration of organic material in the sediments at some time t_0 is C_0. At that time, the mass emissions or composition of the effluent is changed. At some later time, the concentration of organic material in the sediments will reach some new steady-state concentration, C_1. The difference in the steady-state concentrations is C_1-C_0. From equation 3.10, we see that in the *DECAL* model, the change between the two concentrations is controlled by the factor:

$$t_r = h_s / k_s \qquad (2.1)$$

where k_s is the "apparent interfacial removal rate coefficient" for sedimented organic material and h_s is the mixing depth for those sediments. This factor has the characteristics of a response time; it is a measure of the

time required for the difference between the two steady-state concentrations to be reduced by 1/e (ca. 37%). Based on a literature review of sediment studies, Tetra Tech (1987) deduced that an approximate value for the "interfacial removal rate coefficient" (see equation 3.10) was about 0.015 cm d^{-1}. Assuming a mixed layer depth in the range of 5-15 cm, the response time would be on the order of 1-3 yr.

For the simulations at the Los Angeles County outfall site, we chose to use the average values of the discharge parameters for a three year period preceding the sampling carried out in 1981 (i.e. from 1978 to 1980). The average mass emissions during this period was 97,950 (± 6,750) mt per year. Since the samples for the Orange County and San Diego simulations were collected in 1990, the corresponding averaging period would be from 1987-1989. Assuming that mass emissions in 1989 were equal to those in 1988, the average mass emissions of suspended solids for both discharges is about 17,500 mt yr^{-1}.

Suspended solids concentrations at the latter two sites were relatively constant during this period, averaging 49 mg l^{-1} for the Orange County effluent and 67 mg l^{-1} for the San Diego effluent. The volumetric discharge rates during the period averaged 11.3 $m^3 s^{-1}$ (260 mgd) and 8.3 $m^3 s^{-1}$ (189 mgd) for the Orange County and San Diego discharges, respectively. The concentration of suspended solids in the Los Angeles County effluent from 1978 to 1980 averaged 197 (± 22) mg l^{-1}. The volumetric discharge rate averaged 15.8 $m^3 s^{-1}$ (360 mgd). We apportioned this flow between the 90-inch and the 120-inch outfalls according to their design maximum capacities (160 and 235 mgd, respectively).

The two trace constituents used for the simulations are lead and cadmium. The history of the concentrations of these two trace metals is shown in Figures 2.12 (Pb) and 2.13 (Cd). Both metals show a persistent downward trend, reflecting increased solids removal in the effluent and the effects of source control programs. Lead concentrations in the San Diego effluent were constant at 10 $\mu g\ l^{-1}$ in 1987 and 1988.

The concentration of Pb in the Orange County effluent decreased between 1986 and 1988. By assuming a steady decline, we estimated the concentration in the 1990 effluent to be 8.3 $\mu g\ l^{-1}$. The average concentration for effluent for the period from 1988-1990 would then be 16 $\mu gm\ l^{-1}$. The average Pb concentration in the Los Angeles County effluent from 1978-1980 was 152 $\mu g\ l^{-1}$.

The average Cd concentrations were 2, 3.3, and 9.3 $\mu g\ l^{-1}$ for the San Diego, Orange County and Los Angeles County effluents, respectively. The input values used to characterize the effluent in the *DECAL* simulations are summarized in Table 2.10.

II.B.1.b. Simulation Area. *DECAL* computes the deposition of particulates, and their effects on the sediments, within a two-dimensional grid of cells. The parameters required to define this simulation area are:

1. Orientation of Y-axis (relative to N_{true})
2. Length (X-axis, km)
3. Length (Y-axis, km)

At each simulation site, the orientation of the x-axis of the simulation grid was chosen to be parallel to the principal axis of the variations of subtidal frequency in the ocean currents (the decomposition into subtidal, tidal, and supertidal frequency bands is discussed later). This axis usually parallels the general trend of the isobaths (contours of constant depth). Positive values of x are chosen to correspond to the direction of the long-term net flow. The y-axis of the grid is oriented ninety degrees in a counter-clockwise direction from the x-axis. Table 2.11 summarizes the orientation of the simulation grids at each of the simulation areas:

The dimensions of the cells in the *DECAL* simulation grid are determined by the simulation program. However, the overall dimensions of the simulation area must be supplied as input. Specification of these dimensions determines the number of cells in the "longshore" and "cross-shore" directions (within the limits of the program). All the *DECAL* simulations used a length of 32 km (longshore) and a width of 8 km (cross-shore). These grids are shown in Figure 2.14a,b,c. Note: These grids are shown as rectilinear. In practice, a better correspondence will be obtained by distorting the grid so that the longshore row of cells containing the

discharge follows the principal major axis of variation for the midwater currents of subtidal frequency. In areas with relatively simple bathymetry, this roughly corresponds to the axis following the isobath passing through the terminus of the discharge.

II.B.1.c. Water Column. The characteristics of the water column are defined by the thicknesses of the three layers used in the simulation:

1. Depth of upper layer (m)
2. Thickness of middle layer (wastefield, m)
3. Thickness of lower layer (m)

The *DECAL* simulation program does not estimate these values and they must be supplied as input to the simulations. Numerous simulation models of initial dilution have been developed (e.g. EPA 1988) that can be used to provide estimates of these quantities. The selection of the model to be used should be made on the characteristics of the discharge and the receiving water environment, and the suitability of the model for these conditions. For our simulations, we used the *SED2D* submodel TSLINE to compute these parameters. Output from this model includes the distribution of values of the wastefield boundaries and thickness (as well as the minimum and average dilutions). Median values for the position of the lower bound of the wastefield and its thickness were used to supply the water column information for the *DECAL* simulations. These values are summarized in Table 2.12.

II.B.1.d. Diffuser. The parameters that define the diffuser are:

1. Number of diffuser segments
2. For each segment:
    a. Diffuser distance from origin (x-axis, km)
    b. Diffuser distance from origin (y-axis, km)
    c. Length (m)
    d. Orientation of diffuser from x-axis

The Los Angeles County 90-inch and the San Diego outfalls terminate in a "vee" shaped diffuser with an included angle of about 120 degrees. The Los Angeles County 120-inch outfall and the Orange County outfall terminate in diffusers in the shape of a "bent L." All of these configurations were approximated by using two segments to represent the diffuser. The latter were joined either at the apex of the vee, or at the bend in the ell, as appropriate.

The Los Angeles County simulation area contains both the 90-inch and the 120-inch outfalls. The distance between the two diffusers (i.e. the "ell" to "bend" distance) is approximately 1.6 km. Thus four diffuser segments are required to simulate the discharge. Multiple diffuser segments can be used in *DECAL*. However, because of the method used to calculate the extended source, it is not appropriate to combine separated segments into a single simulation. We assumed that the wastefields discharged from the two outfalls would not interact. In that case, simulations of the discharges from the two outfalls can be independently generated and then added to represent the composite discharge.

The lengths and orientations of the diffuser segments at each site are summarized in Table 2.13.

The origin of the diffuser (center of the ell or bend) within the grid was chosen as x=10 km and y=4 km for the San Diego, Orange County, and Los Angeles County 90-inch outfalls. The origin of diffuser for the Los Angeles County 120-inch outfall was at x=8.4 km and y=3.5 km.

II.B.1.e. Currents. The parameters characterizing the ocean currents are:

1. The number of tidal current components (i.e. by period)
2. For each component:

a. Principal major axis, relative to N(degrees)
b. Period (hours)
c. Magnitude (x-component, m s^{-1})
d. Magnitude (y-component, m s^{-1})
e. Phase, x-component (degrees)
f. Phase, y-component (degrees)

3. The number of long-term (subtidal frequency) currents
4. For each subtidal current component:
   a. Direction of flow relative to N (degrees)
   b. Speed (m s^{-1})
   c. Frequency of occurrence (percent)

We used current measurements from each of the simulation sites to estimate appropriate values for these parameters. Records from midwater current meters were used for the analysis since the wastefield is generally trapped below the thermocline. On infrequent occasions, the thermocline may be weak, or absent, resulting in a surface wastefield. During these conditions, the shear in the currents is generally reduced and the deeper measurements may still provide a reasonable representation. The dates of the current meter data sets are summarized in Table 2.14

Variations in the strength and direction of flow of the coastal currents in southern California cover a wide range of time-scales. These time-scales were examined by representing the original time-series (i.e. the "time domain") by an independent set of sine and cosine functions of varying frequency using a "digital fast Fourier transform" (e.g. Otnes and Enochson 1978). The distribution of the amplitudes associated with each discrete frequency provide an alternate, but equivalent, description of the variations in the "frequency domain." This information is commonly presented in terms of the "spectral energy density". The spectral energy density is equal to the square of the amplitude (for a single frequency within the spectrum of frequencies) divided by the bandwidth between frequencies in the spectrum (the bandwidth is determined by the duration of the deployment). Since the ordinate is proportional to the square of the current velocity, it is a measure of the kinetic energy associated with each frequency, thus giving rise to the term: "spectral energy density."

Figures 2.15, 2.16, and 2.17 show the spectral energy density for the longshore and cross-shore components of the flows measured at each site. Both similarities and differences between the characteristics of the flows in the two directions are evident. In both directions, the amplitude of the variations associated with frequencies greater than the tidal frequencies (i.e. $>>2$ cycles per day) decrease rapidly with increasing frequency. Both the longshore and cross-shore flows also show two "peaks" in the spectrum at frequencies corresponding to the diurnal (1 cpd) and semidiurnal (2 cpd) tidal frequencies. The amplitude(s) near the semidiurnal frequency are somewhat greater than those near the diurnal frequency (approximately 2.7 times greater for the longshore flow, about a factor of 1.4 for the cross-shore component).

The principal difference between the flows is in the subtidal frequencies (i.e. frequencies $<<1$ cpd). Here the difference in spectral energy density between the two components increases with decreasing frequency (increasing periodicity). This is indicative of the predominant along shore character of these slowly varying components of the flows.

An alternative representation of the distribution of energy (or, equivalently, the variance in the flow) is obtained by plotting the cumulative energy as a function of increasing periodicity (i.e. decreasing frequency). The cumulative energy is obtained by summing the spectral energy density associated with each frequency. An example is shown in Figures 2.18a,b, which are the equivalents of Figures 2.16a,b. At frequencies in excess of about 2 cpd, the energy decreases at a roughly constant rate with increasing (log) frequency. The total variances associated with the fluctuations of supertidal frequency are about 9.5 and 6.5 cm^2 s^{-2} in the longshore and cross-shore directions, respectively.

Two abrupt increases in the cumulative variance are evident at the diurnal and semidiurnal tidal frequencies and represent the contributions associated with the two tidal peaks in the spectral energy distribution. The total

variances in the frequency band between the supertidal frequencies and a frequency slightly below 1 cpd are about 18 $cm^2 s^{-2}$ (i.e. 27.5-9.5) and 9.5 $cm^2 s^{-2}$ (16-6.5) for the longshore and cross-shore flows respectively.

The total variance in the longshore flow (Figure 2.18a) associated with frequencies <1 cpd is about 90 $cm^2 s^{-2}$. This corresponds to about 75% of the all the variance in the longshore motions. In contrast, the subtidal variance in cross-shore direction (Figure 2.18b) is only about 4 cm s^{-2}, or about 20% of the total variance in this direction.

We used spectral energy densities and cumulative variances to estimate the strength of the longshore and cross-shore tidal flows at each site. The variance associated with the tidal motions was assumed to be the variance associated with the frequency interval between 0.9 and 2.3 cpd. After computing this variance, an associated "rms amplitude" was computed. This amplitude is equal to the square-root of the variance. A corresponding "peak" amplitude, representing an oscillation with a single frequency, (or periodicity, e.g. semidiurnal = 12.42 hr), was estimated by multiplying the rms amplitude by 1.4 ($\sqrt{2}$). For example, in the preceding paragraphs we estimated the variance for the longshore motions of tidal periodicity to be about 18 cm s^{-1}. The corresponding rms amplitude is 4.2 cm s^{-1} and the peak amplitude is 6.0 cm s^{-1}. In the cross-shore direction, the peak amplitude is 4.3 cm s^{-1}. These peak values were used to characterize the tidal fluctuations in the *DECAL* simulations.

The fluctuations of diurnal frequency are smaller than those of semidiurnal frequency at the San Diego and Orange County sites. For simplicity, it was assumed that a single oscillation of semidiurnal tidal frequency (i.e. the M2, or "principal lunar semidiurnal" frequency, with a period of 12.42 hr) could be used to represent the tidal flows in those areas. The diurnal fluctuations were stronger in the Los Angeles County outfall area, and both semidiurnal and diurnal (24.00 hr) fluctuations were used for the simulations in that area. The tidal amplitudes used at each of the outfall sites are summarized in Table 2.15.

Multiple "net" currents can be used in the *DECAL* simulations to estimate subtidal variability in the currents. We elected to represent these motions by two components--a single upcoast movement and a corresponding downcoast flow. Estimates of the strength and frequency of occurrence of each of these flows was estimated from time-series representing fluctuations in the currents of subtidal frequency. These low frequency time-series were generated by applying a "running-average" (or "boxcar") filter to the original velocity time-series. In this process, at each time, t, in the series, "n" values surrounding that time are averaged to yield a new, "average" value for that time. The number of values averaged, n, determines which variations will be suppressed by the averaging process, and which will be passed on to the new time-series. Variations with a frequency equal to multiples of the averaging time are efficiently rejected by this filter, and periodicities shorter than the averaging period are suppressed.

In our analysis, the strongest source of variance in the tidal and supertidal bands are the fluctuations of semi-diurnal periodicity (M2, period = 12.42 hr). We selected a value of "n" that corresponded to an averaging time that was as close as possible to twice the M2 tidal period (i.e. 24.84 hr). For the Orange and Los Angeles County measurements, which were sampled at 45 min intervals, this corresponded to 24.75 hr; for the San Diego measurements (sampled at 30 min intervals) the average extended over 25 hr. After generating the new time-series, they were examined for the frequency of upcoast versus downcoast movements. At the same time, the average speeds in both flow directions were calculated. The results of this analysis are summarized in Table 2.16.

II.B.1.f. Simulation Parameters. Various information on the rates of aggregation, decomposition, natural particle production, and loss of particle mass in the sediments are required to carry out the simulation. If a trace constituent is simulated, the partitioning coefficient between particle and water is also required. The specific parameters are:

1. Phytoplankton productivity (gm-C $m^{-2} d^{-1}$)
2. Second order coagulation/settling rate coefficients (top, middle layers, L $mg\text{-}d^{-1}$)

3. Floc settling velocity coefficients (differential settling, $[cm\ s^{-1}][mg\ l^{-1}]^{1.78}$; brownian motion, $[cm\ s^{-1}][mg\ l^{-1}]^{0.38}$)
4. First-order decay coefficients (upper, middle, lower layers; d^{-1})
5. First-order interfacial sediment decomposition rate coefficient ($cm\ d^{-1}$)
6. Trace constituent partition coefficient ($[mg\ kg^{-1}]/[mg\ l^{-1}]$)

We selected a phytoplankton productivity rate of 2 gm-C $m^{-2}\ d^{-1}$. This is near the upper range of productivities measured in the Southern California Bight (Eppley *et al.* 1983), but a relatively high value was suggested in Tetra Tech (1987) because productivity may be enhanced by the discharge of nitrogen from the outfall (Thomas 1972). We assumed an upper layer thickness of 30 m, a decay coefficient of 0.1 d^{-1}, and a second-order aggregation coefficient of 2×10^{-6} l mg s^{-1}. These values result in a predicted settling flux of total organic carbon of about 1 gm $m^{-2}\ d^{-1}$ (Tetra Tech 1987). Using a factor of 2.5 to convert carbon mass to total mass (Tetra Tech 1987), results in a total mass flux of 2.5 gm $m^{-2}\ d^{-1}$, or about 90 mg $cm^{-2}\ yr^{-1}$.

The second order coagulation/settling coefficient, B (see equations 1.3 and 1.25) varies as the 0.23-power of the wastefield thickness and the 0.3-power of the (average) concentration of suspended solids. For a 30 m thick wastefield and an anticipated total suspended solids concentration in the wastefield of about 1 mg l^{-1}, the magnitude of this coefficient is estimated to be about 0.35 (mg $l^{-1}\ d^{-1}$), or about 4.1×10^{-6} mg $l^{-1}\ s^{-1}$. This is about twice the default value in the *DECAL* program (2×10^{-6}). A value of 4×10^{-6} was used for the wastefield layer. For other wastefield thicknesses, or initial suspended solids concentrations, the coagulation/settling coefficient should be modified to be:

$$B = 4.1 \times 10^{-6} (h_w/30)^{0.23} (C/1.0)^{0.3} \qquad (2.2)$$

where h_w is in meters and C is in mg l^{-1}.

The floc settling speed coefficients suggested as default values in *DECAL* are based on a wastefield thickness of 10 m. In order to convert these to the wastefield thicknesses appropriate to our simulations (26.5-30 m), the default *DECAL* settling speed parameter values need to be multiplied by the factors:

Differential settling:	$(h_w/10)^{1.74}$
Brownian motion:	$(h_w/10)^{0.46}$

For a wastefield thickness of 30 m, the two coefficients become about 1.1×10^{-5} and 0.098 for the aggregation associated with Brownian motion and differential settling, respectively.

Tetra Tech (1987) suggests a decay coefficient of 0.1 per day for organic material in the upper layer and 0.05 d^{-1} for the lower layers. Studies of effluent particle decay in the laboratory and in the ocean (Myers 1974) suggest a value of about 0.52. Since the effects of this decay may be significant for the time scales characterizing wastefield particle deposition , we carried out simulations for values of 0.1 and 0.52 at each of the simulation sites.

The first-order interfacial removal rate is a composite rate representing the combined effects of sediment resuspension, decomposition, and burial. The relative contributions of each of these processes to the composite rate can be expected to vary with water depth, sediment composition, and season at a single site. The magnitude can also be expected to vary from site-to-site. In general, measurements at each study site should be used to select an appropriate value. Tetra Tech (1987) suggests a value of 0.015 cm d^{-1}, based on a review of organic carbon turnover rates in surface sediments (Hopkinson 1985 and associated references). This value was used for the *DECAL* simulations in this study. Uncertainties in this parameter affect only the accumulation rate and mass of organic and trace material in the sediments--they do not affect the sedimentation rate of particulate mass from the water column. The effects of varying this parameter between 0.005 and 0.045 cm d^{-1} were examined at the Orange County outfall site.

Appropriate values for the partitioning coefficients for lead and cadmium are difficult to estimate. Tetra Tech (1987) used data reported on the residence times of trace metals in the ocean (Balistrieri *et al.* 1981) to deduce that the coefficients for trace metals can vary over several orders of magnitude, with:

$$K_p(\text{lead}) > K_p(\text{copper}) >>> K_p(\text{cadmium})$$

In their simulations of the Los Angeles County and Orange County outfall sites with the two-layer version of *DECAL*, they assumed that K_p(lead) was $>10^7$ and K_p(cadmium) = 3×10^5. We used values of 10^7 for Pb, and 3×10^5 for Cd in all our *DECAL* simulations.

While Tetra Tech (1987) used a value of 0.015 cm d^{-1} for the interfacial removal rate of organic material from the surface layer of the sediments, they use an interfacial removal rate of 0.007 cm d^{-1} for both lead and cadmium. This selection was based on a comparison between the predicted and observed distributions at the two sites. The three-layer version of *DECAL* does not provide for separate interfacial removal rates for organic material and a trace constituent, so all our results correspond to a interfacial removal rate of 0.015 cm d^{-1} for both organic material and the trace constituent.

II.B.2. SED2D

SED2D consists of a suite of submodels. The input data and parameters used in the *SED2D* simulations for the three simulation sites are listed in this section in the approximate order that the information is required for the simulations.

II.B.2.a. Initial Dilution (TSLINE). Calculations of initial dilution using TSLINE require information on:

1. discharge depth
2. orientation of the diffuser
3. volumetric discharge rate
4. diffuser length
5. effluent density
6. receiving water density at the diffuser depth (avg)
7. simultaneously collected time-series of ocean currents and density stratification of the water column

The discharge and diffuser characteristics used in the simulations are summarized in Table 2.17. All the simulations used an effluent density of 0.9995 gm cm^{-3} and a receiving water density (at the diffuser port) of 1.02588.

The initial dilution calculations are based on simultaneous measurements of ocean currents and water temperature measured in the vicinity of the San Diego (Point Loma) ocean outfall by Engineering Science from March to September 1990 (Engineering Science 1990). The observations were collected at moorings C2 (currents) and T2 (temperature) in 56 m of water (Figure 2.19). The characteristics of this data set (as well as data collected at other moorings in the study area) are discussed in Engineering Science (1990) and Hendricks (1990).

Although temperature gradients generally control the density stratification of the water column, salinity gradients also make a contribution--particularly when the temperature stratification is minimal. Time-series of temperatures at 5 m intervals in the water column were converted to density equivalent time-series using (roughly) monthly CTD data from the area. This conversion was made by developing piece-wise quadratic equations between temperature and salinity for each deployment period. These analytical relationships were then used to generate the density time-series from the temperature time-series.

The temperature and current meter time-series from the San Diego area were also used to simulate the initial dilutions at the Orange County and Los Angeles County simulation sites. In doing so, we assumed that the characteristics of the currents and density structure of the water column are comparable in all three areas.

Thus the differences in the dilutions predicted for each site are the result of differences in the discharge depth, diffuser orientation, and hydraulic loading (volumetric discharge rate per unit length).

The orientation of the coast, and hence the dominant direction of flow of the ocean currents changes from site to site. Therefore it was necessary to rotate the orientation of the San Diego currents (or, alternatively, the diffuser alignment) to maintain the correct angle between the ocean currents and the diffuser at the Orange County and Los Angeles County outfall sites.

The TSLINE calculations use a single alignment for the outfall diffuser. However, the diffusers at these sites consist of two legs, either in the form of a wye or "bent L." Therefore it was necessary to represent each of the outfall diffusers by two segments, and compute the initial dilutions for each of the segments. Within a single simulation site, the initial dilution and wastefield characteristics (distributions of wastefield-averaged dilution, rms-averaged concentration, wastefield thickness, and depth to the bottom of the wastefield) were calculated at 30 min intervals for each diffuser leg and each data period. The results were then weighted by the number of observations and averaged to produce a "long-term average" distribution for each characteristic. The median values of the wastefield thickness, and depth to the bottom of the wastefield were used as input into both the *DECAL* and *SED2D* simulations. The median rms value of the spatially averaged initial dilution (based on the rms change in concentration) was used to estimate the wastefield concentration of effluent suspended solids in the *SED2D* simulations.

The other information required to carry out aggregation simulations with the *SED2D* submodel DPA is:

1. initial wastefield concentration of effluent suspended solids
2. initial wastefield concentration of natural suspended solids
3. composition of the effluent and natural particles
    a. inorganic fraction
    b. organic-refractory fraction
    c. organic-labile fraction
4. flux of natural particles settling into the wastefield
5. wastefield thickness
6. depth to the bottom of the wastefield
7. bottom depths in the simulation grid
8. decay rate of the organic-labile material
9. total simulation time
10. output time-series interval
11. computation time-step

The initial wastefield concentration of effluent suspended solids was computed from the initial dilution computed from the TSLINE simulations and the concentration of suspended solids in the effluent (Table 2.10).

II.B.2.b. Composition of Effluent Suspended Solids. The mass of total volatile solids (TVS) in primary treated effluent is about 70% of the total mass (Myers 1974; this report). We assumed that this corresponds to the total organic content of the particulates. Studies of the decay of organic material in primary treated effluent (this study; Myers 1974) suggest that there are at least two components to the organic material. One of these is characterized by decay time-scales on the order of days; the other, by time-scales in excess of 10 d. We anticipate that sedimentation within the simulation area will be dominated by deposition that occurs within a few days of discharge, hence only the first component is likely to undergo significant decay. We refer to this rapidly decaying component as the organic-labile ("labile") fraction, and the slow decaying component as the organic-refractory ("refractory") fraction.

From the decay experiments in this study, we estimate that about 15% of the organic material may be refractory or subject to slow decay, with the remaining 85% subject to rapid decay. Therefore, for the simulations of particle aggregation and settling in the water column, we assumed that:

$f_{inorganic}$	= 0.300
$f_{organic\text{-}refractory}$	= 0.105
$f_{organic\text{-}labile}$	= 0.595

Based on the studies of the decomposition of organic material under simulated and in-situ conditions (Myers 1974), we assumed a decay coefficient of 0.52 for organic-labile material. This rate is about 5-10 times greater than the rate of 0.05 to 0.1 d^{-1} suggested by Tetra Tech (1987). Two simulations were carried out for each site--one for each decay rate.

II.B.2.c.Initial Concentration of Natural Particles. The entrainment of natural particles into the plume during the initial dilution process contributes to the initial suspended solids load of the wastefield. In order to estimate this contribution, we used measurements of suspended solids collected offshore from Dana Point and the Los Angeles County outfalls (Myers 1974); at various locations in the Los Angeles County simulation area (LACOSAN, unpub. data); in the coastal waters off Encinitas, about 20 nm (38 km) north of the San Diego simulation area (Kinnetics 1988); and monthly observations off Mission Beach (ca. 10 km upcoast from Point Loma) between January 1989 and December 1991 (City of San Diego, unpub. data). Since entrainment is usually limited to the lower half of the water column, we focused on the concentrations of suspended solids at midwater depths.

The LACOSAN data shows that midwater concentrations of suspended solids in water depths of 30 m, 60 m, and 300 m in the Los Angeles County simulation area were on the order of 2.5-3 mg l^{-1}, 2-3 mg l^{-1}, and 1.5-2.5 mg l^{-1}, respectively (one collection). Myers(1974) measured similar concentrations offshore from the Los Angeles County outfall (i.e. 1-2 mg l^{-1}) and in the Dana Point area (ca. 1.7 mg l-1). The suspended solids measurements off Encinitas spanned a six month period from April to September 1987. Midwater suspended solids concentrations ranged from 2.4-10.5 mg l^{-1} in 15 m of water, and 1-10.3 mg l^{-1} in 36m of water. The average values were 6.5 mg l^{-1} in 15 m, and 4.5 mg l^{-1} in 36 m of water.

The City of San Diego measurements were made at depths of 24 m (85 ft) and just above the bottom in 61 m of water. Concentrations measured in 1989-90 at both depths ranged from 0.6-4.6 mg l^{-1}. The average concentration at 24 m was 1.7 mg l^{-1}, while the near-bottom concentrations averaged 2.5 mg l^{-1}. The average for all observations was 2.0 mg l^{-1}. From January to November 1991, ambient suspended solids were about six times higher than in 1989-90. At 24 m, suspended solids ranged from 9.0-14.5 mg l^{-1}, averaging 11.0 mg l^{-1}. Near the bottom, the concentrations ranged from 9.9-14.5 mg l^{-1} (excluding one observation of 51.3 mg l^{-1} that was likely due to resuspension of bottom sediments). The average was 15.8 mg l^{-1}.

There is a trend towards decreasing suspended solids concentrations with increasing water depth. Considering normal variability (and neglecting the apparent change in oceanographic conditions off Point Loma during 1991), depth-adjusted ambient suspended concentrations are remarkably similar from site to site. Typical concentrations in 55-65 m of water are on the order of 2 mg l^{-1}, and this value was used in the *SED2D* simulations.

II.B.2.d. Composition of Natural Particles. The next step is to estimate the composition of the natural particles. We used data from sediment trap studies in the water column that were carried out over Santa Monica Basin, lying offshore from the Los Angeles County outfall site (LANDRY et al.21.,1991). Particles were collected in sediment traps at mean depths of 119, 199, 499, and 850 m during a set of deployments over slightly more than a year. The solid line in Figure 2.20 shows the concentration of organic material (taken as twice the organic carbon concentration) in the trap material as a function of the collection depth. The dashed line shows the regression line for a power-law fit to this data. Extrapolating this trend line into shallower water depths yields predicted organic concentrations of 0.7 at a depth of 25 m, and 0.6 at a depth of 40 m. Since these concentrations are similar to those of effluent particles, we assumed that the organic composition of natural and effluent particles were the same.

II.B.2.e. Sedimentation of Natural Particles from Overlying Layer. The other source of natural particles is the sedimentation of natural particles from the overlying water column. The CABS sediment trap studies found

that the total mass flux into the sediment traps was nearly independent of depth. The lowest average flux (at 499 m) was 580 mg m^{-2} d^{-1}--only 7.5% lower than the highest value of 627 mg m^{-2} d^{-1} (at 199 m). We assumed a depth-independent natural particle flux of 600 mg m^{-2} d^{-1}.

For an organic carbon concentration of 35% , this would correspond to TOC flux about 210 mg m^{-2} d^{-1}, or roughly one-fifth of the flux that we used in the *DECAL* simulations (1000 mg-C m^{-2} d^{-1}). We elected to use the smaller flux for the *SED2D* simulations because this rate is probably more representative of the average phytoplankton productivity in the southern California bight (Tetra Tech 1987, Figure 3). Enhanced productivity resulting from the discharge of nutrients is likely to be minimal in the upper layer of the ocean, due to the inhibition of vertical exchange with the wastefield by the thermocline.

II.B.2.f. Simulation Grid. The *SED2D* primary simulation grid is a 32 x 32 array of cells. In the San Diego and Orange County simulation areas, the length (longshore dimension) of each cell was 500 m; in the Los Angeles County simulations the length was increased to 1 km. The width (cross-shore dimension) of the cells in each of the simulations was 125 m. Thus the area covered by the simulations for the San Diego and Orange County sites was 64 km^2 (16 x 4) and 128 km^2 for the Los Angeles County site (32 x 4). The orientation and placement of the simulation grid in each of the simulation area is shown in Figures 2.21a,b,c.

II.B.2.g. Water Depth. DPA computes the time-dependent sedimentation of particles from the wastefield to the bottom in a column moving along each of the alongshore rows of cells. The time-dependent deposition rate is dependent on the water depth for each row and this information is required as input. The depths at the boundaries of the cells along a cross-shore transect are shown in Figure 2.22 for each of the simulation sites. Note that the grids were placed so that the water depth at the innermost boundary was on the order of 12-16 m.

II.B.2.h. Duration of the Simulated Deposition. In all the simulations, the total simulated time for particles to settle from the wastefield to the ocean bottom after discharge from the outfall was one week (168 hr). The interval at which the deposition and transport simulation results were written to files was chosen to be equal to the sampling interval in the ocean currents measurements at each site. For the Orange County and Los Angeles County simulations, this interval was 45 min; for the San Diego simulations, 30 min. The computation time step used within the DPA and DPS (settling) computations ranged from 15 to 22.5 min.

II.B.2.i. Advective Transport. Current meter time-series are used to estimate the advective transport of the settling particles. Current meter data collected by SCCWRP was used for the Orange County and Los Angeles County simulations; data collected by Engineering Science was used for the San Diego simulation. The dates of these deployments were summarized in Table 2.14

The San Diego transport calculations use data for the same seven month period as was used in the initial dilution calculations. The transport data was collected at a depth of 30 m in 56 m of water. The Orange County simulations used 13 months of data collected at a depth of 36 m in 56 m of water. The Los Angeles County simulations used data collected in water depths ranging from 30 m to 62 m. The properties of the currents in the San Diego data set are discussed in Engineering Science (1990) and Hendricks (1990). The Orange County data set is discussed in Hendricks (1992). No overview of the set of measurements used in the Los Angeles County simulations is available, however the general features of the currents in this area are discussed in Hendricks (1980).

II.B.2.j. Representation of Diffusers as Multiple Sources. The output files generated by PRX and PRY correspond to the time-dependent distribution probability for wastewater discharged from a point source. Since the cell dimensions of the grid cells are less than, or comparable to, the diffuser lengths, simulations were generated for multiple discharge points. In each case, three discharge points were used to represent the extended diffuser. Two of these points were located inboard from the end of the diffuser at a point equal to one-third of the diffuser segment length. The third was positioned at the connection between the two diffuser segments.

In the simulations for the Los Angeles County site, only the discharge from the 90-inch outfall was simulated using the full suite of simulation submodels. After this pattern was computed, the pattern associated with the 120-inch outfall was estimated using the submodel PXYADD.

II.B.2.k. Mass Emissions. The mass emissions and suspended solids concentrations used in the *DECAL* simulations were also used for the *SED2D* simulations. As before, the sediment quality and accumulation rate in 1990 was the goal of the simulations for the San Diego and Orange County simulations. The simulation date for the Los Angeles County simulations was 1981.

We also carried out some simulations for the Los Angeles County site for a target date of 1972. This roughly corresponds to the period of peak emissions (ca. 168,000 mt yr^{-1}, versus 97,950 mt yr^{-1} for the 1981 simulations, and 34,300 mt yr-1 in 1990). Prior to June, 1972, the concentration of suspended solids in the effluent leading to the 90-inch outfall were greater than in the effluent leading to the 120-inch outfall. For aggregating particles, this means that a greater fraction of the wastefield particles from the 90-inch outfall will settle to the bottom within some fixed period of time than will reach the bottom in the same period of time from the 120-inch outfall. In addition, for both aggregating and noncohesive particles, the mass emissions from the 90-inch outfall will be enhanced. As a result, the accumulation of wastefield-related particles in the sediments in the area can be expected to be biased towards the discharge from the 90-inch outfall.

For both simulations, we assumed that the total flow to the Los Angeles County outfalls was partitioned between the 90- and 120-inch diffusers according to their design capacities (160 mgd and 235 mgd, respectively). For the 1981 simulations, the ratio of the mass emissions of suspended solids from the two outfalls is the same as the flow rates. For the 1972 simulations, we assumed that the mass emissions from the 90-inch outfall were twice those from the 120-inch outfall.

II.B.2.l. Combining Data Periods and Effluent Components. The distributions generated using each current meter data set were combined into a temporally averaged distribution for each site. Some additional data manipulations was required for the Los Angeles County simulations. Here the current meter data was not uniformly distributed in time (spring was heavily sampled; late summer was poorly sampled). Therefore the extended source depositional probability files were partitioned according to the seasons (winter, spring, summer, fall) in which the current meter was collected. Within each season, the depositional patterns were weighted and combined to yield the average distributional probability for the season. The seasonal average time-dependent depositional patterns were then weighted equally and combined to yield the average depositional pattern for the Los Angeles County outfall site.

The simulations of the initial sedimentation of wastefield particles to the ocean bottom computed the depositions associated with each of the components (inorganic, labile, refractory) of the effluent and natural particles. For the remaining portion of the simulation (sediment processes), we assumed that the refractory and labile organic material could be combined into the single category "organic". We also combined the effluent and natural particle fluxes into a single "total" flux. Thus the remaining simulations calculated the flux of only two components.

II.B.2.m. Sediment Resuspension and Transport. The depositional patterns, concentrations, and accumulation of particulate material originating in the wastefield can be modified by sediment resuspension, transport, and redeposition. The input information required by the submodels TRANS, DISPER, ACCUM, and SEDR to simulate these processes are:

1. threshold current speed for resuspension
2. threshold current speed for deposition
3. accumulation fraction

We do not know appropriate values to use for the threshold resuspension and threshold deposition speeds--or even if such values exist. Washburn et al. (1991) conducted studies of the properties of the water column near the Los Angeles County outfalls and noted evidence for sediment resuspension when the currents were about 7

cm s^{-1}, but no evidence of sediment resuspension when the currents were 1 cm s^{-1}. These observations provide some guidance on suitable values for the threshold speeds. However, we note that measurements with an *in situ* resuspension water tunnel (Hendricks 1976) indicate that the threshold resuspension stress is probably related to the organic content of the sediments--as well as particle size. Thus the threshold resuspension speed may vary with location in the simulation area, decreasing in areas with organically enriched sediments, and increasing in areas less affected by the discharge.

For the purposes of these simulations, we assumed a threshold resuspension speed of 9 cm s^{-1}, and a threshold deposition speed of 4.5 cm s^{-1}. One simulation run was made for the discharge from the Los Angeles County 90-inch outfall using threshold speed of 6 and 3 cm s^{-1}.

II.B.2.n. Near-Bottom Transport. The sediment trap studies indicate the distribution of resuspended particles follows an equation of the form:

$$f(z) = f(z=0)\, e^{-z/h_r} \qquad (2.3)$$

where f(z) is the flux of particle mass into a trap position at a distance z above the bottom, and h_r is a characteristic thickness. Typical values for *hr* are 2-4 m, indicating that roughly 63% of mass of resuspended particles are within this distance from the bottom. Fluxes into the traps generally decrease exponentially with increasing distance from the bottom.. We used current meter data collected 2 m above the bottom to simulate the resuspension and transport of surficial sediments at the Orange County and Los Angeles County sites. Unfortunately, the bottom meters on the moorings at the San Diego site were 4 m above the bottom. Measurements by SCCWRP indicate that there are some potentially significant changes in the properties of the currents between an elevation of 2 m and an elevation of 5 m. The most important difference is the possibility that offshore transport at the San Diego site may be underestimated in our simulations. This introduces some additional uncertainty into the resuspension and transport estimates for the San Diego simulations.

II.B.2.o. Accumulation Fraction. The conceptual model used to simulate resuspension describes the process in terms of a series of resuspensions and depositions before the average particle becomes part of the surface layer of sediments. At each stage, a fraction of the particles lying in the surficial layer of easily resuspended sediments is transferred into the more resuspension resistant surface layer. This fraction is termed the "accumulation fraction" f_a. In the absence of wastewater particles, the average value of this parameter can be estimated from the ratio between the net accumulation rate of natural particles in the sediments and the flux of these particles into the near bottom sediment traps. If the average depositional flux into the traps is F_d, and the average accumulation rate of particle mass in the sediments is F_a, the average value of the accumulation fraction is approximately:

$$f_a = (F_a / F_d)\,(1-C_a)\,/(1-C_t) \qquad (2.4)$$

where C_t and C_a are the concentrations of organic material in the sediment trap material in the surface sediments, respectively.

Annual average near-bottom fluxes of particle mass into sediment traps range from about 1000 mg cm^2 yr^{-1} (Orange County) to 4,500 mg cm^{-2} yr^{-1} (Los Angeles County) in water depths of 55-60 m (Figure 2.23). Published estimates of the accumulation rate of particle mass in the sediments prior to the outfall discharges in this area range from 9 mg cm^{-2} yr^{-1} (Emery 1960) to 20-60 mg cm^{-2} yr^{-1} (e.g. Schwalbach and Gorsline 1985). Concentrations of organic material in the traps tend to be higher than in the underlying sediments, but both concentrations are relatively low. Therefore if we assume a typical accumulation rate of particles in the sediments of 20 mg cm^{-2} yr^{-1}, the accumulation fraction would be on the order of 0.005 to 0.020. For our simulations, we assumed values of 0.01 ("resuspension") and 1.00 ("no resuspension") at all the sites. However, it is not known if a value of 0.01 for the accumulation fraction is appropriate if effluent particles are present or the flux (or abundance) of organic material is increased in near bottom waters. We also made parametric studies with the accumulation fraction ranging from 0.005 to 1.00 for discharge from the Los Angeles County 90-inch outfall.

II.B.2.p. Accumulation and Composition of Particles in Surface Sediments. The remaining portion of the simulation process addresses the processes that determine the accumulation rate of particles in the sediments and the concentration of organic material in the surface sediments. We need two additional pieces of information for these simulations:

1. the flux and composition of natural particles into the surface sediments that are not associated with deposition from the wastefield
2. the decomposition flux of organic material in the decay layer of the sediments.

We estimated this flux of natural particles from the estimates of the accumulation rate of natural sediments in the absence of a discharge. The organic content of these particles is estimated from the organic content of the surface sediments in the absence of the discharge. Note that the organic content of these natural particles may be much less than that of the natural particles settling from water column since they include particles from coastal erosion and runoff. Estimates of the flux rate and initial organic content are obtained by systematically selecting values and carrying out simulations with PXYACC until the modeling results approximately reproduce the observed accumulation rates and composition.

Two parameters characterize the decay layer of the sediments--the mass (per unit area) and the rate of loss of organic material. If fluxes are used to characterize the loss of organic material, it is not necessary to know the mass of material in the layer. However, the mass of material per unit area in the mixed layer of the sediments (i.e. the surface layer), is required if the transient response of the sediments is required. Since *SED2D* presently only calculates steady-state conditions, we only need to supply the decay flux as input information.

Measurements of the remineralization rate of total organic carbon have been reported for a variety of sites (Table 2.18). Rates vary from site to site and range over approximately two orders of magnitude. To estimate this flux for our simulations, we calculated the geometric average remineralization rate for three sites: (1) Skan Bay, (2) Cape Lookout, and (3) the average of the southern California basins. The result was a rate of 0.55 milli-moles C cm^{-2} yr^{-1} (or 6.6 mg C cm^{-2} yr^{-1}). If we assume that the concentration of organic carbon in these sediments averages 5-6%, the decay flux (which is based on 100% organic material) is about 120 mg cm^{-2} yr^{-1}. We used this value for the *SED2D* simulations. Table 2.19 summarizes estimates of the corresponding decay rates (k_d) in sediments.

II.B.2.q. Simulations with Settling Column Data. Simulations were also carried out for the case of noncohesive particles. For these simulations, the submodel DPS replaces the aggregation simulation submodel DPA. Our predictions are based on estimates of settling speeds obtained in laboratory studies using settling columns. The settling column measurements of Los Angeles County effluent reported by Myers (1974) were used for the simulations. (Figure 2.24). These results were obtained from studies using low dilutions of Los Angeles County final effluent (at that time), but are comparable with the results obtained by Herring and Abati (1978) using Los Angeles County final effluent for the year 1977 and a dilution of 500:1. We elected to use Myers' results instead of those of Herring and Abati since the latter contains more variability (understandable in view of the complications associated with the high dilution). Differences between the two distributions are generally small (Figure 2.24).

We used the equation:

$$F(V_{sr}) = 0.01 / (V_{sr})^{0.5} \qquad (2.5)$$

where $F(V_{sr})$ = fraction of the total mass with a settling speed greater than v_{sr}, to represent this mass distribution of settling speeds.

III. RESULTS

III.A. FIELD STUDIES

III.A.1. Effluent

III.A.1.a. General properties (TSS, TOC, TN). Table 3.1 provides data on the suspended solids concentration of effluent samples. Data are given for filtrations in which both 47 mm and 25 mm glass fiber filters were used. The latter were employed for TOC and TN analyses, whereas the former were used to determine TSS, principally because of their higher capacity. In general, the results obtained by different analysts using the two filter sizes are quite similar for a given date and effluent. However, a few discrepancies between results for the two filter sizes were observed, and where appropriate these differences have been noted.

Three of the four effluents (Hyperion, JWPCP, OCSD) exhibit TSS concentrations in the range of 50-80 mg l^{-1}. For the JWPCP and OCSD this range is similar to the mean annual concentrations reported by the treatment plants in 1989 (SCCWRP 1991b). However, our measurements for effluent samples from the Point Loma and Hyperion treatment plants appear to be higher than the monitoring data generated by the sanitation districts by a factor of approximately two (e.g. monitoring data: Hyperion-33 mg l^{-1}, Point Loma-60 mg l^{-1}; SCCWRP 1991b). Moreover, the TSS concentrations we obtained for the PLTP effluent (ca. 70-120 mg l^{-1}) fall in a somewhat higher range than those observed for the other effluents. This difference may be attributable to the fact that the PLTP is the only plant whose effluent receives exclusively advanced primary treatment (no secondary). The effluents from Hyperion, JWPCP and OCSD plants are 48.5, 54.5 and 53.4% secondary, respectively, the remainder being advanced primary.

Table 3.2 gives results of the TOC and TN analyses of effluent particles. The data are presented both in terms of elemental abundance (percent organic carbon and percent nitrogen) and as POC (particulate organic carbon) and PN (particulate nitrogen) concentrations. Effluent particles contain approximately 25-40% organic carbon and 2.5-6% nitrogen. There is considerable variation between samples for a given effluent. Coefficients of variation range from 15-23% for TOC and 15-27% for TN. The TOC concentrations reported here are similar to those found in JWPCP effluent particles by Myers (1974) in the early 1970s (ca. 28-41%), by Sweeney *et al.* (1980) in the late 1970s (30.8-31.8%) and by Venkatesan and Kaplan (1990) in 1987 (25.3%). In contrast, the average nitrogen content of the JWPCP effluent particles collected in this study (3.9%) is significantly greater than that reported by Sweeney *et al.* (1980; 2.36%). Because of the higher suspended solids concentration of the PLTP effluent, the concentrations of POC and PN in this effluent are approximately 30% greater than those in the JWPCP and OCSD effluents.

The effluent particles generally exhibit C/N ratios of 6.5-10. These are similar to ratios found by Eganhouse (1986) in final effluent from the South Essex Sewage District (Salem Harbor, MA; 8.3) and by Eganhouse and Sherblom (1991) in combined sewer overflow effluent to Boston Harbor; 6.5-8.9).

III.A.1.b. Stable isotopes. Table 3.2 lists the stable carbon and nitrogen isotope ratios of effluent particles collected from the three treatment plants. The data presented here are few. Thus, our ability to interpret these results remains limited until further analyses can be performed.

The stable carbon isotope ratios for the JWPCP, OCSD and PLTP effluent particles range from -21.76 to -23.26‰. The lowest of these ratios is only slightly more depleted in ^{13}C than suspended and sinking marine particulate organic matter in the southern California Bight which ranges from about -20.5 to -22.5‰ (Williams *et al.* 1992). Comparison of the present JWPCP data with results obtained earlier by Myers (1974), Sweeney *et al.* (1980) and Eganhouse *et al.* (1983c) indicates little, if any, difference. However, the $\delta^{13}C$ values for the PLTP and OCSD effluents appear to be more enriched in ^{13}C today than they were a decade ago. This enrichment reduces the value of the stable carbon isotope ratios as a means of discriminating between marine and effluent particulate organic carbon at these sites.

The stable nitrogen isotope ratios of the three effluents are similar and close to atmospheric nitrogen (0‰). The only reliable data with which the present data can be compared are those reported by Sweeney *et al.* (1980) for the JWPCP effluent. Judging from these few data, the isotopic composition of the effluents are all more like terrestrial nitrogen (near 0‰) than marine particulate nitrogen in southern California (7-10‰; Liu 1979;

Sweeney *et al.* 1978; Sweeney and Kaplan 1980; Eganhouse and Kaplan 1988; Williams *et al.* 1992). Thus, nitrogen isotopes should provide a more reliable tracer of waste organic matter in the nearshore coastal zone.

III.A.1.c. Trace metals. The particulate matter in bimonthly effluent samples from the JWPCP, OCSD and PLTP was analyzed for Pb and Cd by ICP-MS. In addition, a subset of these samples (two per discharge per year) were analyzed for an extended list of 13 elements. The results of these analyses are given in Tables 3.4 and 3.5. Lead concentrations for the OCSD and PLTP effluents ranged from <20-73 μg dry g^{-1}, whereas the concentrations in the JWPCP effluent were distributed over a somewhat higher range (<20-124 μg dry g^{-1}). Cadmium concentrations for all effluents were typically below 12 μg dry g^{-1}. However, the OCSD 5/17/90 effluent sample yielded an unusually high concentration. Reanalysis of the digest of this sample indicated that the anomaly was most likely a feature of the sample itself or a result of its handling prior to instrumental analysis. Comparison of the cadmium data for the five replicate filters obtained from the same sample and analyzed for the suite of 13 metals (Table 3.5) indicates that the 5/17/90 filter analyzed for Cd and Pb alone (Table 3.4) was most likely contaminated prior to instrumental analysis. Similarly, the cadmium results from the multielement scan on the JWPCP 7/6/90 sample (Table 3.5) would appear to be anomalously high when compared with the other data.

It is difficult to generalize about the multielement scan because of the limited number of samples that were analyzed. Figure 3.1 illustrates the distribution of the 13 trace elements for these six samples. These bar diagrams are presented with a logarithmic scale for the ordinate. There are no obvious major differences among the three discharges with respect to trace metal composition.

III.A.1.d. Trace organics. Six effluent samples (two per discharge) were analyzed for the linear alkylbenzenes. Table 3.6 lists the effluent particulate concentrations of the long-chain linear alkylbenzenes. Data are presented based on individual congeners, as homolog groups (i.e. a given chain length) and as total LAB. Table 3.7 presents total extractable organics and total LAB concentrations. The former measurement is given in particulate-based units, whereas the LAB data are computed on both particulate and volume-based units as well as normalized to particulate organic carbon. These various units facilitate comparison of this data set with previous work on these effluents and effluents from other areas. Table 3.8 lists data for the fecal sterols, coprostanol and epicoprostanol, along with data derived from other sources.

The total extractable organics concentration of the three effluents examined in this study are comparable (140-300 mg g^{-1}). It is interesting to note that the TEO concentrations of the JWPCP effluent particles are not significantly different from what they were in 1979. This may suggest that the decline in oil and grease mass emissions noted over the last decade (SCCWRP 1991b) has more to do with overall reductions in solids emissions than source control. It is also worth noting that the particulate TEO concentrations of the southern California effluents are similar to those determined by Eganhouse (1986) and Sherblom (1990) for East Coast treatment plants.

The ΣLAB concentrations on a particulate basis range between 94-400 $\mu g\ g^{-1}$ for the three treatment plants examined in this study. There would appear to be considerable between-sample variability in the LAB concentration for a given effluent, and this observation is supported by data obtained for the JWPCP on a monthly basis by Eganhouse *et al.* (1983a) in 1979. At that time, the JWPCP had higher particulate LAB concentrations (470-1340 $\mu g\ g^{-1}$) than it does today. The three treatment plants contain LABs at concentrations that are bracketed by measurements from the East Coast. For example, the South Essex Sewage District (Salem, MA) final effluent yielded a concentration of ca. 50-140 $\mu g\ g^{-1}$, whereas the Nut Island treatment plant (Boston, MA) had LABs in concentrations of 150-780 $\mu g\ g^{-1}$. The reasons for the change in LAB concentration for JWPCP between 1979 and 1990 as well as the differences between the different effluents will be discussed below.

Figure 3.2 illustrates the composition of the secondary phenyldodecanes in the effluent samples tested here. The patterns for all of the effluents are typical of the so-called "flat" distribution, whereby roughly equal amounts of each of the phenyldodecane isomers are present. This is characteristic of unaltered (i.e.

undegraded) LABs as they are synthesized and found in surfactants (Eganhouse *et al.* 1983b; Takada and Ishiwatari 1989).

Table 3.8 gives results of the effluent sterol analyses. Concentration data are provided on dry mass, volume and organic carbon bases to facilitate comparisons with other data sets. Also given are data from earlier studies of Eganhouse (1982, 1986), Venkatesan and Kaplan (1990) and Sherblom (1990) for effluents in southern California and Boston.

Coprostanol concentrations for the three effluents examined here overlap each other, ranging from 53-250 μg l^{-1}, 970-3050 μg g^{-1} and 2.4-12.3 mg g OC^{-1}. These concentrations appear to be similar to that reported for effluents from other parts of the world (cf. Grimalt *et al.* 1990; McCalley *et al.* 1981). They also compare well with data reported for effluents from the East Coast (Eganhouse 1986; Sherblom 1990) and for southern California effluents as reported by others (Eganhouse 1992; Venkatasen and Kaplan 1990). Variations in coprostanol concentrations from one effluent to the next are due, in part, to differences in the quality of the influent (e.g. percent domestic *vs.* industrial) as well as the type and extent of treatment (McCalley *et al.* 1981; Walker *et al.* 1982). Comparing the results obtained by Eganhouse (1992) for the JWPCP, OCSD and PLTP effluents in 1979 with those found in the present work, it seems possible that the OCSD and PLTP effluents have experienced a decline in coprostanol content during the intervening decade. Unfortunately, the paucity of data and large concentration ranges typical of these samples prevents us from making more definitive statements. By contrast, when expressed on a dry mass or organic carbon basis, the concentration of coprostanol in the JWPCP effluent would appear to be higher today than it was in 1979. On a volume basis, however, the concentrations found in 1979 and 1990 are comparable. This apparent discrepancy may reflect the effect of improved source control of industrial wastes, whereby the input of solids and, especially, particulate organic carbon would be affected. Again, however, the scarcity of data makes it difficult to draw firm conclusions.

The abundance of epicoprostanol in the 1990 effluent samples from all three treatment plants is consistently lower than it was in samples collected in 1979. Moreover, the coprostanol:epicoprostanol ratio increased dramatically during this interval. McCalley *et al.* (1981) have shown that both coprostanol and epicoprostanol are generated (via biohydrogenation) during anaerobic digestion of sludge. However, the ratio of coprostanol/epicoprostanol tends to decline when sludge is incubated in the absence of oxygen (i.e. epicoprostanol is accumulates more rapidly under these conditions). Thus, the increase in coprostanol:epicoprostanol during the 11 yr interval may signal a significant change in the character of waste treatment. In this context, it is interesting to note that in 1979 the JWPCP and OCSD effluents had coprostanol/epicoprostanol ratios of 4-8, whereas the PLTP exhibited ratios in the range 20-28. Today the fecal sterol ratios of these effluents are similar.

III.A.2. Sediment traps

III.A.2.a. Intercomparison of sediment trap designs. Prior to deploying sediment traps in the field, we developed a new prototype based on the earlier design of Hendricks (SCCWRP 1987). The new prototype has the same trap geometry as the "Hendricks trap," but was modified to improve sample collection and handling for purposes of trace analysis. The design of the new sediment trap is described in the METHODS section. As a preliminary effort to compare the performance of the two trap designs in the field, we deployed six moorings each of which held three traps (at 0.5, 2.0 and 5.0 m above the sea floor) off Point Loma in October of 1989. Three of the moorings were equipped with the Hendricks traps whereas the other three were equipped with the new traps. The moorings were placed as indicated on Figure 2.4 and were approximately 20 m away from each other along a transect in the longshore direction. The traps were recovered 31 d after deployment. Because we were primarily interested in comparing the trapping efficiencies of the two designs and general chemical characteristics of the trapped particles, we only measured four parameters: 1) dry mass flux, 2) total volatile solids, 3) TOC, and 4) TN. The results of the intercomparison are given in Table 3.9.

The flux of particulate matter decreases with increasing elevation of the trap from the ocean bottom. For both trap designs, the TOC content of the trapped particles generally ranges from about 2.3-2.9%. TN content is approximately an order of magnitude lower (0.14-0.34%). No trend in TOC (or TN) with respect to trap

elevation is evident. Total organic matter as measured by TVS, however, appears to increase with elevation above the bottom. This may indicate that the organic-rich fine grain sized particles are in greater abundance in the upper traps than in the traps nearest the bottom. Why the same trend is not noted for TOC and TN is unclear.

Table 3.10 provides a summary of the trap intercomparison results. The data indicate that the mean solids fluxes at a given depth (n=3 for the new traps, n=2 for the Hendricks traps) for the two trap designs can differ by as much as a factor of two. Although the fluxes measured at 0.5 m above the bottom are essentially identical for the two designs, the traps at shallower depths in the water column (greater elevations relative to the bottom) differ from each other, with the new trap yielding higher fluxes in both cases. The variability in the fluxes measured by the Hendricks trap appear to be somewhat greater than that for the new traps. However, there is no reasonable explanation for this difference given the fact that the construction of exterior and critical trapping components of the two designs are nearly identical. All coefficients of variation (CV) for the new traps fall within 15%, and there appears to be an inverse relation between reproducibility (measured by the CV) and the magnitude of vertical flux of solids. Comparison of the total volatile solids, TOC, and TN concentrations of trapped particles indicate that the composition of the material in both types of traps (at a given depth) is quite similar. The variability among traps at a given depth, and among traps of the same design, is generally below 10% (CV). The only exception was for particles collected in the 0.5 m traps of the Hendricks design, where the elemental analyses (TOC, TN) for one of the traps yielded very different results from the other and from the values measured in the Eganhouse traps.

III.A.2.b. General properties (Solids fluxes, TOC, TN). Table 3.11 gives the mass flux of solids (in units of dry g cm^{-2} yr^{-1}) in the near-bottom traps at each of the three outfall sites. Concentrations of TOC and TN in the trapped particles are also provided. These data are illustrated in Figure 3.3. The ordinate scales for plots corresponding to each site were adjusted to improve readability.

In general, the highest mass fluxes at all elevations for a given period were observed at the White Point site. Fluxes for the 0.5, 2.0 and 5.0 m traps at White Point ranged from 3.9-8.6, 1.9-2.4, and 0.9-1.4 g cm^{-2} yr^{-1}, respectively. At the Point Loma site, mass fluxes were somewhat lower: 2.0-6.3 g cm^{-2} yr^{-1} (0.5 m), 0.8-2.4 g cm^{-2} yr^{-1} (2.0 m), and 0.2-0.9 g cm^{-2} yr^{-1} (5.0 m). Fluxes at the Orange County site were approximately one-half those observed at Point Loma and one-third those at White Point: 0.8-3.0 g cm^{-2} yr^{-1} (0.5 m), 0.4-1.9 g cm^{-2} yr^{-1} (2.0 m), 0.1-1.0 g cm^{-2} yr^{-1} (5.0 m). The results at the White Point and Orange County sites are similar to those reported by Hendricks (SCCWRP 1987 and Figure 2.23) for the same areas based on long-term deployments of the Hendricks traps. The fluxes observed at Point Loma represent the first near-bottom sediment trap data to be collected at this site.

Variations in fluxes over time at a given elevation are not well correlated between the sites. However, for Orange County and Point Loma sites, variations in the fluxes at each elevation for a given site appear to be coherent. The time series is not long enough to discern whether or not a seasonal pattern exists. However, the fluxes do vary by factors of two to three over the period investigated. This is consistent with the findings of Hendricks for traps deployed off White Point and Orange County in 1986-87 (SCCWRP 1987).

The particles collected off White Point also appear to have higher organic carbon and nitrogen contents than at either of the other sites. The organic carbon content of the particles tends to increase with elevation of the traps above the sea floor. At the same time the C/N ratio remains relatively constant for particles collected at all elevations (9.7-11.0). There is no obvious trend in the organic content or quality (as judged by C/N) over time. By contrast, the particles collected off Orange County and Point Loma generally exhibit lower and more variable organic matter contents with a noticeable enrichment in organic carbon (relative to nitrogen) at most times during the year. Trends in the organic carbon and nitrogen content of the particles with respect to trapping elevation are not as evident as in the case of the White Point site.

III.A.2.c. Stable isotopes. Table 3.12 lists results of the analyses of sediment trap particles for stable isotopic composition. In general, the organic carbon in the White Point and Orange County sediment trap particles is more depleted in ^{13}C than for particles collected off Point Loma. All ratios fall within the range for marine

plankton and marine particulate organic matter (Williams *et al.* 1992). The composition of particles collected during different seasons does not appear noticeably different, and except for the White Point samples collected in November 1989, the differences between particles trapped at different elevations are small and show no consistent trends.

A different pattern emerges for the stable nitrogen isotopes. The isotope ratios of particles collected off Point Loma are close to but somewhat lighter (i.e. more depleted in ^{15}N) than marine sedimentary nitrogen (Eganhouse and Kaplan 1988; Williams *et al.* 1992; cf. references in Eganhouse and Venkatesan 1992). By contrast, particles collected near Orange County and White Point are much more depleted in ^{15}N indicating a significant input of terrestrial (i.e. wastewater effluent and/or terrigenous debris) nitrogen. For these latter locations, the ratios are significantly lighter during the summer than during the winter. Again, however, there are no trends in stable nitrogen isotopic composition with elevation above the bottom.

III.A.2.d. Trace metals. Table 3.13 provides results of the analysis of sediment trap particles for the trace metals, Cd and Pb. Table 3.14 gives data for the ICP-MS multielement analyses on selected samples, and Figure 3.4 summarizes the multielement results for particles collected in the 0.5 m traps.

At the White Point site, concentrations of Pb and Cd are similar to those found in the JWPCP effluent particles (cf. Tables 3.13 and 3.4). There is no strong discernable temporal variation in the concentrations of these metals in the trapped particles at a given elevation. Results obtained for traps at different elevations for a given site show that the concentrations are likewise comparable. However, in five out of six cases, there is a continuous decrease in Pb content with elevation above the sea floor.

The concentrations of Pb and Cd in particles trapped off Orange County and Point Loma are lower and more variable than those collected from the Palos Verdes shelf. The Pb concentrations are similar for the two former sites, but Orange County particles are apparently somewhat more enriched in Cd than those collected from Point Loma. The concentrations of both metals are significantly lower (ca. 2-4 times) in the particles from Orange County and Point Loma than the effluent particles discharged to those sites (cf. Tables 3.13 and 3.4). There are no obvious trends in Pb and Cd content with time or trap elevation.

Examination of data in Figure 3.4 and Table 3.14 indicates that the relative (and absolute) abundances of the 13 elements determined by ICP-MS for a given effluent are essentially the same at different times and for different trap elevations. Comparison of the bar diagrams for the multielement scans of the trapped particles (Figure 3.4) and those for the respective effluents (Figure 3.1) reveal some similarities. In particular, the JWPCP effluent particles and the White Point trapped particles show comparable patterns. However, the abundances of most metals are lower in the trapped particles than the corresponding effluent particles. The same is true for the other two sites. One of the two elements targeted for use in the verification phase of this project, Cd, as well as Ag, are at very low concentrations in the trap particles compared with the effluent.

III.A.2.e. Trace organics. Table 3.15 lists data for the linear alkylbenzenes in sediment trap particles. These data are summarized as total LAB concentrations normalized both to dry mass and organic carbon in Table 3.16 along with data for the total extractable organics. Distributions of the phenyldodecane isomers are also provided in Figures 3.5-3.7. We anticipated low concentrations of the LABs in the sediment trap particles. As a result we underestimated the amount of LAB recovery surrogates to be added. This prevented us from correcting the concentrations given in Tables 3.15 and 3.16 for recovery. Consequently, we cannot assure that high recoveries were obtained. Consequently, the data listed in Tables 3.15 and 3.16 represent minimum concentrations.

The data presented here are sparse and only a few generalizations can be drawn. The concentration of TEO in sediment trap particles ranges from 2-35 mg g^{-1}. In general, the TEO concentrations correlate with the total LAB concentrations at different elevations at a given site. TEO concentrations are much lower than those found in the effluent particles (i.e. 136-304 mg g^{-1}). At all sites and all elevations the chain length distributions of the LABs are dominated by the phenyldodecanes. This distribution is typically observed for waste-contaminated sediments and effluents (Eganhouse *et al.* 1983a; Eganhouse 1976; Eganhouse and Sherblom

1991) because the LAB distribution of the source material (effluent particles) is generally dominated by the phenyldodecanes (cf. Table 3.6). In reference to the total LAB concentrations (Table 3.16), particles trapped off White Point are much more contaminated than those off Orange County and Point Loma. This is probably due to the fact that the JWPCP receives influent from a LAB manufacturing facility and, hence, has in the past had unusually high concentrations of LABs in its effluent (Eganhouse *et al.* 1983a; Eganhouse and Sherblom 1991). Although the dataset is incomplete, it would appear that the White Point traps collected particles that were more enriched in LABs with increasing elevation above the bottom. This trend is not seen at the other sites. It is also obvious that the particles collected off White Point have total LAB concentrations that are similar to, albeit slightly lower than, those found in the present-day effluent (cf. Tables 3.16 and 3.7). By contrast, the OCSD and PLTP effluent particles have total LAB concentrations (dry mass basis) that exceed those of the sediment trap particles collected at the respective sites by factors of approximately one to more than two orders of magnitude. Normalization of effluent particle LAB concentrations to organic carbon reduces the discrepancy, but the differences between plants are maintained.

Inspection of Figures 3.5, 3.6, and 3.7 reveals another difference between the sediment trap LAB distributions. Particles collected off White Point exhibit phenyldodecane isomer plots that approach the "flat" distributions found in the effluent particles (cf. Figure 3.2). During the November 1989 deployment, particles collected in the 5.0 meter trap showed the greatest relative abundance of external isomers (2-, 3- and 4-phenyldodecanes) with the 2.0 m and 0.5 m traps showing lesser amounts. The significance of this result is that the external isomers are degraded more rapidly than the internal isomers (6- and 5-phenyldodecanes) under aerobic conditions (Takada and Ishiwatari 1989, 1991; Bayona *et al.* 1986). All things being equal, this would suggest that the particles collected in the upper trap were less degraded. Moreover, when these patterns are compared with those typically observed in sediments near the JWPCP waste outfalls (Eganhouse *et al.* 1983a) and the effluents responsible for the sediment contamination (Figure 3.2), it is apparent that the sediment traps are collecting relatively unaltered (i.e. fresh) LABs. Thus, the inverse relation between degree of alteration of the phenyldodecane isomer pattern and total LAB concentration may indicate a strong influence of present day effluent emissions on the near bottom (readily resuspended) particles. The distributions noted for the June 1990 deployment off White Point also show relatively unaltered LAB isomer patterns. However, the distributions look similar at all elevations.

By contrast, the isomer patterns exhibited by particles trapped off Orange County and Point Loma are significantly more altered than their effluent particle counterparts (cf. Figures 3.6 and 3.2). In the case of Orange County, the apparent degree of degradation with respect to elevation is inverse to that observed off White Point, with the lowest relative abundances of the external isomers seen at the 5.0 m trap. The differences between the LAB distributions found in the trapped particles and the respective effluents suggest variations in the effluent sedimentation processes and sediment dynamics at each site.

Table 3.17 gives results of the sterol analyses. It must be recognized that these data have not been recovery-corrected because (as mentioned earlier) insufficient recovery surrogate standard was introduced to the sediment trap samples. Consequently, the concentrations listed in Table 3.17 must be interpreted with caution. In general, however, particles collected near the bottom off White Point have higher concentrations of the fecal sterols than do particles trapped at either of the other two sites. This appears to be true even after normalization to organic carbon content. There is no consistent relationship between trap elevation and sterol concentration. The concentrations of coprostanol on a dry mass basis at all sites are much lower than those found on the effluent particles (1000-3000 $\mu g\ g^{-1}$; Table 3.8). However, normalization of the coprostanol concentrations to organic carbon, in this case, significantly reduces the magnitude of the difference. This indicates dilution of effluent particles by lithogenic material during and after sedimentation.

The coprostanol/epicoprostanol ratio is not sensitive to the quantitation problems associated with recovery correction. Ratios obtained for the sediment trap particles are quite variable (6-170). However, the ratios are generally lower than those reported for the respective effluents (26 to >580; Table 3.8). Given that effluent fecal sterol ratios were lower in the past (see discussion above), it is possible that the lower ratios found in these sediment trap particles may indicate the presence of (waste-derived) sterols deposited at an earlier time. This assumes that the ratio is conservative, an hypothesis that is as yet untested, and that no other additions of fecal

sterols exhibiting a different ratio are important. Unfortunately, the present data are too few to differentiate among these possibilities.

III.A.2.f. Summary of Fluxes. Table 3.18 summarizes the mass fluxes of solids, organic carbon, nitrogen, Pb, Cd and the marker compounds to the near bottom traps off White Point, Orange County and Point Loma. Several trends are obvious. First, in almost every case the fluxes of all constituents decrease with increasing trap elevation off the bottom (exception: fecal sterols). Second, the fluxes of all constituents are significantly greater at the White Point site than they are at the other two sites. Both of these trends largely reflect the patterns in solids fluxes.

The mass fluxes of solids reported here can be compared with data developed by Williams *et al.* (1992) for paired Soutar traps deployed 45 m above the shelf bottom (water depth 395 m) in Santa Monica Bay. They found fluxes in the range of 0.087 to 0.102 g cm^{-2} yr^{-1}. [Fluxes of solids measured in the water column (100-850 m) within the central part of Santa Monica Basin were substantially lower (0.009-0.030 g cm^{-2} yr^{-1}).] The fluxes measured in the uppermost traps, particularly those deployed off Orange County, approach the highest fluxes reported by Williams *et al.* (1992) for the shelf area of Santa Monica Bay. Similarly, the fluxes of organic carbon and nitrogen to the near-bottom traps of this study generally exceed those found by Williams *et al.* (1992) for the traps positioned 45 m above the shelf in Santa Monica Bay (TOC: 2.9-5.8 mg cm^{-2} yr^{-1}; TN: 0.63-2.3 mg cm^{-2} yr^{-1}). No comparable data are available for fluxes of trace metals to near-bottom traps on the shelf off southern California. However, Bruland *et al.* (1974) and Bruland Franks (1979) reported results for trapping experiments done in several inner basins off southern California (Santa Barbara, San Pedro and Santa Monica basins). They found fluxes of Pb and Cd ranging from 0.4 to 2.7 μg cm^{-2} yr^{-1} and 0.04 to 0.13 g cm^{-2} yr^{-1}, respectively. Again, our results show significantly higher fluxes near the bottom in these shallow shelf areas.

No comparable data presently exist for the flux of linear alkylbenzenes in the southern California bight. The flux of coprostanol to the near bottom traps is highly variable with respect to trap elevation, time of year and site. No consistent trends are obvious save the greatly increased fluxes found off White Point (ca. 30-400 μg cm^{-2} yr^{-1}). This difference between sites is attributable to both the higher fluxes of solids off White Point and the substantially greater concentrations of fecal sterols on the particles at this site (Table 3.17). Because the concentrations of fecal sterols on present-day effluent particles from all three plants are similar (Table 3.8), the differences in coprostanol fluxes between sites must be due to processes affecting the effluent particles prior to and/or following sedimentation. The only other data presently available within the southern California Bight come from Venkatesan and Kaplan (1992). They measured a fecal sterol (coprostanol + epicoprostanol) flux of 0.4 μg cm^{-2} yr^{-1} to sediment traps positioned in the deep waters of Santa Monica Basin (850 m). Maximum fluxes on the Palos Verdes Shelf would appear to be three orders of magnitude higher, whereas those obtained off Orange County and Point Loma are within a factor of ten of the Santa Monica Basin trap fluxes.

III.A.3. Sediments

III.A.3.a. Water content, TOC, TN. Table 3.19 lists general properties of the surface sediments and sediment cores collected in this study. The concentrations of TOC and TN in surface sediments from Orange County offer little evidence of impact by the outfall, save for station OC-0 (for location see Figure 2.4). The concentrations of TOC and TN are apparently at or near background levels at all other stations. The unusually high C/N ratio at station OC-37 may signal a contribution from terrigenous debris. The structural polymers of land plants characteristically have low nitrogen contents (Stuermer *et al.* 1978), and this station is nearest the mouth of the Newport Canyon where such debris might collect.

The same (lack of) features are seen off Point Loma where the concentrations of TOC and TN range from 0.46 to 0.70% and 0.057 to 0.100%, respectively. There is no obvious pattern of sediment contamination as a result of the waste discharge from the PLTP outfall system. Examination of the sediment cores, however, reveals the existence of subsurface maxima in TOC and TN concentrations at both coring sites (Figure 3.8). At SD A-16, the station immediately adjacent to the northwest leg of the Y-outfall, the subsurface maxima occur at depths of 10-12 cm and 18-20 cm. The TOC maxima at both sites would appear to be no greater than 1.4 times the lowest concentration which was encountered in the deepest sub-bottom section (ca. 0.7%). The C/N ratios in the core

sediments (11.3 to 16.1) are significantly greater than those found for the effluent particles (8.1±1.5%; Table 3.2), and there is a general trend toward higher ratios at greater sub-bottom depths. This may reflect diagenetic alteration whereby nitrogen-bearing organic substances are preferentially remineralized. There also seems to be a discrepancy between the C/N ratios of the uppermost (0-2 cm) sections of the cores and those obtained for sediments collected by Van Veen grab at stations SD A-16 and SD A-5, with the core yielding higher ratios. The reason for this difference is not immediately obvious although the collection of surface sediments and cores occurred at different times. Another feature of the data is that in all cases, the surface sediments off Orange County and Point Loma have lower TOC and TN contents than the particles collected in sediment traps deployed at these sites (cf. Tables 3.19 and 3.11). A similar relationship was reported for Orange County based on trap/surface sediment collections performed in 1986-87 (SCCWRP 1987). However, this is opposite of the relationship reported for TVS (total volatile solids) by Hendricks (1987) for surface sediments and trapped particles collected off White Point. The intersite difference may reflect variations in the dominant sources of particles to near-bottom traps in the respective areas. The C/N ratios of the surface sediments off Orange County and Point Loma overlap those of particles collected in the near-bottom traps at these two sites.

III.A.3.b. Stable isotopes. Table 3.20 lists the results of the stable isotope analyses of the surface sediments. Shown in this table are data for sediment grabs taken at stations OC-0 and OC-ZB2 off Orange County, the upper sections (0-2 cm) of the cores taken at stations SD A-5 and SD A-16 off Point Loma and five replicate grabs collected off White Point at the sediment trap station (cf. Figure 2.6). The White Point samples were not part of this contract but were collected to enhance the value of the existing dataset.

The stable carbon isotope ratios of the surface sediments from White Point are all near -21.7 °/₀₀. This is slightly heavier (i.e. enriched in ^{13}C) when compared with the sediment trap samples (ca. -22.5 °/₀₀; cf. Table 3.12) and significantly heavier than the effluent particles (-23.3 °/₀₀; cf. Table 3.3). By contrast, the nitrogen isotope ratios of the sediments range from +3.0 to +3.6 °/₀₀. These are similar to or lighter (i.e. more depleted in ^{15}N) than the ratios found for the sediment trap particles (+4.3 to +5.1 °/₀₀) and slightly heavier than those obtained for the effluent particles (+1.68 °/₀₀, +2.37 °/₀₀).

Sediments collected off Orange County are isotopically lighter (both elements) than the particles collected in near-bottom sediment traps. The OCSD effluent particles have heavier carbon isotope ratios and lighter nitrogen isotope ratios than the sediments collected off Orange County.

Sediments from the Point Loma site have stable carbon isotope ratios that are essentially indistinguishable from either the effluent or the sediment trap particles. However, the nitrogen isotope ratios of the sediments are lighter and heavier, respectively, than the sediment trap particles and PLTP effluent particles.

III.A.3.c. Trace metals. Tables 3.21 and 3.22 list results of the analyses of surface sediments and core sediments for Pb and Cd and other elements determined by ICP-MS. Figure 3.9 depicts the vertical distribution of Pb and Cd in the SD A-5 and SD A-16 cores, whereas Figure 3.10 illustrates the distribution of 13 trace elements in core tops from these same stations as well as surface sediments collected at OC-control (cf. Table 2.3 and Figures 2.4 and 2.5 for locations). Off Orange County there is no evidence of a gradient in Pb and Cd concentrations relative to the location of the outfall in either longshore or cross-shelf directions. The same is true for the Point Loma outfall with the possible exception of an apparent enrichment of Pb at station SD X-2, immediately off the northwest leg of the wye outfall. No enrichment is observed for Cd at this location, however, suggesting the enrichment of Pb may be anomalous.

As Figure 3.9 illustrates, Pb and Cd appear to reach highest concentrations in sediments deposited approximately 7-15 cm below the sediment-water interface at both stations. Concentrations decline to their lowest levels at the core bottoms (24-28 cm). The subsurface maxima may reflect effects of the wastewater effluent discharges in earlier times when treatment and source control measures were not as well developed as they are today. Figure 3.11 depicts a plot of Pb and Cd against TOC for the two sediment cores. In the case of Pb, the equations for the least squares lines are very close for the two cores, and the correlation coefficients are high. The correlations for Cd *vs.* TOC are not as strong and the slopes and intercepts for the two cores are less similar. The slopes of the Pb *vs.* TOC linear regressions are higher than Pb/TOC ratios observed for the

sediment trap particles (7-13) and much higher than those exhibited by the effluent particles (<0.5 to 3.9). The same holds true for cadmium. These differences most likely reflect the preferential mobilization of effluent-derived organic matter (i.e. degradation) relative to lead (Kettenring 1981) and cadmium (Sweeney *et al.* 1980).

III.A.3.d. Trace organics. Table 3.23 lists the results of analyses of surface sediments from stations SD A-5 and SD A-16 for linear alkylbenzenes, whereas Table 3.24 summarizes the trace organics data for total extractable organics, LABs and the fecal sterols. The concentration of TEO in the core tops from Point Loma are approximately 0.5 to 0.6 mg g^{-1}. These concentrations are more than 3 to 10 times lower than those observed in the sediment trap particles (cf. Table 3.16) and 290 to 580 times lower than the concentrations found in effluent particles (cf. Table 3.7). Similarly, the total LAB concentration in the sediments are 0.07 $\mu g\ g^{-1}$ as compared with 0.5-1.3 $\mu g\ g^{-1}$ and 150 $\mu g\ g^{-1}$ for sediment trap particles and effluent particles, respectively. Normalization of the LAB concentrations to organic carbon content does not measurably reduce these differences.

As in the case of the PLTP effluent particles and particles collected in sediment traps deployed off Point Loma, the surface sediments from stations SD A-16 and SD A-5 exhibit LAB chain length distributions dominated by the phenyldodecanes (cf. Tables 3.6, 3.15 and 3.23). Figure 3.12 illustrates the isomer distribution of the phenyldodecanes in the surface sediments (core tops). This can be compared with similar plots for the sediment trap particles (Figure 3.7) and the PLTP effluent particles (Figure 3.2). The distributions in the sediment samples exhibit a greater degree of depletion of the external isomers (2- and 3-phenyldodecanes) than the sediment trap and the effluent particles. This again signals a greater degree of organic degradation and less influence from recently discharged effluent than particles collected in the traps.

Coprostanol concentrations in the top sections of cores A-16 and A-5 are 0.6 and 0.3 $\mu g\ g^{-1}$, respectively. Again, these data are not recovery-corrected and must, therefore, be considered as minimum concentrations. The sediments exhibit coprostanol concentrations similar to those in particles collected with sediment traps at the 0.5 m elevation off Point Loma (ca. 0.4-0.5 $\mu g\ g^{-1}$; Table 3.17). By contrast, the present-day PLTP effluent concentrations we obtained were in the range 1000-3000 $\mu g\ g^{-1}$. Normalization of the coprostanol concentrations to organic carbon tends to reduce the difference between the effluent particles and sediments. However, it is clear that the sediment trap particles more closely resemble the sediments than the effluent. Epicoprostanol concentrations are about 10% that of coprostanol. Thus, the fecal sterol ratio (coprostanol/epicoprostanol) is about 9. Again, this is closer to ratios exhibited by the sediment trap particles (Table 3.17) than by the effluent particles (Table 3.8).

III.A.4. Effluent Degradation Studies

In the course of this project we conducted more than 20 experiments, the long-range goal of which was the development of an exposure system for measuring the decomposition kinetics of effluent particles. Unfortunately, we were unsuccessful at establishing a satisfactory system, and, for this reason, the details of each and every experiment will not be described here. Nevertheless, we did obtain results that prompted the development of new hypotheses concerning the behavior and fate of effluent particles. Moreover, some of the data arising from this work bears directly on the interpretations to be presented later in the DISCUSSION section. For these reasons, we feel it is worthwhile to provide a chronology of the experiments and describe some of the more important results.

III.A.4.a. Preliminary experiments. Our initial efforts were directed toward the development of a field-deployable incubation chamber patterned after the system used by Myers (1974) to study the decomposition of JWPCP effluent particles in the early 1970's. Because of dramatic reductions in the suspended solids concentrations of all southern California effluents over the last two decades (SCCWRP 1991b), we could not use effluent particles for these experiments. We, therefore, chose to use a surrogate that offered unlimited access to waste particles closely similar to those found in final effluent: undigested primary sludge.

In December of 1989 we launched a preliminary field experiment in which four moorings were deployed at a site off Orange County. Each mooring had 21 individual incubation vessels held within nylon mesh bags. The vessels consisted of glass centrifuge bottles capped with Whatman GF/C filters using a lid similar to that employed on the sediment trap bottle (cf. Figure 2.5). The 21 incubation vessels corresponded to seven

replicate samples of three sludges (JWPCP, OCSD, PLTP). Within a few days after deployment, several of the incubation vessels were recovered and centrifuged, and the supernatants were tested for dissolved oxygen content. Dissolved oxygen was not detected in any of the vessels. We, therefore, immediately abandoned the experiment and retrieved all of the moorings.

The depletion of oxygen in the incubation vessels during this preliminary field exercise identified oxygen supply as a critical requirement for any successful kinetics experiment. We therefore, began to conduct a series of experiments, the ultimate goal of which was the development of a field-deployable system that would remain oxygenated and, hopefully, mimic the behavior of effluent particles undergoing decomposition during sedimentation. Before embarking on these experiments, we examined a number of problems related to handling of primary sludge. Without elaborating details of these studies, suffice it to say that we established protocols for sieving, diluting and accurately dispensing known quantities of sludge into incubation vessels. These procedures were developed prior to initiating any of the experiments described below.

The first experiment was designed to assess the effect of sludge solids loading on oxygen demand using the same centrifuge bottles and glass fiber filters (Whatman GF/C) employed in the original field trial. We wanted to determine if there was a sludge loading level below which oxygen depletion did not occur. After homogenization and dilution of the sludge sample, aliquots corresponding to dry particle masses of 0-245 mg were dispensed into vessels which were immediately capped and placed into an aerated aquarium maintained at 12°C. Two bottles were charged with degassed filtered seawater for the purpose of estimating the diffusive flux of oxygen into the bottles (from the aquarium) in the absence of any biological oxygen demand. The results of this experiment are shown in Table 3.25.

After only one day (corresponding to sample T_0) all vessels containing sludge particles exhibited significant depletion of oxygen. During the same period, the degassed water sample attained a concentration of 2 mg O_2 l^{-1} (tank water = 8.4 mg l^{-1}). These results suggested to us that the rates of oxygen depletion within the dosed bottles exceeded the rate at which oxygen could diffuse into the containers, partly as a result of the small pore size of the filter covering the bottle mouth. We, therefore, decided to run a second experiment in which three types of barriers were used: 1) the GF/C filter, 2) Nitex screen with 20 μm pore size, 3) Nitex screen with 110 μm pore size. Centrifuge bottles were loaded with nominal masses of sludge solids ranging from 50 to 250 mg. (Subsequent analyses showed the actual solids loadings to be 20 to 100 mg.) The bottles were incubated for up to 13 d with samples taken at intervals of 1 d (T_0), 3 d (T_2), 8 d (T_7) and 14 d (T_{13}) following preparation of the bottles.

The results (Table 3.26) indicated that all of the barriers were ineffective in preventing depletion of oxygen with longer incubations (i.e. $\geq$3 d). The only observable difference between the samples covered with the different materials occurred after one day, particularly at the higher loadings. We concluded that oxygen simply could not diffuse into the vessels fast enough to compete with the activities of heterotrophic microorganisms. Therefore, we decided to increase the interfacial surface area to volume ratio of the container to increase the rate of oxygen supply. For this purpose we used a "culture dish" which had a interfacial surface area/volume ratio of 0.12 cm^{-1} (as compared to that of the centrifuge bottle which was 0.021 cm^{-1}). In this experiment we loaded the culture dishes with 50 to 500 mg of sludge solids, covered them with either the 20 μm or 110 μm Nitex screens and incubated them for periods of 1, 3 and 6 d (T_0, T_2 and T_5, respectively). The results are given in Table 3.27.

The data suggest that increasing the interfacial surface area/volume ratio tended to increase the rate of supply of oxygen to the incubation vessels (cf. Tables 3.25 and 3.26) such that after 6 d there were reasonably high amounts of oxygen in the vessels loaded with 250 mg of solids (even for the 20 μm Nitex screen-covered vessels). However, only those vessels covered with the 110 μm Nitex screen were able to maintain the original oxygen concentration throughout the experiment at all sludge loading levels. Although the vessels covered with the 110 μm screen and loaded with 500 mg of sludge solids were not run for the full 6 d, the 1 d incubation showed no evidence of oxygen depletion.

On the basis of these results we conducted a fourth experiment to examine the question of particle loss from the experimental vessels through the 110 μm Nitex screen. In this experiment we used glass jars whose bakelite lids had holes cut into them in lieu of the culture dish vessels. Although the capacity of the jars was smaller (ca. 200 ml) than the culture dishes (ca. 420 ml), the interfacial surface area/volume ratios of the two vessels were the same. Jars were charged with 250 mg sludge solids, sealed with 110 μm Nitex screens, poisoned with $HgCl_2$ (to inhibit biological activity) and placed in a thermostated aquarium (12°C). The jars were positioned in a rack that rocked gently to simulate the motion that might be expected to occur during incubation at sea. Samples (jars) were sacrificed at 4, 6, and 8 d intervals. The contents (water + particles) were placed into a centrifuge bottle and centrifuged at 500 g for 20 min. Total solids was determined by filtering the supernatant on a GF/C filter and reweighing and transferring the settled solids onto a filter and reweighing. The results of this experiment are given in Table 3.28.

With the exception of one sample (jar #7) at the 4 d interval, all of the jars showed a loss of about 12-18 mg solids during the experiment. Assuming no biodegradation had occurred, this loss must have been due to diffusion of small particles through the screen and/or adhesion of particles to the screen. Whatever the cause, the losses were complete within the 4 d period as no differences were observed in subsequent samplings. At this point, the data were viewed with caution because we had not ascertained whether the quality of the "lost" particles was identical to that of the particles remaining in the jars. Moreover, it was felt that the losses, although reasonably reproducible, were small enough that they might have been due to handling or other analytical problems. Turbidity had been observed in the aquaria in which the jars were placed. However, it was unclear whether this reflected the presence of "escaped" particles or a buildup of microorganisms in the tank in response to diffusion of soluble nutrients and dissolved organic matter across the screens.

We, therefore, decided to run another experiment in which Nitex-covered jars containing 250 mg of sludge solids were placed inside of a beaker (containing seawater) for 4 d. The beaker water was poisoned with a small amount of $HgCl_2$, and after 4 d, the water from the beaker was filtered. The Nitex screen was removed and rinsed with seawater, and the rinses were filtered. Finally, the contents of the jar were centrifuged and treated as in the preceding experiment (i.e. supernatant filtered and solids placed on a filter). In addition to estimating the amount of solids on the screen, in the beaker and in the supernatant and settled solids within the jar, elemental analysis was performed on each of the particulate fractions. The results, shown in Table 3.29, indicate that an excellent mass balance was achieved (within ca. 2% of added solids) and that only ca. 1.5-2% of the solids adhered to the screen. Approximately 13.6% of the solids escaped through the screen. This was in good agreement with the previous experiment (cf. Table 3.28) where ca. 85% of the solids had remained in the jar. These data gave us confidence that the amount of solids being lost from the jars was limited and reproducible.

Examination of the results for the elemental analysis (Table 3.30), however, revealed other trends. Approximately 92% of the particulate organic carbon (POC) and 90% of the particulate nitrogen (PN) were retained within the jar. Again, only minor amounts of POC and PN were retained by the screen (<0.2%). There appeared to be some fractionation during the diffusion of small particles from the incubation vessels. The small particles escaping the jars had lower organic carbon and nitrogen contents that those remaining inside. This was contrary to expectations since it is usually observed that organic matter content is inversely related to particle size. At the same time the C/N ratio of the former particles were lower (i.e. enriched in nitrogen) than the retained sludge solids. It is interesting to note that the particles remaining in suspension after centrifugation also had lower C/N ratios than those that settled.

It is appropriate at this point to introduce some measurements made earlier on JWPCP (Los Angeles County) final effluent particles and primary sludge solids from the same plant. These analyses were intended to determine whether primary sewage sludge could be considered a viable surrogate of effluent particles. Table 3.31 lists these results. The replicate samples for which data are presented in these tables were taken from a single grab sample (in the case of the sludge) and a single 24-hr composite (in the case of the effluent). It is seen that (at least on this occasion) the sludge had a higher organic carbon and nitrogen content than the settled sludge particles in the incubation vessels (cf. Tables 3.31 and 3.30). The same is true of JWPCP final effluent. The C/N ratio of the settled solids in the incubation vessel was intermediate between those obtained

for the sludge and effluent samples. It is difficult to interpret these data with so few samples. However, it would appear that the sludge particles retained by the Nitex screen are of approximately the same quality (judging from C/N ratio) as the particles in the final effluent. Whether these particles are less organically enriched than "representative" effluent particles is unclear.

As a final effort to test whether sample handling could account for the apparent losses of particles from the incubation vessels, we examined the recovery of solids by centrifugation. In this experiment jars were charged with 250 mg of sludge solids. The samples were then transferred directly to a centrifuge bottle and centrifuged for either 30 min and 60 min at ca. 500 g. The supernatant was filtered, and the settled solids were weighed by placing them on a filter. The results of this experiment, shown in Table 3.32, indicate that the 30 min centrifugation was effective in removing (through sedimentation) all but ca. 0.5-3.5% of the solids. Centrifugation for an additional 30 min had marginal effects (i.e. only 1% more of the solids was removed). Again, the mass balance was excellent, indicating that we could successfully recover all of the particles charged to or remaining in the incubation vessels despite some minor handling.

The elemental analyses performed in this experiment revealed that the vast majority of the particulate organic carbon and nitrogen was removed by centrifugation after 30 min (OC:>98%, N:>96.5%). As demonstrated earlier (Table 3.31), the fine suspended particles appeared to contain less organic carbon and nitrogen than their settled counterparts. At the same time, they were enriched in nitrogen such that their C/N ratios (ca. 5.2-5.7) were significantly lower than the settled solids (ca. 8.1-9.2).

III.A.4.b. Attempted field tests. Having established a working prototype of the sludge decomposition vessel we carried out two further experiments to examine the effects of 1) particle invasion , 2) chamber geometry, and 3) solids loading. In the case of the first effect, we were concerned about the large pore size of the barrier being used (110 μm Nitex) and its ability to prevent particles from invading the incubation vessel from the surrounding seawater.

In the first experiment, four empty 8 oz jars equipped with 110 μm Nitex screens were placed into two exposure chambers having different sized openings (above the jar tops). Thus, four jars per chamber were deployed as shown in Figure 3.13. The opening of the "tall" chamber was the height of a jar (ca. 80 mm), and the opening of the "short" chamber was one half the height of a jar. The empty jars were placed in the top and middle positions of the chamber while the bottom slot of each chamber was occupied by a jar that contained 50 mg of previously screened (250 μm) and kilned beach sand. This jar was also equipped with a 110 μm screen lid. The exposure chambers were deployed at the Los Angeles County pier (San Pedro, CA) at a distance of approximately 3 m off the bottom (water depth approx. 7 m). The chambers were allowed to remain on station for 5 d.

Upon retrieval, the contents of the empty jars were filtered through a 47 mm GF/C filter to isolate the "invaded" solids. The supernatant in the sand-spiked jars were also filtered, and the sand was sampled to estimate the amount of "invaded" solids captured by the sand. Total organic carbon and total nitrogen contents were measured on the sand exposed in the jars as well as the original sand. Although the amount of intruded particles appears high, the chambers were purposely exposed to an environment expected to have high standing stocks of fine suspended matter. The data for the empty jars (no sand) showed no apparent discrimination between the short and tall openings with regard to particle invasion (Table 3.33). Likewise, there did not appear to be a position-in-chamber effect on solids invasion. The C/N ratio of the particles captured in the sand-spiked containers was close to the Redfield ratio (16) and caused a measurable increase in organic content of the sand. These results indicated that particle invasion could occur, but that chamber geometry would have little, if any, effect on the flux of solids *into* the incubation vessels.

In the second experiment, we were primarily interested in examining the potential effects of exposure chamber design and sludge loading on decomposition kinetics at an open coastal site. If either of these experimental conditions were found to influence the rate at which sludge particles decomposed, a meaningful simulation of the behavior of ocean-discharged effluent particles would be impossible. A primary undigested sludge sample from the JWPCP was collected, screened (1 mm) and diluted. Twenty 8 oz jars were charged with sludge, ten

with the equivalent of 100 mg (nominal) and the other ten with 250 mg (nominal) of dry sludge solids. Each of the jars was filled to capacity with filtered (GF/C) seawater and capped with 100 μm Nitex screen. A total of four exposure chambers was used, two with "tall" openings and two with "short" openings. Each of the chambers, thus, held four jars. Two jars at each of the two loading levels (100 mg and 250 mg) were randomly placed into the exposure chambers (total of 16 jars). The chambers were immediately transferred to a refrigerator (approx. 5°C) where they remained until deployment at sea the following morning. Chambers of each design were also filled with jars that contained only seawater. The purpose here was to measure *in situ* particle invasion for purpose of correcting the solids mass balance for physical exchange. The remaining four jars (two at each loading level) were placed into the refrigerator at the same time as the chambers and were allowed to remain there overnight. These jars represented the T_0 time period.

Following collection, each sample was treated as follows: The dissolved oxygen content of the overlying water in the jar was determined by Winkler titration. The remaining overlying water was filtered through a 25 mm GF/C filter, and the plug of solids on the bottom of the jar was transferred to a 47 mm GF/C filter (both filters pre-weighed). The solids recovered on the filters were determined as well as TOC, TN and TVS. Calculations were made to determine whether the amount of solids lost during incubation could be explained by the loss of organic material *via* degradation.

As shown in Table 3.34 the dissolved oxygen content of the water inside the jars remained high (5.0-8.8 mg l^{-1}) regardless of chamber type or loading level. The mass of solids that intruded into the empty jars ranged from 8 to 12.6 mg. (9 mg was used in subsequent mass balance calculations where corrections for "background intrusion" was required.) The recovery of the solids showed two trends. The replication within chamber type and loading level was generally good, and recovery was generally higher for the lower loading level. However, the recovery for both chamber types declined after 4 d and remained somewhat constant throughout the eight day period.

Total volatile solids was measured on these samples in order to estimate the percentage of particulate organic matter represented by the TOC. By multiplying the mass of recovered carbon by the TVS/TOC ratio we were able to estimate the rate at which organic matter was lost (Table 3.35). TVS was somewhat higher in particles at the lower loading level and showed fairly good replication with chamber type and loading level. By contrast, the TOC content of the recovered solids was usually lower in the lower loading level. Replication within chambers and loadings was variable. The TOC and TN contents of the T_4 and T_8 samples were also generally lower than those of the T_0 samples. Carbon to nitrogen ratios were quite variable throughout the experiment, and it was difficult to identify any patterns. However, particles contained in the jars with higher loadings showed greater increases in their C/N ratios from T_0 to T_4 than those in the lower loading level jars. This seems the inverse of trends in the change of TVS over time. The jars in the "short" chambers tended to yield higher amounts of solids at both loading levels.

After calculating the mass of solids that was lost during the experiment, we attempted to estimate how much of this mass could be accounted for by loss of organic matter. Adjustments were made for the physical losses and gains across the screen. Using the TOC and TVS data, we calculated the mass of organic matter lost during exposure and compared these estimates with the data for recovered solids (Table 3.36). The results of these calculations were quite variable. In some cases we were able to account for almost all of the mass of solids that was lost (by loss of organic matter), but in other cases the calculations did not agree well with the experimental results (Table 3.36). Generally speaking, a better mass balance was achieved with the jars loaded with less sludge. The discrepancies may reflect analytical errors, limitations of the assumptions and empirical data being employed or a loss (or gain) of particulate inorganic matter in the course of the exposures. The experimental results indicate that there is a high probability of a particle concentration, and to a lesser extent, chamber design effect on degradation rate. This raised concerns in our minds about the validity of obtaining representative effluent particle decomposition kinetics from a system that would appear to be sensitive to (at least two) experimental conditions. For this reason we decided to abandon the field-based simulations using sludge as a surrogate.

III.A.4.c. Decomposition of final effluent. The final experiment described here was undertaken as a preliminary step toward developing a laboratory-based system for establishing an "approximate" rate of degradation of effluent particles through a laboratory exposure system. The experiment was designed to approximate dilutions of 25:1 (effluent/seawater) far lower than is likely to be encountered in the natural environment. However, this low dilution was imposed by limitations on our ability to reliably measure small quantities of suspended particles by gravimetric methods (and carry out TOC and TN analyses on same).

Twenty-four hour composite effluent samples were collected from the JWPCP and Hyperion treatment plants. Each effluent was diluted 25:1 with filtered (GF/C) seawater. One of the jugs containing diluted effluent from each treatment plant was designated as T_0. The other two jugs of diluted effluent from each treatment plant were allowed to incubate for 4 d in a water bath at approximately 12°C. The incubating effluents were aerated through a pipette at a rate of 5-10 ml min^{-1}. The T_0 samples were also placed in the water bath and allowed to come to thermal equilibrium before being sacrificed. Two incubation blanks (filtered seawater) were placed into the water bath and allowed to incubate (aerated) alongside the effluent samples. Two separate seawater samples were filtered twice successively (i.e. refiltered) in order to determine the mass of solids likely to be contributed to the samples of once-filtered seawater at T_0 as a result of particle aggregation. Total suspended solids, TOC and TN were determined on all samples including the starting effluent.

The results, listed in Table 3.37, showed that after correction for the seawater blank, the mean suspended solids concentration decreased for the Hyperion effluent and increased for the JWPCP effluent. At the same time, the mean TOC content (both before and after appropriate blank correction) decreased for the Hyperion effluent and increased for the JWPCP effluent. The C/N ratios of the effluent particles decreased for both treatment plants tested. These data suggest that there may be at least two different processes at work. If particle degradation was the only process involved, the corrected suspended solids and the TOC content of the diluted effluents from both plants would be expected to decrease with time. This decrease is observed in the Hyperion but not the JWPCP samples. The filtered seawater blanks, aerated over 4 d, show a measurable TSS content as do the refiltered seawater samples. The former exceeds the latter by 0.5 mg l^{-1}. This indicates that particles sufficiently large to collect on the filters after aeration may be forming as a result of bubble-induced aggregation and/or conversion of DOM to POM. Alternatively, the effect may be due to adsorption of dissolved organic matter on the filters. Support for the aggregation hypothesis is found in the C/N ratio data.

If particle degradation were the only process occurring, one would expect the C/N ratio to increase over time. This is because nitrogen-bearing organics are preferentially metabolized by bacteria. Instead, the C/N ratio of the suspended particles decreases. Results from previous experiments show conclusively that following centrifugation, filterable sludge particles remaining in the supernatant have lower C/N ratios than particles deposited on the bottom (Tables 3.30 and 3.32). Thus, fine particles (and/or filter-adsorbable DOM) have chemical characteristics appropriate to a source for the filterable particle pool.

It remains to explain why such different results should be obtained for the JWPCP and Hyperion effluents. If one invokes both particle formation and organic degradation and assumes that the rate of particle aggregation (which depends primarily on the particle concentration) is similar for the two effluents, the difference in behavior could be ascribed to variations in biodegradability. The Hyperion effluent is not chlorinated prior to discharge, whereas the JWPCP effluent is. This raises the intriguing possibility that effluent chlorination could significantly inhibit the activity of microbial communities on effluent particles such that they are not significantly degraded, at least over a matter of days. In this case, chlorination, a measure used for control of pathogenic microorganisms, would have the effect of enhancing the probability of effluent particle survival and, hence, deposition.

The results of this experiment convinced us that effluent degradation kinetics in an aerated bottle system could not be measured without (and perhaps even with) first isolating the particles themselves. We, therefore, embarked upon an effort to design a system for exposing filter-collected effluent particles to aerated seawater. Regrettably, the successful completion of this task was never realized. For this reason, no description of our experimentation will be attempted here.

III.B. SIMULATION STUDIES

III.B.1. DECAL

III.B.1.a. San Diego. The *DECAL* simulations for the San Diego discharge predict a peak concentration of effluent suspended solids in the wastefield of 0.473 mg l^{-1} during periods of upcoast flow, and 0.790 mg l^{-1} during downcoast flow (k_d=0.10). Neglecting the effects of decay, the corresponding average initial dilutions are 142:1 and 84:1 for up- and downcoast flow, respectively. The direction-weighted average initial dilution is 116:1.

DECAL provides two types of output. The first is a file containing a summary of the parameter values used in the simulation and a set of printer plots. The second output is a file containing a summary of the deposition of natural and accumulation of material along a longshore transect. The latter includes the deposition of: (a) total suspended solids, (b) effluent particles, (c) a trace constituent, and (d) the accumulation of total organic material.

Figure 3.14a shows the two-dimensional pattern of the deposition of total suspended solids (wastewater + natural) in the simulation grid for a decay coefficient of 0.1 d^{-1}. *DECAL* scales the range of values in the grid and assigns them to a series of ranges, or levels. Each level is assigned a number and displayed in this printer-plot. In the present case, the depositional rate (g m^{-2} d^{-1}) has been contoured into seven levels (0->6). Various parameters listed in the output indicate the number of levels, the minimum and maximum values, and the incremental change in the value associated with each level change.

In this figure, each level corresponds to an increase of 3.427 g m^{-2} d^{-1} [see (a) in Figure 3.14a] in the deposition rate. The background level (0) includes the deposition of natural particles from the upper layer of the water column (in the absence of sedimentation from the wastefield). This natural flux is 1.71 mg m^{-2} d^{-1} [see (b) in Figure 3.14a]. The peak deposition (level 6) occurs in the immediate vicinity of the outfall diffuser (x,y = 10,4) and has a value of 21.0 g m^{-2} d^{-1} [see (c) in Figure 3.14a]. These units can be converted to mg cm^{-2} yr^{-1} by multiplying by 36.5. In these units, the background and peak fluxes are 62.5 and 768 mg cm^{-2} yr^{-1}, respectively. The maximum cross-shore width of the depositional pattern is approximately 1.6 km. Enhanced values of the deposition of suspended solids (corresponding to level 1, or greater) are confined within the downcoast end of the grid (10 km), but extend beyond the upcoast end of the grid (22 km).

Figure 3.14b shows the corresponding depositional pattern for a decay coefficient of 0.52. With this increased decay rate, the background depositional flux is reduced from about 63 mg cm^{-2} yr^{-1} to less than 1×10^{-11} mg $cm^{-2}yr^{-1}$. Each level in this figure corresponds to a change of 0.691 gm m^{-2} d^{-1} in the depositional rate. The peak rate is 5.53 gm m^{-2} d^{-1} (202 mg cm^{-2} yr^{-1}), or about one-quarter (0.26) of the peak depositional rate predicted for a decay coefficient of 0.10.

Figure 3.15a shows the depositional flux of total suspended solids in a longshore transect passing through the outfall diffuser (y=4.09 km) for the two values of the decay coefficient.. For a decay coefficient of 0.10, we note that although the depositional rate at the downcoast end of the grid has fallen below the level 1 range in Figure 3.14, it is still well above the background deposition rate of about 63 mg cm^{-2} yr^{-1}. For a decay coefficient of 0.52, the deposition rate at the downcoast end of the grid is essentially at the background level. At the upcoast end, there is still enhanced sedimentation, although the rate is quite low (ca. 1 mg cm^{-2} yr^{-1}). The full width of the enhancement (longshore axis) at half maximum for the depositional rate is about 3.6 km for a decay coefficient of 0.10, and about 1.4 km for a value of 0.52.

Figure 3.15b shows the longshore distribution of the deposition of wastewater suspended solids. Peak values are about 485 and 192 mg cm^{-2} yr^{-1} for decay coefficient values of 0.10 and 0.52, respectively. Thus the deposition of wastewater suspended solids is predicted to account for about 63 to 95% of the enhanced deposition in the immediate vicinity of the outfall diffuser.

Figures 3.16a,b show the deposition rates of Pb and Cd, respectively, along the transect. The secondary peak at 1.4 km appears to be an artifact of the computational process. The depositional rate of lead is less sensitive to the selection of the decay coefficient than is the depositional rate of cadmium. The ratio of the flux of Pb to the

flux of wastewater suspended solids to the bottom in the immediate vicinity of the diffuser is about 0.15 mg g^{-1} for a decay coefficient of 0.10; for a decay coefficient of 0.52, it is about 0.20. In the effluent,. the ratio was about 0.20 mg g^{-1}. For Cd, the depositional ratio is about 0.009 mg g^{-1} for both decay coefficients. In the effluent, the ratio was about 0.04 mg g^{-1}.

Since the accumulation of organic and trace material is proportional to the corresponding depositional fluxes, the distributions of the organic and trace constituent accumulations are identical to those shown in Figures 3.14a,b through 3.16a,b. The accumulation of wastewater material peaks at 89.2 and 35.0 gm l^{-1} for decay coefficients of 0.10 and 0.52. Peak accumulations of Pb are 13.17 and 7.18 mg l^{-1} (k_d = 0.10, 0.52 respectively). The ratios of lead accumulations to the accumulation of wastewater suspended solids are 0.15 and 0.20, or the same as for the depositional fluxes. For Cd, the peak accumulations are 0.82 and 0.32 mg l^{-1} (k_d=0.10, 0.52). The ratio of Cd accumulation to the wastewater suspended solids accumulation in the surface sediments is again the same as the depositional flux ratio (0.009 mg g^{-1}).

Figure 3.17 shows the concentration of organic material in the upper layer of the sediments. The peak value is nearly 140 gm l^{-1} for a decay coefficient of 0.10, and about 36 gm l^{-1} for a decay coefficient of 0.52. Conversion of these concentrations to a concentration expressed in terms of percent organic material on a dry mass basis is discussed in section IV.B.3. *DECAL* output does not include information that can be used to construct equivalent profiles of the accumulation of the two trace constituents.

The effects of changing the concentration of effluent suspended solids were also investigated in the San Diego site simulations. Simulation runs were carried out for suspended solids concentrations of 0, 49, 67, 85, and 102 mg l^{-1}. The peak concentration of wastewater suspended solids in the wastefield was found to be proportional to the effluent suspended solids--as expected.

In the absence of any natural particles, the depositional rate would be expected to increase approximately as the square of the effluent suspended solids concentration (Hendricks and Eganhouse, 1990). Since natural and effluent particles interact during the aggregation process, this relationship will be modified in the presence of natural particles. Figure 3.18a shows that a quadratic equation is required to describe the relationship between the flux and the effluent SS concentration. Figure 3.18b shows the relationship between the accumulation of organic material in the surface sediments and the effluent suspended solids concentration. As might be expected, the relationship is similar to that of the depositional flux.

Figure 3.19a shows the depositional flux of lead to the sediments as a function of the concentration of suspended solids in the effluent. Note that the depositional flux of Pb does not go to zero as the concentration of SS goes to zero in the effluent. This is due to the absorption of dissolved Pb on the natural particles and the subsequent deposition of the natural particles on the ocean bottom. Increases in the concentration of SS in the effluent, however, appear to bring about a linear increase in the deposition rate and accumulation (Figure 3.19b) of Pb in the sediments.

III.B.1.b. Orange County. The maximum effluent suspended solids in the Orange County wastefield are predicted to be 0.45 mg l^{-1} and 0.62 mg l^{-1} for periods of upcoast and downcoast flow, respectively (k_d=0.10). The corresponding average initial dilutions are 109:1 (upcoast) and 79:1 (downcoast), with a direction weighted average of about 96:1.

Figure 3.20a shows the two-dimensional depositional pattern of total (natural + effluent) suspended solids in the simulation area for a decay coefficient of 0.10. The background depositional rate is 1.83 gm m^{-2} d^{-1} (67 mg cm^{-2} yr^{-1}). The maximum deposition (level 4) occurs in the immediate vicinity of the outfall, with a peak rate of 16.4 gm m^{-2} d^{-1} (597 mg cm^{-2} yr^{-1}). Each level corresponds to an increase of 3.66 gm m^{-2} d^{-1} (134 mg cm^{-2} yr^{-1}). The cross-shore width of the discharge enhanced deposition is about 1.3 km.

Figure 3.20b shows the corresponding depositional pattern for a decay coefficient of 0.52. The contour interval is 0.494 gm m^{-2} d^{-1} (18 mg cm^{-2} yr^{-1}). The background depositional rate is reduced to only about

10^{-9} gm m^{-2} d^{-1}. The peak deposition is reduced to 3.95 gm m^{-2} d^{-1} (144 mg cm^{-2} yr^{-1}), or about one-quarter (0.24) of the peak rate for a decay coefficient of 0.10.

Figure 3.21a shows the depositional flux of total suspended solids in a longshore transect passing through the outfall diffuser (y=4.00 km) for the two values of the decay coefficient. The full width of the depositional peak (at ½ maximum) along the transect is about 8.2 km for a decay coefficient of 0.10, declining to about 2.4 km as the decay coefficient increases to 0.52.

Figure 3.21b shows the longshore distribution of the deposition of wastewater suspended solids. Peak values range from 133 to 338 mg cm^{-2} yr^{-1}, and the full width at one-half maximum, from 2.3 to 5.2 km (k_d = 0.52->0.10).

Figures 3.22a,b show the deposition rates of Pb and Cd, respectively, along the transect. Pb depositional rates range from 60 to 108 μg cm^{-2} yr^{-1}, and Cd depositional rates range from 2.2 to 6.4 μg cm^{-2} yr^{-1} as the decay coefficient, k_d, changes from 0.52 to 0.10. The ratio of the flux of Pb to the flux of wastewater suspended solids in the immediate vicinity of the diffuser is about 0.32 to 0.45 mg g^{-1} (k_d = 0.10, 0.52); while the ratio for Cd is about 0.018 mg g^{-1}.

Figure 3.23 shows the concentration of organic material in the upper layer of the sediments. The peak value is about 114 gm l^{-1} for a decay coefficient of 0.10. Increasing the decay rate to 0.52 (d^{-1}) reduces the accumulation to about 26 gm l^{-1}--slightly more than a four-fold reduction.

The effects of changing the phytoplankton productivity and the sediment interfacial removal rate were also examined for the Orange County site. Figure 3.24a shows the variation in the longshore distribution of the deposition of total suspended solids for phytoplankton productivities of 0.5, 1.0 and 2.0 gm-C m^{-2} d^{-1}. A doubling of the productivity rate from 0.5 to 1.0 gm-C m^{-2} d^{-1} increases the peak depositional rate in the longshore transect from about 303 mg cm^{-2} yr^{-1} to about 407 mg cm^{-2} yr^{-1}, about a 34% increase. An additional doubling, from 1 to 2 gm-C m^{-2} d^{-1}, increases the depositional rate to about 600 mg cm^{-2} d^{-1}--about a 48% increase. The effect on the depositional rate of effluent suspended solids, through coaggregation, is smaller. Figure 3.24b shows that doubling the productivity from 0.5 to 1 gm-C m^{-2} d^{-1} produces only about a 13 percent increase in the deposition rate of effluent suspended solids. Another doubling, to 2 gm-C m^{-2} d^{-1}, produces about a 19 percent increase in the depositional rate. Figure 3.24c shows the dependence of the deposition of Pb to the bottom on the productivity. The doubling from 0.5 to 1 gm-C m^{-2} d^{-1} produces a 14% increase, while another doubling to 2 gm-C m^{-2} d^{-1} generates an additional 21% increase. These results suggest that the simulation predictions are not particularly sensitive to the selection of the phytoplankton productivity.

Figure 3.25a shows the longshore distribution of the deposition of effluent suspended solids for sediment interfacial removal rates between 0.015 and 0.045 cm d^{-1}. Since this parameter should only affect material already deposited on the sediments, the depositional pattern should be independent of the magnitude of the interfacial removal rate. Although this is nearly the case, there is a slight variation. The source of this difference is unknown at the present time. Figure 3.25b shows the accumulation of organic material in the surface layer of the sediments as a function of the interfacial removal rate. Here the effect of changing the removal rate is clear--increased rates bring about a significant reduction in the concentration of accumulated organic material. Increasing the interfacial removal rate three-fold, from 0.005 cm d^{-1} to 0.015 cm d^{-1} reduces the peak concentration along the transect from nearly 185.3 gm l^{-1} to slightly less than 61.8 gm l^{-1}--a three-fold reduction. An additional three-fold increase in the interfacial removal rate, from 0.015 cm d^{-1} (the default simulation value) to 0.045 cm d^{-1} produces nearly another three-fold reduction (2.9) in the concentration of accumulated organic material (to about 21.2 gm l^{-1}). Thus the accumulation of organic material in the surface sediments is predicted to be approximately inversely proportional to the interfacial removal rate.

The accumulation of Pb is also sensitive to the interfacial removal rate--although not as sensitive as the assimilation of organic material. Increasing the rate three-fold from 0.015 to 0.045 cm d^{-1}, reduces the peak concentration of Pb in the surface layer of the sediments from 6.78 to 2.95 mg l^{-1}. This is a reduction of about a factor of 2.3 (versus 2.9 for organic material).

3.1.c. Los Angeles County. Individual simulations were carried out for each of the Los Angeles County alls (90-inch, 120-inch), then the depositional patterns and accumulation concentrations were combined into gle pattern.

background concentration of natural suspended solids in the water at the wastefield depth is predicted to .42 mg l^{-1} (decay coefficient = 0.1 d^{-1}). The maximum effluent suspended solids concentration in the efield from the 90-inch outfall was 0.654 mg l^{-1} for the average upcoast flow, and 0.925 mg l^{-1} for the age downcoast flow. The latter concentrations correspond to average initial dilutions of 301:1 and 213:1 periods of upcoast and downcoast flow, respectively). The direction-weighted average dilution is 262:1. the 120-inch outfall, the average dilutions for upcoast and downcoast flows were 179:1 and 130:1, yielding a tion weighted average dilution of 158:1. Weighting the direction-weighted average initial dilutions for the ch and 120-inch discharges by their respective flows yields a site-average dilution of about 188:1.

3.1.c.i. *90-Inch Outfall*. Figure 3.26a shows the two-dimensional pattern of the deposition of total suspended s (effluent + natural) for the 90-inch outfall (k_d = 0.10). The peak deposition occurs in the immediate ity of the outfall diffuser (10,4 km). This deposition rate is about 26.63 g m^{-2} d^{-1} (972 mg cm^{-2} yr^{-1}). Each in the contour corresponds to an increase of 3.5 gm m^{-2} d^{-1} (128 mg cm^{-2} yr^{-1}) in the flux rate. Figure 1 shows the corresponding deposition of effluent particles. The peak deposition rate is 18.66 g m^{-2} d^{-1} (681 m^{-2} yr^{-1}), and the cross-shore width of the wastefield and depositional pattern is about 2.1 km (the contour val remains at 3.5 g cm^{-2} d^{-1}).

res 3.26b and 3.27b show the corresponding depositional patterns for a decay coefficient of 0.52. Each ase in level in Figures 3.26 and 3.27 corresponds to an increase of 1.01 gm m^{-2} d^{-1} (37 mg cm^{-2} yr^{-1}) in the sition rates. The peak deposition rate of suspended solids is 8.08 gm m^{-2} d^{-1} (295 mg/cm^2/year) and the mum rate of deposition of effluent solids is 7.59 gm m^{-2} d^{-1} (277 mg cm^{-2} yr^{-1}). These rates are about 30 nt (total SS) to 40% (effluent SS) of the maximum flux rates for the lower decay coefficient. Although still ficant, these changes are not as great as in the simulations for the San Diego and Orange County sites. is due to the increase in total suspended solids concentration in the Los Angeles County wastefield, which ts in faster aggregation and a shorter residence time in the water column.

re 3.28a shows the depositional pattern of total suspended solids in a longshore transect passing through 0-inch outfall (y = 4.09 km) for both values of the decay coefficient. The full width of the peak in the hore direction at one-half the maximum deposition rate is 5.0 km for a decay rate of 0.10, and 2.8 km for a y rate of 0.52. Figure 3.28b shows the corresponding depositional pattern for effluent suspended solids, and es 3.29a,b show the depositional patterns for Pb and Cd, respectively. Note that changes in the decay icient have a lesser impact on the deposition of Pb (and to a lesser degree, Cd) than they have on the sition of suspended solids.

peak deposition rates for Pb are about 546 and 339 μg cm^{-2} yr^{-1} for k_d = 0.10 and 0.52 respectively. For Cd, eak rates are 12.3 and 5.6 μg cm^{-2} yr^{-1}. The ratios of the trace constituent depositional rates to those of ffluent suspended solids are 0.80 and 1.2 mg g^{-1} (Pb; k_d = 0.10,0.52) and 0.02 mg g^{-1} (Cd, both decay rates).

e 3.30 shows the longshore distribution of total organic mass in the surface layer of the sediments. The accumulation is slightly upcoast (ca. 0.8 km) from the apex of the 90-inch outfall (x = 10 km) and sponds to a concentration of 183 gm l^{-1} (for a decay coefficient of 0.10). For the faster decay rate (0.52), ccumulation falls to about 51 gm l^{-1}. The full width of the accumulation in the longshore direction at one- naximum is about 4.7 for k_d = 0.10, decreasing to about 3.0 km for a decay coefficient 0.52.

3.1.c.ii. *120-Inch Outfall*. Figure 3.31a shows the two-dimensional pattern of the deposition of total nded solids (effluent + natural) for the 120-inch outfall (k_d = 0.10). The peak deposition rate is 56.09 $^{-2}$ d^{-1} (about 2045 mg cm^{-2} yr^{-1}), or slightly more than twice (2.1) the peak depositional flux in the diate vicinity of the 90-inch outfall. Each contour level in this plot corresponds to an increase of 7.25 $^{-2}$ d^{-1} (265 mg cm^{-2} yr^{-1}) in the flux rate. Figure 3.32a shows the corresponding deposition of effluent les. The peak deposition rate is 45.46 g m^{-2} d^{-1}, or 1660 mg cm^{-2} yr^{-1} (the contour interval remains at 7.25

yr^{-1}). Thus the deposition of effluent particles in the vicinity of the 120 is predicted to be about 2.4 times
k sedimentation rate of effluent particles near the 90-inch outfall. The cross-shore width of the
eld and the depositional pattern is about 2.1 km.

3.31b and 3.32b show the corresponding depositional patterns for a decay coefficient of 0.52. Each
e in level in Figures 3.31b and 3.32b corresponds to an increase of 3.52 g m^{-2} d^{-1} (128 g cm^{-2} yr^{-1}) in the
ion rates. The peak deposition rate of total suspended solids is 28.2 gm m^{-2} d^{-1} (1030 mg cm^{-2} yr^{-1}) and
ximum rate for the deposition of effluent solids is 27.4 g m^{-2} d^{-1} (1001 mg cm^{-2} yr^{-1}). These rates are
50% (total SS) to 60% (effluent SS) of the maximum deposition rates for $k_d = 0.10$. Although an increase
lecay rate still produces a significant reduction in the rate of deposition of suspended solids, the
ons are not as large as predicted at the San Diego and Orange County sites. This is due to the increase
ent suspended solids (and consequently the total suspended solids) concentrations in the wastefields
ted by the Los Angeles County discharges. These increased suspended solids concentrations produce
aggregation and a shorter residence time in the water column, so there is less time for decay to contribute
loss of organic mass.

3.33a shows the depositional pattern of total suspended solids in a longshore transect passing through
)-inch outfall. The peak deposition rate is about 1320 mg cm^{-2} yr^{-1} if $k_d = 0.10$, and about 600
$^{-2}$ yr^{-1} if $k_d = 0.52$. These values are somewhat higher than the peak values associated with the 90-inch
rge (Figures 3.28a,b) since this outfall terminates in shallower water (56 m vs. 62 m) and has a lower
ted initial diulution. Figure 3.33b shows the corresponding depositional pattern for effluent suspended
The trace constituent depositional patterns along the transect are illustrated in Figures 3.34a,b. The
deposition rates for Pb are about 820 and 610 μg cm^{-2} yr^{-1} ($k_d = 0.10, 0.52$). For Cd, the peak rates are 23
μg cm^{-2} yr^{-1}. The ratios of the trace constituent depositional rates to those of the effluent suspended
are about 0.62 and 1.0 mg g^{-1} (Pb; kd = 0.10,0.52), and 0.02 mg g^{-1} (Cd, both decay rates).

3.35 shows the longshore distribution of total organic mass in the surface layer of the sediments. The
ccumulation is slightly upcoast from the bend of the 120-inch outfall (x = 8.4 km) and corresponds to a
ntration of 240 gm l^{-1} ($k_d = 0.10$) to 110 gm l^{-1} ($k_d = 0.52$). The full width of the accumulation peak at one-
aximum is about 4.7 km for $k_d = 0.10$. This width shrinks to about 3.0 km for a decay coefficient 0.52.

1.c.iii. *Combined 90- and 120-Inch Outfalls*. Figure 3.36a shows the deposition of total suspended solids on
a transect lying 4.09 km offshore from the inner edge of the grid (i.e. in about 62.5 m of water). Peak
ition rates are on the order of 700 to 1950 mg cm^{-2} yr^{-1} ($k_d = 0.52, 0.10$ respectively). The corresponding
deposition rates of effluent suspended solids (Figure 3.36b) are about 680 and 1440 mg cm^{-2} yr^{-1}. In both
, the major peak is composed of two minor peaks representing the local peak depositions associated with
)- and 120-inch outfalls. For suspended solids, the depositions in the vicinity of the 90-inch outfall are
ly greater than in the vicinity of the 120-inch outfall. The situation is reversed in the case of trace
ituent depositions (Pb, Cd; Figures 3.37a and 3.37b, respectively), where the rates are slightly higher near
20-inch diffuser. The peak accumulation of organic material in the surface layer of the sediments (Figure
varies from about 130 gm l^{-1} ($k_d = 0.52$) to 360 gm l^{-1} ($k_d = 0.10$).

combined effects of the 90-inch and 120-inch discharges were also simulated using four segments (two
ps of two legs) to represent the two outfalls as a single discharge. The average initial dilution for this
ined discharge was 195:1 during periods of upcoast flow, and 142:1 during down coast flow. The direction-
ited average flow was 167:1. This is about 11% lower that the average initial dilution obtained by
dering the two discharges separately (188:1).

results of the base simulations at all three sites are summarized in Table 3.38.

III.B.2. SED2D

III.B.2.a. San Diego.

III.B.2.a.i. *Aggregate Particle Sedimentation*

The average concentration of effluent suspended solids in the wastefield following completion of the initial dilution process is predicted to be 0.134 mg l^{-1} for an effluent with a concentration of 67 mg l^{-1}. This corresponds to an average initial dilution of about 485:1. During the initial dilution process, ambient water containing a natural particle suspended solids concentration of 2 mg l^{-1} is also entrained into the plume and wastefield, resulting in an initial wastefield concentration of total suspended solids of 2.134 mg l^{-1}.

Figure 3.39 shows the time-dependent accumulation of total suspended solids on the bottom as a function of the elapsed time since the particles were discharged (or entrained into the plume). This deposition is for a constant water depth of 66.5 m. The solid curve represents the deposition for an initial total suspended solids concentration of 2.14 mg l^{-1}. The dashed line represents the deposition for non-cohesive particles (using the distribution of particle settling speeds determined from measurements with a settling column). Approximately one-half (47%) of the aggregate particles settle to the bottom within one week (168 hr) after they enter the wastefield. Slightly more than one-half of these particles (and about one-quarter of the original particle mass) is deposited within the first 24 hr after discharge.

The spatial distribution of the predicted flux of sedimenting aggregate particles is shown in Figure 3.40a in undistorted, and magnified in the cross-shore direction in 3.40b. The peak deposition rate lies in the immediate vicinity of the outfall diffuser and reaches about 2440 mg cm^{-2} yr^{-1}. Natural particle sedimentation contributes about 2290 mg cm^{-2} yr^{-1} to this flux; effluent particle sedimentation contributes the remaining 150 mg cm^{-2} yr^{-1}. About 69% of the sedimenting material is organic. If particles settling from the water column undergoes an average of 100 resuspensions, the peak flux of wastefield particles into the surface layer of the sediments is reduced to 88 mg cm^{-2} yr^{-1} (Figure 3.41). This is only about 3.6% of the flux in the absence of resuspension.

The rate at which particle mass accumulates in the sediments is equal to the difference between the flux of particle mass into the surface sediments and the loss of particle mass associated with the decay of organic material. The input flux consists of two sources: (a) the net deposition of particles from the wastefield and, (b) the deposition of natural particles that are not part of the wastefield-related deposition. The latter includes natural particles resuspended from adjacent areas, and natural particles settling from the water column in the absence of wastefield related deposition. Since the degree of surficial sediment resuspension in the presence of a discharge is unknown, we present estimates of the accumulation rate of particle mass in the sediments, and their composition, for the cases of: (1) no resuspension ($f_a = 1.00$), and (2) assuming the average particle undergoes 100 resuspensions ($f_a = 0.01$). Figure 3.42a shows the accumulation rate of total suspended solids mass (from all sources) in the absence of resuspension. The peak accumulation rate is 2369 mg cm^{-2} yr^{-1}, or only about 70 mg cm^{-2} yr^{-1} less than the input flux into the surface sediments. Therefore the mass of organic material lost to decay in the immediate vicinity of the diffuser is only about 3% of the sedimenting mass (and about 4% of the sedimenting organic material). Concentrations of organic material in excess of 60% cover an area of approximately 12 km^2; less than 5 km^2 are predicted to have an organic concentration that is less than 10%.

The concentration of organic material in the immediate vicinity of the outfall is predicted to peak at 68.1% Loss of material due to decay (on a percentage basis) in the area significantly affected by the deposition of particles from the wastefield is minimized by the small value of the decay flux (ca. 120 mg cm^{-2} yr^{-1}--see section II.B.2.p) relative to the input flux of organic material (ca. 1683 mg cm^{-2} yr^{-1} near the diffuser). In areas unaffected by the deposition of wastefield particles, the effects of decay become more significant. Here the concentration of organic material is reduced from 15% (in the input flux) to an average concentration of 1.4% in the surface sediments. This represents a loss of about 92% of the organic material in the deposited particles.

Figure 3.42b shows the predicted accumulation of particle mass and organic content of particles in the surface sediments if the average particle undergoes 100 resuspensions. The peak accumulation rate is about 57 mg cm^{-2} yr^{-1}, and the organic content peaks at 35.1%. In this case, approximately 38% of the input flux in the immediate

y of the diffuser is lost due to decay. Concentrations of organic material in excess of 20% are predicted to in an area of approximately 15 km^2.

2.a.ii. *Non-Cohesive Particles*

redicted cumulative fraction of non-cohesive particle mass deposited on the bottom as a function of d time following discharge is indicated by the dashed line in Figure 3.39. The fraction deposited over the e of a week (11%) is only about one-quarter of the fraction deposited for aggregating particles (with an suspended solids concentration of 2.14 mg l^{-1}). However, about one-half of this mass (5.8% of the initial is deposited within the first 24 hr following discharge. This one-day/one-week ratio is virtually the same the aggregating particles.

e 3.43a shows the deposition rate of effluent suspended solids in the simulation area. The peak rate is 92 mg cm^{-2} yr^{-1}. This is about 60% of the predicted rate of the deposition of effluent particles in the ace of aggregation (150 mg cm^{-2} yr^{-1}). Since there is no aggregation with natural particles (and it is ed that natural particle aggregation is not enhanced within the wastefield), there is no increase in particle entation associated with natural particles present in the wastefield. Even after accounting for the tion in effluent and natural particle fluxes to the bottom, it is evident that the deposition of wastefield-d, noncohesive particles is confined to a smaller area around the outfall than the deposition of aggregating les. In the presence of resuspension (Figure 3.43b), the peak flux of wastefield related particles into the e sediments is predicted to be reduced to about 3.4 mg cm^{-2} yr^{-1}. Again, this is about 4% of the flux in sence of resuspension.

ccumulation rate of total particle mass in the absence of resuspension is shown in Figure 3.44. The peak ulation rate is predicted to be about 53.4 mg cm^{-2} yr^{-1}, or about 58% of the flux to the surface of the ents. The organic content of the sediments peaks at about 36% in the vicinity of the outfall diffuser. The vith a predicted organic concentration in excess of 20% is about three-eighths of a square kilometer; ntrations in excess of 10% are predicted to occur in an area of about 0.75 km^2. If the noncohesive les undergo an average of 100 resuspensions, the peak organic content of the sediments is predicted to be .1%, or an additional 1.7% above the (estimated) background value of 1.4%. Predicted concentrations in of 2% occur in an area slightly greater than 4 square kilometers. The peak rate of accumulation of total nded solids (effluent and natural) is predicted to be 11.7 mg cm^{-2} yr^{-1}. This is only 14% greater than the ated) accumulation rate of 10.3 mg cm^{-2} yr^{-1} in the absence of the discharge.

2.b. Orange County

2.b.i. *Aggregating Particles*

verage initial dilution predicted for the wastefield generated by the Orange County discharge is 593:1. verage concentration of suspended solids in the effluent for the period from 1987 to 1989 was 49 mg l^{-1}; the wastefield average concentration of effluent solids for this period is 0.083 mg l^{-1}. The entrainment of l suspended solids (assumed concentration: 2 mg l^{-1}) into the plume during the initial dilution process the concentration of total suspended solids in the wastefield to 2.083 mg l^{-1}.

umulative fraction of wastefield suspended solids predicted to be deposited on the bottom after elapsed of one day and one week are predicted to be 21% and 43%, respectively. Deposition simulations were d out for an annual mass emission rate of effluent suspended solids equal to 17,500 mt yr^{-1}, representative period from 1987-1989. Figure 3.45 shows the predicted depositional pattern of wastefield suspended in the simulation area. The deposition peaks near the outfall diffuser at 950 mg cm^{-2} yr^{-1}. The organic nt of these particles is 69.5%. Effluent particles contribute approximately 38 mg cm^{-2} yr^{-1} (4%) of this The remaining 911 mg cm^{-2} yr^{-1} is associated with the deposition of natural particles entrained into the field or settling from the overlying water column.

e 3.46 shows the net depositional pattern if the average particle undergoes 100 resuspensions. The peak predicted to be reduced to 28.4 mg cm^{-2} yr^{-1}, or about 3% of the deposition in the absence of pension. Mixing with sediments resuspended from adjacent areas reduces the peak predicted organic nt from 0.695 to 0.674.

:umulation of total suspended solids in the absence of resuspension is shown in Figure 3.47a. The ılation rate peaks at 885 mg cm^{-2} yr^{-1}. Away from the influence of the discharge, the accumulation rate ral particles is 12.6 mg cm^{-2} yr^{-1}. The organic content of the surface sediments peaks at 66%. (Figure Concentrations in excess of 60% are predicted to occur in an area of 4.5 km^2.

:ase of resuspension, the peak accumulation rate is predicted to be 24.7 mg cm^{-2} yr^{-1} (Figure 3.48a). one-half of this rate (12.6 mg cm^{-2} yr^{-1}) results from the wastefield-independent deposition of natural s, the remaining 12.2 mg cm^{-2} yr^{-1} is associated with the deposition of both natural (96%) and effluent articles from the wastefield. The reduced flux of wastefield particles means that wastefield-independent particle deposition makes a greater contribution to the total deposition. Since these particles have a rganic content, and the reduced fluxes increase the effects of decay, the peak predicted organic content ediments is about 15.5% (Figure 3.48b) Concentrations in excess of 10% are predicted to occur in an 3.4 km^2.

b.ii. *Non-Cohesive Particles*

imately 12.5% of the wastefield mass of suspended solids settles to the ocean bottom (in 55 m of water) l week of their discharge. As in the case of aggregating particles, about one-half of the mass (3.3% of l) is deposited within the first day.

:dicted deposition of effluent suspended solids is shown in Figure 3.49a for the case of no resuspension. position peaks at 78 mg cm^{-2} yr^{-1} in the immediate vicinity of the diffuser. This is slightly more than ie predicted rate of deposition of aggregating effluent particles (although the combination of natural and particle flux from the wastefield is nearly 10 times greater than this rate). The organic content of the s settling near the diffuser is predicted to be 69.2%. If the particles undergo an average of 100 nsions, the peak deposition rate is reduced to only 2.0 mg cm^{-2} yr^{-1} (Figure 3.49b).

:umulation of non-cohesive suspended solids in the surface layer of the sediments in the case of no nsion is shown in Figure 3.50a. The peak accumulation rate is 32.6 mg cm^{-2} yr^{-1}, with an organic content % (Figure 3.50b). Concentrations in excess of 20% are predicted to occur in an area of ?? km^2.

ıresence of resuspension, the peak accumulation rate falls to 13.3 mg cm^{-2} yr^{-1} (Figure 3.51a). This is % greater than the accumulation rate in the absence of a discharge (estimated 12.6 mg cm^{-2} yr^{-1}). : content of the surface layer of the sediments is now predicted to peak at 2.8% (Figure 3.51b). In the : of the discharge, the estimated concentration is 2.0%.

:. Los Angeles County (1978-1980)

:.i. *Aggregate Particle Sedimentation*

:dicted average initial dilution for the LA County 90-inch outfall is 463:1. For an effluent suspended ɔncentration of 197 mg l^{-1} (representative of 1978-1980), this corresponds to a initial wastefield ration of 0.425 mg l^{-1}. Adding in 2 mg l^{-1} of natural particles due to entrainment during the initial process results in an initial concentration of total suspended solids in the wastefield of 2.43 mg l^{-1}.

ɔosition of total suspended solids in 1981 peaks at 938 mg cm^{-2} yr^{-1}. Deposition rates of wastefield s are predicted to exceed 500 mg cm^{-2} yr^{-1} over an area in excess of 14 km^2. The concentration of material in the vicinity of the two diffusers is predicted to be about 68.4%. Ten kilometers farther , the concentration is predicted to be 65%; 20 km upcoast, the concentration is still 63%. If the average undergoes 100 resuspensions before becoming part of the surface sediments, the peak flux of particles ; layer is predicted to fall to 34.4 mg cm^{-2} yr^{-1} (3.7% of the rate in the absence of resuspension). Fluxes s of 20 mg cm^{-2} yr^{-1} cover an area of about 22 km^2.

umulation rate of particle mass in the sediments in the absence of resuspension is shown in Figure The maximum rate is 880 mg cm^{-2} yr^{-1}, or about 93% of the inpuf flux of natural and effluent particles surface sediments. The concentration of organic material in the surface sediments is predicted to peak

› (Figure 3.52b). Concentrations in excess of 60% cover an area of 8 . 0 km^2; concentrations in excess of
:e predicted to cover an area of 50.4 km^2. The background concentration of organic material is
ted to be 4.5%. If resuspension occurs (f_a = 0.01), the peak concentration of organic material is predicted
to 19.5% (Figure 3.53b). Ten kilometers farther upcoast the peak concentration falls to 8.9%; after
r 10 km, it falls to 6.3%. The accumulation rate of particles peaks at 30.9 mg cm^{-2} yr^{-1} (Figure 3.53a). In
ence of a discharge, the (estimated) accumulation rate is 15 mg cm^{-2} yr^{-1}.

.c.ii. *Non-Cohesive Particles*

ak depositional rate of noncohesive effluent suspended solids in the absence of resuspension is 208 mg
$^{-1}$. If the average particle undergoes 100 resuspensions, the peak depositional flux into the surface layer
sediments is reduced to 5.3 mg cm^{-2} yr^{-1}). In the absence of resuspension, the peak concentration of
c material in the surface sediments is predicted to be 52% (Figure 3.54a). The corresponding rate of
ulation of effluent and natural particles is predicted to be 166 mg cm^{-2} yr^{-1} (Figure 3.54b).
ntrations of organic material in excess of 10% are predicted to extend 5.5 km upcoast from the peak, and
lowncoast. In the presence of resuspension, the predicted peak concentration falls to only 6.9% (Figure
, and the corresponding accumulation rate is 17 mg cm^{-2} yr^{-1} (Figure 3.55b).

.d. Los Angeles County (1971)

.d.i. *Aggregating Particles*

3.56a shows the predicted initial flux of total suspended solids for the discharge conditions in 1971.
entation peaks in the vicinity of the 90-inch diffuser at 2240 mg cm^{-2} yr^{-1}. Fluxes in excess of 1000 mg
$^{-1}$ are predicted over an area of 15 km^2. With resuspension (f_a = 0.01), the peak flux of wastefield related
ded solids into the surface layer of the sediments is 80.5 mg cm^{-2} yr^{-1} (Figure 3.56b).

ak rate of accumulation of effluent and natural suspended solids in the absence of resuspension is
ted to be 2137 mg cm^{-2} yr^{-1} (Figure 3.57a). The concentration of organic material in the surface
nts reaches 67% in the vicinity of the 90-inch diffuser. Concentrations in excess of 60% are predicted to
an area of 16.4 km^2; concentrations in excess of 30% extend to the downcoast end of the simulation area
from the 90-inch diffuser) and 18 km upcoast (Figure 3.57b). In the presence of resuspension, the peak
tration falls to 34% (Figure 3.58a). Concentrations in excess of 10% extend about 4.5 km downcoast,
› km upcoast from this peak. Resuspension reduces the peak accumulation rate to slightly less than 60 mg
$^{-1}$ (Figure 3.58b).

.d.i. *Non-Cohesive Particles*

ak depositional flux of effluent particles settling to the bottom is predicted to be 393 mg cm^{-2} yr^{-1} (Figure
. If resuspension occurs (f_a = 0.01), the flux rate of effluent particles into the surface sediments falls to
g cm^{-2} yr^{-1} (Figure 3.59b).

absence of resuspension, the organic content of the surface sediments in the immediate vicinity of the 90-
iffuser is predicted to be 60% (Figure 3.60a). This falls to 10% about 8 km upcoast, and 4.5 km
oast from the diffuser. The peak accumulation rate of total suspended solids in the sediments is
ted to be 341 mg cm^{-2} yr^{-1} (Figure 3.60b). Resuspension reduces the peak concentration of organic
ial to 9.3% (Figure 3.61), and the peak accumulation rate to 19.2 mg cm^{-2} yr^{-1}. The estimated
ulation rate in the absence of the discharge is 15 mg cm^{-2} yr^{-1}, with a concentration of 4.5% organic
ial.

.e. Sensitivity to Resuspension

nsitivity of sediment characteristics to the magnitude of the accumulation fraction, f_a, was examined in
tions for the Los Angeles County simulation area. Figure 3.62 shows the change in the peak depositional
f wastefield suspended solids as the accumulation fraction is changed from 1.00 to 0.005. A ten-fold
tion in the accumulation fraction from 1.00 to 0.100 reduces the peak flux by a factor of 3.7. An additional
of 10 reduction in the accumulation fraction (to 0.010) produces an additional factor of 8.4 reduction in
depositional flux. At small accumulation fractions (f_a < 0.01), the change in peak depositional flux is
rtional to the change in the accumulation fraction.

Figure 3.63a shows the sensitivity of the pattern of deposition along a longshore transect to the magnitude of the accumulation fraction. This pattern is much less sensitive to changes in this parameter than is the peak depositional rate. For a fixed value of the accumulation fraction, the ratio between the peak deposition rate (x=4 km) and the far-upcoast (x=32 km) deposition rate only falls by a factor of 2.6 for a 200-fold decrease in the accumulation fraction.

The shape of the cross-shore depositional pattern (Figure 3.63b) is initially sensitive to changes in the accumulation fraction (i.e., as it falls from 1.00), but this sensitivity rapidly diminishes as the accumulation fraction falls below 0.100. The ratio of the peak flux (y=2 km) to the "far-offshore" (y=4 km) flux falls from around 55:1 to about 4:1 as the accumulation fraction changes from 1.0 to 0.1. However, as the accumulation fraction falls from 0.1 to 0.005 (20-fold change), the ratio only falls by an additional factor of 1.4 (from 3.9 to 2.7).

The peak accumulation flux is especially sensitive to the accumulation fraction; sensitivity increases with falling values for this parameter. On the other hand, the pattern of deposition in cross-shore (in the vicinity of the diffuser) is sensitive to initial reductions in the accumulation fraction (from 1.00), but this sensitivity is greatly reduced for accumulation fractions below 0.100. The longshore depositional pattern is only weakly sensitive to changes in the accumulation fraction.

III.B.2.f. Summary

The rate of accumulation of sediments at each simulation site for the four basic simulation conditions (aggregation/non-cohesive and resuspension/no resuspension) are summarized in Table 3.39. Table 3.40 summarizes the concentration of organic material in the surface sediments for the same conditions.

IV. DISCUSSION

IV.A. FIELD STUDIES

The discussion has been divided into two parts: 1) Effluent Characteristics and 2) Sediment Dynamics. The first part considers what we have learned about the chemical characteristics of the JWPCP, OCSD, and PLTP effluents. The second part deals with the short- and long-term fate of waste particles and their potential interactions with other non-waste derived particles in the water column and on the sea floor. To simplify matters, we have presented the Sediment Dynamics discussion into three subsections corresponding to each of the study sites. The discussion does not rely upon nor is it intended as an exhaustive review of the literature.

IV.A.1. Effluent Characteristics

In terms of bulk properties there is nothing that distinguishes the waste effluents in southern California from those in other parts of the United States or world. However, when one examines the detailed chemical composition of treated wastewaters, it becomes evident that although they all contain the same materials, the relative abundances of these constituents vary from effluent to effluent (cf. Eganhouse and Kaplan 1982b). These differences are offset to some extent by the inherent temporal variability in chemical composition of a given effluent. With these limitations in mind, we now consider the unique features of the three effluents studied here.

The PLTP effluent has the highest concentration of suspended solids of the four effluents we examined. This probably reflects the lower level of treatment effected by the PLTP (advanced primary). We also observed higher concentrations of TSS for the PLTP and Hyperion effluents than have been reported by the monitoring groups of the respective agencies in their annual reports. The explanation for this apparent discrepancy may lie in the fact that protocols for determination of suspended solids in wastewaters are not specific about the filter to be used (APHA 1991). We employed a Whatman GF/C glass fiber filter for determination of all four effluents because this is the most widely used filter in oceanographic studies of (suspended) particulate organic matter (Cauwet 1978; Williams 1986). A significant fraction (30-60% by volume) of the suspended particulate matter in wastewaters has a diameter less than 10μm (Faisst 1976). Thus, filters of varying pore size will retain different fractions of the standing stock of suspended particles (cf. Sheldon 1972; Williams 1986). (The smaller the pore size the higher the TSS concentration, all other things being equal.) Thus, if methods currently in use

lyperion Treatment Plant and PLTP do not employ the same filter as we did and perform filtrations in the
e fashion, it is likely that the difference between our data and those of the monitoring groups can be
ibed to variations in filter pore size. From this discussion it should be evident that the methods used by
age treatment plants for monitoring of such basic parameters as total suspended solids may well not be
ndardized." To our knowledge, this represents the only study in which these four effluents have been tested
suspended solids content over an extended period of time using the same filtration procedure.

: organic carbon and nitrogen contents of the filterable particulate matter in all three effluents are about
% and 4%, respectively. (Consequently, POC concentrations are 8 mg l^{-1} and PN concentrations are
ig l^{-1}.) Whereas the abundance of organic carbon and nitrogen on effluent particles has not changed
matically during the last decade, POC and PN concentrations appear to be two to four times lower today
n they were in 1979. This is clearly due to the reduction in solids emissions that has resulted from improved
ırce control and treatment upgrades (SCCWRP 1989, 1991b). If we assume that the organic carbon content
he extractable organic matter in waste effluent is similar to that found in urban runoff (ca. 75%, Eganhouse
2), it can be shown that approximately 40% of the POC in wastewater effluent is extractable by organic
vents (TEO). Of this extractable POC, approximately 25% is made up of hydrocarbons, 45% by fats, and the
nainder by a complex assemblage of solvent-soluble polar compounds (Eganhouse 1982). Thus, more than
f of the POC in municipal wastewaters is composed of substances not easily separated by solvent extraction.
ese most likely include carbohydrates, proteins, lignin and other high molecular weight and/or strongly polar
)genic substances.

evious work (Eganhouse 1978; Eganhouse and Kaplan 1988; Eganhouse and Gossett 1991) has demonstrated
it after entering the marine environment, waste-derived organic matter undergoes rapid transformation with
ly the most stable molecular species surviving microbial attack. The effluent data developed in this study did
t reveal major differences in bulk composition among the three effluents. Consequently, one would not
pect the three effluents to vary with respect to their biodegradability. Based on our effluent degradation
periments, however, it would appear that other factors, such as pre-discharge chlorination, may play a role in
termining the kinetics of biodegradation during the sedimentation process.

general, the stable carbon isotopic composition of effluent particles is similar to, or slightly lighter than,
tural marine sedimentary organic matter in the southern California coastal zone (cf. Tables 3.3 and 3.20). In
incipal, this isotopic difference can be exploited to estimate the contribution of effluent-derived particulate
ganic carbon (or nitrogen) to waste-impacted sediments (e.g. Myers 1974; Eganhouse and Kaplan 1988;
veeney *et al.* 1980; Williams *et al.* 1992). The resolution of isotopic tracers, however, depends on the
fference in isotopic composition between the endmembers (i.e. marine POC and effluent POC) relative to the
riation in endmember compositions. Comparison of results obtained for effluent samples collected in 1990
ith those obtained by Eganhouse (1992) for 1979 effluent samples indicates that the carbon isotopic
)mposition of the PLTP and OCSD effluents has become isotopically heavier over the 11 yr span by as much
; 1-2 °/oo (i.e. approaching that of natural marine sediments). The change for the JWPCP effluent appears to
: less dramatic (ca. 0.5 °/oo). The explanation for this change is not obvious. One possibility is that a
:duction in the discharge of carbon-rich lipoidal or petroleum residues may have occurred as a result of source
)ntrol measures implemented over the last decade. Since these substances typically are more depleted in ^{13}C
ıan other forms of solvent-insoluble organic matter (carbohydrates, amino acids, etc.; Degens 1968), the POC
ould be expected have higher isotope ratios if less were present. However, comparison of data for the OCSD
nd PLTP effluent particulate TEO concentrations in 1979 (Eganhouse 1982; Eganhouse and Kaplan 1982b)
ith the present data (Table 3.7) does not reveal a consistent temporal trend. (Average TEO concentrations
)r the OCSD and PLTP effluents in 1979 were 215 mg g^{-1} and 360 mg g^{-1}, respectively.) Thus, we are left
ithout an acceptable explanation for the change in stable carbon isotopic composition of effluent particles over
ime. Moreover, use of carbon isotopes at the Orange County and Point Loma sites for estimation of effluent
npacts is no longer possible.

he nitrogen isotopes are a different matter. Here the isotopic composition of the effluent TN, although
ariable, is in the range of 0 to +3 °/oo. Marine particulate organic matter in the southern California Bight
ypically exhibits ratios of +7.5 to +10 °/oo (Eganhouse and Kaplan 1988; Sweeney *et al.* 1978; Sweeney and

1980a; Williams *et al.* 1992). The higher ratios of marine particulate nitrogen result from uptake (by lankton) of isotopically heavy nitrate inherited from the eastern tropical North Pacific where fication within the oxygen minimum zone is an important heterotrophic process (Cline and Kaplan 1975; d Kaplan 1989; Peters *et al.* 1978). Thus, there is a 4.5-7 per mil difference between endmember sitions. Sweeney *et al.* (1980), Sweeney and Kaplan (1980a, 1980b) and Eganhouse and Kaplan (1988) sed this difference to estimate the contribution of waste-derived nitrogen to outfall sediments off Palos s. Unfortunately, nitrogen isotope data for the OCSD and PLTP effluents did not exist prior to the time study. Judging from the data obtained for the JWPCP effluent in the late 1970s by Sweeney *et al.* (1980) r data for 1990, however, there does not appear to have been any change in nitrogen isotopic composition e last decade. In the subsequent discussion (Sediment Dynamics) we will attempt to estimate the ution of effluent-derived nitrogen to sediment trap particles and surface sediments at the three sites.

ace metal measurements made in this study, particularly the multielement scan, were expected to reveal al compositional variations among the effluents or between the effluents and uncontaminated sediments coastal zone. As in the case of the stable isotopes, such differences could be useful in differentiating from effluent-derived particles (e.g. Olmez *et al.* 1991). Despite the limitations of our data, there seems ttle difference in the trace metal composition among the three effluents examined here. The only major s the generally higher concentrations of all metals (by a factor of approximately two) found in the P effluent. This finding is consistent with results reported by SCCWRP (1991b) in which routine ring data supplied by the sanitation districts' in their respective annual reports were used. The latter e for total metal concentrations (i.e. dissolved + particulate). If one converts the particulate trace metal trations in these effluents (our data) to a volumetric basis (i.e. $\mu g\ l^{-1}$) and compares them with the total concentrations measured directly by the sanitation districts (Table 4.1), it is clear that the former usually nts a minor fraction of the total. This comparison assumes that the methods used by SCCWRP/WCAS the various sanitation agencies are comparable. If this assumption is correct, the comparison suggests e majority of the metals presently being discharged from these three plants are in the dissolved phase. ntrasts with the results of Galloway (1979) and Faisst (1976) who demonstrated in the early 1970s that t majority of most of the trace metals considered here (exception: Ni) were associated with filterable s (effluent and sludge, respectively). Based on equilibrium modeling, the dominance of the particulate was postulated to result from the formation of insoluble sulfides during anaerobic sludge digestion *et al.* 1975). Further experimental work by Chen *et al.* (1974) showed that the metals Cd, Cr, Cu, Hg, d Fe were principally found in the particulate phase of primary effluent (60-80% using 0.2 μm filter), s in secondary effluent the majority of the mass of these metals was found in the dissolved phase. Thus, ssible that the higher than expected dissolved phase fraction in contemporary southern California ts may reflect the dramatic improvements in waste treatment effected over the last two decades. This include the removal of sludge centrate from the waste steams of all three treatment plants.

of the extremely complex mixture of organic substances in wastewater effluent (cf. Eganhouse and 1982b), only two classes of trace organic compounds were identified and quantitated in this particular These substances have unique structures which carry very specific information. The linear alkylbenzenes fecal sterols, coprostanol and epicoprostanol, have been used as markers of anthropogenic ination in a wide variety of aquatic environments (Eganhouse *et al.* 1983a; Walker *et al.* 1982). They are ed in distinctly different ways, the former being a synthetic industrial product whereas the latter is ed biologically. However, they have been detected in all municipal wastewater effluents investigated thus

esence of long-chain linear alkylbenzenes in municipal wastewater effluent results directly from ant usage because these hydrocarbons are synthetic precursors of the most widely used anionic ants, the linear alkylbenzenesulfonates-LAS (Eganhouse and Kaplan 1982b; Eganhouse *et al.* 1983a). sulfonation, a small fraction of the LABs is left as a residue (<1%) and is carried with the LAS into nt formulations (Eganhouse *et al.*1983b; Takada and Ishiwatari 1987). In specific instances, inputs to streams due to surfactant usage can be augmented by industrial sources. Just such a case exists in rn California. During the studies of Eganhouse *et al.* (1983a), mass balance calculations were attempted r to evaluate whether domestic detergent use could account for the concentrations of LABs in the

P effluent. Only 13% of the LABs in the effluent could be attributed to domestic detergent usage. quently, it has been learned that the JWPCP serves one of only two LAB manufacturing plants in the United States. This industrial source undoubtedly accounts for the unusually high concentrations ed in JWPCP's effluent in 1979 (see Table 3.7) when compared with other effluents, such as the South Sewage District (SESD) plant in Salem, Massachusetts, and the poor mass balance mentioned above. A r situation exists in Boston Harbor where one of the two treatment plants discharging to harbor waters, it Island Plant (Table 3.7), receives influent from a LAB sulfonating facility. Not surprisingly, effluent his plant has highly variable and unusually large (peak) concentrations of LABs (Eganhouse and lom 1991; Sherblom 1990).

ination of data in Table 3.7 reveals that the present day LAB concentrations in the JWPCP effluent are cantly lower than they were in 1979. Possible explanations for this may be: 1) reduced suspended solids ntrations due to improved treatment, 2) source control of the LAB manufacturing plant effluent or 3) ed production rates by the LAB manufacturing plant. We cannot entirely exclude any of these possibilities present time. However, it is clear the particulate-based LAB concentrations have also declined since For this reason and because the isomer patterns of the phenyldodecanes (Figure 3.2) do not indicate cant degradation of the LABs (Takada and Ishiwatari 1987), it is more likely that direct source control r reduced industrial production are responsible for the decline than enhanced treatment. An analogous on now exists in Boston Harbor where effective source control measures have brought about a dramatic tion in oil and grease (and presumably particulate LAB) emissions from the sulfonating plant discharging Nut Island facility (M. Ross 1991, personal communication). Corresponding decreases in effluent LAB ntrations have been observed at the Nut Island Plant (cf. Battelle Ocean Sciences 1991; Sherblom 1990).

. Sediment Dynamics

rous researchers in southern California have undertaken studies of the behavior and fate of ocean- rged wastewater particles (Eganhouse and Kaplan 1988; Faisst 1976; Galloway 1979; Hendricks 1978, Herring and Abati 1978; Jackson 1982; Kettenring 1981; Morel *et al.* 1975; Myers 1974; Rohatgi and Chen Stull *et al.* 1986; Sweeney *et al.* 1980; Wang 1988; among others). The purpose of this section is not to v in detail the results of these various studies. Instead, we attempt to interpret the geochemical data oped in this project in terms of the fate of effluent particles during sedimentation. For practical reasons scussion is divided into subsections corresponding to each of the three study sites.

2.a. White Point. The only analyses performed on surface sediments from the Palos Verdes Shelf in this were for $\delta^{13}C$ and $\delta^{15}N$. Consequently, most of the following discussion must rely upon data we ted for sediment trap and effluent particles along with historical (literature) data for sediments.

ediment trap particles have TOC and TN concentrations that are approximately 8-10 times lower than the CP effluent particles. This difference cannot be explained by biodegradation alone as Myers' (1974) iments showed a reduction in TOC content of only 30%. It is more likely that the sediment trap particles porate lithogenic materials derived from the land *via* runoff, aeolian transport or coastal erosion (e.g. the guese Bend landslide). The effluent particles are, thus, diluted. The consistent trend of higher organic r concentrations with increasing trap elevation indicates that either the upper trap receives a greater input ganic-rich particles and/or that finer grained sediments resuspended from the sea floor are more abundant upper traps. The latter would be expected to bring about higher TOC concentrations because of the se relationship between particle size and organic matter content (Thompson *et al.* 1987) and the tendency er particles to remain in suspension longer than large particles. Since finer grained particles seem to have C/N ratios in sludge (Table 3.32), it is perhaps not surprising that the C/N ratio of the sediment trap les decreases with increasing trap elevation.

ediment traps deployed off White Point were located between stations 5C and 6C of the LACSD toring grid (Figure 2.6). The most recent TOC data for the 60 m stations on this grid were developed by nring (1981) who collected box cores in 1977. In the upper 1 cm of sediments collected at stations 5C and Kettenring found TOC concentrations of 6.8 and 8.7%, respectively. It is not clear that these concentrations epresentative of surface sediments today, nor is it known if the particles collected in the near-bottom traps

derive from these locations. However, the higher TOC concentrations found in these nearby sediments (when compared with the trap particles) is consistent with observations made by Hendricks (1987) for TVS (total volatile solids) and DDT. Hendricks ascribed the disparity between sediment trap particle and surface sediment TVS concentrations to the fact that trapped particles were sourced from a wide area, not just in the immediate vicinity of the trap moorings.

The TOC concentration of the sediment trap particles most closely resembles that of flocculent material collected in shallower waters off Palos Verdes by Myers (1974) and Sweeney and Kaplan (1980b). Sweeney and Kaplan (1980b) reported concentrations ranging from 0.8-5.2% TOC, whereas Myers (1974) found concentrations of 1.8-3.2%. Sweeney and Kaplan (1980b) found an inverse relationship between the C/N ratio and $\delta^{15}N$ value of the flocculents. Most of the samples having low isotope ratios, indicative of the presence of effluent nitrogen (i.e. $\delta^{15}N = +3$ to $+5‰$), exhibited C/N ratios in the range of 8 to 12. These ratios are, likewise, consistent with the present data (Table 3.11). Recently, Williams *et al.* (1992) reported results of elemental analyses on sediment trap particles collected at a depth of 100 m (a short distance below the euphotic zone) over the shelf and central portions of Santa Monica Basin (water depths: 395 and 910 m, respectively). Based on its isotopic composition, the organic matter in the sediment trap particles is believed to have only a small contribution from terrestrial sources (7-8%, including municipal wastes) being largely autochthonous (derived from marine production). The C/N ratios for these particles range from 6.5-7. Thus, it may be concluded that a third possible cause for the lower C/N ratios of the upper traps is a greater influence of sinking marine particulate matter at higher trap elevations.

The organic carbon content and C/N ratio provide only a gross assessment of the possible sources of particulate matter to the sediments and sediment traps. In order to draw more definitive conclusions, other indicators such as isotopic composition or the presence of marker compounds must be exploited. Data shown in Tables 3.3, 3.12 and 3.20 can be used to estimate the contributions of effluent and marine organic matter according to the following mixing equation:

$$F_w(X) = (\delta_s - \delta_m)/(\delta_w - \delta_m) \qquad (4.1)$$

where: $F_w(X)$ is the fraction of waste-derived organic matter based on the isotopic composition of element X,

δ_s is the isotopic composition of the sample,

δ_w is the isotopic composition of the refractory fraction of waste effluent, and

δ_m is the isotopic composition of the refractory fraction of marine particulate matter.

Computations of this sort have been made previously for sediments and flocculents collected off Palos Verdes (Eganhouse and Kaplan 1988; Myers 1974; Sweeney and Kaplan 1980b). In these cases several assumptions have usually been made: 1) only two sources of organic matter, marine and effluent, are present, 2) the isotopic compositions of the two endmembers are different and 3) these differences are maintained (i.e. isotopic composition is conservative) following deposition of the particles on the sea floor. The first assumption appears to be valid based on evidence of only minor amounts of terrestrially-derived, non-waste organic matter (exemplified by the higher plant waxes) in contaminated sediments from the Palos Verdes Shelf (Eganhouse and Kaplan 1988). As for the second assumption, the precision of isotope-based estimates will be determined by the variations in endmember isotopic composition (δ_w, δ_m) *versus* the difference between their isotopic compositions ($\delta_w - \delta_m$). Consequently, the carbon isotopes offer much less ability to detect the influence of effluent particulate matter than do the nitrogen isotopes ($[(\delta_w - \delta_m)_N] \sim 5.5‰$; $[(\delta_w - \delta_m)_C] \sim 2‰$). The third assumption is largely supported by studies carried out by Peters *et al.* (1978) that show the isotopic composition of sedimentary organic matter in the coastal zone to be largely inherited from that of the inorganic nutrients from which the organic matter was produced (e.g. carbon: CO_2, HCO_3^-; nitrogen: N_2, NO_3^-). Nevertheless, diagenetic alteration of organic matter would likely tend to cause further variations in the isotopic composition of the source materials.

lata in Tables 3.3, 3.12 and 3.20 indicate that the surface sediments collected off White Point are not nced by the effluent on the basis of stable carbon isotopic composition. This result is undoubtedly due in o the previously mentioned increase in $\delta^{13}C$ of the JWPCP effluent particulate matter over the last le (decreasing $[\delta_w - \delta_m]$). By contrast, the nitrogen isotope ratios of the sediments and trap particles ly show the influence of effluent nitrogen. Moreover, particles collected during the trap deployment of 0 exhibit consistently lower nitrogen isotope ratios at all elevations than those collected during the 3/89 deployment. This suggests that the particles collected on these two occasions either came from ent areas of the shelf (cf. Sweeney *et al.* 1980) and/or were receiving varying contributions of relatively uted effluent (*versus* resuspended sediments). There is no apparent trend in the isotope data with trap tion. This is not surprising given the variability in the source compositions (Table 3.3) and the weak trends l for TOC and TN concentration *versus* trap elevation (Table 3.11).

e 4.2 provides estimates of the fraction of effluent-derived nitrogen and carbon based on data given in es 3.3, 3.12, and 3.20. In the case of the carbon estimates, the assumption was made that a 0.5 °/oo tion of ^{13}C occurs during early diagenetic alteration of effluent carbon (cf. Eganhouse and Kaplan 1988; rs 1974). A marine endmember composition of -22 °/oo was chosen in order to be consistent with house and Kaplan (1988). In the case of nitrogen, estimates are presented based on two endmember positions: 1) $\delta_m = +7.8$ °/oo, $\delta_w = +3.15$ °/oo, 2) $\delta_m = +7.6$ °/oo, $\delta_w = +2.0$ °/oo. These compositions are what arbitrary but they should safely bracket the range of possible estimates for F_w (cf. Eganhouse and an 1988). The results based on the carbon isotopes indicate that a significant fraction of the sediment trap culate carbon (ca. 30-40%) is derived from the effluent. This is in contrast to the $\delta^{13}C$ data for sediments cted near the traps. The estimates based on nitrogen isotopes show a much greater influence of the ent particles (45-100%) on both sediment trap particles and nearby sediments. The estimates for the 90 deployment indicate a greater contribution of effluent nitrogen than the 11/28/89 deployment.

her information concerning the origin of the sediment trap particles is obtained from the trace metal yses. Comparison of the lead (Pb) and cadmium concentrations in the sediment trap particles indicates that are approximately 6-10 and nearly 20 times higher, respectively, than "average background" concentrations elf sediments (Katz and Kaplan 1981). These concentrations are, however, quite similar to, albeit slightly r than, those determined for the JWPCP effluent particles (compare Tables 3.4 and 3.13). Katz and lan (1981) indicated that the ratio of the "average background" concentrations of Pb and Cd in the southern fornia Bight was about 24. This is in contrast to the mean annual JWPCP effluent concentration ratio rted by Shafer (1978) of 7.6 and data developed in this study (Table 3.4; Pb/Cd=8.4-10.8). Kettenring 1) carried out analyses on sediment cores from the LACSD monitoring stations along the 60 meter isobath. results show that near the outfalls (e.g. stations 7C, 6C) the Pb/Cd ratios were low (5-10) and similar to the ent ratio. At greater distance from the outfalls, the ratios increase (5C: 7-11.5; 4C: 10-26; 3C: 10-20; 2C: 7). This trend is consistent with simple mixing of "background" sediments and effluent-derived particles tz and Kaplan 1981). However, higher ratios are often found in the upper portions of these cores. This ern may reflect some preferential loss of Cd relative to Pb from effluent particles following discharge (Chen Hendricks 1974; Kettenring 1981). Kettenring (1981) noted that the apparent onset of Cd mobilization urred between stations 4C and 5C. This corresponded approximately to the outer boundary of the reducing e (sulfide field) at that time. Comparison of the sediment trap Pb/Cd ratios in Table 3.13 with data for the uent particles and sediments from the vicinity of the outfall system (Kettenring 1981) all indicate that ticles collected in the near bottom traps are heavily contaminated with effluent-derived material. No trends h respect to time of collection or trap elevation are evident, but this again is to be expected considering the iability in effluent compositions.

e effluent and sediment trap multielement distributions (Tables 3.5 and 3.14) are essentially identical (please e that the Cd result for JWPCP sample collected on 7/6/90 is anomalously high). Of the elements ermined in this study, Ni is one of the most likely to be mobilized by oxidation during sedimentation of uent particles (Chen and Hendricks 1974; Faisst 1976; Lu and Chen 1977; Morel *et al.* 1975; Rohatgi and en 1975). If effluent particles settled rapidly through the water column without significant trace metal ease, one might expect to see Ni/Pb ratios that were similar for the two materials. The data in Tables 3.5

14 indicate that the effluent particles have Ni/Pb ratios of 0.51-0.69 whereas the sediment trap particles atios in the range 0.51-0.63. Galloway (1979) and Faisst (1976) reported Ni/Pb (particulate) ratios for P final effluent and sludge in the early 1970s of 0.42 and 0.44, respectively. By contrast, Kettenring (1981) Ni/Pb ratios for sediment cores collected along the 60 meter isobath that never exceeded approximately These results suggest that the trace element burden of the sediment trap particles is largely derived from ly-discharged effluent, not resuspension of older sediments. The definition of recently discharged is matic (i.e., one does know the time required for release of Ni), but the lack of evidence of Ni zation is consistent with the hypothesis that particles collected in the near-bottom sediment traps are not ly influenced by resuspension of historical deposits.

ncentrations of linear alkylbenzenes in the effluent range from 170-390 $\mu g\ g^{-1}$. By comparison, the um concentration found in sediment trap particles is an order of magnitude lower (cs. 29 $\mu g\ g^{-1}$). When lized to organic carbon, however, the ΣLAB concentration ranges of sediment trap and effluent particles p (300-760 $\mu g\ g\ OC^{-1}$ *versus* 490-1280 $\mu g\ g\ OC^{-1}$). Furthermore, when the similarity of the effluent and nt trap isomer distributions are considered along with the fact that ΣLAB, ΣLAB_{OC} and TOC trations all increase with trap elevation (while $\delta^{15}N$ decreases) it is apparent that recently-discharged t is being introduced to the traps.

nd line of evidence pointing to the influence of recently-discharged effluent *versus* older sediments is the e abundance of LABs when compared with the tetrapropylene-based alkylbenzenes (TABs). The latter is of highly branched C_9- through C_{15}-benzenes synthesized by alkylation of tetrapropylene (Eganhouse The sulfonated derivatives of the TABs were used between ca. 1950 and the mid-1960s as surfactants ouse *et al.* 1983a). The TABs were abruptly phased out (and replaced by the LABs) because of the ence of their sulfonated analogs which led to foaming problems in wastewater treatment plants and water receiving waste effluents (Figure 4.1). Both the LABs and TABs have been found in the sediments off Verdes (Eganhouse *et al.* 1983a).

wn in Figure 4.1, the vertical distribution of the TABs off Palos Verdes is characterized by a subsurface tration maximum below depths at which the highest LAB concentrations are found. The overlapping s somewhat resemble the historical production and usage patterns during the 1950-1981 period ouse *et al.* 1983a) and document the history of waste emissions from the LACSD plant. The effluent ed in 1979 by Eganhouse and Kaplan (1982b) bore no traces of the TABs. The same is true of effluent s collected in the present study. Consequently, the observation of TABs in sediment trap particles be direct and unequivocal evidence of the resuspension of historically deposited sediments dating back at far as the mid-1960s. [Note: This does not require the resuspension of deeply buried sediments because vertical sediment mixing that has occurred off Palos Verdes (Eganhouse *et al.* 1983a).] Figure 4.2 shows fragmentogram (m/z = 119) of the F2 fraction isolated from particles collected in the sediment trap ed 6/8/90 (0.5 m elevation). Also shown is a mass fragmentogram (m/z=119) for the LAB calibration rd. This m/z=119 ion ($C_9H_{11}^+$) is diagnostic for the highly branched TABs (Eganhouse 1985; ouse *et al.* 1983b). Because of the dominant cleavage at the beta position, the 3-phenylalkanes produce gest 119 peaks among the LABs. Comparison of these mass fragmentograms shows that the composition lkylbenzenes in the sediment trap sample is considerably more complex than the LAB calibration (although the LABs, noted as filled peaks, are clearly present). Furthermore, the assemblage very y resembles a 1:1 mixture of unaltered LABs and TABs as illustrated in Eganhouse *et al.* (1983b-see 4, m/z 119). For confirmation that TABs were present, we examined the mass spectra of several peaks ng the one labelled TAB_1 in Figure 4.2a (sediment trap sample). The mass spectrum of this peak did not molecular ion. However, its retention time and mass spectrum were otherwise identical with a major B identified in Palos Verdes sediments by Eganhouse *et al.* (1983a-see Figure 2a). The mass spectrum ot resemble that of an LAB (where beta cleavage yields two diagnostic ions), and the retention time s a branched alkyl side chain (i.e. elution of a C_{12}-benzene before any of the secondary phenyldodecane s-see Figure 4.2). This represents clear evidence of the presence of TABs in the sediment trap samples.

.3 provides data on the ratio of 3-phenyldodecane, a LAB isomer, to that of TAB_1 in the sediment trap s collected in this study and sediments collected in 1981 by the LACSD from station 3C (for location see

re 2.6). Both of these compounds are significant components of their respective alkylbenzene classes and ree of intergroup (i.e. LAB/TAB) interferences (Eganhouse 1985; Eganhouse *et al.* 1983b). The 3ϕ-cane/TAB_1 ratio is used here as an index of the relative contributions of recently-discharged effluent and spended older sediments. (Higher ratios imply a greater influence of the former.) Although we do not yet 3ϕ-dodecane/TAB_1 ratios for sediments collected off White Point in 1990, the ratios observed in the 3C ice sediments (0-6 cm) collected in 1981 (Eganhouse *et al.* 1983a) fall in the range of 1-1.6. At greater sub-om depths in this sediment core the ratios decline as the TABs become more abundant (due to higher e rates in earlier times and possible degradation of the LABs-see Figure 4.1). The ratios found in the nent trap particles collected during the 11/28/89 and 6/8/90 deployments fall in the range of 1.4-2.3 and -0.84, respectively. In the specific case of the 11/28/89 deployment, the ratio tends to increase with trap ation. The 1981 surface sediment ratios and the sediment trap particle ratios overlap, indicating a ificant influence from resuspension of historically-deposited surface sediments.

ortunately, it is not possible from these data to quantify the relative abundance of the older contaminated ments in the sediment trap samples (as opposed to effluent that was more recently discharged) because the) of the source material is not accurately known. Also, there are uncertainties related to the relative ilities of the LAB and TAB compounds. However, Eganhouse *et al.* (1983a) have shown that the LABs in ace sediments at station 3C are degraded as indicated by the depletion of the external isomers. Therefore, ixture of resuspended surface sediments with contemporary undegraded effluent particles would likely duce an LAB isomer pattern intermediate between the effluent and the sediments. To facilitate this parison we introduce a parameter proposed by Takada and Ishiwatari (1987), the I/E ratio (Table 4.3). s ratio equals the summation of 6-phenyl and 5-phenyldodecanes divided by the summation of 4-phenyl-, 3-nyl- and 2-phenyldodecanes. Higher ratios indicate a greater degree of biodegradation (Eganhouse *et al.* 3a; Takada and Ishiwatari 1987, 1989).

effluent I/E ratios are approximately 0.8 whereas the sediment trap particle ratios range from 0.8 to 1.1. comparison, the surface sediments collected from station 3C in 1981 had ratios of 1.4 to >2.3 with values easing at greater sub-bottom depths (as a result of biodegradation). If it is assumed that the I/E ratios nd by Eganhouse *et al.* (1983a) at station 3C in 1981 are representative of those of present-day surface iments off Palos Verdes, the sediment trap samples would appear to be dominated by recently-discharged . undegraded) effluent. Moreover, the higher I/E ratios found for the traps at lower elevations (e.g. 0.5 m) icates a higher proportion of the more heavily degraded materials derived from the sediments. The increase he 3ϕ-dodecane/TAB_1 ratio and corresponding decrease in the I/E ratio with trap elevation for the '28/89 trap deployment strongly suggests a vertical gradient in relatively unaltered effluent particles *vs.* older liment inputs near the sea floor.

kada and Ishiwatari (1989) have shown that under aerobic conditions the LABs in wastewater effluent are idly degraded within a matter of days. The degradation can be monitored by the change in I/E ratio as own in Figure 4.3. In the succeeding discussion we assume that the degradation experiments of Takada and iwatari (1989) are generally applicable to the LACSD effluent and the waters off Palos Verdes. If all of the LBs associated with the sediment trap particles were derived from contemporary JWPCP effluent, the served difference in I/E ratio (0.8-$\leq$1.1) would imply a degree of degradation of $\leq$20-25% and a residence ie in the ocean of no more than about 2 d. The latter is consistent with model predictions for the transport of luent particles (*via* settling and possible resuspension). However, the presence of significant amounts of LBs in the sediment traps at all elevations clearly indicates a contribution of particulate matter from older diments (predating current discharges by at least 25 yr) I/E ratios $\geq$1.4) it is clear that a significant portion of e difference between effluent and sediment trap I/E ratios could be explained by simple mixing of recently-scharged effluent and older sediments. Given these facts, it is difficult to conceive how the I/E ratio of the fluent particles could have changed very much during sedimentation. In other words, the effluent particles do ot appear to have undergone much, if any, biodegradation. Here, the results of the degradation experiment able 3.37) may provide a key.

the experiment summarized in Table 3.37 we found that the POC content of the JWPCP effluent increased ther than decreased over time. This behavior was opposite that observed for the Hyperion final effluent

whose POC concentration declined by about 16% over 4 d. The trends were interpreted as being the net result of competing processes of particle aggregation and decay, whereby the former exceeded the latter in the case of the JWPCP effluent. One major difference between the treatment of these two effluents is that chlorination is used more or less continually by the JWPCP to reduce the abundance of pathogenic microorganisms. Although other causes may be involved, we hypothesize that the process of chlorination may have served to inhibit microbial activity on the JWPCP effluent particles thereby reducing their rate of degradation over the period of the experiment. Such inhibition could help explain the undegraded character of the LABs collected in the near-bottom traps. If such a process is operative off Palos Verdes, it would mean that measures presently being taken to reduce the emission of pathogenic microorganisms could be having the undesirable side effect of increasing the deposition of effluent particles (and attendant contaminants) to the nearby shelf.

IV.A.2.b. Orange County. The dataset for Orange County is limited because we were unable to obtain sediment cores at this site. Consequently, no vertical profiles of TOC, TN, Pb and Cd are available. Moreover, we did not carry out analyses of surface sediments for trace organics.

When compared with the other two effluents examined here, the OCSD effluent particles have somewhat higher TN concentrations. This has the effect of yielding lower C/N ratios for the OCSD effluent particles. The concentration of organic matter in the effluent is approximately 10-20 times higher than that of particles collected in the sediment traps. At the same time, the C/N ratio of the sediment trap particles (7.7-10) is significantly higher than that of the effluent (6.6-7.9). In addition, unlike the situation off White Point, the surface sediments have lower concentrations of TOC and TN than the sediment trap samples (by factors of 2-10). Generally speaking, there is a trend of increasing TOC and TN and lower C/N ratios with increasing trap elevations (similar to White Point). Together, these relations may signal the rapid decomposition and/or dilution of sinking effluent particles followed by resuspension of the organic-rich fines to waters overlying the sediments.

Unfortunately, the stable carbon isotopes are of little use in estimating the impact of effluent POC on the sediment trap particles. Nitrogen, on the other hand, provides a means for making such calculations. One feature of the present data is that the sediment trap particles are more enriched in ^{15}N than are the near-outfall surface sediments we examined (cf. Tables 3.12 and 3.20). This would seem to indicate that the source of the sediment trap particles is not exclusively the surface sediments near outfall. As in the case of the White Point trapping experiments, we found lower $\delta^{15}N$ values in the summer than in the winter deployment. These temporal relations are based on only a few data, and there are no obvious seasonal trends among the other measured parameters that would suggest a mechanism for such an isotopic shift. Until more data are collected the explanation for this variation in isotopic composition will remain obscure.

Computation of the fraction of effluent-derived nitrogen can be performed using endmember compositions of $\delta^{15}N_m = +7.6\ ^{o}/_{oo}$ and $\delta^{15}N_w = +0.55\ ^{o}/_{oo}$. The latter ratio was developed from the average of only two measurements made on the OCSD effluent (Table 3.3). The results show that from 31-46% of the TN in the sediment traps could be derived from the effluent and approximately 67% of the near-outfall sediment TN comes from the effluent. This result is most interesting because the stations at which the largest elevation in TN is observed are OC-0 and OC-ZB2. At these locations there are increases over "apparent background" TN concentrations (ca. 0.33%) of about 35-75%.

Little can be said of the trace metal data other than the fact that both lead and cadmium concentrations follow the order effluent > sediment trap > sediments. The Pb concentrations in surface sediments show little variation with location, and no enrichment of Pb is noted for the near-outfall site, OC-ZB2. Cadmium, on the other hand, appears to be more abundant in the vicinity of the outfall. Both elements are present at or near "background" levels for the southern California Bight (Pb = $15.0 \pm 2.0\ \mu g\ g^{-1}$, Cd = $0.3 \pm 0.2\ \mu g\ g^{-1}$) as judged by the data summarized by Katz and Kaplan (1981).

The concentration of LABs in the sediment trap particles (0.8-6.3 $\mu g\ g^{-1}$) ranges from 15 times to more than two orders of magnitude lower than that of the effluent particles (94-240 $\mu g\ g^{-1}$). Normalization of ΣLAB concentrations to TOC greatly reduces the discrepancy. Obviously, the sediment trap particles incorporate a

nificant amount of lithogenous material. No TABs were detected in the Orange County sediment trap nples, despite the fact that the LABs were easily measured in these samples and the discharge of TABs by OCSD in the past is a virtual certainty (Eganhouse *et al.* 1983a). One possible explanation for the absence TABs in the trap samples is that the OCSD first began discharging wastes from the present outfall (some 5 offshore at a depth of 60 m) in 1974. Prior to that time (1954-74) treated wastes were discharged from a le-long outfall discharging upcoast of the present pipe into 18 m of water (M. Moore 1991, personal nmunication). Consequently, it is unlikely that TAB-bearing effluent particles carried in OCSD waste eams from 1950 to the mid-1960s (when TABs were produced) would have accumulated in the vicinity of the sent-day outfall. Unfortunately, we have no sediment analyses for the long-chain alkylbenzenes with which compare the sediment trap results. As noted earlier, the sediment trap samples show degraded LAB isomer ofiles (I/E ratios of 1.16 to 2.22). The effluent I/E ratios were 0.88 and 1.05. As compared with the White int results, it would appear that the effluent particles collected by the sediment traps off Orange County have en reworked. Without further sediment analyses, however, it is impossible to say whether the residues are ming from resuspended older sediments or recently-discharged effluent particles that have been rapidly graded during sedimentation.

A.2.c. Point Loma. Sediment trap particles collected off Point Loma have TOC and TN concentrations 10-12 nes lower than those in the PLTP effluent particles. However, the C/N ratio is higher (8.6-10.7 for sediment ips; 6.5-10 for effluent-see Tables 3.2 and 3.11). These relationships are similar to those observed for the hite Point and Orange County sites and their respective effluents. Unlike the other sites, however, there does it seem to be a consistent trend in TOC, TN or C/N *versus* trap elevation. The TOC and TN concentrations surface sediments are uniformly lower than the sediment traps by factors of 2-4. C/N ratios are also nerally lower in the surface sediments, and they fall in a narrow range (7.0-8.9). One difficulty in this dataset the poor comparability between the TOC, TN concentrations and especially the C/N ratio for the surface diments (stns. SD A-5, SD A-16) and surface (0-2 cm) sections of cores taken at the same locations (Table 19). Given the relative uniformity of the C/N ratios for surface sediments collected throughout the Point oma outfall area, it is hard to understand why the C/N ratio in the upper sections of the cores are so different om sediments collected by the Van Veen grab. One possibility is that the corer may have blown away a gnificant portion of the surface sediments, revealing (and coring) older, more diagenetically-altered sediments. he only support for this hypothesis is the generally decreasing C/N ratios seen in both cores with increasing ib-bottom depth. This trend almost certainly reflects organic diagenesis (i.e. remineralization of sedimentary rganic matter).

he stable nitrogen isotope composition of both surface sediments and sediment trap particles is significantly ore enriched in ^{15}N than was found for the other two sites. Since the effluent $\delta^{15}N$ values fall in a similar nge (+1 to +3 °/oo), it can only be assumed that this indicates a smaller contribution of effluent particulate itrogen. Although there is no consistent relationship between $\delta^{15}N$ and trap elevation (similar to other sites), ie relationship between $\delta^{15}N$ and season previously noted for White Point and Orange County is again bserved. We computed F_w values for the Point Loma sediment trap samples and the upper sections of ediment cores SD A-5 and SD A-16 using endmember compositions as follows: $\delta^{15}N_w = +1.85$ °/oo, $^{15}N_m = +7.6$ °/oo (Table 4.4). From these calculations, only 10-20% of the nitrogen in sediment trap particles, nd 20-30% of the "surface" sediments near the outfall, appear to be derived from effluent. These estimates ndicate that the marine environment off Pt. Loma is significantly less impacted by the discharge of municipal astes than either the White Point or Orange County sites. The observation of higher isotope ratios in the ediment traps compared with the near-outfall sediments implies that effluent is effectively dispersed and that he effluent particles that reach the near-outfall bottom are not a major, long-term source of contamination to lowncurrent sites.

The concentration of Pb in sediment trap particles is about 3-5 times lower than in the effluent particles, but nearly twice that found in the surface sediments. As in the case of Orange County, the Pb and Cd concentrations measured in the surface sediments are very near the "average background" levels reported for he Southern California Bight by Katz and Kaplan (1981). Not surprisingly, it is difficult to discern any pattern n the distribution of Pb and Cd around the outfall, with the possible exception of an elevated Pb concentration at station SD X-2, just off the northwest leg of the wye (Figure 2.4, Table 3.21). Comparison of the core

nts, sediment trap particles, surface sediments and effluent particles on a Pb *vs.* TOC diagram (e.g. 3.11) reveals some interesting trends. The surface sediment data (not shown) plots to the left but very) the regression line for the core data. By contrast, the sediment trap particle data plots to the right of e and the effluent data are distributed to the far right. These relationships are contrary to what might be ed if simple mixing of effluent and "background" sediments was the dominant process. The enrichment of ⊃ in sediments when compared with the sediment trap and effluent samples indicates there may be a lary source of Pb and/or that the organic carbon-normalized Pb concentrations in the PLTP effluent ıigher in earlier times. The *greater* similarity between sediment trap and present-day effluent ıtrations (Pb/OC) when compared with the sediments collected in this study also implies that although pact of the outfalls is lower for the sediment traps than the near-outfall sediments, a greater proportion effluent-derived Pb in the sediment trap particles is probably coming from recently-discharged effluent ı the case of the sediments. Given the higher subsurface concentrations of Pb in the near-outfall ent cores, this might be explained by the introduction of older effluent-derived Pb residues to the ent-water interface. These statements will remain speculative until further data are collected.

oncentration of ΣLABs in the sediment trap particles is more than 100 times less than in PLTP effluent les. After normalization to organic carbon, the difference is only reduced to a factor of 10. This indicates ither the LABs are very extensively degraded (relative to effluent organic carbon) or that the effluent les are highly diluted by non-effluent particulate matter. Both hypotheses are consistent with the stable ıic results which indicate that only 10-20% of the TN is effluent-derived. The I/E ratios of the ıldodecanes in the two effluent samples tested were 0.84 and 0.92, similar to those observed for the ⊃P and OCSD effluents. By contrast, the sediment trap particles yielded I/E ratios in the range 1.2-2.1. ; same time, small amounts of TABs were found in the sediment trap and sediment samples (Table 4.5). ϕ-dodecane/TAB_1 ratios determined in the sediment trap samples range from 2.2-7.0, whereas the ;e (core) sediments yielded ratios of 1.45 and 1.05. This indicates that the LABs in the sediment trap ;les are probably largely derived from recently-discharged effluent (as opposed to historical sediment ;its), and that the extent of degradation indicated by the high I/E ratios may have resulted from rather ive breakdown of the effluent POC during sedimentation. Because trapping took place over long periods ıe relative to the kinetics of LAB decomposition (Figure 4.3), we cannot entirely rule out the possibility ome of the apparent degradation occurred subsequent to particle trapping. Such a process, however, ł not explain the relatively unaltered composition of the LABs in White Point sediment traps.

SIMULATIONS

liscussion of the simulation models and their predictions can be divided into two parts. First, we use the lations to examine some of the differences between the two models and the uncertainties introduced into imulation process by uncertainties in the input data. Second, we compare the characteristics of sediments icted by the models with the characteristics of sediments obtained from measurements.

.1. Model Differences and Consequences

.1.a. Wastefield Suspended Solids Concentrations. For aggregating particles, the rate of aggregation, cle settling speeds, and depositional flux all depend on the concentration of suspended solids in the efield. For typical southern California coastal waters, the fraction of the wastefield particles deposited in a area in the immediate vicinity of an ocean outfall is approximately proportional to the square of the initial entration of suspended solids in the wastefield (Hendricks and Eganhouse 1990). Two sources contribute e concentration of suspended solids in the wastefield: (1) effluent particles discharged from the outfall and ıatural particles settling into the wastefield from the overlying water column or entrained into the wastefield ng the initial dilution process.

3.1.a.i Effluent Suspended Solids Concentration. The two models use different methods to estimate the al concentration of effluent suspended solids in the wastefield. *DECAL* uses a mass balance approach d on the mass emissions of effluent suspended solids, the length and orientation of the diffuser relative to ocean currents, the vertical extent of the wastefield, and a simplified description of the tidal and slowly- ing components of the ocean currents to estimate this concentration. On the other hand, *SED2D* uses a ılation model of the initial dilution process (TSLINE) to produce a statistical summary of the dilution

teristics. These characteristics are then used, in combination with the concentration of suspended solids effluent, to compute the initial concentration of suspended solids in the wastefield.

nation of the initial concentrations of suspended solids in the wastefield predicted by the two models this study show that the two methods produce significantly different results for southern California ipal wastewater ocean outfalls. Table 4.6 compares the "average" initial dilutions predicted by TSLINE D) with those predicted by *DECAL*. The average initial dilutions predicted by TSLINE are about 2-6 larger than the average initial dilutions predicted by *DECAL*.

ver, these two average initial dilutions may not be directly comparable. The "average dilution" can be d in several ways. One measure is based on the spatially-averaged concentration:

$$\frac{1}{S_a} = \frac{C_s}{C_0} = \frac{1}{C_0} \frac{\int_{h_l}^{h_u} C(z)\, dz}{h_u - h_l} \tag{4.2}$$

h_u and h_l are the upper and lower "boundaries" of the wastefield and C_s is the average concentration. If ncentration of effluent in the wastefield is unity, then we define the spatially averaged initial dilution as the regulatory definition for the dilution often corresponds to $[1+C_s]^{-1}$ --but the difference is minor for 1). The two wastefield boundaries, h_u and h_l, are defined as the upper and lower boundaries of the ield where the concentration falls to 5% of the maximum concentration within the wastefield (Roberts et 9a). The concentration C_s is the value obtained by collecting equal volumes of wastefield water at m intervals across the wastefield, mixing them together, and then measuring the concentration. For on subthermocline ocean current speeds in southern California coastal waters, the spatial average initial n is about twice the dilution at the level of maximum concentration of effluent within the wastefield rts *et al.* 1989a).

ernate measure is the flow-averaged initial dilution, defined by:

$$\frac{1}{S_v} = \frac{C_v}{C_0} = \frac{1}{C_0} \frac{\int_{h_l}^{h_u} C(z)\, V(z)\, dz}{\int_{h_l}^{h_u} V(z)\, dz} \tag{4.3}$$

v(z) is the discharge-induced flow at the depth, z, within the wastefield and C_f is the flow averaged ntration. The flow-averaged initial dilution is often used in regulatory requirements. This is the dilution ied by sampling in the same manner as before, but at each depth collecting a sample volume proportional discharge-induced flow at that depth. Roberts (1990) estimates that the flow-averaged initial dilution is 1.15-1.20 times greater than the minimum dilution within the wastefield. Thus the flow-averaged initial on will be about 58-60% of the spatial average dilution..

DECAL formalism, it is assumed that there are no gradients in the suspended solids concentration or the elocity within the wastefield. Thus the spatial and flow averaged initial dilutions are identical. Table 4.7 ares the flow-averaged initial dilutions predicted by TSLINE with the average initial dilutions predicted by *AL*.

redicted flow-averaged initial dilutions are clearly in better agreement than are the spatial-average initial ons. However, the values predicted by TSLINE for the San Diego and Orange County outfall sites are .5-3.5 times greater than those predicted by *DECAL*. Only for the Los Angeles County site are the two ons comparable.

ot clear if the spatially-averaged or flow-averaged initial dilution (or some other value) should be used to ate the "effective" concentration of suspended solids within the wastefield. For the low values of current

n the ocean, aggregation should be dominated by differential settling and Browinan motion (Farley and 1990). If aggregation associated with Brownian motion dominates (low suspended solids trations), the aggregation rate is approximately proportional to the concentration of suspended solids the wastefield. In this case, the spatially-averaged value of the initial dilution is appropriate and the ion rate of effluent particles predicted by *DECAL* would be expected to be about 1.8-6.2 times greater at ites than the rate predicted from the TSLINE estimates. If aggregation due to differential settling ites (high suspended solids concentrations), the aggregation rate is roughly proportional to the square of ncentration. In this case the flow averaged dilution is the appropriate measure (i.e. the concentration and y tend to covary within the wastefield so the integrand of the numerator in equation 4.2 provides an e of the average value of c^2). In that case, the deposition predicted by *DECAL* would be expected to that predicted by *SED2D* by a factor ranging from of 1.1-19. Thus if the effluent discharge is the sole of suspended solids in the wastefield, the deposition predicted by *DECAL* can frequently be significantly than that predicted by *SED2D*.

a.ii Natural Suspended Solids in the Wastefield. Natural particles also contribute to the suspended solids wastefield through sedimentation from the overlying layer of water and by entrainment into the plume the initial dilution process. The potential significance of these sources can be estimated by comparing oncentration with the concentration of effluent solids within the wastefield.

tial concentrations of effluent suspended solids in the wastefield for our base simulation periods range .083 mg l^{-1} (Orange County) to 0.43 mg l^{-1} (Los Angeles County) using the TSLINE predicted initial as, and from 0.51 mg l^{-1} (Orange County) to 0.75 mg l^{-1} (Los Angeles County, 90-inch) using the *DECAL* ions. Concentrations of natural suspended solids in the wastefield in the vicinity of the outfall diffuser dicted by *DECAL* to range from 0 to 0.42 mg l^{-1}, depending on the location and the rate of decay of material. Thus if the decay rate is slow (e.g. on the order of 0.1 d^{-1}), the concentration of natural s due to sedimentation from the overlying layer may be comparable to the concentration of effluent ded solids in the vicinity of the diffuser, and exceed the effluent particle concentration farther away from user.

her source of natural particles in the wastefield is associated with the entrainment of dilution water the initial dilution process. In *DECAL*, it is assumed that this concentration is negligible compared with ncentration of effluent suspended solids and natural suspended solids from the overlying water. However, er measurements of suspended solids in southern California coastal waters in water depths comparable tfall depths indicate that typical concentrations are on the order of 1-3 mg l^{-1}. For typical initial dilution the concentration of entrained natural suspended solids in the wastefield will be virtually the same as in ural waters. The potential significance of these entrained natural particles in the aggregation process can nined by comparing the contributions of suspended solids from the three sources. These concentrations nmarized in Table 4.8.

his table, we see that the entrainment of natural suspended solids into the wastefield contributes more percent of the initial total suspended solids concentration in the *SED2D* simulations, and would ute more than 55 percent of the total suspended solids concentration in the *DECAL* simulations if ment were included into the simulation process.

ase of the *SED2D* simulations, the inclusion of entrained natural suspended solids will increase the ion rate in the immediate vicinity of the outfall to roughly 13-40 times higher (Los Angeles County, County, respectively) than the corresponding rate if entrainment had not been included. From these trations, we also estimate that the deposition rates would have been increased by a factor of about seven ngeles County, 120-inch) to nine (Orange County) if the initial suspended solids concentration had been ed by an additional 2 mg l^{-1}. Since the entrainment of natural particles makes such an important ution to the deposition of wastefield suspended solids in the *SED2D* simulations, but is not included in *CAL* simulations, the *SED2D* predicted deposition rates exceed the rates predicted by *DECAL* at each imulation sites--even though the concentration of effluent suspended solids in the wastefield was higher *DECAL* simulations.

3.1.b. Initial Distribution of Particle Settling Speeds. *DECAL* and *SED2D* simulations for aggregating icles use equations 1.25 and 1.27 to compute the flux of particle mass out of the wastefield and their settling eds. These equations were derived under the assumption that the initial distribution of particle sizes ranges n 0.06-1.5 μm. Particles of this size have exceedingly slow settling speeds (e.g. $<4x10^{-9}$ cm s^{-1}, or $3x10^{-6}$ $^{-1}$). Because of these small settling speeds, they essentially will not settle to the bottom until they aggregate faster settling particles. The use of settling columns to estimate effluent particle settling speeds is often icized on the basis that aggregation is not adequately simulated within the column (due to its short length the lack of mixing), so that the deposition of particles in the effluent will be underestimated.

mmediately following initial dilution, the effluent particles have the distribution of particle sizes assumed in derivation the aggregation equations, virtually no deposition would be expected in the column (or at least regation and the accompanying deposition should proceed at a very slow rate). The mass distribution of ling speeds of Los Angeles County final effluent (in 1973), as measured with a short settling column, is wn in Figure 2.24. Approximately 3.7% of the particle mass was associated with settling speeds in excess of cm s^{-1} (86 m d^{-1}), and about 13% was associated with settling speeds in excess of 0.01 cm s^{-1} (8.6 m d^{-1}). is indicates that a significant fraction of the particle mass initially is associated with particles that have ensions that greatly exceed the dimensions of the initial distribution in the aggregation simulations. These ling speeds are sufficiently rapid to produce a significant flux of effluent particles to the ocean bottom within vicinity of the outfall diffuser. Consider, for example, the case of a wastefield that lies 10 m above the ocean tom moving with an ocean current of 2-3 cm s^{-1} and tidal excursions of about 1 km. In the absence of sequent aggregation, approximately 3.7% of the effluent suspended solids will settle to the bottom within ut 1200 m of the diffuser (i.e. within 2.8 hr after discharge), and 13% will settle within about 5 km of the charge.

he concentration of suspended solids in the wastefield is low, or the wastefield is thin, the deposition rate in vicinity of the outfall diffuser predicted from settling column measurements may exceed the rate predicted m the aggregation equations. Even for the relatively high suspended solids concentrations used in the *D2D* simulations (>2 mg l^{-1}), there is a brief initial period when the sedimentation of particles predicted ng the distribution in Figure 2.24, exceeds the rate predicted from the aggregation equations (see Figure 9). It is probably reasonable to interpret the depositional fluxes of wastefield-related suspended solids based settling column studies as a lower bound estimate for the actual depositional rates. At the present time, re is no way to modify the aggregation rate and settling speed equations to represent the actual initial tribution of particle sizes. Until an appropriate representation is developed, perhaps an ad hoc approach can used to produce an adequate estimate. In this approach, the distribution of settling speeds measured with a tling column is used for the initial stages of the simulation. The computational procedure would then shift to aggregation equations when the settling speed predicted for of the aggregating particles exceeds the ximum (settling column) speed of the particles still remaining in the wastefield.

.B.1.c. Wastefield Thickness. The aggregation equations also assume that the properties of the wastefield are nstant within its boundaries. In both the *SED2D* and *DECAL* simulations, we used the median thickness of e wastefield (as predicted by TSLINE) to estimate this thickness. Examination of the distribution of dicators of wastefield constituents in the water column (e.g., Figures 1.4a,b,c,d) indicates that the wastefield es not consist of a homogeneous region with sharply defined upper and lower boundaries. Therefore, the ecise thickness of the wastefield is not well defined from the standpoint of using this dimension in the gregation simulations. In the absence of specific studies of the aggregation process under these rcumstances, we estimate that the use of the 5% concentration level to define the wastefield thickness oberts *et al.* 1989a) probably is an overestimate of the wastefield thickness from the standpoint of the gregation simulations. Use of a smaller wastefield thickness would result in smaller predicted deposition tes.

n the other hand, since the initial thickness of the wastefield varies with changes in the density structure of the ater column (and the aggregation rate equation depends on this thickness in a nonlinear manner), some ldditional inaccuracies may be introduced by using the median thickness. For aggregation dominated by

ntial settling, we would expect that use of the median thickness of the wastefield would underestimate the ition rate. Thus, to some extent, the effects of these two uncertainties will probably tend to offset each

ver the initial thickness of the wastefield, the thickness of the wastefield may change as it moves away he outfall. Processes that can result in a thicker wastefield include vertical mixing and the return of the ield to the vicinity of the diffuser by a reversal in the ocean currents. Processes that can thin the ield include current shear (e.g. changes in the strength and direction of the cross-shore motion with ng position in the water column--Hendricks 1990) and the gravitational collapse and spreading of the ield due to density imbalances (e.g. Wu 1969; Amen and Maxworthy 1980; Roberts *et al.* 1989b). A nt wastefield thickness is assumed in the *DECAL* simulations. The *SED2D* model allows for a thinning of stefield, using an approximate relationship describing gravitational collapse (Hendricks 1990). The site tions with *SED2D* assumed a thinning wastefield, with the rate of collapse computed from the density ire of the ambient water column at typical wastefield depths as recorded in the San Diego data. There is oncern that an actual wastefield will not collapse as rapidly as indicated in the studies mentioned above igure 1.3). The laboratory studies also indicate that as the density stratification becomes weaker (and epresentative of ocean conditions), frictional effects become more important and reduce the rate of ing. In the executing the *SED2D* simulations, we assumed that some thinning of the wastefield was likely ue to current shear), but thickening was less likely. This assumption will result in an underestimation of osition rate if the wastefield thickness actually remains constant. An example of this difference is ed in the following section (Figure 4.7). In the absence of thinning, the fraction of the wastefield particle eposited on the bottom will be on the order of two times the rate estimated in the *SED2D* simulations elapsed time of 2 d, and about 50-65% greater for an elapsed time of 1 week.

d. Effective Wastefield Thickness. There is a potentially much more serious uncertainty involved with ig the magnitude of the middle layer (westfield) thickness. As we noted earlier, the aggregation ns were derived on the assumption that the wastefield layer is fully mixed. A consequence of this mixing naintenance of a uniform concentration of suspended solids within the layer and vertical recirculation of ating particles. This recirculation carries aggregate particles back to the top of the wastefield, where n resettle and continue the aggregation process. If mixing within the layer of water is suppressed, the in the distribution of suspended solids within the layer, and the reduction in the recirculation of ate particles, can be expected to reduce both the rate of production and the settling speed of these s.

duced flux rate and diminished settling speed can be partially accounted for in the aggregation ions by using a smaller value for the "wastefield thickness." However, we note that since the flux from tefield layer and the settling speed of those particles have different dependencies on this thickness, this are will not be precise. In the subsequent discussions, we will use the term "effective thickness" for the f the layer thickness, H, that approximately yields the correct value for the flux rate of aggregate particles he wastefield layer. This effective layer thickness will be equal to, or less than, the actual vertical extent ayer--depending on the strength of the mixing. In the subsequent discussion, we will refer to the actual dimension of the wastefield as the "physical thickness" or simply the "thickness."

ing out both the *DECAL* and DPA (*SED2D*) simulations, we used the physical thickness of the ld layer for the aggregation calculations. It is not clear, however, that mixing within the wastefield is tly strong to justify this assumption. Figures 1.4a,b,c,d show the distribution of various water quality ters at four stations in the vicinity of an ocean outfall. From these distributions, it is evident that a ld was present in the depth interval between about 20m and 40 m at stations HR1, HR7, and HR50, but rom the water column at station HR11. Figure 4.5 shows the distribution of density (in sigma_t units) d from the salinity and temperature profiles in Figures 1.4a,b. It is difficult to distinguish significant in density gradients due to the presence or absence of the wastefield. The absence of a significant n in the density gradient within the wastefield, combined with the inhomogeneous distribution of the f water quality parameters, suggests that aggregation processes within this region of the water column proceeding less rapidly than assumed in our *DECAL* and *SED2D* simulations.

We tested the consistency of our aggregation calculations in the *SED2D* simulations by attempting to reproduce the observed concentration of natural suspended solids in the middle layer in the absence of a discharge. First, we assumed that the density stratification in the middle layer is independent of the presence or absence of a wastefield. In that case, we can use the aggregation equations in DPA to determine the steady-state concentration of natural particles in this layer for a specific flux of natural particles from the overlying water column. In our earlier *SED2D* simulations, we assumed a natural suspended solids concentration in the water column at this depth of 2 mg l^{-1}. If our use of a thickness of 25-30 m for the thickness of the wastefield region of the water column in the aggregation equations is correct, the concentration would remain constant since the flux of natural particles settling from the overlying layer into the middle layer is balanced by the loss of aggregate natural particles from the middle layer into the underlying (lower) layer of the water column and the decay of organic material.

Figure 4.6 shows this concentration as a function of simulated time after "starting" the simulation. The solid line represents the deposition assuming a sedimentation rate of 600 mg m^{-2} d^{-1} from the overlying layer of water (as used in the *SED2D* site simulations); the dashed line is for a flux of 2400 mg m^{-2} d^{-1} (the latter is probably represents an upper bound for this flux). It is immediately evident that the suspended solids concentration does not remain constant at 2 mg l^{-1}. Instead, it rapidly decays to a value of about 0.25 mg l^{-1} for a flux of 600 mg m^{-2} d^{-1} from the overlying water column, or 0.52 mg l^{-1} for a flux of 2400 mg m^{-2} d^{-1}. These asymptotic values are indicated by the two lower solid and dashed lines. In order to sustain a natural suspended solids concentration of 2 mg l^{-1}, the "effective thickness" of the middle layer would have to be reduced to about 0.4 m for a flux of 600 mg m^{-2} d^{-1}, or 1.9 m for a flux of 2400 mg m^{-2} d^{-1}. The upper solid and dashed lines indicate the middle layer suspended solids concentrations for these two effective mixing thicknesses (the slight drop at the beginning to about 1.98 mg l^{-1} is associated with a change in the composition of the middle layer suspended solids from the initial composition as they leave the overlying layer to the equilibrium composition in the middle layer).

Therefore, if the density structure of the water column is essentially independent of the presence or absence of a wastefield, the deposition rates predicted by both our *DECAL* and *SED2D* simulations may have been greatly overestimated. To examine the magnitude of this potential error, we calculated the time-dependent deposition of suspended solids from a layer with a thickness of 25 m, 17 m above the ocean bottom. The initial suspended solids concentration in the layer was 2.21 mg l^{-1}. Figure 4.7 shows the results of this simulation for three different simulation conditions. The solid line represents the deposition using the full thickness of the wastefield as the effective thickness--but the thickness of the layer is allowed to subsequently diminish due to gravitational spreading. This was the situation condition used in our earlier *SED2D* simulations. The dashed line represents the deposition for the same conditions--except that the thickness of the wastefield is held constant. In the absence of collapse, approximately 36% of the particle mass settles to the ocean bottom within the first day after they are discharged from the outfall, and about 59% of the mass settles within the first week. If the wastefield collapses, these values fall to 16% and 36%.

The dot-dash line represents the sedimentation for a layer with a physical thickness of 25 m, but an effective thickness for the aggregation process of only 1.9 m. The flux of natural particles into the wastefield from the overlying layer was 2400 mg m^{-2} d^{-1} so that steady-state conditions would be maintained in the absence of the discharge. No deposition occurs within the first 6 d after the particles leave the outfall. The first deposition occurs near the beginning of the seventh day, leading to about 8% of the initial mass of suspended solids in the wastefield deposited on the ocean bottom during the first week after they are discharged. This is only about 22% of the deposition that occurs during the first day if the initial effective thickness is 25 m.

Because of the long delay between when the particles are discharged, and when they reach the bottom, they will be spread over a large area. For example, Figure 4.8 shows the longshore depositional probability for the Orange County area (during a 45 min interval) beginning with an elapsed time of 151.50 hr. The distribution is nearly flat, with some hint of a broad peak approximately five cells (2 km) upcoast from the diffuser. This distribution is far different from the strong depositional peak associated with an effective wastefield thickness of 25 m (e.g., see Figure 3.46a). At the same time, the flux is greatly reduced. For an effective thickness of 1.9 m,

the depositional flux in the immediate vicinity of the discharge is estimated to be about 2-4 mg cm^{-2} yr^{-1}. This is about $1/300^{th}$ the flux of 950 mg cm^{-2} yr^{-1} when the full wastefield thickness is used. If the depositional flux from the overlying waster column is 600 mg cm^{-2} yr^{-1}, and the effective thickness is only about 0.4 m, no deposition will occur under these conditions during the first week after discharge (neglecting, of course, the deposition of particles in the effluent that have settling speeds in excess of about 0.003 cm s^{-1} before aggregation).

Let us now consider the implications if the presence of the wastefield introduces turbulence into a nearly quiescent region of the water column. This condition would have profound implications for the effects of wastewater discharge on the sediments around the outfall. For example, in the Orange County simulations the initial concentration of total suspended solids in the wastefield was 2.08 mg l^{-1}. Of this concentration, 0.08 mg l^{-1} was contributed by the effluent particles, while the remaining 2 mg l^{-1} was associated with the entrainment of natural particles. The fraction of the wastefield suspended solids deposited near the outfall diffuser is approximately proportional to the square of the initial wastefield suspended solids concentration. Therefore if suspended solids are completely removed from the effluent (e.g., distilled water is discharged), the deposition of suspended solids in the vicinity of the diffuser will still be about 885 mg cm^{-2} yr^{-1}. This is only about 7% lower than the deposition rate of suspended solids if the effluent contains 49 mg l^{-1} of suspended solids. This large flux is the result of the increased mixing associated with the presence of the wastefield; in the absence of discharge, diminished mixing could reduce the depositional rate to less than a few tens of mg cm^{-2} yr^{-1}. The presence of turbulence in the wastefield may increase the sedimentation of particles from the water column by one to two orders of magnitude.

IV.B.1.e. Inorganic Material. The *DECAL* calculations assume that both natural and effluent particles consist entirely of labile organic material. TVS concentrations in effluent particles are on the order of 70%, indicating that about 30% of the mass is inorganic material. We are less certain about the composition of natural particles, but certainly some of the mass is also inorganic. As long as the aggregation process is fast compared with the decay of organic material, the failure to decompose the particle mass into organic and inorganic fractions probably will not introduce significant errors into the simulation process--although at some point, the deposition of inorganic material must be incorporated into the simulation since it represents the bulk of the sediments.

We examined the significance of inorganic material on the deposition process by computing the distance a particle settles in the water column as a function of the elapsed time after it settles out of the wastefield. This calculation was made for decay coefficients ranging from 0.1 to 1.0 d^{-1}. The results, for decay rates of 0.1, 0.3, 0.5, 0.7, and 0.9 d^{-1} are shown in Figures 4.9a,b. The vertical axis is an indication of the particle depth. It is normalized by the initial settling speed of the particle when it first leaves the wastefield. Thus if this speed was 1 cm s^{-1}, the vertical axis represents the settling distance in meters; if the initial speed is 0.01 cm s^{-1}, the values should be multiplied by 0.01 (alternatively, the scale will now indicate the settling distance in centimeters).

For a particle consisting entirely of organic labile material, the settling speed of the particle tends to an asymptotic value of zero as the time that has elapsed since it settled out of the wastefield increases. As a result, there will be a limit to the depth that the particle can settle. This depth, Z_{max}, is equal to:

$$Z_{max} = (3\ V_o) / (2\ k_d) \qquad (4.4)$$

where V_o is the initial settling speed of the particle, and k_d is the decay rate. This limit is evident in the settling depth curves shown in Figure 4.9a for the higher decay rates (e.g. k_d=0.7-0.9). Now consider the case of a particle consisting of a mass fraction, m_o, of organic material and a mass fraction, m_i, of inorganic material at the time it settles out of the wastefield. In this case, the asymptotic limit for the particle settling speed is:

$$V_{min} = V_o\ (m_i)^{2/3} \qquad (4.5)$$

For a particle consisting of 70% organic material and 30% inorganic material, this limiting settling speed will still be nearly 45% (0.448) of the initial settling speed. Thus the slope of the curves in Figure 4.9b will approach about 45% of the initial slope.

If the residence time of particles in the water column is comparable to, or exceeds, the characteristic time for the decay of organic material, the associated loss of particle mass may have significant effects on the deposition. For the sake of illustration, consider two hypothetical groups of particles that are identical in mass and settling speed at the time they settle out of the wastefield. However, one particle group consists entirely of labile organic material, while 30 percent of the mass in the other group is inorganic material. We also assume that the decay rate for the organic material is 0.5 day^{-1} (characteristic decay time of 2 days). The masses of the two types of particles diminish while they settle through the water column are:

$$m(t_d)/m(0) = m_i + m_o e^{-k_d t} \qquad (4.6)$$

where t is the time that has elapsed since the particles settled out of the wastefield. We assume that the initial mass of particles in both groups is such that the organic particle settles to the bottom seven days (168 hours) after discharge (in a net current of 2 cm s-1, the deposition would be about 12 kilometers downstream, or in the vicinity of station 1C at the White Point outfall--Figure 4.18). The mass of the organic particle at the time of deposition is about 3 percent of its original mass in the wastefield. The composite particle (30 percent inorganic, 70 percent organic) settles to the bottom in 92 hours, or about one-half the time (deposition is about 7 kilometers downstream, or station 3C at the White Point discharge). At the time of deposition, the composite particle mass is about 40 percent of its mass in the wastfield, and about 13 times greater than the mass of the organic particle at its time of deposition.

At the times of deposition, the ration of the settling speeds for the two types of particles will be about $(0.3/0.40)^{2/3}$ or 0.18. Thus particles consisting entirely of organic material will be spread out over an area that is about 5.6 times as large as the area affected by the deposition of the composite particles. Hence the depositional flux (rate per unit area) of *total* particle mass for the composite particles, will be about 74 times greater than the *total* depositional particle flux of organic particles. The depositional flux of organic mass associated with organic particles is equal to their deposition flux of *total* particle mass. For the mixed composition particles, the depositional flux of *organic* material will be about one-quarter (0.26) the depositional flux of total particle mass. Thus the flux of *organic* mass to the bottom for the composite particles will be about 19 times greater than for the particles consisting entirely of organic material--even though the *organic* flux associated with composite particles out of the wastefield is only 70 percent of the flux associated with the organic particles.

Particles with faster settling speeds will have smaller differences; particles settling more slowly will have a greater difference. This means that the deposition rates of particles can be substantially underestimated if effluent particles are considered as consisting entirely of organic material if substantial decay of organic material occurs during the deposition process. This error may be relatively minor close to the outfall diffuser, but it can be significant farther away (such as in the Los Angeles County simulations).

IV.B.1.f. Near-Bottom and Benthic Processes. Near-bottom and benthic processes incorporated into the two simulation models include the resuspension of sediment particles, loss of particle mass due to the decay of organic material, and burial. Mass balance relationships are used in both models to represent these processes--but the conceptual approach and equations used to describe these processes are completely different.

DECAL combines all three processes in to a single process--the interfacial removal flux. This flux is described in terms of a single, first-order rate equation in which the removal rate is equal to the product of the concentration of organic mass in the surface sediments (dry mass/wet volume) and a parameter known as the interfacial removal rate, k_r, (equation 3.9). This representation implicitly assumes that each of the three processes (resuspension, decay, burial) can also be represented as independent, first-order rate equations.

steady-state conditions (i.e. $t >> h_s/k_r$--eqn. 1.10), the concentration of organic material in the surface nents is proportional to the depositional flux of wastefield particles to the sediments:

$$C(\text{gm l}^{-1}) = C(\text{mg cm}^{-3}) = J_s(\text{mg cm}^{-2}\,\text{d}^{-1}) \,/\, k_r\,(\text{cm d}^{-1}) \qquad (4.7)$$

the loss fluxes associated with decay, resuspension, and burial are proportional to the concentration of ic material, they are also proportional to the depositional flux. This means that the concentrations of ic and trace constituents, as well as the decay, burial, and resuspension fluxes are unbounded. They are d only by the magnitude of the depositional flux. There are some philosophical, if not practical, problems his result. For example, an interfacial removal rate of 0.015 cm d^{-1} was used in the *DECAL* simulations, ggested in Tetra Tech (1987). In that case, the concentration of organic material in the surface sediments e equal to:

$$C(\text{gm l}^{-1}) = 66.7\ J_s(\text{mg cm}^{-2}\,\text{d}^{-1}) \qquad (4.8)$$

depositional flux exceeds about 40 mg cm^{-2} d^{-1} (14,000 mg cm^{-2} yr^{-1}), the concentration of organic ial in the surface sediments will exceed 2700 gm l^{-1}. This density is equal to that of solid quartz. From a cal standpoint, this flux is much greater than any of the rates predicted in the simulations. On the other the example indicates the potential limitations in using a simple rate equation to represent these ses.

D2D, the three processes do not take on a single form. The process of resuspension is considered to be ndent of the processes of decay and burial, but the latter two processes are mutually coupled. In the case spension, if the accumulation fraction (f_a) is constant (e.g. independent of sediment composition), the nt loss flux of sediment material due to resuspension will be proportional to the initial deposition rate of ield suspended solids from the from the water column. This is the same relationship as used in *DECAL*, conceptual approach is different--in *SED2D*, the flux of wastefield suspended solids is reduced by ension processes prior to their incorporation into the surface sediments.

ons 1.51 and 1.52 represent the processes of burial and decay in the *SED2D* model. Although equation pears similar to the mass balance equation in *DECAL* (eqn. 1.9), there are three fundamental nces: (a) the equation is nonlinear, (b) there are two components to this flux--(the total flux, and the flux nic material) and, (c) the decay of organic material is limited to a layer of surface sediments (see section ese differences substantially alter the effects of the two processes. These differences are evident from ation of Figure 1.11. First of all, the concentration of organic material in the surface sediments is d, approaching that of the particles entering the surface sediments when the flux of the latter is greater e maximum decay flux of organic material. A value of 120 mg cm^{-2} yr^{-1} was used for this flux in the site simulations. At lower depositional fluxes, the concentration is roughly proportional to the ional flux--as in the *DECAL* formalism. The depositional flux rates predicted by *SED2D* for the ate vicinity of the three outfall diffusers are greatly in excess of the maximum decay flux--unless there ensive resuspension (e.g. $f_a = 0.01$). In the latter case, the peak flux rates were comparable to the m decay rate. This indicates that the rate of loss of organic material estimated by the *DECAL* model in simulations can be significantly greater than those in computed by the *SED2D* model for at least some onditions encountered in these simulations.

1.11 shows the burial flux of particles in the *SED2D* model as a function of the ratio of the net onal flux of particles into the maximum decay flux. The burial flux of *total* particle mass is nately proportional to the net depositional flux into the surface sediments if the ratio is greater than)-30, or less than about 0.1. For the site simulations with *SED2D*, this corresponds to net depositional s that exceed about 3000 mg cm^{-2} yr^{-1}, or are less than about 12 mg cm^{-2} yr^{-1}. All of the cases ed in the *SED2D* simulations (three sites, aggregation/noncohesive, no resuspension/resuspension) d depositional fluxes into the surface sediments that lie between these two limits. Thus the loss of *total* mass due to burial will not be proportional to the deposition flux--the rate of burial will increase faster increase in depositional flux.

The burial flux of organic material is equal to the product of the concentration of organic material in the surface and the burial flux of total particle mass. Since the concentration of organic material is proportional to the deposition flux for depositional fluxes smaller than about 200 mg cm^{-2} yr^{-1}, the relationship between the burial flux of organic material and the depositional flux will be even less linear than the burial flux of *total* particle mass at these lower flux rates. The effect of the differences in the representation of the losses due to burial between the *DECAL* and *SED2D* representations will lead to increased concentrations of organic material in the sediments predicted by *SED2D*, relative to those predicted by *DECAL*.

IV.B.1.g. Uncertainties in the Input Data and Processes.

IV.B.1.g.i. *Accumulation of Natural Particles with no Discharge*. The gross rate of accumulation of sediment material is the sum of the rates associated with the accumulation of effluent particles, natural particles originating in the water column, and natural particles resulting from coastal erosion or runoff. *DECAL* does not attempt to predict the deposition of inorganic material and *SED2D* only attempts to predict the accumulation of the inorganic material associated with the production of particles in the water column (the flux associated with other natural sources is supplied as input data to the simulation). Nevertheless, at all three sites the accumulation rate of inorganic particle mass in the surface sediments is 5-50 times the rate of accumulation of organic mass. In the deeper sediments, representative of deposition before the period of discharge, the ratio increases to about 20 to 100:1. Thus although the sediments are dominated by the accumulation of inorganic material, neither model attempts to completely account for this accumulation.

This would not be as serious a problem for the simulation process if we knew this rate with some degree of certainty. In the *SED2D* simulations, we assumed that the gross accumulation rate of sediment mass in the absence of a wastewater discharge is in the range of 10-50 mg cm^{-2} yr^{-1}. This selection was based on the studies of Emery (1960) and Schwalbach and Gorsline (1985). However, there is the possibility that accumulation rates could be substantially higher--at least in the Los Angeles County simulation site area.

It has been suggested (e.g., Bandy 1960; Nardin *et al.* 1981; Pierson *et al.* 1987; SDW 1987) that the deposits overlying the bedrock off the Palos Verdes peninsula (Los Angeles County simulation site) are post-Wisconsin deposits (i.e. within the last 10,000 yr). In the vicinity of the 90- and 120-inch outfalls, the thickness of these deposits is on the order of 22 m (Pierson et al. 1987; SDW 1987). Assuming a sediment density of 2 dry g wet cm^{-3} (e.g., Figure 4.12b), the average accumulation rate of total particle mass over this period would be about 440 mg cm^{-2} yr^{-1}. This is about 25-45 times greater than the rates we used in the simulations. If the higher accumulation rate is representative of the actual accumulation rate, the validity of the simulations generated with *SED2D* is questionable.

There are two potential sources of error. First, the magnitude and composition of the sediments supplied to the model to represent the accumulation of natural particles that did not originate in the water column will be substantially different. The other source of error is in estimating the accumulation fraction, f_a. The value of 0.01 used to represent resuspension in the *SED2D* simulations was based on average sediment trap fluxes of 1000 to 4500 mg cm^{-2} yr^{-1} and an accumulation flux of 10-45 mg cm^{-2} yr^{-1} in the absence of a discharge. If the true accumulation rate is on the order of 450 mg cm^{-2} yr^{-1}, a better estimate of the accumulation fraction may be on the order of 0.20-0.50. This change would greatly reduce the effects of sediment resuspension, increasing the net depositional flux into the surface layer and hence on the rate of accumulation of wastefield suspended solids and their organic content.

It is not certain, however, that this average accumulation rate is representative of the current accumulation rate. For example, there were climatic changes between time of glaciation and the present, and sea level rose by about 33.5 m. During this change, the erosion and deposition rates of natural particles may have been substantially different from those at the present time.

The situation is further complicated by the fact that the thickness of the deposits varies by more than an order of magnitude along the Palos Verdes Peninsula. Downcoast from the two outfalls, near San Pedro Canyon, the thickness peaks at about 26 m (Pierson, 1987). On the other hand between 6 and 12 km upcoast from the 90-

inch outfall (e.g. transect 3 to transect 1), the accumulation is on the order of 2 m. Farther upcoast, in the vicinity of transect 0 (between Redondo Canyon and the peninsula) the thickness again increases, peaking at about 36 m. Thus the average accumulation rate within the Los Angeles County simulation site varies from about 44 mg cm^{-2} yr^{-1} to 800 mg cm^{-2} yr^{-1}. These variations add considerable complexity and uncertainty in selecting appropriate values for the accumulation fraction.

IV.B.1.g.ii. *Accumulation Fraction*. Although we have suggested a mechanism for estimating the magnitude of the accumulation fraction, we cannot demonstrate that the magnitude of this parameter will be independent of the composition of the particles settling into the surficial layer or the surface sediments. Therefore, a value representative of resuspension in the absence of a discharge may not be appropriate in the presence of a discharge. In fact, studies of the resuspension of sediments in the vicinity of the Orange County and Los Angeles County outfalls using an in-situ resuspension tunnel indicate that the stress required to erode surface sediments decreases as the organic content of the sediments increases (Hendricks, 1976). Whether a similar qualitative relationship also exists for the resuspension of surficial sediments is still conjecture--but it is certainly possible, and perhaps probable. Changes in particle bonding may result directly from changes in the surface properties of the particles, or indirectly through changes in the abundance and composition of filter and ingestion feeding organisms living in, or on the sediments. If the magnitude of this parameter does change in the presence of a discharge, or locally in response to gradients in the discharge-related effects, we do not have any *a priori* method for estimating appropriate values.

IV.B.1.h.iii. *Resuspension Processes*. We do not have a definitive and quantative description of the processes that actually dominate the resuspension, transport, and deposition of sediment particles. This is particularly true for the cohesive particles associated with the discharge of municipal wastewaters and in the case of silty or clayey natural sediments. The representations used in *SED2D* are only a mathematical description of a simple conceptual model that was designed to be consistent with the sediment trap observations. Since the dominant processes have not been identified, it is impossible to assess the uncertainty in the predictions associated with the simulation of resuspension processes in the two models.

Real resuspension processes are certain to be substantially more complex than the simple representation used in the *SED2D* simulations. For example, in the ocean the interaction of wave-induced flows with the ocean currents is a better measure of the potential for the physical resuspension of sediments. Resuspension may also be induced by the biota, so that resuspension fluxes may not be correlated with the strength of the waves and currents. Conversely, the redeposition of particles may represent a dynamic balance between resuspension, aggregation, disaggregation, settling, and filter feeding processes. Since we do not know the relative importance of these processes, we are unable to evaluate how well the transport estimates generated by TRANS represent the actual transport of resuspended sediments. Uncertainties in this transport distance will add to the uncertainties associated with the resuspension process.

IV.B.2. Comparison of Model Predictions with Sediments

A true predictive sediment simulation model should be able to reproduce the properties of the sediments without the use of any parameters. Models that require some information on these properties to "adjust" (or "fit") parameter values in the model provide a lower level of predictive capability. Both *DECAL* and *SED2D* fall into the latter category (e.g. through the interfacial removal rate, accumulation fraction, etc.). In the simulations described in RESULTS section, we have attempted to simulate the characteristics of the sediments at the three test sites with a minimum of parameter "fitting." In this section, we discuss the differences between the sediment characteristics predicted by the models and the actual sediment characteristics. Processes and uncertainties that may contribute to differences between the predicted and observed values have been described in the preceding paragraphs. In some cases, it may be possible to obtain better agreement between the predicted and measured characteristics of the sediments, but the improved agreement is not necessarily an indication that the simulation process is correct.

We break down the comparison into two groups, based on sediment characteristics. The first group consists of the simulations for the San Diego and Orange County sites. In these two areas discharge-related changes in the characteristics of the sediments are small, and difficult to detect within natural variability. On the other hand,

discharge-related changes are readily evident in the sediments at the Los Angeles County site (the second "group"), and thus provide a different kind of test for the models.

Within each group, we will compare the following predicted and measured and characteristics of the sediments:

1. *DECAL*
    a. Concentration of organic material in the surface layer
    b. Concentration of the trace metals Pb and Cd in the surface layer

2. *SED2D*
    a. Concentration of organic material in the surface layer
    b. Rate of accumulation of discharge-related particles ("burial rate")

There are other characteristics of the discharge that are predicted by the models, but are difficult to measure in the field and hence were not included in this study. These include the long-term average values of:

(a) the concentration of suspended solids in the wastefield, including the concentrations of Pb and Cd on these particles(*DECAL*),

(b) the initial flux of natural and effluent particles from the wastefield to the bottom (*DECAL* and *SED2D*),

(c) the flux of natural particle from the upper layer into the middle (wastefield) layer (*DECAL* and *SED2D*) and,

(d) the horizontal flux of resuspended particles near the ocean bottom (*SED2D*).

IV.B.2.a. *SED2D* Simulations for San Diego and Orange County.
We did not directly measure the concentration of organic material in the sediment samples collected at the San Diego and Orange County sites, therefore we used the concentration of total organic carbon (TOC) as a surrogate measure of this concentration. In order to make the conversion, we assumed that total volatile solids (TVS) is a measure of the organic concentration. Then we compared historical measurements of TVS in the surface sediments with TOC measurements in this study. Thie historical station locations were selected to coincide, to the maximum extent possible, with the locations sampled in our studies. The TVS measurements reported by Bascom (1978) were used for this conversion process. Since the mass emissions of suspended solids in 1978 were higher than in 1990, we assumed that the concentration of organic material in the grab samples collected in 1978 may have been higher than in the samples collected in 1990. Therefore, we reduced the 1978 TVS values by 18 percent before computing the ratio between TVS and TOC (1990). This reduction was selected based on the profile of TOC in the cores from San Diego. The conversion factor from TOC to TVS for the San Diego grab samples was estimated to be 3.68; for the Orange County grab samples, the ratio was 5.24. These ratios are significantly higher than in the effluent (ca. 2.0). Both TVS and TOC were measured in the sediment trap material collected during the sediment trap intercomparison study in the San Diego area. For the Hendricks trap design, the ratio was 3.7 (±1.1); for the Eganhouse modification, the ratio was 3.4 (±0.3). These values are comparable with the ratio deduced from the comparison of the 1978 and 1990 grab samples.

IV.B.2.a.i. *San Diego*. The solid circles in Figure 4.10a show the distribution of organic material in the grab samples collected along a transect in 60 m of water in the San Diego area. The curves represent the longshore distributions predicted by *SED2D* for the same transect. Four simulation conditions are illustrated:

(1) aggregating particles with no resuspension,
(2) aggregating particles with resuspension ($f_a = 0.01$),
(3) noncohesive (settling column) particles with no resuspension and,
(4) noncohesive particles with resuspension.

The concentration of organic material in the sediments ranges from about 1.7-2.6%. There is no clear evidence for a localized increase in the immediate vicinity of the outfall diffuser. Figure 4.10b shows the cross-shore distribution of organic material along a transect passing through the diffuser. Again, all the predicted enhancements are greater than observed in the grab samples.

There is a hint of two trends in this data:

(a) an increase in the organic content with increasing water depth and,
(b) a similar trend proceeding from upcoast to downcoast from the outfall.

In contrast to this offshore enhancement in the sediment samples, the effects of resuspension are predicted to enhance concentrations inshore of the diffuser relative to those offshore. The predicted onshore enhancement is probably an artifact of using current measurements from an elevation of 4 m (instead of 1-2 m) to estimate the transport of resuspended particles. Limited measurements of currents at an elevation of 2 m above the bottom in this area show a net offshore flow, and the transport of resuspended material would be expected to follow this trend.

Out of the four cases simulated (e.g. aggregation/noncohesive, resuspension/no resuspension), only the prediction for noncohesive particles undergoing resuspension yields a peak organic concentration that is comparable with the measured levels (2.2%). For the other three cases, the predicted concentrations are in the range of 34-68%, or about 15-31 times higher than the observed level. For noncohesive particles with resuspension, the predicted peak concentration (3.1%) is about 1.7% higher than the "predicted" background concentration of 1.4%.

There is a difference of about 0.9% between the highest (2.58%) and lowest (1.70%) values measured in the grab samples. This is about one-half the increase predicted for noncohesive particles (1.6%). However, examination of Figures 4.10a,b does not show the model predicted localized peak in the immediate vicinity of the outfall diffuser that is predicted by the model. Instead, there is a broad enhancement in the vicinity of the discharge and farther downcoast, relative to the concentrations 8 km upcoast from the outfall. Thus, the predicted enhancement in the immediate vicinity of the diffuser does not appear to be manifested in the sediments.

The accumulation rate of natural particles in the absence of a discharge is "predicted" (i.e. fixed by the values used for the natural flux and composition) to be 10.3 mg cm^{-2} yr^{-1}. The deposition of noncohesive effluent particles, combined with resuspension processes, is predicted to increase this flux in the immediate vicinity of the outfall to about 11.7 mg cm^{-2} yr^{-1}--a 14% increase.

We examined the distribution of TOC, Pb, and Cd in the two cores collected from the San Diego site to see if we could find any evidence that could be used to validate these accumulation rates. Figure 4.11a shows the vertical distribution of TOC in these cores. This figure is analogous to Figure 3.8, but here the depth is expressed in terms of the mass (per cm^2) of material lying above the reference depth, instead of the physical distance to that depth. This conversion reduces the potential for artifacts that may be introduced into the analysis by differences in the compression of the sample during the sampling process and facilitates estimates of accumulation rates of particle mass in the sediments. This mass is calculated from the equation:

(4.9)

We did not measure the density of the sediments in this study. We estimated the wet density (grams of sediment mass, including water, per unit volume) from the water content of the sediments using data collected at the Los Angeles County site in 1981. Figure 4.12a shows the density of the sediments as a function of percent water and the concentration of TVS. It was found that 92% of the variance in the density could be related to changes in the moisture content. This relationship is shown in Figure 4.12b, and can be expressed as:

$$\text{density (wet)} = 8.37 P_w^{-0.456} \quad (4.10)$$

where P_w is the moisture content in percent. The average moisture content of the cores from the San Diego site is about 59%, resulting in an estimated wet density of 1.3 g cm^{-3}. The density in dry-g wet cm^{-3} is:

$$\text{density (dry)} = \text{density (wet)} * (1\text{-}\%\text{water}/100) \quad (4.11)$$

For the San Diego grab samples, the average dry density is 0.53 g cm^{-3}.

At the bottom of the core (ca 7-8 g cm^{-2}), the TOC concentration is on the order of 0.71-0.73%. The concentration in the upper 2 cm is slightly higher at about 0.76%. There appears to be a small enhancement at intermediate depths where the TOC concentration peaks at about 0.95-1.02% (in the depth interval between 3-6 g cm^{-2}). This concentration is about 37% higher than in the surface sediments. The present mass emission rate of suspended solids is about one half the rate in 1978, so we assumed that the peak concentration of TVS in the surface sediments in 1978 may have been 7-19% higher than the present value. We used an estimated increase of 18% in developing the conversion factor from TOC to TVS.

Similar subsurface peaks are observed in the core profiles of lead and cadmium (Figures 4.11b,c), although the enhancements are somewhat greater. At the bottom of the cores, lead concentrations are on the order of 4.0 to 4.5 mg kg^{-1}. The concentration in the upper 2 cm is nearly twice as high at about 8 mg kg^{-1}. Lead concentrations peak at about 11.8 mg kg^{-1} at a depth of about 3.2 g cm^{-2} in the core from station A-16, and at 13 mg kg^{-1} at a depth of 3.5 g cm^{-2} in the core from station A-5. These peak concentrations are about 2.9 times higher than at the bottom of the core, compared with the 37% increase in the TOC concentrations.

The cadmium profile from station A-5 is similar to the profile of lead concentration at this station. The concentration increases from about 0.12 mg kg^{-1} at the bottom of the core (a depth of 8 g cm^{-2}) to about 0.55 mg kg^{-1} at a depth of 3.7 g cm^{-2}. The cadmium profile from station A-16 also is similar to the lead profile at that station--except that there is a sharp peak at a depth of 2.1 g cm^{-2}. The concentration of this peak is 0.85 mg kg^{-1}), or about 55% higher than the peak in the core from station A5. If this peak is an artifact and we ignore it, the concentration peaks at about 0.51 mg kg^{-1} at a depth of about 3.1 g cm^{-2}. This concentration is comparable in magnitude and location to the peak in the core from A5. The ratio of the concentration of cadmium at a depth of about 3 to 3.7 g cm^{-2} is about 4.4 times higher than at the bottom of the core. This ratio is about 50% higher that the corresponding increase for the lead concentrations, and about 3.3 times higher than the change in the TOC concentration.

We used these profiles to estimate the magnitude of the accumulation rate of sediments--assuming that they are associated with the commencement of the discharge. The discharge commenced in 1961, so the period of accumulation period is about 30 years. Thus the average accumulation rate of wastefield-affected sediments would be about 250 mg cm^{-2} yr^{-1}.

Next, we note that the concentration of lead and cadmium in the San Diego effluent peaked in 1975 and 1976 (Figures 2.12 and 2.13). If we assume that the subsurface peak in these concentrations (at a depth of about 3.5 gm cm^{-2}) is associated with the peak in the lead and cadmium concentrations in the effluent, the accumulation rate between 1990 and 1975 would average about 235 mg cm^{-2} yr^{-1}, or roughly the same as during the entire period of discharge.

Let us compare these accumulation rates with the rates predicted by the *SED2D* simulations. In the simulations, we assumed a background accumulation rate (in the absence of a discharge) of about 15 mg cm^{-2} yr^{-1}. The introduction of the wastewater discharge will increase this accumulation rate in the vicinity of the outfall, with the magnitude of the enhancement dependent on the conditions assumed for the simulation. Figures 4.13a,b show the rate of accumulation of sediment material predicted by *SED2D* along the longshore and cross-shore transects. The predicted peak accumulation rate is about 10 times greater than 235-250 mg cm^{-2} yr^{-1} suggested by core profiles for aggregating particles without resuspension. The core-based estimate is, however, about four times the accumulation flux predicted for either a) aggregating particles with

resuspension (f_a=0.01), or b) noncohesive particles in the absence of resuspension. The peak accumulation rate for noncohesive particles undergoing resuspension is nearly the same as the (assumed) accumulation rate in the absence of a discharge (ca. 12 mg cm^{-2} yr^{-1}), and more than an order of magnitude less than the 250 mg cm^{-2} yr^{-1} estimated from the cores. However, this was the only case among the four, where the predicted increase in the organic content was comparable with the measured concentrations.

These results demonstrate that the *SED2D* simulations cannot reproduce both the accumulation rate and composition of the sediments with the input data set used for the simulations. One change that might produce better agreement is to assume that the accumulation rate of natural particles in the absence of the discharge is on the order of 200-250 mg cm^{-2} yr^{-1}. In that case, for a limiting decay flux of about 120 mg cm^{-2} yr^{-1}, the concentration of organic material in the sediments should be approximately the same as in the particles entering the surface sediments (e.g., see Figure 1.11c). Let us assume that the concentration of TOC in the absence of a discharge is 0.71 mg cm^{-2} yr^{-1}, and that this concentration is increased to about 1 mg cm^{-2} yr^{-1} by the discharge in the period between 1974 and 1979. We further assume that deposition rate of natural particles in the absence of the discharge is 200 mg cm^{-2} yr^{-1} (the accumulation rate will be about the same because of the high inorganic content of the particles and the high depositional rate). If the particles settling from the wastefield have a TOC concentration of 18% TOC (68% TVS for a conversion ratio of 3.7), the ratio of wastefield flux to ambient natural flux of particle mass will be about 0.023. Thus we would expect the wastefield particle flux to be on the order of 4-5 mg cm^{-2} yr^{-1}. This peak discharge-associated increase in the accumulation rate is much lower than rate predicted for aggregating particles with, or without, resuspension, and for noncohesive particles in the absence of resuspension.

On the other hand, it is about 1.5-3 times greater than the predicted increase in accumulation rate for the case of noncohesive particles with resuspension. (2.8 mg cm^{-2} yr^{-1} for the mass emissions in the mid 1970s, 1.4 mg cm^{-2} yr^{-1} for the mass emissions in the late 1980s.) In order to produce a predicted accumulation rate of wastefield suspended solids of about 4.5 mg cm^{-2} yr^{-1}, we estimate that the accumulation fraction should be 0.030-0.056. In that case, we would expect an average flux of particles into the sediment traps that is between 04200-8000 mg cm^{-2} yr^{-1}. These fluxes are 1.1-2.1 times greater than the average flux into the sediment traps during the San Diego study (3740 mg cm^{-2} yr^{-1}). However, the two rates are probably comparable, given the remaining uncertainties in the simulation process. Therefore, it appears that it is probably possible to approximately reproduce the characteristics of the sediments by changing the flux of natural particles in the absence of a discharge to about 200 mg cm^{-2} yr^{-1}. The organic content of these particles would be about 1.7%.

IV.B.2.a.ii. Orange County. Next we examine the predictions for the Orange County simulations. Since we were unable to collect any cores at this site, we can only compare the predicted and measured concentrations of organic materials and trace constituents in the surface sediments.

Figures 4.14a,b show the organic content of the sediment along longshore and cross-shore transects passing through the diffuser of the Orange County outfall. Background concentrations appear to be 1.3-1.5% (a sample with an estimated TVS concentration of 0.9% was collected on the edge of Newport Canyon, but may not be representative of shelf sediments). Although the number of samples is limited, there is a hint of a small increase in the organic content of the sediments in the vicinity of the diffuser, and perhaps a few kilometers upcoast. Close to the diffuser, the estimated TVS concentration reaches about 2.8%. All the other concentrations are less than 2%. Thus general enhancements in the concentration of organic material in the area may be on the order of 0.2-0.4%. In the absence of direct measurements of TVS, it is difficult to determine if the increase in the immediate vicinity of the diffuser (1.4-2.8%) is real, or is an overestimate of the TVS to TOC ratio.

As in the *SED2D* simulations for the San Diego area, the best agreement between the predicted and measured organic content of the sediments occurs for the case of noncohesive particles undergoing resuspension. For this case, the organic content in the sediments is predicted to increase from a ("predicted") background concentration of 2.1% to 2.5%. This change of 0.4% is comparable with the general change suggested in the sediment measurements. For the other simulation cases, the change in concentration in the immediate vicinity of the outfall ranges from about 13.5-65%.

The background concentration is "predicted" to be about 2.1%. The word "predicted" is enclosed in quotation marks when referring to the background concentration since it is determined solely by net depositional flux and composition of natural particles in the absence of a discharge. These parameter values are supplied as input to the model and should be selected to reproduce the concentration of the natural sediments in the absence of a discharge. Although it probably would have been appropriate to change the input data to better reproduce the background concentrations in this simulation, the predicted and measured effects of the discharge can be adequately examined by comparing the increases above the background value. The peak and background concentrations of organic material in the sediments at the two sites are summarized in Table 4.9. The predicted longshore and cross-shore accumulation fluxes are shown in Figures 4.15a,b.

IV.B.3. DECAL simulations for San Diego and Orange County

DECAL predicts the concentration of organic material in the surface sediments in units of gm l^{-1}. We converted the grab sample concentrations into these units by multiplying the concentrations based on a mass per unit mass basis by an estimate of the dry density of the surface sediments. The average moisture content of the grab samples at the San Diego site was 36.0% (±1.2); at the Orange County site, it was 31.8% (±2.3). Using the same relationship between moisture content and sediment density as we used for the San Diego cores, we estimate that the wet densities of the sediments in the San Diego and Orange County grab samples are 1.63 and 1.73 wet-gm l^{-1}, respectively. Converting these to dry density yields 1.04 and 1.18 dry-gm l^{-1}.

IV.B.3.a. San Diego. *DECAL* predicts the concentration of *effluent* organic material in the surface sediments, but not the concentration of *total* organic material (i.e., the combination of material of both effluent and natural origin). In order to obtain the total organic concentration so that we may make comparisons with the sediment samples, we note that for steady-state conditions the concentration of organic material is proportional to the depositional flux (eqn. 1.11). If we assume that steady-state conditions exist, the concentration of total organic material in the sediments is related to the predicted concentration of effluent organic material by the equation:

(4.12)

A analogous form of this equation can also be used to estimate the concentration of natural organic material in the background sediments.

The peak and background concentrations predicted with *DECAL*, as well as the maximum and minimum concentrations in the grab samples, are listed in Table 4.10. Also summarized is the difference between the maximum (or peak) and minimum (or background) values, and the ratio of these differences for the *DECAL* predictions and the grab samples. For general reference, we also include the maximum and minimum values found in the cores collected at stations A5 and A16.

The predicted peak concentration of organic material in the surface sediments for a decay coefficient of 0.10 d^{-1} is about 5.1 times greater than the measured concentration. For a decay coefficient of 0.52 d^{-1}, the predicted peak concentration is about 2.0 times greater than measured. On the other hand, the predicted background concentration for a decay coefficient of 0.52 d^{-1} is essentially zero. For a decay coefficient of 0.10 d^{-1}, the predicted background concentration is roughly 44% of the measured minimum concentration.

The predicted enhancement in the organic content resulting from the discharge is predicted to be about 5-14 times larger than the observed increase above the minimum measured concentration (decay coefficient = 0.52, 0.10 d^{-1}, respectively). Figure 4.16 compares the longshore distribution of the predicted and measured organic content of the surface sediments. This transect lies along the 60 m isobath and passes through the outfall diffuser.

The lead and cadmium concentrations show a similar trend, but in varying degrees. We note that the predicted peak concentration of lead for a decay coefficient of 0.52 d^{-1} is slightly lower than the maximum measured value. However, we also note that the maximum lead concentration (measured at station--X2 in Figure 2.4 is nearly 80% higher than the next highest measured value. Some of these other stations are equally close to the

diffuser, and within 400 m of station X2. This suggests the possibility that the value for station X2 may be anomalously high. Again, the background concentrations of lead and cadmium are predicted to be zero for a decay coefficient of 0.52 d^{-1}, and the predicted values for a decay coefficient of 0.10 d^{-1} are roughly 16-44% of the measured minimum value.

The predicted enhancements in the lead and cadmium concentrations associated with the discharge range from about 1.8 (lead) to 14 (organic) times the difference between the maximum and minimum measured concentrations for a decay coefficient of 0.10 d^{-1}, the ratios fall to roughly one-half these ratios for a decay coefficient of 0.52 d^{-1}.

IV.B.3.b. Orange County. Table 4.11 contains a summary of the predicted and measured concentrations for the Orange County study site.

The differences between the predicted and measured concentrations for the Orange County area are similar in many ways to the differences observed in the San Diego area. Figure 4.17 compares the predicted concentration of organic material with the measured concentrations in the sediments along a longshore transect passing through the outfall diffuser. Again the predicted peak concentrations of organic material and lead for a decay coefficient of 0.10 d^{-1} substantially exceed the peak concentrations measured in the grab samples (5.2x 3.2x, respectively), and the predicted values for a decay coefficient of 0.52 d^{-1} are 1.4-1.8 times higher than the maximum measured concentrations. Although the peak predicted concentration of cadmium for a decay coefficient of 0.10 d^{-1} is 1.9 times greater than the maximum measured concentration, the predicted concentration for a decay coefficient of 0.52 d^{-1} is about 64 percent of the maximum measured value (0.70 vs 0.76).

Again the predicted background concentrations for organic material, lead, and cadmium are essentially zero for a decay coefficient of 0.52 d^{-1}. The predicted background concentrations of lead is lower than the minimum measured value for a decay coefficient of 0.10 d^{-1}, but the predicted minimum concentration of cadmium is about twice the measured value. The predicted discharge-related enhancements in the concentrations are greater than the measured changes by factors of up to nine, although the changes are essentially identical for the case of cadmium and a decay coefficient of 0.52 d^{-1}.

IV.B.3.c. Sediment Interfacial Removal Rate - San Diego and Orange County. Since the fluxes associated with the decay of organic material in the surface sediments, resuspension, and burial of sediment material are all lumped into a single parameter (the interfacial removal rate), it is impossible to determine the net rate of accumulation (burial) of the sediments. However, some insight may be gained by comparing the loss flux computed for all three processes in the *DECAL* simulations with reported the reported accumulation rates and the results of the core analysis in this study.

We compute the total loss rate from the rate of deposition of particle mass into the sediments by assuming steady-state conditions and using equation 1.9. Since the depositional flux depends on the rate of decay of organic material in the water column (k_d), we will obtain two different estimates for this loss rate. For the San Diego simulations and a decay rate of 0.10 d^{-1}, the peak loss flux will be about 765 mg cm^{-2} yr^{-1}; for a decay rate of 0.52 d^{-1}, the peak flux will be 300 mg cm^{-2} yr^{-1}. The corresponding loss fluxes for the Orange County simulations will be about 595 and 235 mg cm^{-2} yr^{-1}.

Let us first examine what these fluxes mean if there are no losses associated with the decay of organic material in the sediments and resuspension. The fluxes will be equal to the burial rate (accumulation rate) of organic mass. To get the accumulation rate of total sediment mass, we must add the burial flux of inorganic material. The measured maximum concentration of organic material in the surface sediments in the San Diego area is 2.6%; at the Orange County site the maximum measured concentration is 2.8% in the Orange County sediments. For an average value of 2.7%, approximately 37 g of inorganic particle mass will be deposited for each gram of organic mass. Therefore, peak burial fluxes of **total** sediment material are 11,000-28,500 mg cm^{-2} yr^{-1} (for k_d=0.52 and 0.10 d^{-1} respectively) for the San Diego sediments, and 8,500-22,000 mg cm^{-2} yr^{-1} for Orange County sediments.

The studies by Emery (1960) and Schwalbach and Gorsline (1985) suggest that the accumulation rate of total sediment material is 10-60 mg cm^{-2} yr^{-1}. Analyses of the cores from the San Diego area suggest that the total accumulation rate may be as high as 235-250 mg cm^{-2} yr^{-1}. In the Los Angeles County simulation area, assuming that accumulation of sediments on the underlying bedrock of the Palos Verdes Shelf occurred uniformly in the post-Wisconsin period, localized accumulation fluxes (in the absence of discharge) range between 40-700 mg cm^{-2} yr^{-1}.

Although the rates based on Palos Verdes natural sediments yield the highest burial flux estimates, they are more than an order of magnitude lower than the loss flux calculated for *DECAL* simulations. This suggests that decay and/or resuspension processes must make a substantial contribution to the total loss flux. Since decay processes in the sediments will not cause a loss of inorganic material, this process will not contribute significantly to the loss of total sediment material--although it may play an important role in determining the organic content of the surface sediments. Therefore, we conclude that resuspension processes dominate the loss of material from the surface sediments within the *DECAL* formalism. This would be consistent with the results of the *SED2D* simulations, in which significant resuspension was required to: a) produce surface sediment concentrations of organic material that are comparable with the observed values, and b) account for the disparity between the fluxes of particulate material into the sediment traps and the accumulation rate of mass in the adjacent sediments. In the latter case, however, we note that the total loss fluxes that we computed for a decay rate of 0.52 d^{-1} for organic material in the water column are still 2-10 times greater than sediment trap fluxes.

IV.B.4. Los Angeles County Simulations

Discharge-associated changes in the concentrations of organic material are relatively minor in the surface sediments at the San Diego and Orange County sites. In contrast, enhancements in the concentration of organic material are readily evident in the surface sediments in the area of the Los Angeles County outfalls. As we noted earlier, we selected 1981 as the target simulation date for the simulations at the Los Angeles County outfall site. There were two factors motivating the choice of this year, instead of 1990 (used for the San Diego and Orange County simulations). First, by 1988 the mass emissions of suspended solids declined to only about 20-25% of the emissions in the early to mid 1970s (e.g., Figure 2.11). This decline has the potential to significantly alter the accumulation and concentration of organic material in the surface sediments in a manner that would not be simulated in either the *DECAL* or *SED2D* models.

The rate of accumulation of sediment mass can be written as a mass balance:

$$F_A = F_D - (F_{Ld} + F_{Lr}) \qquad (4.13)$$

where F_A is the accumulation flux, F_D the deposition flux of particles, and F_{Ld} and F_{Lr} are the loss flux associated with decay and resuspension respectively. As we noted earlier, changes in the composition of the sediments will lag changes in the deposition due to mixing of the surface sediments by physical and biological processes. During a period of declining deposition, the organic content of surface sediments will be higher than the steady-state concentration.

In studies of sediment resuspension with an *in situ* water tunnel, Hendricks (1976) found that the stress required to erode sediments declined as the organic content of the sediments increased. Thus at any given time during a period of declining deposition, the loss flux associated with sediment resuspension will be higher than the equilibrium value for the deposition rate at that time. As a result, the accumulation rate will be reduced below the equilibrium value for that depositional rate. If the disparity between the steady-state loss rate due to resuspension and the loss rate during steady-state conditions is sufficiently large, the accumulation flux may become negative, resulting in a loss of sediment material.

Neither *DECAL* nor *SED2D* was intended to simulate these conditions. Therefore, we tried to pick a simulation period when these concerns could be minimized. Although simulations for a time in the mid-1970s would probably have been most appropriate, the first data set available that was suitable for testing the model

predictions was collected in 1981. Between 1975-1976 and 1980, the mass emissions of suspended solids declined by about 33%. This is less than the reduction in the reduction of suspended solids mass emissions in the Orange County effluent between 1978 and 1990 (54%), but essentially the same as the reduction in the San Diego effluent between 1978 and 1990 (35%). Simulation conditions for the Los Angeles County area are similar to those for the San Diego and Orange County simulations.

The simulation model tests in the Los Angeles area are based on cores collected by SCCWRP and the County of Los Angeles in 1981. Stull *et al.* (1986) discusses the properties of this data set. Figure 4.18 shows the locations of the coring stations. Each station is designated by a number and a letter. The number indicates the location of a cross-shore transect along the coast. Transect 0 is located in the outer portion of the southern end of Santa Monica Bay; approximately 18 km upcoast from the wye of the 90-inch outfall. Transect 10 lies 4 km downcoast from the wye. Both stations are close to the boundaries of the grids used in the Los Angeles County simulations.

Within a transect, a letter designator indicates the water depth at the station (A=305 m, B=150 m, C=60 m, D=30 m, Z=480 m, BA=870 m). Each core was subsampled at 2 cm increments and analyzed for a variety of physical and chemical properties. TVS values were directly measured in all cores and at all depths; TOC values were measured in a subset of the samples. The ratio between TVS and TOC concentrations in 15 samples collected within the 0-6 cm depth interval at stations along the 60 m isobath ("C" stations) was 3.40 (±0.63). This is comparable with the ratios found in the San Diego cores and sediment traps, and inferred from historical grab sample data collected in the San Diego and Orange County areas.

IV.B.4.a. *SED2D* Concentrations - 1981. Figure 4.19a compares the *SED2D* predicted concentration of organic material in the surface sediments along the 60m isobath ("C" stations) with the values measured in the 1981 cores. The solid circles represent the concentrations in the upper 2 cm of the cores; the curves, the predicted values for the four simulation cases. The measured concentrations rise from about 7% 18 km upcoast from the discharge (transect 0), peaking at about 19% in the vicinity of the 90-inch outfall diffuser (transect 8), then falling to about 5.5% at transect 10, 4 km farther downcoast.

In the San Diego and Orange County simulations, only the predicted concentrations of organic material for the case of noncohesive particles undergoing resuspension were comparable with the measured concentrations. The concentration of organic material in the surface sediments predicted for this case at the Los Angeles County site falls far below the measured concentration. This was not the situation for the *SED2D* simulations of the Los Angeles County sediments. Comparison of the measured and predicted concentrations in the vicinity of the diffusers indicates that the best agreement is obtained for the cases of either: (a) aggregating particles with resuspension or, (b) noncohesive particles in the absence of significant resuspension. However, at distances greater than 4 km upcoast from the 90-inch diffuser, the measured concentrations consistently exceed the predicted values, averaging 34% higher than the prediction for aggregating particles with resuspension, and 56% higher than for noncohesive particle without resuspension.

Figure 4.19b shows the predicted and measured cross-shore distributions in transect 8. It is dangerous to deduce any points of agreement, or discrepancy, between the predicted an measured concentrations offshore from the 60 m isobath (i.e. >2.35 km) since there is some indication that the sediments may have slumped between stations 8B and 8Z (4.7 km) resulting in substantially less accumulation of discharge related material at stations 8A and 8B than at the offshore station 8Z. It is clear, however, that the concentration of organic material in 30 m of water (station 8D, 1.3 km) is predicted to be higher than the actual concentration. This difference may be due to increased resuspension in the shallower water due to the increased effects of sea and swell. The use of a single value for the accumulation fraction, however, ignores this increased resuspension in shallower water.

IV.B.4.b. *DECAL* Concentrations - 1981. Figure 4.20a compares the predicted and measured concentrations of organic material in the surface sediments along the 60m isobath for 1981. The measured concentrations average 54.2 (±13.4) g l^{-1} along a 22.5 km section of the coast. This is about 2.4-2.7 times higher than the average 1990 concentrations in the Orange County (20.4 g l^{-1}) and San Diego (22.7 gm l^{-1}) areas. There is no

clear trend to the concentrations in the Los Angeles County sediments. The highest concentration (79.0 g l^{-1}) was measured in one of two samples collected at station 6C; the second sample had a concentration that was less than the average (48.6 g l^{-1}). The lowest concentration was measured in one of two samples collected at station 3C (36.9 g l^{-1}--second sample: 44.5 g l^{-1}). Although there is not a clear pattern in the concentration of organic material in the surface sediments when measured in gm l^{-1}, there is a clear trend of an enhancement that peaks in the vicinity of the 90-inch diffuser if the concentration is expressed in dry-gm of organic material per dry-gm of sediments (black circles in Figure 4.20). The difference in the two trends is associated with changes in the density of the surface sediments (in dry-gm of sediment per wet cubic centimeter), as illustrated by the open circles in Figure 4.20b.

The concentration of organic material in the cores in the vicinity of the two diffusers was substantially less than predicted (ca. 10 and 50%, for decay coefficients of 0.10 and 0.52 d^{-1}, respectively). Since the measured concentrations of organic material (in g l^{-1}) remain relatively constant with position upcoast from the diffuser, the predicted concentration for a decay coefficient of 0.52 d^{-1} becomes comparable to the measured value a few kilometers upcoast, and the value predicted for a decay coefficient of 0.10 d^{-1} becomes comparable about 10-18 km upcoast. The maximum and minimum predicted and measured concentrations along the 60m isobath are summarized in Table 4.9.

Figure 4.21a shows the predicted and measured concentrations of lead in the surface sediments. In the vicinity of the diffuser for the 90-inch outfall, the concentrations predicted for a decay coefficient of 0.52 d^{-1} are comparable with the measured values. A few kilometers upcoast from the diffuser, the predicted concentrations fall off more rapidly than the measured values. Ten to 18 km upcoast from the outfall, the predicted concentrations for a decay coefficient of 0.10 d^{-1} become somewhat lower than the measured values.

Figure 4.21b shows the predicted and measured concentrations of cadmium in the surface sediments. The predicted concentrations for both decay coefficients tend to be significantly lower than the measured concentrations in the vicinity of the diffuse. The measured concentration at station 10C is comparable to the predicted concentration for a decay coefficient of 0.10 d^{-1}.

The predicted enhancements in the concentration of organic material in the sediments are on the order of 4.5-11 times the measured enhancement. For lead, the predicted enhancements range from comparable to the measured increase ($k_d = 0.52\ d^{-1}$) to twice the measured enhancement ($k_d = 0.10\ d^{-1}$). The concentrations for cadmium continue a trend also observed in the simulations for the San Diego and Orange County sites--the predicted enhancements are comparable with, or less than the observed enhancement.

IV.B.4.c. *SED2D* Accumulation Rates - 1981. Figures 4.22a,b show profiles of TVS in the sediments along the 60 m isobath upcoast and downcoast from station 8C, respectively. Deep in the cores (ca. depths >22 g cm^{-2}), the concentrations approach a depth-independent value of about 4-7%. We assume that concentrations in excess of these values are the result of the discharge. The mass of this "excess" organic material in each core is:

$$M_{excess} = M_{cummulative} \times (TVS_{avg} - TVS_{deep}) \qquad (4.14)$$

Contours of this excess accumulation of organic material are illustrated in Figure 4.23. This distribution is based on the combined cores collected in 1981 (Stull *et al.* 1986) and in 1987 (Hendricks 1987). The two samplings have been combined to provide greater spatial detail. A comparison between the accumulations at stations that were sampled in both 1981 and 1987 yield nearly the same masses (1987 values average about 0.85 times the 1981 values). The accumulation of excess organic material peaks at about 3.3 g cm^{-2} at station 8C, located between the 90-inch and 120-inch outfalls. The total mass of sediments above the "discharge horizon" in the 1981 core at this station is about 20-21 g cm^{-2}.

We used the accumulations of total mass and organic mass above the discharge horizon to estimate the average fluxes of natural and wastefield-associated particles in the sediments since the commencement of the deep

discharge (i.e. post 1955). The accumulation fluxes are related to these natural and wastefield fluxes by the equations:

$$F_{total} = F_n + F_w$$
$$F_{organic} = C_n \times F_n + C_w \times F_w \quad (4.15)$$

where:

F_n = natural flux of total particle mass in the absence of discharge
F_w = wastefield associated flux
C_n = fraction of organic material in the natural particles
C_w = fraction of organic material in the wastefield particles

The accumulation fluxes of total particle mass and organic mass are estimated from the cummulative total and organic masses in the core above the discharge horizon. Bioturbation of the sediments introduces some uncertainty into selecting the location of the latter--and hence into the estimates of the accumulation fluxes. These uncertainties are greatest for the coring stations with the smallest accumulations. The accumulated total mass and excess organic mass during the period of discharge for a "reasonable" estimate of the location of the discharge horizon in each core are summarized in Table 4.13.

The total organic mass above the discharge horizon is equal to sum of the product of the total particle mass and the concentration of natural particles (eqn. 4.15). We assumed that the concentration of organic material in the natural particles was approximately equal to the concentration measured well below the discharge horizon (i.e. in the deep portion of the cores). This is equivalent to assuming that $F_n >> F_d$ (see Figure 1.11b). Based on the results of the *SED2D* simulations, we assumed that the concentration of organic material in the wastefield associated during the discharge period (1956 -> 1981) are summarized in Table 4.13. The relationship between the natural and wastefield associated fluxes for each core in this example is illustrated in Figure 4.24a. The relationships for other estimates of the location of the discharge horizon are shown in Figures 4.24b, c, d. The results shown in Figure 4.24c represent a selection that deliberately underestimates the effects of bioturbation; the results of Figure 4.24d, an overestimate of these effects.

One characteristic evident in this analysis is that the calculated flux of natural particulate material is not a constant. Instead there is a trend of increased natural particle flux accompanying an increase in wastefield particle flux. The magnitude of this relationship varies depending on the selection of the mass of wastewater-related particle mass. The magnitude of the natural particle flux in the absence of a discharge also depends on the selection of the discharge horizon, ranging from about 65 to 290 mg cm^{-2} yr^{-1}, averaging 210 mg cm^{-2} yr^{-1}. This average natural particle flux is about 3 to 20 times greater but comparable to the 260 mg cm^{-2} yr^{-1} average post-Wisconsin accumulation rate in the vicinity of the outfall diffusers (Pierson et al. 1987, Kolpack 1987).

We used a natural flux of 20 mg cm^{-2} yr^{-1} for the *SED2D* simulations. Therefore the predicted total accumulation fluxes should be significantly lower than those deduced from the cores. However, since the natural flux in these simulations is added to the flux associated with deposition from the wastefield, the predicted accumulation of wastefield-associated particles should still be approximately comparable with the measured accumulation (at least where the total deposition rate in the simulations is $>F_d$). Figure 4.25 shows the wastefield-associated rate of accumulation of sediments along the 60 m isobath predicted for the four simulation cases, and the fluxes deduced from the cores.

The accumulation rates of wastefield-associated particles predicted by *SED2D* show a more "peaked" distribution than that calculated from the cores. In the immediate vicinity of the 90-inch outfall, the accumulation rate of wastefield-associated particle mass in the cores is estimated to be about 200 mg cm^{-2} yr^{-1}. Fifteen to 20 km farther upcoast, the accumulation rate estimated from the cores has declined to about 43-52 mg cm^{-2} yr^{-1}. Thus the peak accumulation rate is about 3.7-4.5 times greater than the accumulation rate 15-20 km upcoast from the 90-inch diffuser. *SED2D* predicts peak accumulation rates of about 25, 180, and 710

mg cm^{-2} yr^{-1} for aggregation with resuspension (fr = 0.01), noncohesive particles without resuspension, and aggregation with no resuspension, respectively. Fifteen to 20 km upcoast from the 90-inch outfall, the corresponding predicted rates of accumulation of wastefield particles are on the order of 2-30 mg cm^{-2} yr^{-1}. The ratio of peak predicted accumulation rate to the rate predicted 22.5 km upcoast from the 90-inch outfall ranges from 7:1 (resuspension) to 33:1 (no resuspension) for aggregating particles, and about 86:1 for non-cohesive particles without resuspension. The distribution predicted for aggregating particles with resuspension is the closest to the distribution estimated from the cores, but the predicted accumulation rates are only about 6%-14% of the core rates.

IV.B.4.e. *DECAL* Accumulation Rates - 1981. *DECAL* does not compute the rate of accumulation of wastefield-associated particles in the sediments. The total loss rate of organic material can be estimated from equation (1.9) and the average concentration of organic material in the sediments, but this loss represents the combined processes of burial (accumulation), resuspension, and decay. An upper bound to the accumulation rate can be generated by assuming that most of the loss is due to burial. The average concentration of TVS in the sediments (above the discharge horizon) at station 8C is about 14.6% and the average density (dry-g wet cm^{-3}) is 0.48 gm cm^{-3}. Therefore the average concentration of organic material in the sediments (C_s in equation 1.9) is about 70 mg l^{-1}. An interfacial removal rate of 0.015 cm d^{-1} was used for the *DECAL* simulations. This yields an interfacial removal flux of about 0.4 mg cm^{-2} yr^{-1} for organic material. For an average concentration of organic material of 14.6%, this corresponds to an interfacial removal rate for total particulate mass of about 2.6 mg cm^{-2} yr^{-1}. This predicted upper bound is only about 1-2% of the peak accumulation rate of wastefield-associated particles estimated from the cores (195 mg cm^{-2} yr^{-1}), and only about 10% of the accumulation rate 15-20 km upcoast from the 90-inch diffuser.

V. SUMMARY OF MODEL RESULTS

This study consisted of two components: a) refinement and testing of two numerical simulation models of sedimentation, *DECAL* and *SED2D* and b) laboratory and field studies to provide input for the modeling and to provide insight into the processes that determine the fates of effluent and natural particles in the vicinity of an ocean outfall discharging treated municipal wastewaters. The modeling component began with studies of the dynamics of particle aggregation for water column conditions similar to the case of a submerged wastefield. This work was conducted by Mr. Palo Castro under the direction of Dr. Kevin Farley (Clemson University). The results were incorporated into a revised version of *DECAL* by Dr. Farley, and into a new subprogram within the suite of subprograms forming the *SED2D* simulation model.

The revised models were used to simulate the characteristics of sediments around three ocean outfalls that discharge into the coastal waters of southern California (City of San Diego, Orange County Sanitation Districts, Los Angeles County Sanitation Districts). In addition to site simulations, representations of the processes determining the fates of the suspended solids in both models were examined and studies were carried out to determine the sensitivity of model predictions to the choice of input values, and to determine the internal consistency of some model predictions.

The aggregation dynamics studies showed that the aggregation and settling of cohesive particles could be adequately described by two equations. One of the equations describes the rate of production of aggregate particles; the second (and new) equation provides an estimate of the settling speed of these particles. These equations were incorporated into both models for simulations of aggregating particles. Apart from this similarity, the two models differ in their approach and process representations in a number of important ways. Some of these differences are summarized in Table V.A.

These differences can produce significantly different results for the same basic input information. For example, *DECAL* estimates the initial concentration of effluent suspended solids in the wastefield using a mass balance approach. The approximations used in estimating the spatial dimensions of the wastefield, and its transport away from the vicinity of the diffuser, implicitly assume that the transport associated with the daily average flow is less than the transport associated with the tidal currents or the dimensions of the diffuser. On the other hand, the *SED2D* simulations use a simulation model of the initial dilution process to estimate this concentration. This approach assumes that the transport associated with the daily average flow is greater than that associated

with the tidal currents or diffuser dimensions. The dilutions, and hence the initial effluent particle concentrations, generated by *DECAL* differ from those predicted during the *SED2D* simulations by factors ranging from 1.8 to 6.2. Investigations of the sedimentation of particles in the immediate vicinity of the diffuser showed that the sedimentation flux is approximately proportional to the square of the initial concentration of suspended solids in the wastefield. Thus if the concentration of natural suspended solids in the wastefield is negligible, the sedimentation fluxes predicted by *DECAL* in the vicinity of the diffuser will be on the order of 3.2-38 times greater than the rates predicted using *SED2D*. However, both these calculations assume that the concentration of suspended solids within the wastefield is homogeneous. Physical model studies and measurements in the ocean show that this is not the case. If the initial concentration of effluent suspended solids is based on the flow-averaged initial dilution, rather than a spatially-averaged dilution, the ratio between the *DECAL* and *SED2D* predicted concentrations falls to values ranging from 1.03-3.6. Since the aggregation dynamics studies were carried out assuming a uniform concentration within the wastefield layer, it is not clear how to relate the concentration of suspended solids predicted from the initial dilution calculations to an appropriate concentration for the aggregation rate equations.

Both the rate of particle aggregation and the aggregate particle settling speeds depend on the concentration of *total* suspended solids in the wastefield. The *DECAL* model assumes that the concentration of natural particles in the water column at the depth of entrainment during the initial dilution process is negligible compared with the initial concentration of effluent particles in the wastefield. In the *SED2D* simulations, this concentration is supplied as input information. Examination of limited historical measurements of suspended solids concentrations at typical entrainment depths in the coastal waters of southern California indicates that typical concentrations may range from one to a few milligrams per liter. In the *SED2D* simulations, the contribution of natural suspended solids to the concentration of total suspended solids in the wastefield ranges from substantially greater than the effluent suspended solids concentration (San Diego and Orange County, present discharge) to comparable to the effluent suspended solids concentration (Los Angles County, 1979-1980 effluent). The *SED2D* simulations assume that all of this natural particle suspended solids mass can participate in the aggregation process. Therefore, the initial concentration of total suspended solids in the wastefield in the *SED2D* simulations was greater than in the *DECAL* simulations--even though the initial dilutions predicted by the latter model were lower than those in the *SED2D* simulations. The contribution of natural particles to the aggregation process has potentially important consequences for assessing the impact of wastewater discharges, but this role is not known at the present time.

The equations representing the aggregation process were developed for aggregation within a completely mixed layer of water. The *DECAL* and *SED2D* simulations were carried out assuming that the thickness of this layer is equal to the thickness of the wastefield. However, examination of the distribution of temperature, salinity, dissolved oxygen, transmissivity, and density within the wastefield generated by the discharge from the ocean outfall operated by the City of Los Angeles suggests that, except in the immediate vicinity of the diffuser, mixing within the wastefield may be relatively weak and profiles of various indicators of the wastefield are not constant across the wastefield. The strength of vertical mixing is related to the density stratification of the water column and shear in the currents. Comparison of the density structure within the wastefield with that of the same region of the water column outside the wastefield revealed no substantial differences, suggesting that mixing within the wastefield and in the natural waters may be comparable (the comparison was, however, not precise because of the effects of internal waves and internal tides on the profiles). Simulations were carried out for the wastefield region of the water column, but in the absence of a discharge. During these simulations it was assumed that the strength of mixing was the same as was assumed within the wastefield during the *DECAL* and *SED2D* simulations. It was found that the observed concentrations of natural suspended solids could not be maintained (i.e. steady-state conditions) without an order of magnitude, or greater, reduction in the thickness of the layer in which aggregation is taking place. This suggests that reduced mixing within the wastefield means that the "effective" thickness of the layer for the purposes of particle aggregation may be much less than the physical thickness of the wastefield. This change could result in a one to two order-of-magnitude reduction in the sedimentation fluxes predicted by the *DECAL* and *SED2D* simulation models.

The *DECAL* model assumes that effluent and natural particles are too small to settle until they undergo aggregation. *SED2D* makes the same assumption during simulations of aggregating particles. Alternatively,

simulations can be carried out with *SED2D* by assuming that particles undergo minimal aggregation, but have an initial distribution of particle sizes and settling speeds. However, the results of exploratory simulations discussed above, combined with the site-specific simulations, suggests that it may be more appropriate to use a "mixed" representation. One possibility would be to compute an initial particle settling speed by assuming that all the particles are small and using the aggregation equations. Effluent particles with settling speeds greater than this value (e.g. from settling column measurements) would settle without requiring aggregation, while particles with slower settling speeds would undergo aggregation and subsequent settling. The changes in sedimentation flux and sediment distributions and characteristics associated with such a representation were not, however, examined during this study.

The settling of particles within the water column was also examined. *DECAL* assumes that the particles consist entirely of organic material. In the presence of decay of this organic material, it was found that there is an asymptotic limit to the depth that these particles will settle. The value of this depth is dependent on the initial particle settling speed and the rate of decay. For a decay coefficient of 0.5 d^{-1} and an initial particle settling speed of 0.1 cm s^{-1}, the limiting settling distance is only about 17 m, so this process could be significant. In spite of this decay, the particle will, however, consist entirely of organic material. *SED2D* allows for an inorganic component to the effluent (and natural) particles. Analysis of the effluent carried out during the study, and during other studies, shows that about 30% of the particle mass is associated with inorganic material and thus not subject to decay. In this case, there is no limiting settling depth, but the particle settling speeds approach an asymptotic limit. However, the organic content of the particles can become very small if the settling time is long compared with the characteristic decay time. These considerations will become increasingly important for higher water temperatures, reduced concentrations of total suspended solids, and reductions in the mass of effluent particles that have high settling speeds in the absence of aggregation.

Once organic particles reach the sediments, they can undergo additional decay. The *DECAL* calculations compute the flux of material lost due to decay using a first-order rate equation. The *SED2D* simulations use a similar approach, but with a limiting flux. Exploratory simulations carried out during this study show that these two approaches can yield significantly different results once the flux of particle mass settling from the water column becomes comparable with the decay flux. Although the magnitude of the latter flux is not known, data from a variety of sources suggests that these fluxes may become comparable in the immediate vicinity of the diffuser (and over a broader area if the rate of natural particle accumulation in the sediments as high as suggest in our analysis of cores during this study).

In addition to decay, sediment particles can also undergo resuspension, transport, and redeposition. In the *DECAL* simulations, these processes are represented by the same first-order rate equation used to simulate particle decay. The effect of resuspension is manifested by a change in the rate constant. It is assumed to be independent of position and sediment composition. The magnitude of this parameter must either be "fitted" to the simulation site, or estimated from studies in other areas. In contrast, *SED2D* assumes that, on the average, part of the particles deposited on the surface sediments are resuspended during the next resuspension event, while the remainder become part of the "permanent" sediments. The magnitude of this fraction is estimated from near-bottom sediment trap measurements and the rate of accumulation of natural particles in the sediments in the absence of a discharge. However, examination of core data during this study indicates that the latter rate may not be well known for the simulation sites. Natural particle sedimentation rates deduced from this analysis suggest rates that may be 4-25 times greater than the estimates used in the simulations carried out at the three test sites. The latter values were based on measurements from sites lying offshore and in deeper water from the outfall diffusers. A further difference between the representation of resuspension processes is that in *SED2D*, these processes can change the composition of the sediments (reflecting the composition of the particles resuspended elsewhere and settling at a specific location) and the rate of accumulation (e.g. increasing the apparent sedimentation rates downstream from the location of the peak in the sedimentation flux from the water column).

From this summary of the characteristics of the two simulation models, it is evident that:

1. The predictions generated by the two simulation models may be substantially different. If the two predictions are comparable, they are likely to produce the same results for different reasons.

2. Uncertainties in the representations of the processes that determine particle fates are likely to result in significant errors in the predictions.

The simulations carried out with *SED2D* generally predict substantially larger enhancements in the organic content of the sediments in the vicinity of the test outfalls than are measured. Only for the case of noncohesive particles and substantial resuspension do the predicted enhancements approach the observed conditions. The same situation is observed in the *DECAL* simulations. Here the closest agreement is obtained if the decay rate of organic material in the water column is large (ca. 0.52 d^{-1}). However, increasing this rate also results in a predicted organic concentration for the natural sediments of essentially zero instead of within 50-70% of the peak measured concentration.

The situation is somewhat different at the White Point site. Here the organic concentrations predicted by *SED2D* are similar to those predicted for the San Diego and Orange County sites (e.g WP: 5-65%; SD and OC: 2-68%, depending on the choice of input parameters), but the measured concentrations in the vicinity of the outfall have risen to 3-4 times the White Point background level (and 7-10 times the background levels at the San Diego and Orange County sites). However, input parameter values that lead to predictions that yield approximately the observed concentrations in the immediate vicinity of the diffuser tend to underestimate the concentrations in the sediments by a factor of 0.5-0.7 at distances of 10-15 km downstream.

The enhancement predicted by *DECAL* for the White Point site is about 2.3-3.3 times greater than the enhancements predicted for the San Diego and Orange County areas, 15-20%. The predicted peak concentration for a decay rate of 0.1 d^{-1} is 356 mg l^{-1}, or about 5.4 times greater than the peak measured value in the surface sediments. However, the predicted background concentration is comparable to the measured value (predicted: 49 mg l^{-1}; observed: 39 mg l^{-1}). On the other hand, for a decay rate of 0.52 d^{-1}, the predicted peak concentration is only about 1.9 times the measured value (126 mg l^{-1} vs. 66 mg l^{-1}), but the predicted background concentration is much less than observed (0.6 mg l^{-1} vs. 39 mg l^{-1}).

The enhancements of lead predicted by *DECAL* for the San Diego and White Point sites are within a factor of 2.8 of the observed concentrations. At the Orange County site, they are 8-12 times greater than the measured concentrations. On the other hand, the enhancement in the concentration of cadmium predicted for the San Diego site is 3-7 times the observed enhancement, while the predicted enhancement for the Orange County site is only 1-3 times the observed value. The predicted concentration of cadmium at the White Point site is unusual in that it is less than the observed increase (e.g. a ratio of 0.3-0.5).

VI. CONCLUSIONS

VI.A. FIELD STUDIES

The geochemical studies described in this report provide information on the characteristics and fate of effluent particles discharged to the shelf off southern California. Although the composition of the wastewater effluents examined here appear to be quite similar, the fate and transport of the particles being discharged from the respective outfall systems is not. This is best exemplified by dramatic differences in the abundance and composition of the linear alkylbenzenes in sediments and sediment traps at each of the three sites. Off White Point, the particles collected in sediment traps contain a mixture of materials derived *via* resuspension of older, historically deposited sediments (as far back as 25 or more years) and effluent particles that could not have been discharged from the JWPCP (prior to trapping) much earlier than a few days to weeks. At the other two sites, and particularly off Point Loma, the particulate LAB concentrations are greatly attenuated (i.e. much lower sediment trap/effluent concentration ratios), and the distribution of C_{12} isomers indicates that the effluent particles have undergone extensive biodegradation. Whether this biodegradation occurs during or subsequent to deposition in the sediments/sediment traps is unclear. In the case of Point Loma, at least, the higher 3ϕ-dodecane/TAB_1 ratios (when compared with surficial sediments) indicates that a significant fraction of the LABs does not originate from resuspension of the older sediments alone. Laboratory data developed during this project on effluent particle degradation kinetics are preliminary and must, therefore, be viewed with

caution. Nevertheless, the results suggest that wastewater treatment processes (such as pre-discharge chlorination) may have important *secondary* effects on the accumulation rates of effluent particles in nearby sediments, principally by reducing the efficiency with which the particles are degraded. The high sediment trap/effluent concentration ratio and the undegraded character of the LABs off White Point when compared with those found at the other outfall sites may, thus, be explained by a reduction in the metabolism of these marker compounds during the process of sedimentation of *chlorinated* JWPCP effluent particles. This hypothesis remains to be tested.

Although significant differences exist in the depositional patterns at the three sites, some generalizations can be made. At all three sites, there is evidence of contamination from wastewater effluent both in surficial sediments and particles collected in the sediment traps. This means that effluent has and/or is reaching the sediments, and some fraction of this material is being resuspended and transported across the shelf as represented in the models. Evidence comes from the presence of sewage marker compounds (the linear alkylbenzenes and the fecal sterols), low stable nitrogen isotope ratios and, in some cases, from elevated concentrations of other constituents that are enriched in effluent particles (e.g. Pb, Cd, TOC, TN). The latter (elemental) indicators are not as sensitive as the sewage marker compounds in delineating the areal extent of contamination because other (non-effluent) sources exist, and the signal-to-noise ratio is not as favorable when compared with the molecular markers. Nevertheless, based on measured $\delta^{15}N$ values, the percent of nitrogen in the sediment trap particles ranges from 45-100% off White Point, 30-45% off Orange County and 7-20% off Point Loma.

We frequently observed differences between the composition of surficial sediments and particles collected in nearby sediment traps. Obviously, resuspension events can lead to redistribution of surficial sediments that varies both spatially and temporally, whereas sediment traps integrate sedimenting particles derived from a broad, and as yet undefined, area of the shelf. Thus, the geochemical data presented here do little to illuminate the relationship between hydrodynamics and the processes of resuspension and redeposition.

VI.B. Modeling Studies

The simulations conducted during this study show that the two numerical models, *DECAL* and *SED2D*, cannot accurately predict the sediment characteristics near ocean outfalls that discharge treated municipal wastewaters off southern California. Although the ultimate goal of the simulation process is to obtain an accurate and reliable predictions, these models can serve another important and useful purpose--a quantitative test of our understanding of the processes affecting the fates of natural and effluent particles in coastal waters. This study has provided important guidance on questions that must be answered before a reliable predictions can be obtained.

These questions can be divided into three categories:

1. Uncertainties in the magnitudes of parameters required to conduct the simulations.

2. Uncertainties about the proper representation or interpretation of processes incorporated into the models.

3. The role and importance of processes not incorporated into the models

Uncertainties in the magnitudes of parameters required for the simulations:

1. Rate of accumulation of natural particles in the absence of wastewater discharge.

2. Concentration of natural suspended solids in the wastefield at the completion of initial dilution and the fraction of this mass that undergoes particle aggregation.

3. Rates of decay of effluent and natural particles in the water column, and the rate of decay, or the decay flux, of particles in the sediments; the composition of natural and effluent particles in terms of inorganic and organic components with different decay rates.

4. Frequency, duration, and intensity (resuspended mass) of resuspension events and the conditions leading to these events.

Uncertainties in the process representations incorporated into the model:

1. Estimates of the "average" concentration of effluent suspended solids in the wastefield after initial dilution. Part of this problem arises from the non-uniform distribution of effluent particles within the wastefield.

2. Extent of vertical mixing within the wastefield and a description of the aggregation dynamics of particles in a non-uniform distribution.

3. The validity of the mutually exclusive assumptions that either: a) all the particles are initially so small that they settle only after undergoing aggregation, or b) the effects of particle aggregation can be neglected (settling column approximation).

4. The processes of resuspension, decay, and burial can be represented by a first-order rate equation. Alternatively, the decay flux has a limiting value and resuspension, transport, and deposition can be represented in terms of a simple "average" accumulation fraction, and "threshold" resuspension and deposition speeds.

Finally, both models neglect the role of the biota in determining the fates of particles. The biota may play a significant role in:

1. Transformation, aggregation, etc. of particles in the water column (e.g., fecal pellet production).

2. Biologically-induced changes in resuspension and particle deposition rates, including passive roles (sediment modification) and active roles (scavenging suspended solids from near-bottom waters, particle resuspension by mechanical means, pumping).

3. Depth and rate of mixing of the "surface" sediments.

Since the abundance and composition of the benthic biota changes in response to wastewater discharges, biologically-induced sediment processes may exhibit spatial and temporal scales that are comparable to those characterizing the properties of the wastewater affected sediments. The importance of the biota in determining the fates of particles in the vicinity of a discharge, relative to the physical processes that form the basis for the two models, is unknown.

Until these simulation uncertainties are addressed, the predictions of sediment characteristics based on these models is qualitative at best, particularly for discharges into new areas. They may be useful in assessing the effects of small changes in the discharge environment or wastewater characteristics if the model parameters are "tuned" to reproduce existing conditions (for small changes, a first-order perturbation linearizes all the rate equations). Their primary usefulness at present is as a means to explore the consequences of the modeling assumptions and the sensitivity of these processes to uncertainties in the input information.

VII. RECOMMENDATIONS

The results of the geochemical studies suggest several new avenues of inquiry. We need to determine the extent to which pre-discharge chlorination of effluent affects the short-term biodegradation potential of effluent particles. If the kinetics of degradation are reduced, the practice of chlorination may need to be re-evaluated in light of its effects on enhancing the preservation and deposition of effluent particles.

Unfortunately, critical information on the degradation rates of natural marine sinking particles and effluent particles is still lacking. Insofar as natural particles interact with effluent, investigations of the frequency and

efficiency of particle-particle collisions are needed. We know little about the role that plankton, especially zooplankton, play in repackaging small effluent particles and releasing them along with other particulate matter as larger, rapidly sinking fecal pellets. Data are just beginning to be generated on diagenesis in the Palos Verdes sediments (W. Berelson, personal communication). This will provide first order estimates of the decomposition fluxes of organic carbon in these waste-impacted sediments. This information was not available during this study, but would have helped reduce uncertainties in model parameterization.

The markers used in this study offer unique opportunities to probe the relative importance of various sedimentation and resuspension processes, and to determine transport pathways. However, we have little understanding of the behavior of effluent particles that reach the sea floor. How frequently are they resuspended (on average) before they accumulate as bedded sediments? What is the redox environment in the upper millimeter of surficial sediments? How are decomposition rates affected by resuspension events? What is the relative importance of aggregation and disaggregation near the sea floor? These and other aspects of the sedimentation process remain obscure. In order for deposition models to make significant advances, a more accurate conceptualization of these processes and their interrelationships must be developed along with a satisfactory set of field measurements that characterize the rates at which they occur.

The results of the modeling studies indicate that additional knowledge is required before *DECAL* and *SED2D* can be used for reliable predictions. Within the water column, the most critical areas requiring further study are: 1) dynamics of aggregation in the ocean, 2) role of natural particles in aggregation processes, and 3) rate of decay of organic material.

The results of this study suggest that the assumptions used in developing mathematical representations of aggregation processes in the ocean environment are not representative. In particular, comparisons of the rate of production of phytoplankton mass with standing stock (in the presence of aggregation) suggests that: a) only a fraction of the natural suspended solids in the ocean aggregate, b) vertical mixing in the ocean below the pycnocline and *within the wastefield* is weak, and c) there are other significant sources of natural particles.

We need more data on the aggregation of natural-natural, effluent-natural, and effluent-effluent pairs of particles in actual or simulated oceanographic conditions. The extent of vertical mixing within the wastefield and the receiving water (at and below wastefield depth) should be determined to see if the assumption of a homogeneously mixed layer of water is justified. If not, new representations that relate the rate of production of aggregate particles and their settling speeds to the strength of vertical mixing, as well as the suspended solids concentration and layer thickness, will have to be developed. The role of the decay of organic material is difficult to assess, but the simulations suggest that the process is important (for particles with a high organic content) if the concentration of total suspended solids in the wastefield (or ambient water) is low, resulting in settling times that are long compared with the decay time.

There is also some question about how the initial concentration of effluent solids in the wastefield should be calculated. This uncertainty is not especially critical unless: a) the concentration of natural suspended solids in the wastefield is comparable with, or less than, the concentration of effluent suspended solids, or b) natural suspended solids do not significantly participate in aggregation with effluent particles. If natural particles aggregate with effluent particles, our analysis suggests that for present discharges in southern California coastal waters, the uncertainty associated with initial dilutions is not critical.

The comparison of initial particle settling speeds predicted from the aggregation equation with direct measurements from a settling column suggested that large, fast-settling particles may be present in the effluent immediately following discharge and before significant aggregation occurs. Although the fraction of total particle mass associated with these speeds may be small, they can make a significant contribution to the deposition of effluent particles in the immediate vicinity of the diffuser. It may be appropriate to modify the models so that simulated sedimentation represents a composite of the settling of discrete particles present in the effluent, and the aggregation of smaller effluent particles into faster settling aggregates.

The rate of accumulation of natural particles on the shelf in water depths comparable with ocean discharges (in the absence of a discharge) may be 2 to 25 times greater than published estimates based on extrapolation from data collected on the slope. The consequences of this uncertainty are: 1) the flux of natural particles directly affects the composition and rate of accumulation of sediment mass, and 2) a corresponding uncertainty in the rate of wastefield (natural + effluent) particle accumulation in the sediments is introduced into the *SED2D* simulations via the effects of sediment resuspension. This natural particle accumulation flux information is another crucial element in understanding and predicting the fates of particles on the shelf.

VIII. ACKNOWLEDGMENTS

Many individuals participated in this project and deserve credit for collecting and analyzing samples as well as contributing to experimental design. From start to finish, Skip Westcott played a central role in organizing the program and seeing that data were properly collected. We thank Pat Hershelman for his many creative contributions and elemental analyses. Azra Khan carried out the fecal sterol analyses as well as elemental analyses, and Marilyn Castillo performed the linear alkylbenzene measurements. The extensive sampling effort was conducted almost entirely by Harold Stubbs and Dario Diehl. Darrin Greenstein provided analyses for dissolved oxygen. We also wish to thank personnel of Hyperian (City of Los Angeles), Joint Water Polution Control Plant (Los Angeles County), County Sanitation Districts of Orange County, and Point Loma Treatment Plant and the personnel of the Joint Water Control Plant for their help in obtaining samples of effluent and sludge sectioning the sediment cores. Special thanks go to Stefan Lorenzato, the project officer, whose keen interest and forbearance throughout this project made all of our jobs more rewarding and less stressful.

We appreciate the discussions the M. Moshiri, B. Hansen, and R. Caballero of Los Angeles County Sanitation Districts (LACOSAN) about the history of flows through the 90" and 120" White Point outfalls. A. Steele, also of LACOSAN, and Patti Vainik and Lori Vereker of the City of San Diego, provided crucial monitoring data on the water column concentrations of suspended solids in their respective discharge areas.

IX. LITERATURE CITED

Amen, R. and T. Maxworthy. 1980. The gravitational collapse of a mixed region into a linearly stratified fluid. J. Fluid Mech. 96:65-80.

Bandy, O.L. 1960. Geological significance of coiling ratios in foraminifer *Globigerina pachyderma*. J. Paleo. 34:671-681.

Balistrieri, L., P.G. Brewer, and J.W. Murray. 1981. Scavenging residence times of trace metals and surface chemistry of sinking particles in the deep ocean. Deep-Sea Res. 28A:101-121.

Bascom, W., J. Mardesich, and H. Stubbs. 1982. An improved corer for soft sediments. *In*: Annual Report 1982, Southern California Coastal Water Research Project, Long Beach, pp. 267-271,.

Battelle Ocean Sciences. 1991. CSO effects on contamination of Boston Harbor sediments. A draft report prepared for the Massachusetts Water Resources Authority, May 1991.

Bayona, J.M., J. Albaigés, A.M. Solanas, and M. Grifoll. 1986. Selective aerobic degradation of linear alkylbenzenes by pure microbial cultures. Chemosphere 15:595-598.

Bruland, K.W. and R.P. Franks. 1979. Trace metal characterization of water column particulates. Annual Report to Bureau of Land Management, Southern California Baseline Study, Benthic, Year 2, Vol. II, Report 7.0.

Bender,M.R., Jahnke, R., Weiss, R., Martin, W. Heggie, D.T., Orchardo, J. and T. Sowers. 1989. Organic carbon oxidation and benthic nitrogen and silica dynamics in San Clemente Basin, a continental borderland site. Geochim. Cosmochim. Acta, 53:685-697.

Berelson, W.M.,Hammond, D.E. and K.S. Johnson Benthic fluxes and the cycling of bqgenic silica and carbon in two southern California borderland basins. *ibd*., 51:1345.1363.

Bruland, K.W., K. Bertine, M. Koide and E.D. Goldberg. 1974. History of metal pollution in southern California coastal zone. Envir. Sci. Technol. 8:425-432.

Burnett, W.C. and O.A. Schaeffer. 1980. Effect of ocean dumping on $^{13}C/^{12}C$ ratios in marine sediments from the New York Bight. Estuar. Coastal Mar. Sci. 11:605-611.

Castro, A.P. 1990. Modeling deposition of particles and particle-bound contaminants in stratified waters. M.S. Thesis, Clemson University, Alabama. 79pp.

City of San Diego. Unpublished data. San Diego, CA.

Carry, C.W. and J.A. Redner. 1970. Pesticides and heavy metals. Progress Report, County Sanitation Districts of Los Angeles County, 51pp.

Cauwet, G. 1978. Organic chemistry of sea water particulates. Concepts and developments. Oceanol. Acta 1:99-105.

Chen, K.Y., C.S. Young, T.K. Jan, and N. Rohatgi. 1974. Trace metals in wastewater effluents. J. Water Pollut. Contr. Fedr. 46:2663-2675.

Cline, J.D. and I.R. Kaplan. 1975. Isotopic fractionation of dissolved nitrate during denitrification in the eastern tropical North Pacific ocean. Mar. Chem. 3:271-299.

Degens, E.T. 1968. Biogeochemistry of stable carbon isotopes. Chapter 12. *In*: Organic Geochemistry, G. Eglinton and M.T.J. Murphy, eds., Springer-Verlag, NY, pp. 304-329.

Eganhouse, R.P. 1982. Organic matter in municipal wastes and storm runoff: Characterization and budget to the coastal waters of southern California. Ph.D. dissertation. University of California, Los Angeles, 230pp.

Eganhouse, R.P. 1985. Long-chain alkylbenzenes: Their analytical chemistry, environmental occurrence and fate. Intern. J. Environ. Anal. Chem. 26:241-263.

Eganhouse, B. Gould, D. Olaguer, P. Sherblom and C. Phinney. 1987. Analytical procedures for the congener-specific determination of chlorobiphenyls in biological tissues. Final Report to the Massachusetts Dept. Environ. Qual. Engin. and U.S. E.P.A. 67pp.

Eganhouse, R.P. 1986. Baseline Assessment of Salem Harbor-Salem Sound and Adjacent Waters. Final Report to the New England Aquarium, October 10, 1986, 28pp.

Eganhouse, R.P. 1992. Unpublished data.

Eganhouse, R.P. and I.R. Kaplan. 1982a. Extractable organic matter in municipal wastewaters. 1. Petroleum hydrocarbons: Temporal variations and mass emission rates to the ocean. Envir. Sci. Technol. 16:180-186.

Eganhouse, R.P. and I.R. Kaplan. 1982b. Extractable organic matter in municipal wastewaters. 2. Hydrocarbons: Molecular characterization. Environ. Sci. Technol. 16:541-551.

Eganhouse, R.P. and I.R. Kaplan. 1988. Depositional history of Recent sediments from San Pedro Shelf, California: Reconstruction using elemental abundance, isotopic composition and molecular markers. Mar. Chem. 24:163-191.

Eganhouse, R.P. and M.I. Venkatesan. 1991. Chemical Oceanography. and Geochemistry. In: Ecology of the Southern California Bight, Chapter 3, University of California Press, Los Angeles. *In press*.

Eganhouse, R.P. and P.M. Sherblom. 1991. Assessment of the Chemical Composition of the Fox Point CSO Effluent and Associated Subtidal and Intertidal Environments: Organic Chemistry of CSO Effluent, Surficial Sediments and Receiving Waters. Final Report to the Massachusetts Dept. Environ. Protect. *In press*, 127pp.

Eganhouse, R.P. and R.W. Gossett. 1991. Historical deposition and biogeochemical fate of polycyclic aromatic hydrocarbons in sediments near a major submarine wastewater outfall in southern California. pp. 191-220, *In*: Organic Substances and Sediments in Water, Vol. 2, R.A. Baker, ed., Lewis Publishers, Boca Raton, FL.

Eganhouse, R.P., B.R. Gould, D.M. Olaguer, C.S. Phinney, and P.M. Sherblom. 1989. Congener-specific determination of chlorobiphenyls in biological tissues using an Aroclor-based secondary calibration standard. Intern. J. Environ. Anal. Chem. 35:175-198.

Eganhouse, R.P., D.L. Blumfield, and I.R. Kaplan. 1983a. Long-chain alkylbenzenes as molecular tracers of domestic wastes in the marine environment. Environ. Sci. Technol. 17:523-530.

Eganhouse, R.P., D.P. Olaguer, B.R. Gould, and C.S. Phinney. 1988. Use of molecular markers for the detection of municipal sewage sludge at sea. Mar. Environ. Res. 25:1-22.

Eganhouse, R.P., E. Unher, and I.R. Kaplan. 1983c. Unpublished data.

Eganhouse, R.P., E.C. Ruth, and I.R. Kaplan. 1983b. Determination of long-chain alkylbenzenes in environmental samples by argentation thin-layer chromatography/high-resolution gas chromatography and gas chromatography/mass spectrometry. Anal. Chem. 55:2120-2126.

Emery K.O. 1960. The sea off southern California--A modern habitat of petroleum. John Wiley and Sons, N.Y.

Engineering Science. 1991. Point Loma outfall extension report -- Volume II, Engineering studies. Report prepared for City of San Diego by Engineering-Science, Inc., La Jolla, CA.

EPA. 1988. Workshop on predicting sediment quality around ocean outfalls. Marine Research Division, U.S. EPA, Newport, OR.

Faisst, W.K. 1976. Digested sludge: Delineation and modeling for ocean disposal. Ph.D. Dissertation, California Institute of Technology, Pasadena. 193pp.

Farley, K.J. 1990a. Personal communication.

Farley, K.J. 1990b. Predicting organic accumulation in sediments near marine outfalls. J. Env. Eng., V116, No. 1, Feb. 1990, p144-165.

Farley, K.J. and A.P. Castro. 1990. Effects of stratification on the deposition of organic material near marine sewage outfalls. Rept. to SCCWRP from Env. Sys. Eng. Dept., Clemson Univ. 46pp.

Farley, K.J. and F.M.M. Morel. 1986. The role of coagulation in the kinetics of sedimentation. Environ. Sci. Tech. 20:187-195.

Galloway, J.N. 1979. Alteration of trace metal geochemical cycles due to the marine discharge of wastewater. Geochim. Cosmochim. Acta 43:207-218.

Grant, W.D. and O.S. Madsen. 1986. The continental shelf bottom layer. Ann. Rev. Fluid Mech. 18:256-305.

Grant, W.D. and O.S. Madsen. 1979. Combined wave and current interaction with a rough bottom. J. Geophys. Res. 87:469-481.

Grimalt, J.O., P. Fernandez, J.M. Bayona, and J. Albaigés. 1990. Assessment of fecal sterols and ketones as indicators of urban sewage inputs to coastal waters. Environ. Sci. Technol. 24:357-363.

Harding, J. and T.J. Hendricks. 1973. The uptake and possible dispersion of ammonia. SCCWRP Technical Memorandum. Southern California Coastal Water Research Project, Long Beach.

Hedges, J.I. and J.H. Stern. 1984. Carbon and nitrogen determinations of carbonate-containing solids. Limnol. Oceanogr. 29:657-663.

Hendricks, T.J. 1976. Current velocities required to move sediments. *In*: Annual Report 1976. Southern California Coastal Water Research Project, Long Beach, pp. 71-76.

Hendricks, 1977. Coastal currents. *In*: Annual Report 1977. Southern California Coastal Water Research Project, El Segundo, pp. 53-62.

Hendricks, T.J. 1978. Forecasting changes in sediments near wastewater outfalls. *In*: Annual Report 1978, Southern California Coastal Water Research Project, pp. 127-143.

Hendricks, T.J. 1980. Currents in the Los Angeles Area. *In*: Annual Report 1980, Southern California Coastal Water Research Project, Long Beach, pp. 243-254.

Hendricks, T.J. 1983. Numerical model of sediment quality near an ocean outfall. Final Rept. to Nat. Oceano. and Atm. Adm. (NOAA Grant # NA80RAD00041) from Southern California Coastal Water Research Project, Long Beach. 149pp.

Hendricks, T.J. 1987. A Study of Sediment Composition, Transport, and Deposition off Palos Verdes. Final Report to County Sanitation Districts of Los Angeles County. 46pp.

Hendricks, T.J. 1987. Seasonal and Spatial Variations in Sediment Resuspension. *In*: Annual Report 1987, Southern California Coastal Water Research Project, Long Beach, pp. 35-39.

Hendricks, T.J. 1990. Analysis of cross-shore transport off Point Loma. Rept. to: Engineering Science, Inc. from Southern California Coastal Water Research Project, Long Beach. 59pp.

Hendricks, T.J. 1992. Orange County Currents: Phase II - SCCWRP Measurements. Report to County Sanitation Dist. of Orange County, CA. from Southern California Coastal Water Research Project, Long Beach. 30pp.

Hendricks, T.J. and R.P. Eganhouse. 1990. Modfification and verification of sediment deposition models: Phase 1 - Modeling component. Prog. Rept. #4 to Calif. State Water Res. Ctrl. Brd. from Southern California Coastal Water Research Project, Long Beach. 83pp.

Herring, J.R. and A.L. Abati. 1978. Effluent particle dispersion. *In*: Annual Report 1978, Southern California Coastal Water Research Project, El Segundo, pp. 113-125.

Hopkinson, C.S., Jr. 1985. Shallow-water benthic and pelagic matabolism: evidence of heterotrophy in the nearshore Georgia Bight. Mar. Biol. 87:19-32.

Jackson, G.A. 1982. Sludge disposal in southern California basins. Environ. Sci. Technol. 16:746-757.

Jackson, G.A., F. Azam, A.F. Carlucci, R.W. Eppley, B. Finney, D.S. Gorsline, B. Hickey, C.-A. Huh, R.A. Jahnke, I.R. Kaplan, M.R. Landry, L.F. Small, M.I. Venkatesan, P.M. Williams, and K.M. Wong, 1989. Elemental cycling and fluxes off the coast of southern California. EOS, Trans., Am. Geophys. Union. 70:146-155.

Jahnke, R.A.1990. Early diagenesis and recycling of biogenic debris at the sea floor, Santa Monica Basin, California. J. Mar. Res. 48:413-436.

Keith, J.O., L.A. Woods, and E.G. Hunt. 1970. Reproductive failure in brown pelicans on the Pacific coast. pp. 56-63, *In*: Transactions 35th North American Wildlife Natural Resources Conference.

Kettenring, K.N. 1981. The trace metal stratigraphy and recent sedimentary history of anthrogenous particulates on the San Pedro Shelf, California. Ph.D. Dissertation, University of California, Los Angeles, 156pp.

Kinnetics. 1988. San Elijo ocean outfall - Basline monitoring program. Report to City of Escondido, CA from Kinnetic Labs, Inc., Carlsbad, CA. Rept. #KLI-R-88-11. (rev. Mar. 1989).

Klein, D.H. and E.D. Goldberg. 1970. Mercury in the marine environment. Environ. Sci. Technol. 4:765-768.

Koh, R.C.V. 1982. Initial sedimentation of waste particulates discharged from ocean outfalls. Environ. Sci. Technol. 16:757-763.

Kolpack, R. L. 1987. Environmental Processes Affecting DDT Contaminated Sediments Off Palos Verdes, California. Proceedings of A Sediment Dynamics Workshop, Pomona, California, October 19-21, 1987, 102pp.

Landry, M.R., W.K. Peterson, and C.C. Andrews. 1991. Particulate flux in the water column overlying Santa Monica Basin: Adventures in sediment trapology. Contribution from School of Oceano and Earth Science 2nd Tech., Univ. of Hawaii, Manoz, Honolulu,HI. 48 pp.

Liu, K.-K. 1979. Geochemistry of inorganic nitrogen compounds in two marine environments: The Santa Barbara Basin and the ocean off Peru. Ph.D. Dissertation, University of California, Los Angeles, 354 pp.

Liu, K.-K. and I.R. Kaplan. 1989. The eastern tropical Pacific as a source of ^{15}N-enrihed nitrate in seawater off southern California. Limnol. Oceanogr. 34:820-830.

MacGregor, J.S. 1974. Changes in the amount and proportions of DDT and its metabolites, DDE and DDD, in the marine environment off southern California, 1949-1972. U.S. Fish. Bull. 72:275-293.

MacGregor, J.S. 1976. DDT and its metabolites in the sediments off southern California. U.S. Fish. Bull. 74:27-35.

McCalley, D.V., M. Cooke, and G. Nickless. 1981. Effect of sewage treatment on faecal sterols. Water Res. 15:1019-1025.

McDermott, D.J., T.C. Heesen and D.R. Young. DDT in Bottom Sediments around Five southern California Outfall Systems. Techn. Mem. 217, Southern California Coastal Water Research Project, El Segundo. 54p.

Minagawa, M., D.A. Winter, and I.R. Kaplan. 1984. Comparison of Kjeldahl and combustion methods for measurement of nitrogen isotope ratios in organic matter. Anal. Chem. 56:1859-1861.

Morel, F.M.M., J.C. Westall, C.R. O'Melia, and J.J. Morgan. 1975. Fate of trace metals in Los Angeles County Wastewater Discharge. Environ. Sci. Technol. 9:756-761.

Myers, E.P. 1974. The concentration and isotopic composition of carbon in marine sediments affected by a sewage discharge. Ph.D. dissertation, California Institute of Technology, Pasadena. 179pp.

Nardin, T.R., R.H. Osborne, D.J. Bottjer, and R.C. Scheidemann. 1981. Holocene sea-level curves for Santa Monica Shelf, California Continental Borderland. Science 213:331-333.

Olmez, I., E.R. Sholkovitz, D. Hermann and R.P. Eganhouse. 1991. Rare earth elements in sediments off southern California: A new anthropogenic indicator. Environ. Sci. Technol. 25:310-316.

Ontnes R.K. and L. Enochson. 1978. Applied Time Series Analysis - Volume I: Basic Techniques. John Wiley and Sons, New York. 449pp.

Peters, K.E., R.E. Sweeney, and I.R. Kaplan. 1978. Correlation of carbon and nitrogen stable isotope ratios in sedimentary organic matter. Limnol. Oceanogr. 23:598-604.

Pierson, L.J., G.I. Shiller, and R.A. Slater. 1987. Archaeological resource study: Morro Bay to Mexican Border. Final Rept. to Minerals Mgmt. Serv., U.S. Dept. Interior (MMS 870025). PS Associates, Cardiff, CA. 199pp.

Roberts, P.J.W., W.H. Synder, and D.J. Baumgartner. 1989a. Ocean outfalls. I: Submerged wastsefield formation. J. Hyd. Eng. 115:1-25.

Roberts, P.J.W., W.H. Synder, and D.J. Baumgartner. 1989b. Ocean outfalls. II: Spatial evolution of submerged wastefield. J. Hyd. Eng. 115:26-48.

Roberts, P.J.W., W.H. Synder, and D.J. Baumgartner. 1989c. Ocean outfalls. III: Effect of diffuser design on submerged wastefield. J. Hyd. Eng. 115:49-70.

Rohatgi, N. and K.Y. Chen. 1975. Transport of trace metals by suspended particulates on mixing with seawater. J. Water Pollut. Control Fed. 47:2297-2316.

Ross, M. 1991. Personal communication, Massachusetts Water Resources Authority, 6/27/91.

SCCWRP. 1973. The Ecology of the Southern California Bight: Implications for Water Quality Managment, TR104, Southern California Coastal Water Research Project, El Segundo. 531p.

SCCWRP. 1987. Seasonal and Spatial Variations in Sediment Resuspension. *In*: Annual Report, 1987. Southern California Coastal Water Research Project, Long Beach, pp. 35-39.

SCCWRP. 1989. Recent changes and long term trends in the combined mass emissions discharged into the southern California Bight. *In*: Annual Report, 1988-89. Southern California Coastal Water Research Project, Long Beach, pp. 20-28.

SCCWRP. 1991a. Potential applications of waste-specific molecular markers. *In*: Annual Report, 1989-90. Southern California Coastal Water Research Project, Long Beach, pp. 38-46.

SCCWRP. 1991b. Characteristics of effluents from large municipal wastewater treatment facilities in 1989. *In*: Annual Report, 1989-90. Southern California Coastal Water Research Project, Long Beach, pp. 8-15.

Schlicting H. 1960. Boundary Layer Theory. Translation by J. Kestin. Fourth Edition. McGraw-Hill, Inc., NY. 635p.

Schwalbach J.R. 1982. Sediment Budget for the California Continental Borderland--Northern Region. Unpubl. M.S. Thesis, Univ. of So. Calif., Los Angeles. 190pp.

Schwalbach J.R. and D.S. Gorsline. 1985. Holocene sediment budgets for the basins of the California continental borderland. J. Sed. Petrol. 55:829-842.

SDW. 1987. Environmental processes affecting DDT contaminated sediments off Palos Verdes, California. Report by: Sediment Dynamics Workshop Group (R.L. Kolpack, ed.). Kellog West Conf. Cntr., Pomona, CA. Oct. 19-21, 1987. 102pp.

Sheldon, R.W. 1972. Size separation of marine seston by membrane and glass-fiber filters. Limnol. Oceanogr. 17:494-498.

Sherblom, P. 1990. Factors affecting the availability and accumulation of long chain linear alkylbenzenes in *Mytilus edulis*. Ph.D. Dissertation. University of Massachusetts, Boston, 195pp.

Sherblom, P.M. and R.P. Eganhouse. 1988. Correlations between octanol-water partition coefficients and reversed-phase high-performance liquid chromatography capacity factors. J. Chromatography 454:37-50.

Stubbs, H.H., D.W. Diehl, and G.P. Hershelman. 1987. A Van Veen grab sampling method. Technical Report 276. Southern California Coastal Water Research Project, Long Beach. 4pp.

Stull, J.K., R.B. Baird, and T.C. Heesen. 1986. Marine sediment core profiles of trace constituents offshore of a deep wastewater outfall. J. Water Pollut. Control Fed. 58:985-991.

Stuermer, D.H., K.E. Peters, and I.R. Kaplan. 1978. Source indicators of humic substances and proto-kerogen. Stable isotope ratios, elemental compositions and electron spin resonance spectra. Geochim. Cosmochim. Acta 42:989-997.

Sweeney, R.E. and I.R. Kaplan. 1980a. Natural abundances of ^{15}N as a source indicator for near-shore marine sedimentary and dissolved nitrogen. Mar. Chem. 9:81-94.

Sweeney, R.E. and I.R. Kaplan. 1980b. Tracing flocculent industrial and domestic sewage transport on San Pedro Shelf, southern California, by nitrogen and sulphur isotope ratios. Mar. Environ. Res. 3:215-224.

Sweeney, R.E., E.K. Kalil, and I.R. Kaplan. 1980. Characterisation of domestic and industrial sewage in southern California coastal sediments using nitrogen, carbon, sulphur and uranium tracers. Mar. Environ. Res. 3:225-242.

Sweeney, R.E., K.K. Liu, and I.R. Kaplan. 1978. Oceanic nitrogen isotopes and their uses in determining the source of sedimentary nitrogen. Stable Isotopes in the Earth Sciences. DSIR Bulletin 220:9-26.

Takada, H. and R. Ishiwatari. 1987. Linear alkylbenzenes in urban riverine environments in Tokyo: Distribution, source, and behavior. Environ. Sci. Technol. 21:875-883.

Takada, H. and R. Ishiwatari. 1989. Biodegradation experiments of linear alkylbenzenes (LABs): Isomeric composition of C^{12} LABs as an indicator of the degree of LAB degradation in the aquatic environment. Environ. Sci. Technol. 24:86-91.

Takada, H. and R. Ishiwatari. 1991. Linear alkylbenzenes (LABs) in urban riverine and coastal sediments and their usefulness as a molecular indicator of domestic wastes. Water Sci. Technol. 23:437-446.

Tetra Tech. 1987. A simplified deposition calculation (DECAL) for organic accumulation near marine outfalls. Final Report to U.S. EPA (Contract # 68-01-6938). Marine Operations Div., Office of Mar. and Est. Protect., U.S. EPA, Washington, DC. 49pp.

Thomas, W.H. 1972. Nutrients, chlorophyll, and phytoplankton productivity near southern California sewage outfalls. Inst. of Mar. Resources Ref. No. 72-19. Univ. of Calif. San Diego, La Jolla. 77pp.

Thompson, B.E., J.D. Laughlin, and D.T. Tsukada. 1987. 1985 Reference site survey. Technical Report #221. Southern California Coastal Water Research Project, Long Beach. 50pp.

Thompson, B.E. 1992. Recovery of Santa Monica Bay from sludge discharge. Report to the City of Los Angeles Bureau of Sanitation. Southern California Coastal Water Research Project, Long Beach.

Venkatesan, M.I. and I.R. Kaplan. 1990. Sedimentary coprostanol as an index of sewage addition in Santa Monica Basin, southern California. Environ. Sci. Technol. 24:208-214.

Venkatesan, M.I. and I.R. Kaplan. 1992. Vertical and lateral transport of organic carbon and the carbon budget in Santa Monica Basin, California. Prog. Oceanogr. *In press*.

Walker, R.W., C.K. Wun, and W. Litsky. 1982. Coprostanol as an indicator of fecal polllution. *In*: CRC Critical Reviews in Environmental Control, CRC Press, Boca Raton, Florida, pp. 91-112.

Wang, R.-F. T. 1988. Laboratory analysis of settling velocities of wastewater particles in seawater using holography. Ph.D. dissertation, California Institute of Technology, Pasadena, 265pp.

Washburn L., B.H. Jones, A. Bratkovich, T.D. Dickey, and M.S. Chem. 1991. Mixing, dispersion, and resuspension in the vicinity of an ocean wastewater plume. Joy. Hyd. Eng. *In Press*.

Williams, P.M. 1986. Chemistry of the dissolved and particulate phases in the water column. *In*: Lecture notes on coastal and estuarine studies. Vol. 15. Plankton dynamics of the Southern California Bight. R.W. Eppley, ed., Springer-Verlag, Berlin, pp. 53-83.

Williams, P.M., K.J. Robertson, A. Soutar, S.M. Griffin, and E.R.M. Druffel. 1992. Isotopic signatures (^{14}C, ^{13}C, ^{15}N) as tracers of sources and cycling of soluble and particulate organic matter in the Santa Monica Basin, California. Submitted to Prog. Oceanogr. 43pp.

Winant, C.D. 1983. Longshore coherence of currents on the southern California shelf during the summer. J. Phys. Oceanogr. 13:54-64.

Wu, J. 1969. Mixed region collapse with internal wave generation in a density-stratified medium. J. Fluid Mech. 35:531-544.

LIST OF FIGURES

Table 2.1. Effluent sampling dates

JWPCP	Hyperion	OCSD	PLTP
11/1/89	11/3/89	10/31/89	11/3/89
12/19/89			
1/17/90	1/12/90	1/17/90	1/18/90
2/21/90			
3/7/90	3/6/90	3/9/90	3/12/90
4/12/90			
5/3/90	5/3/90	5/17/90	5/24/90
6/21/90			
7/6/90	7/7/90	7/5/90	7/6/90
8/22/90			
10/1/90		9/24/90	9/17/90
11/1/90	11/9/90	11/21/90	11/19/90
11/21/90			

2.2. Deployment of sediment traps off Palos Verdes, Orange County and Point Loma during 1989-90.

	Coordinates	Deployment date	# days	Comments
'erdes:				
	33° 42.67 118° 21.82	10/30/89	29	deployment normal
	33° 42.73 118° 21.84	11/28/89	36	deployment normal
	33° 42.70 118° 21.76	1/3/90	--	mooring lost
	33° 42.66 118° 21.83	2/12/90	--	mooring lost
	33° 42.71 118° 21.88	3/12/90	35	deployment normal
	33° 42.71 118° 21.91	4/16/90	28	deployment normal
	33° 42.84 118° 21.90	5/14/90	--	mooring lost
	33° 43.11 118° 21.84	6/8/90	33	deployment normal
	33° 42.90 118° 21.89	7/11/90	--	mooring lost
	33° 42.90 118° 21.89	8/28/90	--	mooring lost
	33° 42.67 118° 21.71	10/25/90	18	deployment normal
County:				
	33° 34.44 118° 01.13	10/27/89	34	deployment normal
	33° 34.48 118° 01.10	11/30/89	35	deployment normal
	33° 34.45 118° 01.10	1/4/90	33	deployment normal
	33° 34.45 118° 01.10	2/6/90	16	deployment normal

continued on next page

Table 2.2 continued

Site	Coordinates	Deployment date	# days	Comments
Orange County:				
	33° 34.46 118° 00.94	2/22/90	29	deployment normal
	33° 34.46 118° 00.94	3/23/90	34	deployment normal
	33° 34.48 118° 00.89	4/26/90	--	mooring lost
	33° 34.50 118° 00.96	5/24/90	--	mooring lost
	33° 34.52 118° 00.96	6/21/90	34	deployment normal
	33° 34.52 118° 00.96	7/25/90	36	deployment normal
	33° 34.40 118° 00.97	8/30/90	29	deployment normal
	33° 34.41 118° 00.98	9/28/90	35	deployment normal
. Loma:				
	32° 40.87 117° 16.96	11/8/89	30	deployment normal
	32° 40.85 117° 16.96	12/8/89	--	mooring lost
	32° 40.85 117° 16.95	1/8/90	31	normal deployment
	32° 40.85 117° 16.95	2/8/90	27	deployment normal, #1[1]
	32° 40.85 117° 16.95	2/8/90	27	deployment normal, #2[1]
	32° 40.90 117° 16.96	3/7/90	34	deployment normal, #1[1]
	32° 40.90 117° 16.96	3/7/90	34	deployment normal, #2[1]

continued on next page

Table 2.2 continued

	Coordinates	Deployment date	# days	Comments
ma:				
	32° 40.90 117° 16.96	4/10/90	28	deployment normal
	32° 40.85 117° 16.90	5/8/90	70	trap lost for one month
	32° 40.88 117° 16.88	6/15/90	32	deployment normal
	32° 40.74 117° 16.80	7/17/90	31	deployment normal
	32° 40.74 117° 16.80	8/17/90	26	deployment normal
	32° 40.74 117° 16.80	9/12/90	--	mooring lost
	32° 40.80 117° 16.85	10/11/90	--	mooring lost

Separate moorings were deployed approximately 50 meters apart on this date.

Table 2.3 Information on the collection of surface sediments (modified Van Veen grab) and gravity cores off Orange County and Pt. Loma.

Station[1]	Coordinates	Date	Water Depth (m)	Comments
		Orange County:		
OC-ZB	33° 34.49 118° 00.20	5/2/89	56	silty clay, slight H_2S smell
OC-ZB2	33° 34.56 118° 00.57	"	56	silty clay
OC-0	33° 34.52 118° 00.51	"	56	silty clay, slight H_2S smell
OC-1	33° 34.64 118° 00.87	"	56	silty clay
OC-2	33° 34.95 118° 00.43	"	49	silty clay
OC-3	33° 34.40 118° 00.61	"	60	silty clay
OC-5	33° 34.72 118° 01.54	"	59	silty clay
OC-7	33° 35.42 118° 00.31	"	38	silty clay
OC-9	33° 34.28 117° 59.43	"	59	silty clay
OC-10	33° 34.95 118° 01.98	"	60	silty clay
OC-11	33° 36.01 118° 00.09	"	30	silty clay
OC-13	33° 35.26 118° 02.91	"	59	silty clay
OC-17.5	33° 33.95 118° 00.31	"	91	silty clay
OC-37	33° 34.88 117° 57.33	"	56	sandy clay
OC-con	33° 35.78 118° 03.80	"	56	silty clay

continued on next page

Table 2.3 continued

Station	Coordinates	Date	Water Depth (m)	Comments
		Pt. Loma:		
SD A-2	32° 39.37 117° 16.68	4/6/89	59	sandy silt
SD A-5	32° 41.32 117° 17.27	"	62	sandy silt
SD A-9	32° 40.83 117° 17.12	"	63	sandy silt
SD A-12.5	32° 40.82 117° 16.53	"	52	silty clay
SD A-15	32° 40.10 117° 16.90	"	61	sandy silt
SD A-16	32° 40.58 117° 17.05	"	60	sandy silt
SD A-17	32° 40.30 117° 17.11	"	66	silty clay
SD B-3	32° 45.42 117° 18.38	"	60	sandy silt
SD B-5	32° 49.25 117° 19.60	"	60	sandy silt
SD X-1	32° 40.67 117° 16.87	"	62.5	silty clay, slight H_2S
SD X-2	32° 40.87 117° 17.08	"	65	silty clay
SD X-3	32° 40.45 117° 17.53	"	71	sandy silt
SD X-4	32° 40.27 117° 18.42	"	83	silty clay
SD X-5	32° 40.00 117° 17.20	"	76	silty clay
SD X-6	32° 38.38 117° 16.63	"	64	sandy silt

1 For locations see Figures 3 and 4.

Table 2.4. Amounts of recovery surrogates and internal (quantitation) standards used for trace organics measurements.

Compound[1]	Class	Volume used (μliters)[2]	Concentration (ng μliter^{-1})
		Effluent:	
androstanol(RS)	Sterols	200	105.
1-phenyldecane(RS)	LABs	40	40.5
1-phenylundecane(RS)	"	40	54.2
1-phenyldodecane(RS)	"	40	50.2
1-phenyltridecane(RS)	"	40	60.4
1-phenyltetradecane(RS)	"	40	40.4
2,4,6-trichlorobiphenyl(RS)	PCB	50	0.0959
2,3,3',5,6-pentachlorobiphenyl(RS)	"	50	0.0565
2,2',3,3',4,5,5',6-octachlorobiphenyl(RS)	"	50	0.0246
naphthalene-D_8 (RS)	PAH	50	0.639
phenanthrene-D_{10} (RS)	"	50	0.549
acenaphthene-D_{10} (RS)	"	50	0.585
perylene-D_{12} (RS)	"	50	0.534
chrysene-D_{12} (RS)	"	50	0.544
5α(H)-cholestane(IS)	Sterols	--	42.4
1-phenylnonane(IS)	LABs	--	26.8
1-phenylpentadecane(IS)	"	--	30.8
3,3'-dichlorobiphenyl(IS)	PCB	--	--
2,2',3,3',4,4',5,6,6'-nonachlorobiphenyl(IS)	"	--	--
hexamethylbenzene(IS)	PAH	--	21.9
benzo[b]fluoranthene-D_{12}(IS)	"	--	10.3
benzo[g,h,i]perylene-D_{12}(IS)	"	--	20.8

continued on next page

Compound[1]	Class	Volume used (μliters)[2]	Concentration (ng μliter^{-1})
	Sediments, Sediment Trap Particles:		
androstanol(RS)	Sterols	100	1.05
1-phenyldecane(RS)	LABs	100	0.405
1-phenylundecane(RS)	"	100	0.542
1-phenyldodecane(RS)	"	100	0.502
1-phenyltridecane(RS)	"	100	0.604
1-phenyltetradecane(RS)	"	100	0.404
2,4,6-trichlorobiphenyl(RS)	PCB	50	1.92
2,3,3',5,6-pentachlorobiphenyl(RS)	"	50	1.13
2,2',3,3',4,5,5',6-octachlorobiphenyl(RS)	"	50	0.492
naphthalene-D_8(RS)	PAH	500	0.639
phenanthrene-D_{10}(RS)	"	500	0.549
acenaphthene-D_{10}(RS)	"	500	0.585
perylene-D_{12}(RS)	"	500	0.534
chrysene-D_{12}(RS)	"	500	0.544

1 Letters in parentheses indicate whether compound was used as a recovery surrogate (RS) or an internal standard (IS).

2 For recovery surrogates, this is the volume of solution added to each sample. No data are provided for internal standards because different volumes were added to each final fraction.

: 2.5. Precision and accuracy of elemental (CHN) analyses of effluent particles and sediments.

ple[2]	N	Concentration (%)[1]					
		Carbon		Nitrogen		Hydrogen	
		mean	CV[3]	mean	CV	mean	CV
ent	5	41.2	1.7	4.79	4.2	7.31	3.2
ge-1	5	35.0	0.5	3.09	3.1	11.4	3.8
ge-2	5	40.0	2.8	3.62	1.8	7.38	1.5
ment-1	10	11.4	1.8	0.42	29.	1.85	1.7
S-1a	5	3.59	0.8	0.28	1.0	0.88	3.1
S-1b	3	3.48	1.1				
S-1c	3	3.61	0.8				
fied value		3.69	3.0				

Concentrations in effluent and sludge samples are for carbonate-free solids; concentration for PACS-1 is for untreated material.

Effluent and sludge samples were obtained from the JWPCP as final effluent and raw sludge, respectively. Sediment-1 was marine sediment from Santa Monica Bay (HR-6-6) run without carbonate removal. PACS-1 is a standard reference material from the National Research Council of Canada. It is an estuarine sediment from Esquimalt Harbor, British Columbia.

CV = coefficient of variation (%).

Table 2.6. Results of intercomparison exercise between SCCWRP and West Coast Analytical Service (WCAS) using Canadian National Research Council standard reference materials.

Metal	Concentrations (μg dry g^{-1})		
	Certified value	SCCWRP	WCAS
		MESS-1	
Cr	71.	34.	27.4
Ni	29.5	21.	21.
Cu	25.1	23.	20.9
Zn	191.	165.	150.
Ag	–	–	0.1
Cd	0.59	0.55	0.52
Pb	34.0	23.	29.7
		PACS-1	
Cr	113.	77.	54.5
Ni	44.1	32.	29.
Cu	452.	459.	328.
Zn	824.	792.	650.
Ag	–	–	1.08
Cd	2.38	2.6	1.44
Pb	404.	384.	396.

Table 2.7. Limits of detection for ICP-MS trace metal measurements.[1]

Element	Limit of Detection (μg dry g^{-1})
Pb	0.06
Cd	0.04
Be	0.09
Cr	0.5
Ni	0.07
Cu	0.2
Zn	0.6
As	2.0
Se	1.0
Ag	0.02
Sb	0.2
Hg	0.05
Th	0.02

1 Data supplied by West Coast Analytical Service, Inc. (Santa Fe Springs, CA).

Table 2.8. Chromatographic conditions of analysis for trace organics.

Parameter	Value
Linear Alkylbenzenes	
Carrier gas	helium
Carrier gas linear velocity	30 cm sec^{-1}
Injector temperature	250°C
Splitless valve activation time	45 sec
Injection volume	1.0 μliter
Initial oven temperature (T_1)	40°C
Initial temperature hold time	5 min
Second oven temperature (T_2)	150°C
Program rate (first ramp)	25°C min^{-1}
Final oven temperature (T_3)	290°C
Program rate (second ramp)	4°C min^{-1}
Final temperature hold time	35 min
Column:	
length	30 meters
inner diameter	0.25 mm
phase	DB-5 (5% phenyl, J&W Scientific)
film thickness	0.25 microns
Fecal sterols	
Carrier gas	helium
Carrier gas linear velocity	30 cm sec^{-1}
Injection method	cool on-column
Initial injector temperature	60°C
Final injector temperature	290°C
Injector temperature program rate	100°C min^{-1}
Final injector temperature hold time	63 min
Initial oven temperature (T_1)	70°C
Initial temperature hold time	5 min
Final oven temperature (T_2)	285°C
Program rate (first ramp)	6°C min^{-1}
Final temperature hold time	50 min
Column:	
length	30 meters
inner diameter	0.25 mm
phase	DB-5 (5% phenyl, J&W Scientific)
film thickness	0.25 microns

Table 2.9. Ions used for GC/MS quantition of the linear alkylbenzenes.

Compound	Ion used (m/z)	Internal standard used
5-phenyldecane	91	1-phenylnonane
4-phenyldecane	91	"
3-phenyldecane	91	"
2-phenyldecane	105	"
1-phenyldecane (RS)	92	—
6-phenylundecane	91	1-phenylnonane
5-phenylundecane	91	"
4-phenylundecane	91	"
3-phenylundecane	91	"
2-phenylundecane	105	"
1-phenylundecane (RS)	92	"
6-phenyldodecane	91	"
5-phenyldodecane	91	"
4-phenyldodecane	91	"
3-phenyldodecane	91	"
2-phenyldodecane	105	"
1-phenyldodecane (RS)	92	"
7&6-phenyltridecane	91	1-phenylpentadecane
5-phenyltridecane	91	"
4-phenyltridecane	91	"
3-phenyltridecane	91	"
2-phenyltridecane	105	"
1-phenlytridecane (RS)	92	"
7-phenyltetradecane	91	1-phenylpentadecane
6-phenyltetradecane	91	"
5-phenyltetradecane	91	"
4-phenyltetradecane	91	"
3-phenyltetradecane	91	"
2-phenyltetradecane	105	"
1-phenyltetradecane (RS)	92	"
1-phenylnonane (IS)	92	—
1-phenylpentadecane (IS)	92	—

Table 2.10
Effluent Characteristics

Location	Flow	SS	Pb	Cd
San Diego	8.3	67	10	2
Orange County	11.3	49	16	3.3
LA County-90°	6.4	197	152	9.3
LA County-120	9.4	197	152	9.3

Table 2.11
Simulation Grid Orientation

Location	x-axis (mag.)	y-axis (mag.)
San Diego	353	263
Orange County	276	186
LA County	278	188

Table 2.12
Simulation Layer Thicknesses

Location	Top(m)	Wfld(m)	Bott.(m)
LA County	18	30.5	14(90) 7.5(120)
Orange County	19	26.5	10.9
San Diego	20	30.5	12

Table 2.13
Diffuser Legs

Location	Leg #	Len.(m)	Align(r)
LA County-90"	1	366	30
	2	366	150
LA County-120"	1	451	330
	2	903	180
Orange County	1	610	240
	2	1220	0
San Diego	1	410	30
	2	410	150

Table 2.14
Current Meter Deployments

Location	Source	Deployment	# Mon.	CM(m)	Water
San Diego	Eng.Sci.Inc.	Jan.90-Sept.90	7	30	56
Orange County	SCCWRP	Oct.89-Oct.90	13	36	56
LA County	SCCWRP	Various 1981-89	10	20-41	30-62

Table 2.15
Properties of the Tidal Component of the Currents

Location	Axis	Period	Amplitude	Phase
LA County	x	1.2.42	6.0	0
	y	12.42	2.4	90
	x	24.00	6.3	45
	y	24.00	3.1	135
Orange County	x	12.42	6.0	0
	y	12.42	4.3	90
San Diego	x	12.42	4.9	0
	y	12.42	4.2	90

Table 2.16
Properties of the Subtidal Component of the Currents

Location	Component	Spd (cm/sec)	% Occur.
LA County	+x (upcoast)	2.9	64.
	-x (dncoast)	1.5	36.
Orange Cnty.	+x (upcoast)	4.8	64.
	-x (dncoast)	3.1	36.
San Diego	+x (upcoast)	3.1	67.
	-x (dncoast)	1.5	34.

Table 2.17
Discharge and Diffuser Characteristics

Location	Dpth (m)	Flow (mgd)	Flow/Len $m^3/sec/m$	Len-Head Leg-1	Len-Head Leg-2
San Diego	62.5	147	0.0079	410m-025	410m-325
Orange County	56.4	215	0.0052	610m-040	1220m-280
LA County	62.5	148	0.0088	366m-130	366m-250

Table 2.18
Remineralization Rates of Organic Material in Sediments

Location	Reference	Rate(C) mmol-C/cm²/yr
Santa Monica Basin	Jahnke (1990)	0.09
San Pedro Basin	Berelson et.al.(1987)	0.07
San Nicholas Basin	Berelson et.al.(1987)	0.08
Santa Cruz Inner Basin	Bender et.al.(1989)	0.04
Cape Lookout Bight	Martens et.al.(1991)	4.1 (0.7->11)
Skan Bay, Alaska	Alperin et.al(1991)	1.8-2.0

Table 2.19
Decay rates of Organic Material in Sediments

Location	Conditions	References	Decay rate day⁻¹
Laboratory	Fresh plank/aerobic		0.024
Laboratory	Aged plankton/aerobic		0.0023
Cape Lookout Bight	Shallow/anoxic		0.006-0.007
Skan Bay	Shallow/anoxic/kelp		0.00008
Skan Bay	Shallow/anoxic/phyto		0.00005
So. Calif. Basins			0.0009-0.0035
Open Ocean			0.00002-0.00007

Table 3.1. Suspended solids content of southern California effluent samples collected during 1989-90.

Date Sampled	Suspended solids (mg liter^{-1})			
	47 mm	mean	25mm	mean
		Hyperion:		
11/3/89	65.0,58.9	61.9	56.1,54.8	55.5
1/12/90	64.3,57.2	60.8	–	–
3/6/90	–	–	61.9,61.4	61.6
5/3/90	–	–	58.9,61.9	60.4
7/7/90	61.4,60.1	60.7	–	–
11/9/90	–	–	–	–
		JWPCP:		
11/1/89	58.3,58.2	58.2	58.5,66.4	62.5
12/19/90	70.8,74.0	72.4	67.1,67.4	67.2
1/17/90	80.6,85.2	82.9	85.1,88.5	86.8
2/21/90	69.2,67.4	68.3	68.7,70.7	69.7
3/7/90	76.1	76.1	76.5,84.0	80.2
4/12/90	76.4,64.9	70.7	68.7,71.3	70.0
5/3/90	84.1,68.7	76.4	51.8,53.3	52.2
6/21/90	83.5,86.7	85.1	85.4,74.0	79.7
7/6/90	65.8,65.0,64.7,51.0	61.8	57.1	57.1
8/22/90	68.9,64.0	66.4	–	–
10/1/90	47.5,52.8,45.9,52.1	49.6	[35.2,23.7]^2	29.4^2
11/1/90	71.6	71.6	66.7	66.7
11/21/90	87.6,91.8	89.7	–	– –
		OCSD:		
10/31/89	65.0,61.8	63.4	62.4,59.7	61.0
1/17/90	54.0,58.0	56.0	57.4,57.3	57.4
3/9/90	–	–	59.6,61.9	60.8
5/17/90	–		46.1,53.5	49.8
7/5/90	54.1,54.7,52.6,56.7	54.5	56.3	56.3
9/24/90	43.6,42.9,31.4,51.7	42.4	[17.7,25.6]^2	21.6^2
11/21/90	81.3,76.7	79.0	[133.1,139.2]^2	139.2^2
		PLTP:		
11/3/89	82.1,78.8	80.5	78.9,83.5	81.2
1/18/90	68.7,94.7	81.7	106.9,125.1	116.0
3/12/90	–	–	95.0,94.5	94.8
5/24/90	–	–	90.8,111.0	100.9
7/6/90	103.6,104.2,98.4,101.4	101.9	97.6,103.0	100.3
9/17/90	121.7,115.5,123.0,108.4	117.2	86.3	86.3
11/19/90	–	–	112.8,127.8	120.3

1 Suspended solids were measured on Whatman GF/C glass fiber filters.

2 Questionable data.

Table 3.2. Elemental composition of effluent particles.

Effluent	Date	TOC (%)	TN (%)	C/N	POC[1]	PN[1]
JWPCP:	1/17/90	30.7	3.29	9.32	25.4	2.73
	3/7/90	28.7	4.02	7.13	21.8	3.06
	4/12/90	31.6	4.16	7.60	22.3	2.94
	7/6/90	35.0	4.32	8.11	21.6	2.67
	10/1/90	39.4	4.68	8.45	19.5	2.32
	11/1/90	37.2	3.90	9.53	26.6	2.79
	11/21/90	25.3	2.96	8.54	22.7	2.66
	Mean	32.6	3.90	8.38	22.8	2.74
	1 std dev	4.9	0.60	0.86	2.4	0.24
OCSD:	1/17/90	30.1	3.80	7.91	16.8	2.13
	3/9/90[2]	28.7	4.04	7.11	17.4	2.46
	5/17/90[2]	38.5	5.79	6.64	19.2	2.88
	7/5/90	39.9	5.75	6.94	21.7	3.13
	9/24/90	41.4[3]	5.47	7.58	17.6	2.32
	11/21/90	22.2[4]	3.38	6.55	17.5	2.67
	Mean	33.5	4.70	7.12	18.4	2.60
	1 std dev	7.6	1.08	0.53	1.82	0.37
PLTP:	1/18/90	24.8	3.19	7.77	20.3	2.61
	3/12/90[2]	32.9	5.06	6.50	31.2	4.80
	5/24/90[2]	35.3	3.55	9.95	35.6	3.58
	7/6/90	32.3	5.13	6.30	32.9	5.23
	9/17/90	35.5	4.07	8.72	41.6	4.77
	11/19/90[2]	23.0	2.45	9.38	27.7	2.95
	Mean	30.6	3.91	8.10	31.6	3.99
	1 std dev	5.4	1.06	1.51	7.2	1.09

1 Concentrations in units of mg liter^{-1}.

2 TSS concentrations based on 25 mm glass fiber filter were used to compute POC and PN concentrations for these samples (cf. Table 10).

3 Questionable due to unusually low TSS measured on this day.

4 Questionable due to unusually high TSS measured on this day.

Table 3.3. Stable isotopic composition of effluent particles from the JWPCP, OCSD and PLTP facilities.

Effluent	Date	$\delta^{13}C$ (‰)	$\delta^{15}N$ (‰)	Source
JWPCP:	7/6/90	-23.29	+1.68	This study
	11/21/90	-23.26	+2.37	This study
	12/4/72	-23.0[1]	--	Myers (1974)
	1/11/73	-22.7	--	"
	2/1/73	-23.4[1]	--	"
	5/12/73	-22.95[1]	--	"
	6/8/73	-23.5[1]	--	"
	6/29/73	-23.7[1]	--	"
	7/6/73	-24.5	--	"
	7/12/73	-23.8	--	"
	7/25/73	-24.0	--	"
	8/29/73	-24.0[1]	--	"
	1/15/79	-23.91	--	Eganhouse *et al.* (1983c)
	2/28/79	-24.31	--	"
	3/14/79	-23.59	--	"
	4/17/79	-23.71	--	"
	5/15/79	-23.72	--	"
	7/16/79	-23.93[1]	--	"
	8/15/79	-23.76	--	"
	9/13/79	-23.80[1]	--	"
	10/15/79	-23.45	--	"
	11/15/79	-24.28	--	"
	12/13/79	-24.02	--	"
	late 1970s	--	+3.0	Sweeney *et al.* (1980)
		--	+2.0	"
		--	+2.4	"
		--	+2.5	"
OCSD:	7/5/90	-22.06	-0.73	This study
	11/21/90	-22.59	+1.82	This study
	1/15/79	-24.04	--	Eganhouse *et al.* (1983c)
	4/12/79	-23.91	--	"
	7/18/79	-23.98	--	"
PLTP:	7/6/90	-21.76	+0.95	This study
	9/17/90	-22.43	+2.75	This study
	4/17/79	-23.05	--	Eganhouse *et al.* (1983c)
	7/17/79	-23.30	--	"
	10/16/79	-23.35	--	"

1 Mean values for several replicate analyses.

Table 3.4. Concentration of lead (Pb) and cadmium (Cd) in particles isolated from the JWPCP, OCSD and PLTP final effluents.

Effluent	Date sampled	Volume filtered (ml)	Particulate Concentration (μg dry g^{-1}) Pb	Cd
JWPCP:	1/17/90	29	84	10
	3/7/90	25	112	11
	5/3/90	20	124	<9
	7/6/90	25	65	6
	10/1/90	--[1]	<20	<10
OCSD:	1/17/90	32	52	9
	3/9/90	27.5	40	6
	5/17/90	20	54	63[2]
	7/5/90	25	23	<6
	9/24/90	--[1]	<20	<8
PLTP:	1/18/90	25	73	<5
	3/12/90	20	45	<5
	5/24/90	20	49	<5
	7/6/90	20	20	7

1 Not determined.

2 This unusually high concentration is considered suspect. The digest was re-analyzed and yielded a concentration of 62 μg dry g^{-1}.

Table 3.5. Concentrations (μg dry g^{-1}) of 13 elements determined in effluent particulate samples by ICP-MS.

Element	JWPCP		OCSD		PLTP	
	7/6/90	11/21/90	7/5/90	11/21/90	7/6/90	11/19/90
Pb	71	50	33	28	25	24
Cd	36[1]	3	18	16	12	4
Be	<2	<2	<2	<2	<2	<2
Cr	122	65	44	23	99	23
Ni	49	26	27	20	24	12
Cu	178	75	402	195	254	151
Zn	700	514	733	257	294	251
As	12	6	6	2	8	7
Se	60	<30	29	<20	<20	<30
Ag	28	19	28	137	32	21
Sb	3	7	4	<2	<2	16
Hg	4	<3	<3	<2	<2	<4
Th	<2	<2	<2	<2	<2	<2

1 Questionable data (cf. Table 13).

Table 3.6. Concentrations of linear alkylbenzenes (μg dry g^{-1}) determined in particles of final effluent.[1]

Compound	JWPCP		OCSD		PLTP	
	1/17/90	7/6/90	1/17/90	7/5/90	1/18/90	7/6/90
5-phenyldecane	9.46	3.35	5.22	0.74	3.28	3.80
4-phenyldecane	8.73	3.26	4.02	0.65	2.83	3.34
3-phenyldecane	9.92	4.41	4.06	<0.62	3.37	3.54
2-phenyldecane	16.6	6.56	7.08	1.37	2.61	5.30
6-phenylundecane	13.3	6.44	8.87	3.51	4.24	6.12
5-phenylundecane	22.8	10.0	14.3	5.97	7.81	10.5
4-phenylundecane	19.8	9.48	12.2	3.76	7.36	8.67
3-phenylundecane	22.9	11.5	13.0	4.12	7.85	8.27
2-phenylundecane	32.7	11.9	16.0	6.22	8.16	11.2
6-phenyldodecane	37.2	19.3	24.9	12.7	15.5	17.2
5-phenyldodecane	30.6	15.9	20.9	10.0	12.3	15.6
4-phenyldodecane	25.2	12.0	15.3	7.35	10.6	11.6
3-phenyldodecane	29.9	12.2	17.5	7.27	12.5	12.2
2-phenyldodecane	39.6	16.9	19.3	6.96	10.3	12.0
7&6-phenyltridecane	15.4	8.26	13.5	6.32	8.13	7.55
5-phenyltridecane	8.85	3.88	8.74	2.75	4.74	4.22
4-phenyltridecane	6.50	2.58	5.83	2.16	3.14	2.70
3-phenyltridecane	7.84	1.70	4.43	2.36	3.31	2.69
2-phenyltridecane	7.08	2.58	5.10	1.47	3.11	2.65
-phenyltetradecane	7.68	2.90	7.08	2.46	3.96	2.72
-phenyltetradecane	6.13	2.00	4.22	1.65	2.71	2.15
-phenyltetradecane	6.00	1.87	4.46	1.29	2.38	1.89
-phenyltetradecane	3.93	1.29	3.29	0.86	1.73	1.53
-phenyltetradecane	5.12	0.86	3.26	1.01	1.23	0.80
phenyltetradecane	<0.12	1.30	<0.17	0.58	1.29	0.95
phenyldecanes	44.7	17.6	20.4	2.77	12.1	16.0
phenylundecanes	111.6	49.4	64.4	23.6	35.4	44.8
phenyldodecanes	162.5	76.3	97.9	44.3	61.2	68.5
phenyltridecanes	45.6	19.0	37.6	15.1	22.4	19.8
phenyltetradecanes	28.9	10.2	22.3	7.84	13.3	10.0
LABs	393.	172.	242.	93.6	144.	159.

Concentrations have been corrected for recovery as described in text.

Table 3.7. Concentrations of total extractable organics and linear alkylbenzenes in final effluent: summary.

Effluent	Date	TEO ($mg\ g^{-1}$)	Total linear alkylbenzenes		
			$\mu g\ g^{-1}$	$\mu g\ liter^{-1}$	$\mu g\ g\ OC^{-1}$
			This work[1]:		
JWPCP:	1/17/90	205.	393.	32.6	1280.
	7/6/90	304.	172.	10.6	491.
OCSD:	1/17/90	271.	242.	13.6	804.
	7/5/90	294.	93.6	5.11	235.
PLTP:	1/18/90	136.	144.	11.8	580.
	7/6/90	291.	159.	16.2	492.
			Eganhouse *et al.* (1983)[2]:		
JWPCP:	1/15/79	180.	614.	108.	1360.
	2/15/79	276.	1220.	242.	–[3]
	3/14/79	275.	612.	98.0	1280.
	4/4/79	227.	686.	140.	–
	5/15/79	279.	472.	78.4	1020.
	6/15/79	231.	1340.	302.	–
	7/16/79	249.	504.	114.	1080.
	8/15/79	250.	651.	142.	–
	9/13/79	219.	728.	155.	1540.
	10/15/79	232.	484.	87.2	1390.
	12/13/79	–	1080.	173.	–
			Eganhouse (1986)[2]:		
SESD[4]:	2/17/86	–	47.8	5.30	89.0
	2/18/86	–	47.2	5.24	–
	2/26/86	–	114.	9.68	–
	3/11/86	–	59.9	6.29	–
	3/18/86	–	95.4	8.20	–
	3/25/86	215.	136.	11.8	–
	4/1/86	166.	70.1	6.38	–
			Sherblom (1990)[1]:		
Nut Island[4]:	9/10/88	–	–	17.9	–
	9/12/88	166.	152.	16.7	569.
	9/27/88	164.	784.	116.	3550.
	10/5/88	196.	267.	38.1	1160.

1 Concentrations are based on filtration of effluent and analysis of particles collected on Whatman GF/C filters.

2 Particulate LAB concentrations based on analysis of unfiltered effluent and assumption that 100% of LABs are associated with particles. Extraction of 1979 JWPCP effluent performed with chloroform.

3 Dashes indicate missing data (e.g. TSS, TOC) preventing calculation of concentrations.

4 SESD is the South Essex Sewage District in Salem, Massachusetts. Nut Island is one of two treatment plants in the Boston metropolitan area.

e 3.8. Concentrations of fecal sterols in final effluents from southern California, 1990.

luent	Date	Coprostanol			Epicoprostanol		
		$\mu g\ g^{-1}$	$\mu g\ liter^{-1}$	$\mu g\ g\ OC^{-1}$	$\mu g\ g^{-1}$	$\mu g\ liter^{-1}$	$\mu g\ g\ OC^{-1}$
				This work[1]:			
PCP:	1/17/90	2350.	234.	7650.	35.6	3.54	116.
	7/6/90	2010.	124.	5740.	76.3	4.71	218.
SD:	1/17/90	2210.	124.	7340.	15.4	0.86	51.2
	7/5/90	972.	53.1	2440.	<5.7	<0.31	<14.
P:	1/18/90	3050.	250.	12300.	66.2	5.41	267.
	7/6/90	1160.	118.	3590.	<2.0	<0.21	<6.2
				Eganhouse (1992)[2]:			
CP:	1/15/79	847.	149.	1870.	163.	28.7	361.
	2/15/79	1150.	229.	--	276.	55.0	--
	3/14/79	600.	96.1	1260.	98.8	15.8	207.
	4/4/79	936.	191.	--	246.	50.1	--
	5/15/79	2080.	346.	4480.	434.	72.1	935.
	6/15/79	1780.	400.	--	415.	93.4	--
	7/16/79	1270.	287.	2720.	349.	78.8	749
	8/15/79	885.	193.	--	317.	69.2	--
	9/13/79	1090.	237.	2300.	238.	50.8	503.
	10/15/79	552.	99.5	1580.	110.	19.8	315.
	12/13/79	1050.	168.	--	275	44.0	--
):	1/16/79	1670.	300.	3950.	252.	45.3	596.
	4/12/79	3650.	438.	9260.	626.	75.1	1590.
	7/16/79	2630.	374.	6730.	337.	47.9	862.
	10/16/79	2920.	353.	--	442.	53.5	--
:	1/16/79	3040.	475.	--	135.	21.1	--
	4/17/79	5030.	523.	9920.	256.	26.6	505.
	7/16/79	4760.	500.	9540.	82.8	17.8	166.
	10/16/79	5200.	546.	--	226.	23.7	--
				Venkatesan and Kaplan (1990)[1]:			
P:	11/87	947.	--	3740.	--	--	--

continued on next page

Table 3.8 continued

Effluent	Date	Coprostanol			Epicoprostanol		
		$\mu g\ g^{-1}$	$\mu g\ liter^{-1}$	$\mu g\ g\ OC^{-1}$	$\mu g\ g^{-1}$	$\mu g\ liter^{-1}$	$\mu g\ g\ OC^{-1}$
			Eganhouse (1986)[2]:				
SESD[4]:	2/17/86	583.	64.7	1090.	--	--	--
	2/18/86	560.	62.2	--	--	--	--
	2/26/86	809.	68.8	--	--	--	--
	3/11/86	677.	71.1	--	--	--	--
	3/18/86	--[5]	--[5]	--[5]	--	--	--
	3/25/86	811.	70.6	--	--	--	--
	4/1/86	443.	40.3	--	--	--	--
			Sherblom (1990)[1]:				
Nut Island[4]:	9/10/88	--	91.5	--	--	--	--
	9/12/88	2340.	257.	8760.	--	--	--
	9/27/88	1060	156.	4800.	--	--	--
	10/5/88	904.	129.	3930.	--	--	--

1 Concentrations are based on filtration of effluent and analysis of particles collected on Whatman GF/C filters.

2 Particulate sterol concentrations based on analysis of unfiltered effluent and assumption that 100% of sterols are associated with particles. Extraction of 1979 JWPCP effluent performed with chloroform.

3 Dashes indicate missing data (e.g. TSS, TOC) preventing calculation of concentrations.

4 SESD is the South Essex Sewage District in Salem, Massachusetts. Nut Island is one of two treatment plants in the Boston metropolitan area.

5 Sample lost.

Table 3.9. Comparison of performance of two sediment trap designs deployed above the sea floor off Point Loma, October, 1989.

Trap design	Elevation off bottom	Solids flux ($g\ cm^{-2}\ yr^{-1}$)	TOC (%)	TN (%)	C/N (%)	TVS (%)
			Buoy #6:			
Hendricks:	0.5 m	4.83	1.29	0.14	9.21	7.60
	2.0 m	1.01	2.41	0.27	8.93	7.75
	5.0 m	0.45	2.49	0.30	8.30	9.00
			Buoy#2:			
	0.5 m	4.11	2.72	0.33	8.24	7.49
	2.0 m	1.59	2.43	0.26	9.35	8.38
	5.0 m	1.45	2.88	0.34	8.47	9.69
			Buoy #5:			
New design:	0.5 m	4.56	2.40	0.26	9.23	7.99
	2.0 m	2.30	2.48	0.28	8.86	8.02
	5.0 m	0.97	2.47	0.28	8.82	9.84
			Buoy #3:			
	0.5 m	4.51	2.35	0.26	9.04	8.26
	2.0 m	2.10	2.41	0.27	8.93	8.56
	5.0 m	0.83	2.65	0.30	8.83	9.40
			Buoy #1:			
	0.5 m	4.58	2.34	0.26	9.00	6.92
	2.0 m	2.49	2.39	0.26	9.19	7.41
	5.0 m	1.07	2.69	0.30	8.97	9.64

Table 3.10. Summary of the sediment trap design intercomparison.

Trap design	Elevation off bottom	Solids flux Mean ($g\ cm^{-2}\ yr^{-1}$)	Solids flux CV[1] (%)	TOC Mean (%)	TOC CV (%)	TN Mean (%)	TN CV (%)	C/N Mean (%)	C/N CV (%)	TVS Mean (%)	TVS CV (%)
Hendricks:	0.5 m	4.47	11.4	2.00	50.5	0.23	56.5	8.72	7.9	7.5	1.3
	2.0 m	1.30	32.3	2.42	0.4	0.26	0.4	9.12	3.2	7.8	5.1
	5.0 m	0.48	8.3	2.68	10.4	0.32	9.4	8.38	1.4	9.3	5.4
New design:	0.5 m	4.56	1.0	2.36	1.3	0.26	0.0	9.09	1.3	7.7	9.1
	2.0 m	2.29	8.3	2.43	2.1	0.27	3.7	8.99	1.9	8.0	7.5
	5.0 m	0.96	12.5	2.60	4.6	0.29	4.1	8.87	0.9	9.6	2.1

1 Coefficient of variation.

Table 3.11. Mass flux of solids and concentration of TOC and TN in particles collected with sediment traps deployed off Palos Verdes, Orange County and Point Loma, 1989-90.

Site	Deployment date	Elevation off bottom	Solids Flux ($g\ cm^{-2}\ yr^{-1}$)	TOC (%)	TN (%)	C/N
Palos Verdes:						
	10/30/89	0.5	7.24	3.74	0.37	10.1
		2.0	2.04	3.90	0.39	10.0
		5.0	1.19	4.12	0.43	9.58
	11/28/89	0.5	5.73	3.55	0.34	10.4
		2.0	2.42	3.60	0.35	10.3
		5.0	1.51	3.73	0.37	10.1
	3/12/90	0.5	3.94	2.99	0.29	10.3
		2.0	1.87	3.46	0.33	10.5
		5.0	0.90	3.95	0.43	9.16
	4/16/90	0.5	5.47	3.37	0.32	10.5
		2.0	2.01	3.21	0.32	10.0
		5.0	1.31	3.83	0.40	9.50
	6/8/90	0.5	8.62	3.66	0.35	10.4
		2.0	2.19	3.80	0.38	10.1
		5.0	1.40	3.95	0.41	9.66
	10/25/90	0.5	--	3.26	0.32	10.3
		2.0	--	3.50	0.32	11.0
		5.0	--	3.62	0.34	10.5
Orange County:						
	10/27/89	0.5	2.97	1.60,1.57	0.22,0.21	7.25,7.32
		2.0	1.87	1.30	0.12	10.4
		5.0	1.04	1.44	0.14	10.3
	11/30/89	0.5	1.95	1.58	0.17	9.29
		2.0	0.70	2.16	0.24	9.00
		5.0	0.37	2.41	0.29	8.31
	1/4/90	0.5	0.83	1.50	0.14	10.4
		2.0	0.38	1.93	0.19	10.1
		5.0	0.13	insufficient sample		
	2/6/90	0.5	1.10			
		2.0	0.49	Data not available		
		5.0	0.35			
	2/22/90	0.5	0.96	2.17	0.24	8.98
		2.0	0.37	2.97	0.27	8.74
		5.0	0.11	3.18	0.48	7.97

continued on next page

Table 3.11 continued

Site	Deployment date	Elevation off bottom	Solids Flux ($g\ cm^{-2}\ yr^{-1}$)	TOC (%)	TN (%)	C/N
Orange County:						
	3/23/90	0.5	1.09	2.46	0.28	8.74
		2.0	0.46	2.97	0.36	8.33
		5.0	0.26	3.18	0.41	7.71
	6/21/90	0.5	1.84	1.81	0.19	9.68
		2.0	1.04	1.80	0.19	9.36
		5.0	0.41	insufficient sample		
	7/25/90	0.5	1.09	[Data not available]		
		2.0	0.64			
		5.0	0.18			
	8/30/90	0.5	1.76	1.44	0.14	9.90
		2.0	0.96	1.20	0.12	9.71
		5.0	0.45	1.32	0.14	9.49
	9/28/90	0.5	1.42	[Data not available]		
		2.0	0.75			
		5.0	0.33			
Pt. Loma:						
	10/8/89[1]	0.5	4.56	2.36	0.26	9.09
		2.0	2.29	2.43	0.27	8.99
		5.0	0.96	2.60	0.29	8.87
	11/8/89	0.5	5.04	2.53	0.29	8.72
		2.0	2.37	2.83	0.32	8.84
		5.0	0.92	3.23	0.37	8.73
	1/8/90	0.5	6.33	2.24	0.22	10.2
		2.0	2.25	2.17	0.20	10.7
		5.0	0.87	2.22	0.21	10.1
	2/8/90-1	0.5	4.75	[Data not available]		
		2.0	0.94			
		5.0	0.84			
	2/8/90-2	0.5	4.86	[Data not available]		
		2.0	0.81			
		5.0	2.26[2]			

continued on next page

Table 3.11 continued

Site	Deployment date	Elevation off bottom	Solids Flux ($g\ cm^{-2}\ yr^{-1}$)	TOC (%)	TN (%)	C/N
Pt. Loma:						
	3/7/90-1	0.5	2.81	2.07	0.24	8.66
		2.0	1.23	1.63	0.18	9.24
		5.0	0.44	1.50	0.17	8.93
	3/7/90-2	0.5	2.72	1.91	0.22	9.14
		2.0	1.73	2.05	0.23	8.88
		5.0	0.52	2.04	0.24	8.38
	4/10/90	0.5	2.17	2.08	0.22	9.23
		2.0	0.84	2.17	0.23	9.26
		5.0	0.26	2.15	0.24	8.80
	6/15/90	0.5	2.01	2.13	0.23	9.31
		2.0	0.93	2.05	0.22	9.28
		5.0	0.25	2.16	0.25	8.55
	7/17/90	0.5	2.05	[Data not available]		
		2.0	0.92			
		5.0	0.49			
	8/17/90	0.5	2.26	2.22	0.24	9.17
		2.0	0.92	2.31	0.25	9.10
		5.0	0.18	2.40	0.26	9.13

1 Mean of three trap measurements (cf. Table 19).

2 Shell debris due to resident organism may have biased sample.

Table 3.12. Stable isotopic composition of particles collected in sediment traps deployed near the ocean bottom off Palos Verdes, Orange County and Point Loma.

Site	Date of deployment	Elevation off bottom	$\delta^{13}C$ (‰)	$\delta^{15}N$ (‰)
Palos Verdes:				
	11/28/89	0.5 m	-22.00	+5.13
		2.0 m	-22.71	+4.33
		5.0 m	-22.55	+4.33
	6/8/90	0.5 m	-22.58	+3.39
		2.0 m	-22.50	+3.06
		5.0 m	-22.40	+3.30
Orange County:				
	1/4/90	0.5 m	-22.57	+5.23
		2.0 m	-22.45	+5.41
	6/21/90	0.5 m	-22.63	+4.34
		2.0 m	-22.50	+4.69
Point Loma:				
	1/8/90	0.5 m	-21.82	+7.17
		2.0 m	-21.63	+6.96
		5.0 m	-21.75	+6.85
	6/15/90	0.5 m	-21.75	+7.16
		2.0 m	-21.70	+6.36
		5.0 m	-21.54	+6.69

Table 3.13. Concentration of lead (Pb) and cadmium (Cd) in particles collected in sediment traps deployed near the ocean bottom off Palos Verdes, Orange County and Point Loma.

Site	Date of deployment	Elevation off bottom	Concentration (μg dry g^{-1}) Pb	Cd
Palos Verdes:				
	10/30/89	0.5 m	73.9	8.7
	2.0 m	73.4	8.8	
		5.0 m	72.8	7.6
	11/28/89	0.5 m	64.7	8.2
	2.0 m	62.8	8.2	
		5.0 m	61.3	7.1
	3/12/90	0.5 m	71.1	9.3
		2.0 m	68.2	10.
		5.0 m	65.9	9.6
	4/16/90	0.5 m	78.2	7.8
		2.0 m	69.9	8.5
		5.0 m	65.6	7.4
	6/8/90	0.5 m	63.0	8.7
		2.0 m	62.6	7.4
		5.0 m	56.9	6.9
	10/25/90	0.5 m	69.2	7.8
		2.0 m	69.9	8.1
		5.0 m	68.6	7.3
Orange County:				
	1/4/90	0.5 m	18.7	0.6
		2.0 m	17.1	0.7
		5.0 m	insufficient sample	
	2/22/90	0.5 m	19.	0.9
		2.0 m	19.2	1.9
		5.0 m	25.7	<0.7
	3/23/90	0.5 m	17.7	1.1
		2.0 m	11.7	1.3
		5.0 m	20.8	3.2
	6/21/90	0.5 m	17.1	1.
		2.0 m	17.5	1.7
		5.0 m	insufficient sample	

continued on next page

Table 3.13 continued

Site	Date of deployment	Elevation off bottom	Concentration (μg dry g^{-1}) Pb	Cd
Orange County:				
	8/30/90	0.5 m	17.5	2.1
		2.0 m	16.4	1.3
		5.0 m	14.3	1.3
Point Loma:				
	1/8/90	0.5 m	17.1	<0.4
		2.0 m	17.1	0.4
		5.0 m	17.7	0.6
	3/7/90-1	0.5 m	13.8	0.4
		2.0 m	13.3	1.2
		5.0 m	12.9	0.5
	3/7/90-2	0.5 m	12.9	0.3
		2.0 m	13.4	0.5
		5.0 m	12.6	0.7
	4/10/90	0.5 m	13.8	0.3
		2.0 m	13.5	0.3
		5.0 m	13.5	<0.2
	6/15/90	0.5 m	15.2	0.9
		2.0 m	13.6	<0.4
		5.0 m	12.1	<0.9
	8/17/90	0.5 m	16.5	0.5
		2.0 m	16.3	0.4
		5.0 m	16.6	0.3

Table 3.14. Concentrations (μg dry g^{-1}) of 13 elements determined in sediment trap particles by ICP-MS.

Element	Palos Verdes						Orange County						Point Loma					
Date[1]:	11/28/89			6/8/90			1/4/90			6/21/90			1/8/90			6/15/90		
Elevation[2] (m):	0.5	2.0	5.0	0.5	2.0	5.0	0.5	2.0	5.0	0.5	2.0	5.0	0.5	2.0	5.0	0.5	2.0	5.0
Pb	64.7	62.8	61.3	63.	62.6	56.9	18.7	17.1	--[3]	17.1	17.5	--[3]	17.1	17.1	17.7	15.2	13.6	12.1
Cd	8.2	8.2	7.1	8.7	7.4	6.9	0.6	0.7	--	1.	1.7	--	<0.4	0.4	0.6	0.9	<0.4	<0.9
Be	<0.7	<0.7	0.9	<0.7	<0.7	0.8	0.8	0.8	--	<0.7	0.7	--	0.8	<0.7	0.8	<0.7	<0.7	<2.
Cr	179.	179.	165.	175.	176.	161.	46.	46.	--	52.	41.	--	48.	47.	48.	40.	37.	39.
Ni	32.6	33.7	34.6	36.7	35.2	35.6	17.8	19.6	--	19.9	17.5	--	19.9	20.3	19.2	16.1	16.8	13.
Cu	109.	110.	104.	111.	111.	105.	46.1	50.3	--	47.9	45.	--	32.3	32.6	32.5	27.	25.8	23.6
Zn	266.	252.	225.	235.	242.	229.	69.	79.	--	91.	84.	--	79.	348.[4]	77.	71.	60.	51.
As	15.	14.	13.	11.	15.	14.	<6	<6.	--	<7.	<6.	--	<8.	11.	14.	<8.	8.	<40.
Se	<4.	7.	<4.	<4.	<4.	7.	<4.	<4.	--	<4.	<4.	--	<4.	<4.	7.	6.	<4.	<10.
Ag	5.1	4.	3.7	3.8	3.3	3.1	2.	1.7	--	1.5	2.	--	0.9	0.7	0.7	0.7	0.8	<1.
Sb	1.3	1.3	1.2	1.4	1.2	1.1	0.5	0.3	--	<0.3	0.3	--	<0.3	<0.3	<0.3	<0.3	<0.3	<0.7
Hg	0.9	0.4	0.5	0.5	0.6	0.6	0.5	<0.3	--	<0.4	<0.4	--	<0.4	0.2	<0.4	<0.4	<0.4	<1.
Th	0.51	0.39	0.44	0.52	0.54	0.54	0.24	0.28	--	0.35	0.44	--	0.2	0.5	0.37	0.3	0.31	<0.3

1 Deployment date (cf. Table 3).

2 Elevation above the sea floor.

3 Insufficient sample.

4 Questionable datum.

Table 3.15. Concentrations of linear alkylbenzenes (μg dry g^{-1}) determined in sediment trap particles.[1]

Compound	11/28/89			6/8/90		
	0.5 m	2.0 m	5.0 m	0.5 m	2.0 m	5.0 m
Palos Verdes:						
5-phenyldecane	0.24	0.43	0.62	0.36	0.90	--[2]
4-phenyldecane	0.19	0.37	0.52	0.32	0.80	--
3-phenyldecane	0.20	0.40	0.56	0.29	0.78	--
2-phenyldecane	0.29	0.63	0.95	0.43	1.11	--
6-phenylundecane	0.42	0.80	1.04	0.60	1.52	--
5-phenylundecane	0.73	1.18	1.67	0.78	1.91	--
4-phenylundecane	0.61	1.09	1.57	0.82	2.08	--
3-phenylundecane	0.62	1.21	1.69	0.86	2.20	--
2-phenylundecane	0.56	1.29	1.96	0.78	2.02	--
6-phenyldodecane	0.88	1.53	2.11	1.05	2.51	--
5-phenyldodecane	0.74	1.31	1.83	0.89	2.14	--
4-phenyldodecane	0.56	1.02	1.59	0.70	1.72	--
3-phenyldodecane	0.49	1.08	1.48	0.68	1.79	--
2-phenyldodecane	0.47	1.13	1.82	0.72	1.66	--
7&6-phenyltridecane	0.86	1.01	1.20	0.47	1.27	--
5-phenyltridecane	0.50	0.61	0.70	0.28	0.73	--
4-phenyltridecane	0.35	0.53	0.54	0.21	0.56	--
3-phenyltridecane	0.25	0.47	0.45	0.15	0.48	--
2-phenyltridecane	0.16	0.26	0.30	0.12	0.26	--
7-phenyltetradecane	0.39	0.32	0.59	0.23	0.61	--
6-phenyltetradecane	0.31	0.50	0.39	0.18	0.47	--
5-phenyltetradecane	0.31	0.38	0.46	0.18	0.51	--
4-phenyltetradecane	0.18	0.34	0.31	0.10	0.34	--
3-phenyltetradecane	0.15	0.30	0.24	0.09	0.36	--
2-phenyltetradecane	0.07	0.09	0.13	0.05	0.10	--
Σ phenyldecanes	0.92	1.84	2.65	1.41	3.59	--
Σ phenylundecanes	2.95	5.57	7.93	3.84	9.73	--
Σ phenyldodecanes	3.15	6.07	8.83	4.04	9.83	--
Σ phenyltridecanes	2.13	2.88	3.19	1.23	3.30	--
Σ phenyltetradecanes	1.41	1.94	2.12	0.83	2.40	--
Σ LABs	10.6	18.3	24.7	11.4	28.8	--

continued on next page

Table 3.15 continued

Compound	1/4/90			6/21/90		
	0.5 m	2.0 m	5.0 m	0.5 m	2.0 m	5.0 m
Orange County:						
5-phenyldecane	0.047	0.146	0.008	0.020	0.029	0.006
4-phenyldecane	0.036	0.108	0.004	0.014	0.020	0.003
3-phenyldecane	0.032	0.097	<0.003	0.014	0.021	0.004
2-phenyldecane	0.035	0.137	0.006	0.019	0.033	0.008
6-phenylundecane	0.117	0.279	0.031	0.069	0.097	0.031
5-phenylundecane	0.142	0.460	0.058	0.082	0.147	0.046
4-phenylundecane	0.120	0.372	0.040	0.069	0.109	0.043
3-phenylundecane	0.111	0.354	0.024	0.072	0.082	0.039
2-phenylundecane	0.087	0.317	0.022	0.070	0.100	0.033
6-phenyldodecane	0.244	0.615	0.119	0.176	0.256	0.111
5-phenyldodecane	0.172	0.500	0.095	0.119	0.192	0.086
4-phenyldodecane	0.136	0.376	0.048	0.091	0.126	0.059
3-phenyldodecane	0.110	0.312	0.026	0.068	0.094	0.047
2-phenyldodecane	0.095	0.274	0.022	0.081	0.109	0.030
7&6-phenyltridecane	0.125	0.467	0.109	0.073	0.107	0.079
5-phenyltridecane	0.070	0.256	0.052	0.040	0.052	0.043
4-phenyltridecane	0.050	0.164	0.027	0.027	0.038	0.027
3-phenyltridecane	0.037	0.161	0.015	0.021	0.031	0.015
2-phenyltridecane	0.022	0.097	0.009	0.014	0.021	0.014
7-phenyltetradecane	0.057	0.212	0.053	0.041	0.083	0.040
6-phenyltetradecane	0.043	0.153	0.035	0.023	0.039	0.028
5-phenyltetradecane	0.043	0.152	0.030	0.023	0.036	0.025
4-phenyltetradecane	0.024	0.106	0.017	0.017	0.029	0.016
3-phenyltetradecane	0.030	0.093	0.010	0.012	0.023	0.011
2-phenyltetradecane	0.014	0.066	0.005	0.007	0.012	0.008
Σ phenyldecanes	0.150	0.489	0.017	0.066	0.102	0.021
Σ phenylundecanes	0.577	1.78	0.175	0.362	0.535	0.192
Σ phenyldodecanes	0.758	2.08	0.309	0.536	0.777	0.332
Σ phenyltridecanes	0.304	1.15	0.212	0.174	0.248	0.178
Σ phenyltetradecanes	0.212	0.783	0.150	0.122	0.223	0.127
Σ LABs	2.00	6.29	0.865	1.26	1.89	0.85

continued on next page

Table 3.15 continued

Compound	1/8/90			6/15/90		
	0.5 m	2.0 m	5.0 m	0.5 m	2.0 m	5.0 m
			Point Loma:			
5-phenyldecane	0.012	0.007	0.019	0.026	0.012	0.005
4-phenyldecane	0.008	0.003	0.012	0.022	<0.004	<0.004
3-phenyldecane	0.006	0.002	0.008	0.020	0.006	<0.004
2-phenyldecane	0.006	0.003	0.007	0.021	0.012	<0.003
6-phenylundecane	0.025	0.019	0.057	0.056	0.038	0.026
5-phenylundecane	0.036	0.029	0.082	0.088	0.067	0.048
4-phenylundecane	0.026	0.020	0.062	0.070	0.041	0.034
3-phenylundecane	0.021	0.018	0.051	0.069	0.045	0.024
2-phenylundecane	0.013	0.012	0.034	0.049	0.040	0.013
6-phenyldodecane	0.056	0.052	0.159	0.144	0.109	0.091
5-phenyldodecane	0.043	0.042	0.116	0.109	0.083	0.075
4-phenyldodecane	0.029	0.028	0.085	0.085	0.056	0.041
3-phenyldodecane	0.020	0.017	0.064	0.072	0.043	0.025
2-phenyldodecane	0.011	0.011	0.035	0.053	0.034	0.013
7&6-phenyltridecane	0.060	0.069	0.151	0.078	0.071	0.086
5-phenyltridecane	0.031	0.036	0.078	0.042	0.027	0.037
4-phenyltridecane	0.021	0.022	0.049	0.028	0.021	0.017
3-phenyltridecane	0.015	0.014	0.030	0.019	0.012	<0.005
2-phenyltridecane	0.007	0.007	0.016	0.025	0.010	0.006
7-phenyltetradecane	0.017	0.032	0.064	0.005	0.023	0.033
6-phenyltetradecane	0.009	0.022	0.058	0.032	0.023	0.022
5-phenyltetradecane	0.020	0.023	0.047	0.023	0.014	0.018
4-phenyltetradecane	0.015	0.015	0.030	0.017	0.012	0.014
3-phenyltetradecane	0.008	0.007	0.012	0.009	<0.004	<0.005
2-phenyltetradecane	0.003	0.003	0.007	0.006	<0.002	<0.003
Σ phenyldecanes	0.032	0.016	0.046	0.089	0.030	0.005
Σ phenylundecanes	0.121	0.099	0.287	0.331	0.231	0.145
Σ phenyldodecanes	0.160	0.150	0.459	0.464	0.326	0.245
Σ phenyltridecanes	0.134	0.148	0.325	0.192	0.141	0.146
Σ phenyltetradecanes	0.072	0.103	0.216	0.092	0.072	0.087
Σ LABs	0.519	0.515	1.33	1.17	0.800	0.627

1 Concentrations are not recovery-corrected. For explanation, see text.

2 Portion of sample lost during processing.

Table 3.16. Concentrations of total extractable organics and linear alkylbenzenes in sediment trap particles: summary.

Site	Date[1]	Elevation off bottom (m)	TEO (mg g^{-1})	Total linear alkylbenzenes $\mu g\ g^{-1}$	Total linear alkylbenzenes $\mu g\ g\ OC^{-1}$
Palos Verdes:	11/28/89	0.5	7.47	10.6	298.
		2.0	8.71	18.3	508.
		5.0	7.92	24.7	662.
	6/8/90	0.5	25.8	11.4	311.
		2.0	34.9	28.8	758.
		5.0	—[2]	—[2]	—[2]
Orange County:	1/4/90	0.5	3.54	2.00	133.
		2.0	13.3	6.29	326.
		5.0	2.22	0.86	—[3]
	6/21/90	0.5	1.87	1.26	69.6
		2.0	2.90	1.89	105.
		5.0	1.98	0.85	—[3]
Point Loma:	1/8/90	0.5	2.13	0.52	23.2
		2.0	1.94	0.52	24.0
		5.0	2.57	1.33	59.9
	6/15/90	0.5	2.62	1.17	54.9
		2.0	4.11	0.80	39.0
		5.0	6.22	0.63	29.2

1 Deployment date.

2 Sample lost during processing.

3 Insufficient sample for TOC determination.

Table 3.17. Concentrations of fecal sterols in sediment trap particles.

Site	Date[1]	Elevation off bottom (m)	Coprostanol		Epicoprostanol	
			$\mu g\ g^{-1}$	$\mu g\ g\ OC^{-1}$	$\mu g\ g^{-1}$	$\mu g\ g\ OC^{-1}$
Palos Verdes:	11/28/89	0.5	4.87	137.	0.75	2.11
		2.0	21.6	600.	0.13	3.61
		5.0	61.5	1650.	4.07	109.
	6/8/90	0.5	47.8	1310.	4.11	112.
		2.0	71.1	1870.	0.70	18.4
		5.0	23.4	592.	3.73	94.4
Orange County:	1/4/90	0.5	4.67	311.	0.29	19.3
		2.0	2.20	114.	--	--
		5.0	0.81	--[3]	0.15	--[3]
	6/21/90	0.5	7.87	435.	1.06	58.6
		2.0	15.7	872.	2.17	120.
		5.0	3.41	--[3]	0.43	--[3]
Point Loma:	1/8/90	0.5	0.43	19.2	0.02	0.89
		2.0	0.36	16.6	0.09	4.15
		5.0	1.62	73.0	0.23	10.4
	6/15/90	0.5	0.49	23.0	--	--
		2.0	18.3	893.	0.26	12.7
		5.0	7.48	346.	1.36	63.0

1 Deployment date.

2 Sample lost during processing.

3 Insufficient sample for TOC determination.

Table 3.18. Summary of fluxes to near bottom traps deployed off Palos Verdes, Orange County and Point Loma during 1989-90.

Site	Deployment date	Elevation off bottom (m)	Solids ($g\ cm^{-2}\ yr^{-1}$)	TOC ($mg\ cm^{-2}\ yr^{-1}$)	TN	Pb ($\mu g\ cm^{-2}\ yr^{-1}$)	Cd	ΣLAB	Coprostanol
Palos Verdes:	10/30/89	0.5	7.24	271.	13.8	535.	63.0	--	--
		2.0	2.04	79.6	8.0	150.	18.0	--	--
		5.0	1.19	49.0	5.1	86.6	9.0	--	--
	11/28/89	0.5	5.73	203.	19.5	371.	47.0	60.7	27.9
		2.0	2.42	87.1	8.5	152.	19.8	44.3	52.3
		5.0	1.51	56.3	5.6	92.6	10.7	37.3	92.9
	3/12/90	0.5	3.94	118.	11.4	280.	36.6	--	--
		2.0	1.87	64.7	6.2	128.	18.7	--	--
		5.0	0.90	35.6	3.9	59.3	8.6	--	--
	4/16/90	0.5	5.47	184.	17.5	428.	42.7	--	--
		2.0	2.01	64.5	6.4	140.	17.1	--	--
		5.0	1.31	50.2	5.2	85.9	9.7	--	--
	6/8/90	0.5	8.62	315.	30.2	543.	75.0	98.3	412.
		2.0	2.19	83.2	8.3	137.	16.2	63.1	156.
		5.0	1.40	55.3	5.7	79.7	9.7	--	32.5
Orange County:									
	10/27/89	0.5	2.97	46.9	6.5	--	--	--	--
		2.0	1.87	24.3	2.2	--	--	--	--
		5.0	1.04	15.0	1.5	--	--	--	--
	11/30/89	0.5	1.95	30.8	3.3	--	--	--	--
		2.0	0.70	15.1	1.7	--	--	--	--
		5.0	0.37	8.9	1.1	--	--	--	--
	1/4/90	0.5	0.83	12.4	1.2	15.5	0.5	1.66	3.88
		2.0	0.38	7.3	0.7	6.5	0.3	2.39	0.84
		5.0	0.13	--	--	--	--	0.11	0.11

continued on next page

Table 3.18 continued

Site	Deployment date	Elevation off bottom (m)	Solids ($g\ cm^{-2}\ yr^{-1}$)	TOC ($mg\ cm^{-2}\ yr^{-1}$)	TN ($mg\ cm^{-2}\ yr^{-1}$)	Pb ($\mu g\ cm^{-2}\ yr^{-1}$)	Cd ($\mu g\ cm^{-2}\ yr^{-1}$)	ΣLAB ($\mu g\ cm^{-2}\ yr^{-1}$)	Coprostanol ($\mu g\ cm^{-2}\ yr^{-1}$)
Orange County:									
	2/6/90	0.5	1.10	--	--	--	--	--	--
		2.0	0.49	--	--	--	--	--	--
		5.0	0.35	--	--	--	--	--	--
	2/22/89	0.5	0.96	20.8	2.3	18.2	0.9	--	--
		2.0	0.37	28.5	2.6	7.1	0.7	--	--
		5.0	0.11	3.5	0.5	2.8	<0.08	--	--
	3/23/90	0.5	1.09	26.8	3.0	19.3	1.2	--	--
		2.0	0.46	13.7	1.7	5.4	0.6	--	--
		5.0	0.26	8.3	1.1	5.4	0.8	--	--
	6/21/90	0.5	1.84	33.3	3.5	31.5	1.8	2.32	14.5
		2.0	1.04	18.7	2.0	18.2	1.8	1.97	16.3
		5.0	0.41	--	--	--	--	0.35	1.40
	7/25/90	0.5	1.09	--	--	--	--	--	--
		2.0	0.64	--	--	--	--	--	--
		5.0	0.18	--	--	--	--	--	--
	8/30/90	0.5	1.76	25.2	0.6	30.6	3.7	--	--
		2.0	0.96	11.5	1.2	15.7	1.2	--	--
		5.0	0.45	1.4	2.4	6.4	0.6	--	--
	9/28/90	0.5	1.42	--	--	--	--	--	--
		2.0	0.75	--	--	--	--	--	--
		5.0	0.33	--	--	--	--	--	--

continued on next page

Table 3.18 continued

Site	Deployment date	Elevation off bottom (m)	Solids ($g\ cm^{-2}\ yr^{-1}$)	TOC ($mg\ cm^{-2}\ yr^{-1}$)	TN ($mg\ cm^{-2}\ yr^{-1}$)	Pb ($\mu g\ cm^{-2}\ yr^{-1}$)	Cd ($\mu g\ cm^{-2}\ yr^{-1}$)	ΣLAB ($\mu g\ cm^{-2}\ yr^{-1}$)	Coprostanol ($\mu g\ cm^{-2}\ yr^{-1}$)
Point Loma:									
	10/8/89	0.5	4.56	108.	11.9	--	--	--	--
		2.0	2.29	55.6	6.2	--	--	--	--
		5.0	0.96	25.0	2.8	--	--	--	--
	11/8/90	0.5	5.04	128.	14.6	--	--	--	--
		2.0	2.37	67.1	7.6	--	--	--	--
		5.0	0.92	29.7	3.4	--	--	--	--
	1/8/90	0.5	6.33	142.	20.2	157.	<3.7	3.29	2.72
		2.0	2.25	48.8	4.5	38.5	0.9	1.17	0.81
		5.0	0.87	19.3	1.8	15.4	0.5	1.16	1.41
	2/8/90-1	0.5	4.75	--	--	--	--	--	--
		2.0	0.94	--	--	--	--	--	--
		5.0	0.84	--	--	--	--	--	--
	2/8/90-2	0.5	4.86	--	--	--	--	--	--
		2.0	0.81	--	--	--	--	--	--
		5.0	2.26	--	--	--	--	--	--
	3/7/90-1	0.5	2.81	58.2	6.7	38.8	1.1	--	--
		2.0	1.23	20.0	2.2	16.4	1.5	--	--
		5.0	0.44	6.6	0.8	5.7	0.2	--	--
	3/7/90-2	0.5	2.72	52.0	6.0	35.1	0.8	--	--
		2.0	1.73	35.5	4.0	30.6	0.9	--	--
		5.0	0.52	10.6	1.2	6.6	0.4	--	--
	4/10/90	0.5	2.17	45.1	4.8	30.0	0.6	--	--
		2.0	0.84	18.5	1.9	11.3	0.2	--	--
		5.0	0.26	5.6	0.6	3.5	<0.05	--	--

continued on next page

Table 3.18 continued

Site	Deployment date	Elevation off bottom (m)	Solids ($g\ cm^{-2}\ yr^{-1}$)	TOC ($mg\ cm^{-2}\ yr^{-1}$)	TN ($mg\ cm^{-2}\ yr^{-1}$)	Pb ($\mu g\ cm^{-2}\ yr^{-1}$)	Cd ($\mu g\ cm^{-2}\ yr^{-1}$)	ΣLAB ($\mu g\ cm^{-2}\ yr^{-1}$)	Coprostanol ($\mu g\ cm^{-2}\ yr^{-1}$)
Point Loma:									
	6/15/90	0.5	2.01	42.8	4.6	30.6	1.8	2.35	0.98
		2.0	0.93	19.1	2.0	12.6	<0.4	0.74	17.0
		5.0	0.25	5.4	0.6	3.0	<0.4	0.16	1.87
	7/17/90	0.5	2.05	--	--	--	--	--	--
		2.0	0.92	--	--	--	--	--	--
		5.0	0.49	--	--	--	--	--	--
	8/17/90	0.5	2.26	50.2	5.4	37.3	1.1	--	--
		2.0	0.92	21.2	2.3	15.0	0.4	--	--
		5.0	0.18	4.3	0.5	3.0	0.05	--	--

Table 3.19. Water content, total organic carbon and total nitrogen concentrations in surface sediments and sediment cores collected of Orange County and Point Loma.[1]

Site	Station	Sub-bottom depth (cm)	Water Content (%)	TOC (%)	TN (%)	C/N
Orange County:						
	OC-0	0-2	34.5	0.54	0.058	9.3
	OC-1	0-2	33.2	0.33	0.031	10.6
	OC-2	0-2	32.1	0.31	0.033	9.4
	OC-3	0-2	33.3	0.32	0.033	9.7
	OC-5	0-2	32.8	0.37	0.041	9.0
	OC-7	0-2	30.4	0.34	0.036	9.4
	OC-9	0-2	31.1	0.26	0.026	10.0
	OC-10	0-2	33.4	0.38	0.039	9.7
	OC-11	0-2	30.5	0.29	0.027	10.7
	OC-13	0-2	32.2	0.33	0.034	9.7
	OC-con	0-2	31.2	0.31	0.033	9.4
	OC-37	0-2	24.6	0.17	0.013	13.1
	OC-ZB2	0-2	33.6	0.38	0.045	8.4
	OC-ZB	0-2	32.1	0.32	0.031	10.3
	OC-17.5	0-2	32.8	0.32	0.029	11.0
Point Loma:						
	SD A-2	0-2	35.5	0.70	0.100	7.0
	SD A-5	0-2	37.7	0.70	0.083	8.4
	SD A-9	0-2	36.9	0.60	0.070	8.6
	SD A-12.5	0-2	36.0	0.54	0.065	8.3
	SD A-15	0-2	35.4	0.63	0.072	8.8
	SD A-16	0-2	34.5	0.57	0.066	8.6
	SD A-17	0-2	35.5	0.54	0.061	8.9
	SD X-1	0-2	35.5	0.55	0.067	8.2
	SD X-2	0-2	35.2	0.65	0.073	8.9
	SD X-3	0-2	37.2	0.65	0.079	8.2
	SD X-4	0-2	37.2	0.57	0.067	8.5
	SD X-5	0-2	36.1	0.57	0.067	8.5
	SD X-6	0-2	36.4	0.62	0.076	8.2
	SD B-3	0-2	33.5	0.46	0.058	7.9
	SD B-5	0-2	38.0	0.48	0.057	8.4

continued on next page

Table 3.19 continued

Site	Station	Sub-bottom depth (cm)	Water Content (%)	TOC (%)	TN (%)	C/N
Point Loma:						
	SD A-16:	0-2	60.9	0.76	0.058	13.1
		2-4	59.8	0.84	0.063	13.2
		4-6	59.1	0.82	0.060	13.7
		6-8	59.0	0.90	0.066	13.7
		8-10	59.0	0.91	0.063	14.4
		10-12	58.9	0.95	0.065	14.6
		12-14	58.9	0.90	0.066	13.7
		14-16	58.9	0.90	0.063	14.2
		16-18	58.4	0.84	0.061	13.8
		18-20	58.4	0.95	0.063	15.0
		20-22	58.2	0.88	0.062	14.2
		22-24	57.9	0.78	0.055	14.2
		24-26	58.4	0.71	0.044	16.1
	SD A-5:	0-2	61.1	0.77	0.061	12.6
		2-4	60.1	0.85	0.062	13.7
		4-6	60.0	0.97	0.086	11.3
		6-8	59.6	0.96	0.080	12.0
		8-10	59.2	0.90	0.068	13.2
		10-12	59.3	0.95	0.071	13.4
		12-14	59.3	1.02	0.078	13.1
		14-16	59.1	0.95	0.070	13.6
		16-18	58.7	0.88	0.062	14.3
		18-20	58.7	0.98	0.072	13.7
		20-22	58.4	0.93	0.066	14.1
		22-24	58.2	0.87	0.065	13.3
		24-26	58.0	0.86	0.061	14.2
		26-28	57.4	0.74	0.049	15.2
		28-30	57.9	0.73	0.047	15.4

1 For station locations see Table 2 and Figures 3 and 4.

Table 3.20. Stable isotopic composition of surface sediments collected off Palos Verdes, Orange County and Point Loma.

Site	Station[1]	Sample type[2]	$\delta^{13}C$ (‰)	$\delta^{15}N$ (‰)
Palos Verdes:				
	PV 1-1	grab	-21.69	+3.31
	PV 1-2	"	-21.69	+2.96
	PV 1-3	"	-21.69	+3.57
	PV 1-4	"	-21.71	+3.32
	PV 1-5	"	-21.74	+3.32
Orange County:				
	OC-0	grab	-23.52	+2.81
	OC-ZB2	"	-23.63	+3.00
Point Loma:				
	SD A-5	core top	-21.98	+5.88
	SD A-16	" "	-21.49	+6.50

1 See Table 2 and Figures 3,4 and 6 for locations.

2 Sample types are: 1) grab-Van Veen grab (0-2 cm), 2) core top-0 to 2 cm section.

Table 3.21. Concentration of lead (Pb) and cadmium (Cd) in surface sediments and cores collected off Orange County and Point Loma.

Site	Station	Sample type	Pb (μg dry g^{-1})	Cd (μg dry g^{-1})
Orange County:				
	OC-1	grab	9.3	0.99
	OC-2	"	8.8	0.56
	OC-3	"	8.9	0.64
	OC-5	"	9.4	0.46
	OC-10	"	9.8	0.55
	OC-11	"	8.5	0.22
	OC-con	"	8.2	0.30
	OC-37	"	5.0	0.16
	OC-ZB2	"	7.7	0.88
	OC-17.5	"	7.8	0.10
Point Loma:				
	SD A-5	grab	9.2	0.25
	SD A-9	"	7.2	0.24
	SD A-12.5	"	7.2	0.39
	SD A-15	"	8.6	0.30
	SD A-16	"	7.7	0.35
	SD X-2	"	17.9	0.27
	SD X-4	"	8.9	0.10
	SD X-5	"	7.6	0.20
	SD X-6	"	10.3	0.18
	SD B-3	"	6.6	0.10
	SD A-16 (core):	0-2 cm	7.84	0.24
		2-4 cm	10.3	0.30
		4-6 cm	9.2	0.39
		6-8 cm	10.6	0.84
		8-10 cm	11.3	0.41
		10-12 cm	11.8	0.51
		12-14 cm	10.6	0.27
		14-16 cm	9.6	0.29
		16-18 cm	8.9	0.33
		18-20 cm	8.3	0.41
		20-22 cm	7.1	0.24
		22-24 cm	4.9	0.19
		24-26 cm	4.1	0.11

continued on next page

Table 3.21 continued

Site	Station	Sample type	Pb (μg dry g^{-1})	Cd (μg dry g^{-1})
Point Loma:				
	SD A-5 (core):	0-2 cm	8.06	0.2
		2-4 cm	8.6	0.16
		4-6 cm	10.0	0.29
		6-8 cm	9.7	0.36
		8-10 cm	11.7	0.48
		10-12 cm	11.8	0.51
		12-14 cm	13.0	0.55
		14-16 cm	11.9	0.36
		16-18 cm	11.1	0.49
		18-20 cm	11.1	0.28
		20-22 cm	10.1	0.36
		22-24 cm	7.2	0.18
		24-26 cm	5.9	0.25
		26-28 cm	4.3	0.12
		28-30 cm	5.2	0.19

Table 3.22. Concentrations (μg dry g^{-1}) of 13 elements determined in sediments by ICP-MS.[1]

Element	SD A-16 (0-2 cm)	SD A-5 (0-2cm)	OC-control (0-2 cm)
Pb	7.60	8.18	8.45
Cd	0.20	0.22	0.30
Be	0.30	0.28	0.27
Cr	23.8	0.25	25.4
Ni	9.34	9.64	11.1
Cu	13.2	13.2	13.6
Zn	41.2	40.6	44.2
As	3.	4.5	3.2
Se	<1	<1.	<1.
Ag	0.41	0.36	0.31
Sb	0.2	<0.2	0.25
Hg	0.06	<0.05	<0.05
Th	0.31	0.32	0.22

1 All concentrations are means of duplicate analyses.

Table 3.23. Concentrations of linear alkylbenzenes (ng dry g^{-1}) in surface sediments (0-2 cm) collected off Point Loma.[1]

Compound	SD A-16	SD A-5
5-phenyldecane	<0.20	<0.24
4-phenyldecane	<0.22	<0.23
3-phenyldecane	<0.26	<0.28
2-phenyldecane	0.40	<0.20
6-phenylundecane	2.12	1.84
5-phenylundecane	3.16	2.14
4-phenylundecane	1.45	0.91
3-phenylundecane	0.61	<0.24
2-phenylundecane	1.20	1.24
6-phenyldodecane	9.48	6.66
5-phenyldodecane	4.72	3.46
4-phenyldodecane	2.67	1.88
3-phenyldodecane	1.55	1.09
2-phenyldodecane	1.31	1.00
7&6-phenyltridecane	7.95	8.74
5-phenyltridecane	3.84	4.09
4-phenyltridecane	1.88	3.08
3-phenyltridecane	2.79	2.41
2-phenyltridecane	1.50	1.48
7-phenyltetradecane	4.34	7.93
6-phenyltetradecane	3.04	5.05
5-phenyltetradecane	3.21	5.02
4-phenyltetradecane	2.50	3.67
3-phenyltetradecane	3.42	3.31
2-phenyltetradecane	1.88	1.88
Σ phenyldecanes	0.40	0.00
Σ phenylundecanes	8.53	6.13
Σ phenyldodecanes	19.7	14.1
Σ phenyltridecanes	18.0	20.0
Σ phenyltetradecanes	18.4	26.9
Σ LABs	65.0	66.9

1 Concentrations are not recovery-corrected. For explanation, see text.

Table 3.24. Concentrations of total extractable organics, linear alkylbenzenes and fecal sterols in top sections (0-2 cm) of sediment cores collected off Point Loma.

Sample	TEO	Total LABs		Coprostanol	
	(mg g^{-1})	$\mu g\ g^{-1}$	$\mu g\ g\ OC^{-1}$	$\mu g\ g^{-1}$	$\mu g\ g\ OC^{-1}$
SD A-16	0.46	0.065	8.55	0.602	79.2
SD A-5	0.63	0.067	8.70	0.292	37.9

Table 3.25. Effect of solids loading on the dissolved oxygen content of waters overlying sludge in the centrifuge bottle/decomposition vessel.

Bottle #	Sample period[1]	Amount solids (mg)	D.O. (mg liter^{-1})
100	initial	243.4	5.9
34	initial	46.4	4.8
-	initial	degassed	0.1
38	T_0	253.3	1.6
31	T_0	250.0	2.0
74	T_0	100.3	3.2
26	T_0	103.8	3.2
104	T_0	50.5	4.4
69	T_0	50.5	4.0
36	T_0	27.4	5.1
86	T_0	26.1	5.1
47	T_0	0.0	6.3
42	T_0	0.0	6.7
91	T_0	degassed	2.0
tank water	—	---	8.4

1 T_0 = one day after introduction of the sludge solids into the centrifuge bottles. Note: All bottles covered with GF/C filters.

Table 3.26. Effect of barrier por size on the dissolved oxygen content of waters overlying sludge particles in the centrifuge bottle/decomposition vessel.

Time Period	Expected Solids[1] (mg)	Actual Solids[2] (mg)	Filter Type	D.O. (mg liter^{-1})
T_0	262.0	93.6	110 μm	3.27
T_0	97.3	41.2	110 μm	4.80
T_0	48.4	19.6	110 μm	5.50
T_2	277.	--	110 μm	0.00
T_2	95.9	--	110 μm	0.10
T_2	46.2	--	110 μm	0.50
T_7	100.	--	110 μm	0.50
T_7	48.9	--	110 μm	0.50
T_{13}	97.8	--	110 μm	0.00
T_{13}	48.9	--	110 μm	0.40
T_0	707.	245.	20 μm	0.20
T_0	257.	101.	20 μm	2.97
T_0	101.	42.4	20 μm	4.80
T_0	50.8	23.2	20 μm	5.50
T_2	250.	--	20 μm	0.10
T_2	97.5	--	20 μm	<0.10
T_2	72.4	--	20 μm	0.30
T_7	99.4	--	20 μm	0.20
T_7	48.9	--	20 μm	0.50
T_{13}	105.	--	20 μm	0.20
T_{13}	62.7	--	20 μm	0.50
T_0	253.	95.60	GF/C	2.77
T_0	97.5	44.0	GF/C	5.10
T_0	54.3	18.5	GF/C	5.10
T_2	268.	--	GF/C	0.00
T_2	123.	--	GF/C	<0.10
T_7	104.	--	GF/C	0.10
T_7	48.6	--	GF/C	0.30
T_{13}	95.9	--	GF/C	0.20
T_{13}	48.9	--	GF/C	0.20

1 Expected solids based on estimation of solids content of diluted sludge using rapid heating method.

2 Actual solids based on centrifugation followed by gravimetric analysis of the oven-dried particles in the centrifuge bottles. Dashes indicate samples for which analyses were not performed.

Table 3.27. Effect of sludge mass loading on dissolved oxygen content of overlying waters in the culture dish.

Nominal Sample Loading (mg)	Mesh Size (μm)	D.O. at T_0 (mg liter^{-1})	D.O. at T_2 (mg liter^{-1})	D.O. at T_5 (mg liter^{-1})
50	20	7.8	6.0	3.2
100	20	7.6	1.7	2.5
250	20	7.5	2.0	1.2
500	20	7.3	0.1	--
50	110	8.0	6.8	7.5
100	110	8.2	8.1	7.0
250	110	7.7	5.4	7.2
500	110	8.1	nd[1]	nd

1 nd = not determined.

Table 3.28. Loss of particulate matter from glass jar incubation vessels covered with 110μm Nitex screens.

Jar#	No. Days incubated[1]		Solids (mg)[2]	Solids lost[3] (%)
-	0		12.0	–
-	0		11.2	–
		Mean[4]	11.6	–
7	4		169.	30.6
6	4		208.	17.4
		Mean	188.	24.0
2	6		211.	13.6
5	6		214.	12.6
		Mean	212.	13.1
1	8		208.	14.8
4	8		202.	17.6
		Mean	205.	16.2

1 This is the number of days the poisoned jars were kept in the aquarium.

2 This is the mass of solids recovered from the jars (suspended + settled).

3 This is the % solids lost based on the mean of the two determinations at 0 days.

4 Mean = mean of two replicates at each time interval.

Table 3.29. Loss of particles from glass jars sealed with 110μm Nitex screen: mass balance.

Repl. #	Time[1]	Sample Type[2]	Solids (mg)	% Original solids
1	start	orig.	278.	100
2	start	orig.	268.	100
1	end	beaker	37.2	13.4
2	end	beaker	37.0	13.8
1	end	screen	4.4	1.6
2	end	screen	4.9	1.8
1	end	jar-sup	4.9	1.8
2	end	jar-sup	5.5	2.1
1	end	jar-set	231.	82.9
2	end	jar-set	225.	84.0
1		**Total:**	277.	99.6
2		**Total:**	273.	102.

1 Time: start-when sample was prepared, end-four days later.

2 Sample type: screen-particles rinsed from Nitex screen, beaker-particles that accumulated in beaker after passing through Nitex screen, jar-sup-particles recovered from supernatant by filtration after centrifuging contents of jar, jar-set-particles settled to bottom of centrifuge bottle.

Table 3.30. Loss of particles from glass jars sealed with 110μm Nitex screens: chemical composition.

Rep. #	Time[1]	Sample Type[2]	TOC (%)	TN (%)	% Total[3] TOC	% Total[3] TN	C/N
1	end	beaker	15.5	2.11	7.9	10.1	7.4
2	end	beaker	14.2	2.23	7.3	10.6	6.4
1	end	screen	1.58	0.052	0.10	0.04	30.4[4]
2	end	screen	1.82	0.093	0.12	0.06	19.6[4]
1	end	jar-sup	19.5	3.61	1.3	2.3	5.4
2	end	jar-sup	19.3	3.68	1.5	2.6	5.2
1	end	jar-set	28.8	2.98	90.7	87.5	9.9
2	end	jar-set	29.2	2.98	91.1	86.4	9.8

1 Time: start-when sample was prepared, end-four days later.

2 Sample type: screen-particles rinsed from Nitex screen, beaker-particles that accumulated in beaker after passing through Nitex screen, jar-sup-particles recovered from supernatant by filtrations after centrifuging contents of jar, jar-set-particles settled to bottom of centrifuge bottle.

3 Percent of total organic carbon or nitrogen recovered in individual fractions (i.e. screen, beaker, jar-sup, jar-set).

4 Results may be questionable due to small sample size.

Table 3.31. Elemental composition of sludge solids and particles isolated from the JWPCP final effluent[1]

Sample	Rep. #	% TOC	% TN	C/N
Sludge:	1	34.8	3.25	10.7
	2	34.9	3.10	11.3
	3	35.3	3.03	11.7
	4	35.1	2.97	11.8
	5	35.0	3.09	11.3
mean		35.0	3.09	11.4
std. dev.		0.19	0.10	0.43
coeff. var. (%)		0.54	3.09	3.8
Final effluent:	1	38.6	4.88	7.91
	2	40.5	4.67	8.67
	3	41.8	4.77	8.76
	4	43.2	4.83	8.94
	5	42.0	4.82	8.71
mean		41.2	4.79	8.60
std. dev.		1.7	0.08	0.40
coeff. var. (%)		4.2	1.7	4.6

1 JWPCP final effluent filtered through a GF/C glass fiber filter which was subsequently analyzed on a Carlo Erba 1108 elemental analyzer. Sludge was homogenized in the wet state using a polytron, and an aliquot was removed and placed into a combustion boat for analysis.

Table 3.32. Distribution of sludge solids between supernatant and settled particles during centrifugation as a function of spin time.

Sample #	Phase	Spin time (min)	% Solids added
1	supernatant	30	2.4
1	settled solids	30	94.0
		Recovery	96.4
2	supernatant	30	2.5
2	settled solids	30	96.4
		Recovery	98.9
3	supernatant	60	1.6
3	settled solids	60	98.0
		Recovery	99.6
4	supernatant	60	1.5
4	settled solids	60	95.1
		Recovery	96.6

Sample #	Phase	Spin time (min)	% Total[1] TOC	% Total[1] TN	C/N Ratio
1	supernatant	30	2.0	3.3	5.4
1	settled solids	30	98.0	96.7	9.16
2	supernatant	30	1.8	2.8	5.2
2	settled solids	30	98.2	97.2	8.14
3	supernatant	60	1.1	1.7	5.7
3	settled solids	60	98.9	98.3	8.81
4	supernatant	60	1.0	1.5	5.8
4	settled solids	60	99.0	98.5	8.62

1 Percent of total organic carbon or nitrogen recovered in individual fractions (i.e. supernatant, settled solids).

Table 3.33. Mass of solids exchanged through 110 μm screen covering empty 8 oz jars and TOC,TN, and C/N ration of invaded particles associated with sand in incubation jars. Deployment of containers at the L.A. County pier (San Pedro, CA).

Container Contents	Chamber Type and Location	Solids Invaded (mg)
Empty	Tall-Top	25.1
Empty	Tall-Middle	24.8
Empty	Short-Top	22.3
Empty	Short-Middle	23.5

Container Contents	Exposure Time (days)	TOC (%)	TN (%)	C/N ratio
Sand[1]	Kilned sand (T=0)	0.026	nd[2]	–
Sand	exposed sand (T=5)	1.530	0.015	17.7

1 50 mg of screened (250 μm) and kilned beach sand.

2 nd = not detected.

Table 3.34. Percent recovery, dissolved oxygen, %TOC, %TN, C:N ratio of sludge solids exposed to ocean waters for 4 and 8 day time periods.

Jar #	Time Period	Chamber Type	Posit.[1] Chamb.	Amt. Loaded (mg)	Amt. Recov. (mg)	Percent Recov. (%)	Mean[2] %	D.O. (mg l^{-1})	Mean[3] (mg l^{-1})	%TOC	%TN	C/N
5	T_0	–	–	292.	280.	96.2	100.1	6.2	6.1	27.7	2.54	10.9
6	T_0	–	–	291.	303.	104.	–	6.0	–	27.6	2.50	11.0
19	T_0	–	–	118.	104.	88.3	89.2	7.5	7.5	28.5	2.67	10.7
20	T_0	–	–	120.	108.	90.2	–	7.5	–	24.3	2.14	11.4
24	T_4	short	4	–	8.9	–	–	–	–	1.92	0.24	7.96
25	T_4	short	3	–	9.3	–	–	–	–	2.40	0.25	9.72
7	T_4	short	1	291.	92.1	31.6	31.6	8.0	6.6	20.6	1.34	15.4
8	T_4	short	4	292.	92.3	31.6	–	5.1	–	25.1	1.75	14.3
9	T_4	short	3	117.	61.1	52.2	58.4	5.7	5.4	19.6	1.57	12.5
10	T_4	short	2	119.	76.9	64.7	–	5.0	–	18.1	1.65	11.0
15	T_4	tall	1	292.	55.5	19.0	20.6	8.8	7.3	22.6	1.03	22.0
15	"	"	"	–	–	–	–	–	–	18.2	0.86	21.2
15	"	"	"	–	–	–	–	–	–	28.1	1.51	18.6
16	T_4	tall	4	292.	64.9	22.2	–	5.8	–	21.0	0.91	23.2
17	T_4	tall	3	120.	41.7	34.8	41.8	7.3	7.0	14.9	0.92	16.2
18	T_4	tall	2	119.	58.2	48.7	–	6.6	–	13.7	1.09	12.5
1	T_8	short	4	292.	72.5	24.8	34.0	7.0	6.3	18.2	1.28	14.2
2	T_8	short	2	292.	126.	43.2	–	5.6	–	21.8	1.87	11.6
3	T_8	short	3	117.	63.3	53.9	49.2	6.6	7.0	13.6	1.33	10.2
4	T_8	short	1	118.	52.5	44.5	–	7.3	–	12.0	1.17	10.2
11	T_8	tall	4	291.	78.2	26.9	29.4	7.0	6.6	17.6	1.46	12.1
12	T_8	tall	2	292.	93.5	32.0	–	6.2	–	19.3	1.72	11.2
13	T_8	tall	3	116.	48.5	41.8	41.9	7.3	7.4	9.32	0.83	11.3
14	T_8	tall	1	118.	49.7	42.0	–	7.4	–	12.1	1.10	11.0
21	T_8	tall	1	–	8.0	–	–	–	–	3.18	0.49	6.46
22	T_8	tall	2	–	9.5	–	–	–	–	2.96	0.36	8.30
23	T_8	tall	3	–	12.6	–	–	–	–	2.76	0.32	8.51
26	T_8	short	2	–	10.4	–	–	–	–	2.08	0.24	8.73
27	T_8	short	1	–	10.1	–	–	–	–	3.75	0.28	13.4

1 Chambers were numbered from the bottom up. Jar locations were randomly selected.

2 Mean percentage of solids recovered for replicates.

3 Mean of dissolved oxygen concentrations for replicates.

Table 3.35. Results of sludge incubation off Orange County: solids and organic carbon mass balance.

Jar #	Time Period (days)	Chamber Type	Amt. Loaded (mg)	Amt. after[1] Physical Losses (mg)	Amount[2] After Invasion (mg)	Recov. Solids (mg)	Percent[3] Recovery (corr'd)	Percent Solids Lost	Mass[4] Solids Lost (mg)	TVS (%)	TOC (%)	TVS/TOC
7	T_4	short	291.	247.	256.	92.1	35.9	64.1	164.	44.4	20.6	2.2
8	T_4	short	292.	248.	257.	92.3	35.9	64.1	165.	43.3	25.1	1.7
9	T_4	short	117.	99.5	108.	61.1	56.3	43.7	47.4	55.6	19.6	2.8
10	T_4	short	119.	101.	110.	76.9	69.9	30.1	33.2	54.5	18.1	3.0
15	T_4	tall	292.	248.	257.	55.5	21.6	78.4	201.	–	23.0	–
16	T_4	tall	292.	248.	257.	64.9	25.2	74.8	192.	53.0	21.0	2.5
17	T_4	tall	120.	102.	111.	41.7	37.6	62.4	69.2	64.9	14.9	4.4
18	T_4	tall	120.	102.	111.	58.2	52.7	47.3	52.3	60.2	13.7	4.4
1	T_8	short	292.	248.	258.	72.5	28.2	71.8	185.	50.9	18.2	2.8
2	T_8	short	292.	248.	257.	126.	49.0	51.0	131.	50.4	21.8	2.3
3	T_8	short	117.	99.8	109.	63.3	58.2	41.8	45.5	57.6	13.6	4.2
4	T_8	short	118.	100.	109.	52.5	48.1	51.9	56.7	65.2	12.0	5.4
11	T_8	tall	291.	248.	256.	78.2	30.5	69.5	178.	47.7	17.6	2.7
12	T_8	tall	292.	248.	257.	93.5	36.4	63.6	164.	44.2	19.3	2.3
13	T_8	tall	116.	98.6	108.	48.5	45.1	54.9	59.1	61.6	9.3	6.6
14	T_8	tall	118.	100.	110.	49.7	45.4	54.6	59.8	62.9	12.1	5.2

Jar #	Time Period (days)	Chamber Type	Amt.[5] TOC Loaded (mg)	Amt. after[6] Physical losses (mg)	Amount[7] after Invasion (mg)	Recov'd Organic Carbon (mg)	Percent[8] Recovery. Corr'd	Percent Carbon Lost	Mass[9] Carbon Lost (mg)	Organic[10] Matter Lost (mg)
7	T_4	short	78.6	72.0	72.2	18.9	26.2	81.1	59.7	115.
8	T_4	short	78.9	72.3	72.5	23.1	31.9	76.9	55.8	85.4
9	T_4	short	31.6	29.0	29.2	11.9	40.8	88.1	19.7	48.9
10	T_4	short	32.1	29.4	29.6	13.8	46.6	86.2	18.3	47.8
15	T_4	tall	78.8	72.2	72.4	12.8	17.7	87.2	66.0	–
16	T_4	tall	78.8	72.2	72.4	13.6	18.8	86.4	65.2	149.
17	T_4	tall	32.4	29.7	29.9	6.2	20.8	93.8	26.2	103.
18	T_4	tall	32.2	29.6	29.8	8.0	26.9	92.0	24.2	95.7
1	T_8	short	78.9	72.4	72.6	13.2	18.2	86.8	65.7	166.
2	T_8	short	78.9	72.3	72.5	27.5	37.9	72.5	51.4	104.
3	T_8	short	31.7	29.1	29.3	8.6	29.4	91.4	23.1	87.6
4	T_8	short	31.8	29.2	29.4	6.3	21.4	93.7	25.5	125.
11	T_8	tall	78.6	72.1	72.3	13.8	19.1	86.2	64.8	158.
12	T_8	tall	78.8	72.3	72.5	18.1	25.0	81.9	60.7	124.
13	T_8	tall	31.3	28.7	28.9	4.5	15.6	95.5	26.8	161.
14	T_8	tall	31.9	29.3	29.5	6.0	20.4	94.0	25.9	122.

1 Multiplied amount loaded by 0.85 (15% loss through the screen).

2 Assumed 9 mg of intrusion - added 9 to the amount in the physical losses column.

3 Divided recovered solids by the amount after invasion and multiplied by 100.

4 Difference between recovered solids and amount after invasion.

5 Used an average of the T_0 TOC concentrations (27%) and multiplied by the amount of solids loaded.

6 Multiplied the amount solids loaded by .0225 (0.15 physical loss x 0.15 TOC) and subtracted from the amount carbon loaded.

7 Added 0.2 to the amount after physical loss (used a mean of the data for jars 24 and 25).

8 [Recovered organic carbon / amount organic carbon after invasion] x 100.

9 Amount carbon loaded - recovered carbon.

10 [Amount organic carbon after invasion - recovered organic carbon] x [TVS/TOC].

Table 3.36. Summary of sludge incubation experiment off Orange County.

Jar #	Time Period (days)	Chamber Type	Mass[1] Solids Lost (mg)	Organic[2] Matter Lost (mg)	Difference (mg)	Percent Difference
7	T_4	short	164.	115.	49.2	29.9
8	T_4	short	165.	85.4	79.6	48.2
9	T_4	short	47.4	48.9	-1.5	-3.2
10	T_4	short	33.2	47.8	-14.6	-44.0
15	T_4	tall	201.	--	201.	--
16	T_4	tall	192.	149.	43.2	22.5
17	T_4	tall	69.2	103.	-34.0	-49.1
18	T_4	tall	52.3	95.7	-43.4	-83.1
1	T_8	short	292.	166.	126.	43.2
2	T_8	short	292.	104.	188.	64.4
3	T_8	short	117.	87.6	29.8	25.4
4	T_8	short	118.	125.	-7.3	-6.2
11	T_8	tall	291.	158.	133.	45.7
12	T_8	tall	292.	124.	168.	57.4
13	T_8	tall	116.	161.	-45.3	-39.
14	T_8	tall	118.	122.	-3.7	-3.1

1 Difference between recovered solids and amount solids after invasion.

2 [Amount organic carbon after invasion - recovered carbon] x [TVS/TOC].

Table 3.37. Summary of results for final effluent degradation experiment.

Sample Description	Suspended Solids (mg liter^{-1})	TOC (%)	TN (%)	C/N Ratio
		Hyperion		
Undiluted effluent:				
Repl. 1	58.9	39.4	6.58	5.99
Repl. 2	61.9	38.8	6.26	6.20
Diluted effluent:				
T_0	2.51	35.0	4.19	8.35
T_4-1	2.98	27.0	4.62	5.85
T_4-2	2.73	24.7	4.02	6.14
		JWPCP		
Undiluted effluent:				
Repl. 1	51.8	42.3	5.05	8.38
Repl. 2	53.3	40.2	4.62	8.78
T_0	2.09	38.0	5.03	7.56
T_4-1	2.88	40.6	7.37	5.43
T_4-2	3.44	41.6	7.52	5.54
		Seawater		
Refiltered SW:				
Repl. 1	0.21	3.14	0.15	20.9
Repl. 2	0.19	3.24	--[1]	--
Incubation blank:				
Repl. 1	0.69	4.69	0.48	9.77
Repl. 2	0.70	3.17	0.25	12.7

1 Not detected.

Table 3.38
Summary of DECAL Predictions

Location		k_d= 0.10			k_d = 0.52		
Avg. I.D.		SD OC 116 96		LA 262, 158	SD OC (235) (189)		LA (321,181)
E-SS	mg / L	67	49	197	67	49	197
E-Pb	ug/L	10	16	152	10	16	152
E-Cd	ug/L	2	3.3	9.3	2	3.3	9.3
DES/DTS	gm/gm	0.635	0.566	0.70, 0.81	0.950	0.924	0.94, 0.97
AES/ATS	gm/gm	0.642	0.542	0.68, *	0.946	0.924	0.94, *
EPb/ESS	mg/gm	0.15	0.33	0.77	0.15	0.33	0.77
DPb/DES	mg/gm	0.15	0.32	0.80, 0.79	0.20	0.45	1.22, 1.04
APb/AES	mg/gm	0.15	0.32	0.81, 0.80	0.21	0.45	1.22, 1.04
DPb/DTS	mg/gm	0.094	0.180	0.56, *	0.195	0.415	1.15, *
APb/AES	mg/gm	0.095	0.174	0.55, *	0.195	0.414	1.15, *
ECd/ESS	mg/gm	0.030	0.067	0.047	0.030	0.067	0.047
DCd/DES	mg/gm	.0092	.0188	.018, .023	.0091	.0165	.020, .022
ACd/AES	mg/gm	.0092	.0194	.018, .023	.0091	.0165	.020, .021
DCd/DTS	mg/gm	.0058	.0106	.013, .018	.0087	.0153	.019, .021
ACd/ATS	mg/gm	.0059	.0105	.012, *	.0086	.0152	.019, *

Table 3.38 continued

Bkg Dep	mg/cm²/yr	62		64, 66	10^{-11}		10^{-12},10^{-7}
		67			10^{-9}		
TSS Dep	mg/cm²/yr	768		972, 2045	202		295, 1030
		597			144		
ESS Dep	mg/cm²/yr	488		681, 1660	192		277, 1001
		338			133		
Pb Dep	ug/cm2/yr	72.1	109	546, 1319	39.3	59.8	339, 1044
Cd Dep	ug/cm2/yr	4.47	6.35	12.3, 37.8	1.75	2.20	5.61, 21.5
TS Acm	gm / L	139		183, *	37		54, *
		114			26.3		
ES Acm	gm/L	89.2	61.8	124, 303	35.0	24.3	51, 183
Pb Acm	mg / L	13.2		100, 241	7.2		62, 191
		19.8			10.9		
Cd Acm	mg / L	0.82		2.2, 6.9	0.32		1.0, 3.9
		1.2			0.40		
Xsh-w	kilometer s	1.6	1.3	2.1	1.6		2.1
					1.3		
TSS-w	kilometer s	3.6		5.0	1.4		2.8
		5.2			2.4		

Avg. I.D. = Average initial dilution based on effluent SS conconcentration
= (upper bound because of decay of organic material)
Bkg Dep = Background deposition of natural particles
TSS Dep = Deposition of total suspended solids (effluent + natural)
ESS Dep = Deposition of effluent suspended solids
Pb/ESS = Ratio: Effluent Pb / Effluent suspended solids
Cd/ESS = Ratio: Effluent Cd / Effluent suspended solids
Pb/EDp = Ratio: Deposition Pb / Deposition effluent suspended solids
Cd/EDp = Ratio: Deposition Cd / Deposition effluent suspended solids
TO Acm = Accumulation of total organic material - sed. surface layer
Pb Acm = Accumulation of Pb - sediment surface layer
Cd Acm = Accumulation of Cd - sediment surface layer
Pb / TO = Ratio: Accumulation Pb / Accumulation total organic material
Cd / TO = Ratio: Accumulation Cd / Accumulation total organic material

Xsh-w = Cross-shore width (max) of wastefield deposition pattern
TSS-W = Longshore full-width at one-half max (total suspended solids)

Table 3.39
Predicted Peak Accumulation Rates ($mg/cm^2/yr$)

Simulation Conditions	San Diego	Orange County	L A County-1978
Aggregation - no resuspension	2369	885	880
Aggregation - resuspension.	57.3	24.7	30.9
No Aggr. - no resuspension	53.4	53.7	166
No Aggr. - resuspension	11.7	13.3	17.0
In absence of discharge*	10.3	12.6	14.6

Table 3.40
Predicted Concentrations of Organic Material (percent)

Simulation Conditions	San Diego	Orange County	LA County
Aggregation-no resuspension	68.1	66.0	64.7
Aggregation-resuspension	35.1	15.5	19.5
No. aggr. - no resuspension	35.9	32.5	51.9
No. aggr. - resuspension	3.1	3.1	6.9
Absence of discharge	1.4	2.0	4.5

Table 4.1. Concentrations (μg liter^{-1}) of trace elements in final effluent: comparison of particulate concentrations determined in this study and total metals measured by respective agencies.[1]

Element	JWPCP		OCSD		PLTP	
	This study	Agency	This study	Agency	This study	Agency
Pb	4.4,4.5	25.	1.8,2.2	13.	2.6,2.9	<50.
Cd	2.2,0.3	2.	1.0,1.3	1.8	1.2,0.5	<5.
Cr	7.5,5.8	31.	2.4,1.8	11.	10.1,2.8	<50.
Ni	3.0,2.3	50.	1.5,1.6	25.	2.4,1.4	15.
Cu	11.0,6.7	35.	21.9,15.4	56.	25.9,18.2	37.
Zn	43.,46.	130.	40.,20.	60.	30.,30.	68.
As	0.7,0.5	5.	0.3,0.2	2.2	0.8,0.8	3.5
Se	3.7,<2.7	13.	1.6,<1.6	1.3	<2.0,<3.6	1.0
Ag	1.7,1.7	8.	1.5,10.8	8.	3.3,2.5	<10.
Hg	0.2,0.3	0.4	0.2,<0.2	0.2	<0.2,1.9	0.2

1 Concentrations from *this study* are particulate concentrations determined by multiplying volume-based concentrations listed in Table 14 by average suspended solids concentrations from Table 10. Mean annual concentrations for total metals determined by respective *agencies* (dissolved + particulate) are taken directly from SCCWRP (1991b).

Table 4.2. Estimates of fraction of effluent-derived organic matter, F_w, in sediment trap particles and surface sediments collected off Palos Verdes.

Sample type	Date Deployed	Elevation (m)	$\delta^{13}C$ (‰)	$\delta^{15}N$ (‰)	$F_w(C)^1$	$F_w(N)^2$	$F_w(N)^3$
Sediment Traps:							
	11/28/89	0.5	-22.0	+5.13	0.0	0.44	0.57
		2.0	-22.71	+4.33	0.41	0.58	0.75
		5.0	-22.55	+4.33	0.31	0.58	0.75
	6/8/90	0.5	-22.58	+3.39	0.33	0.75	0.95
		2.0	-22.50	+3.06	0.29	0.81	1.00
		5.0	-22.40	+3.29	0.23	0.77	0.97
Surface Sediments[4]:							
			-21.7	+3.29	0.0	0.77	0.97

1 Endmember compositions: $\delta^{13}C_m$ = -22.0 ‰, $\delta^{13}C_w$ = -24.25 ‰.

2 Endmember compositions: $\delta^{15}N_m$ = +7.6 ‰, $\delta^{15}N_w$ = +2.0 ‰.

3 Endmember compositions: $\delta^{15}N_m$ = +7.8 ‰, $\delta^{15}N_w$ = +3.15 ‰.

4 Mean of five replicate samples.

Table 4.3. Ratios of 3-phenyldodecane/TAB_1 and internal to external isomers (I/E) in JWPCP effluent particles and sediment trap particles collected off Palos Verdes.

Sample type	Date Deployed/Collected	Elevation (m)	ΣLAB ($\mu g\ g^{-1}$)	ΣLAB_{oc} ($\mu g\ g\ OC^{-1}$)	3ϕ-C_{12}/TAB_1[1] Ratio	I/E[2] Ratio
Effluent:	1/17/90		393.	1280.	—[3]	0.72
	7/6/90		172.	491.	—[3]	0.86
Sediment Traps:						
	11/28/89	0.5	10.6	298.	1.36	1.06
		2.0	18.3	508.	2.07	0.88
		5.0	24.7	662.	2.34	0.81
	6/8/90	0.5	11.4	311.	0.84	0.92
		2.0	28.8	758.	0.84	0.90
		5.0	—[4]	—[4]	0.81	0.90

1 Ratio of 3-phenyldodecane/TAB_1. See text and Figure 23 for explanation.

2 I/E ratio: (6-phenyldodecane + 5-phenyldodecane)/(4-phenyldodecane + 3-phenyldodecane +2-phenyldodecane).

3 No tetrapropylene-based alkylbenzenes (TABs) were found in effluent samples.

4 Sample lost.

Table 4.4. Estimates of the fraction of effluent-derived organic matter, F_w, in sediment trap particles and surface sediments collected off Point Loma.

Sample type	Date Deployed	Elevation (m)	$\delta^{13}C$ (‰)	$\delta^{15}N$ (‰)	$F_w(N)$[1]
Sediment Traps:					
	11/28/89	0.5	-21.82	+7.17	0.07
		2.0	-21.63	+6.96	0.11
		5.0	-21.75	+6.85	0.13
	6/8/90	0.5	-21.75	+7.16	0.08
		2.0	-21.70	+6.36	0.22
		5.0	-21.54	+6.69	0.16
Surface Sediments[2]:					
	SD A-16		-21.98	+5.88	0.30
	SD A-5		-21.49	+6.50	0.19

1 Endmember compositions: $\delta^{15}N_m = +7.6$ ‰, $\delta^{15}N_w = +1.85$ ‰.

2 Upper sections (0-2 cm) of sediment cores.

Table 4.5. Ratios of 3-phenyldodecane/TAB_1 and internam to external isomers (I/E) in PLTP effluent particles and sediment trap particles and surface sediments collected off Point Loma.

Sample type	Date Deployed/Collected	Elevation (m)	ΣLAB ($\mu g\ g^{-1}$)	ΣLAB_{oc} ($\mu g\ g\ OC^{-1}$)	3ϕ-C_{12}/TAB_1[1] Ratio	I/E[2] Ratio
Effluent:	1/18/90		144.	580.	—[3]	0.84
	7/6/90		159.	492.	—[3]	0.92
Sediment Traps:						
	1/8/90	0.5	0.52	23.2	2.23	1.64
		2.0	0.52	24.0	3.87	1.68
		5.0	1.33	59.9	2.49	1.50
	6/15/90	0.5	1.17	54.9	5.59	1.20
		2.0	0.80	39.0	6.96	1.44
		5.0	0.63	29.2	5.22	2.09
Surface Sediments[4]:	SD A-16		0.065	8.55	1.05	2.55
	SD A-5		0.067	8.70	1.46	2.57

1 Ratio of 3-phenyldodecane/TAB_1. See text and Figure 23 for explanation.

2 I/E ratio: (6-phenyldodecane + 5-phenyldodecane)/(4-phenyldodecane + 3-phenyldodecane +2-phenyldodecane).

3 No tetrapropylene-based alkylbenzenes (TABs) were found in effluent samples.

4 These are upper sections (0-2 cm) of sediment cores.

Table 4.6
Predicted Average Initial Dilutions

Average Initial Dilution:	*DECAL*	TSLINE	Ratio (TS/DC)
San Diego	116	485	4.2
Orange County	96	593	6.2
Los Angles County - 90-inch	262	463	1.8
Los Angles County 120-inch	158	na	na

Table 4.7
Estimated Flow-Averaged Initial Dilutions

	DECAL	"TSLINE"	Ratio	Min.ID*
San Diego	116	281	2.4	113
Orange County	96	344	3.6	180
LA County-120-inch	158	-	-	
LA County-90-inch	262	269	1.03	166**

* Min.I.D. = NPDES permit initial dilution value
** Average of the 90-inch and 120-inch outfalls

Table 4.8
Wastefield Suspended Solids Concentrations

Parameter	DECAL	SED2D	Measured
Effluent concentration	0.51-1.25	0.08-0.43	
Natural- Overlying layer	0.32-0.42	<0.25*	
Natural-Entrained	0**	2	2 (60m avg.)
Total	1.0-1.6	2.1-2.4	
Ratio (Nat.Ent./Total)	0	0.82-0.96	

* From the wastefield thickness simulations
** By assumption

Table 4.9
Peak Organic Content of the Surface Layer of the sediments (in percent)

Simulation Conditions	San Diego	Orange County
Aggregation - $f_a = 1.00$	68.2	66.0
Aggregation - $f_a = 0.01$	36.9	15.5
Noncohesive - $f_a = 1.00$	37.6	32.5
Noncohesive - $f_a = 0.01$	5.75	3.08
Predicted Background*	1.4	2.0
Maximum Measured	2.58	2.82
Minimum Measured (Grabs)	1.7	1.4**
Minimum Measured (Cores)	2.2	NA

* Predicted ambient values are semi-arbitrary.(determined by choice of input parameter values). These values simply provide a reference for the predicted increases.

** Neglecting a value of 0.9 on the side of Newport Canyon

Table 4.10
Concentrations - San Diego Sediments

	Organic (gm/L)		Lead (mg/L)		Cadmium (mg/L)	
	Max(Pk)	Min(Bkg)	Max(Pk)	Min(Bkg)	Max(Pk)	Min(Bkg)
DECAL						
kd = 0.10	140.	7.8	20.8	1.16	1.28	0.07
kd = 0.52	55.0	0.00	11.3	0.00	0.50	0.00
Grab Samples	27.3	17.5	19.1	7.3	.41	.16
Cores	(25.1)	17.5	(8.8)	2.8	(0.57)	0.04
	Maximum-Minimum		**Maximum-Minimum**		**Maximum-Minimum**	
DECAL						
kd = 0.10	132.		21.		1.21	
kd = 0.52	55.0		11.3		0.50	
Grab Samples	9.8		11.8		0.25	
Cores	(7.6)		(6.0)		(0.53)	
	Ratio *DECAL*/Grab)		**Ratio (*DECAL*/Grab)**		**Ratio (*DECAL*/Grab)**	
Max-Min (0.10)	13.5		1.8		4.8	
Max-Min (0.52)	5.6		0.96		2.0	

Values enclosed within () are not directly comparable with the predicted maximum concentrations since they may represent deposition that occurred at some time earlier in the discharge

Table 4.11
Concentrations - Orange County Sediments

	Organic (gm/L)		Lead (mg/L)		Cadmium (mg/L)	
	Max(Pk)	Min(Bkg)	Max(Pk)	Min(Bkg)	Max(Pk)	Min(Bkg)
DECAL						
kd = 0.10	109.	12.2	35.0	3.91	2.05	0.23
kd = 0.52	42.9	0.00	19.2	0.00	0.71	0.00
Grab Samples	30.9	13.0	11.0	7.4	1.11	.11
	Maximum-Minimum		**Maximum-Minimum**		**Maximum-Minimum**	
DECAL						
kd = 0.10	97.		31.1		1.82	
kd = 0.52	42.9		19.2		0.71	
Grab Samples	17.9		3.6		1.00	
	Ratio (*DECAL*/Grab)		**Ratio (*DECAL*/Grab)**		**Ratio (*DECAL*/Grab)**	
Max-Min (0.10)	5.4		8.6		1.8	
Max-Min (0.52)	2.4		2.5		0.71	

Table 4.12
Concentrations - LA County Sediments

	Organic (gm/L)		Lead (mg/L)		Cadmium (mg/L)	
	Max(Pk)	Min(Bkg)	Max(Pk)	Min(Bkg)	Max(Pk)	Min(Bkg)
DECAL						
kd = 0.10	356.	48.9	212	3.5	5.65	0.13
kd = 0.52	126	0.62	133	0.00	2.78	0.00
Core Samples	65.9*	38.6*	127	23.5	11.2	1.00
	Maximum-Minimum		Maximum-Minimum		Maximum-Minimum	
DECAL						
kd = 0.10	307		208		5.5	
kd = 0.52	125		133		2.78	
Core Samples	27.3		104		10.2	
	Ratio (*DECAL*/Core)		Ratio (*DECAL*/Core)		Ratio (*DECAL*/Core)	
Max-Min (0.10)	11.2		2.0		0.54	
Max-Min (0.52)	4.6		1.3		0.28	

Table 4.13
Accumulation Rates

Station	Approx. Cum. Mass (gm/cm^2)	Avg. Accum. Rate ($gm/cm^2/yr$)	Xs TVS[1] (gm/cm^2)	F_n ($gm/cm^2/yr$)	F_w ($gm/cm^2/yr$)
0C	6.3	241	.126	233	7.7
1C	9.4	360	.486	314	46
3C	9.7	372	.791	295	26
6C	13.0	499	1.610	361	137
7C	16.2	623	2.006	445	177
8C	17.2	663	3.106	404	259
9C	4.8	185	.396	150	35
10C	5.8	222	.107	211	11

Figures

see page 124 for
index of Figurers

e 1.1 - Some of the processes affecting the fates of
ulates in the ocean.

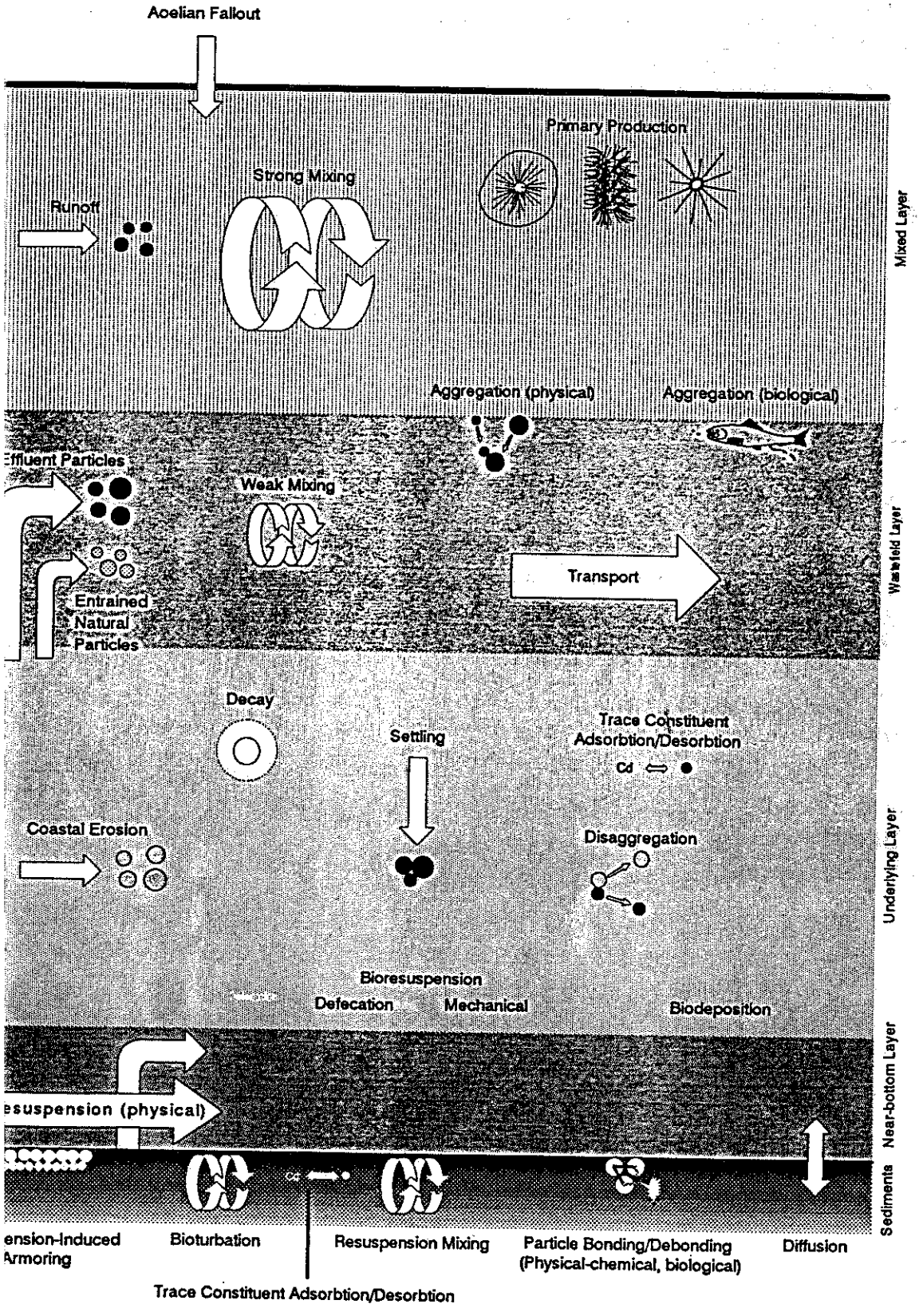

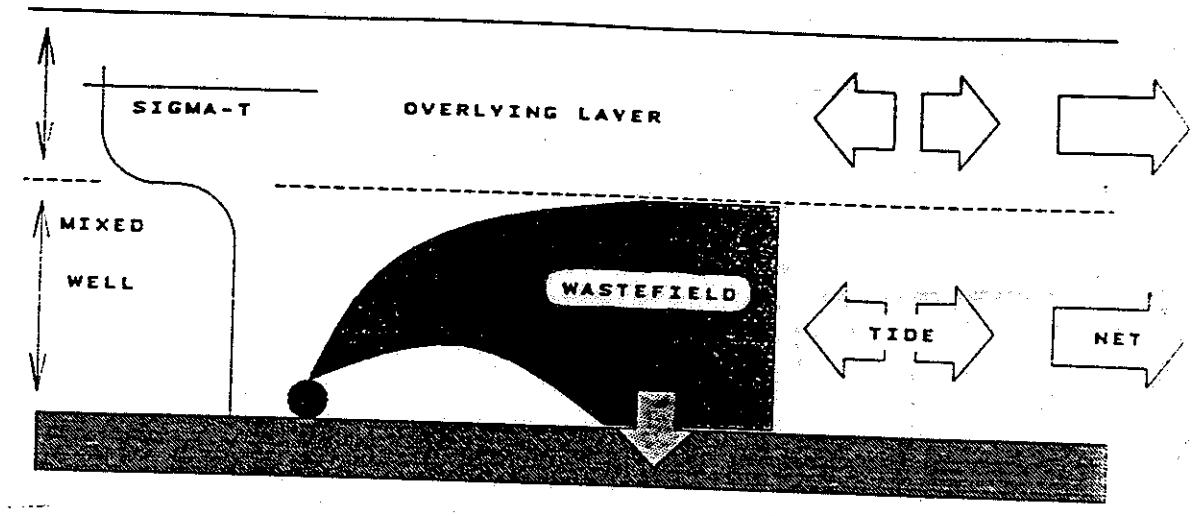

a

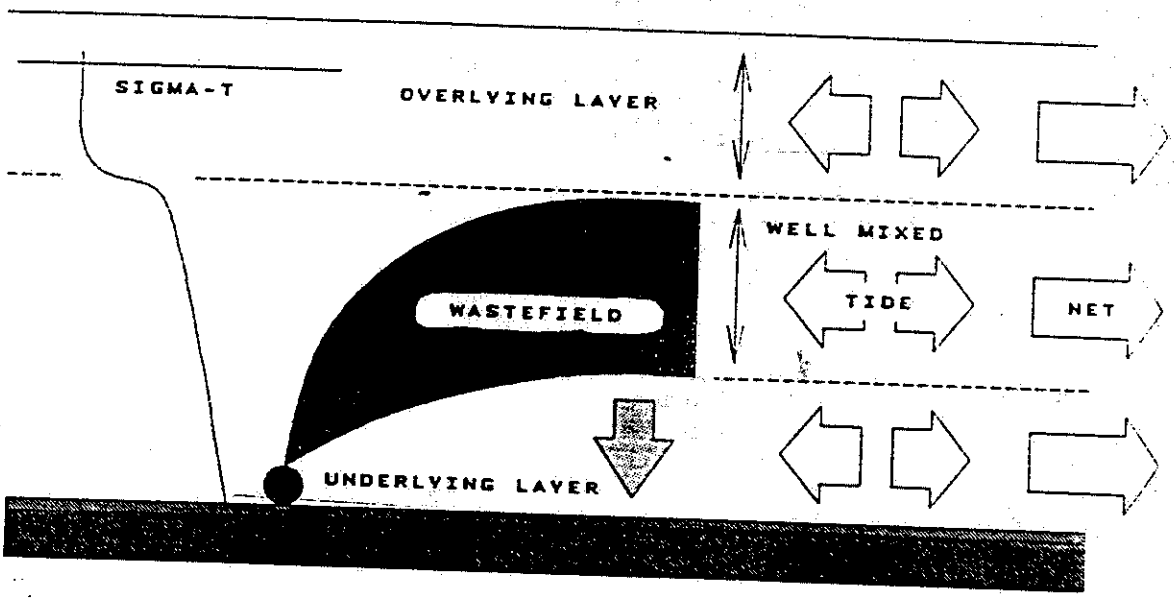

b

Figure 1.2 - Water column stratification in DECAL. (a) 2-Layer, (b) 3-Layer.

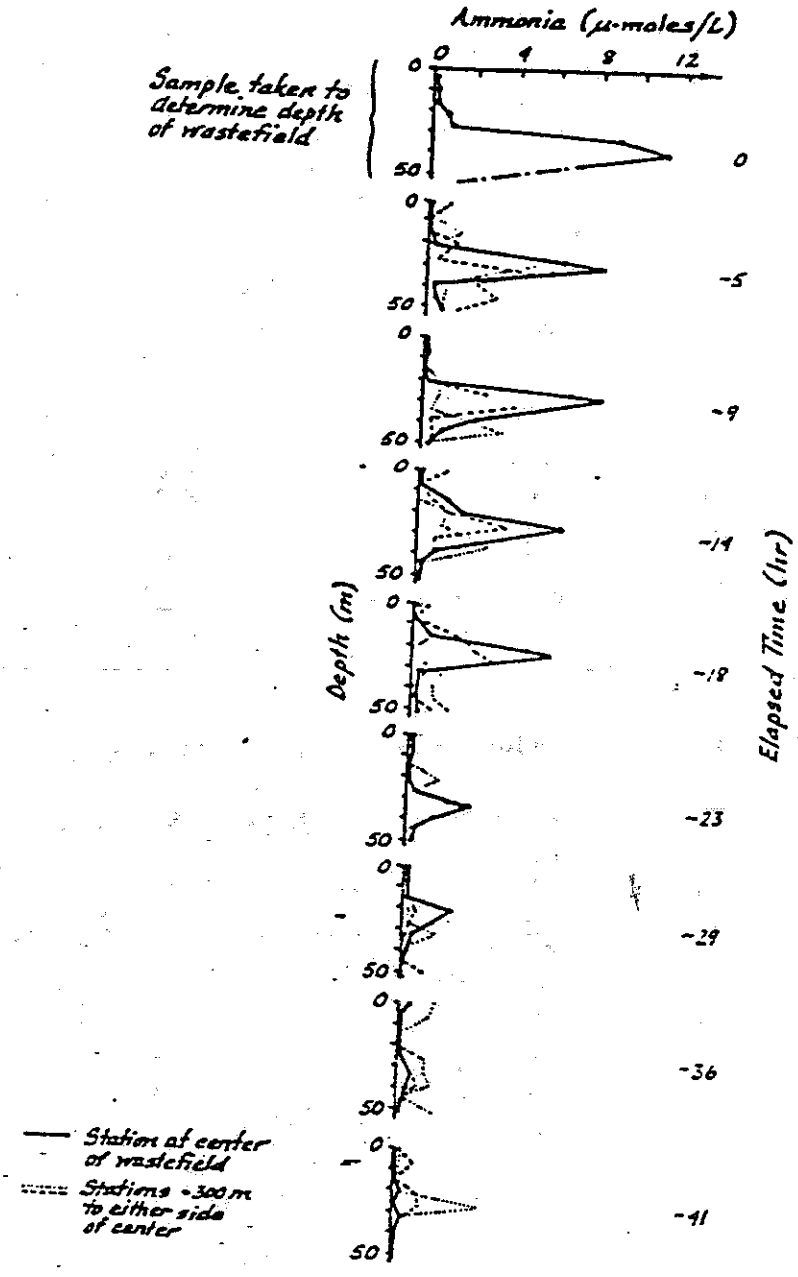

Figure 1.3 - Wastefield ammonia in the water column: Point Loma.

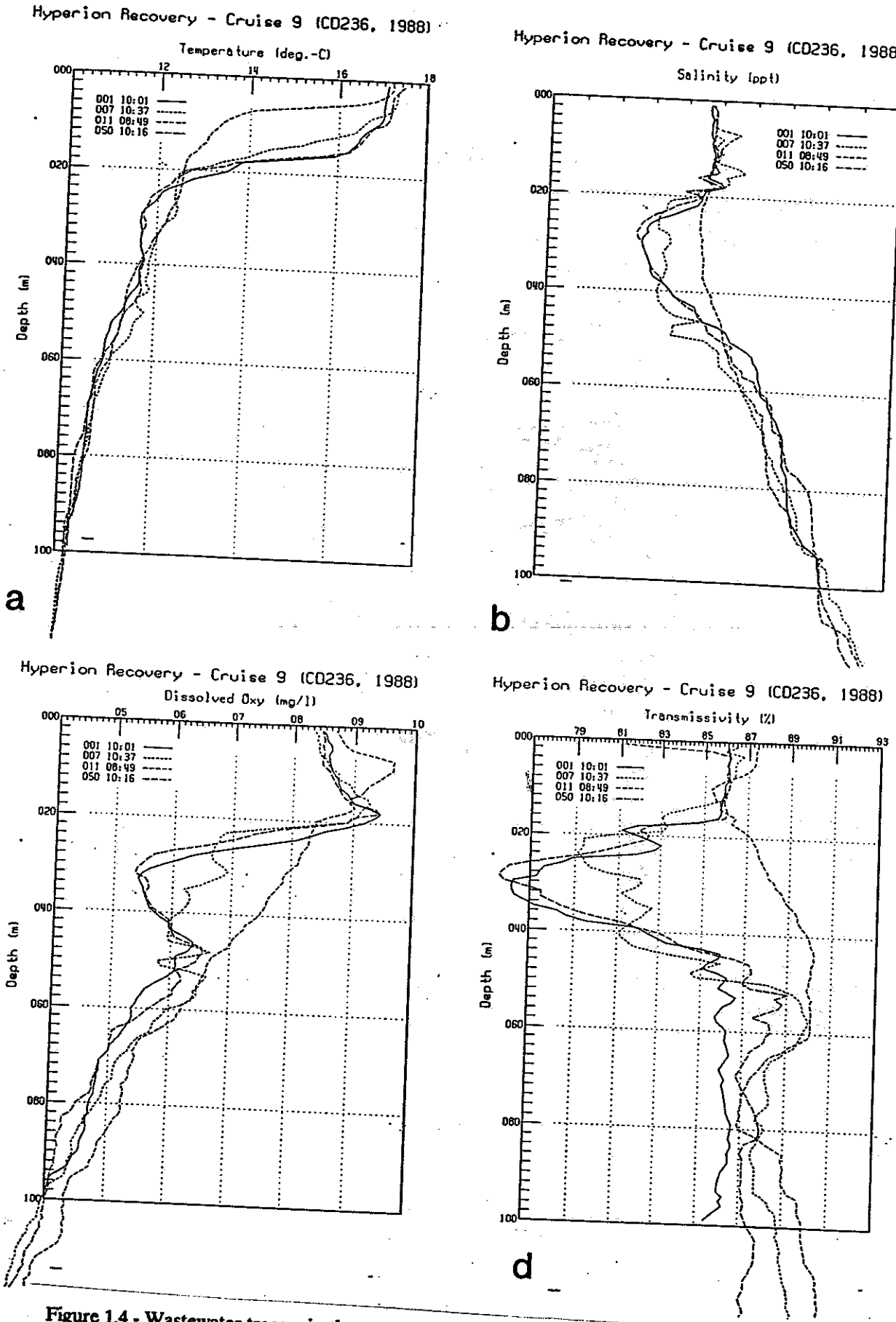

Figure 1.4 - Wastewater tracers in the water column: Santa Monica Bay. (a) temperature, (b) salinity, (c) dissolved oxygen, (d) transmissivity.

gram XTRACT - Ver. 1.0, 7/8/91

racting ROW (xshr) #: 5
put: FLUXES

put file: PVTTXSHR.P05
it files:
PVALLBOT.PR1
PV300BOT.PR1
PV100BOT.PR1
PV030BOT.PR1
PV010BOT.PR1
PV005BOT.PR1

iles:

Val->

.063	.0	13.8	10.4	4.1	1.5	.8
.188	.0	20.2	14.8	5.8	2.1	1.1
.313	77.4	68.1	35.2	12.6	4.4	2.2
.438	204.2	143.3	66.4	22.8	7.9	4.0
.563	361.5	236.0	104.7	35.3	12.2	6.1
.688	546.9	345.1	149.8	50.0	17.2	8.7
.813	745.0	462.5	198.5	65.9	22.7	11.4
.938	953.5	586.9	250.5	82.9	28.5	14.3
1.063	1123.8	693.2	296.1	98.1	33.7	17.0
1.188	1250.7	778.4	334.4	111.0	38.2	19.2
1.313	1380.1	865.4	373.6	124.3	42.8	21.5
1.438	1511.8	952.8	413.1	137.7	47.4	23.9
1.563	1696.4	1065.8	461.9	154.0	53.0	26.7
1.688	1747.5	1108.8	484.5	162.2	55.9	28.2
1.813	1664.8	1080.8	480.1	161.9	55.9	28.2
1.938	1745.1	1133.3	505.2	170.8	59.0	29.8
2.063	1733.6	1135.1	510.6	173.5	60.1	30.3
2.188	1571.3	1055.4	484.8	166.3	57.8	29.2
2.313	1212.8	873.3	420.1	147.0	51.4	26.0
2.438	940.1	732.5	370.2	132.2	46.5	23.6
2.563	719.8	614.5	327.8	119.6	42.3	21.5
2.688	504.1	494.6	283.6	106.3	37.9	19.3
2.813	352.4	405.7	250.4	96.4	34.6	17.7
2.938	256.8	344.3	226.8	89.3	32.3	16.5
3.063	155.6	278.6	201.0	81.5	29.7	15.2
3.188	91.5	230.9	181.5	75.6	27.8	14.2
3.313	10.6	175.1	158.7	68.6	25.5	13.1
3.438	7.9	160.0	150.9	66.2	24.7	12.7
3.563	5.9	146.0	143.3	63.8	23.9	12.3
3.688	5.6	133.0	135.8	61.4	23.1	11.9
3.813	3.9	120.6	128.5	59.1	22.3	11.5
3.938	3.1	109.5	121.6	56.8	21.6	11.1

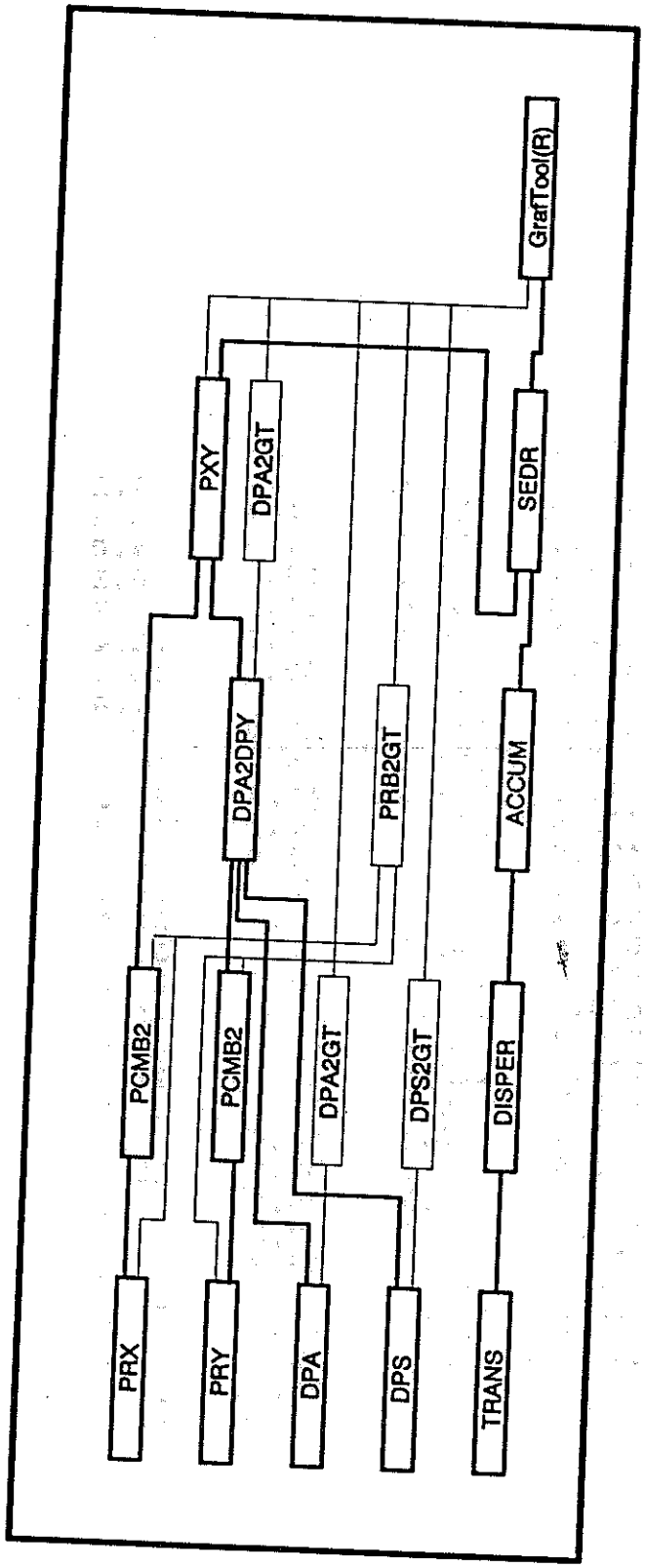

Figure 1.5 - SED2D submodel flow diagram.

Figure 1.6 - Water column stratification in SED2D.

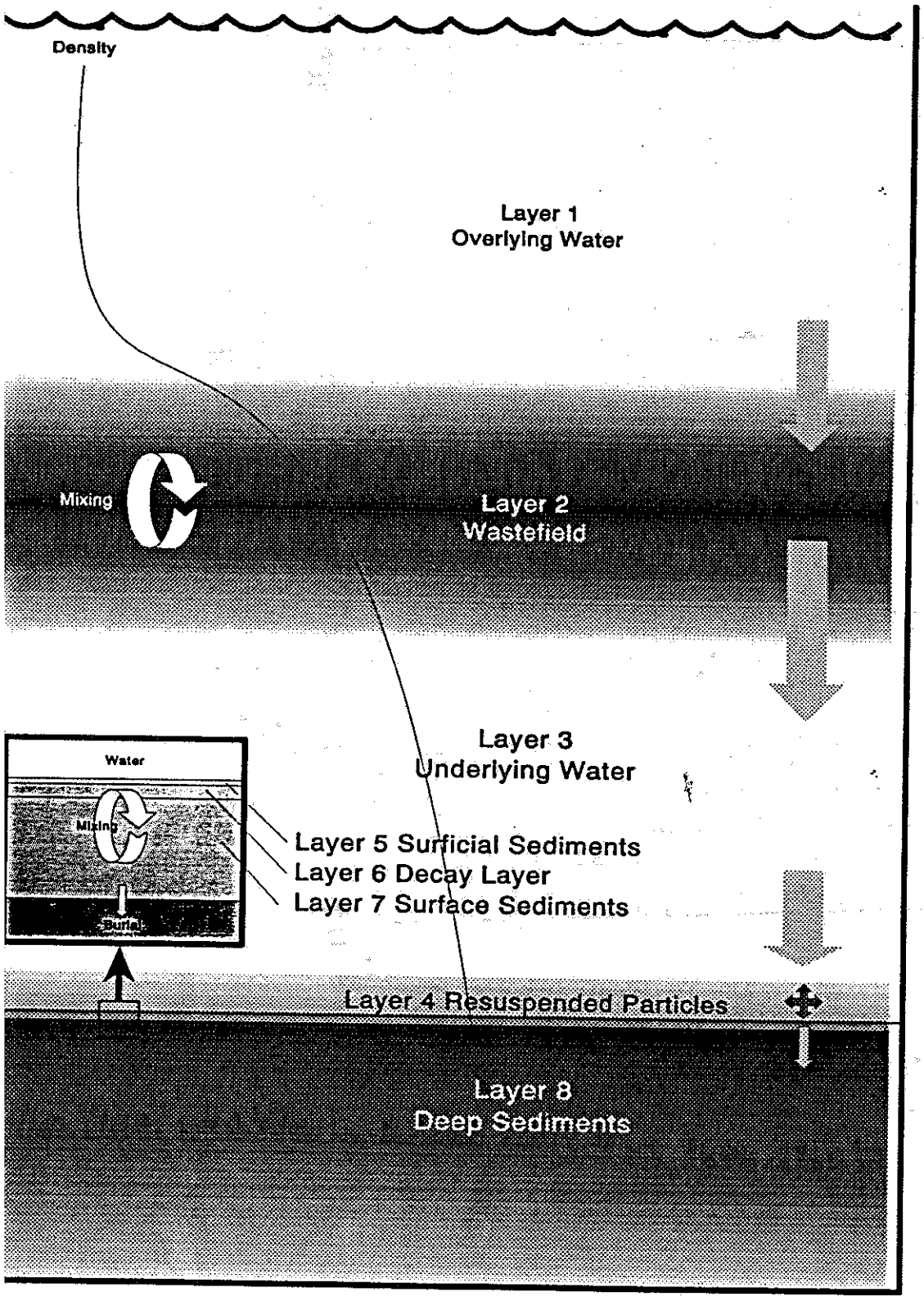

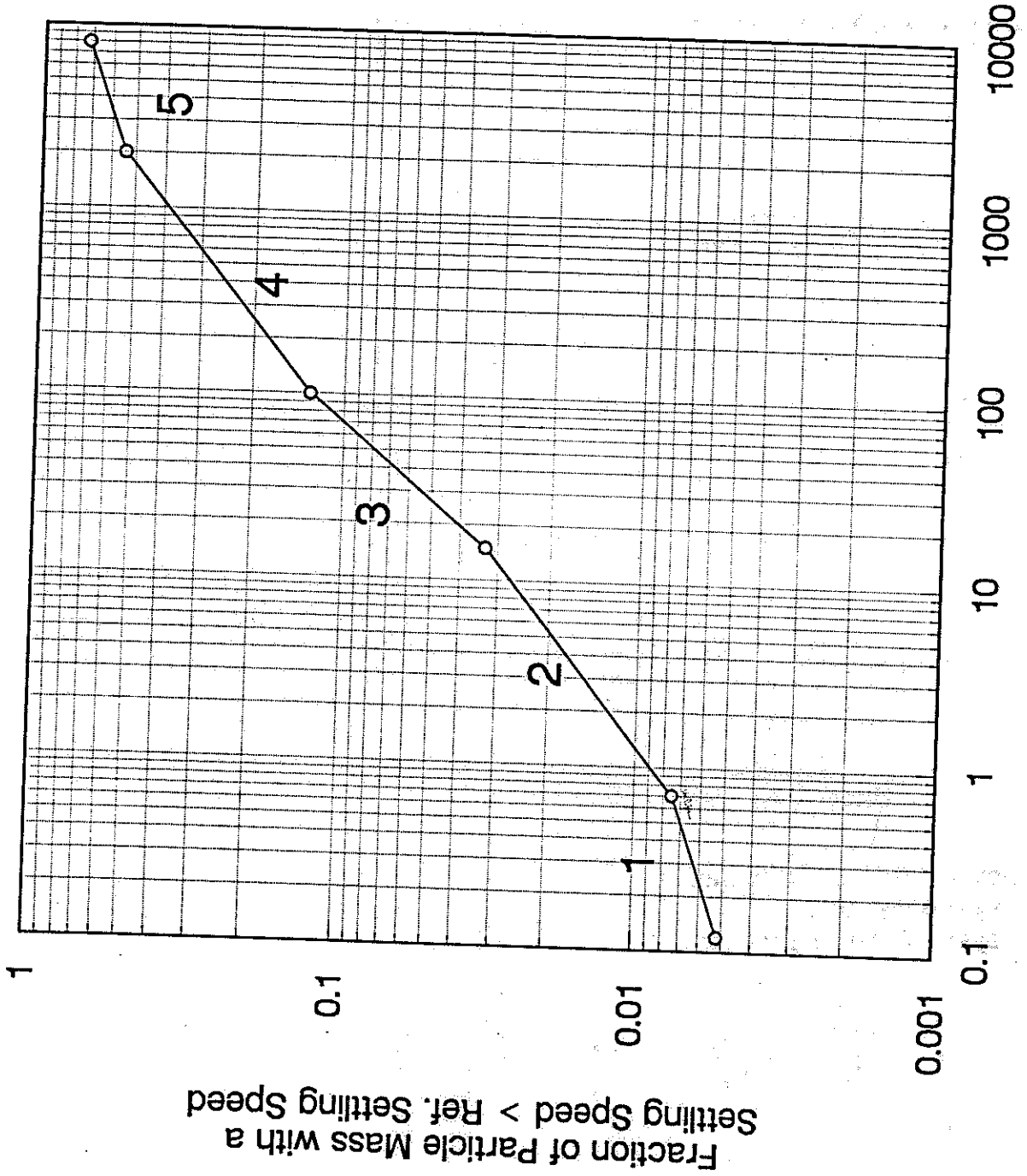

Figure 1.7 - Representation of mass distribution of non-cohesive particle settling speeds.

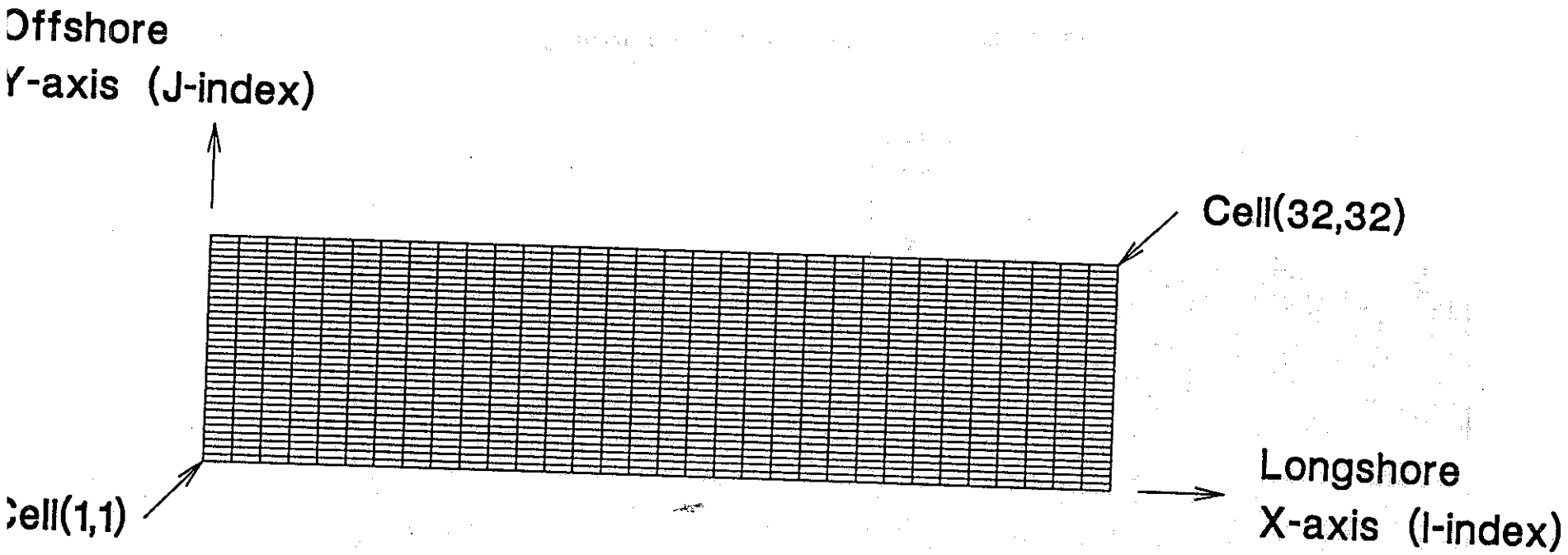

Figure 1.8 - SED2D basic simulation grid.

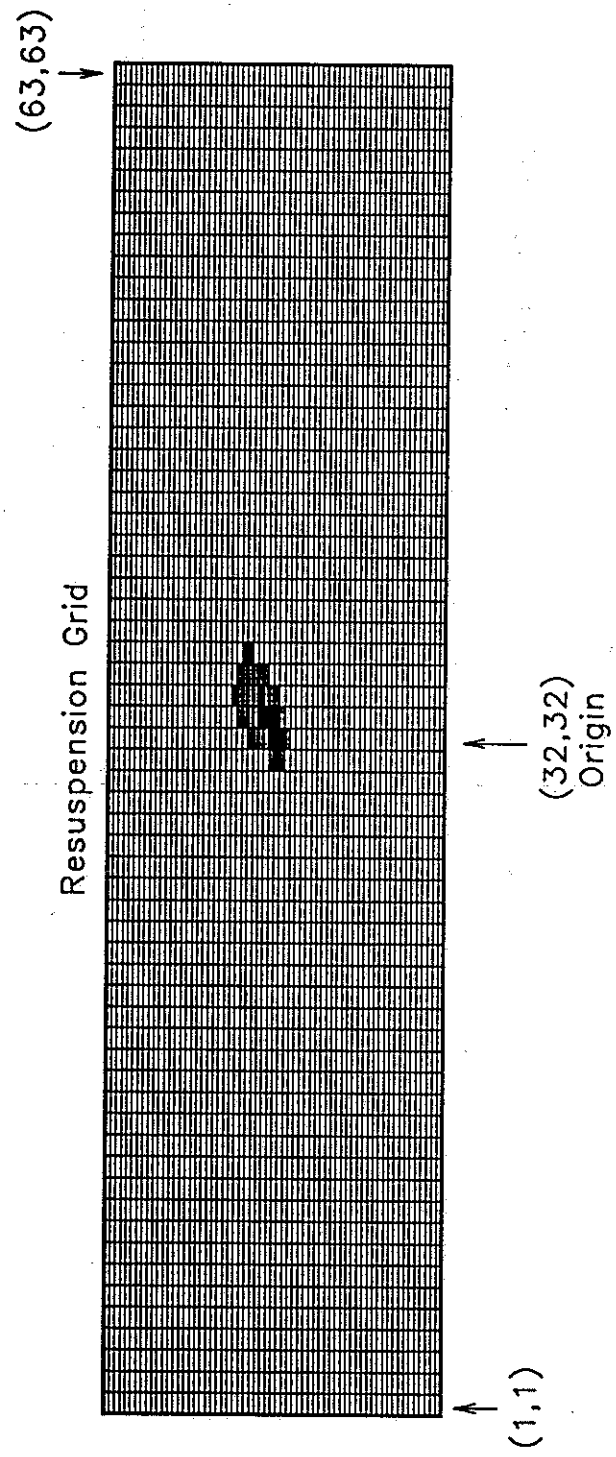

Figure 1.9 - Resuspension redistribution grid - SED2D, one resuspension.

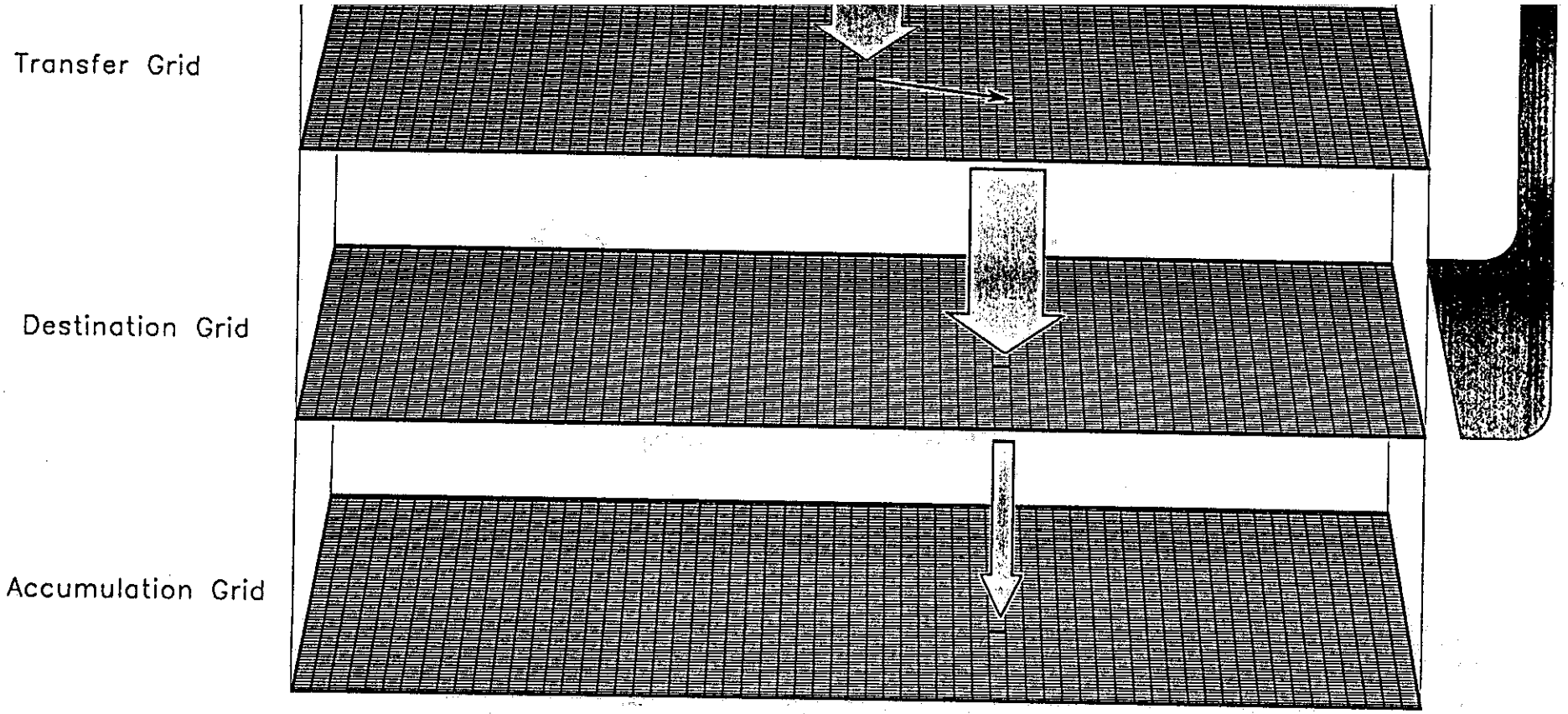

Figure 1.10 - SED2D resuspension simulation grids.

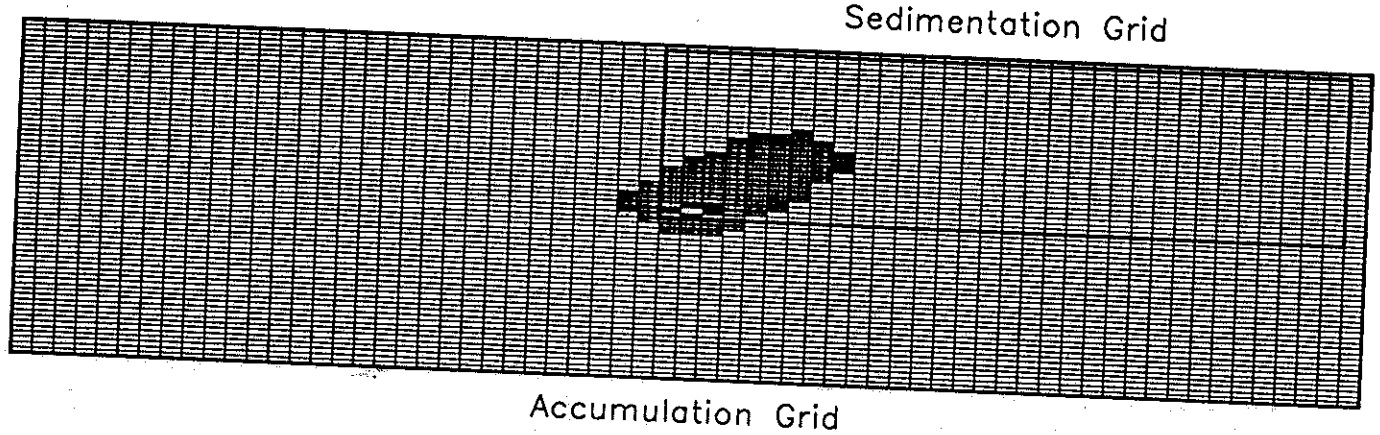

Figure 1.11 - Superposition of SED2D basic ("sedimentation") and "accumulation" grids.

.12 - Effects of the ratio of Sedimentation Flux to
lux. (a) response time, (b) organic fraction, (c)
ation flux.

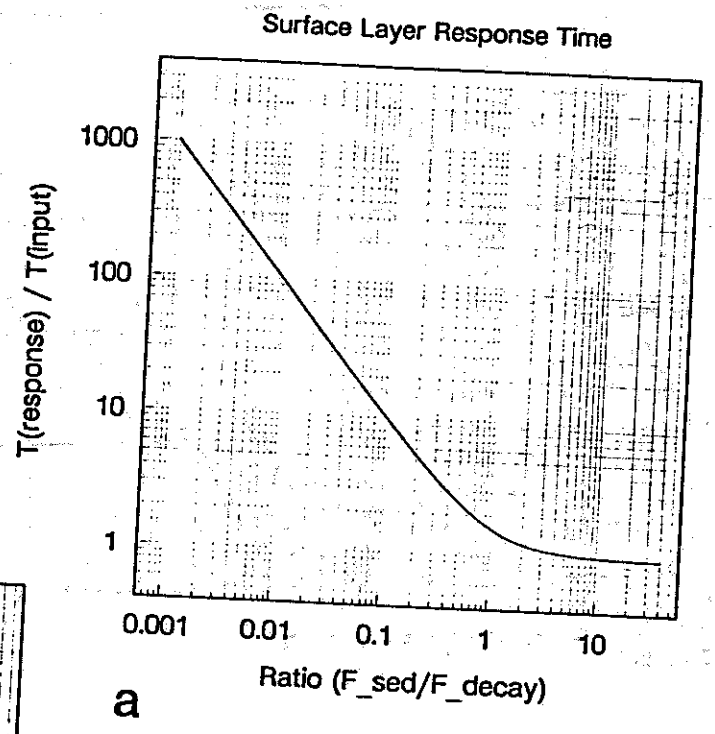

a

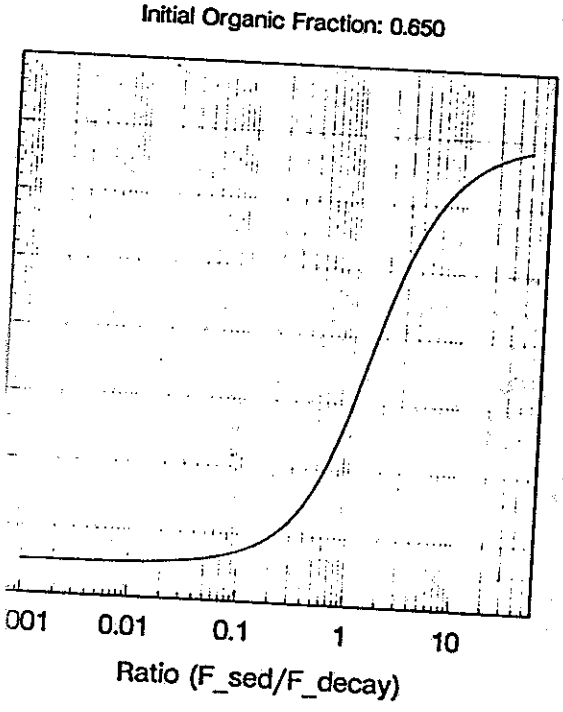

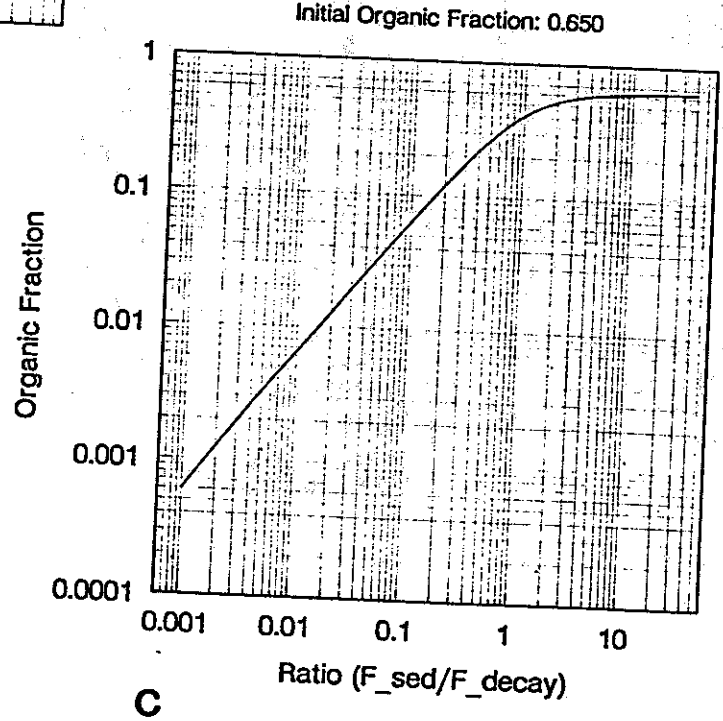

c

Planned Schedule of Effluent Sampling

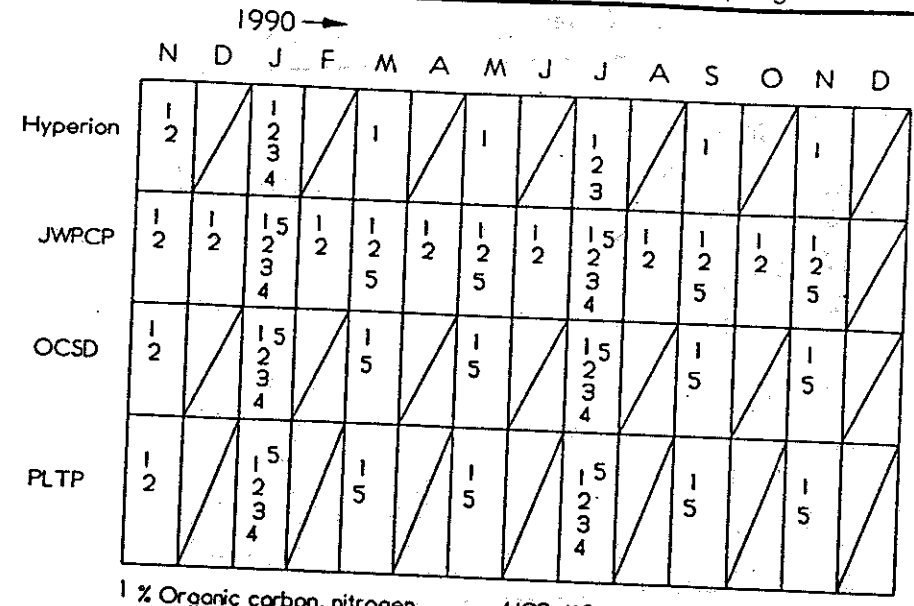

1 % Organic carbon, nitrogen.
2 Linear alkylbenzenes, coprostanol
3 13-C, 15-N.
4 ICP-MS multielement.
5 Cd, Pb.

Actual Schedule of Effluent Sampling

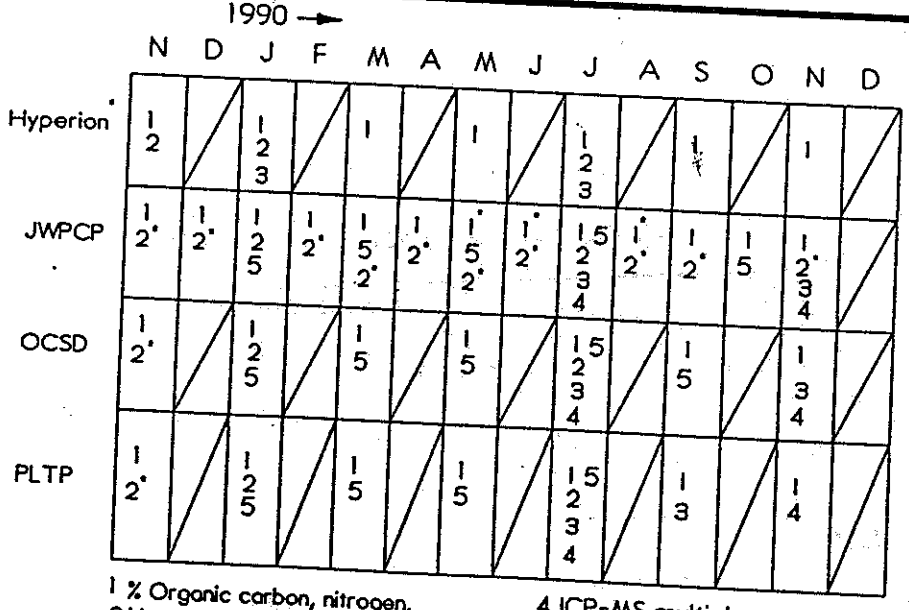

1 % Organic carbon, nitrogen.
2 Linear alkylbenzenes, coprostanol.
3 13-C, 15-N.
4 ICP-MS multielement.
5 Cd, Pb.
• Samples collected, but not analyzed.

Figure 2.1 - Matrices of the planned and actual effluent sampling program.

Planned Schedule of Sediment Trap Retrieval

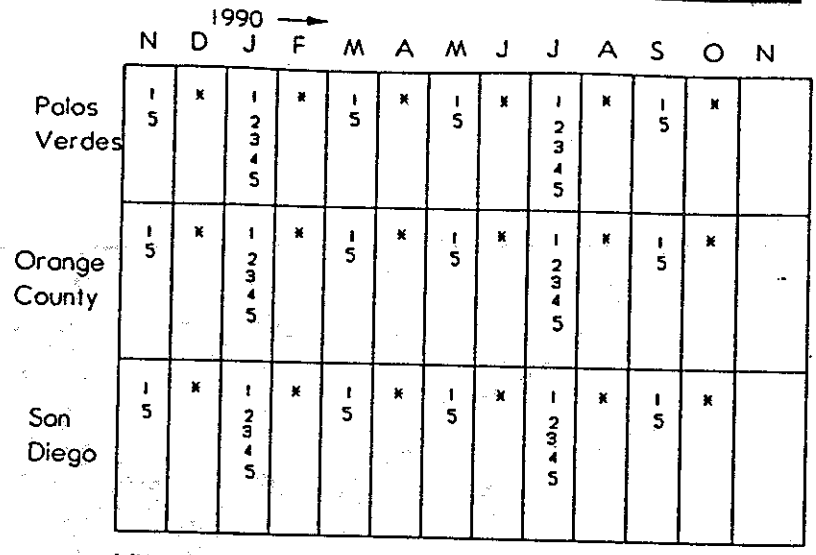

1 % organic carbon, nitrogen.
2 LAB, coprostanol.
3 13-C, 15-N.
4 ICP-MS multielement.
5 Cd, Pb.
* Archive sediments.

Actual Schedule of Sediment Trap Retrieval/Analysis

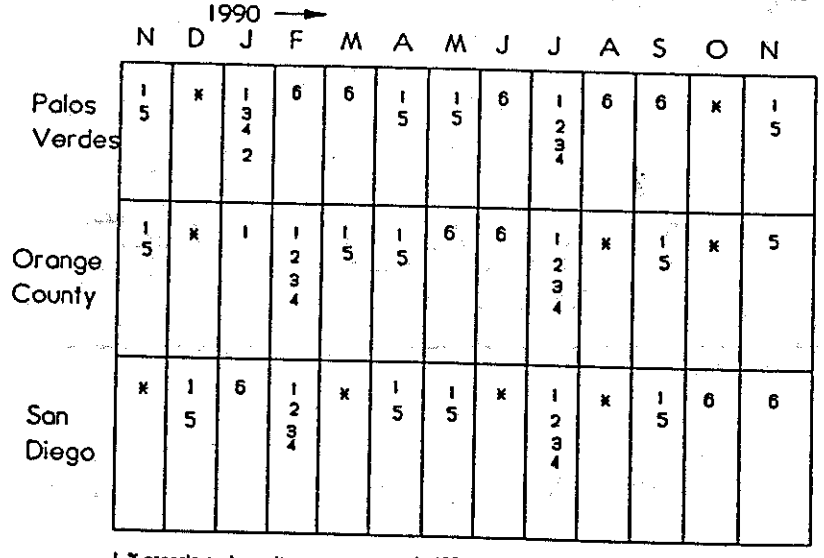

1 % organic carbon, nitrogen.
2 LAB, coprostanol.
3 13-C, 15-N.
4 ICP-MS multielement.
5 Cd, Pb.
6 Mooring lost.
* Archive sediments.

Figure 2.2 - Matrices of the panned and actual sediment trap retrieval schedule.

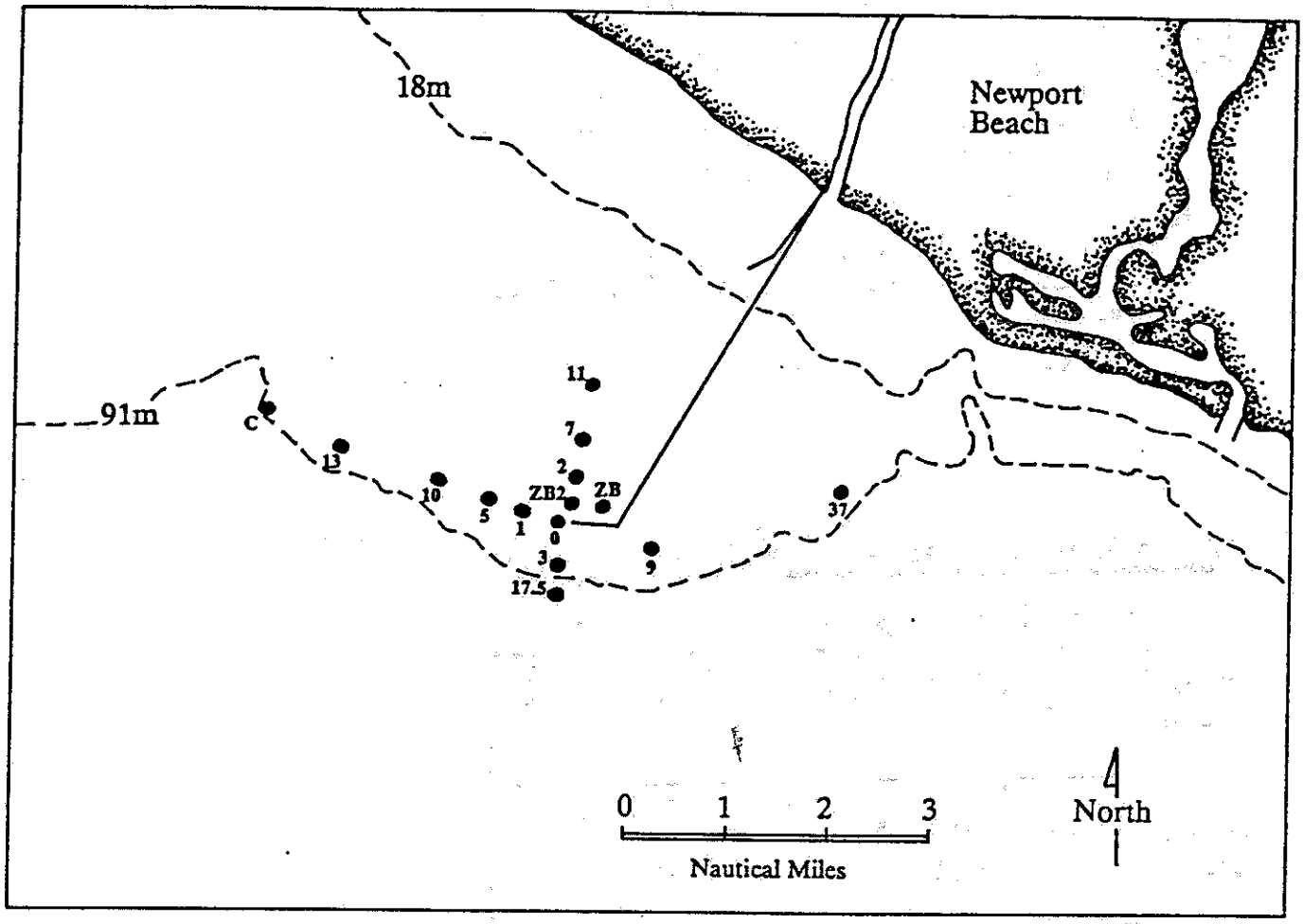

Figure 2.3 - Location map of the site off Orange County showing stations for surface sediment grabs, locations and sediment trap mooring

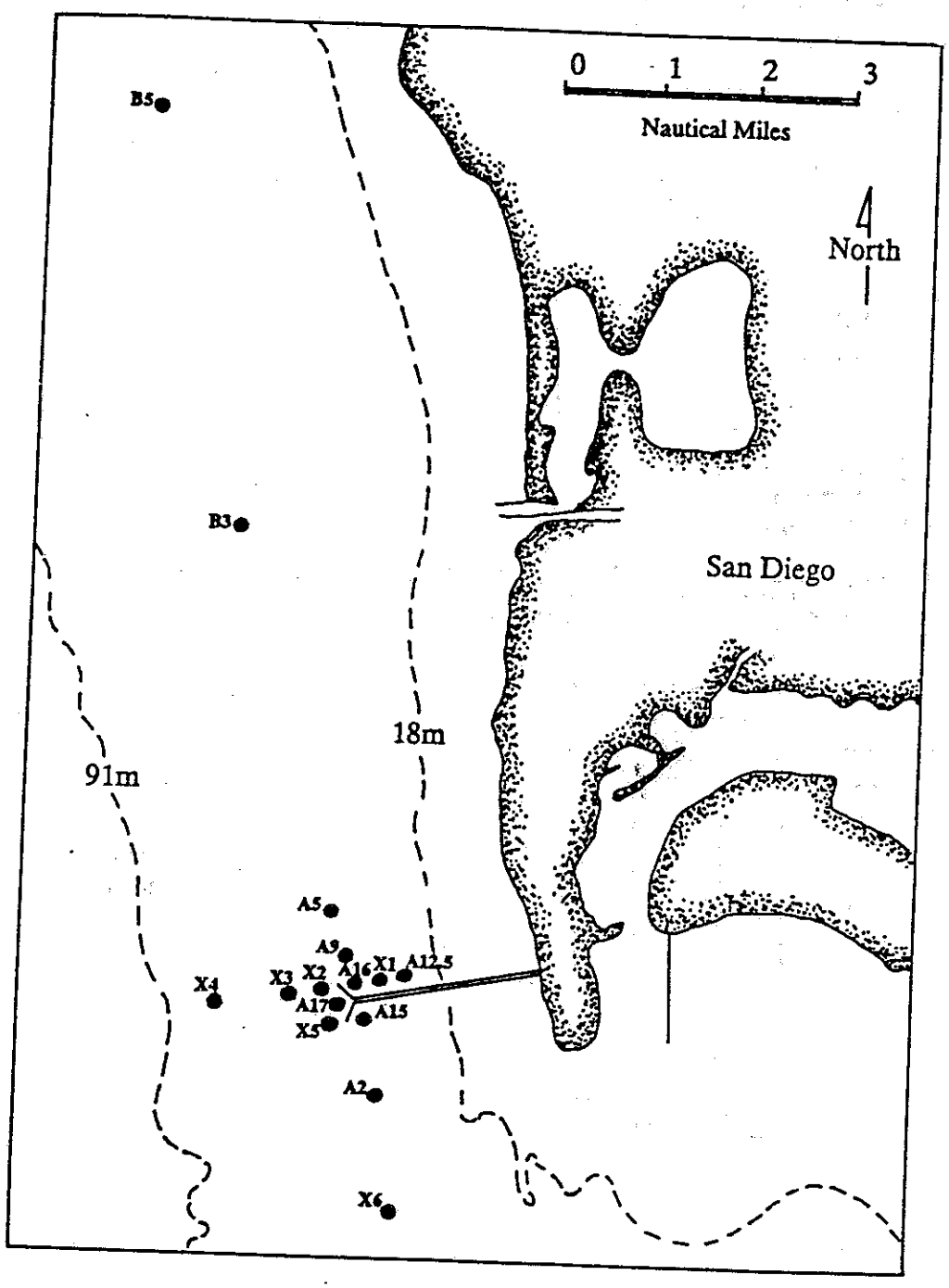

2.4 - Location map of the site off Point Loma showing stations for surface sediment grabs and sediment trap mooring.

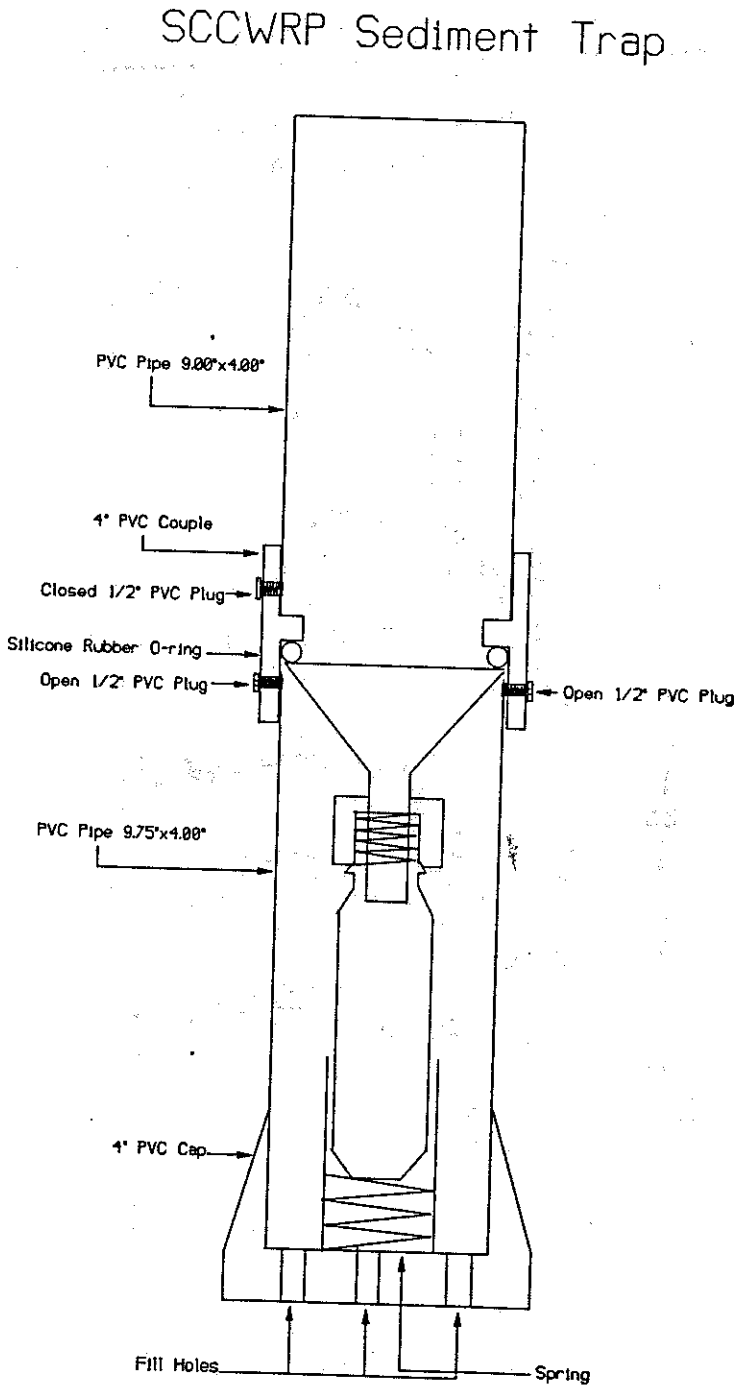

Figure 2.5 - Schematic of the "new" SCCWRP trace constituent sediment trap.

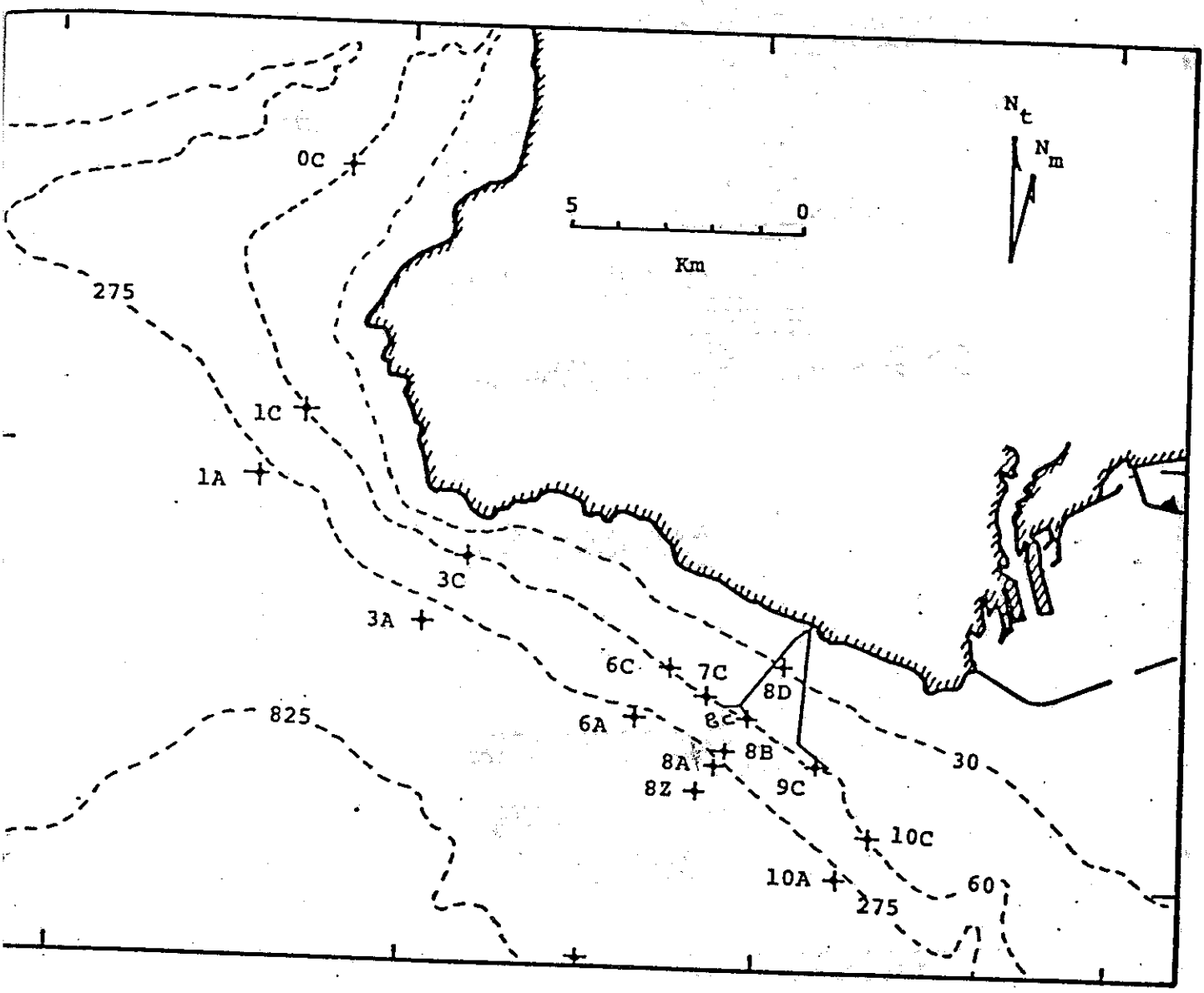

2.6 - Location map of the site off Palos Verdes showing the station at which replicate surface sediment grabs were taken and the
ıt trap mooring was located.

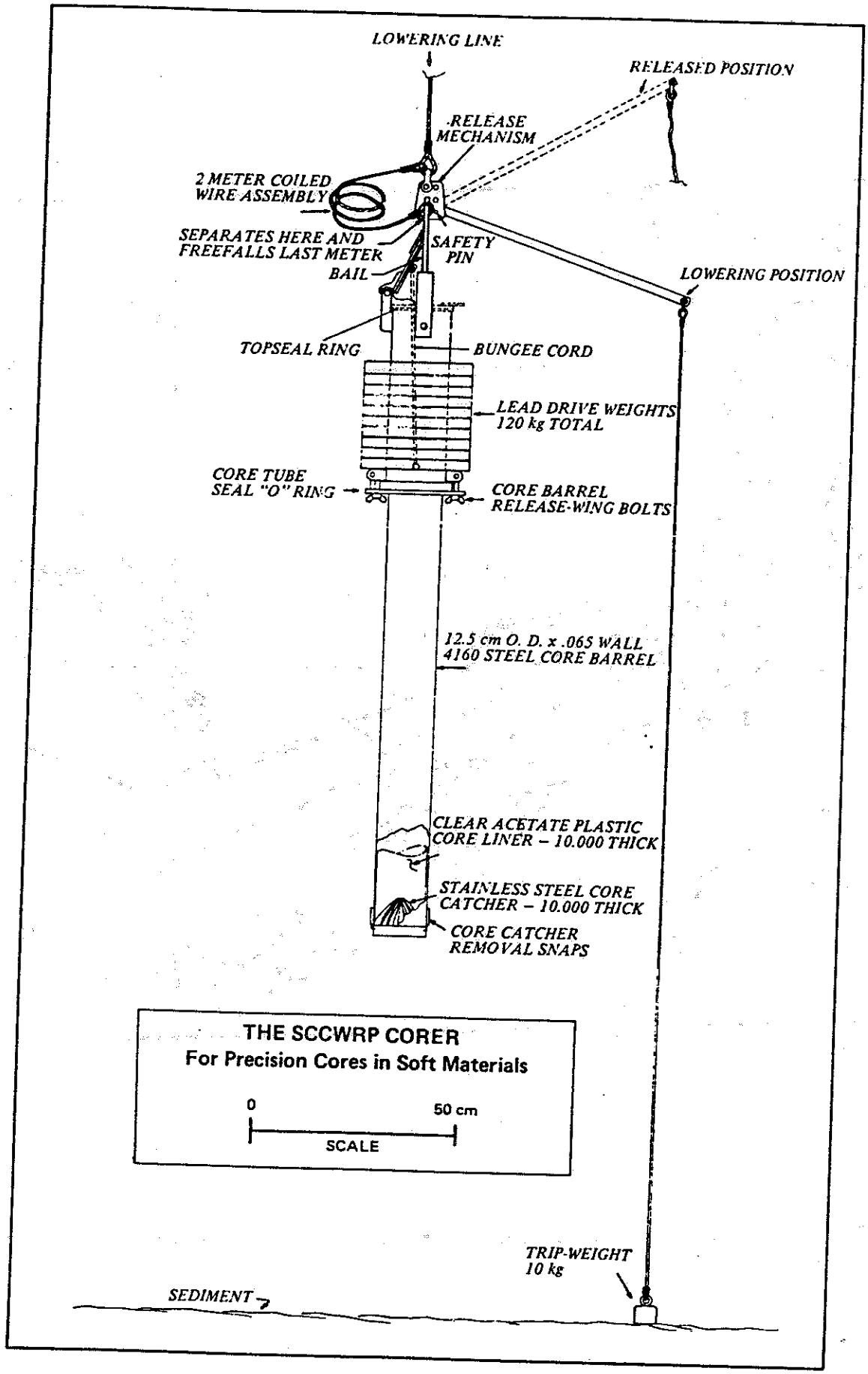

Figure 2.7 - Schematic of the SCCWRP soft sediment gravity corer (after Bascom et al. 1982).

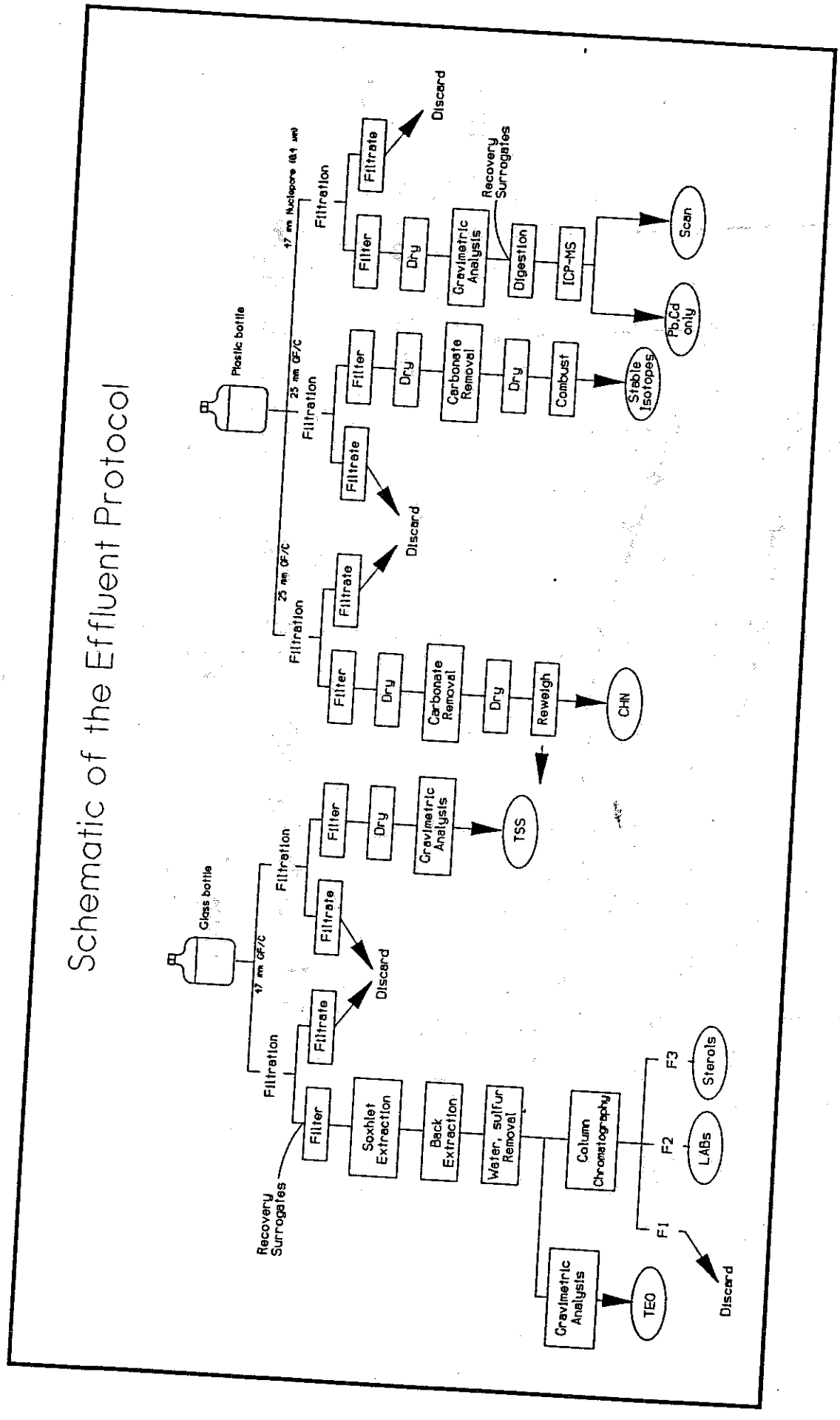

Figure 2.8 - Flow diagram illustrating the protocol used for processing effluent samples.

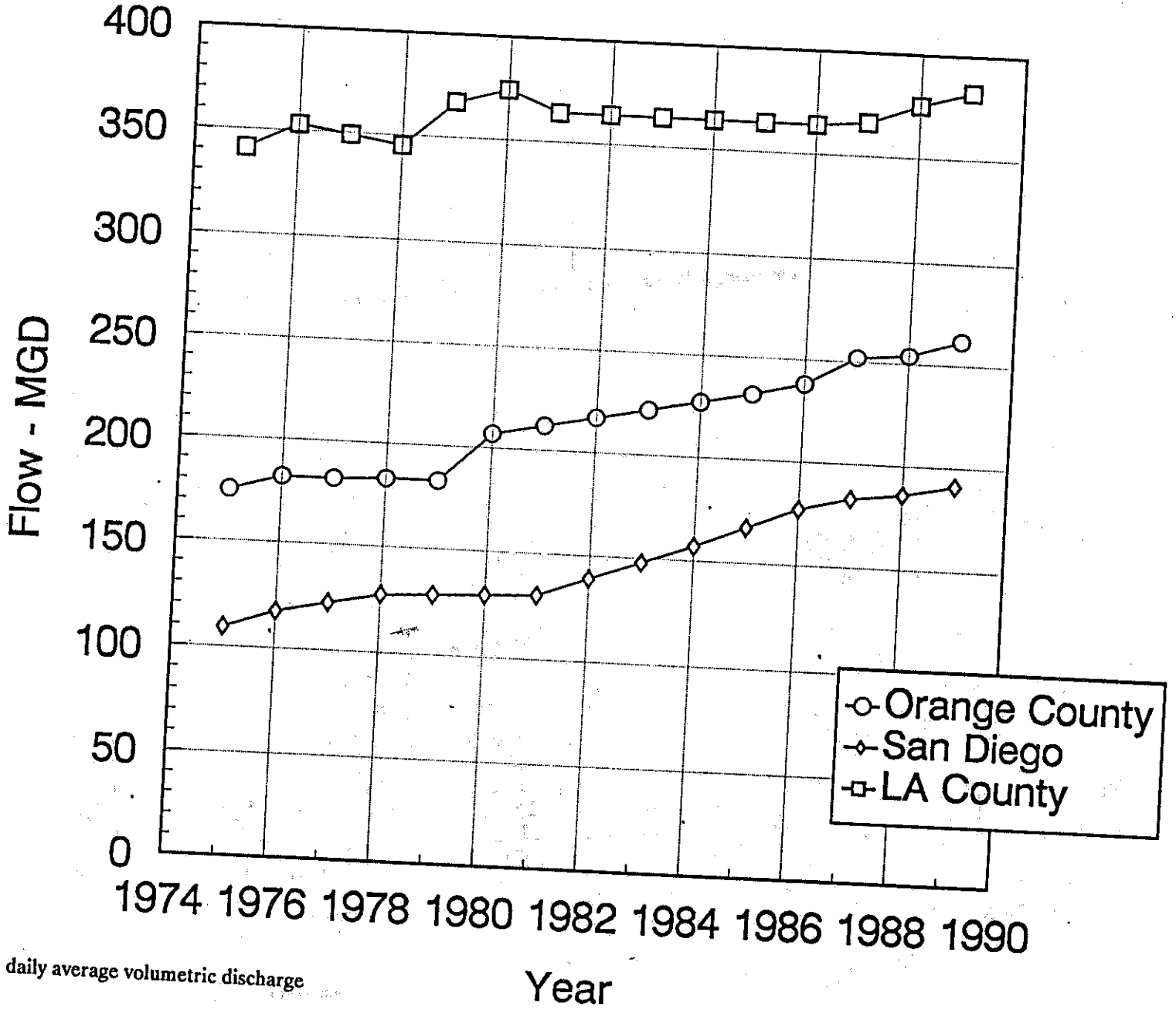

Figure 2.9 - Effluent daily average volumetric discharge rates: 1975-1989.

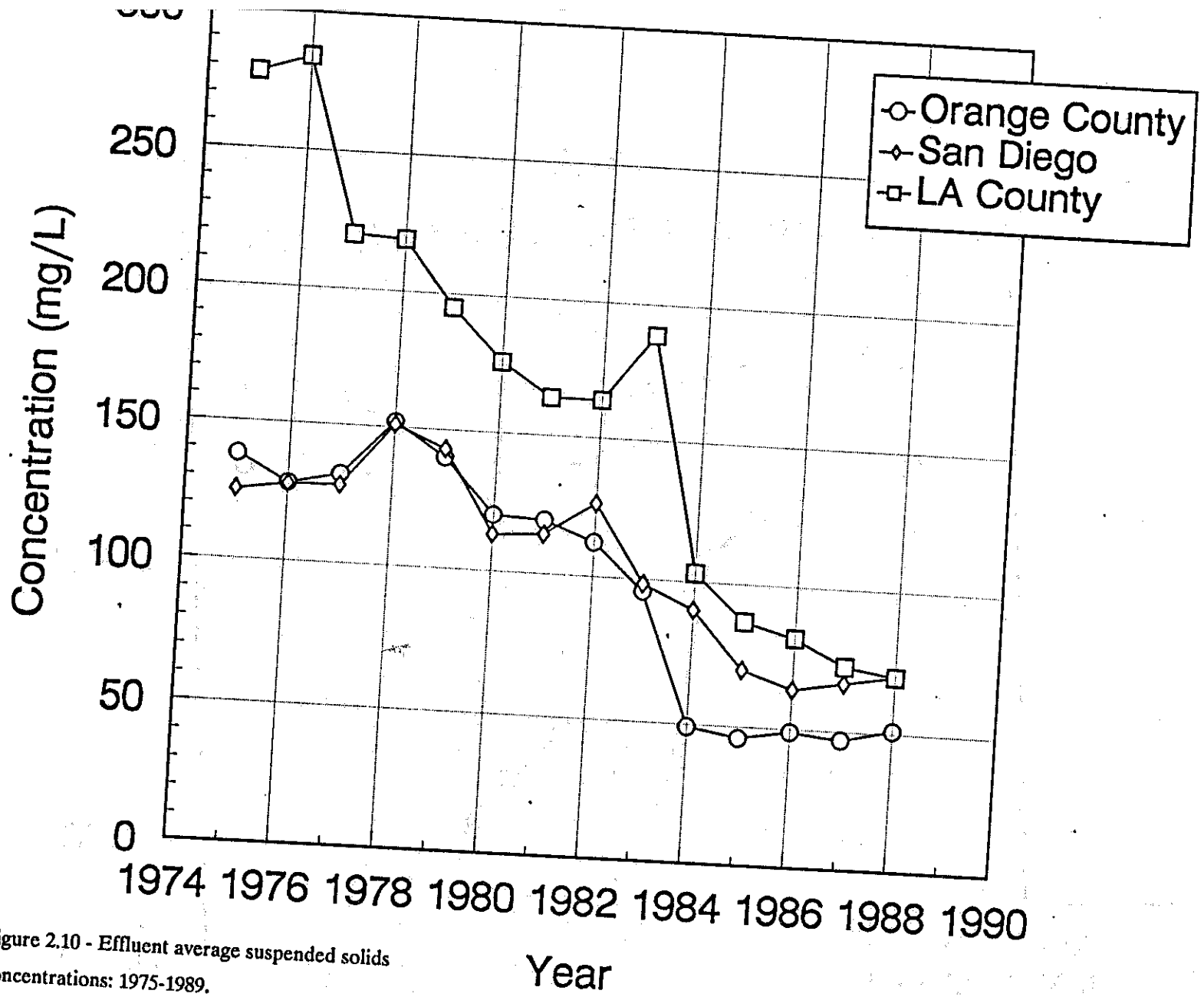

Figure 2.10 - Effluent average suspended solids concentrations: 1975-1989.

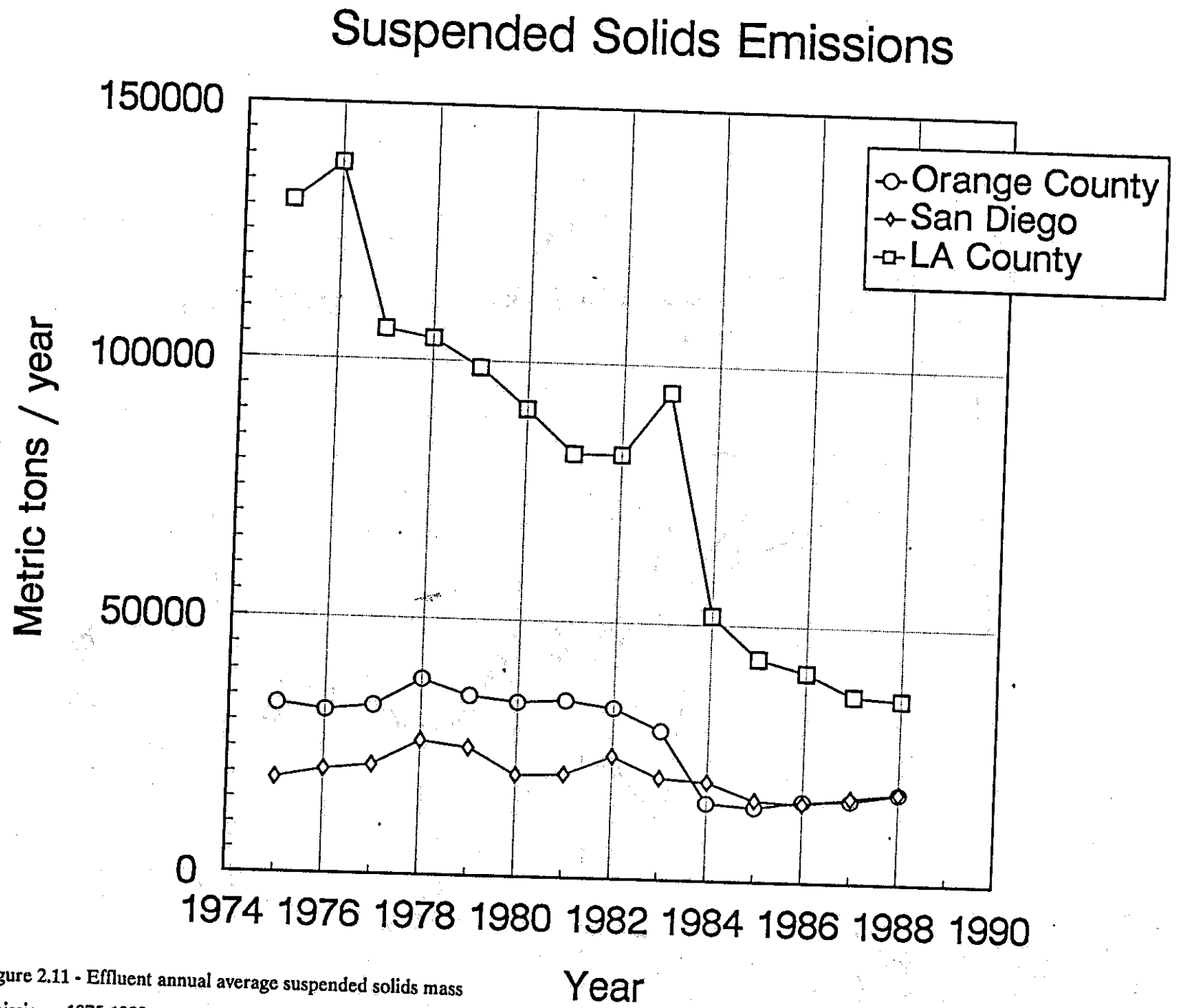

Figure 2.11 - Effluent annual average suspended solids mass emissions: 1975-1989.

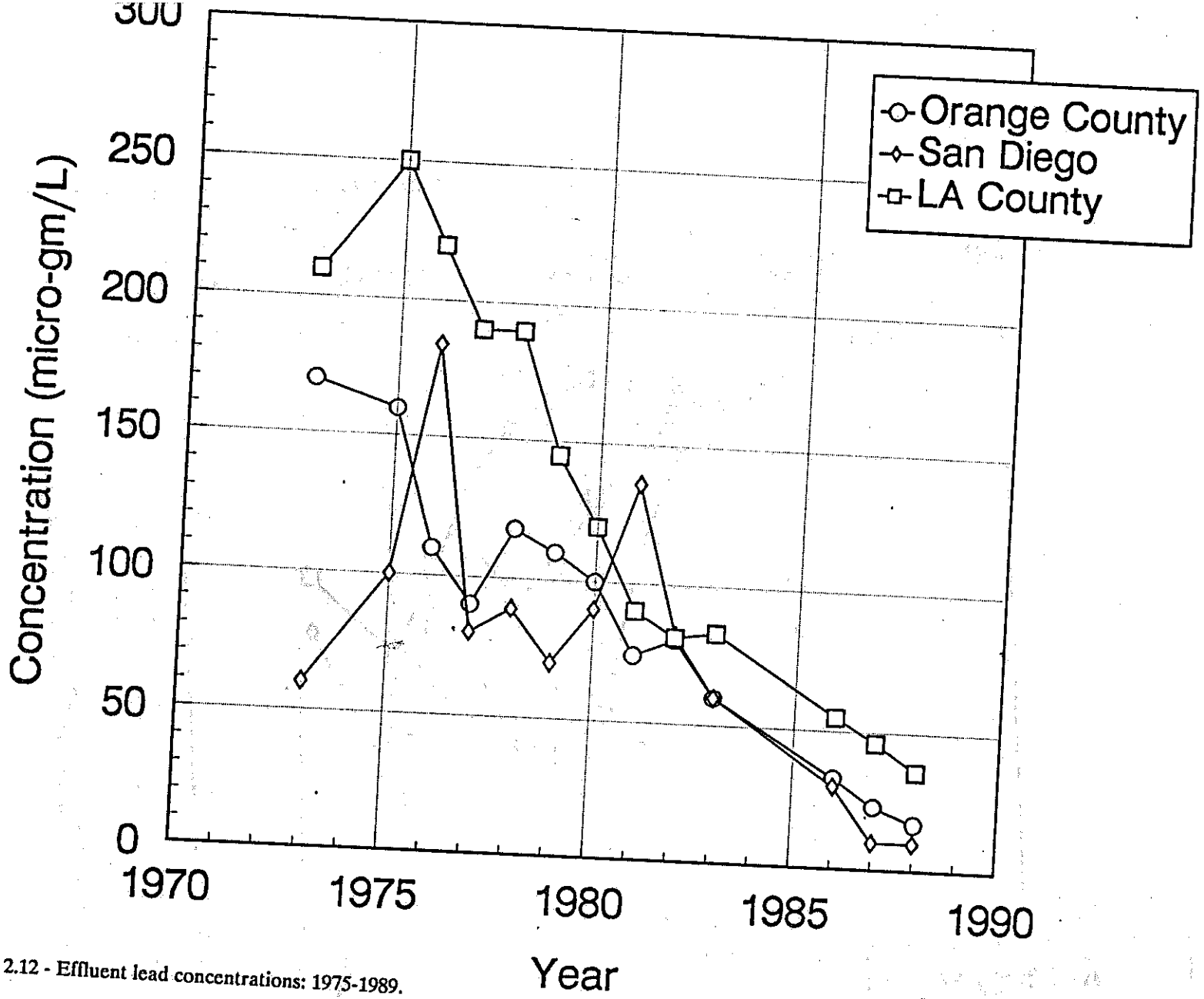

Figure 2.12 - Effluent lead concentrations: 1975-1989.

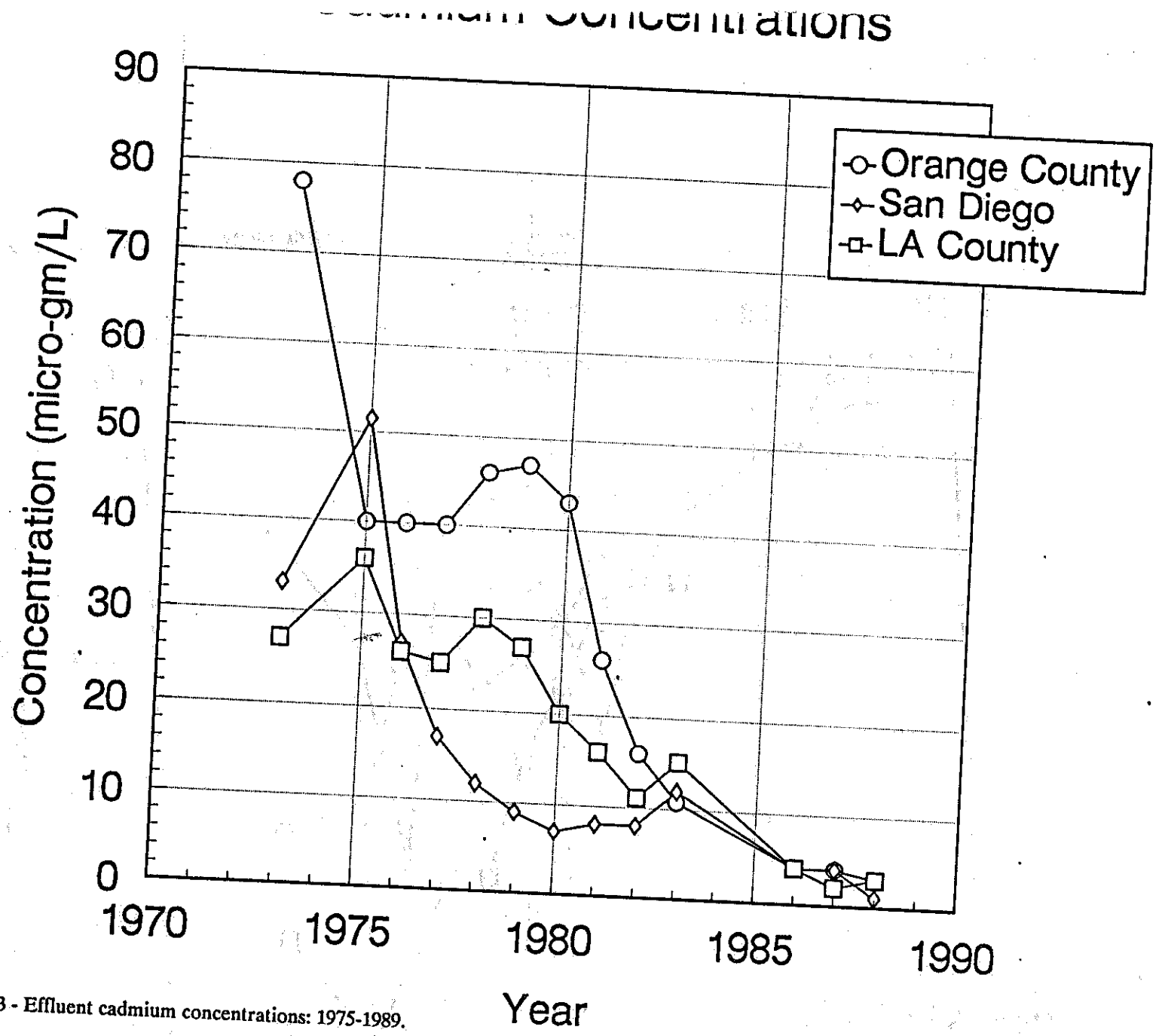

Figure 2.13 - Effluent cadmium concentrations: 1975-1989.

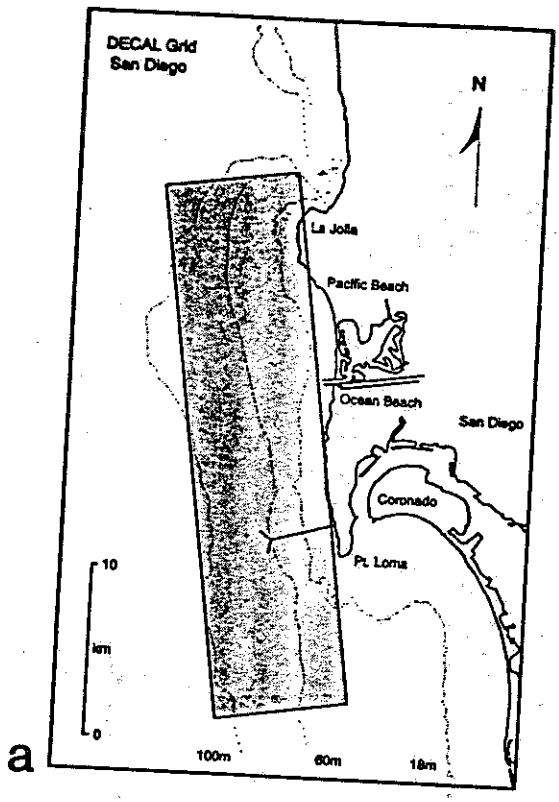

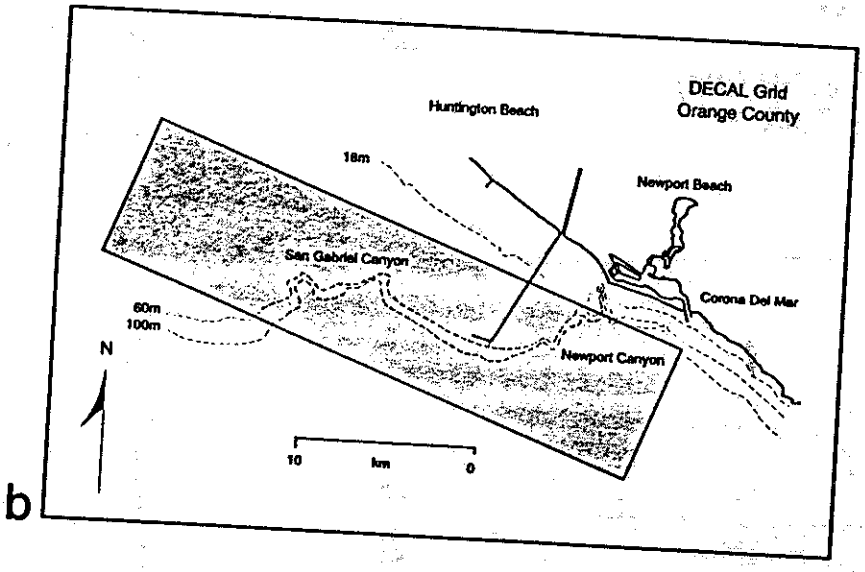

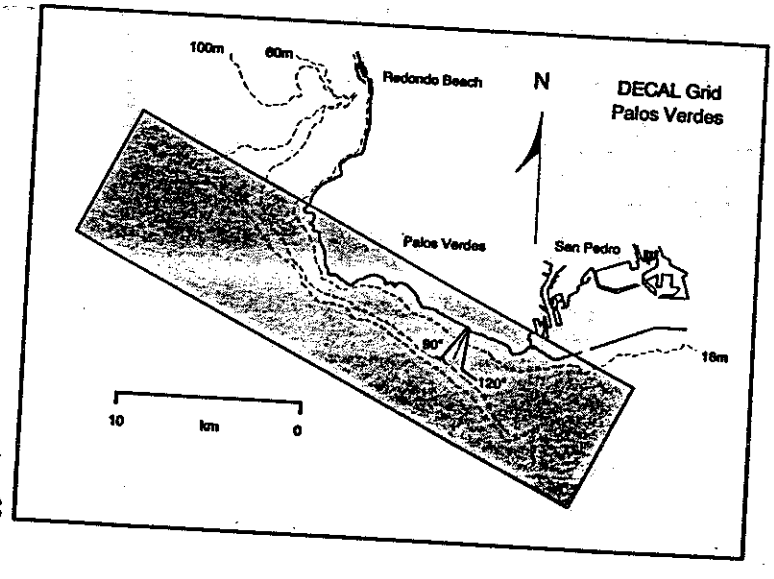

Figure 2.14 - DECAL simulation grids. (a) San Diego, (b) Orange County, (c) Palos Verdes (White Point).

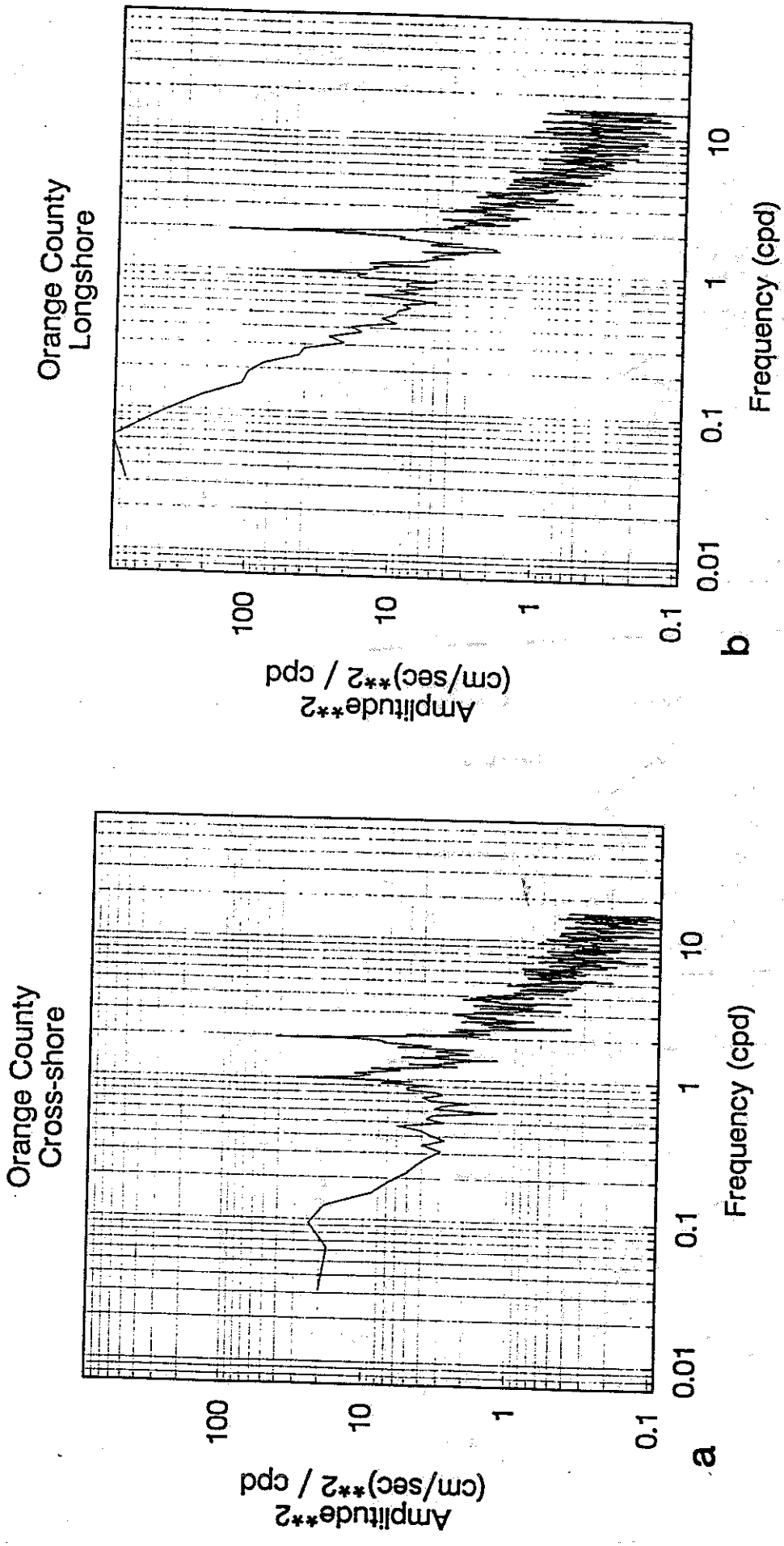

Figure 2.15 - Spectral energy density - Orange County. (a) longshore, (b) cross-shore.

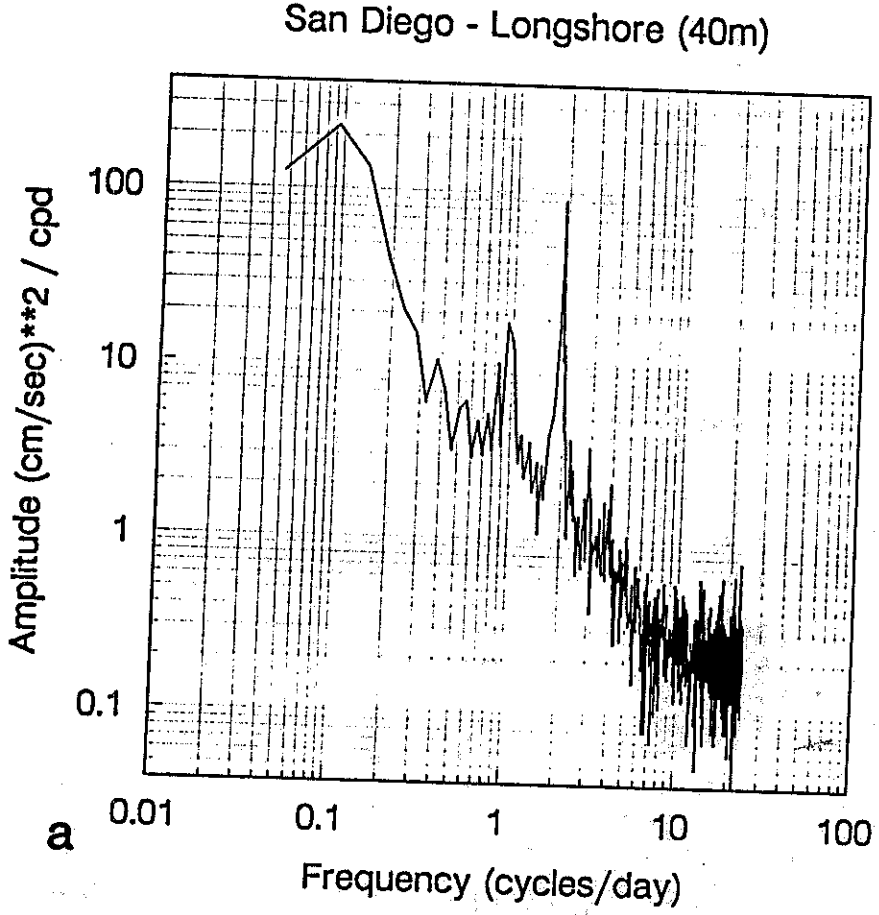

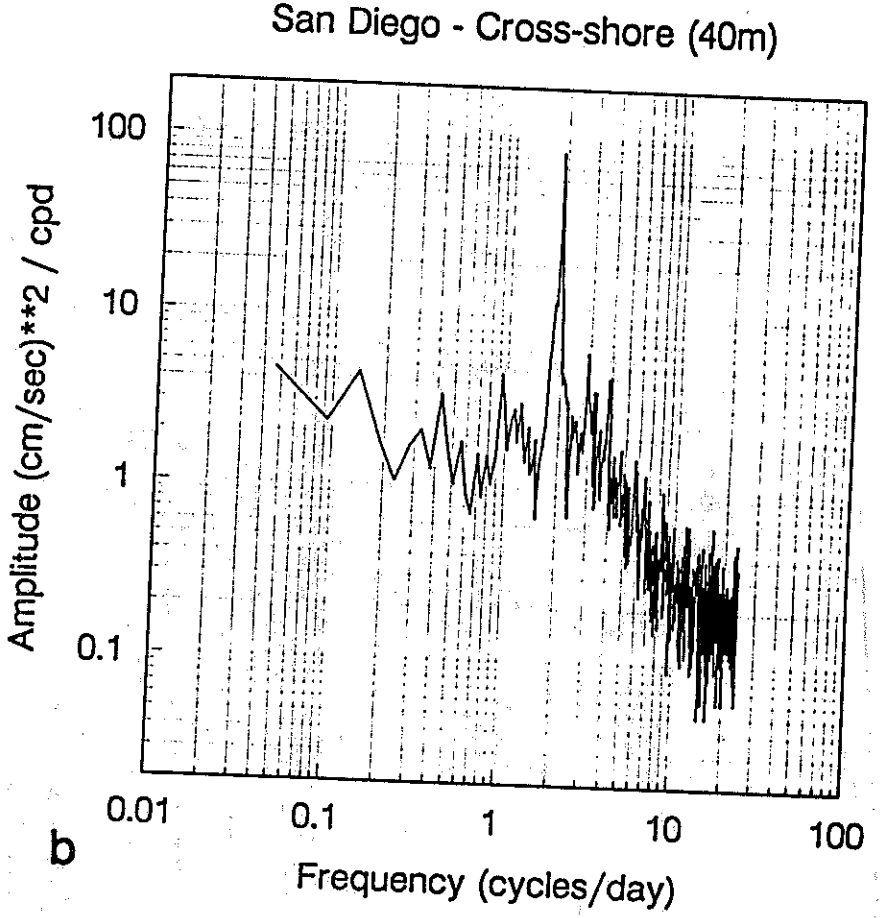

Figure 2.16 - Spectral energy density - San Diego. (a) longshore, (b) cross-shore.

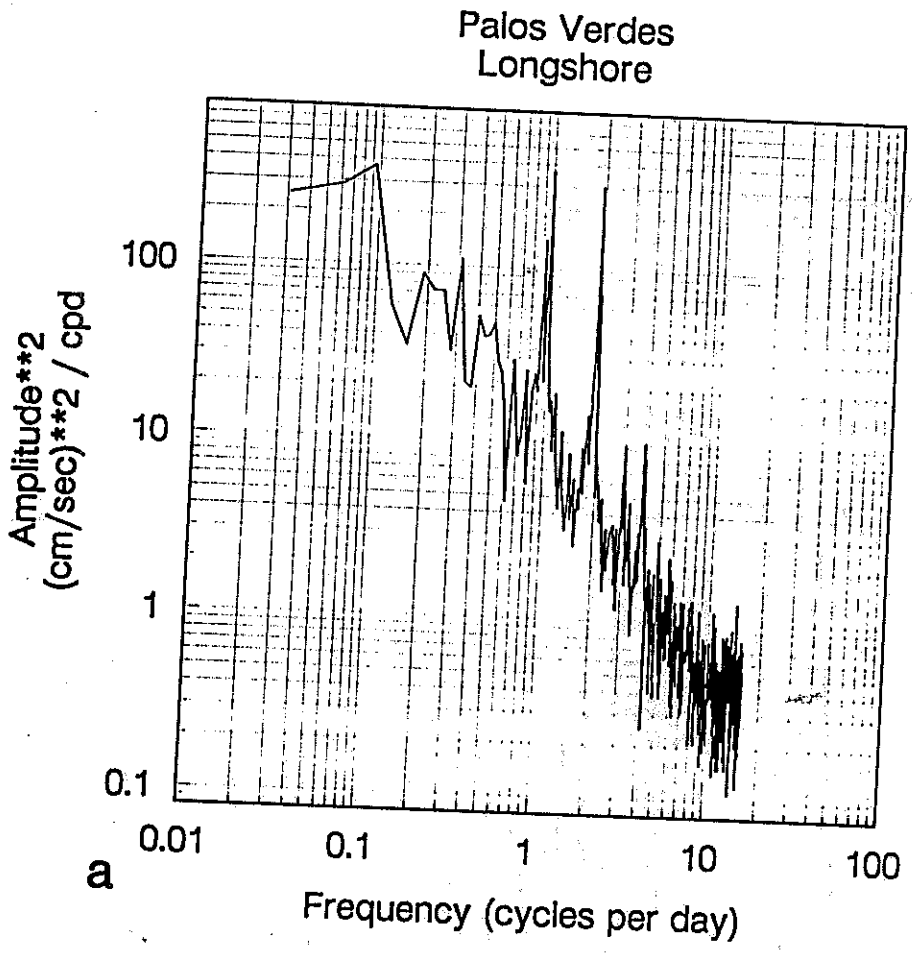

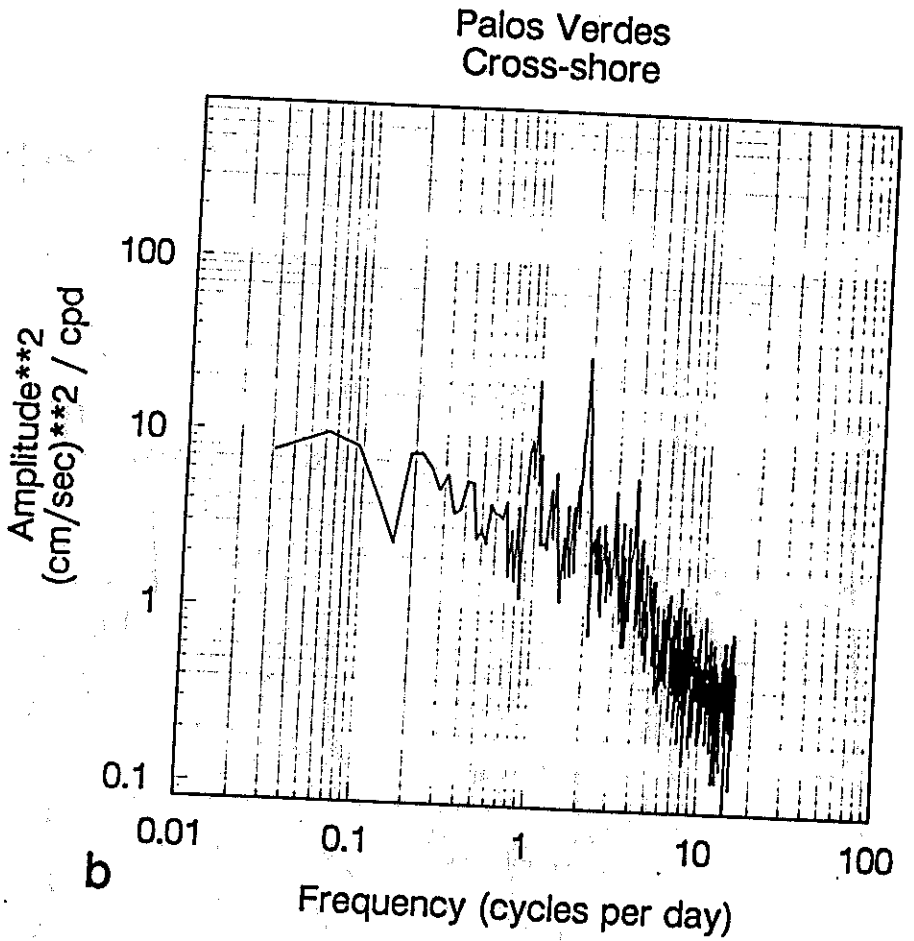

Figure 2.17 - Spectral energy density - Palos Verdes. (a) longshore, (b) cross-shore.

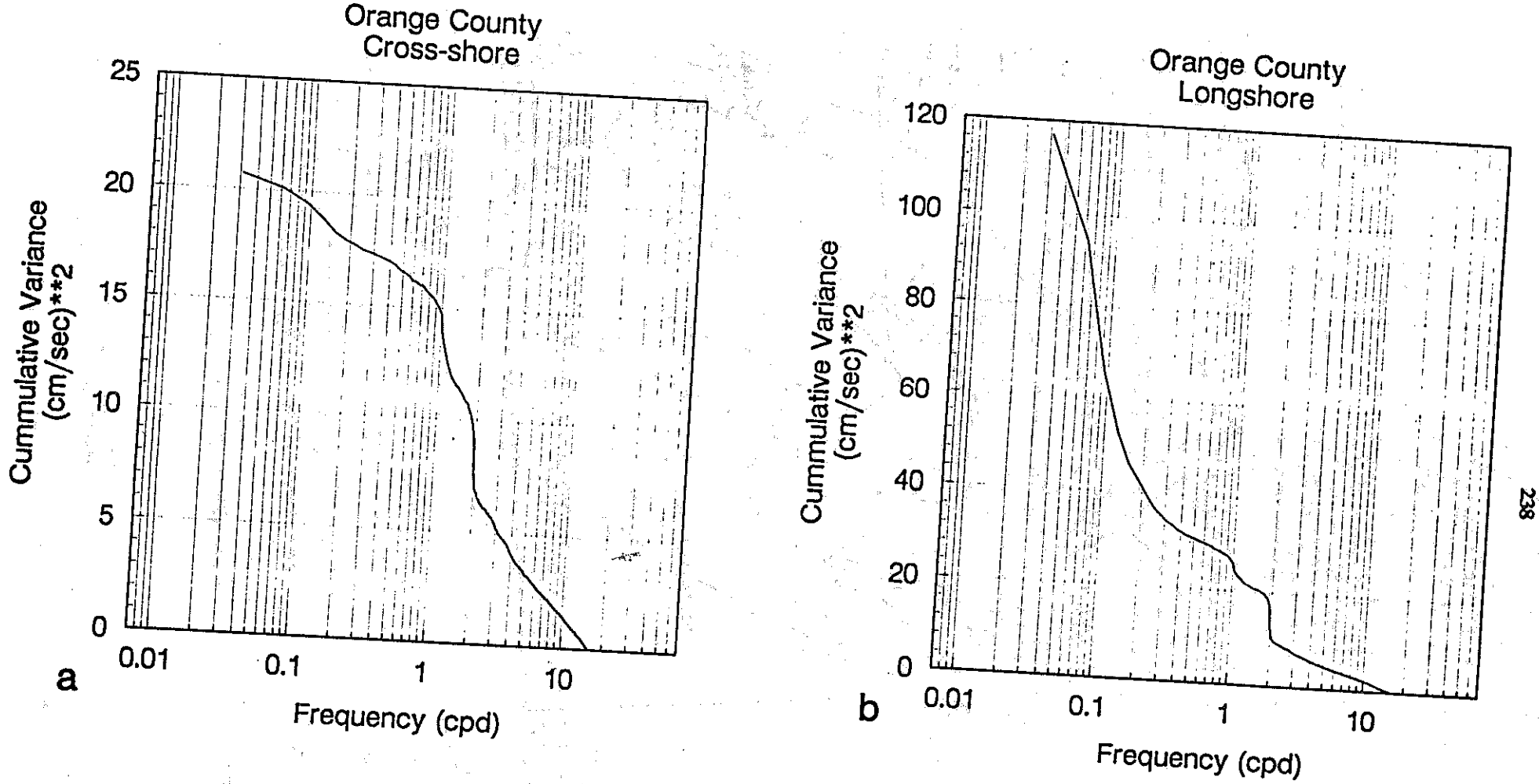

Figure 2.18 - Cummulative variance - Orange County. (a) longshore, (b) cross-shore.

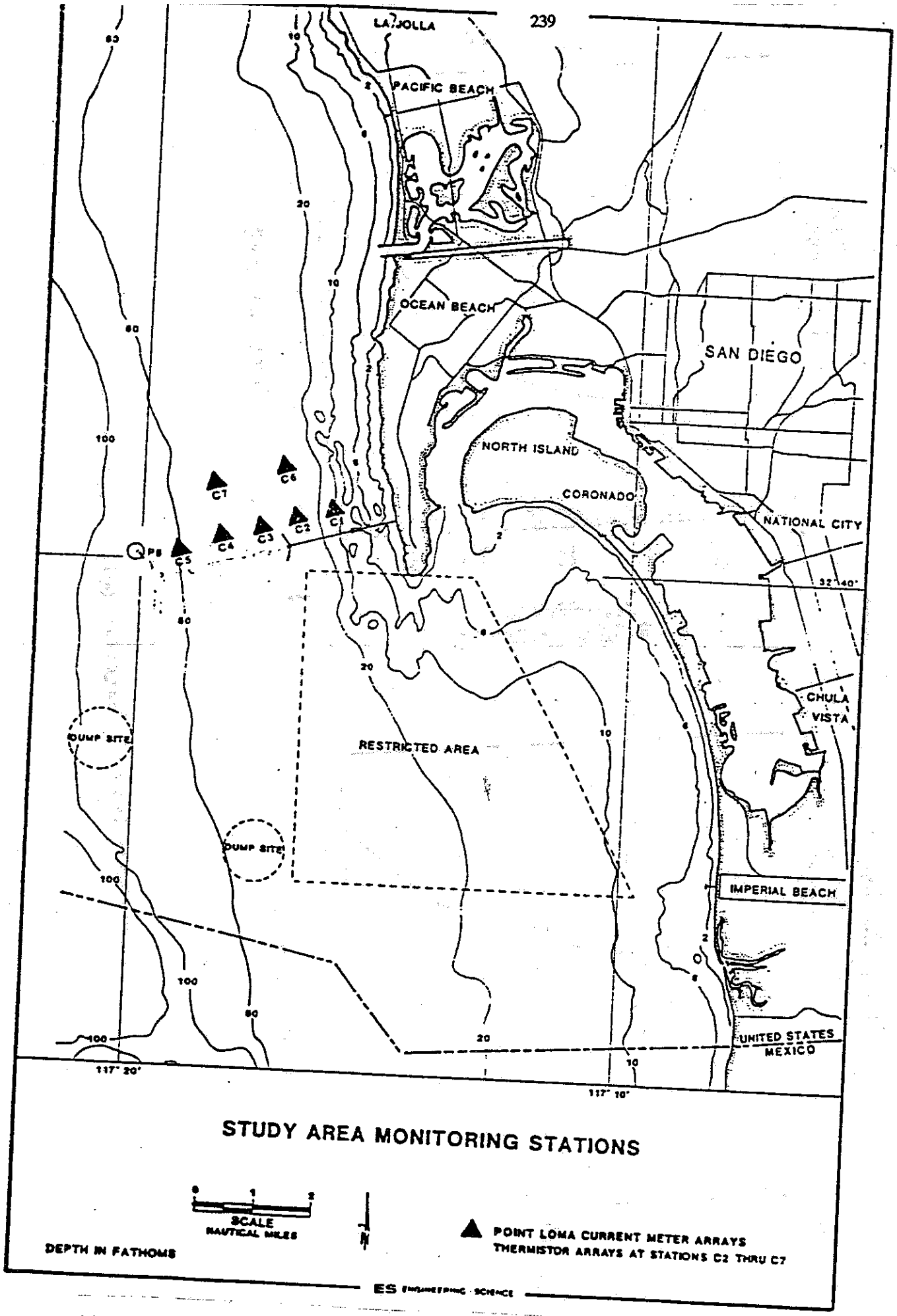

Figure 2.19 - Current meter locations - Point Loma (adapted from [illegible]

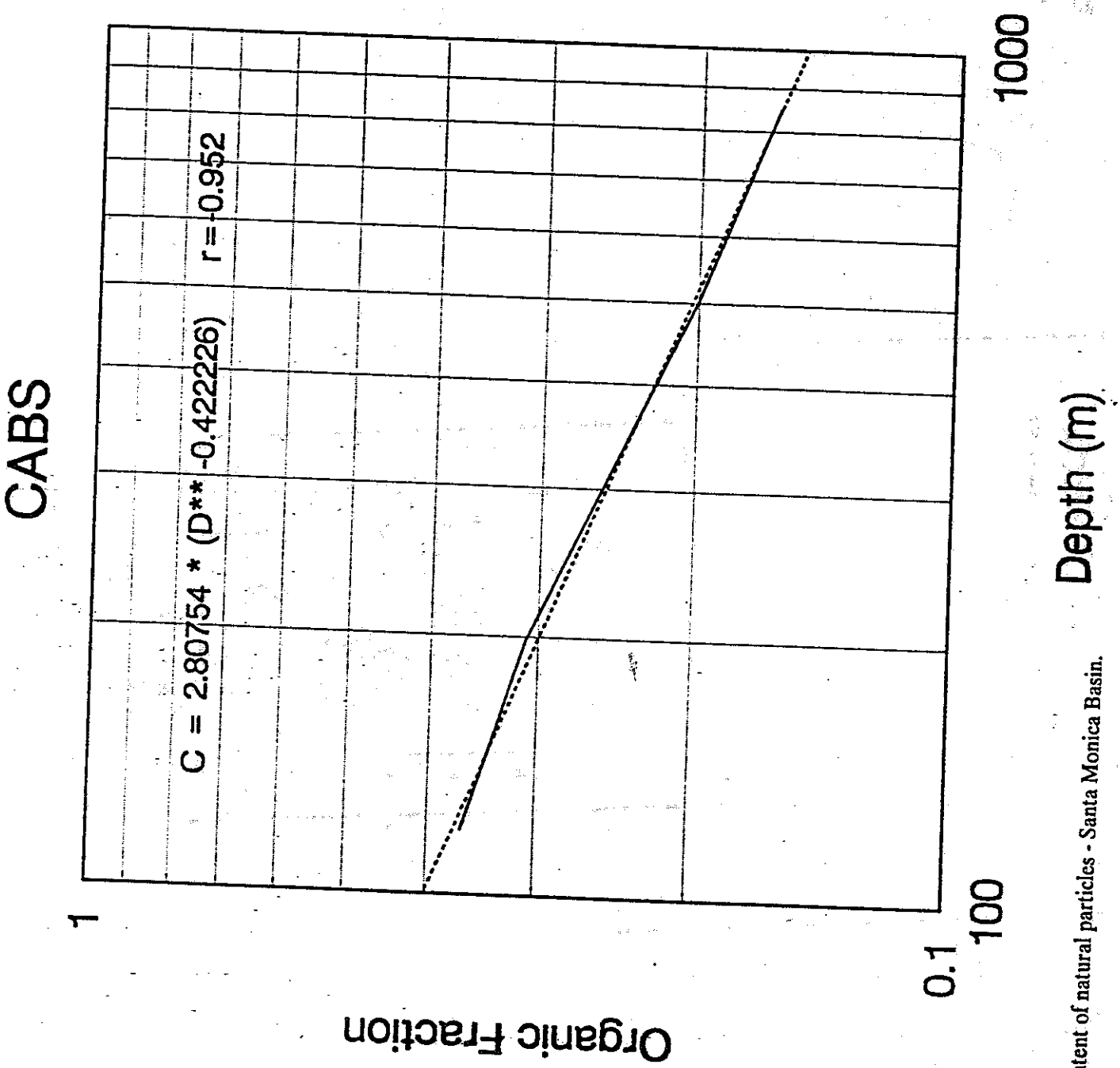

Figure 2.20 - Organic content of natural particles - Santa Monica Basin.

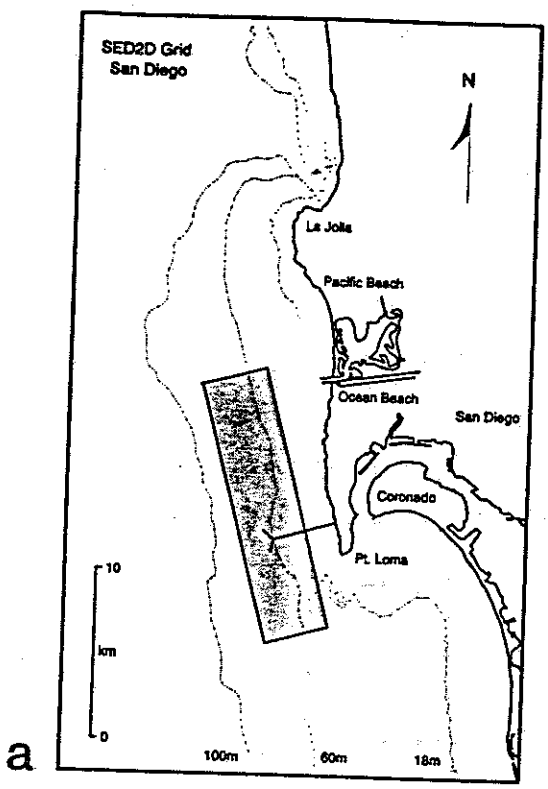

Figure 2.21 - SED2D basic simulation grids. (a) San Diego, (b) Orange County, (c) Palos Verdes.

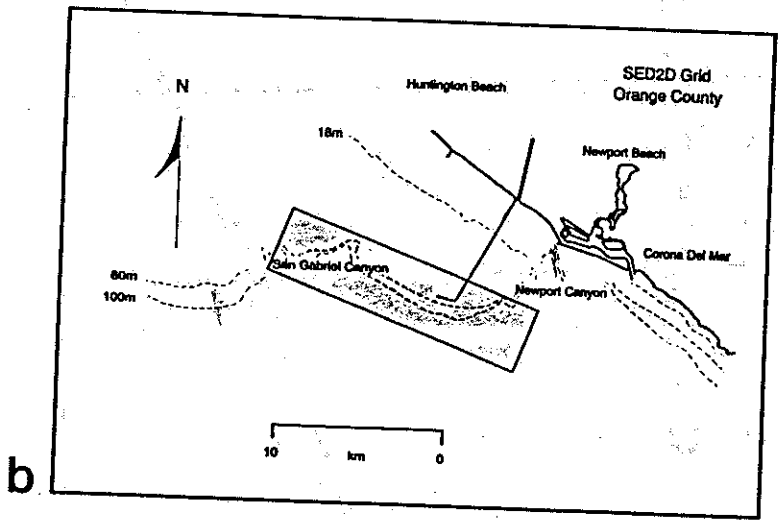

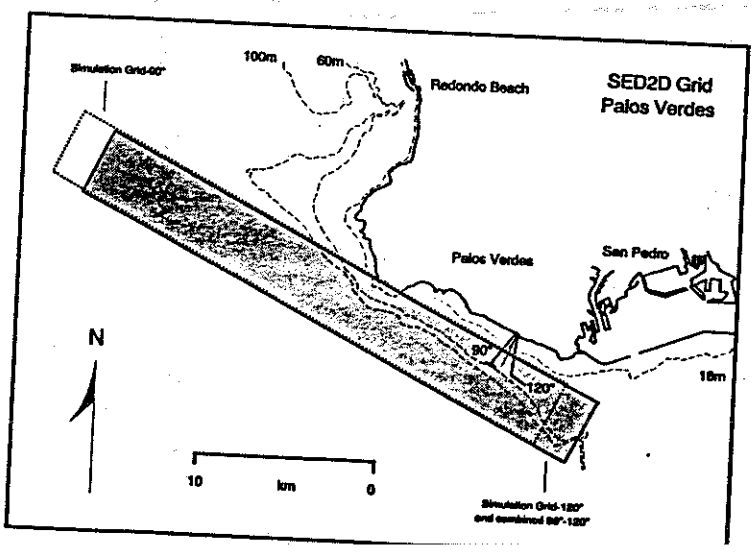

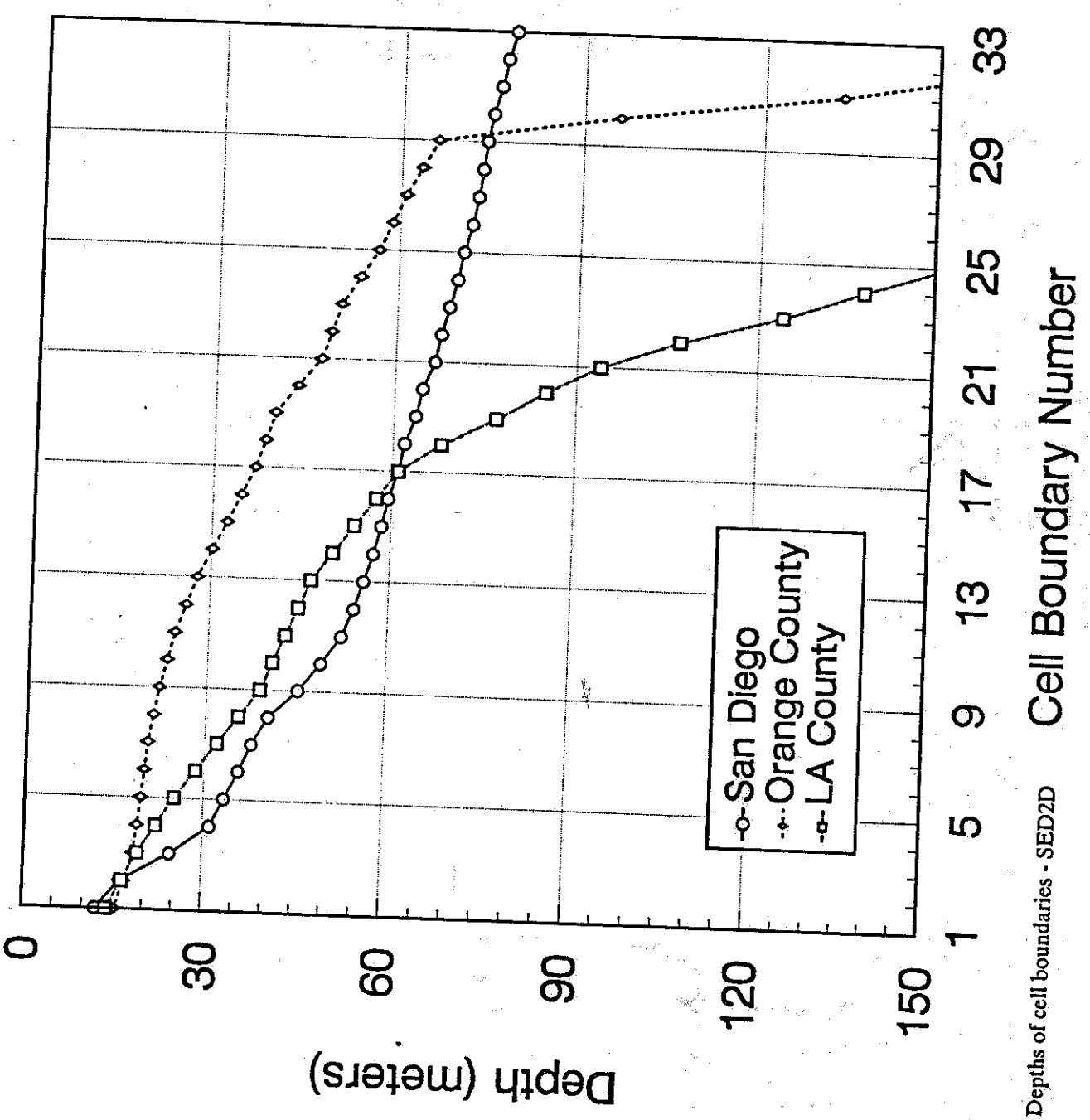

Figure 2.22 - Depths of cell boundaries - SED2D simulations.

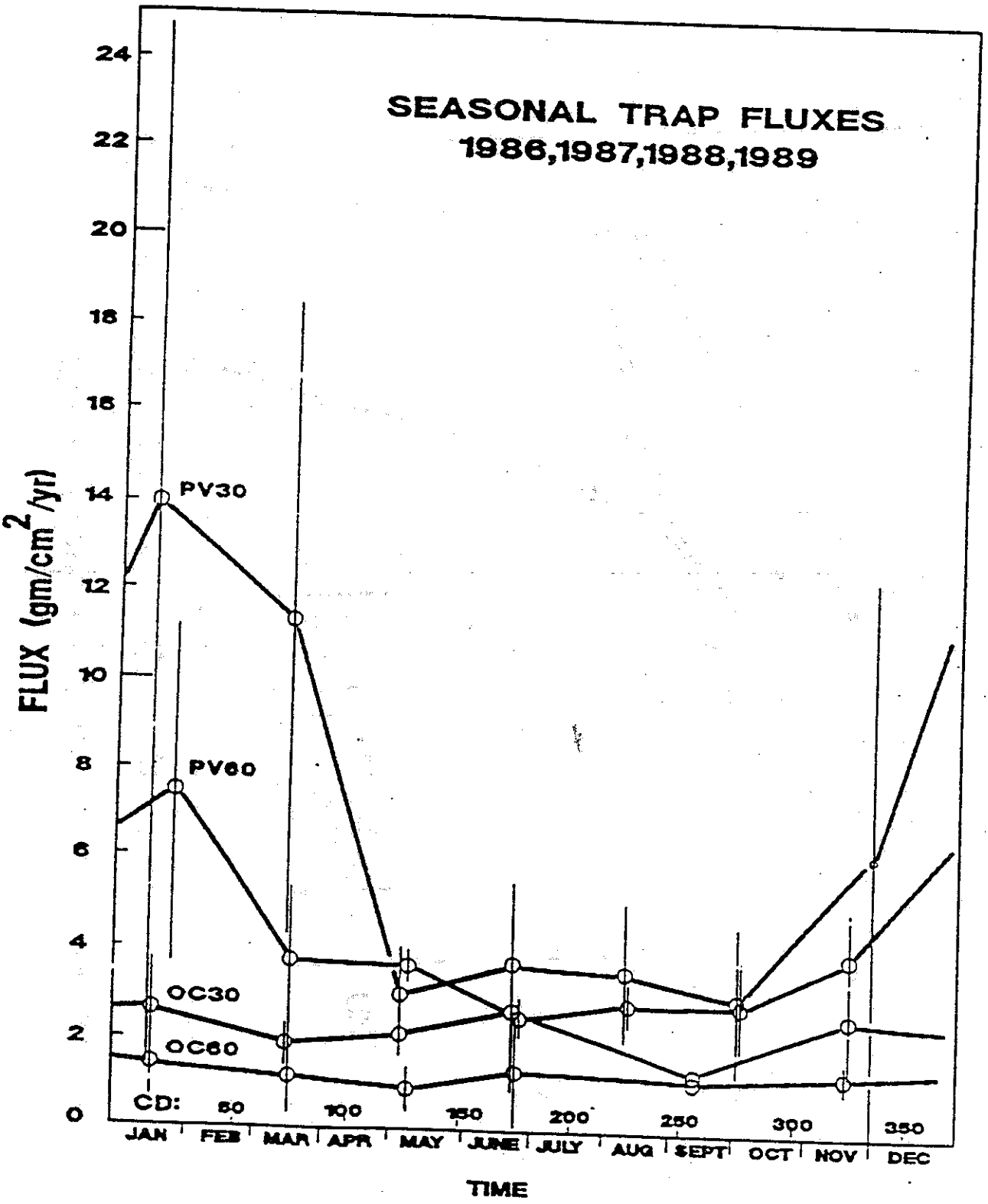

Figure 2.23 - Seasonal variations in near-bottom sediment trap fluxes (from SCCWRP, 1987).

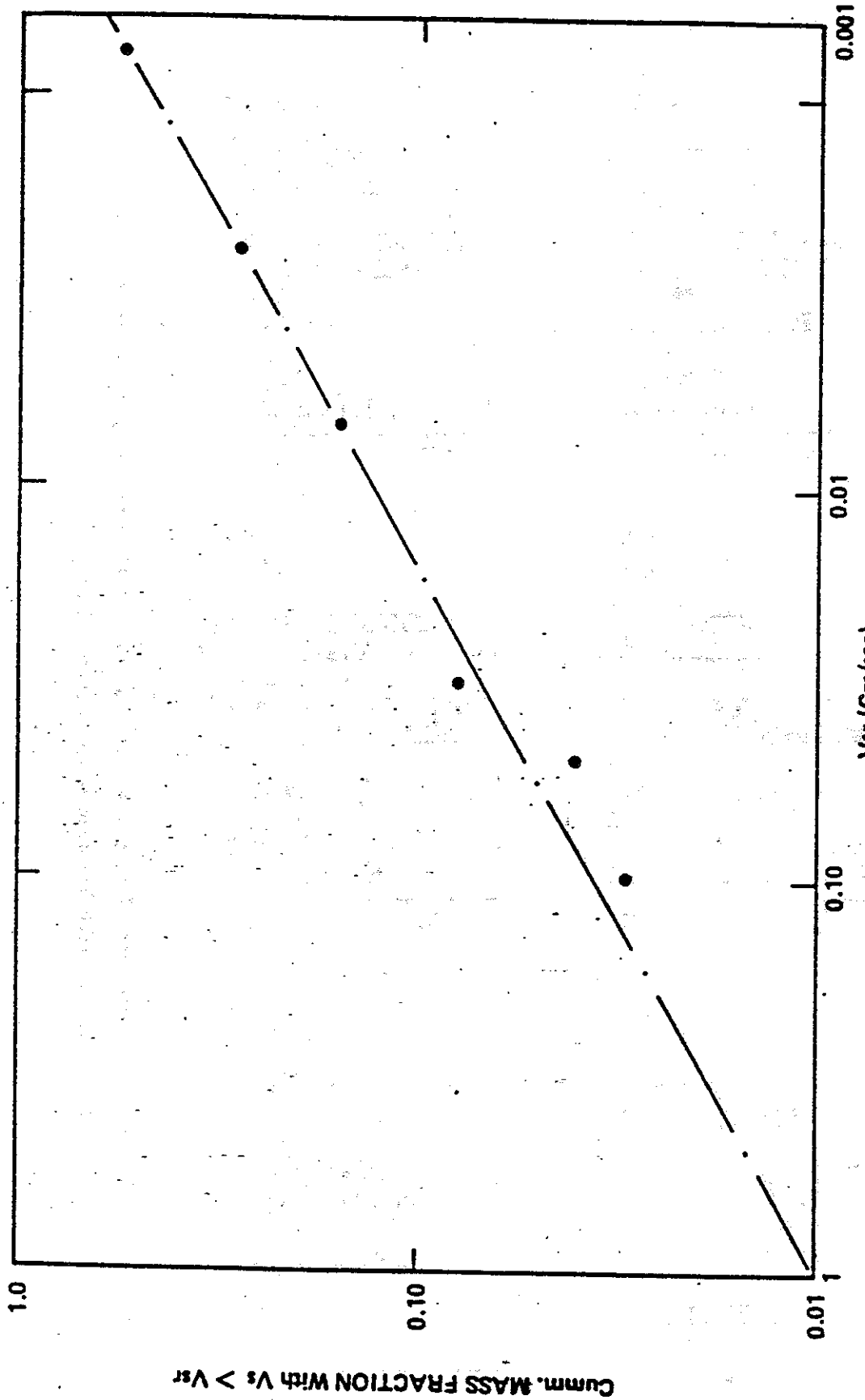

Figure 2.24 - Settling speeds of White Point effluent - 1974, settling column.

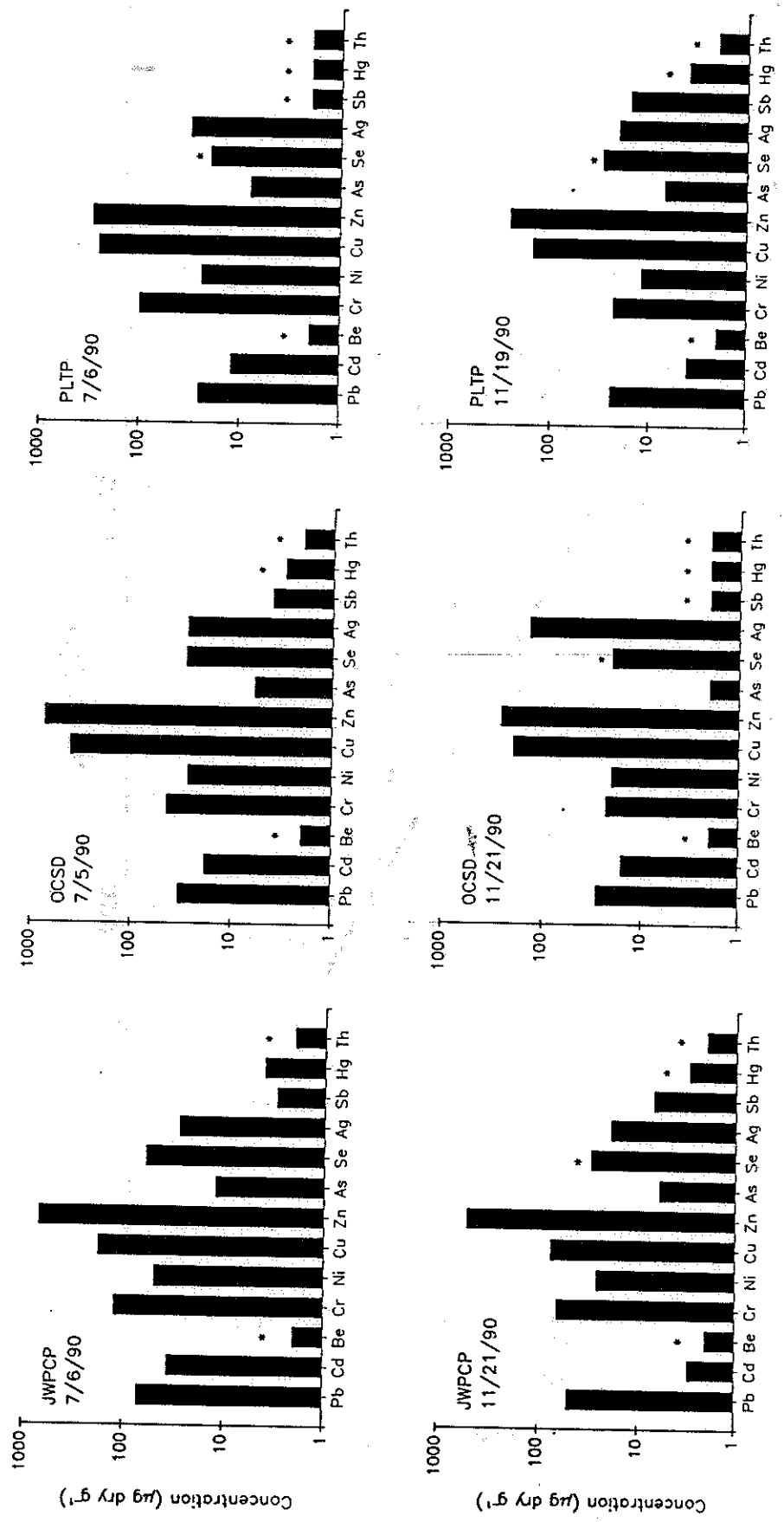

Figure 3.1 - Distributions of thirteen trace elements in effluent particles collected from the JWPCP, OCSD and PLTP facilities, 1990. Asterisks indicate those elements for which data are presented as detection limits.

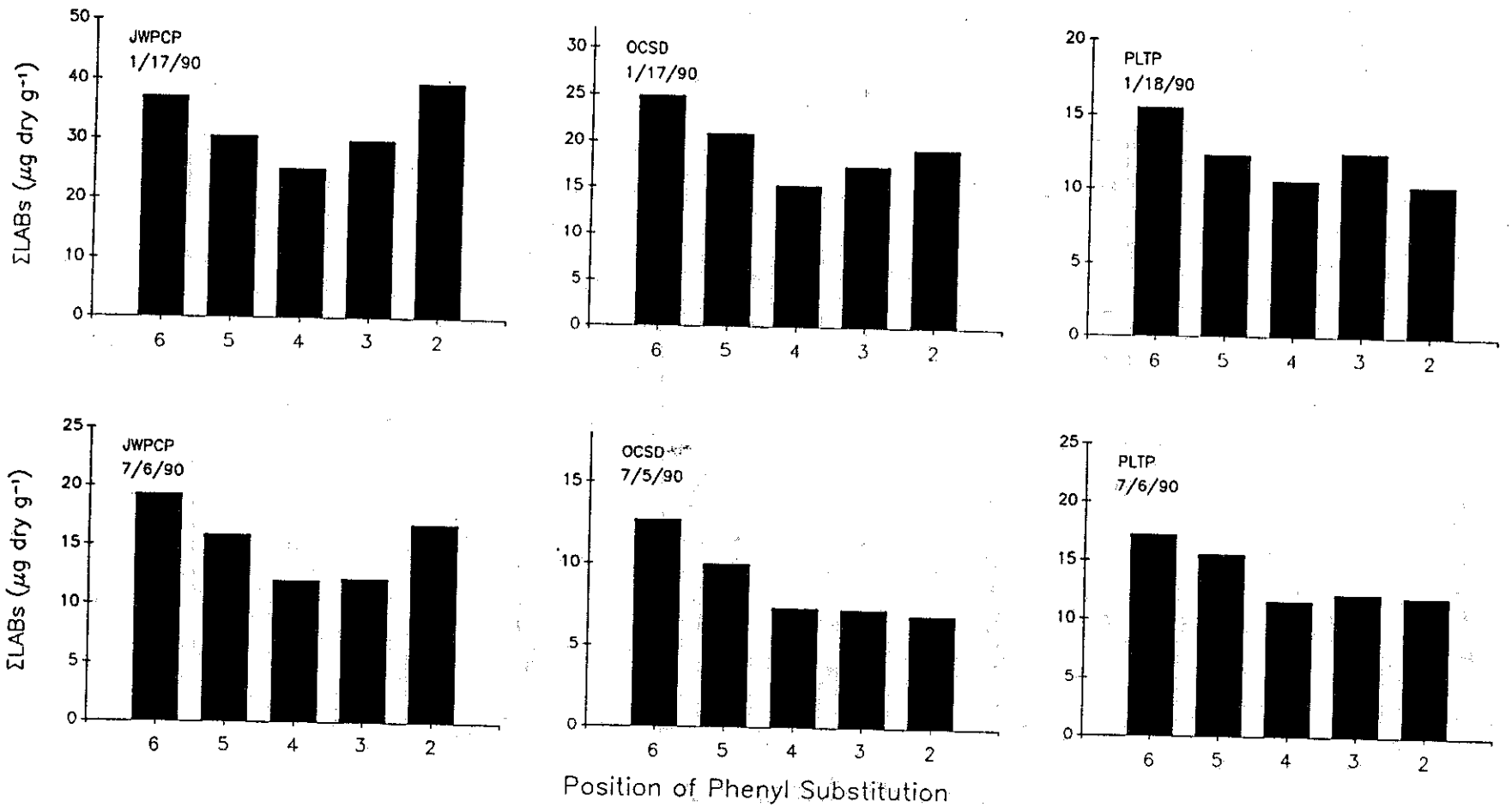

Figure 3.2 - Distribution of phenyldodecane isomers in effluent particles collected for the JWPCP, OCSD and PLTP facilities, 1992.

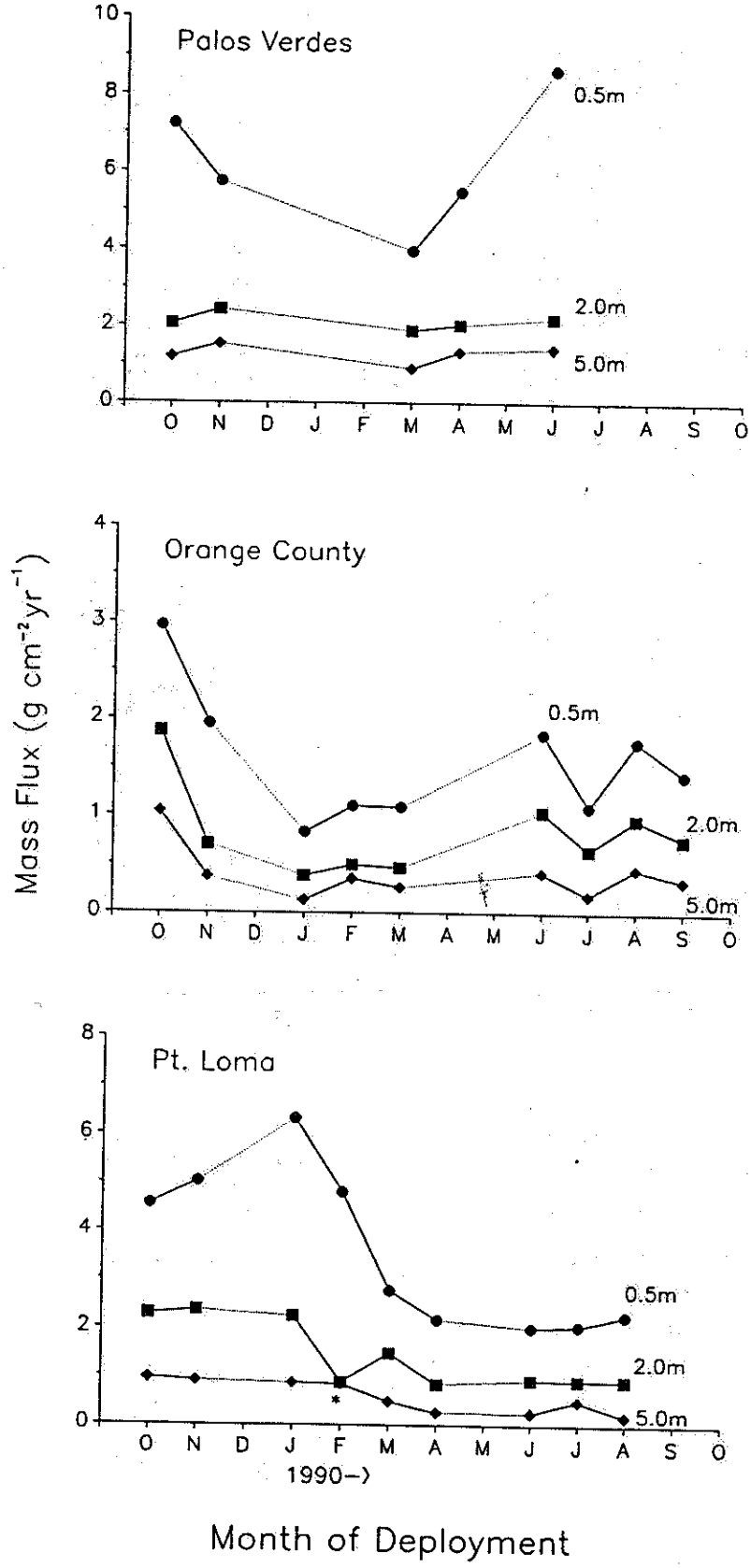

Figure 3.3 - Variation in mass fluxes of solids to near-bottom traps deployed off Palos Verdes, Orange County and Point Loma, 1989-90.

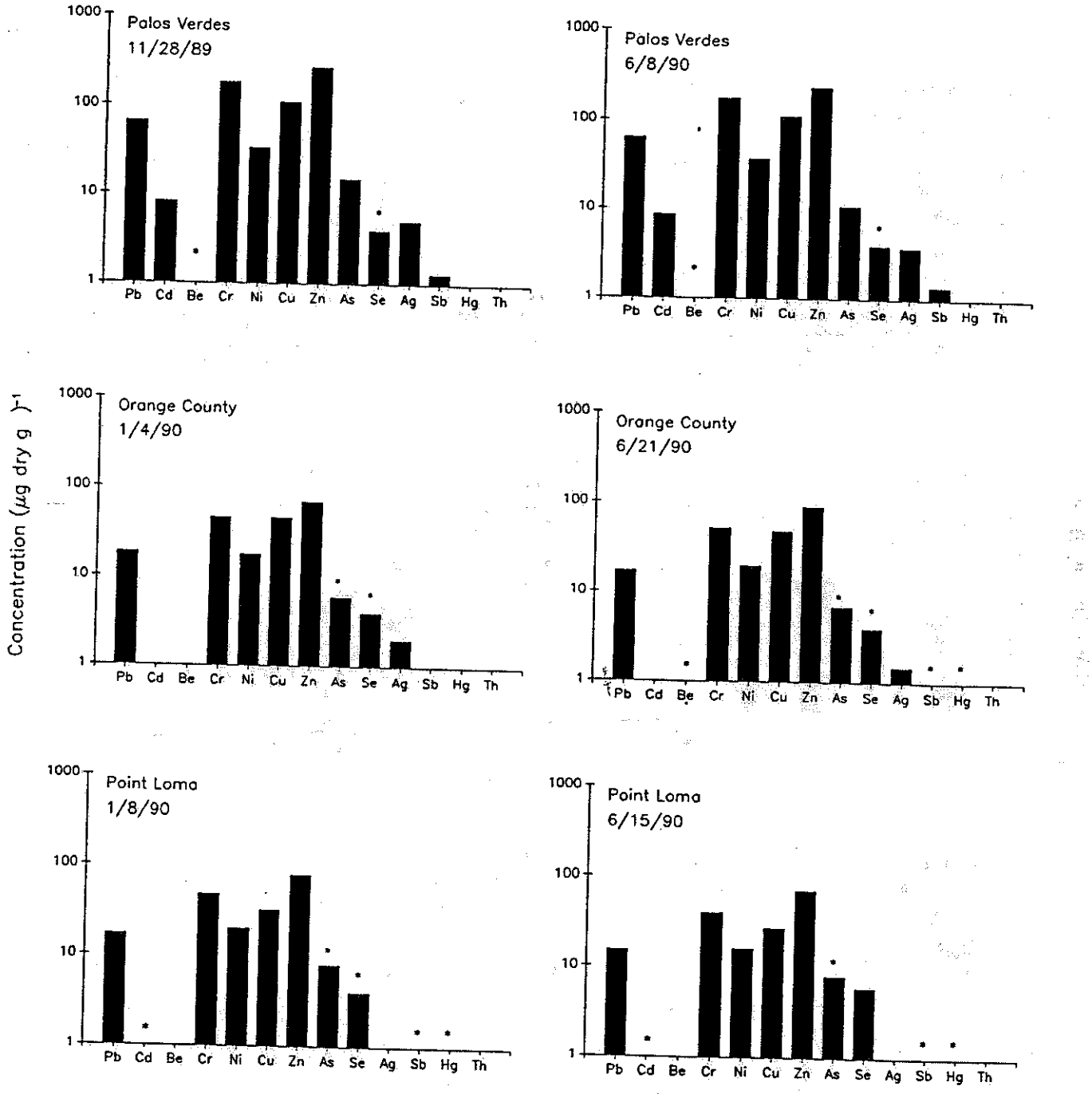

gure 3.4 - Distribution of thirteen trace elements in particles collected in near-bottom sediment traps deployed off Palos Verdes, ange County and Point Loma during two periods in 1989 and 1990. Data are for the trap positioned 0.5 m above the sea floor. terisks indicate those elements for which data are presented as detection limits.

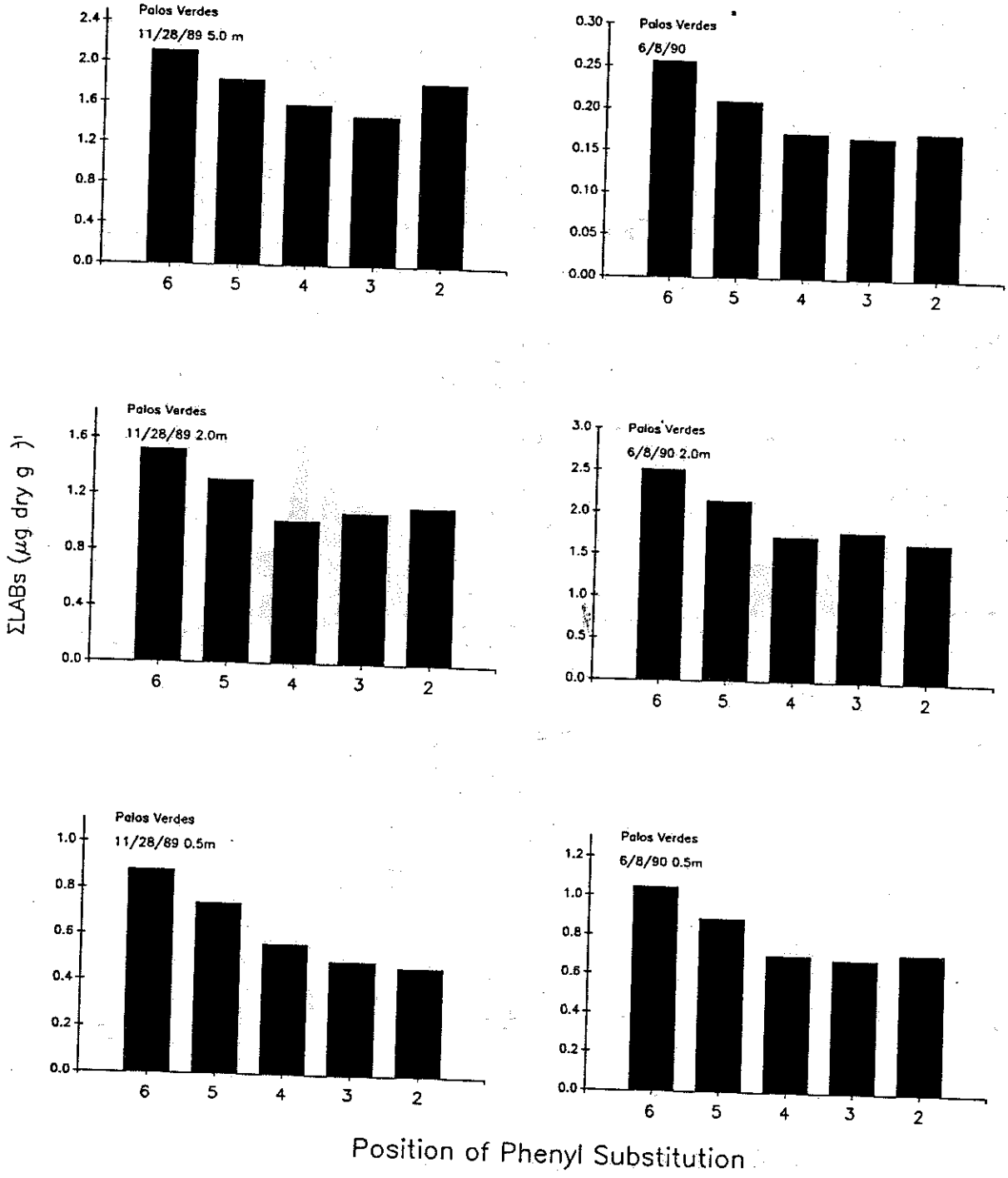

ure 3.5 - Distribution of phenyldodecane isomers in particles collected in near-bottom sediment traps deployed off Palos Verdes ing two periods in 1989 and 1990.

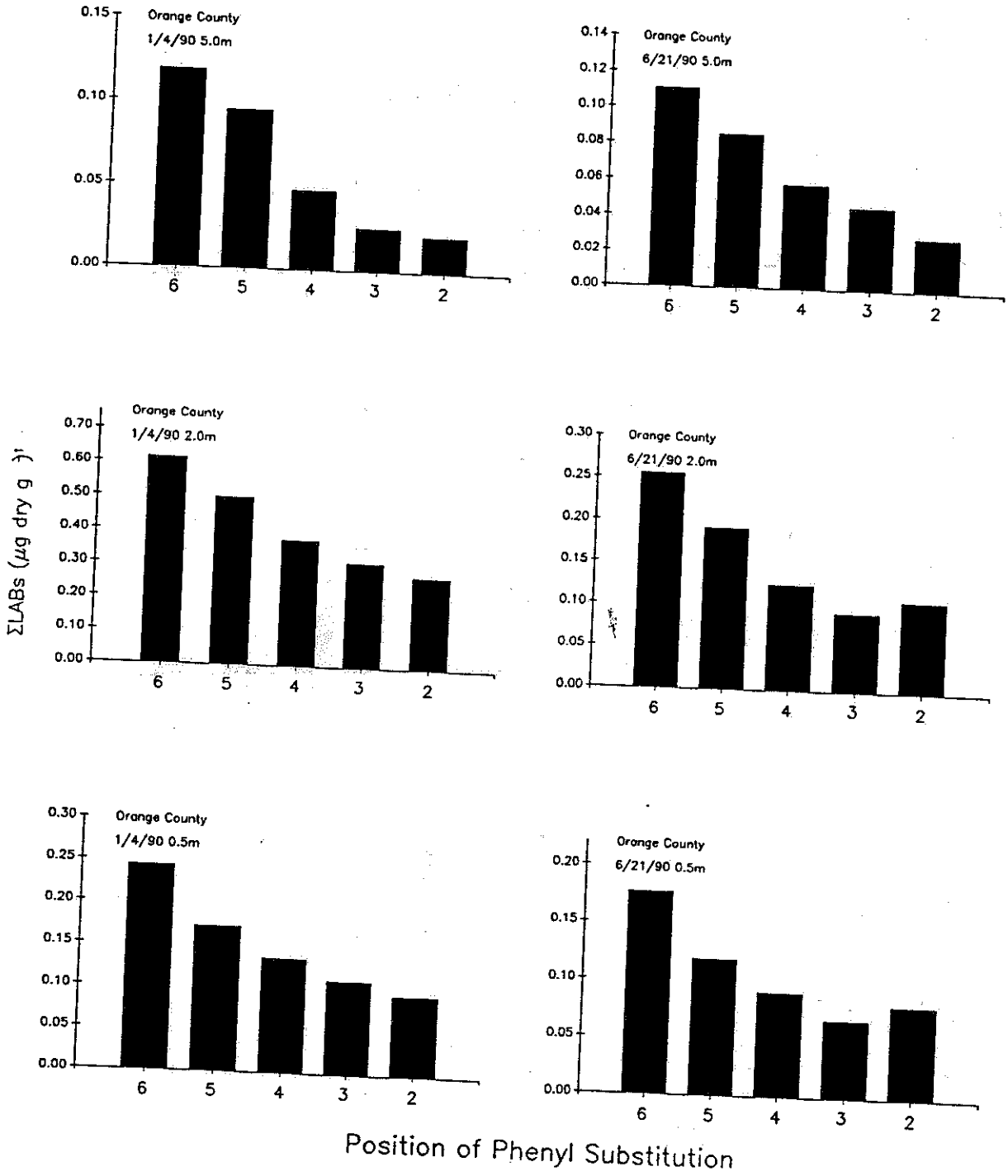

3.6 - Distribution of phenyldodecane isomers in particles collected in near-bottom sediment traps deployed off Orange County wo periods in 1990.

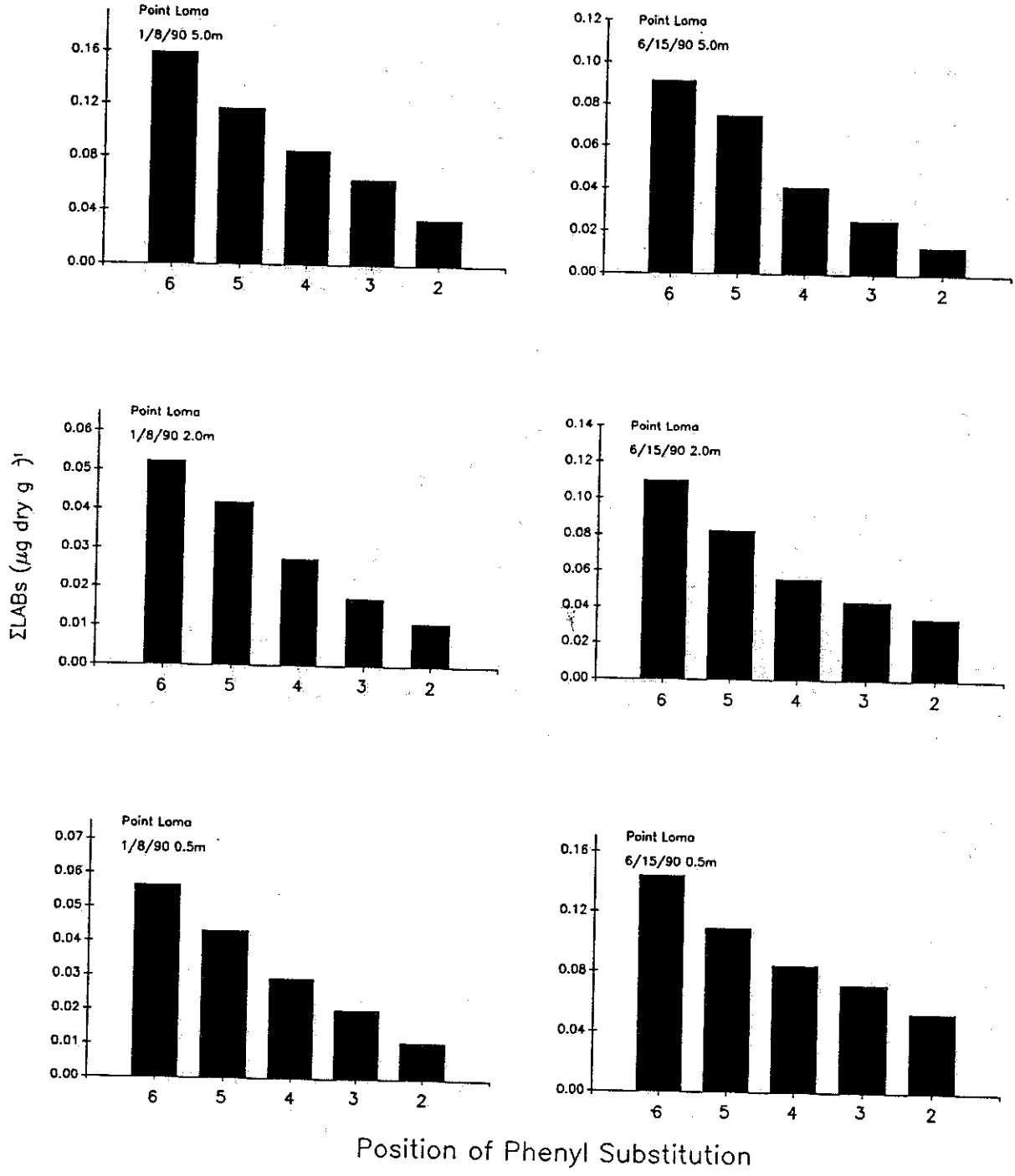

Figure 3.7 - Distribution of phenyldodecane isomers in particles collected in near-bottom sediment traps deployed off Point Loma during two periods in 1990.

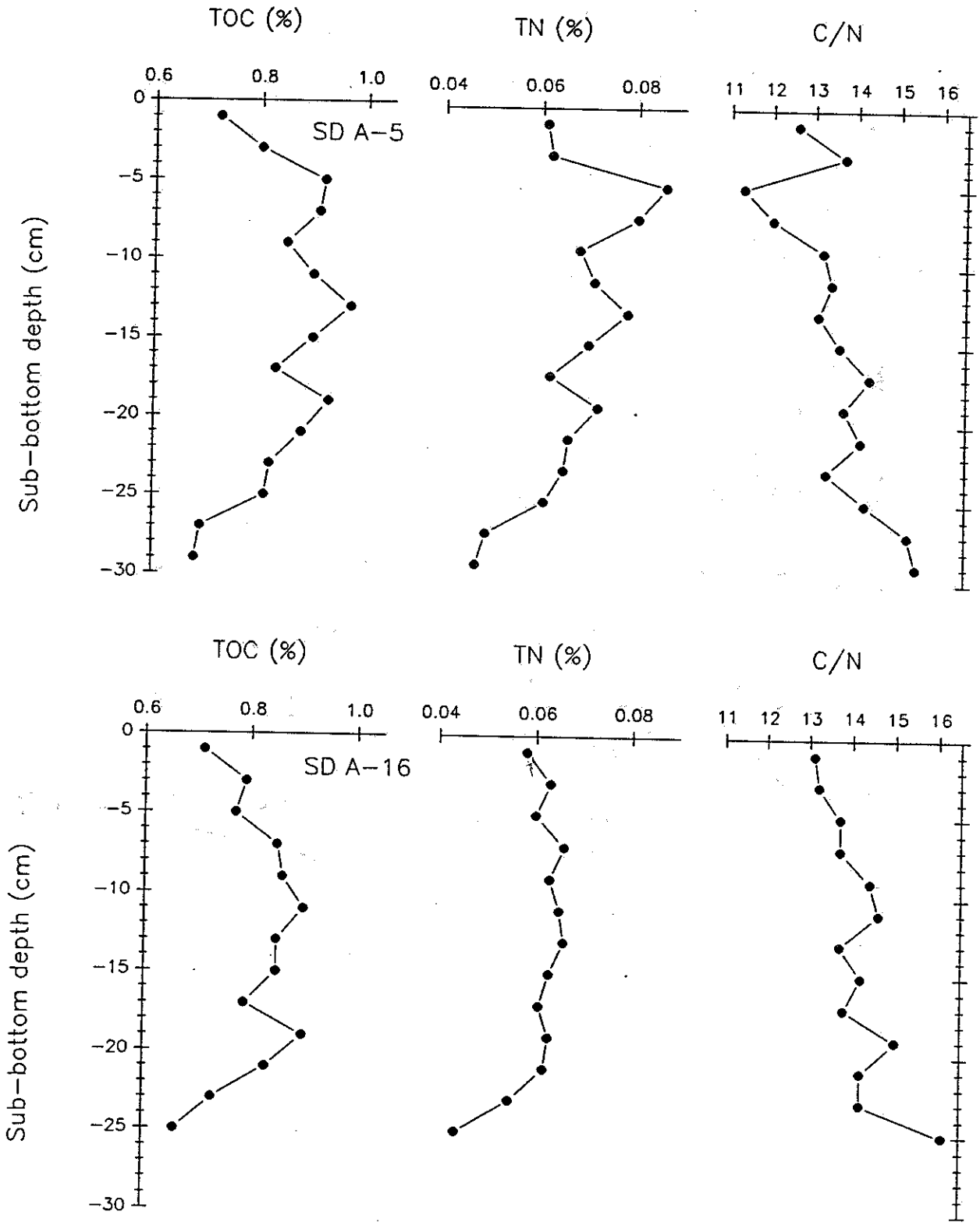

Figure 3.8 - Vertical concentration profiles of total organic carbon (TOC), total nitrogen (TN) and the C/N ration in sediments collected at two stations (SD A-5 and SD A-16) off Point Loma. For locations see figure 2.4.

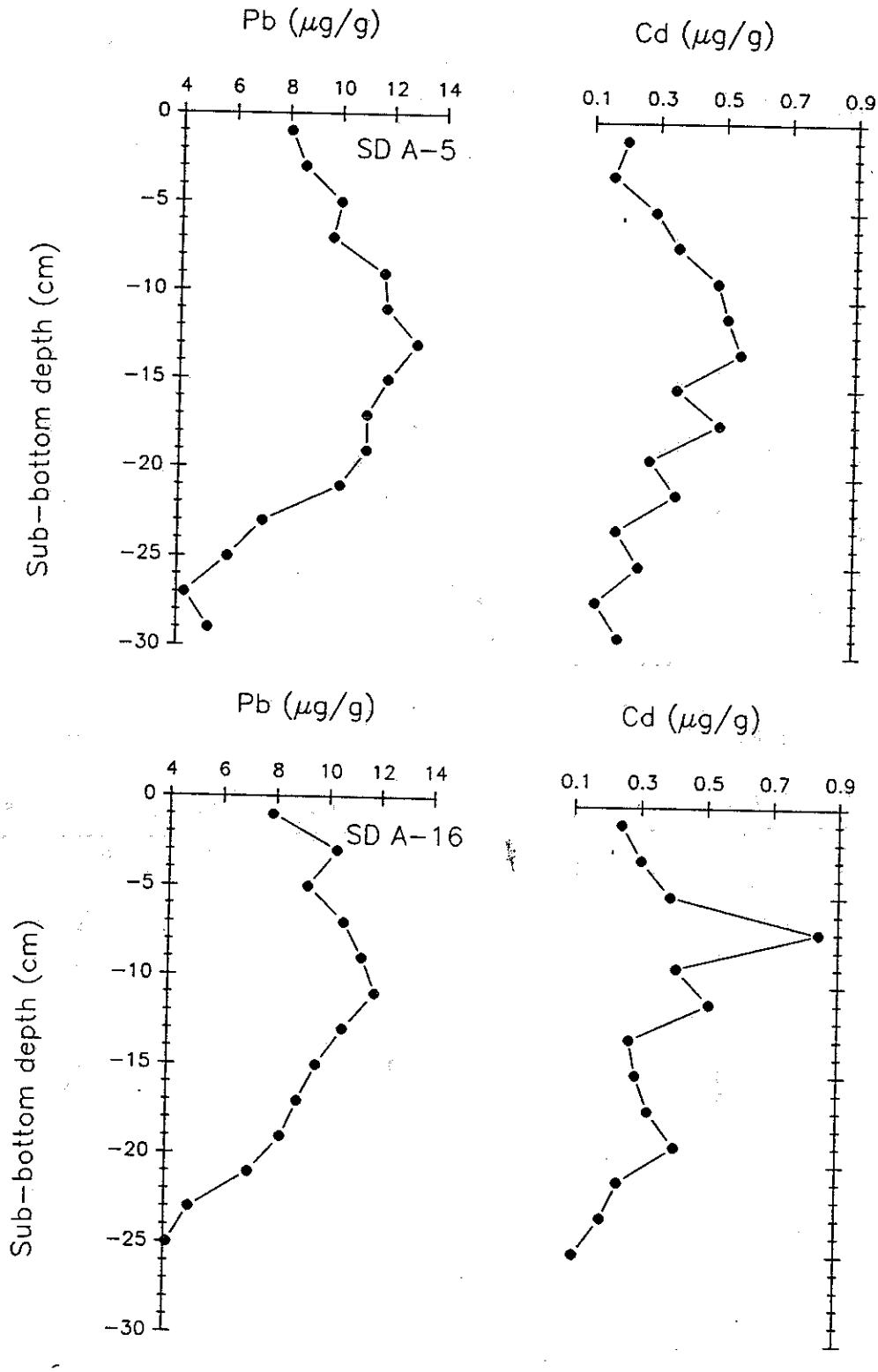

Figure 3.9 - Vertical concentration profiles of lead (Pb) and cadmium (Cd) in sediments collected at two stations (SD A-5, SD A-16) off Point Loma. For locations see Figure 2.4.

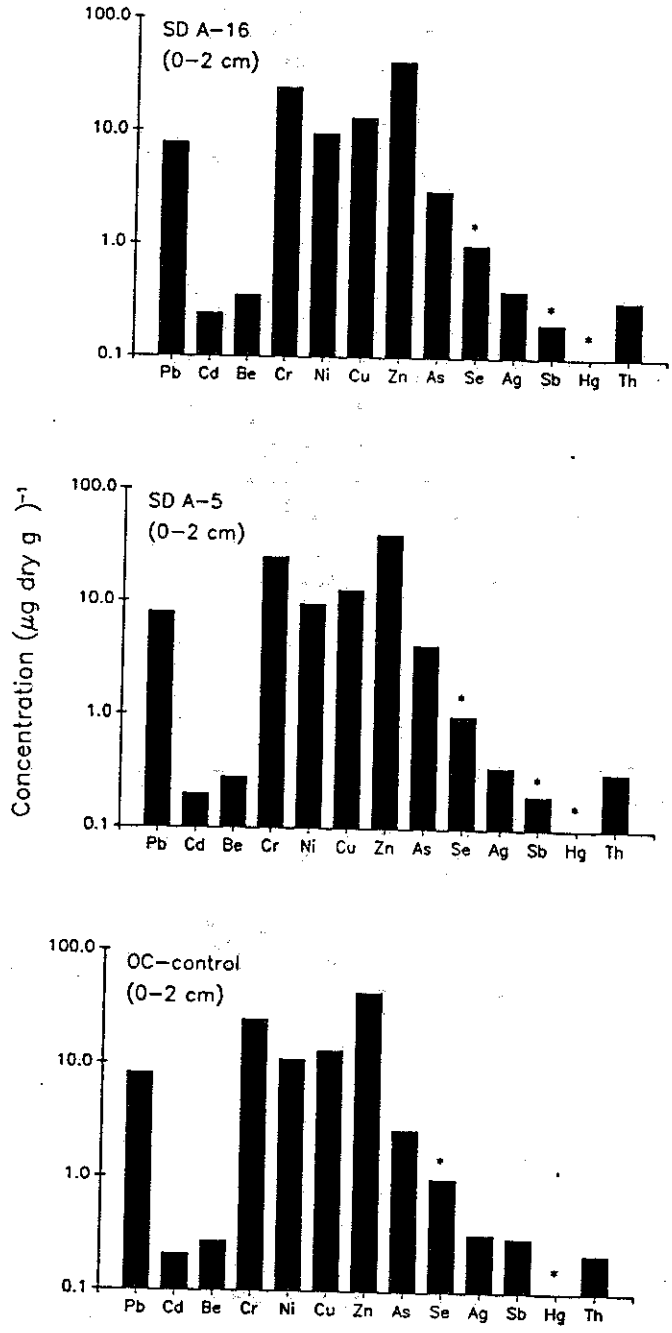

gure 3.10 - Distribution of thirteen trace elements in uppermost section (0-2 cm) of sediment cores taken from the Point Loma (SD -5, SD A-16) and Orange County (OC-control) sites. Asterisks indicate those elements for which data are presented as detection nits. For station locations see Figures 2.3 and 2.4.

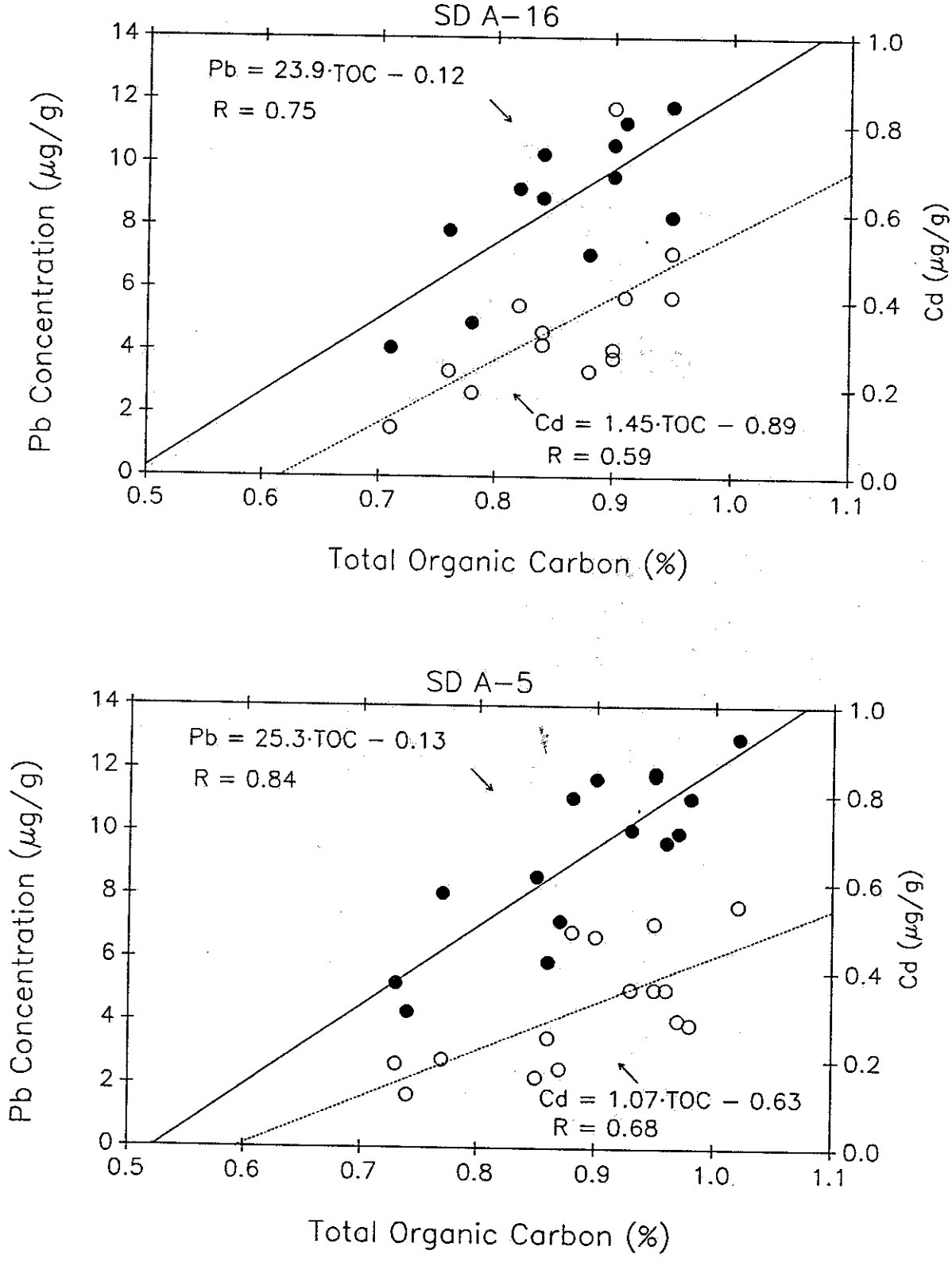

Figure 3.11 - Scatter diagrams for lead (Pb) and cadmium (Cd) *versus* total organic carbon in sediment cores collected off Point Loma.

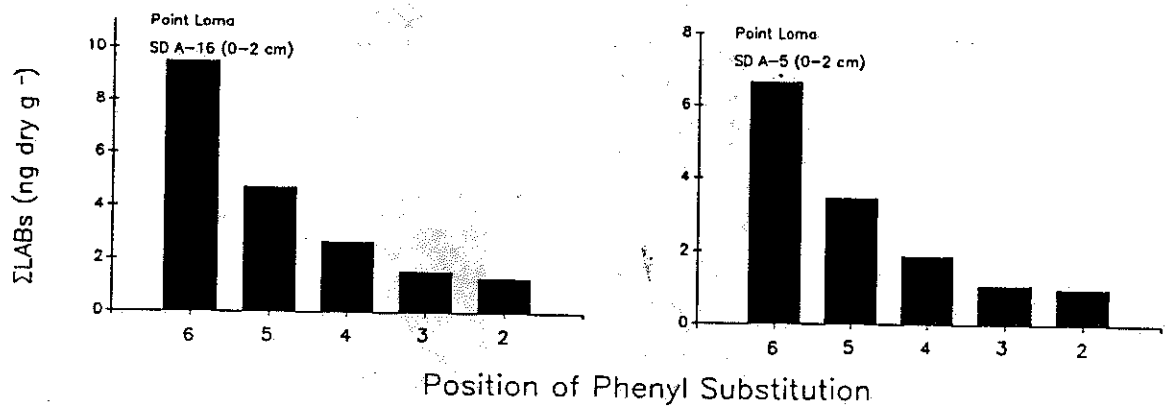

Figure 3.12 - Distribution of phenyldodecane isomers in uppermost sections (0-2cm) of sediment cores taken off Point Loma.

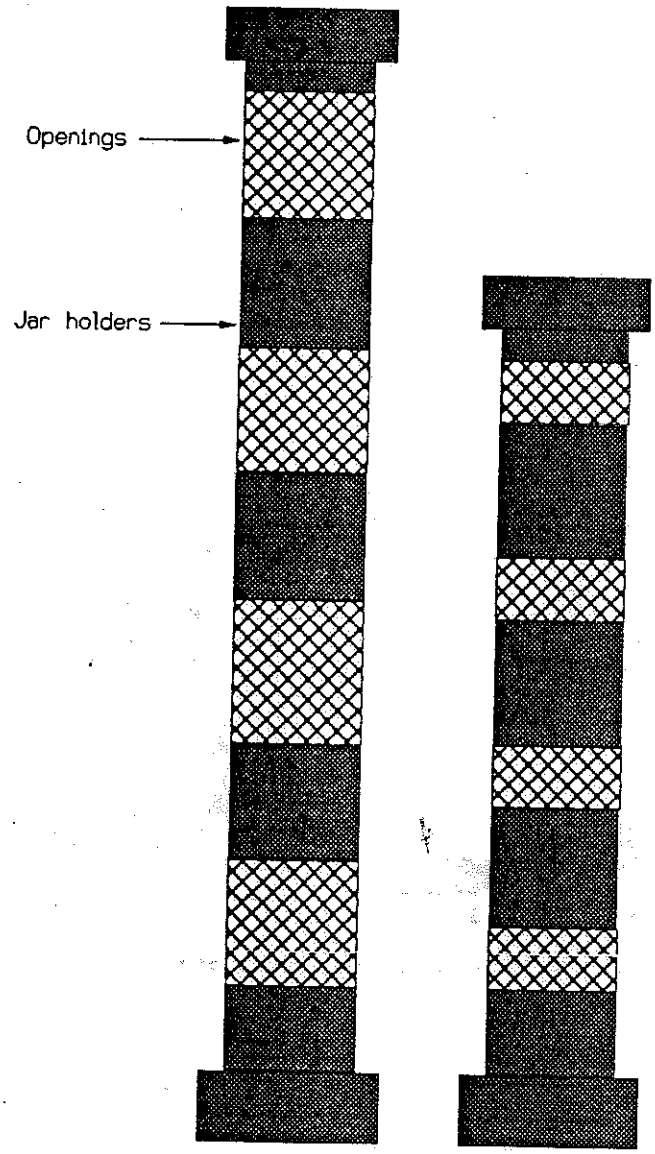

Figure 3.13 - Schematic of exposure chambers in which incubation vessels were placed during the sludge decomposition experiments.

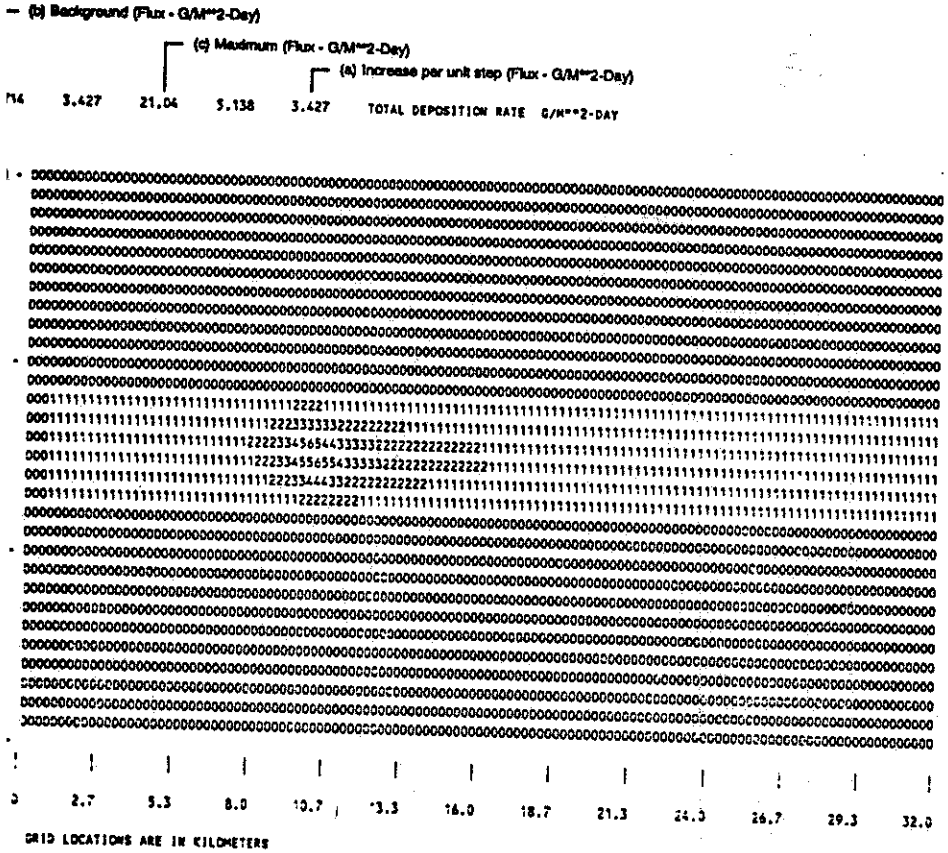

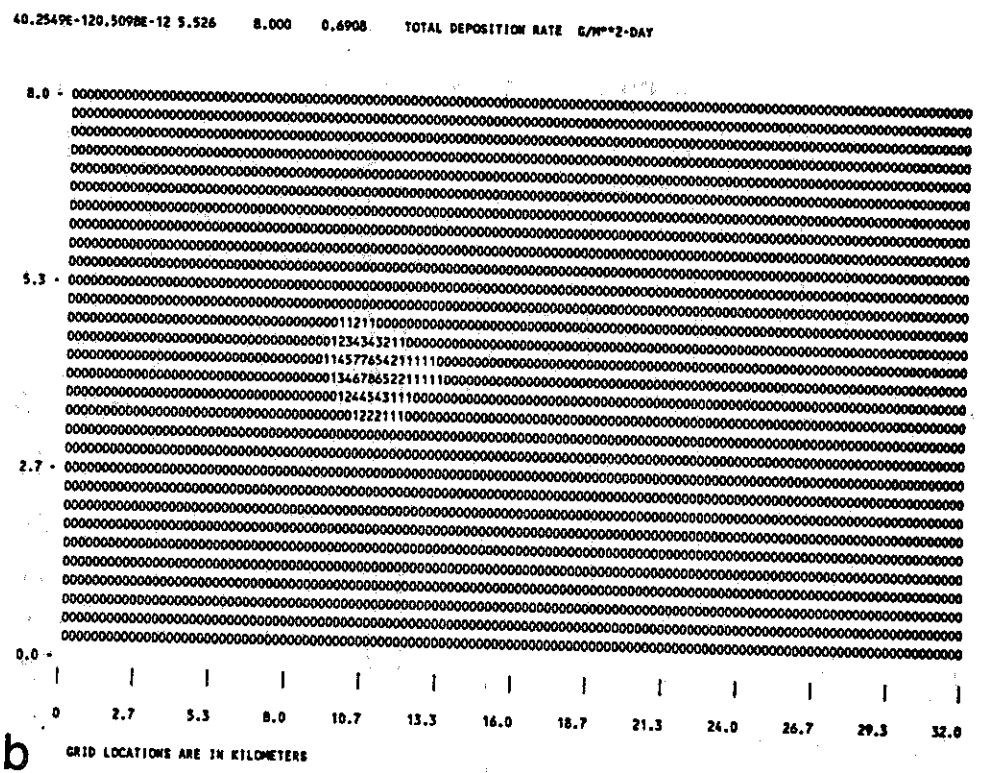

Figure 3.14 - Predicted depositional flux - DECAL, San Diego. (a) $k_d = 0.1\ d^{-1}$, (b) $k_d = 0.52\ d^{-1}$

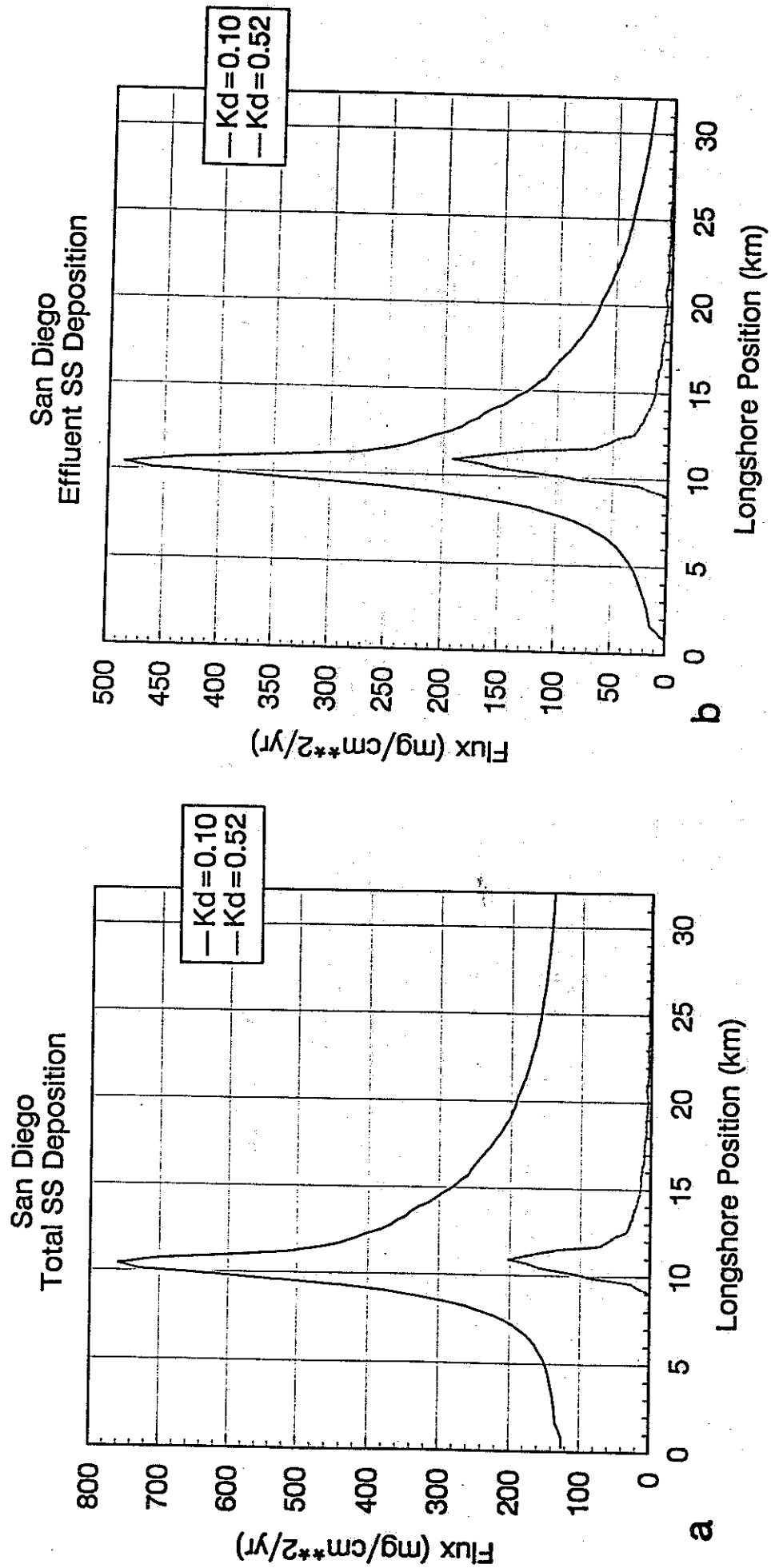

Figure 3.15 - Depositional flux along "60m" transect - DECAL, San Diego. (a) total suspended solids, (b) effluent suspended solids.

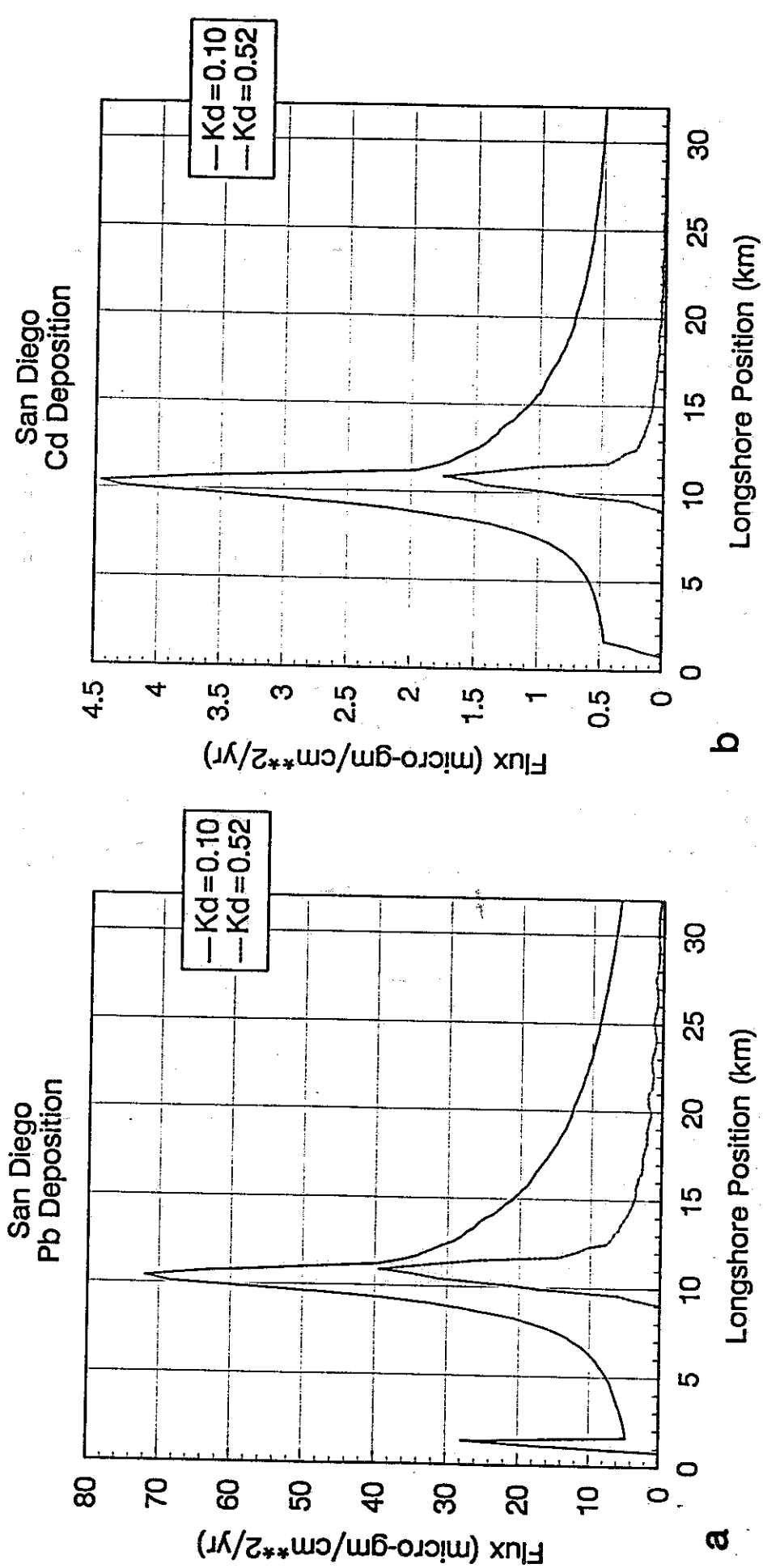

Figure 3.16 - Depositional fluxes of Lead and Cadmium along "60m" transect - San Diego. (a) lead, (b) cadmium.

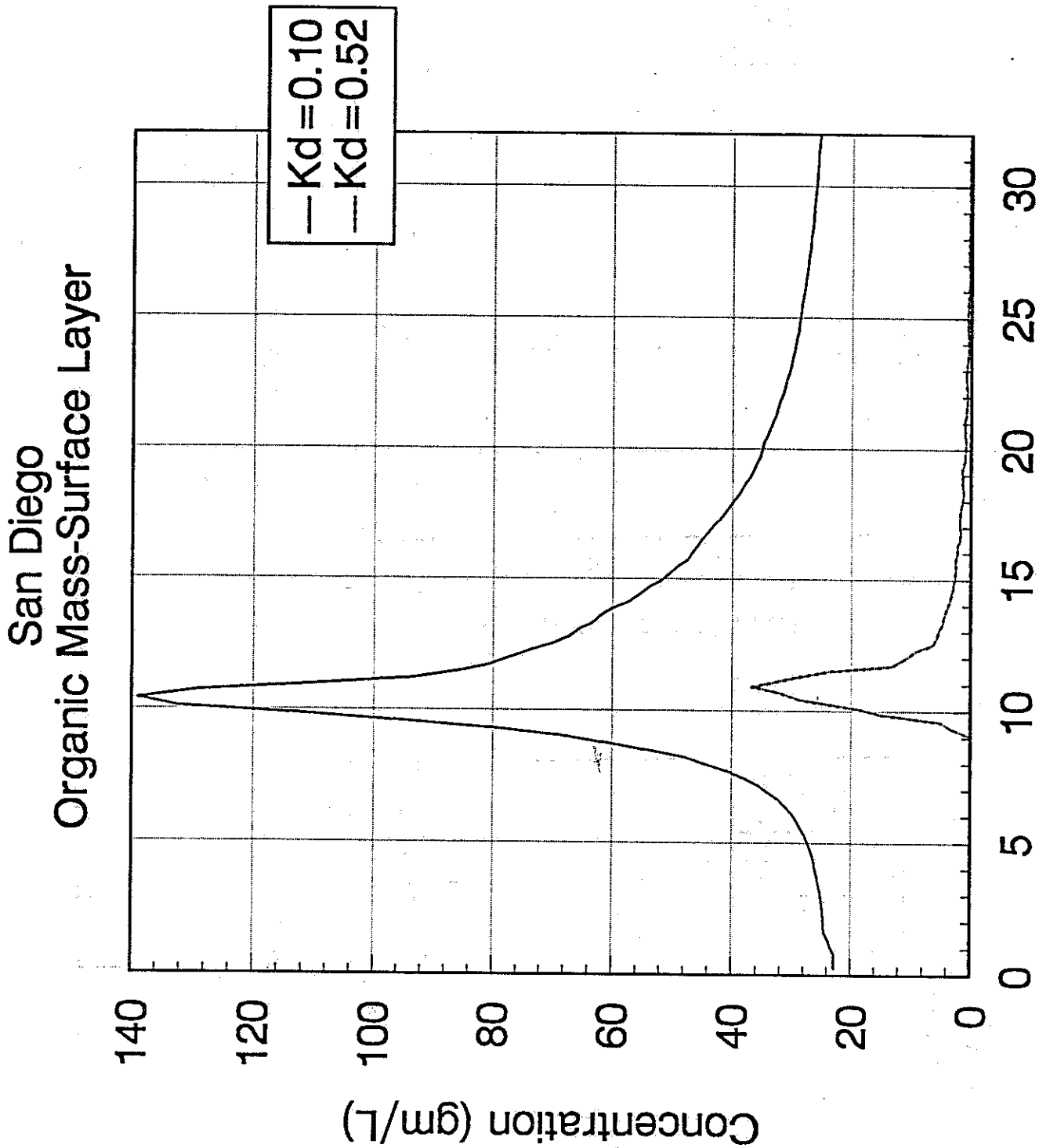

Figure 3.17 - Concentration of organic material in surface sediments - DECAL, San Diego.

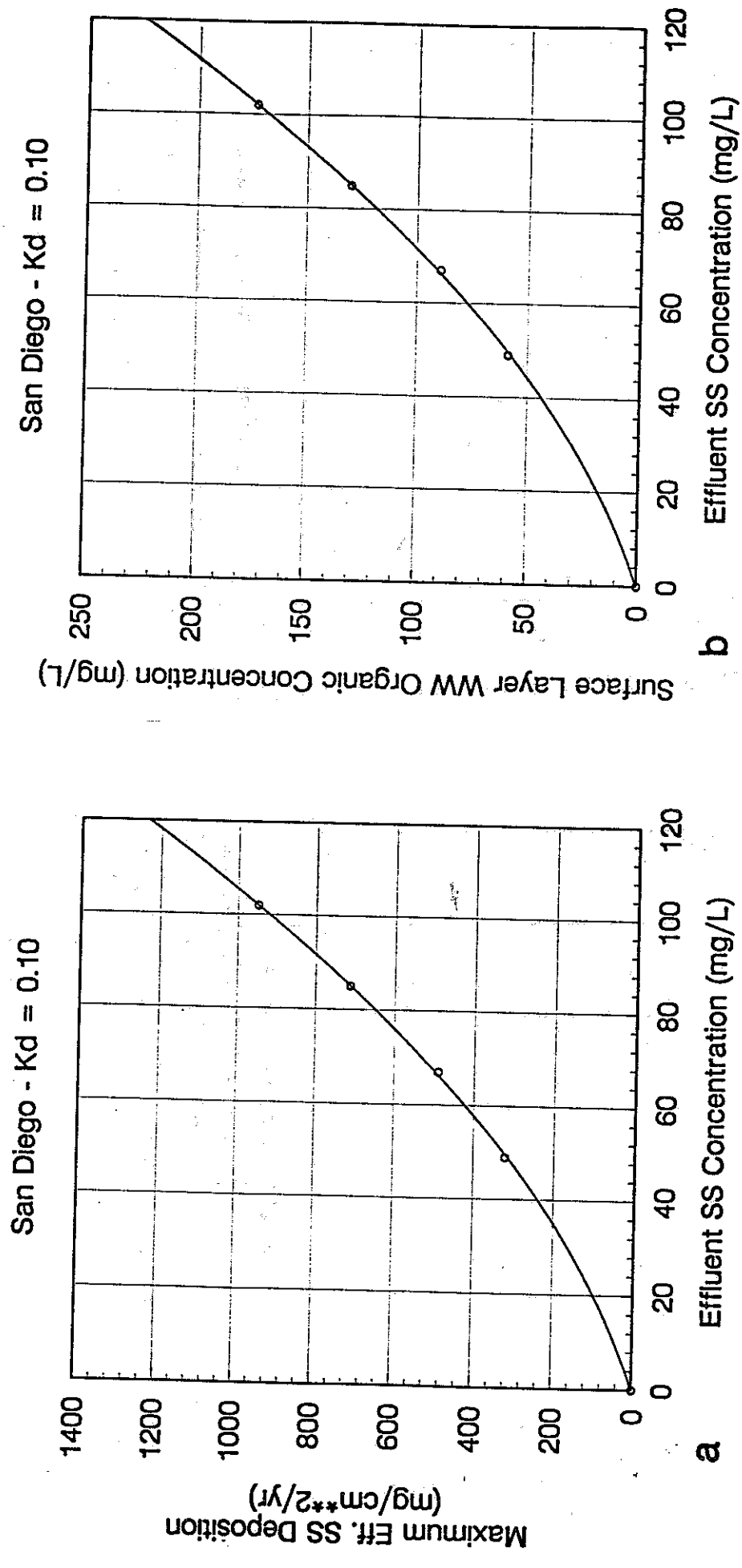

Figure 3.18 - Effects of effluent suspended solids concentrations - DECAL, San Diego. (a) deposition flux, (b) accumulation of organic material.

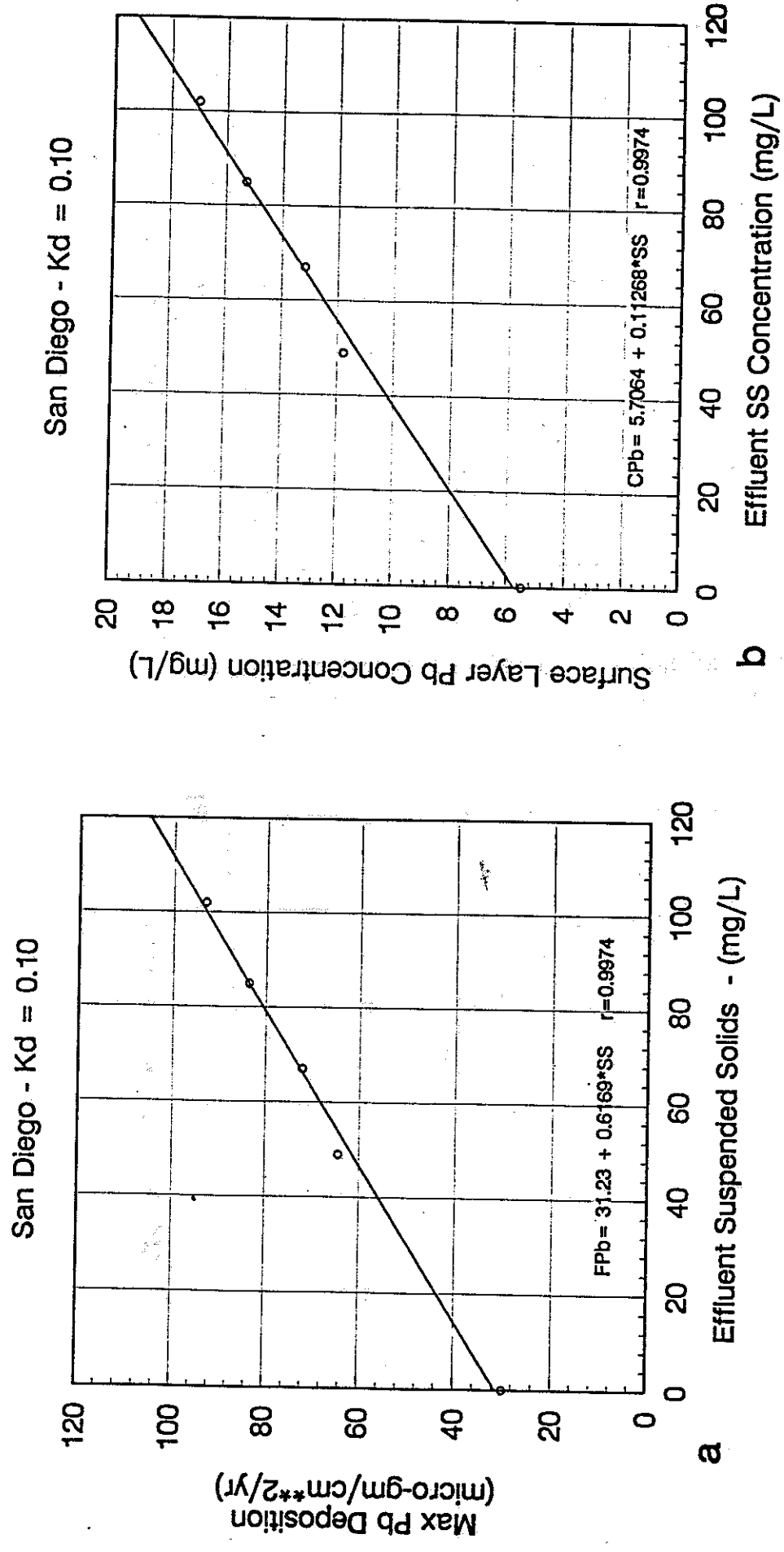

Figure 3.19 - Lead in sediments - DECAL, San Diego. (a) depositional flux, (b) concentration.

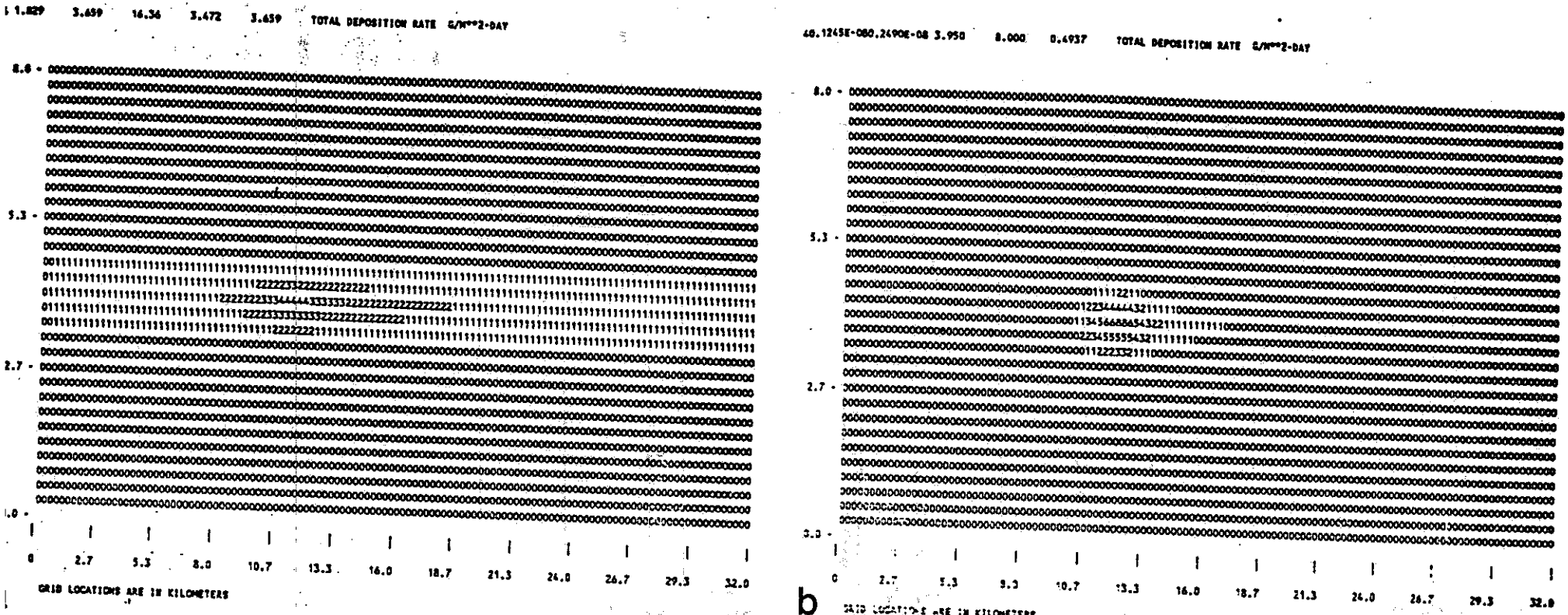

Figure 3.20 - Deposition fluxes - DECAL, Orange County. (a) $k_d = 0.1\ d^{-1}$, (b) $k_d = 0.52\ d^{-1}$

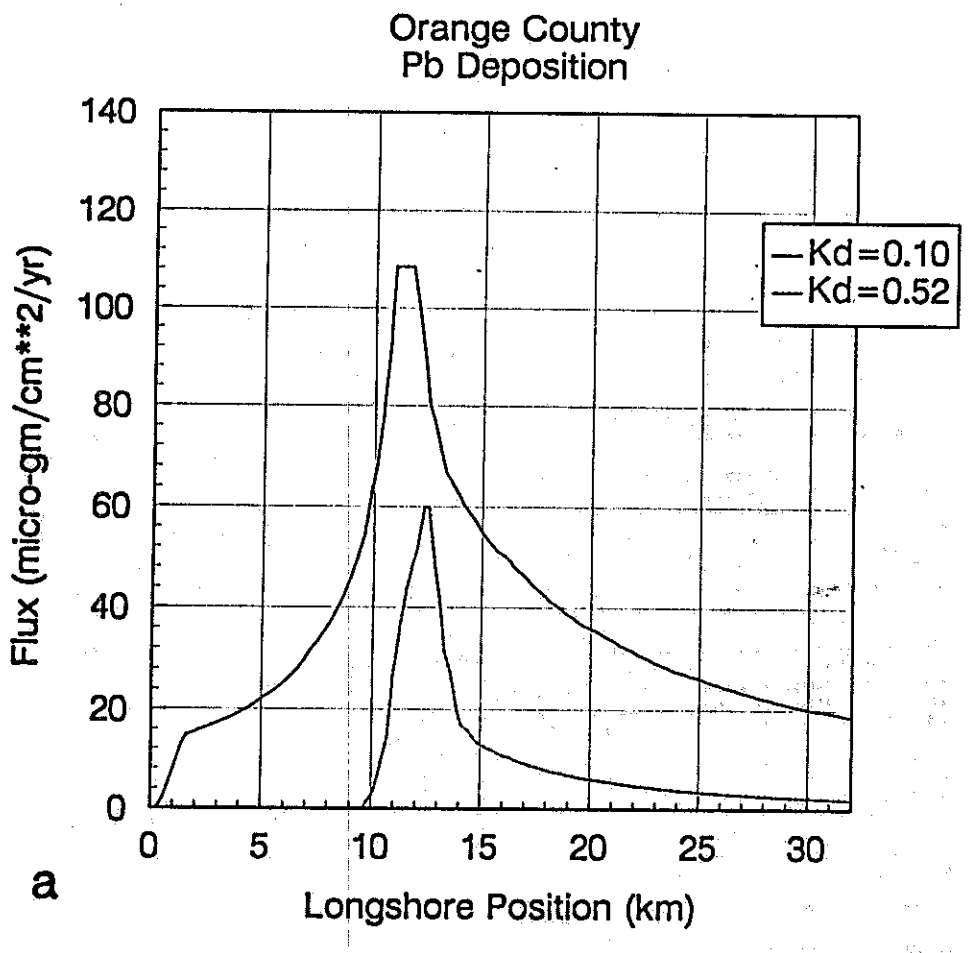

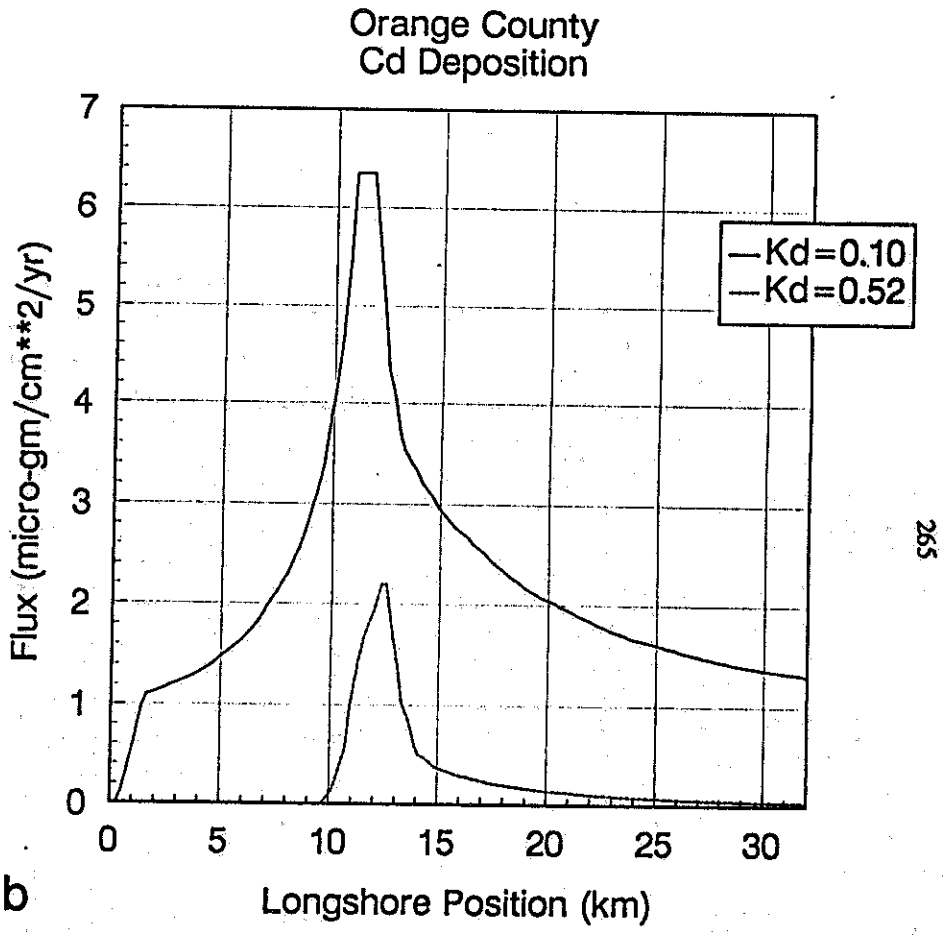

Figure 3.21 - Depositional flux - DECAL, Orange County, 55m isobath. (a) total suspended solids, (b) wastewater suspended solids.

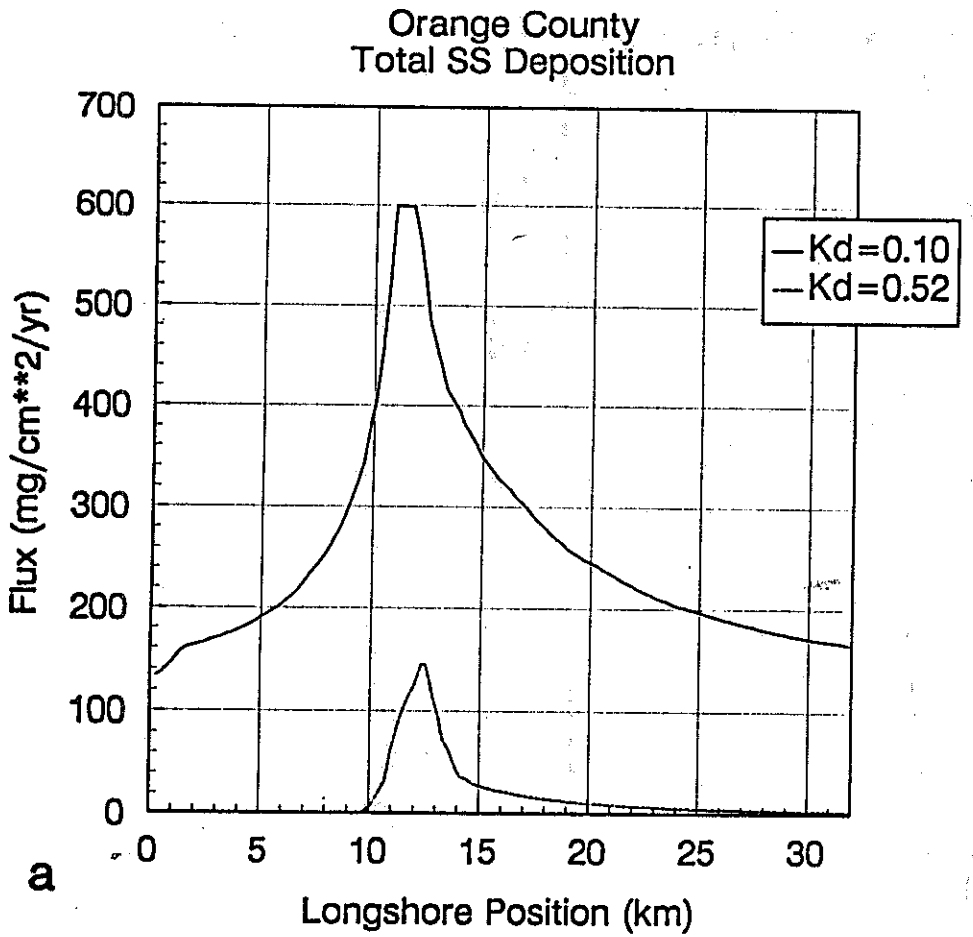

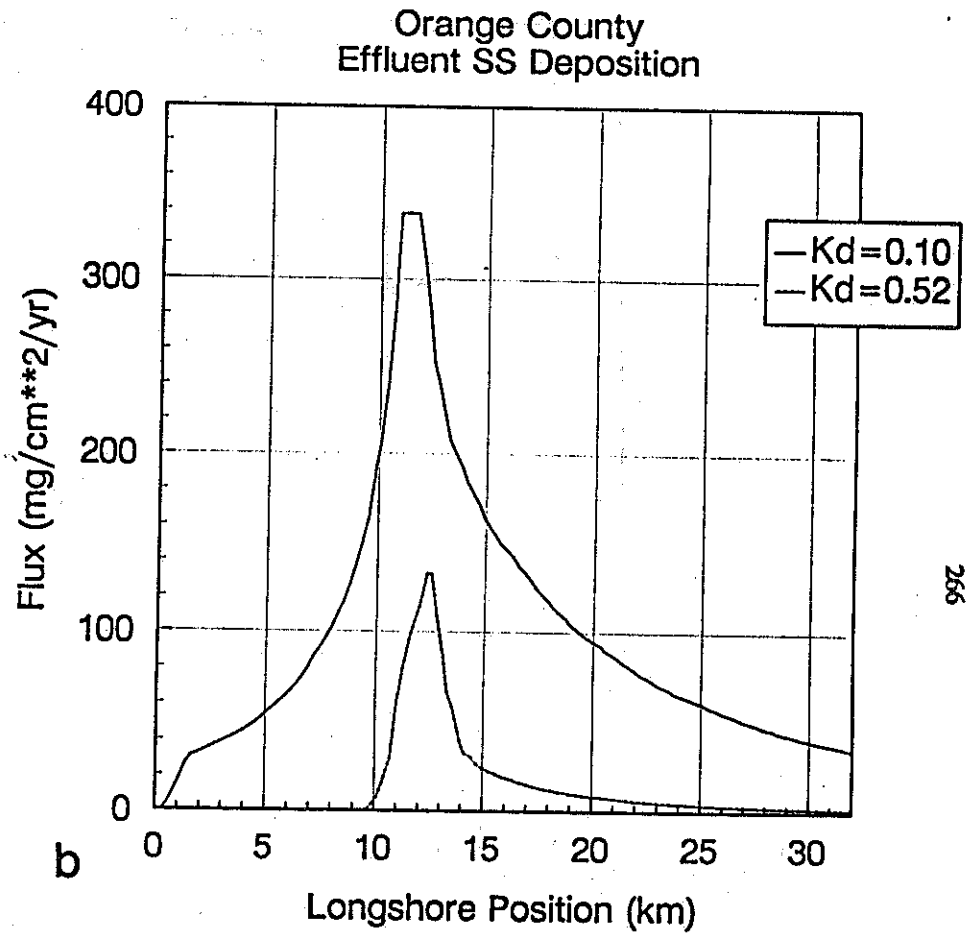

Figure 3.22 - Depositional flux - DECAL, Orange County, 55m isobath. (a) lead, (b) cadmium.

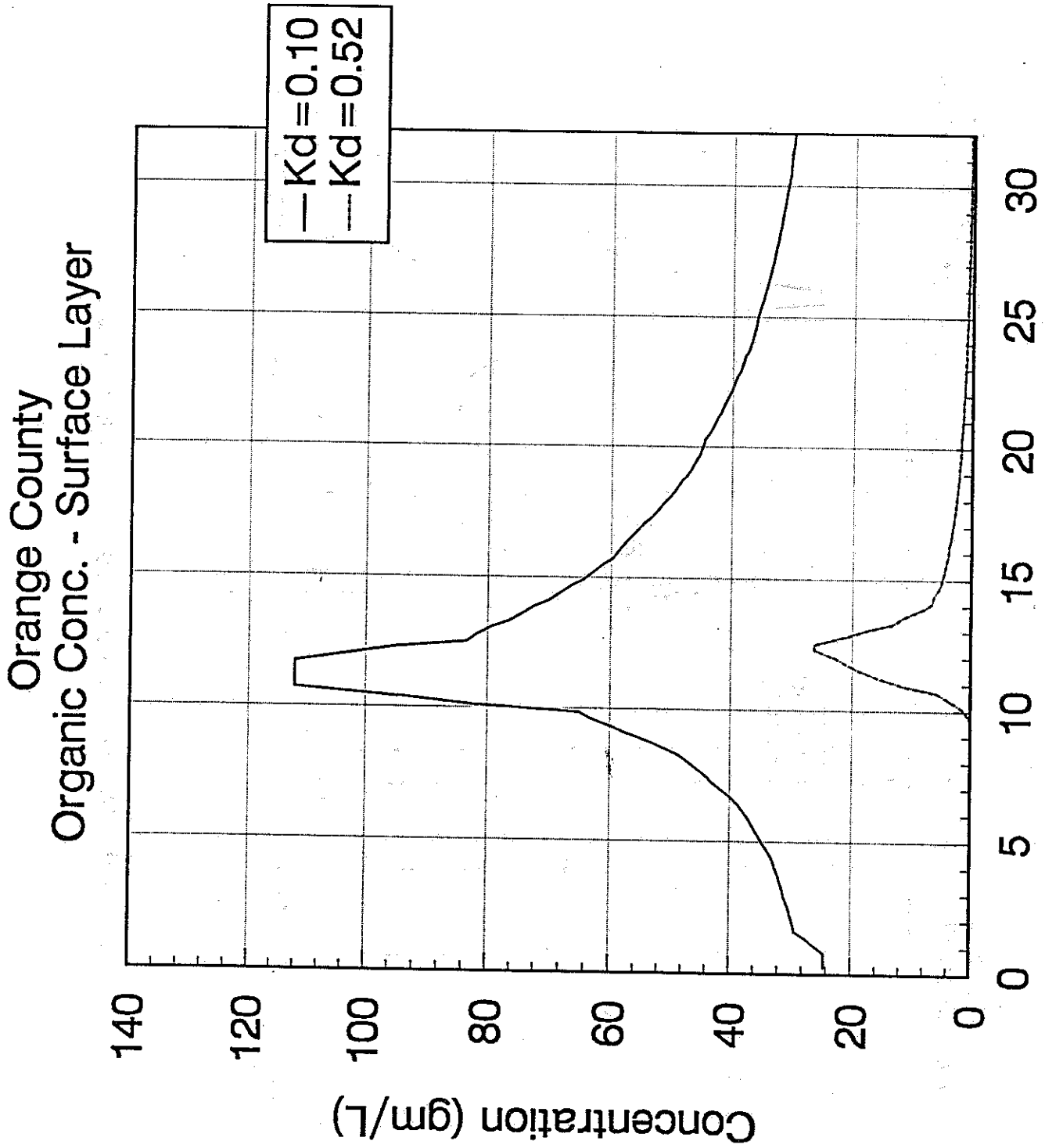

Figure 3.23 - Concentration of organic material - DECAL, Orange County, 55m.

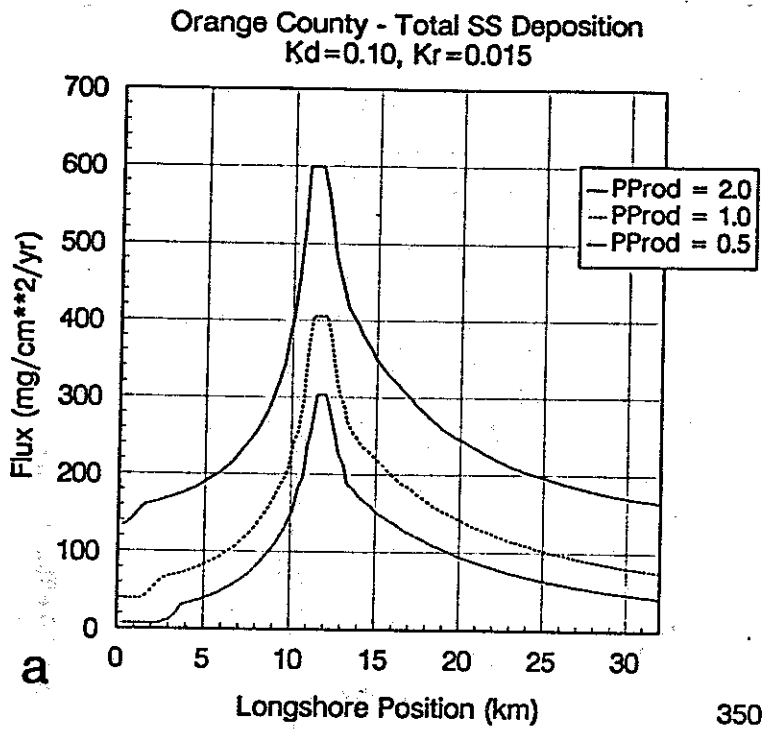

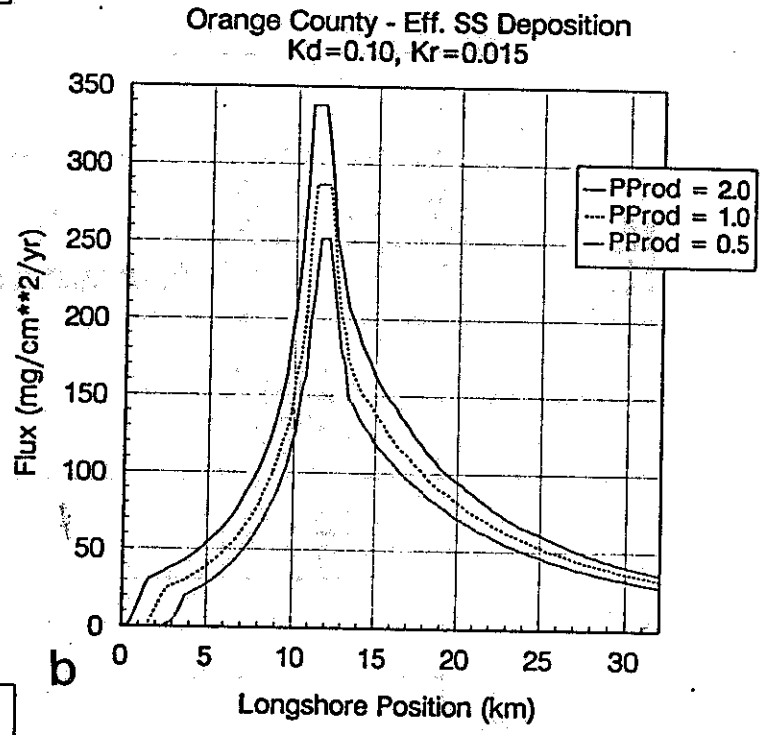

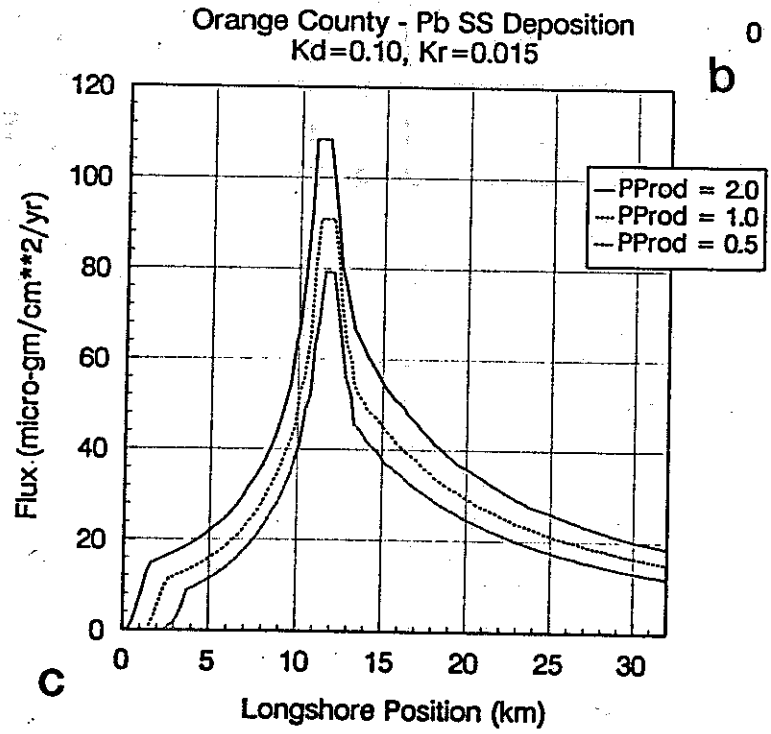

Figure 3.24 - Effects of phytoplankton productivity - DECAL, Orange County, 55m. (a) total suspended solids, (b) effluent suspended solids, (c) lead deposition.

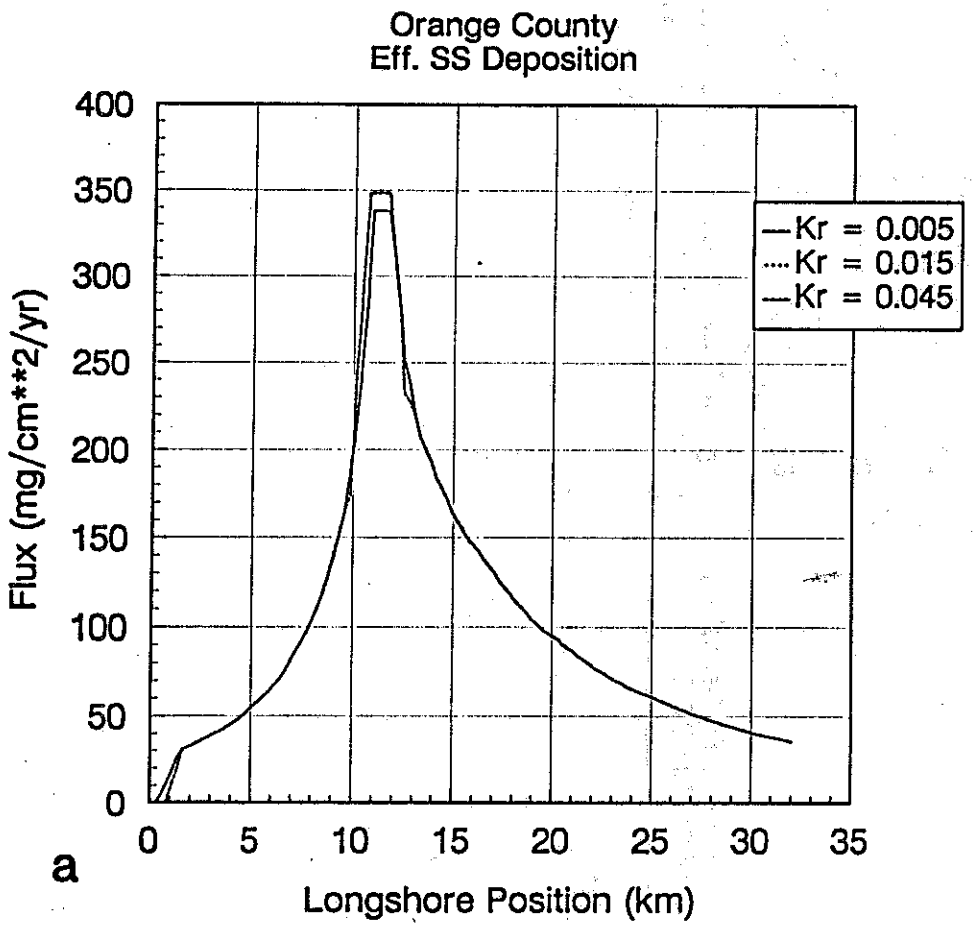

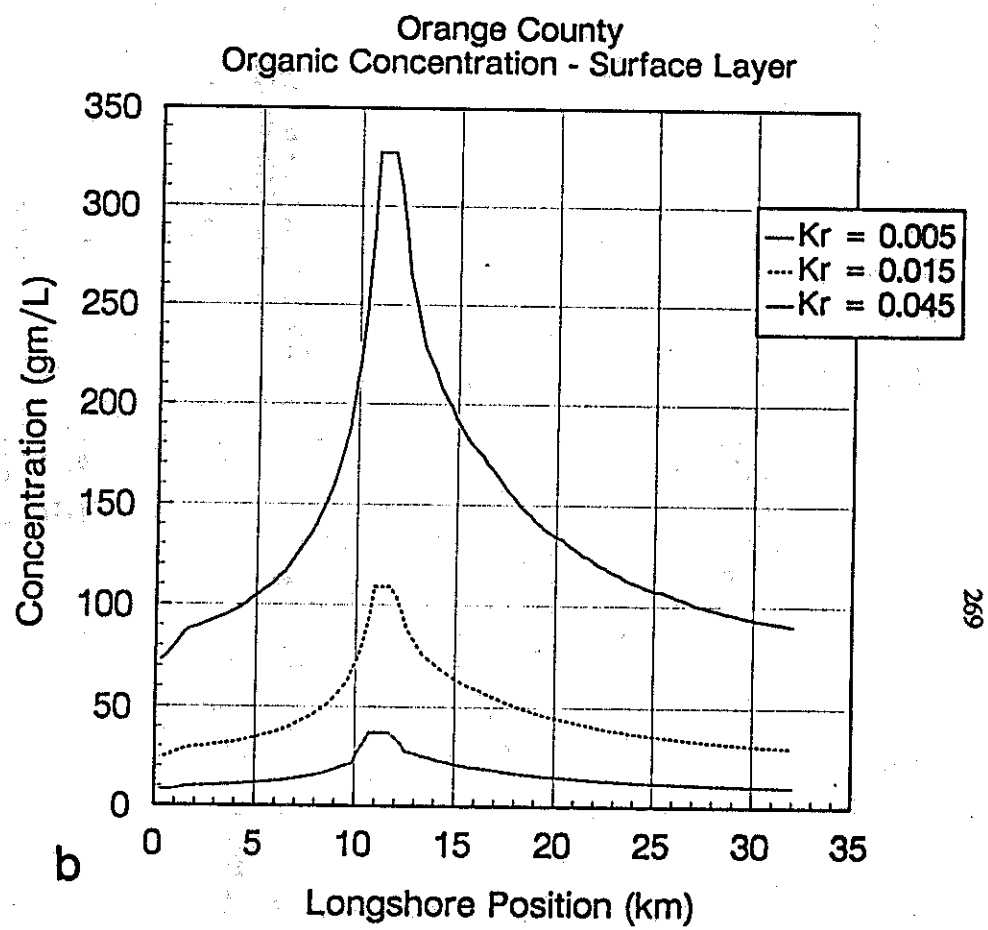

Figure 3.25 - Effects of interfacial removal rate - DECAL, Orange County, 55m. (a) effluent suspended solids, deposition (b) organic material.

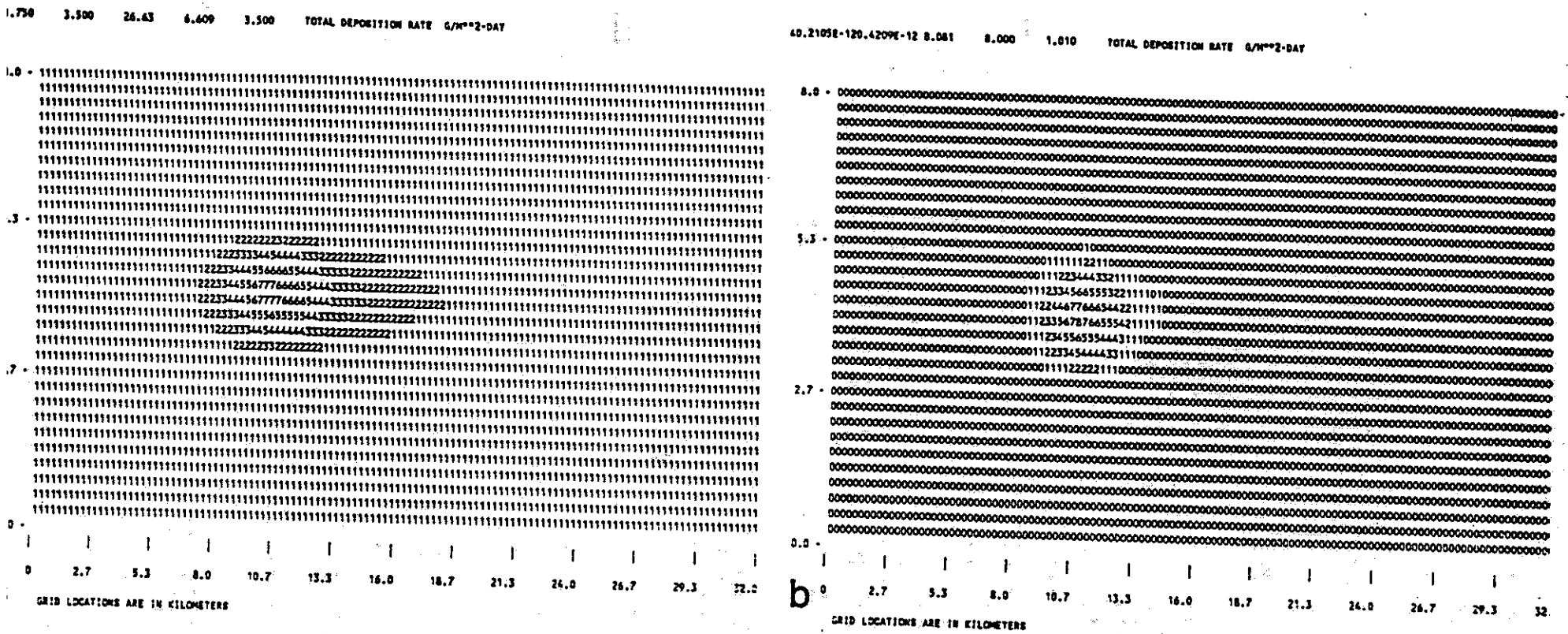

Figure 3.26 - Depositional flux - Total suspended solids, DECAL, Palos Verdes, 90", 1981. (a) kd = 0.1 d-1, (b) kd = 0.52 d-1.

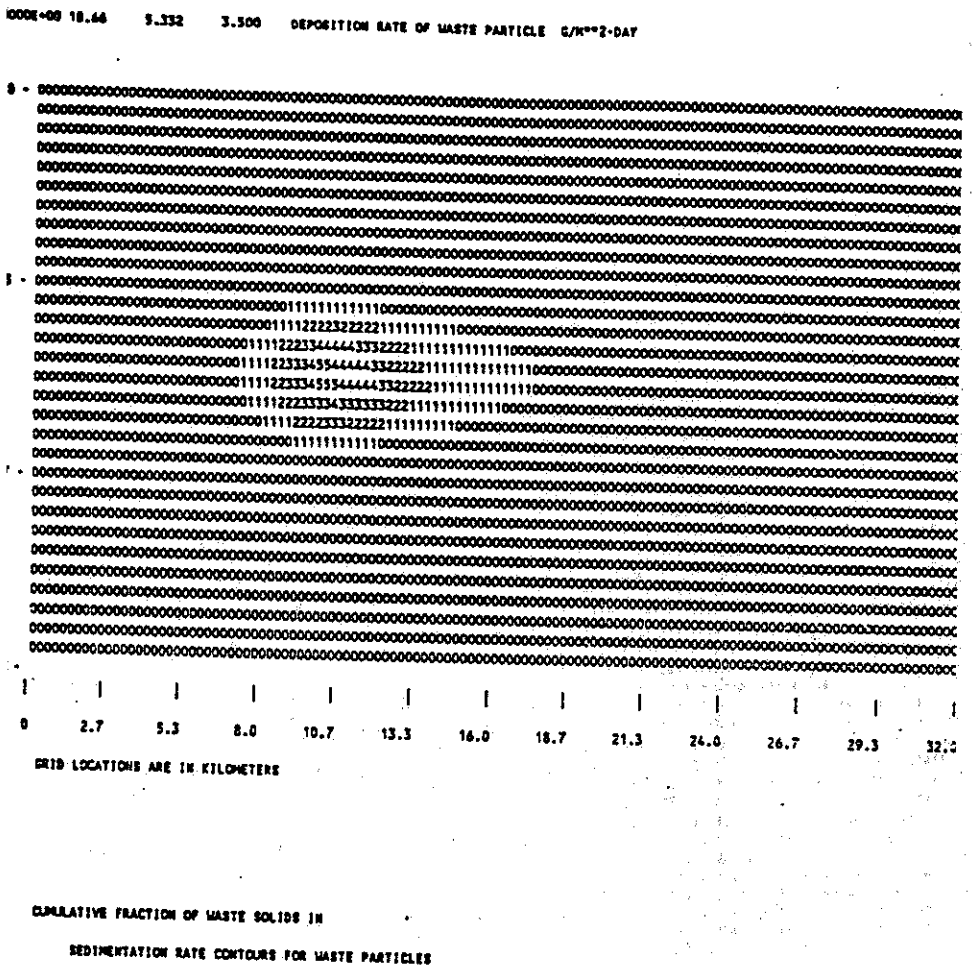

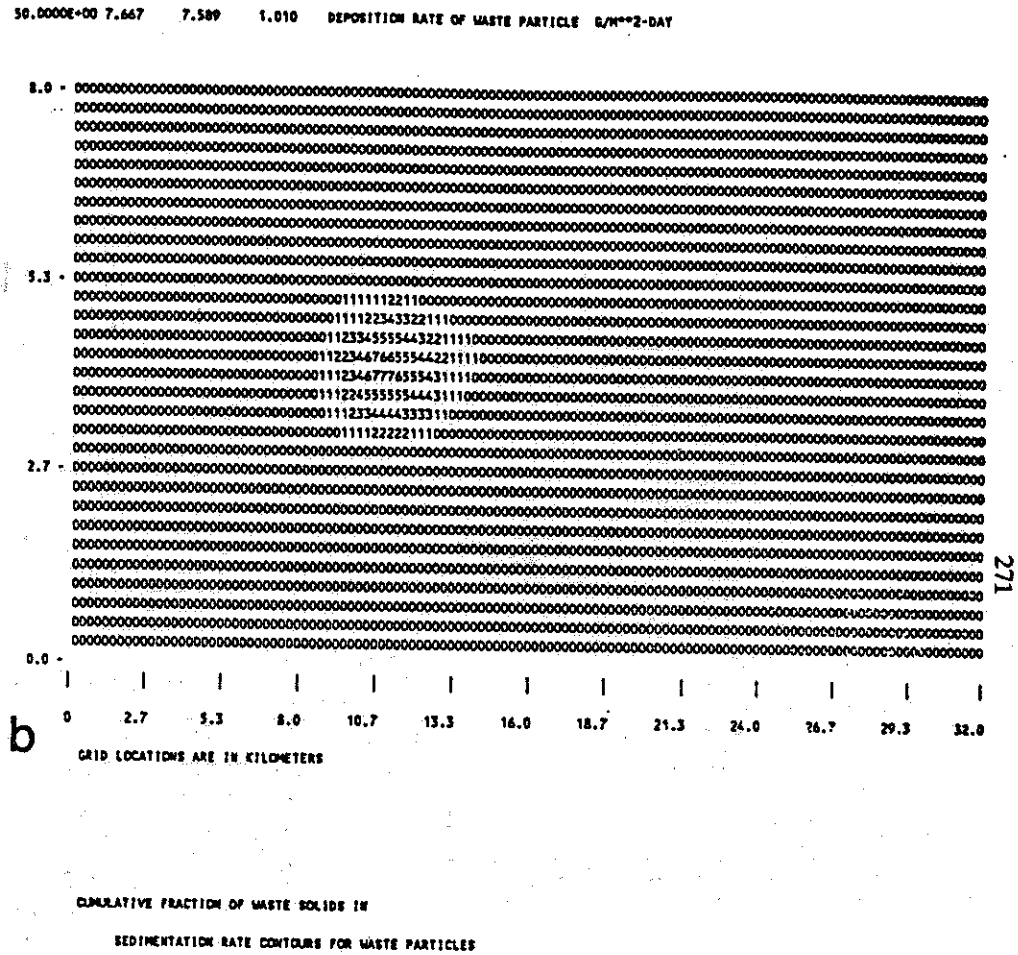

b.

Figure 3.27 - Depositional flux - Effluent suspended solids, DECAL, Palos Verdes, 90", 1981. (a) kd=0.1 d-1, (b) kd=0.52 d-1.

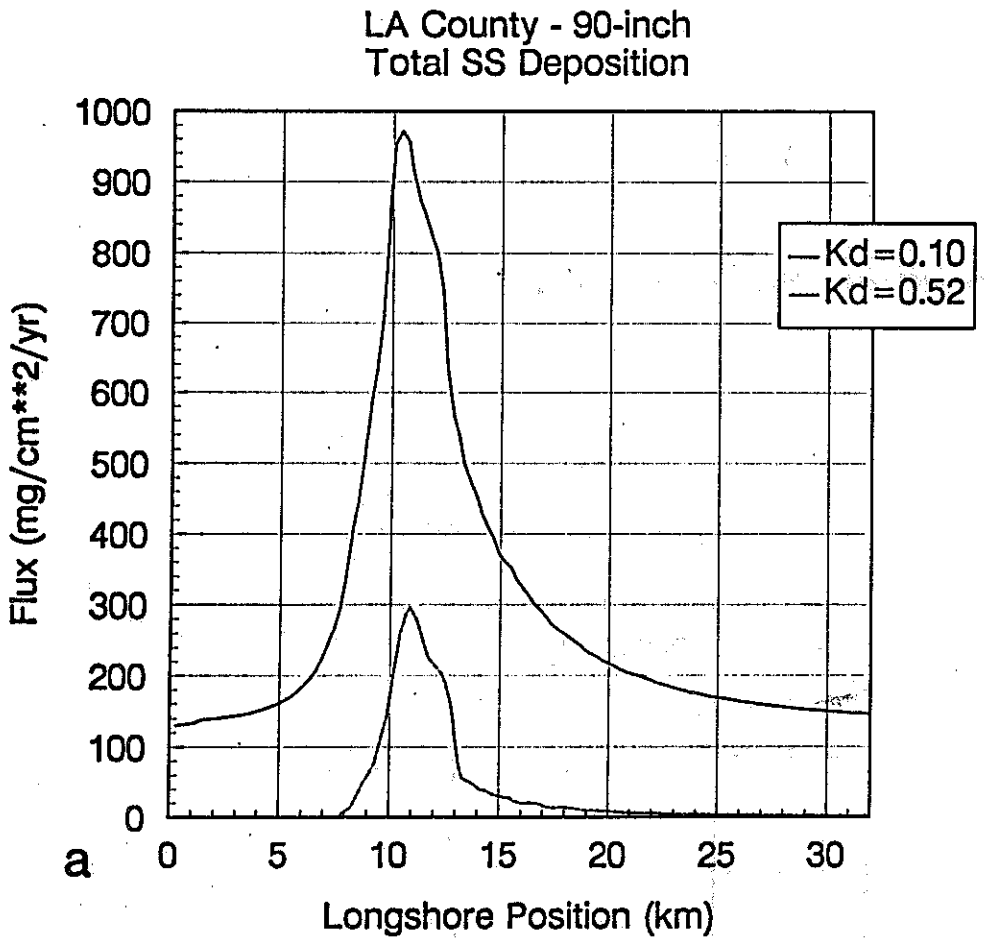

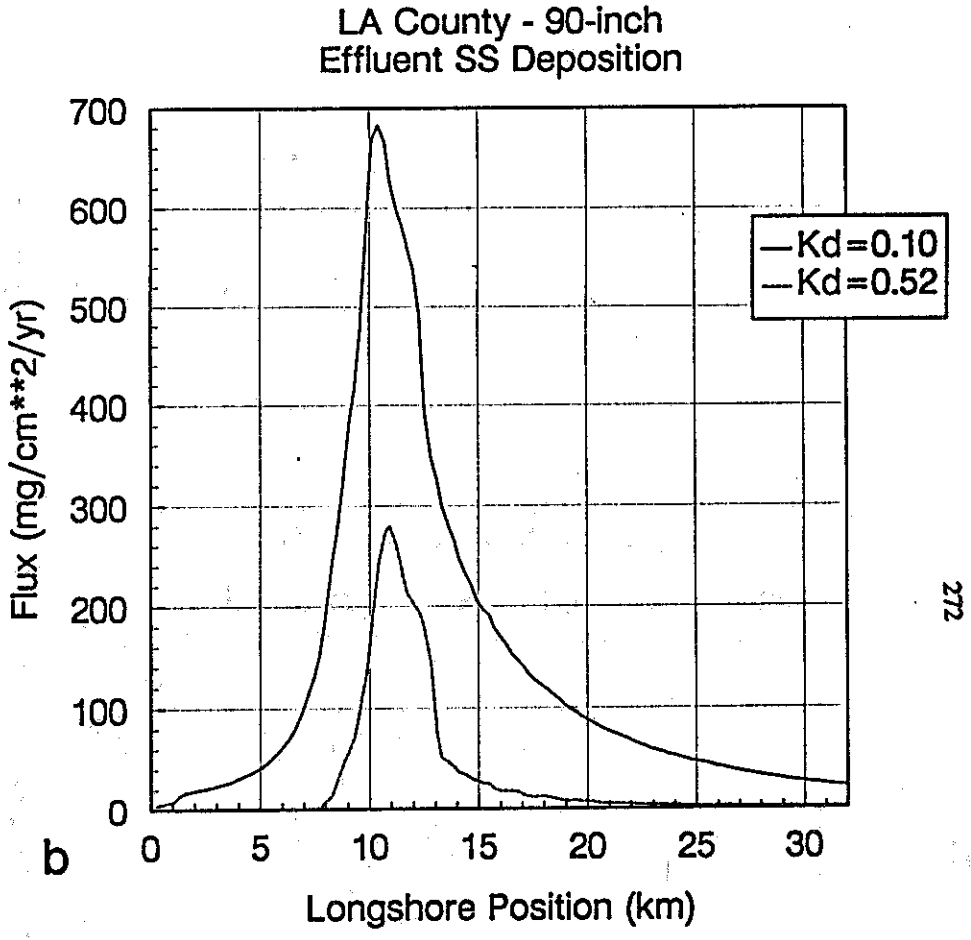

b

Figure 3.28 - Depositonal flux - DECAL, Palos Verdes, 90", 1981. (a) total suspended solids, (b) effluent suspended solids.

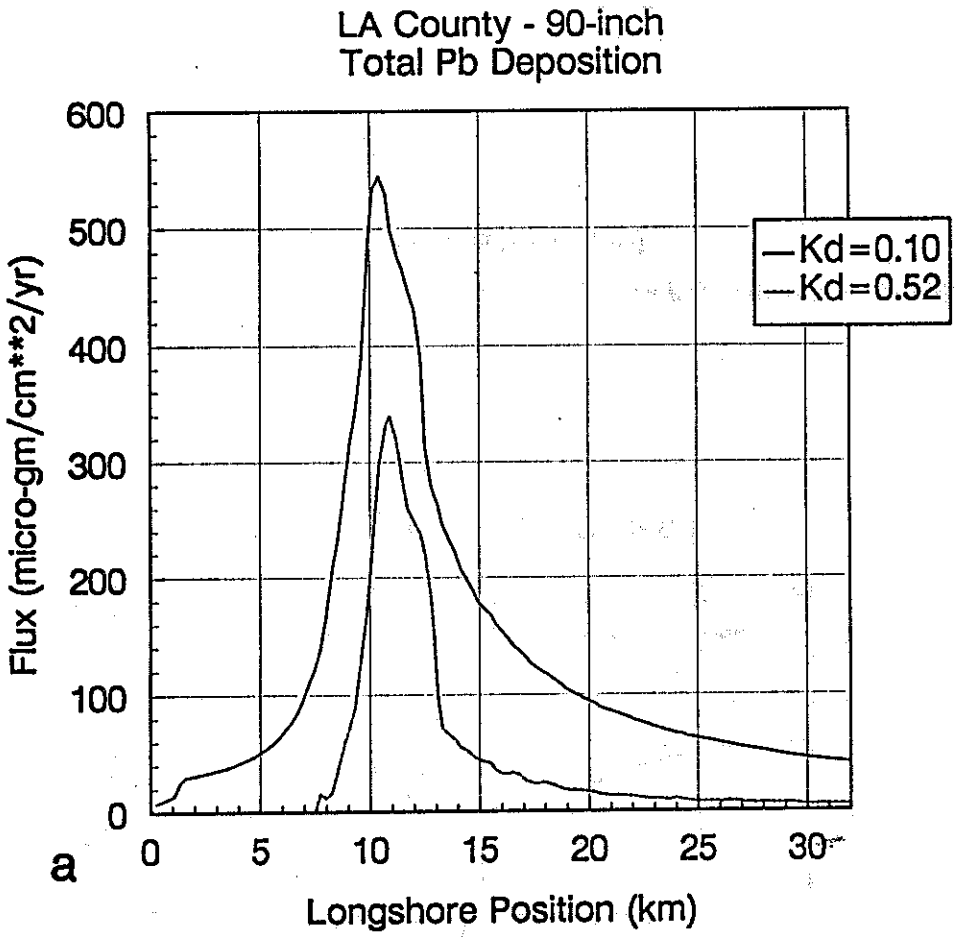

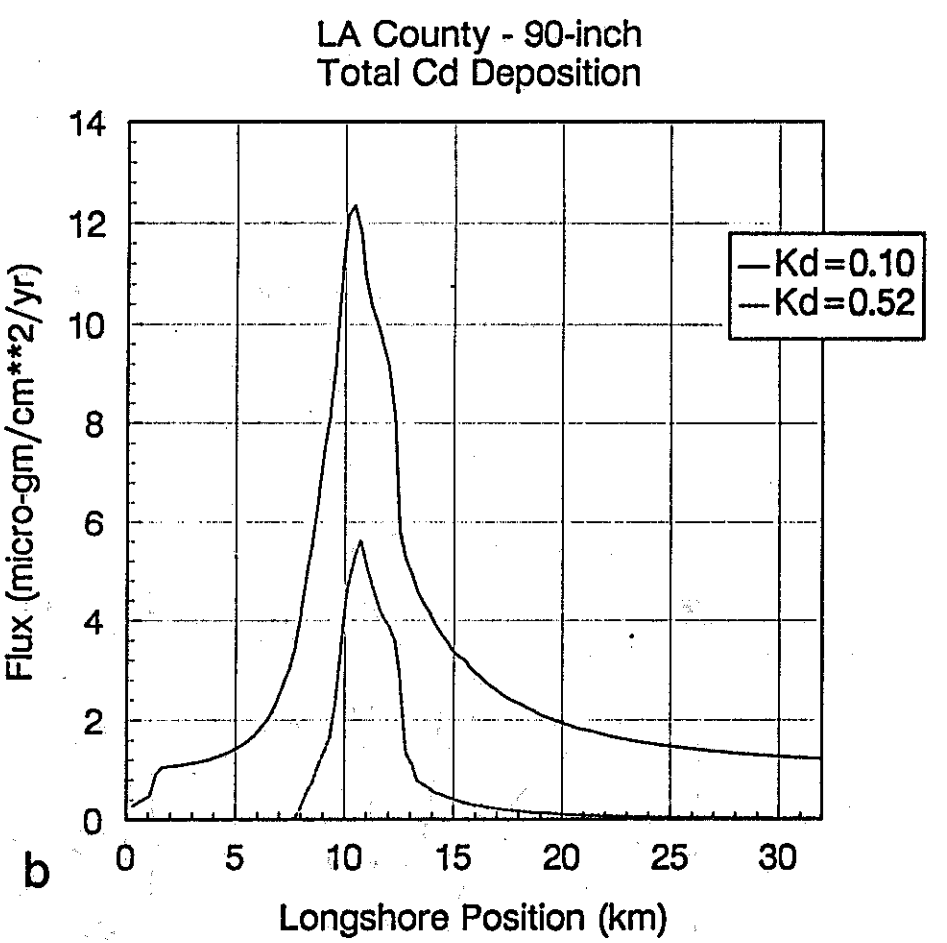

Figure 3.29 - Depositional flux - DECAL, Palos Verdes, 90", 1981. (a) lead, (b) cadmium.

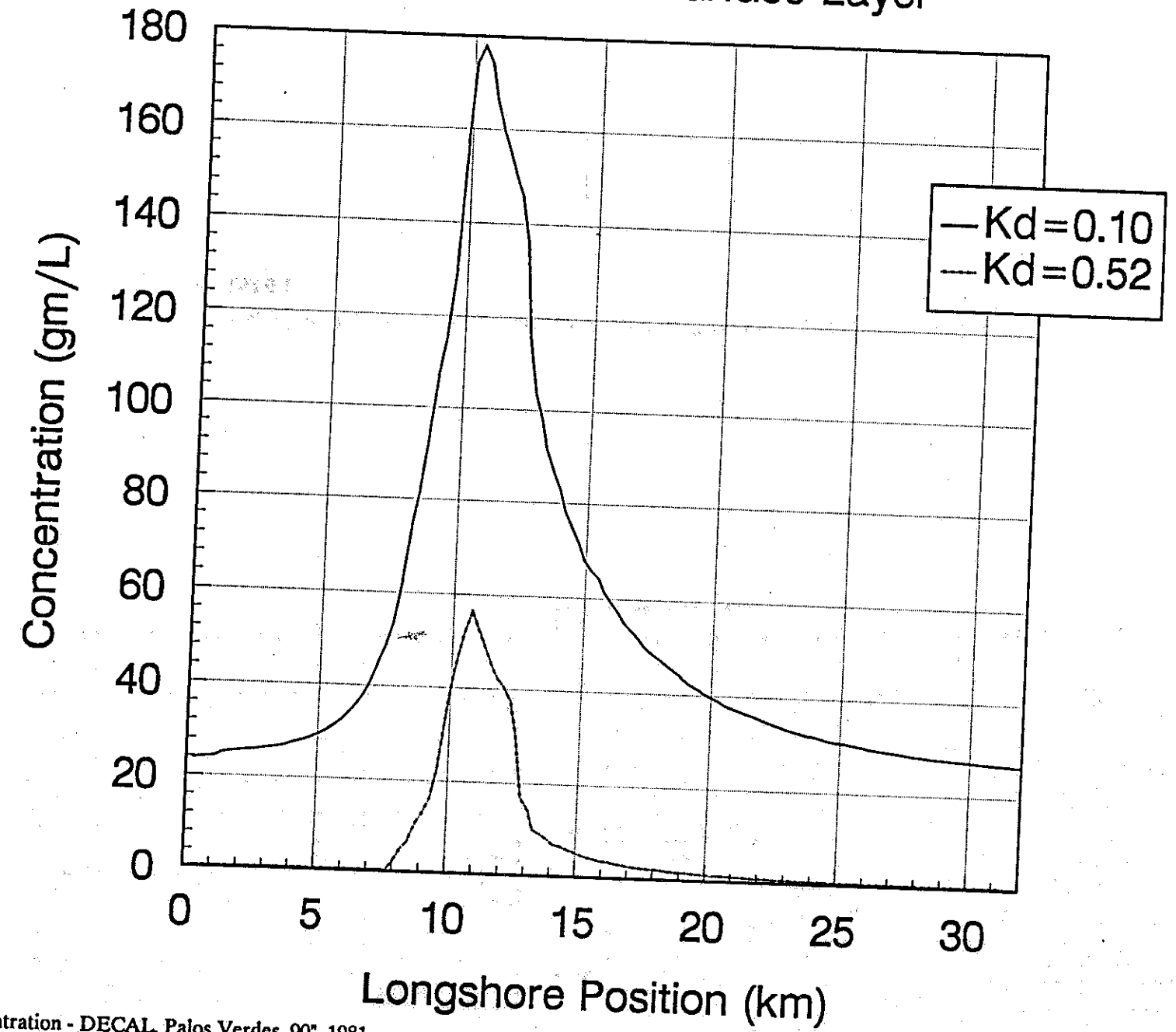

gure 3.30 - Organic concentration - DECAL, Palos Verdes, 90°, 1981.

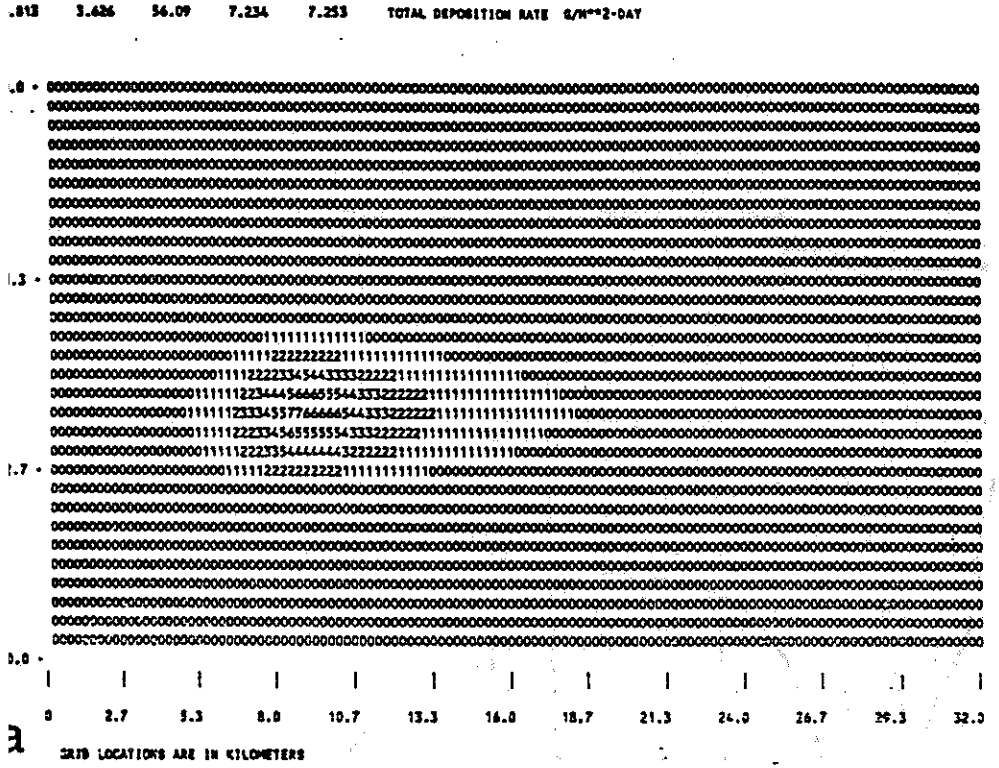

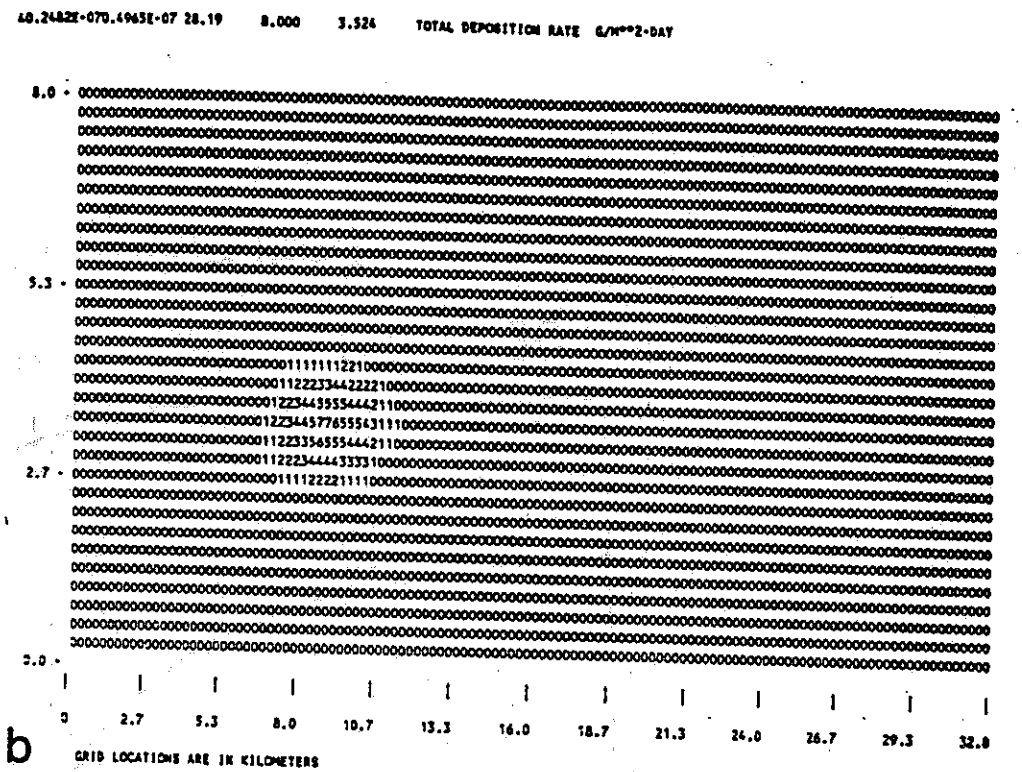

Figure 3.31 - Depositional flux - Total suspended solids, DECAL, Palos Verdes, 120", 1981. (a) kd=0.1 d-1, (b) kd=0.52 d-1.

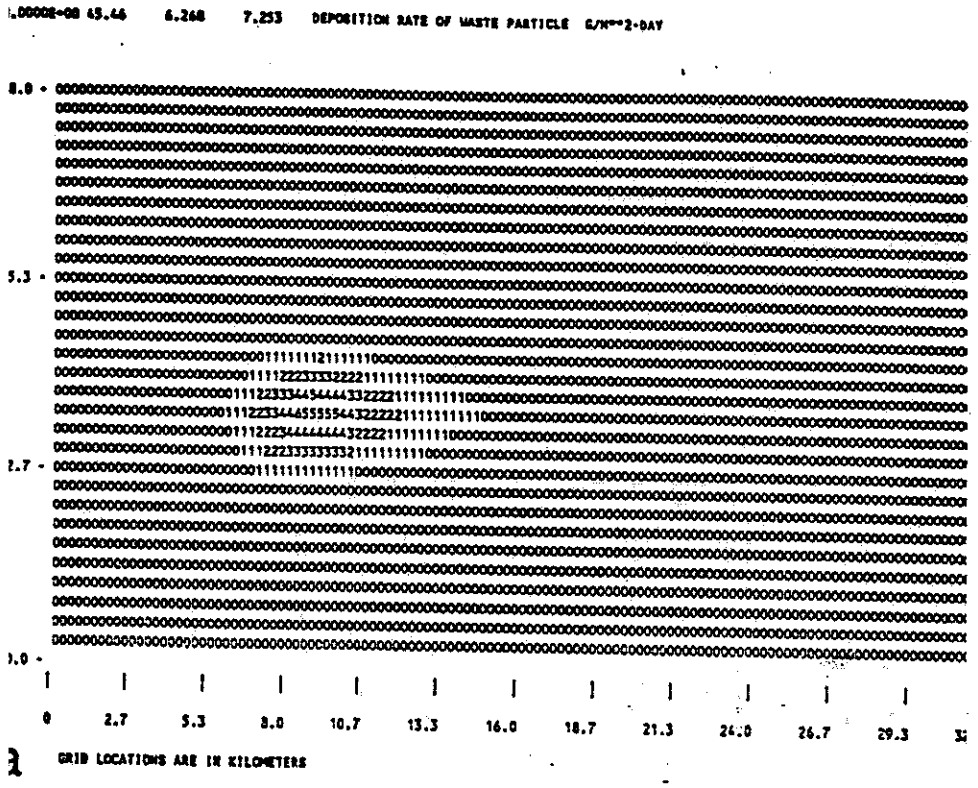

a

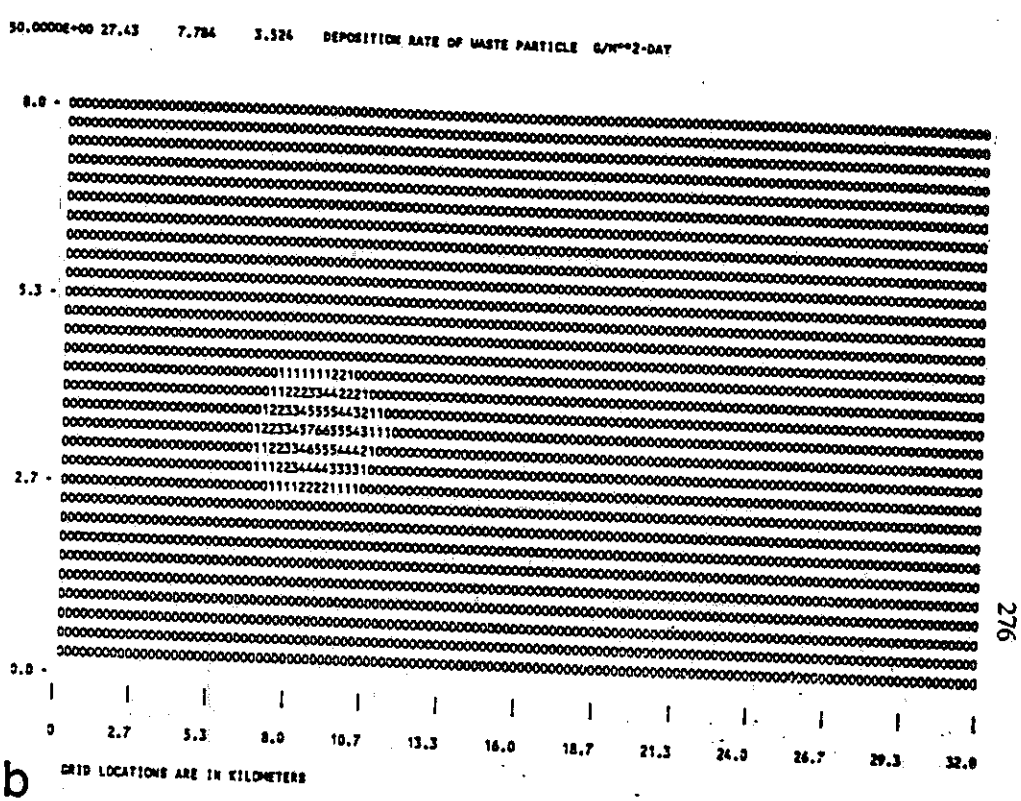

b

Figure 3.32 - Depositional flux - Effluent suspended solids, DECAL, Palos Verdes, 120", 1981. (a) kd=0.10 d-1, (b) kd=0.52 d-1.

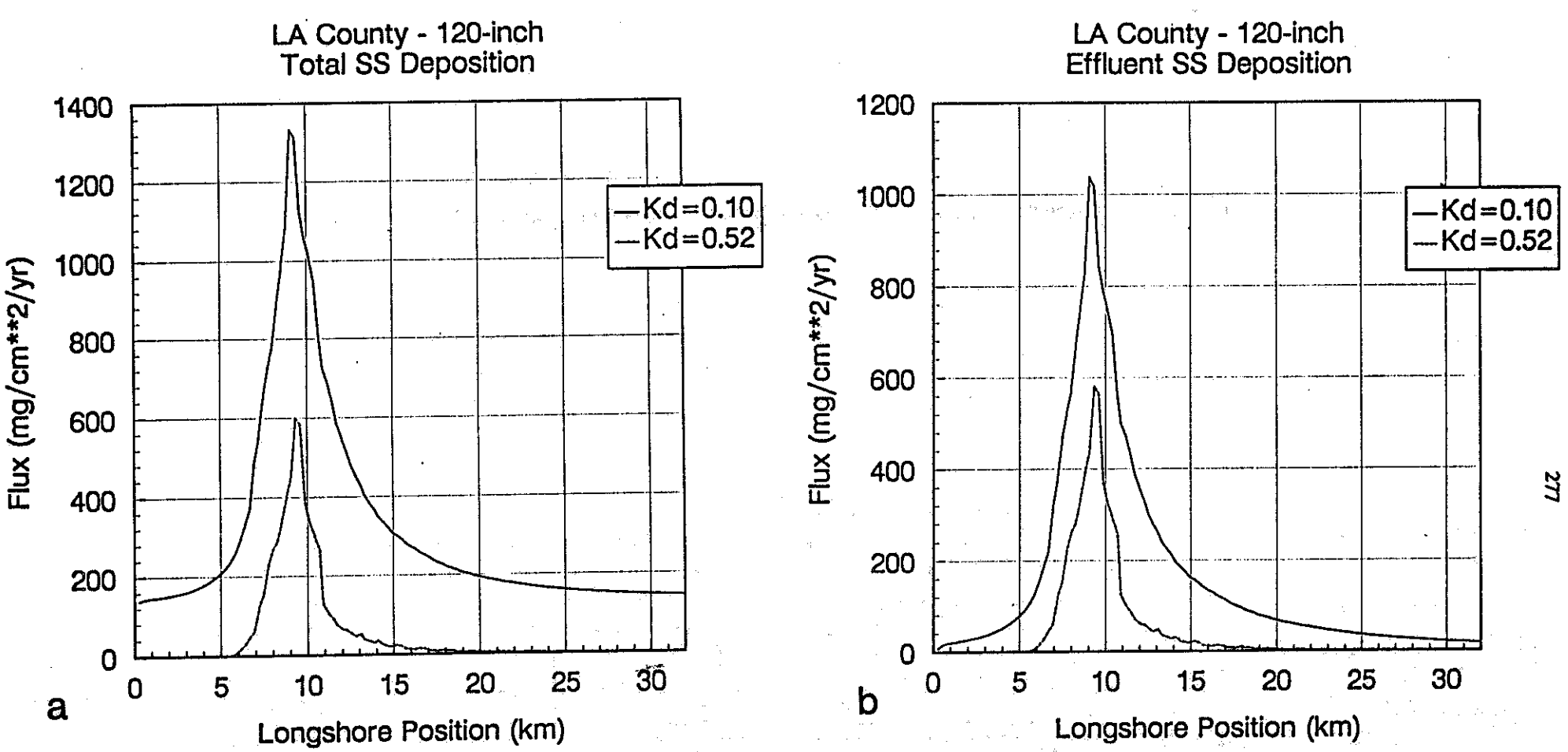

Figure 3.33 - Depositional flux - DECAL, Palos Verdes, 120", 1981, 55m. (a) total suspended solids, (b) effluent suspended solids.

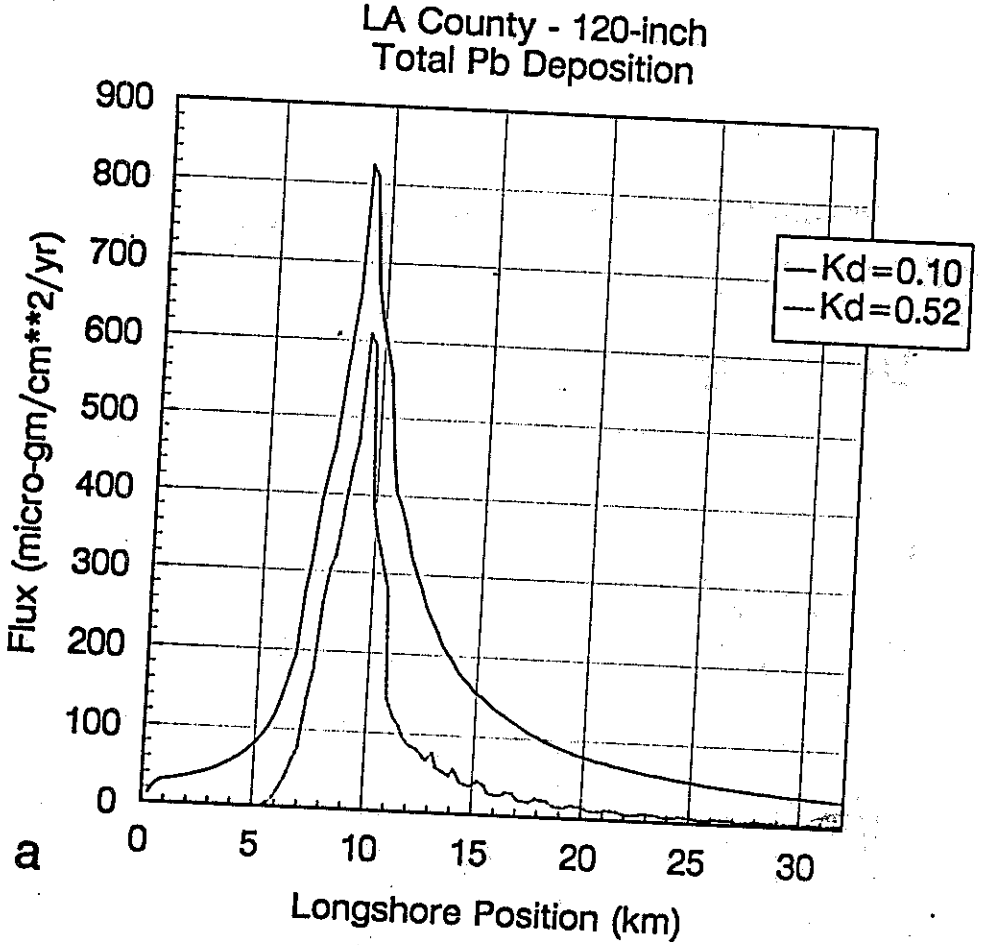

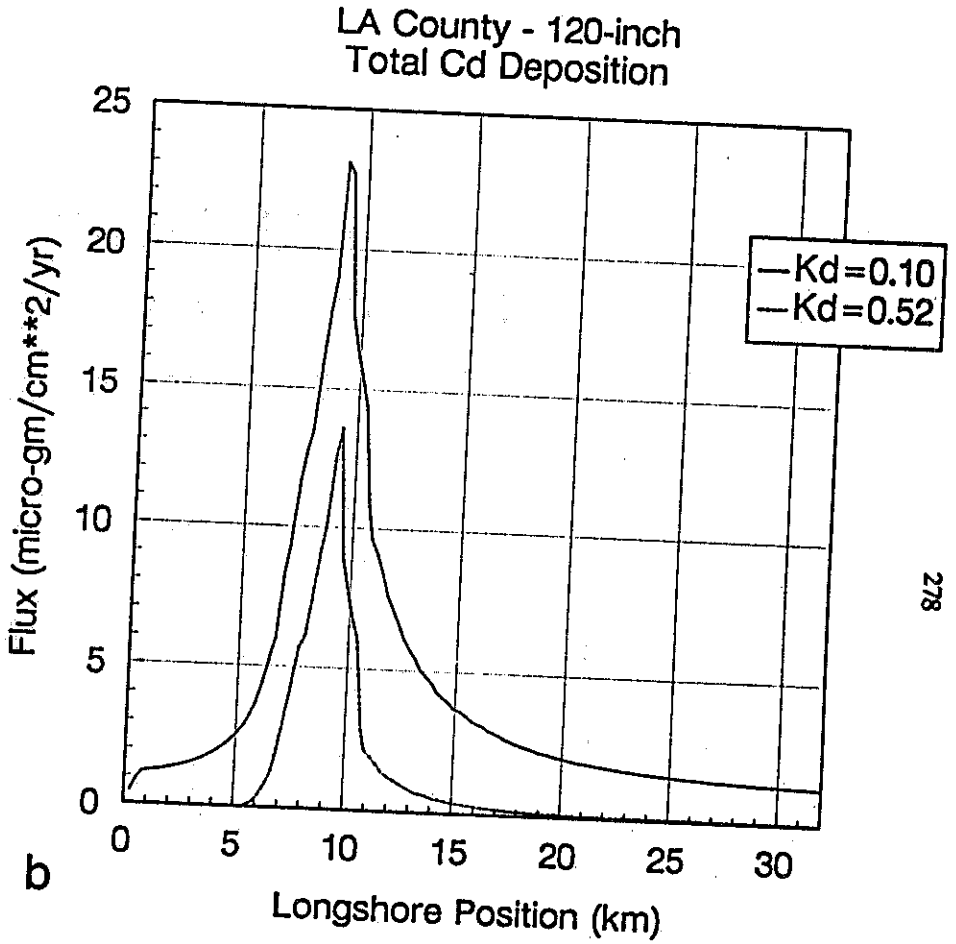

Figure 3.34 - Depositional flux - DECAL, Palos Verdes, 120", 1981, 55m. (a) lead, (b) cadmium.

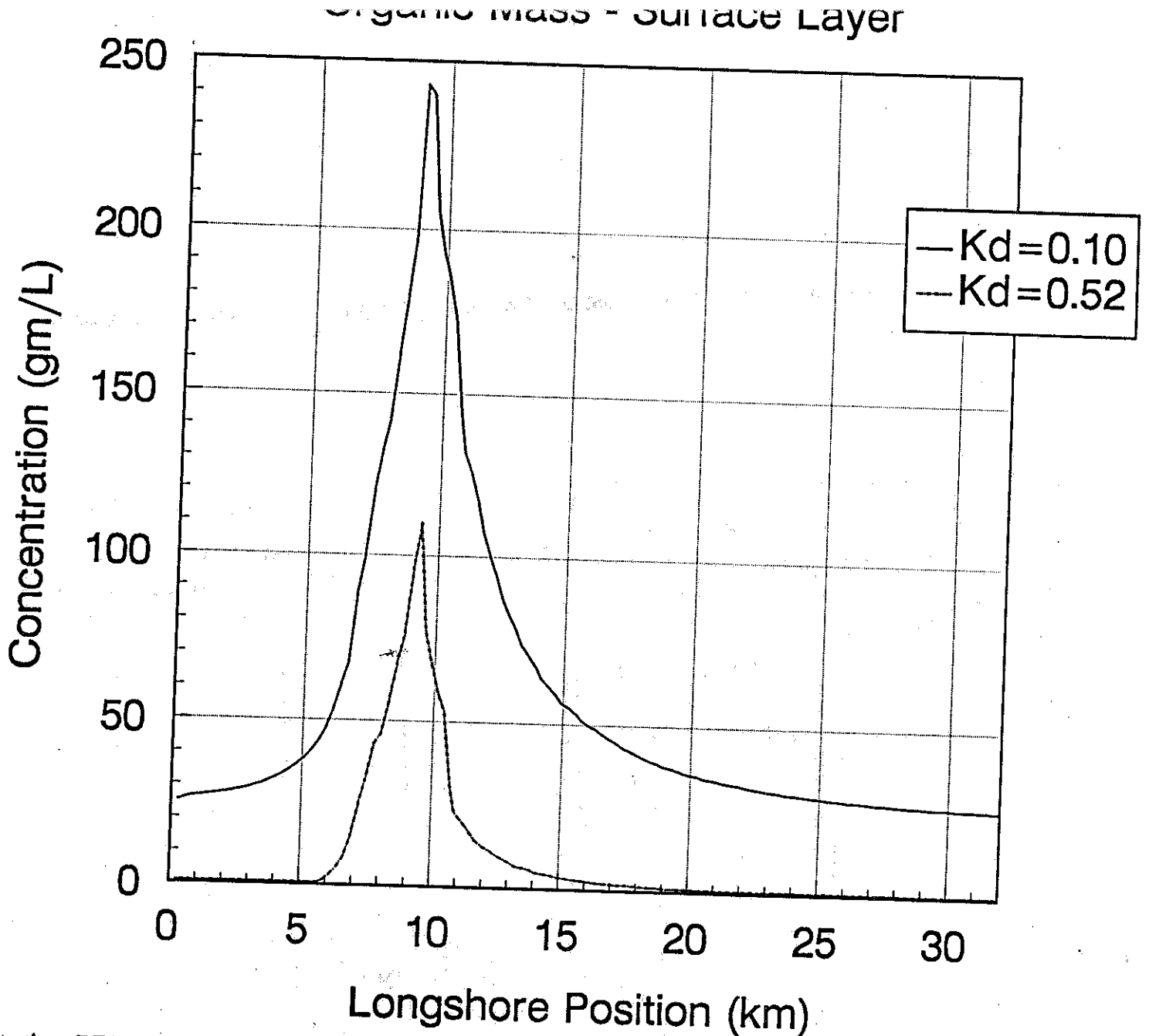

Figure 3.35 - Organic concentration - DECAL, Palos Verdes, 120", 1981, 55m.

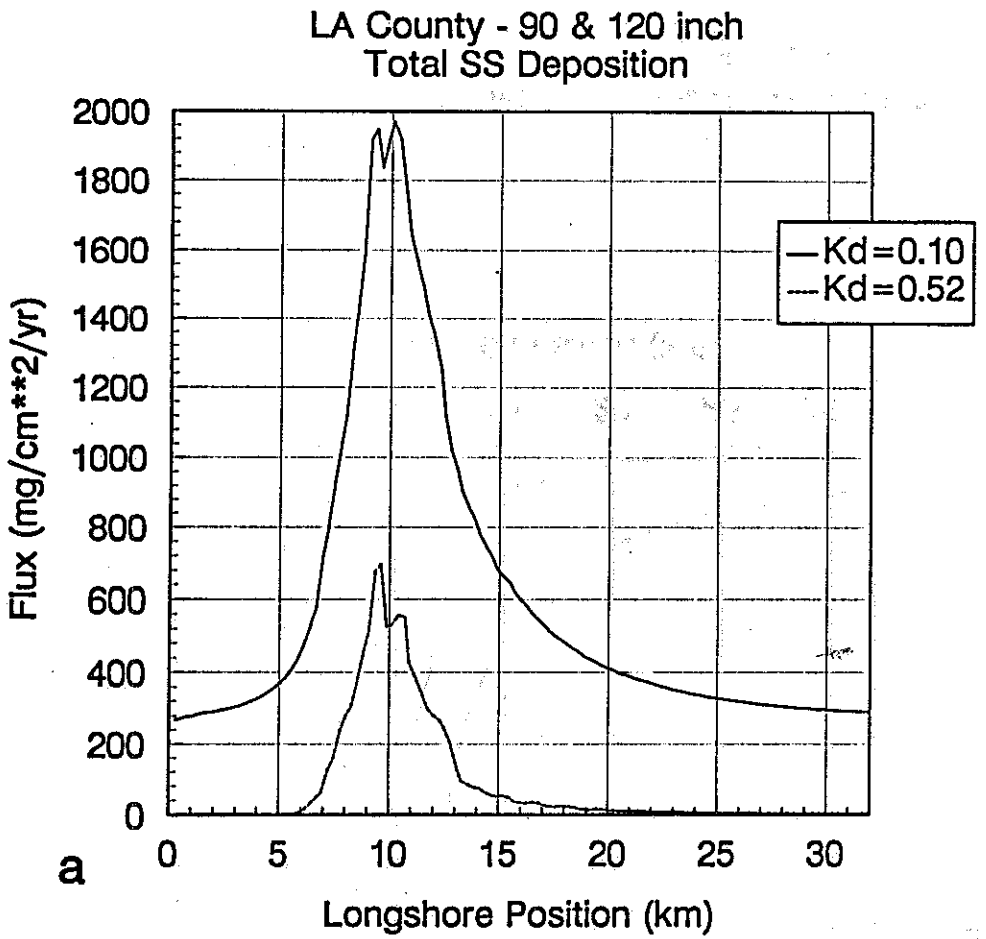

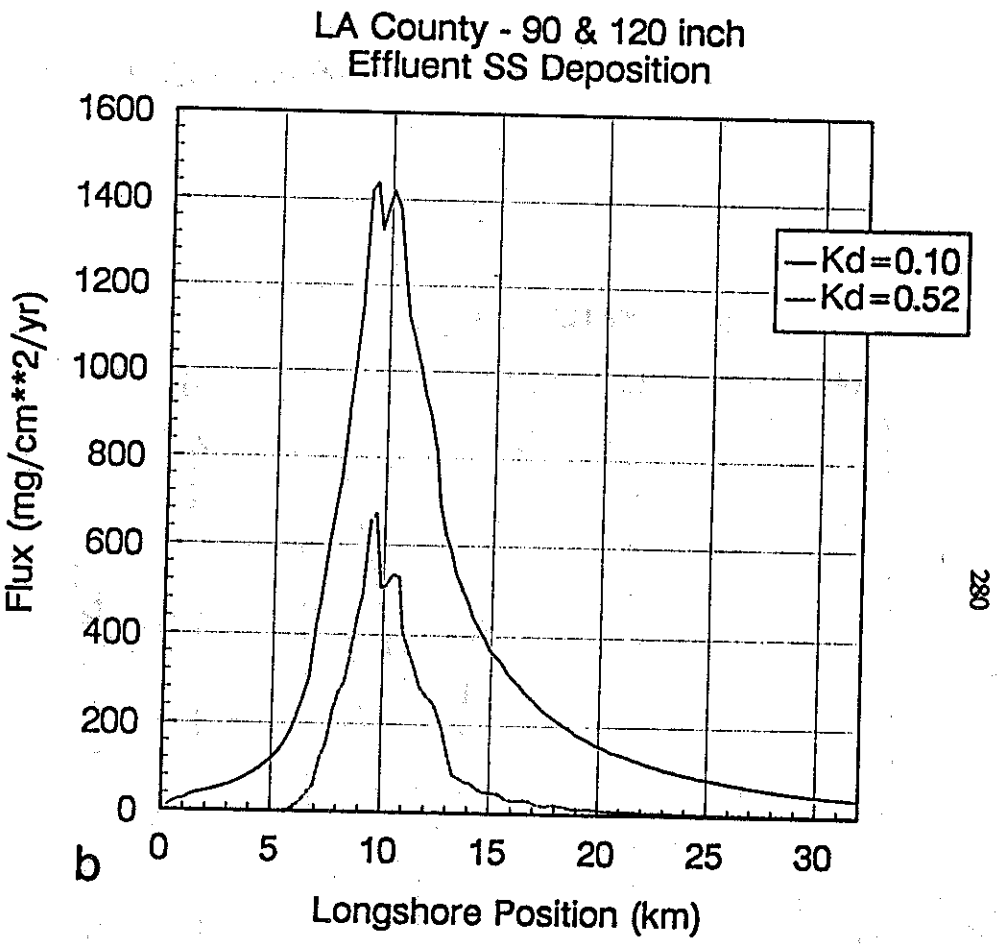

Figure 3.36 - Depositional flux - DECAL, Palos Verdes, 90"+120", 1981, 60m. (a) total suspended solids, (b) effluent suspended solids.

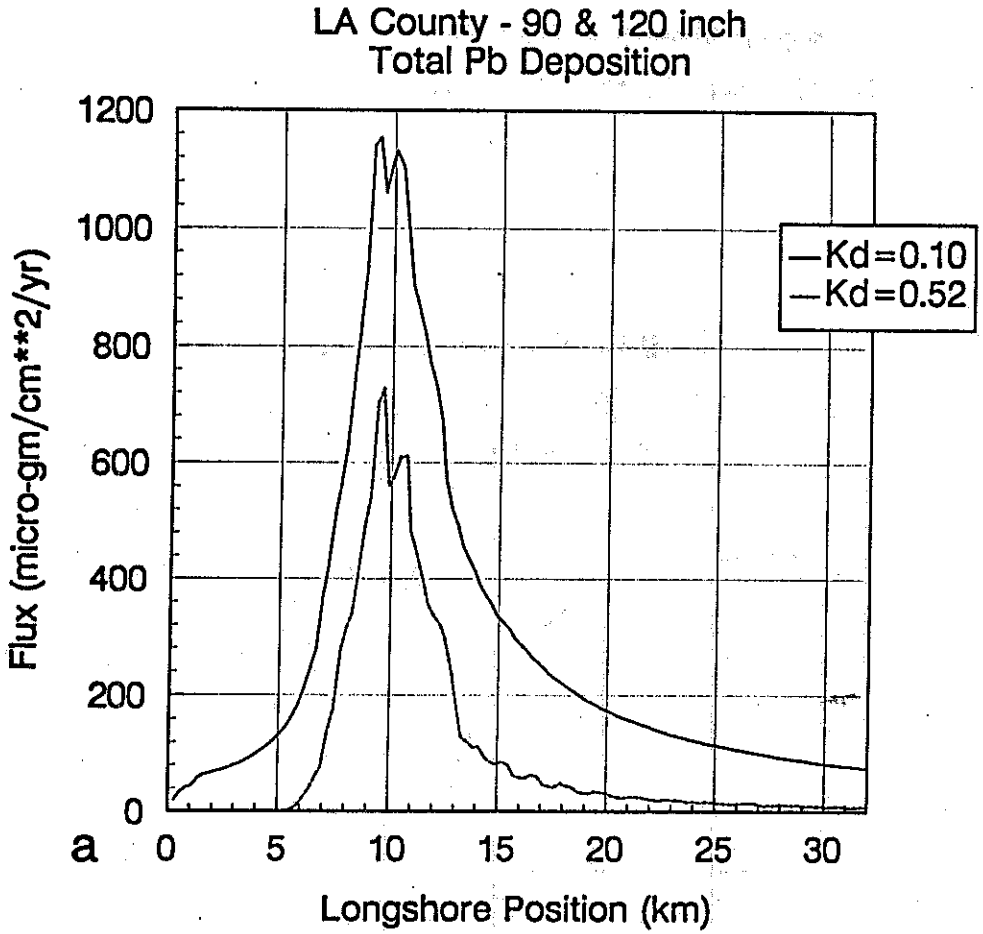

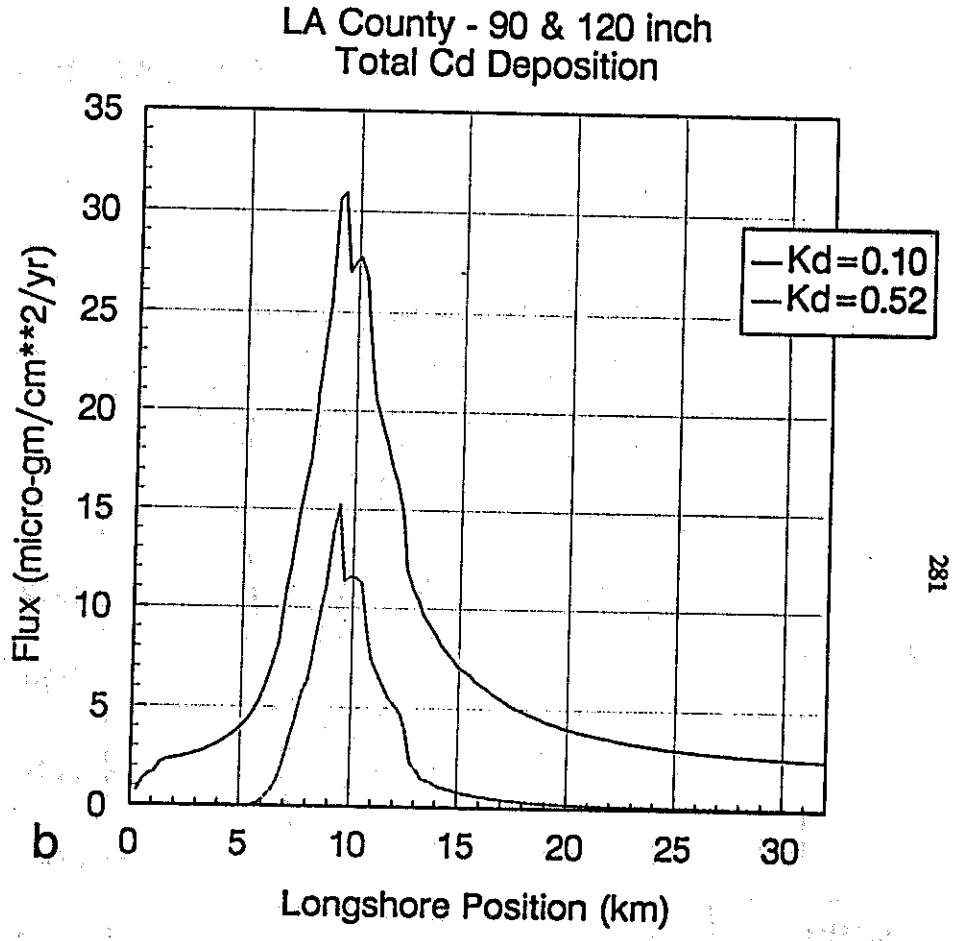

Figure 3.37 - Depositional flux - DECAL, Palos Verdes, 90°+120°, 1981, 60m. (a) lead, (b) cadmium.

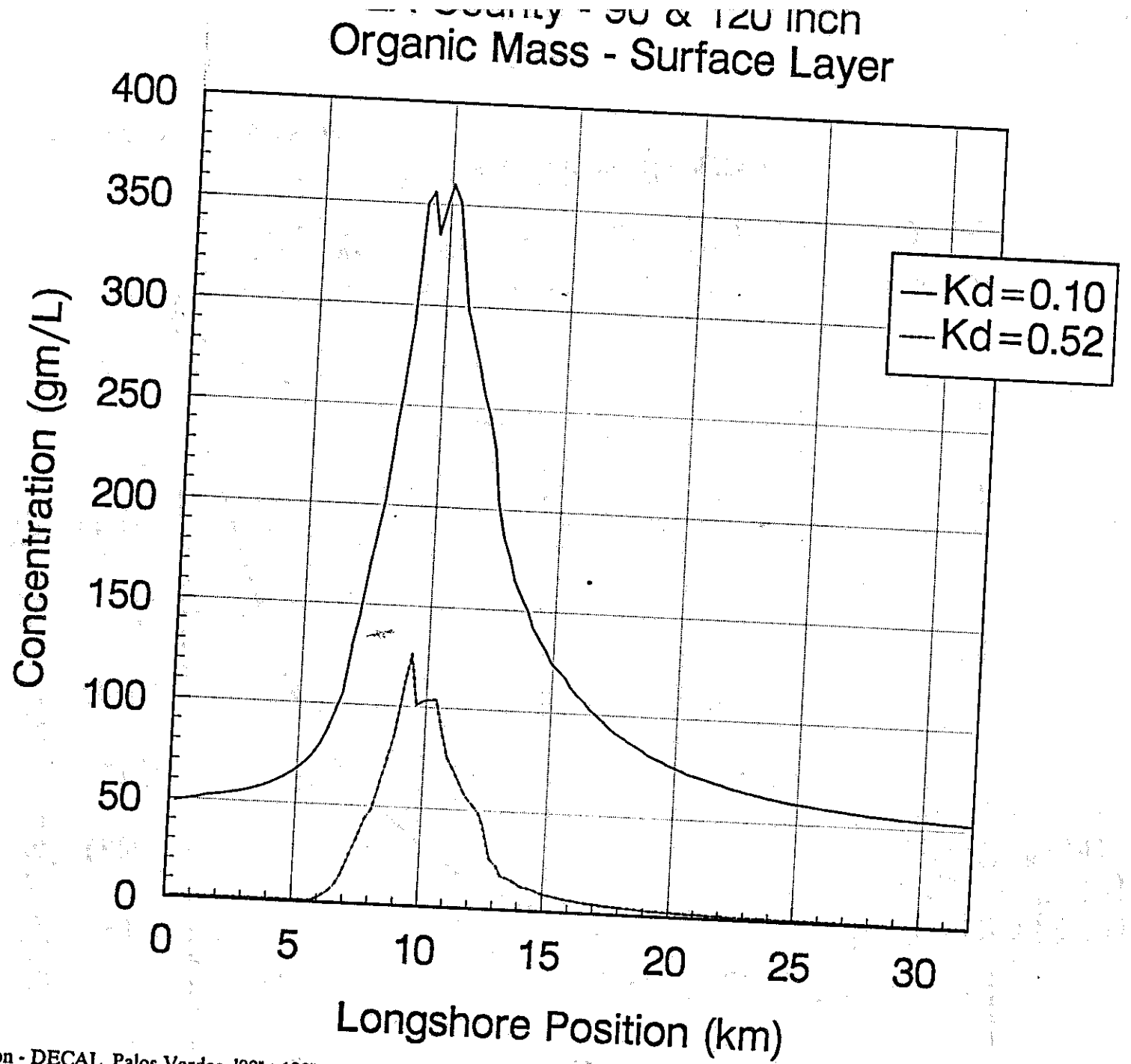

e 3.38 - Organic concentration - DECAL, Palos Verdes, l90"+120", 1981, 60m.

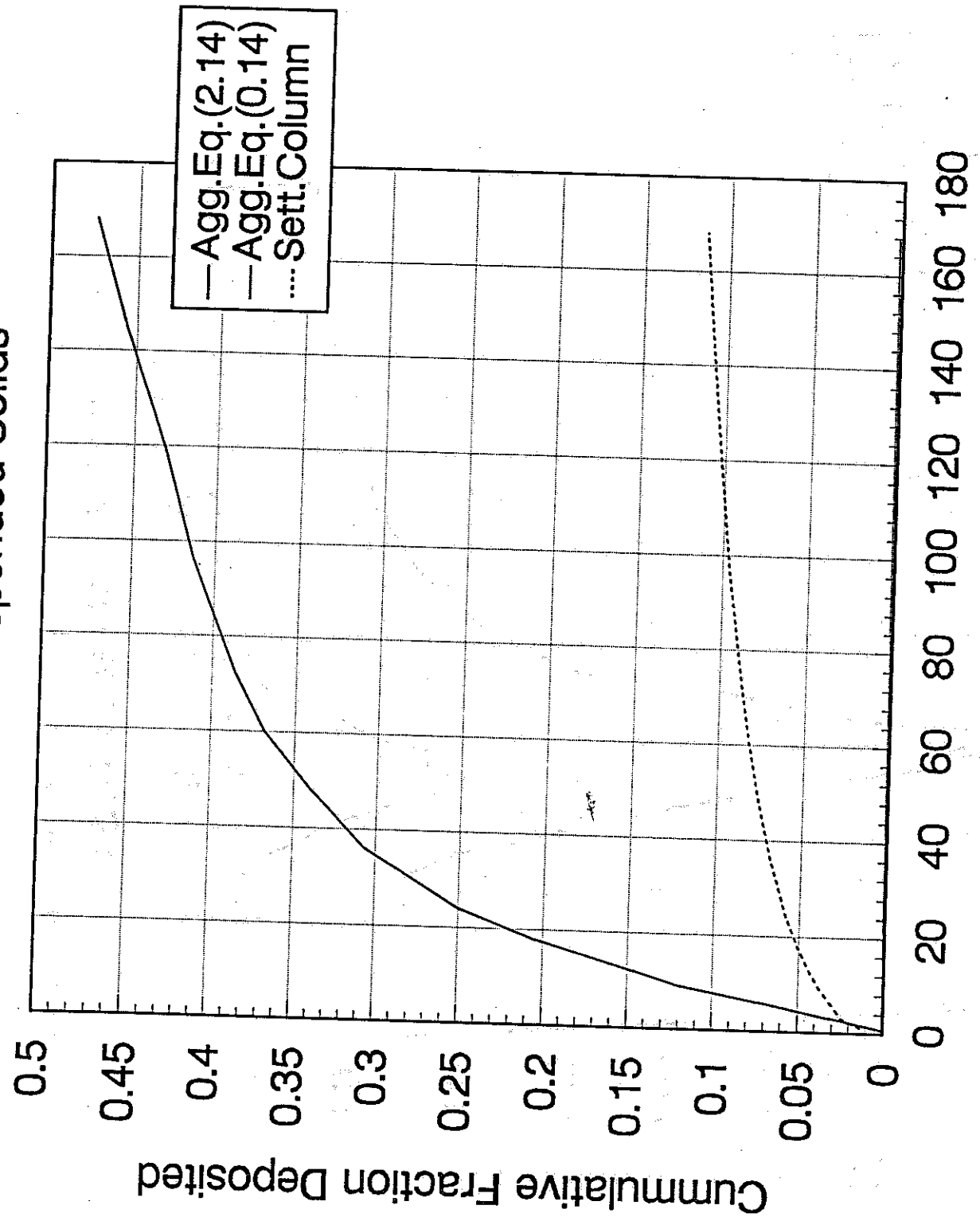

Figure 3.39 - Cummulative deposition - SED2D, San Diego, 1990, 60m.

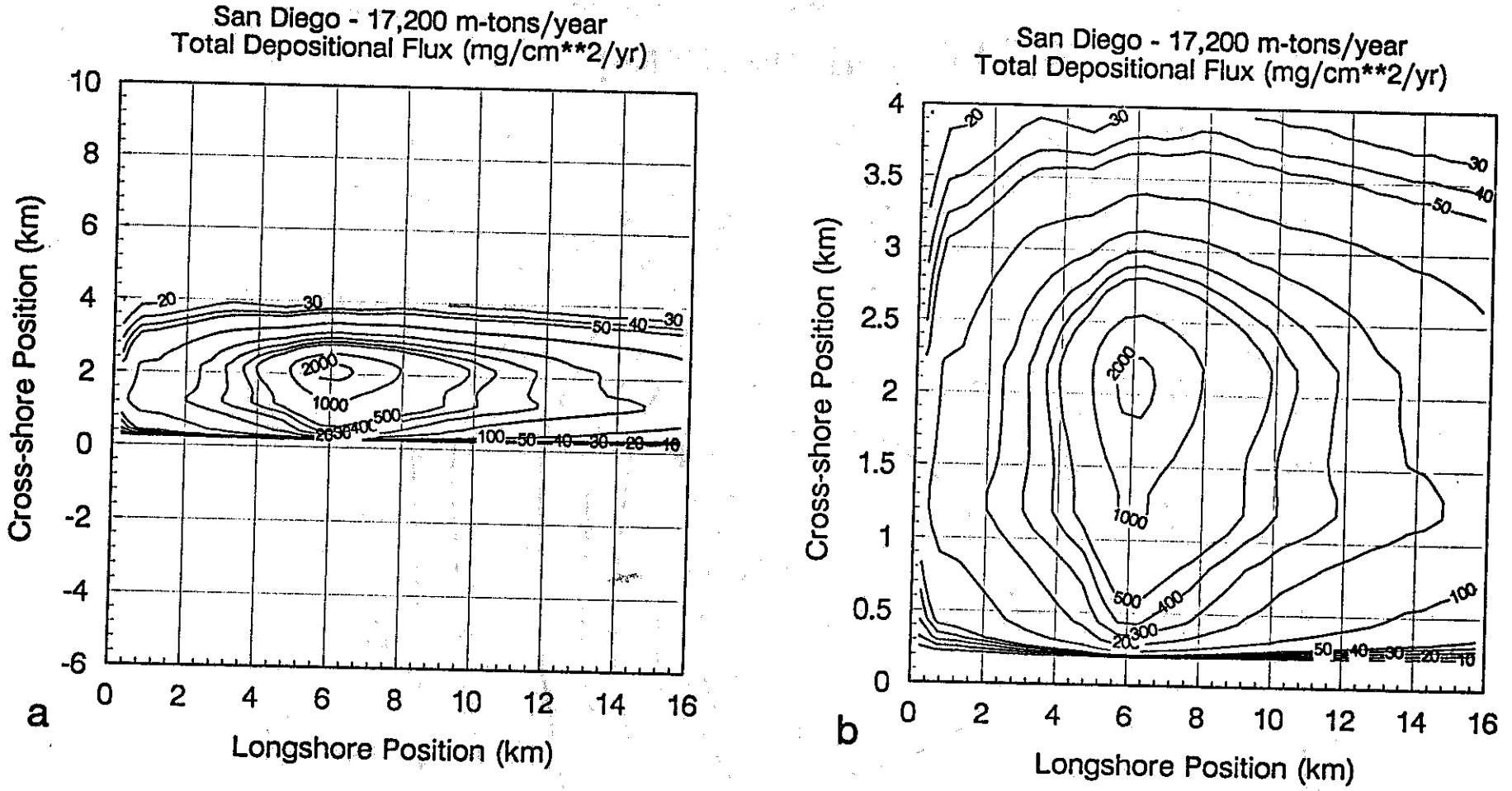

Figure 3.40 - Deposition of aggregate particles - SED2D, no resuspension, San Diego, 1990. (a) undistorted distribution, (b) expanded cross-shore scale.

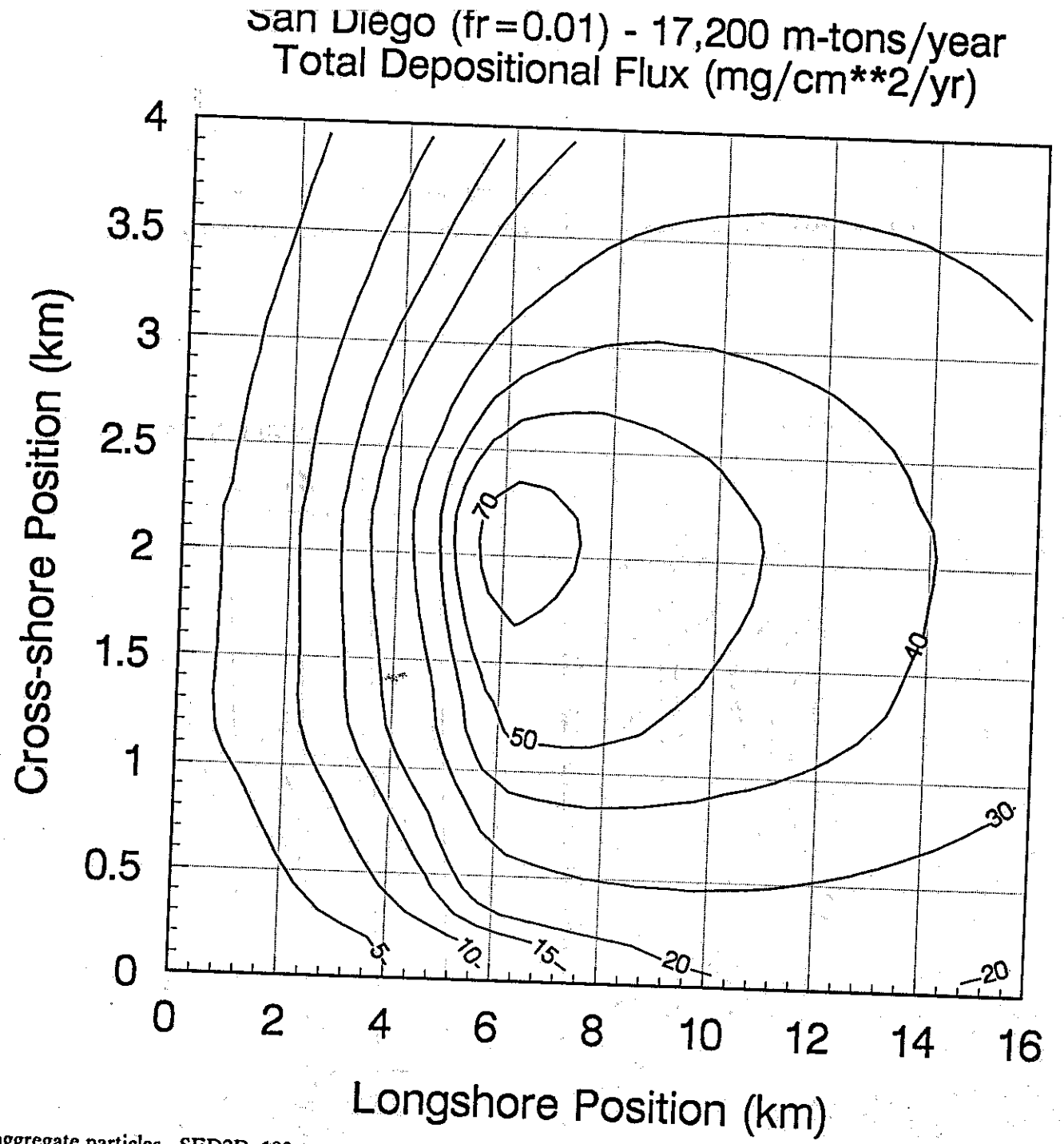

Figure 3.41 - Deposition of aggregate particles - SED2D, 100 resuspensions, San Diego, 1990.

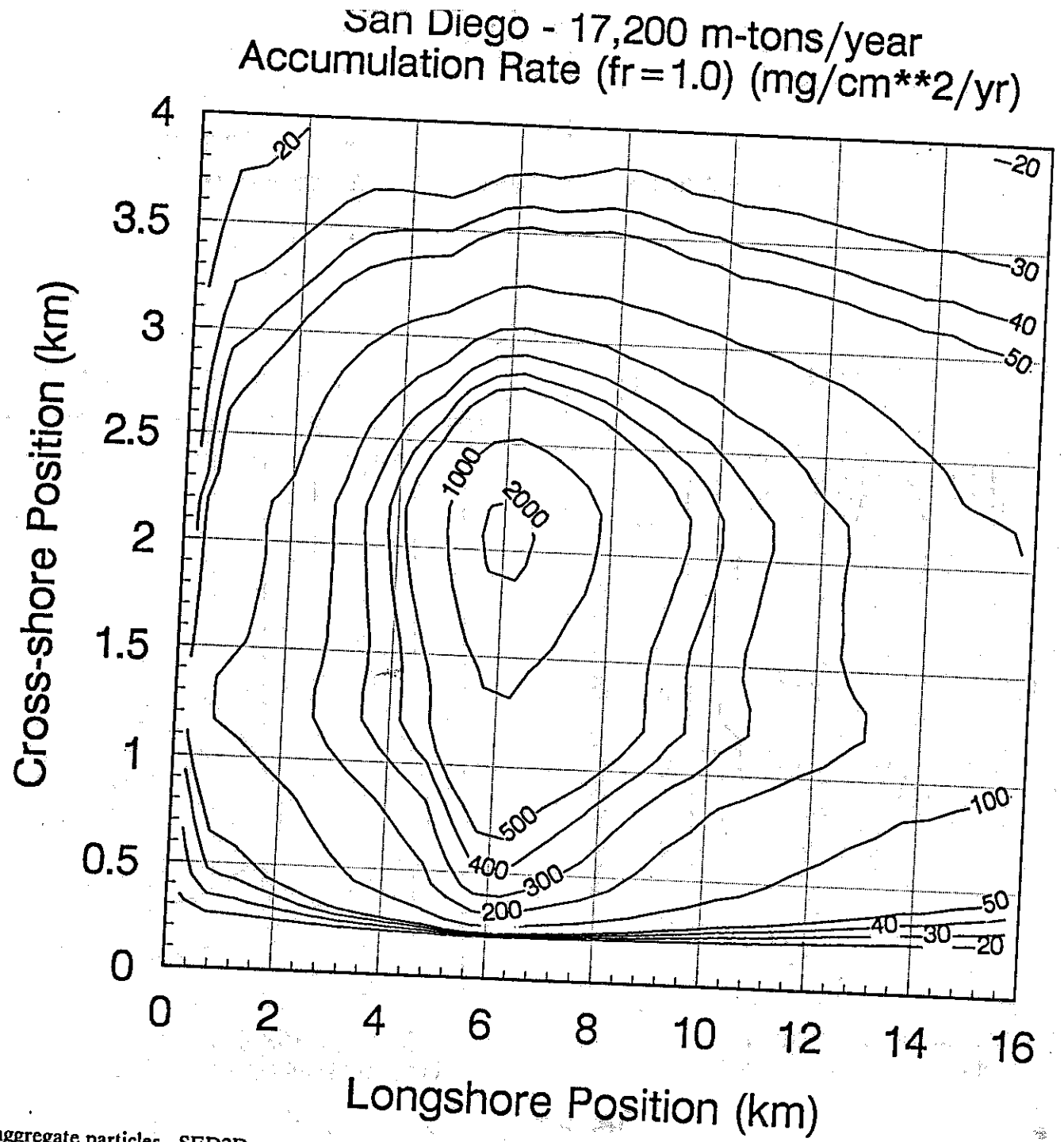

igure 3.42 - Accumulation of aggregate particles - SED2D, no resuspension, San Diego, 1990.

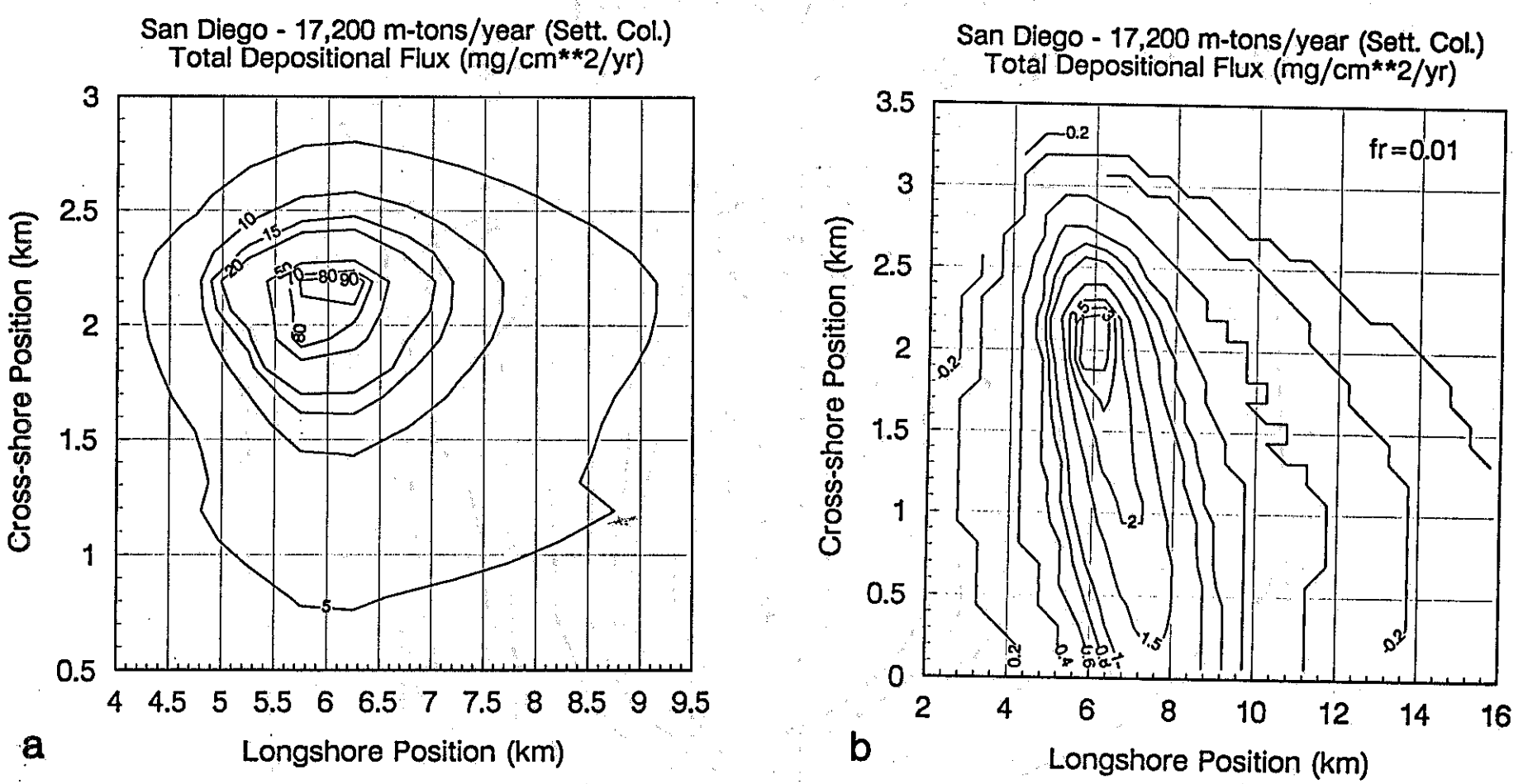

Figure 3.43 - Deposition of aggregate effluent particles - SED2D, San Diego, 1990. (a) no resuspension, (b) 100 resuspensions.

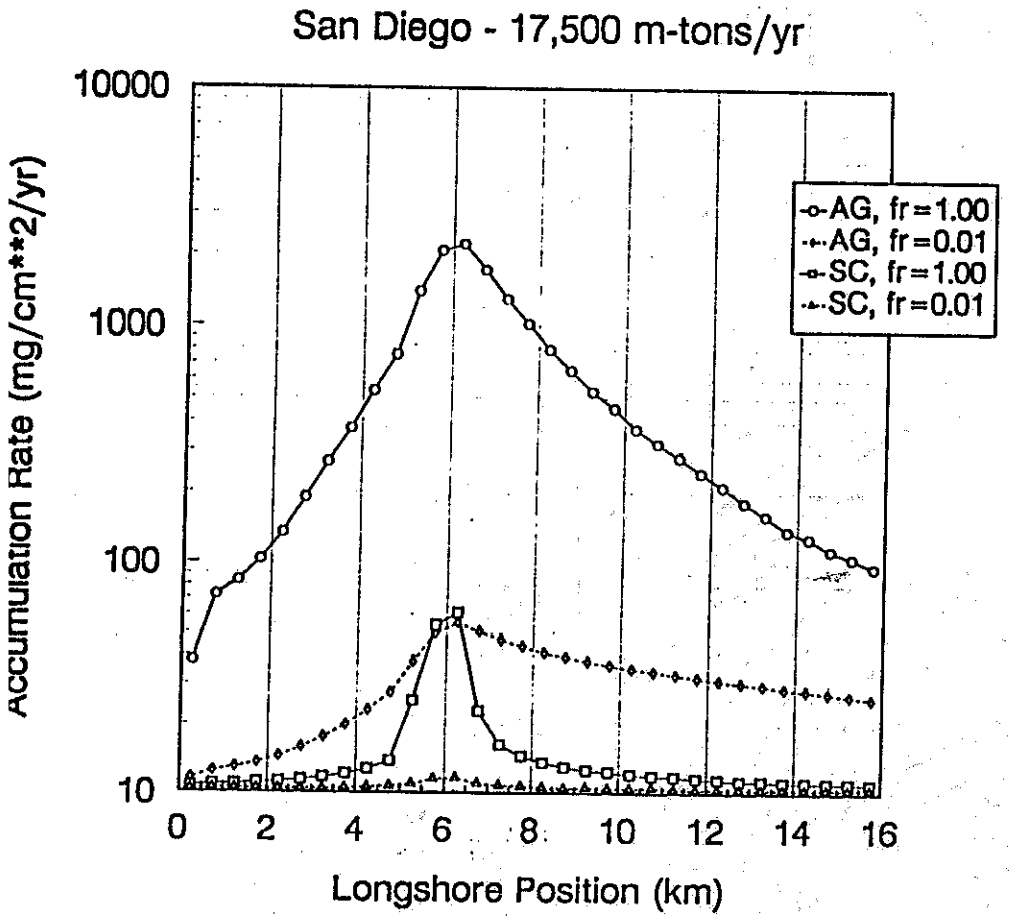

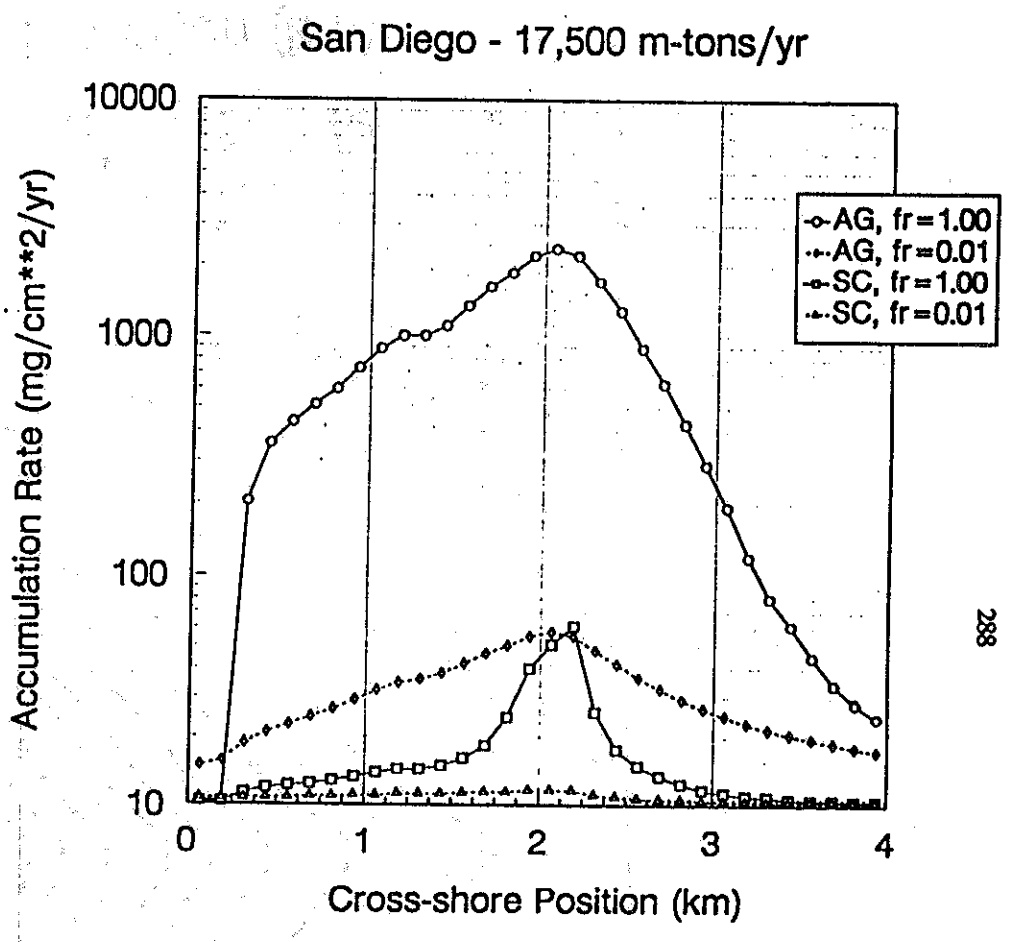

b

Figure 3.44 - Accumulation of total suspended solids - SED2D, San Diego, 1990. (a) longshore transect, (b) cross-shore transect.

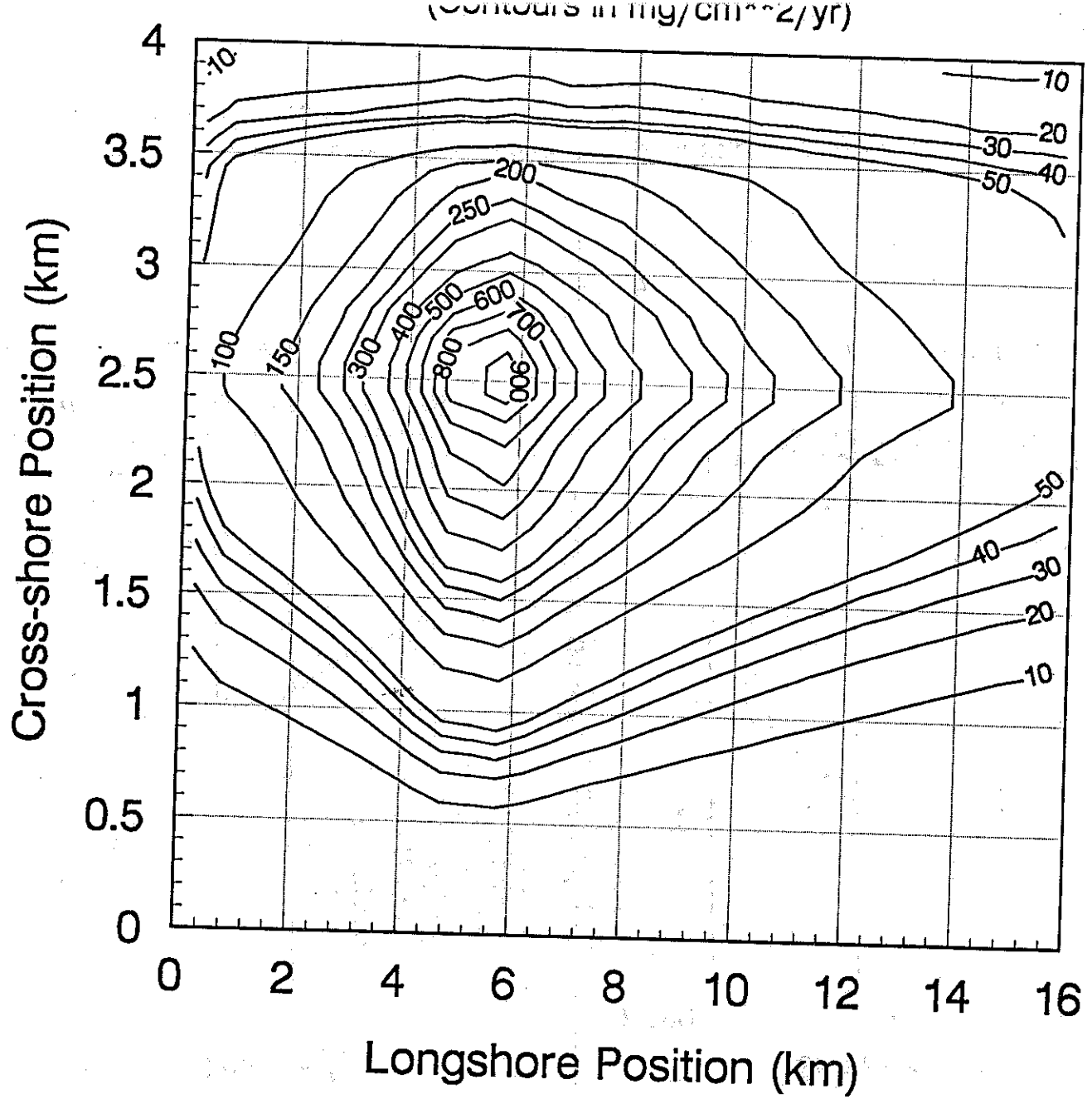

Figure 3.45 - Deposition of aggregate particles - SED2D, no resuspension, Orange County, 1990.

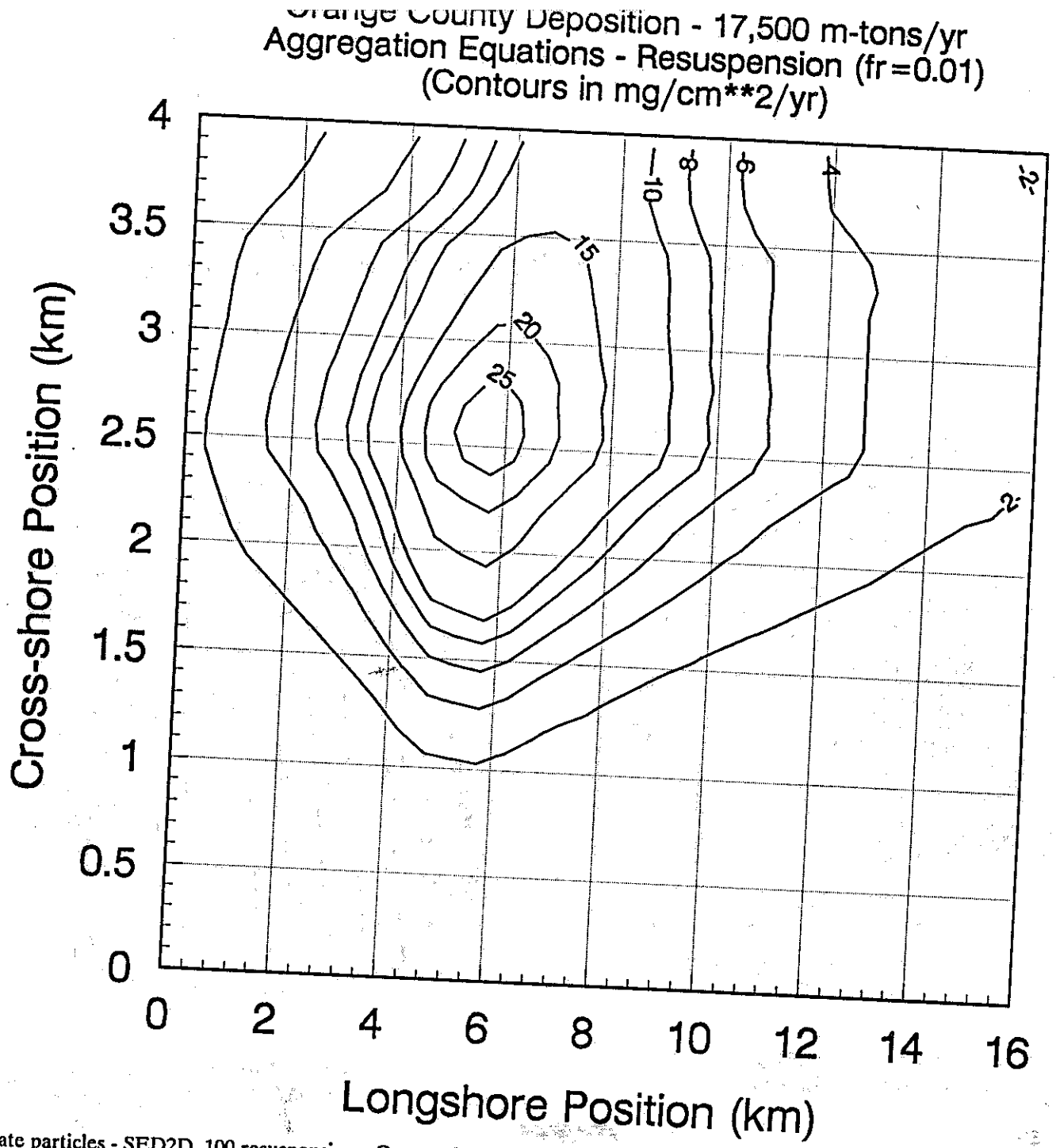

ure 3.46 - Depsoition of aggregate particles - SED2D, 100 resuspensions, Orange County, 1990.

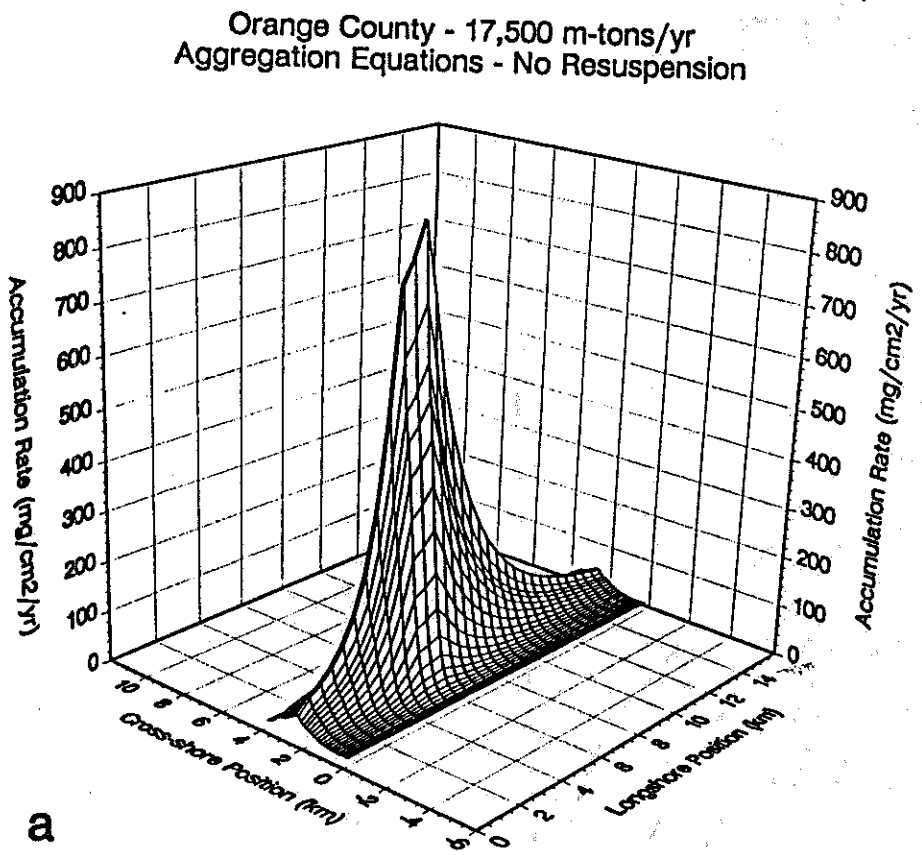

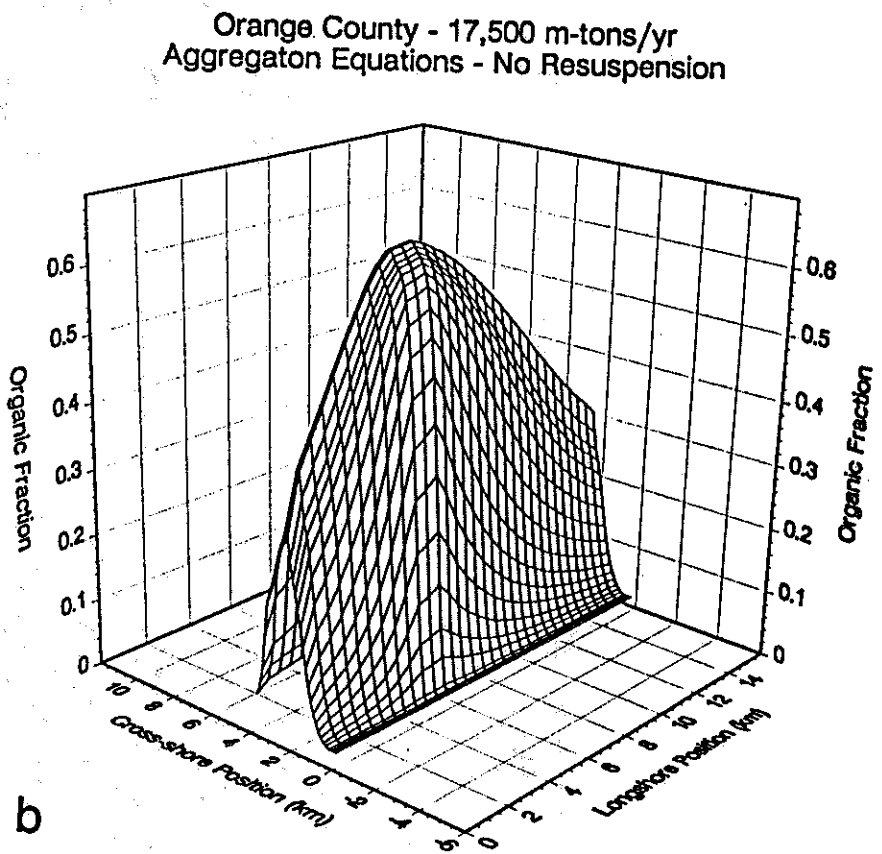

Figure 3.47 - Sediment characteristics - SED2D, no resuspension, Orange County, 1990. (a) accumulation rate, (b) organic fraction.

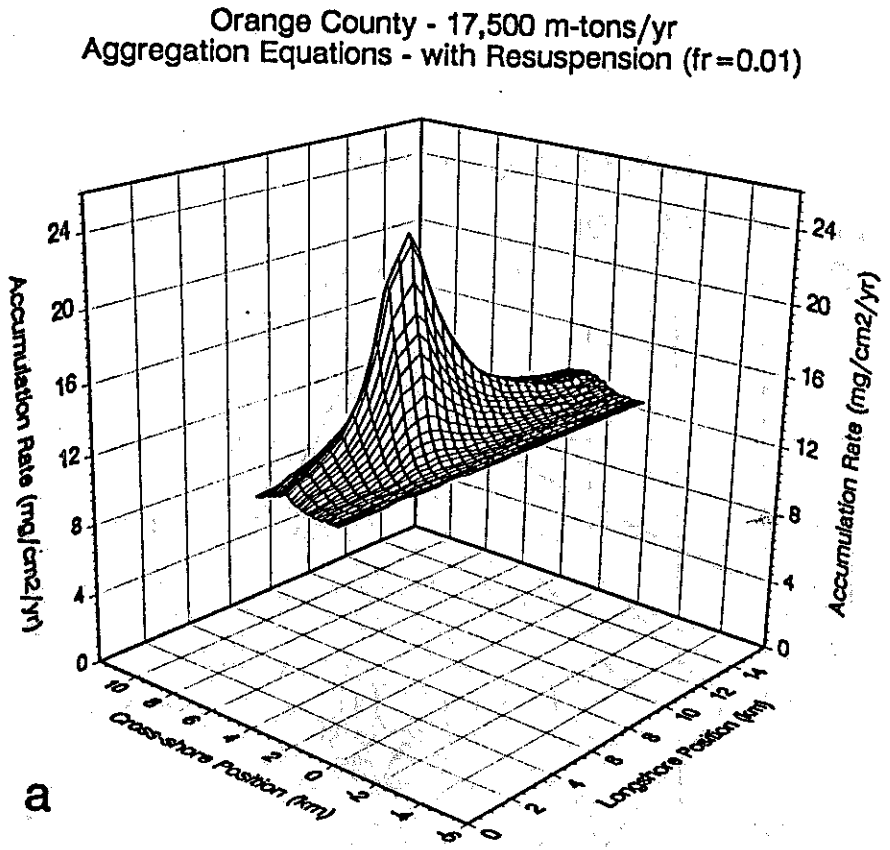

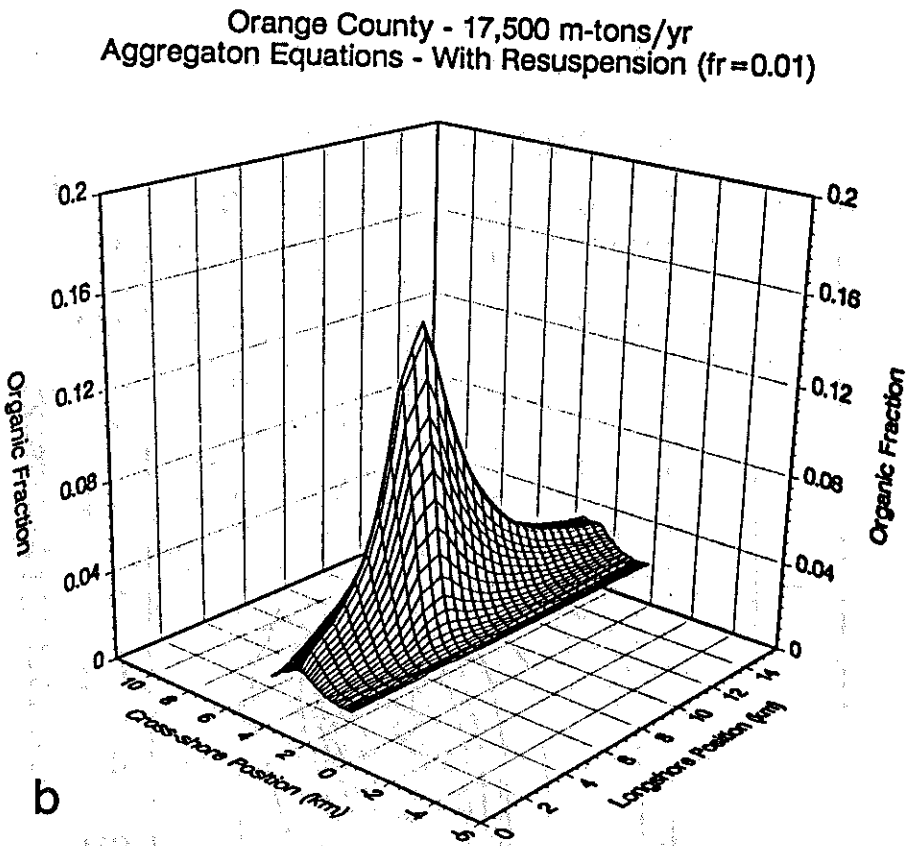

Figure 3.48 - Sediment characteristics - SED2D, 100 resuspensions, Orange County, 1990. (a) accumulation rate, (b) organic fraction.

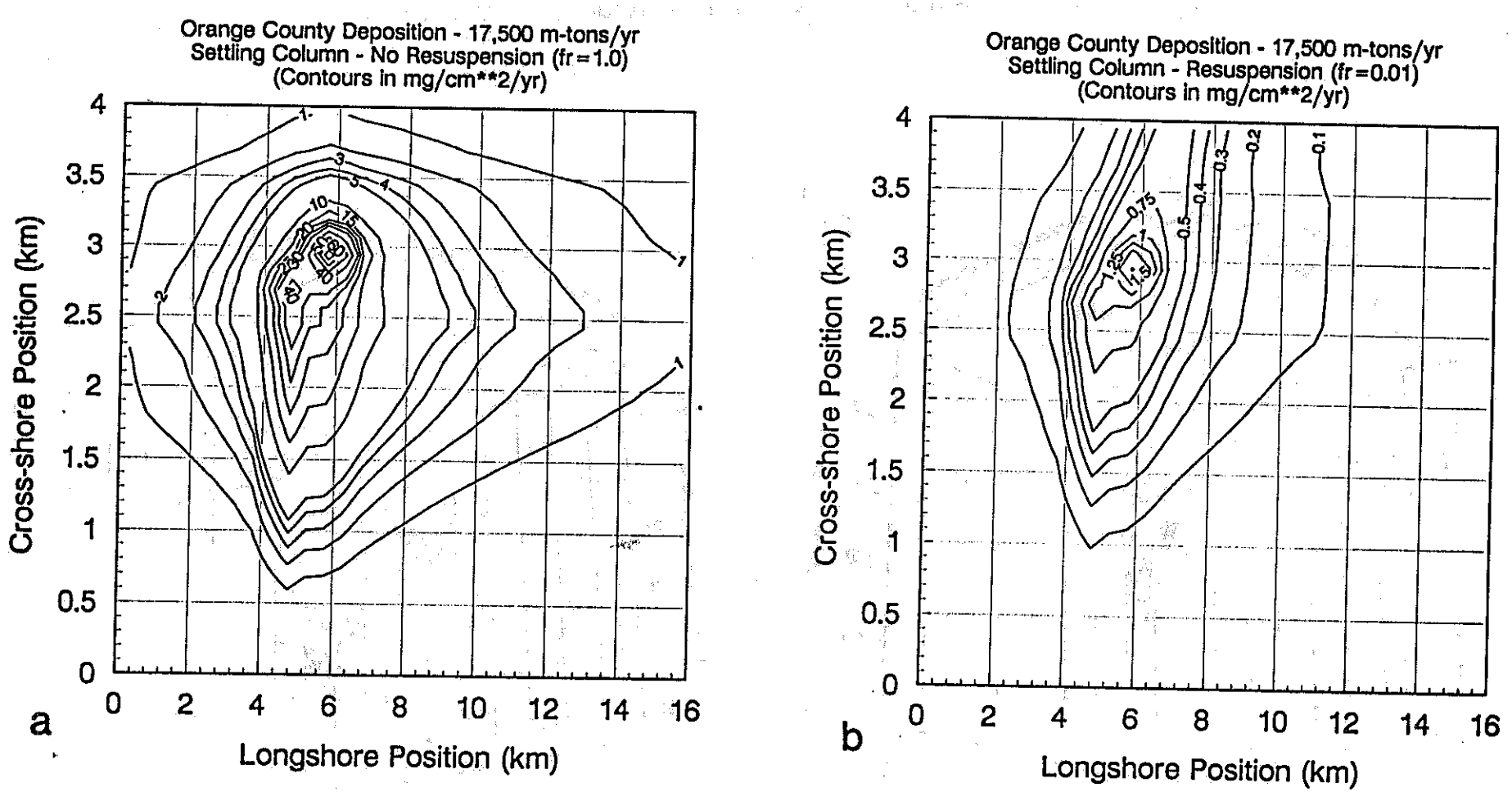

Figure 3.49 - Deposition of non-cohesive effluent particles - SED2D, Orange County, 1990. (a) no resuspension, (b) 100 resuspensions.

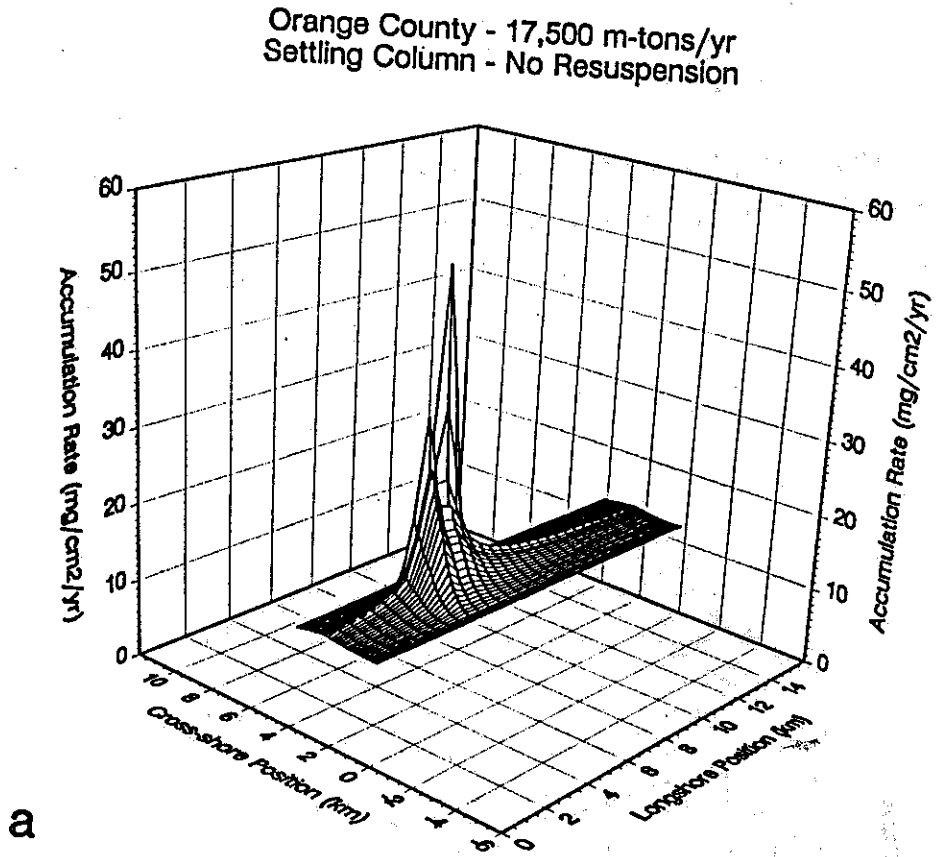

a

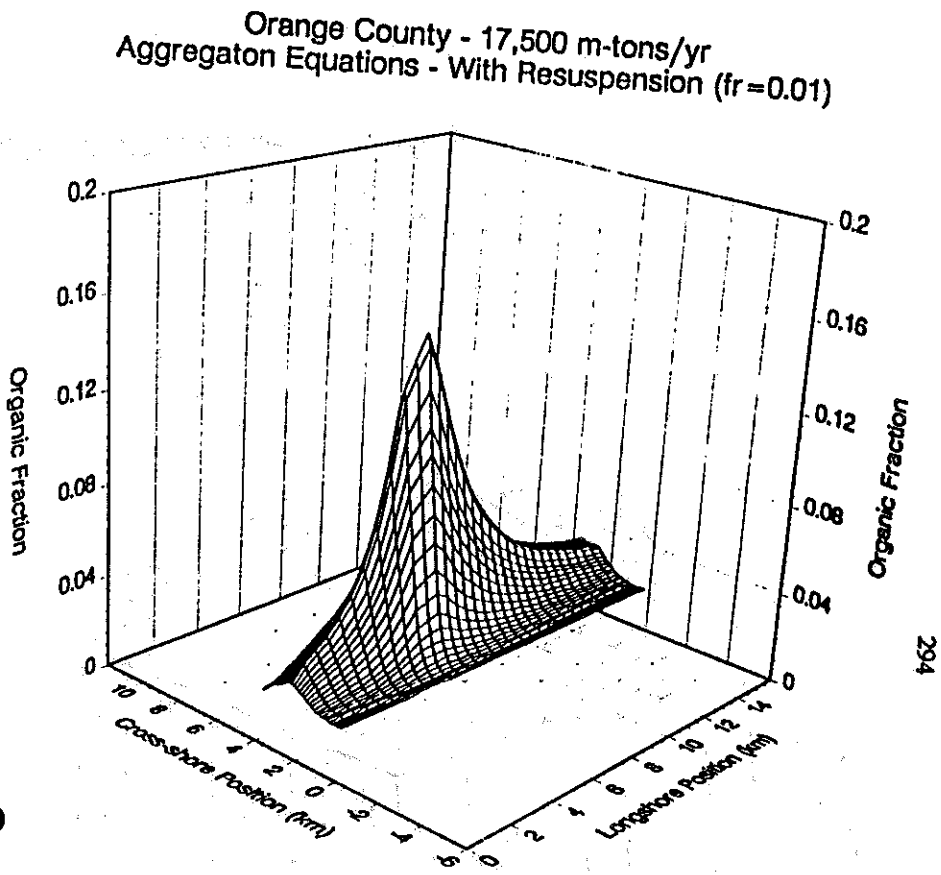

b

Figure 3.50 - Sediment characteristics, noncohesive particles - SED2D, no resuspension, Orange County, 1990. (a) accumulation rate, (b) organic fraction.

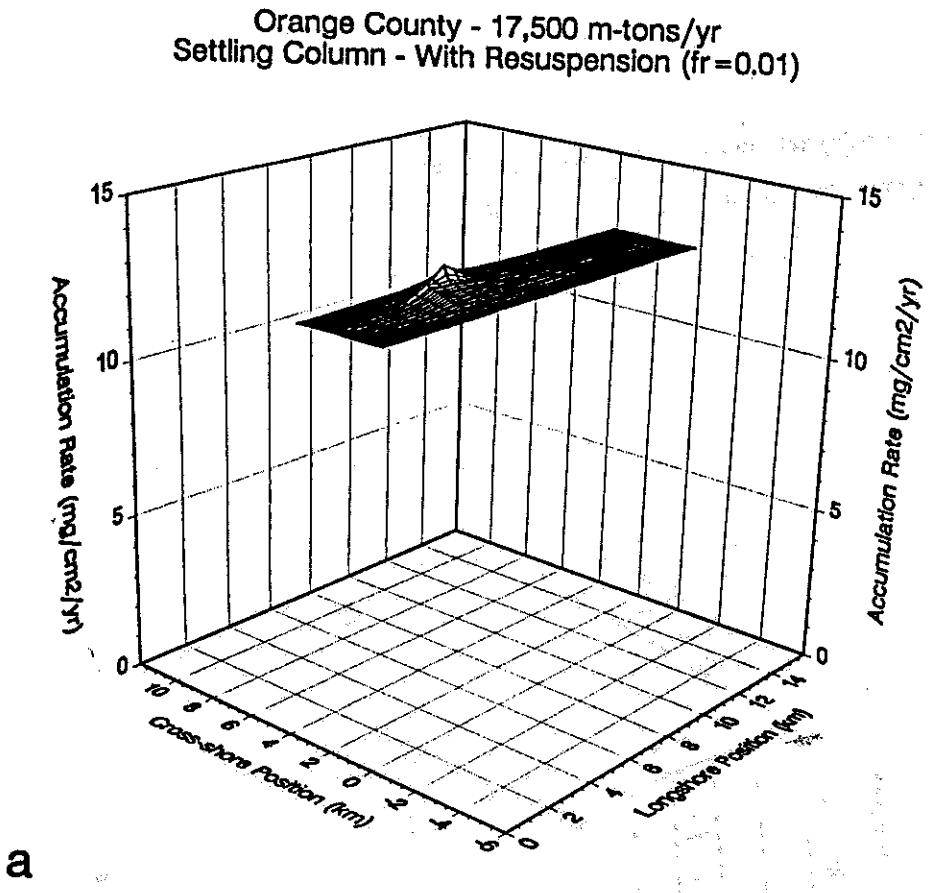

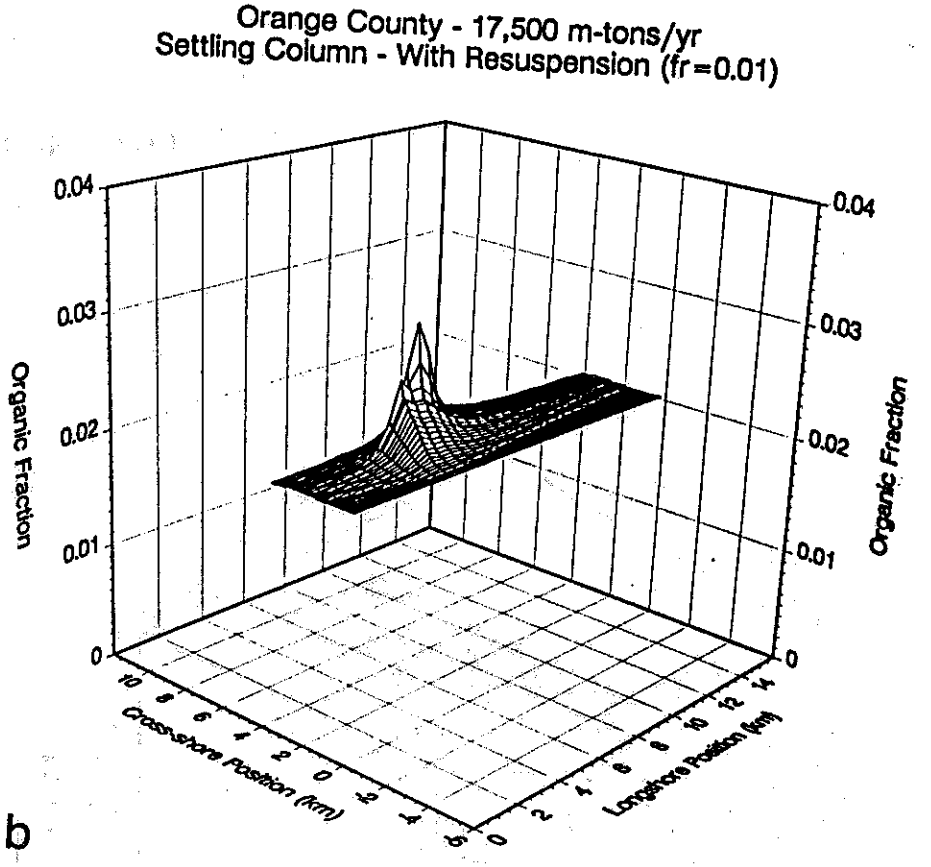

Figure 3.51 - Sediment characteristics, noncohesive particles - SED2D, 100 resuspensions, Orange County, 1990. (a) accumulation rate, (b) organic fraction.

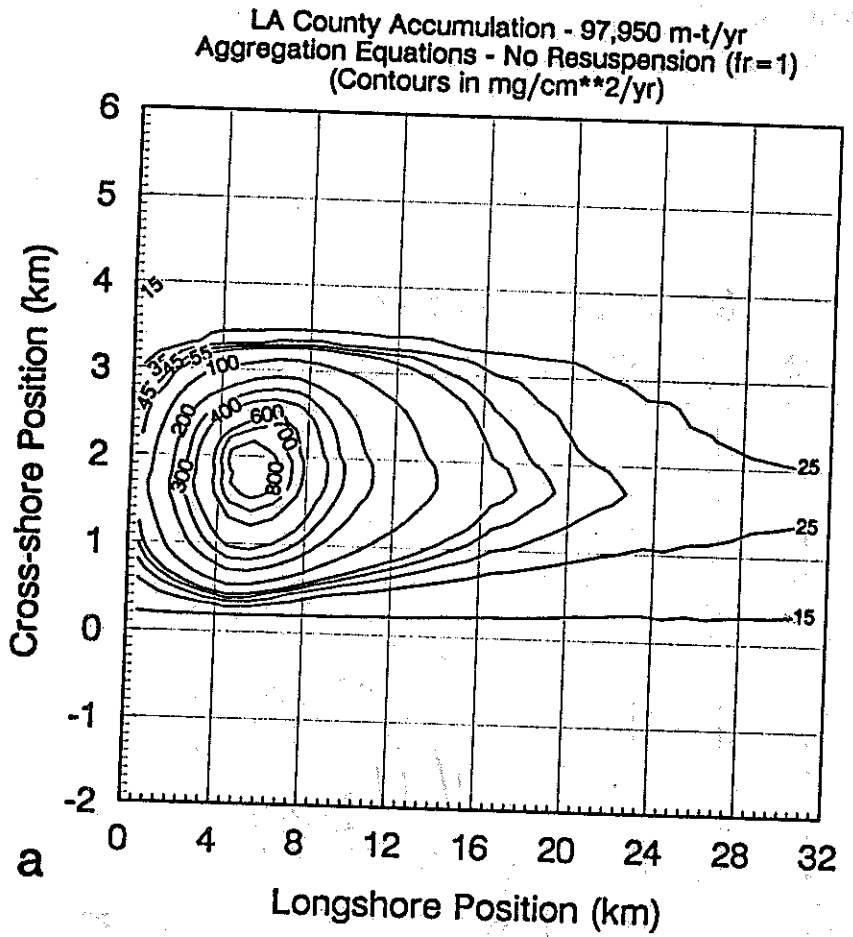

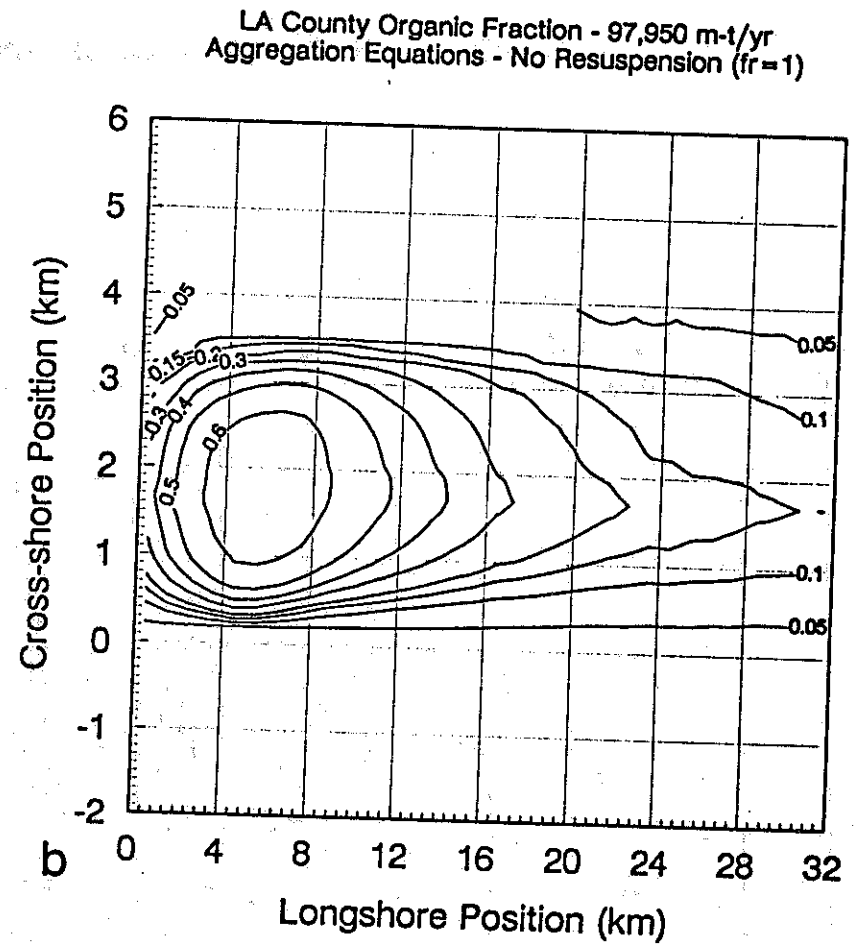

Figure 3.52 - Sediment characteristics, aggregate particles - SED2D, Palos Verdes, no resuspension, 1981. (a) accumulation rate, (b) organic fraction.

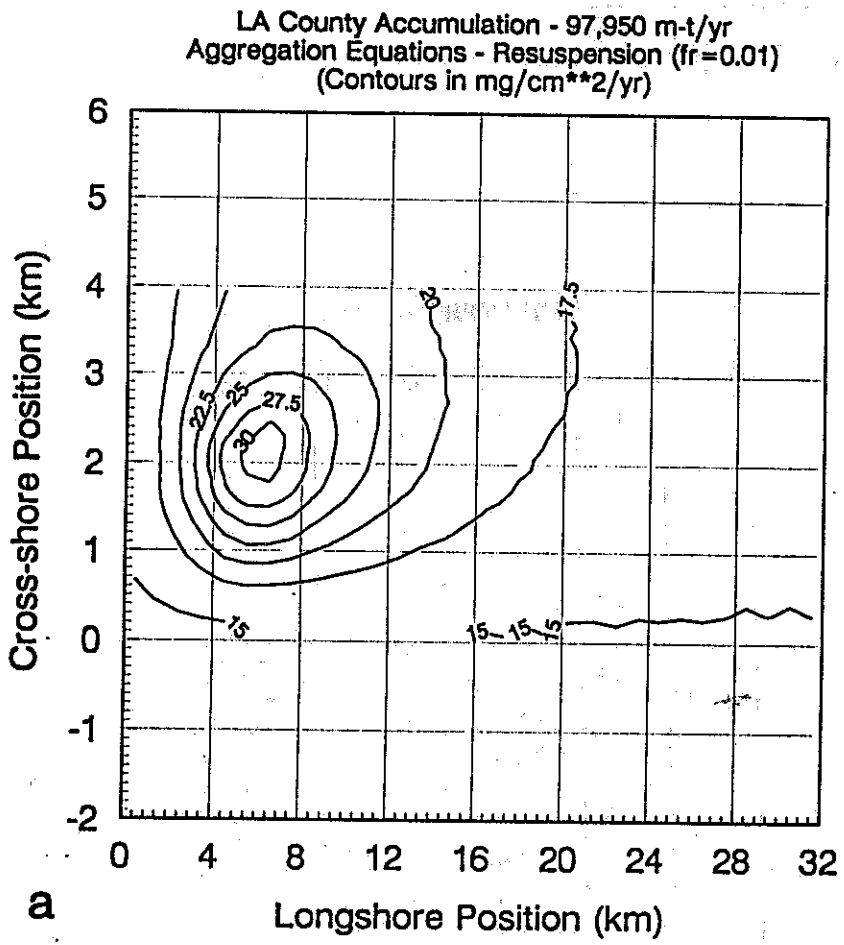

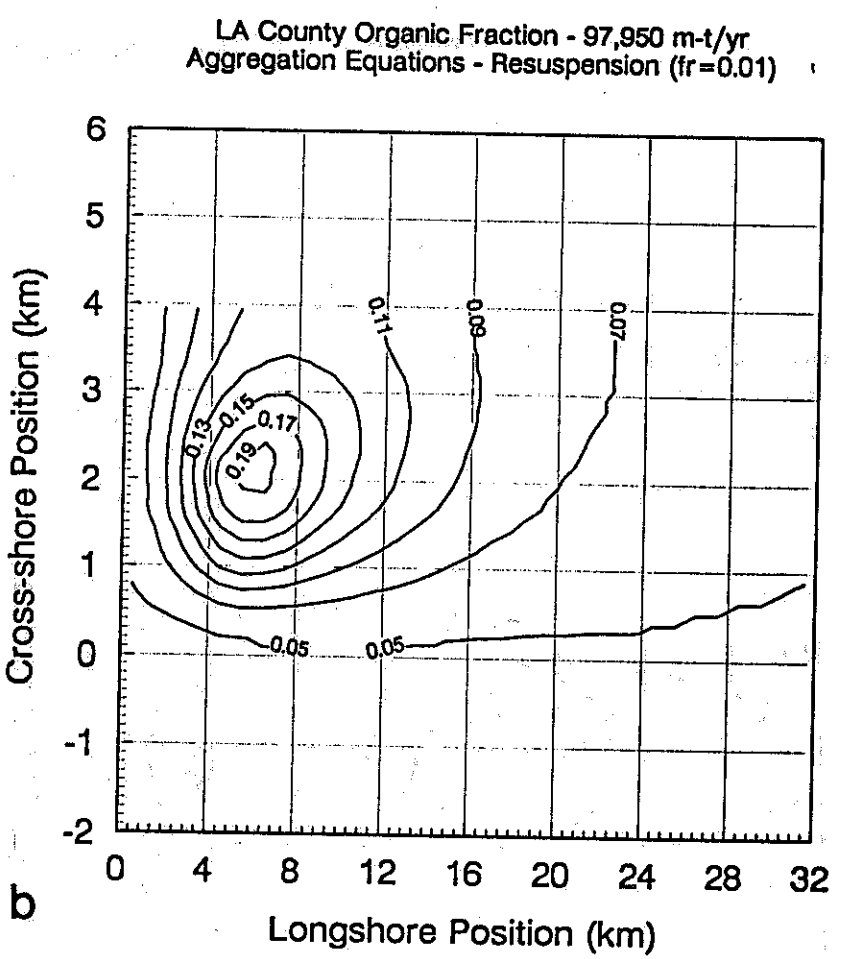

Figure 3.53 - Sediment characteristics, aggregate particles - SED2D, 100 resuspenisons, Palos Verdes, 1981. (a) accumulation rate, (b) organic fraction.

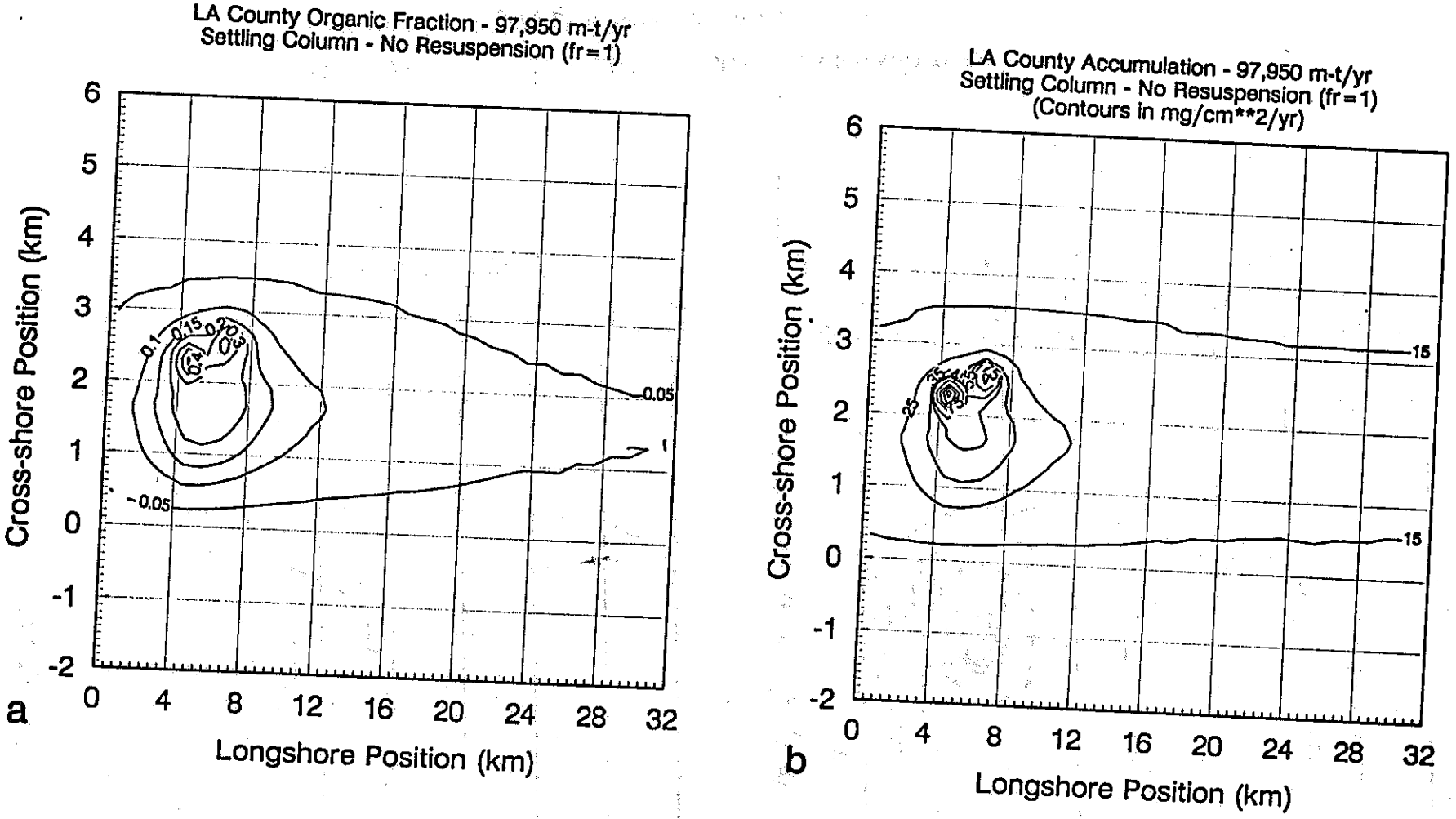

Figure 3.54 - Sediment characteristics, noncohesive particles - SED2D, no resuspension, Palos Verdes, 1981. (a) organic fraction, (b) accumulation rate.

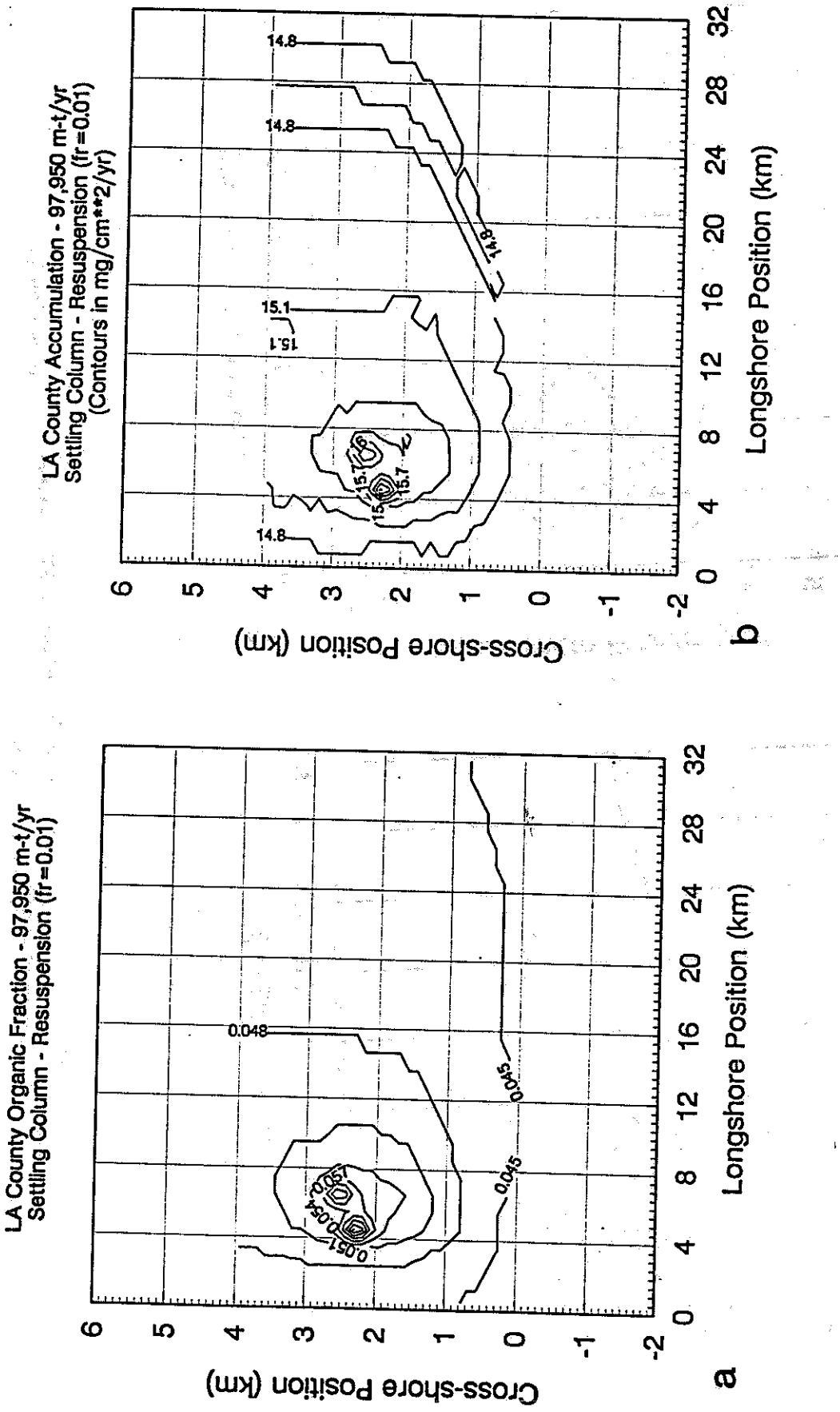

Figure 3.55 - Sediment characteristics, noncohesive particles - SED2D, Palos Verdes, 100 resuspensions, 1981. (a) organic fraction, (b) accumulation rate.

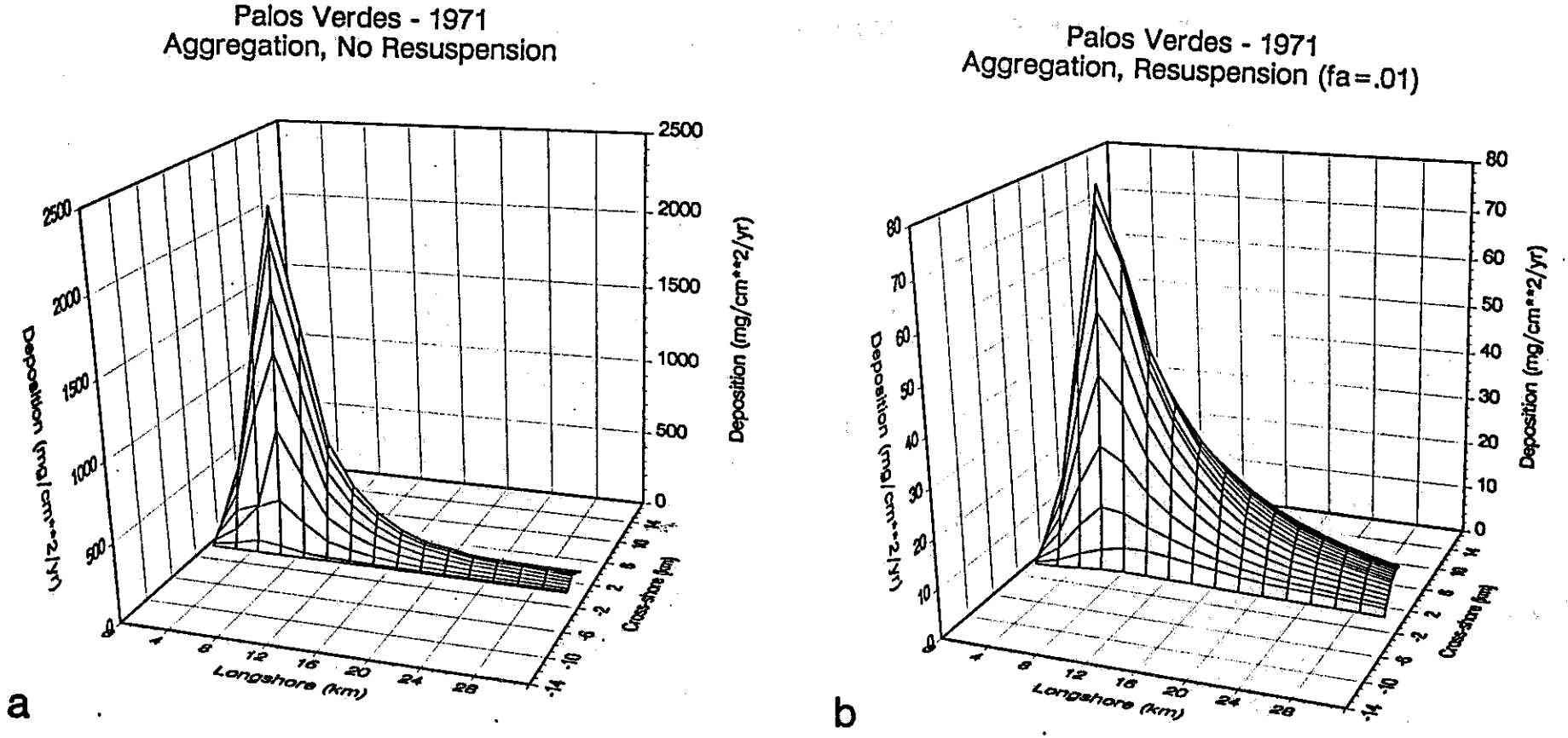

Figure 3.56 - Depositional fluxes, aggregate particles - SED2D, Palos Verdes, 1971. (a) no resuspension, (b) 100 resuspensions.

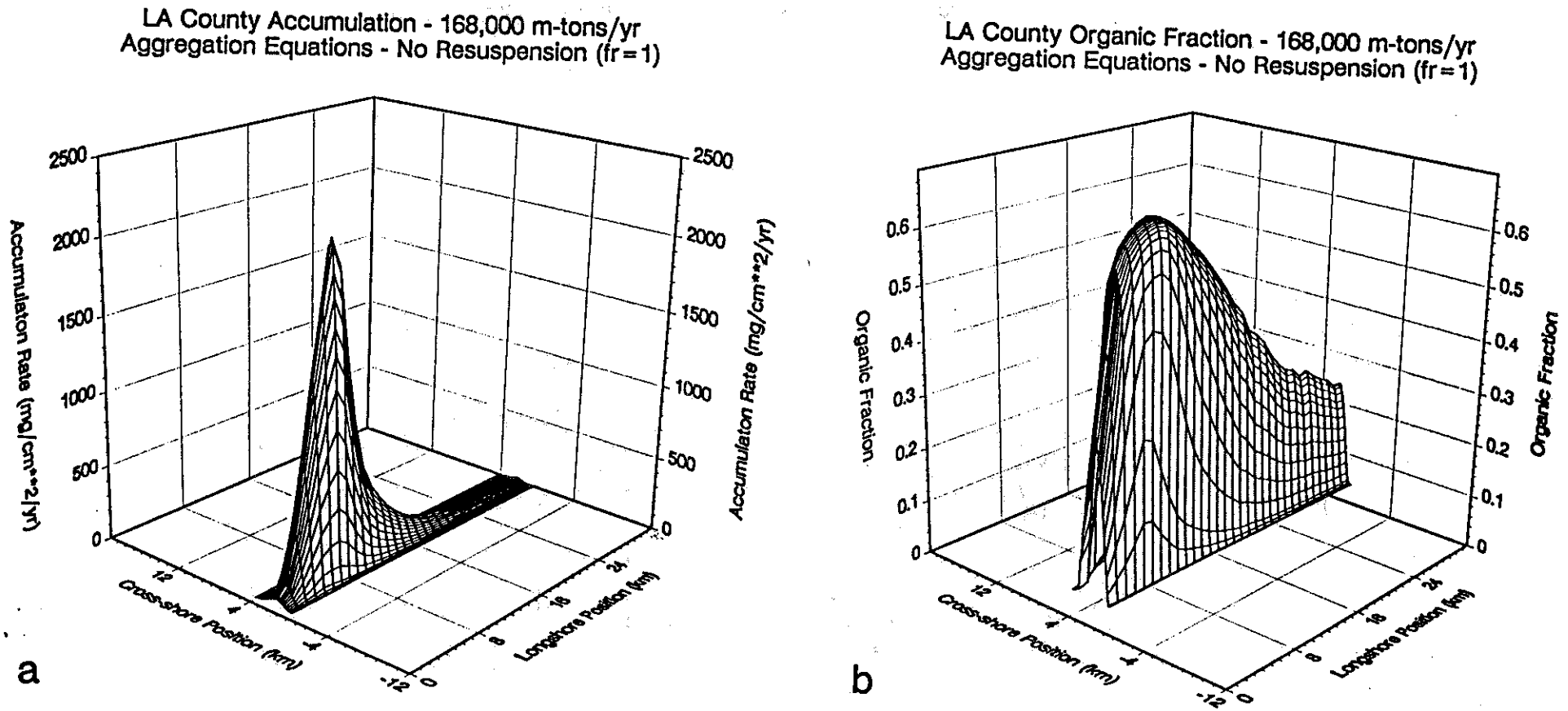

Figure 3.57 - Sediment properties, aggregate particles - SED2D, Palos Verdes, no resuspension, 1971.
(a) accumulation rate, (b) organic concentration.

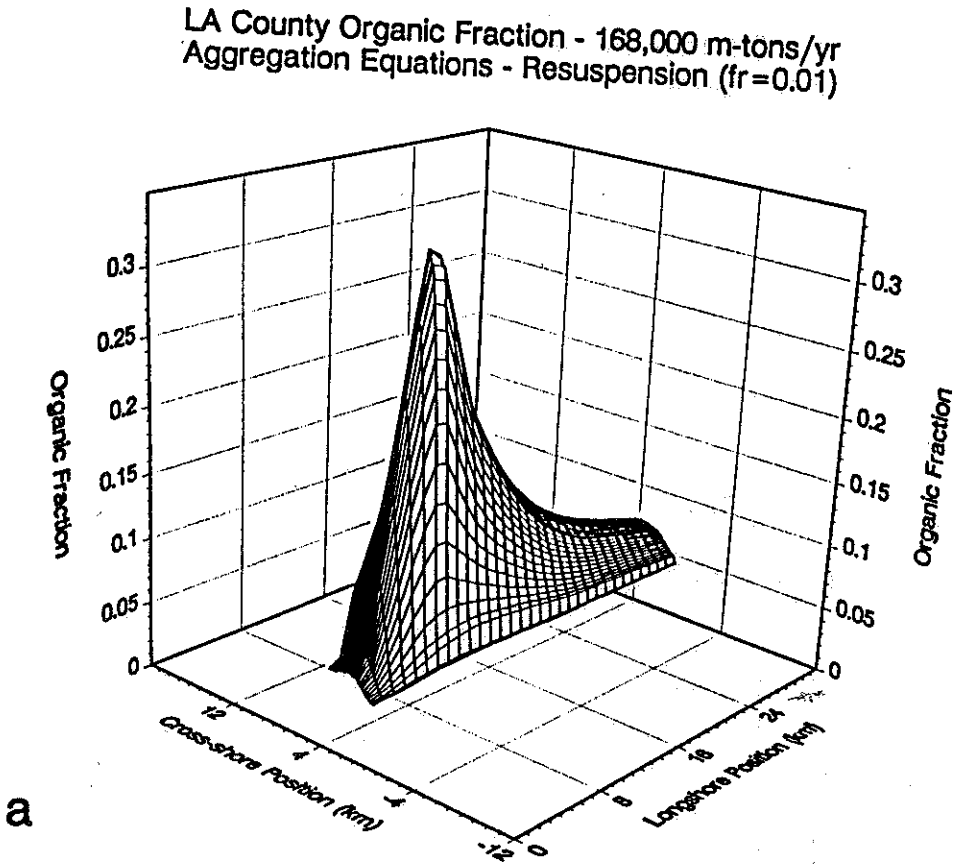

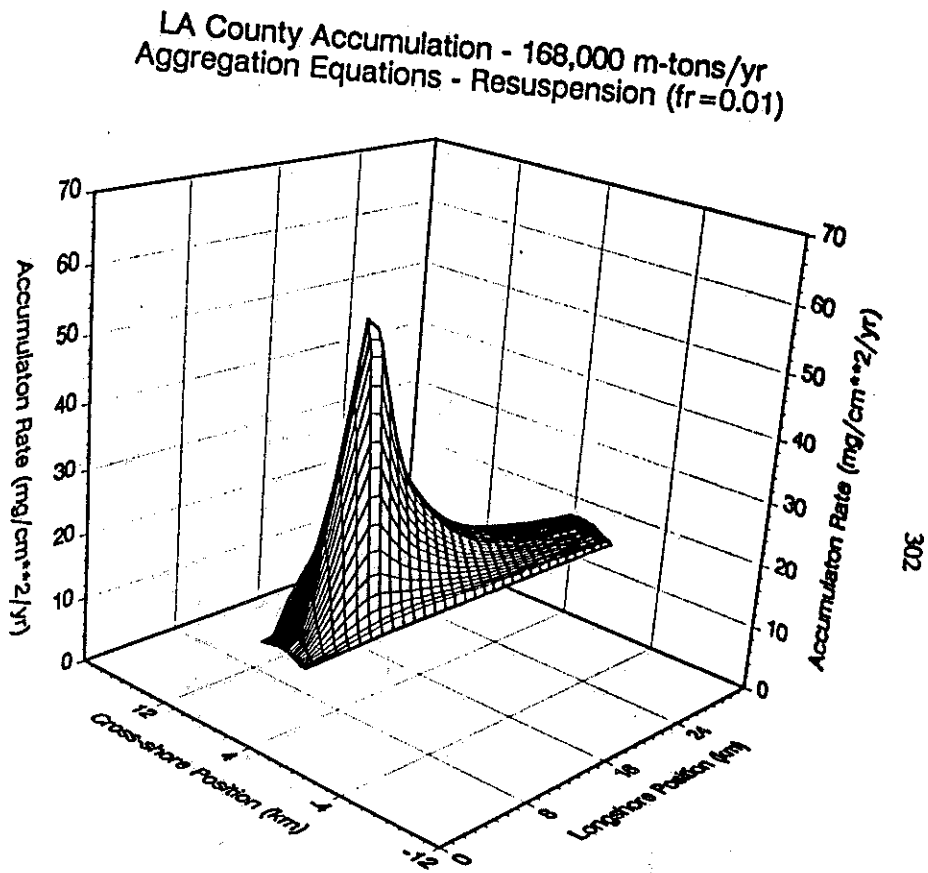

Figure 3.58 - Sediment properties, aggregate particles - SED2D, Palos Verdes, 100 resuspensions, 1971.
(a) organic fraction, (b) accumulation rate.

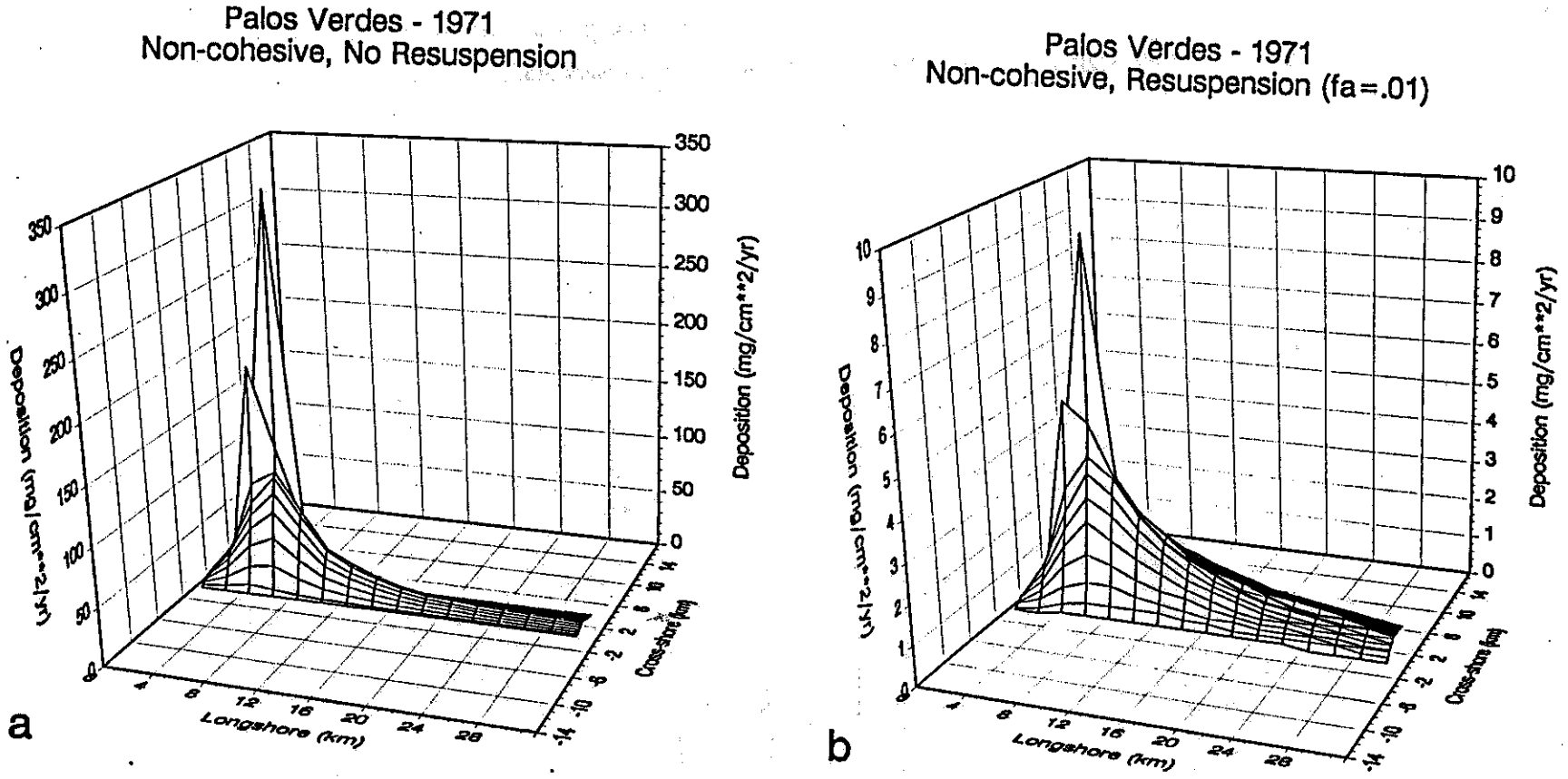

Figure 3.59 - Depositional fluxes, noncohesive particles - SED2D, Palos Verdes, 1971. (a) no resuspension, (b) 100 resuspensions.

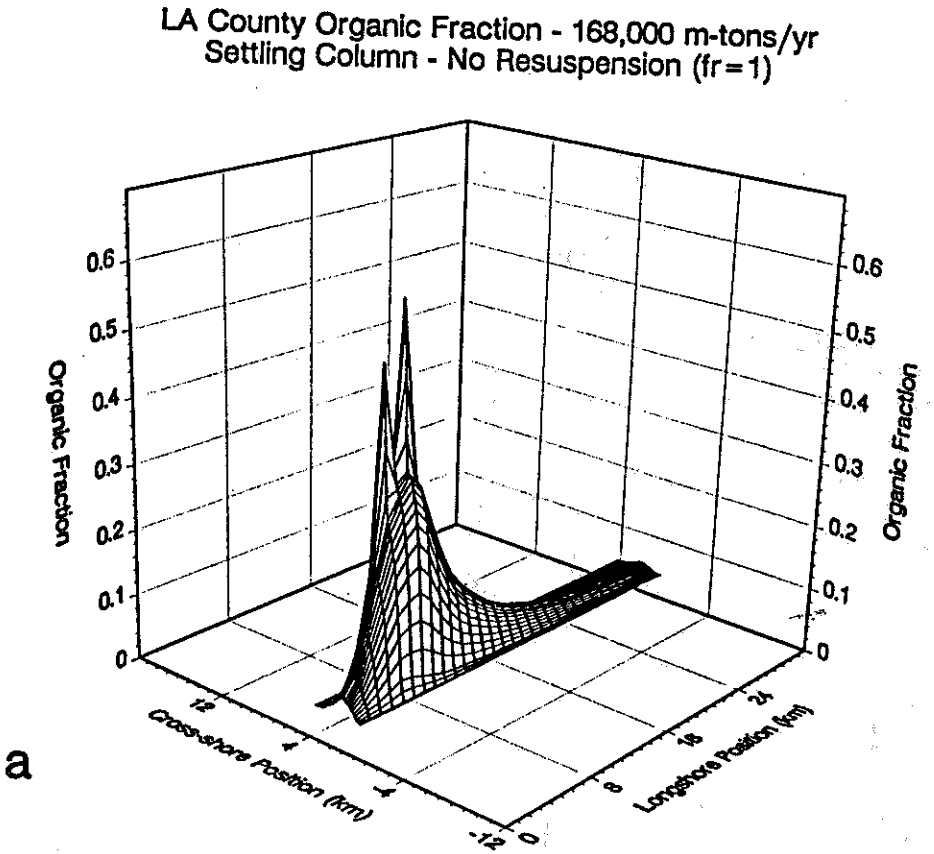

a

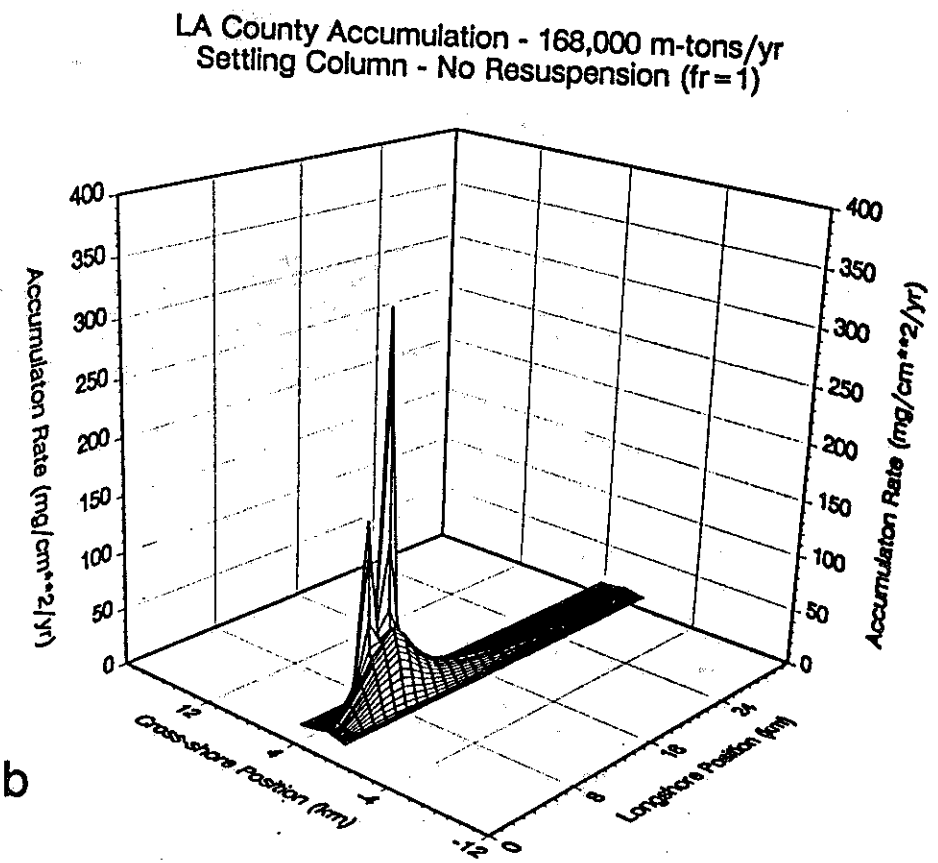

b

Figure 3.60- Sediment properties, noncohesive particles - SED2D, Palos Verdes, no resuspension, 1971. (a) organic fraction, (b) accumulation rate.

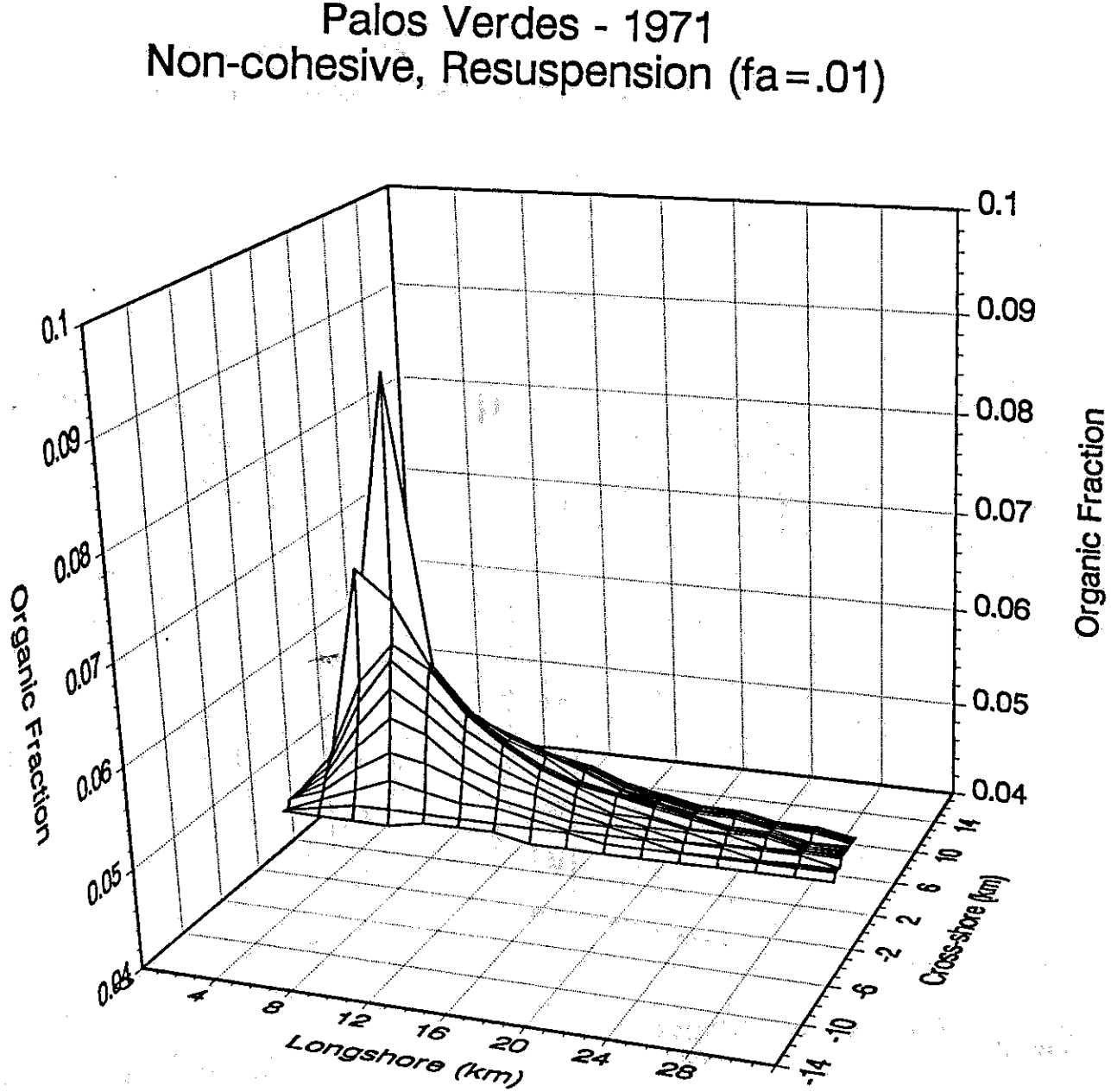

Figure 3.61 - Sediment, - SED2D, Palos Verdes,noncohesive particles 100 resuspensions, 1971.
Organic fraction.

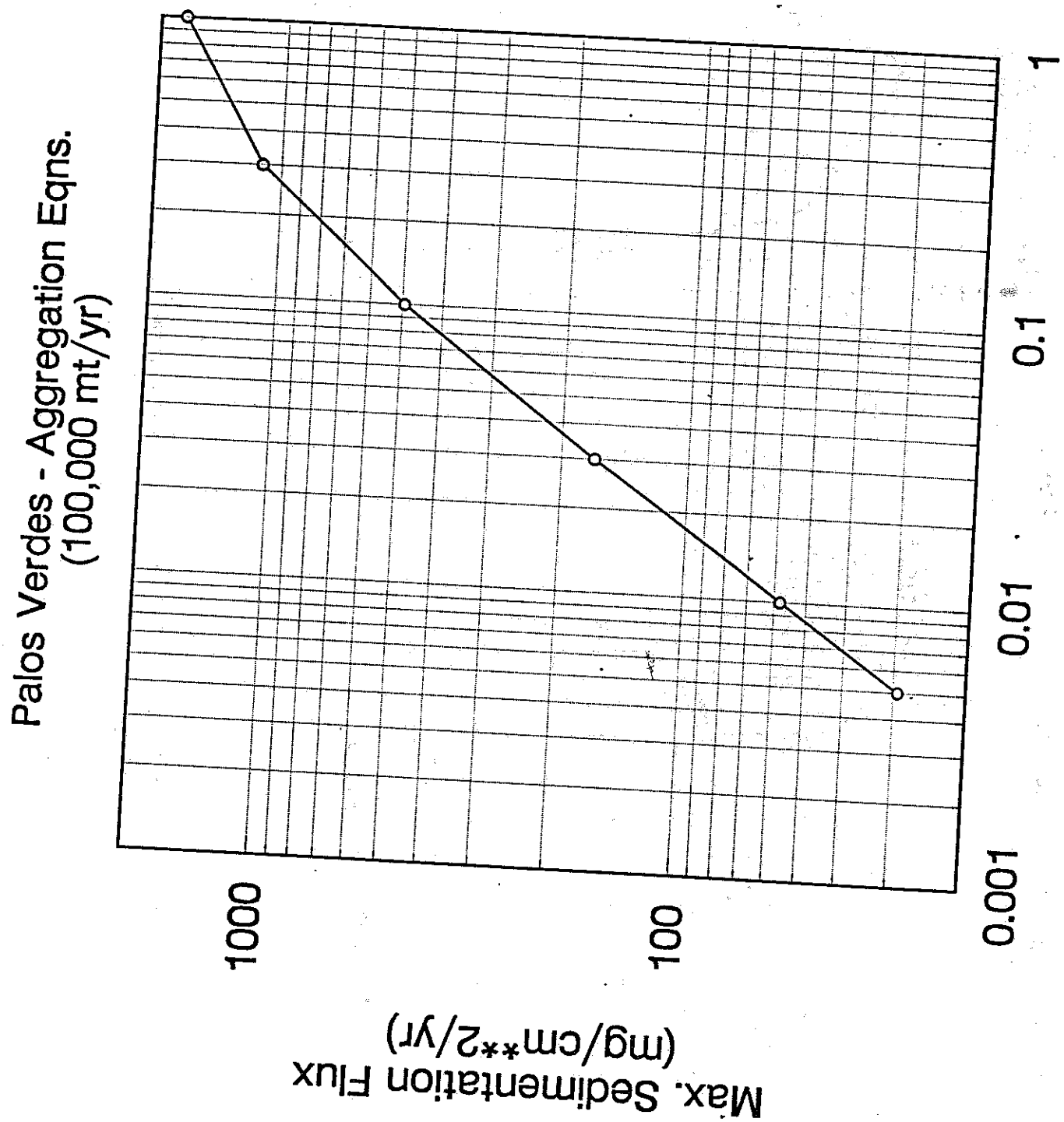

igure 3.62 - Dependence of depositional flux on accumulation fraction - SED2D, Palos Verdes, 1990.

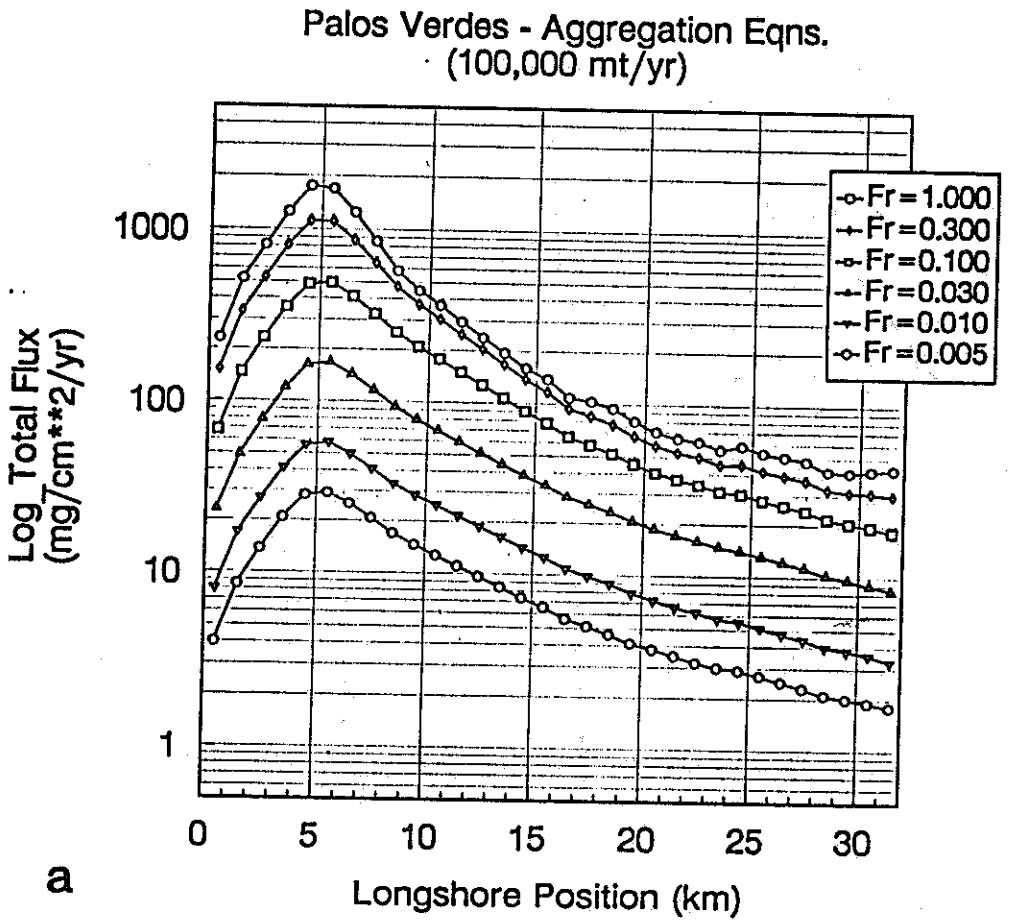

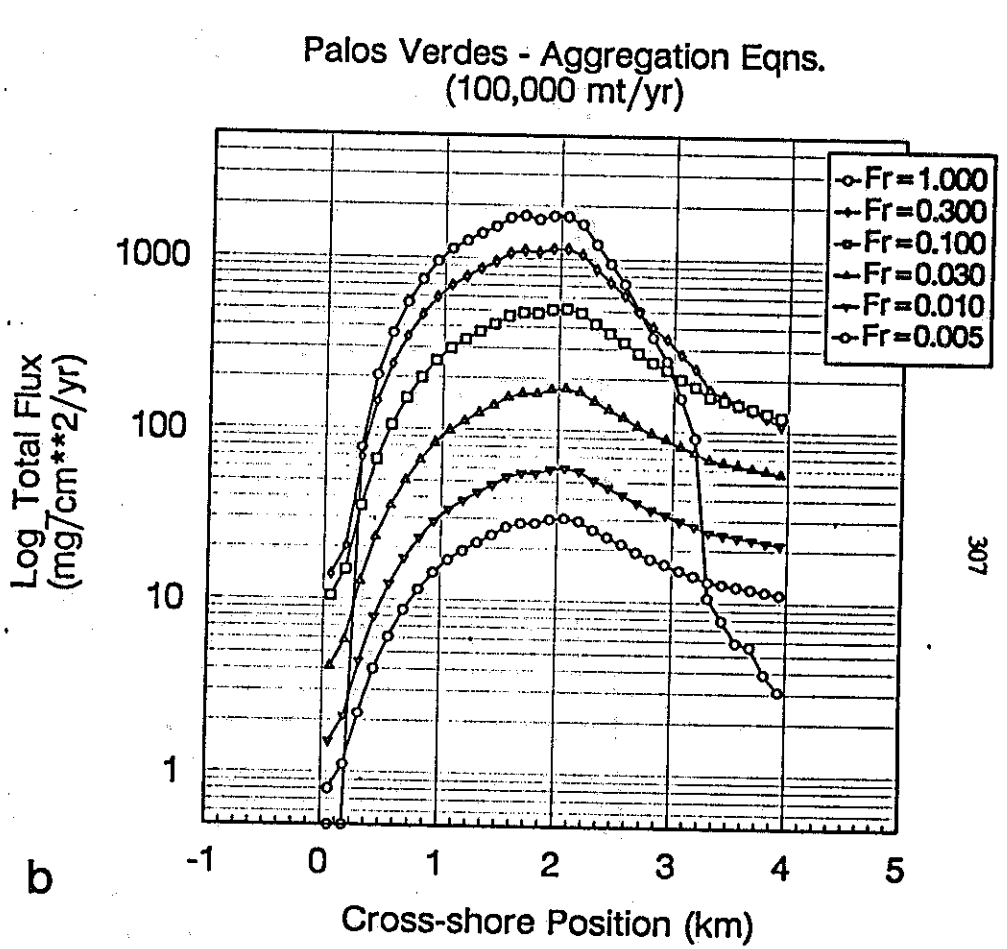

Figure 3.63 - Spatial dependence of aggregate particle depositional flux on the accumulation fraction - SED2D, Palos Verdes, 1990. (a) longshore, (b) cross-shore.

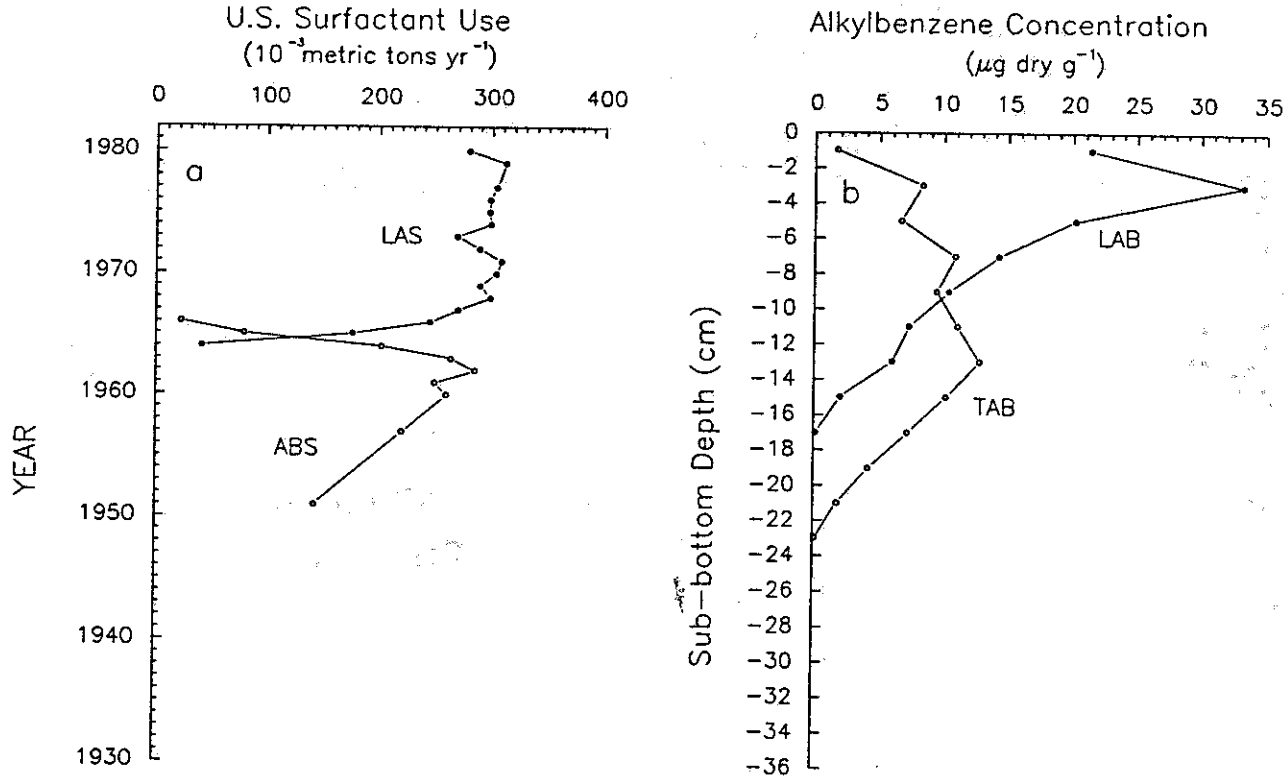

Figure 4.1 - U.S. alkylbenzenesulfonate surfactant usage rates (a) and long-chain alkylbenzene profiles in sediments off Palos Verdes (after Eganhouse *et al.* 1983a).

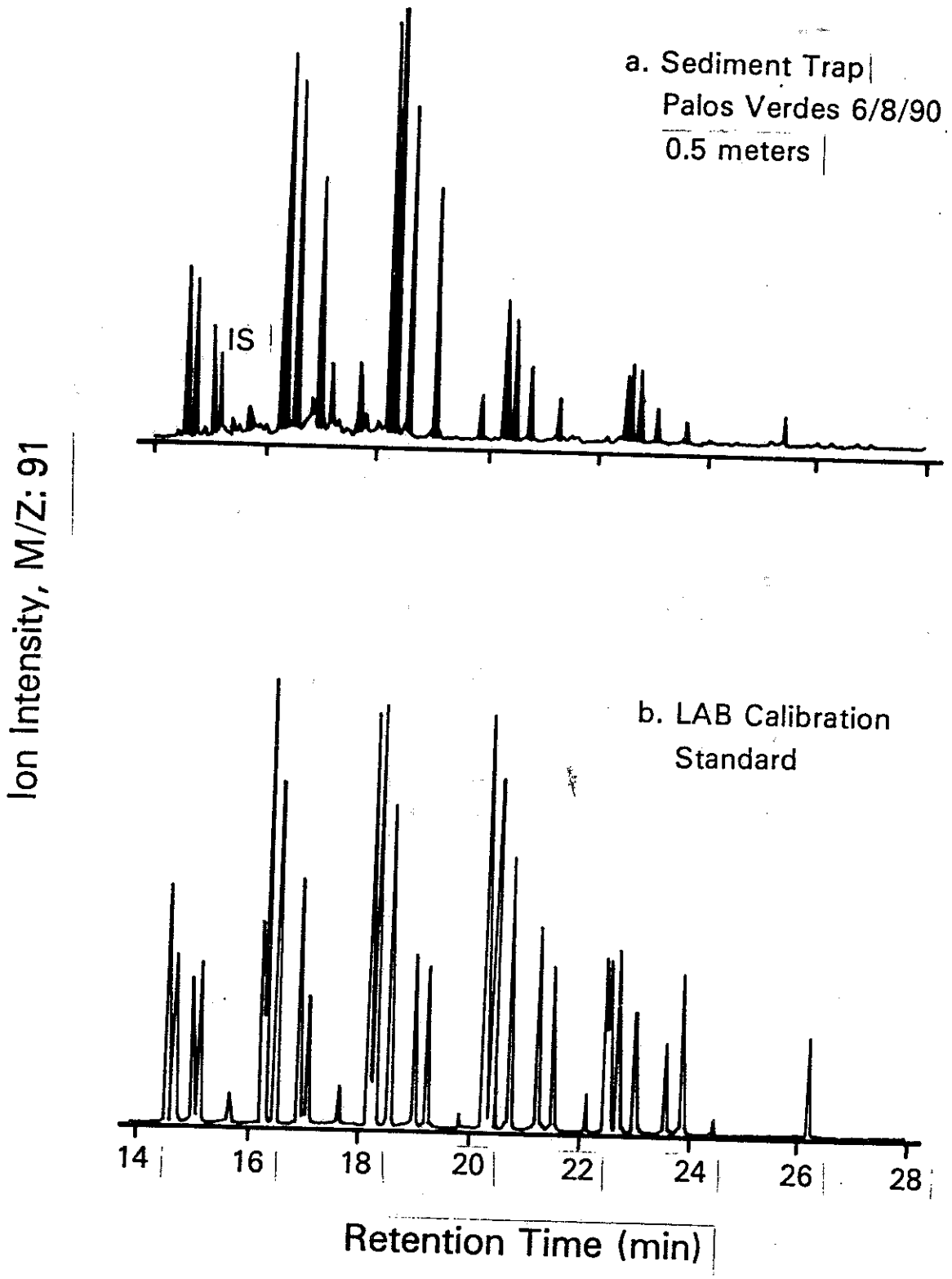

Figure 4.2 - Mass fragmentograms (m/z 119) for a) the F2 fraction from the 0.5 meter sediment trap off Palos Verdes (6/8/90 deployment) and b) LAB calibration standard. Shaded peaks in "a" correspond to LABs.

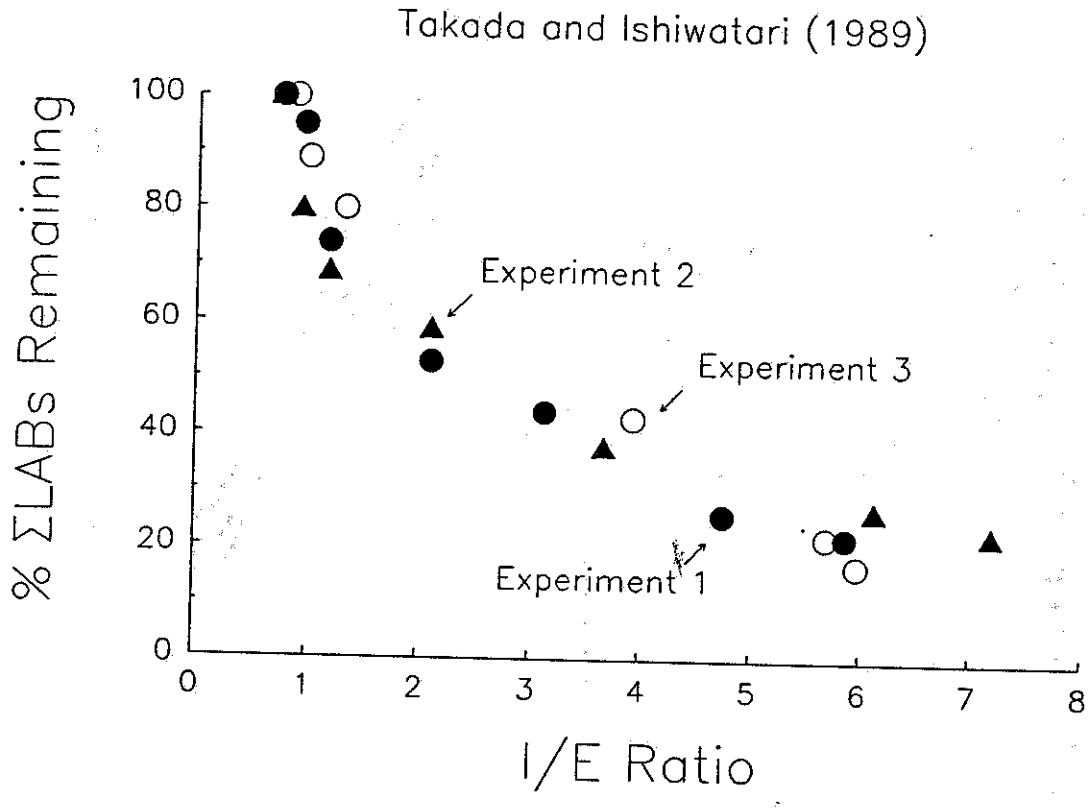

Figure 4.3 - Relationship between extent of LAB degradation and I/E ration during effluent decomposition experiments (after Takada and Ishiwatari 1989).

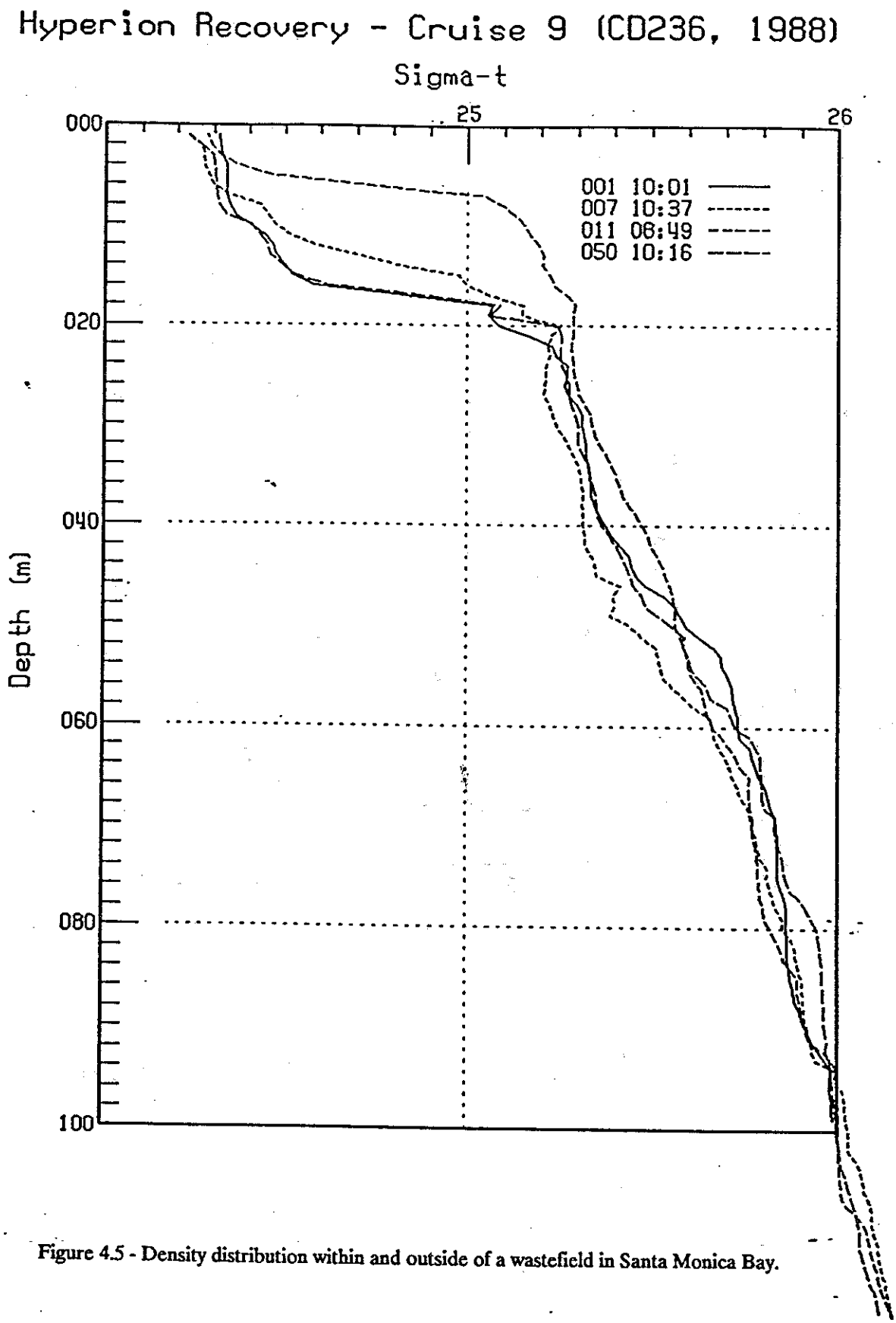

Figure 4.5 - Density distribution within and outside of a wastefield in Santa Monica Bay.

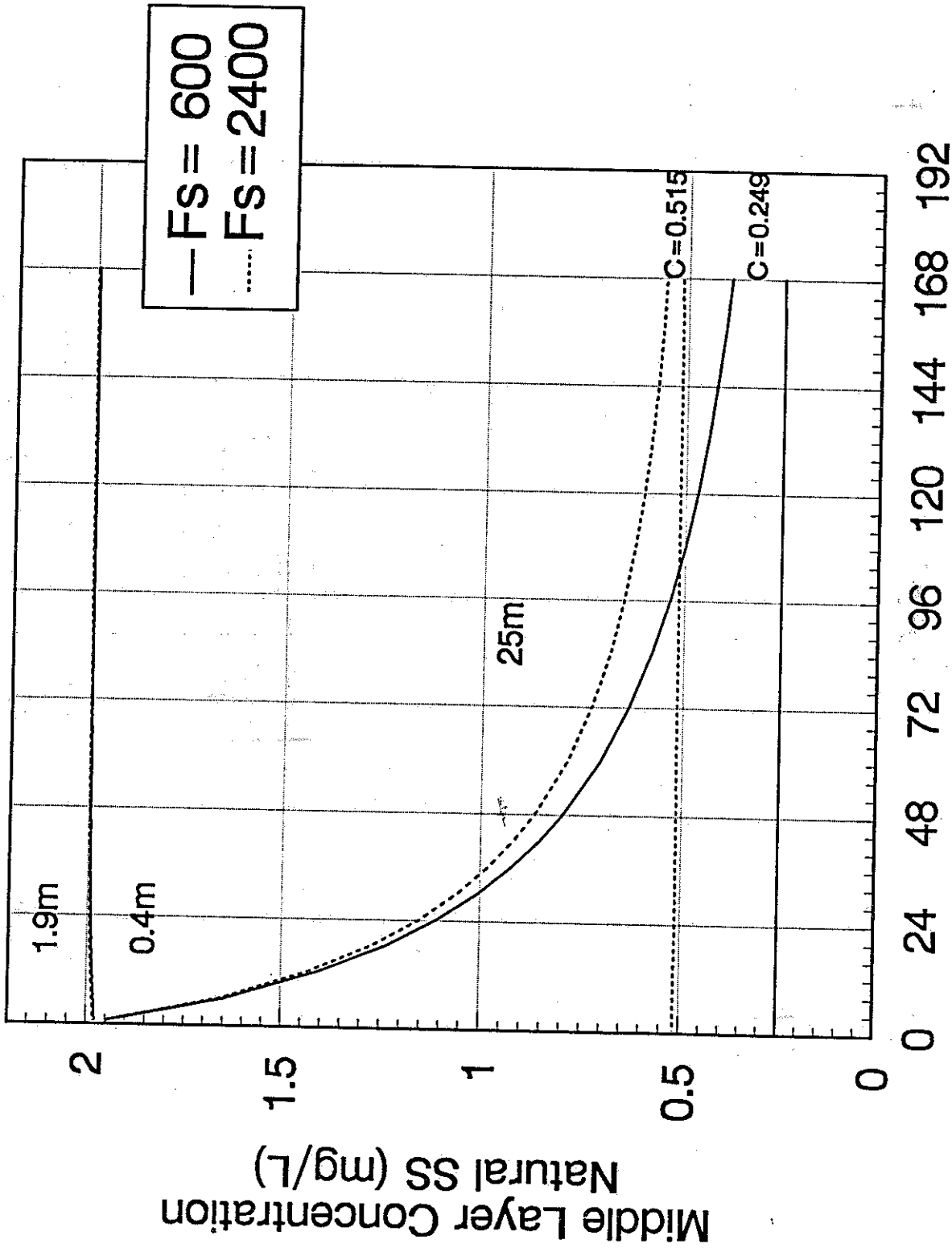

Figure 4.6 - Equilibrium suspended solids concentrations and mixing thickness.

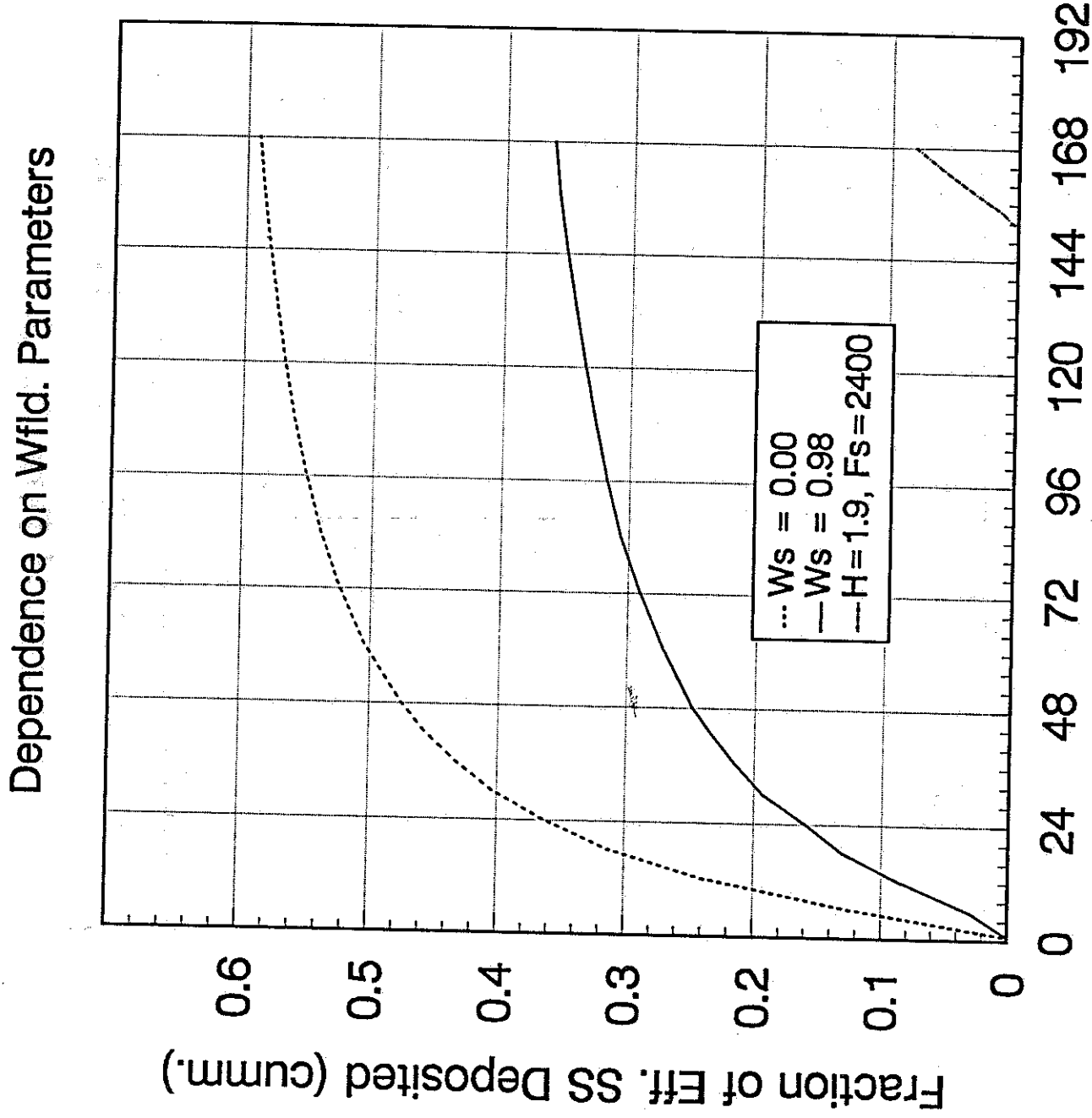

Figure 4.7 - Fraction of mass deposited versus time since discharged. Ws = wastefield spreading factor (wastefield thickness = 25m).

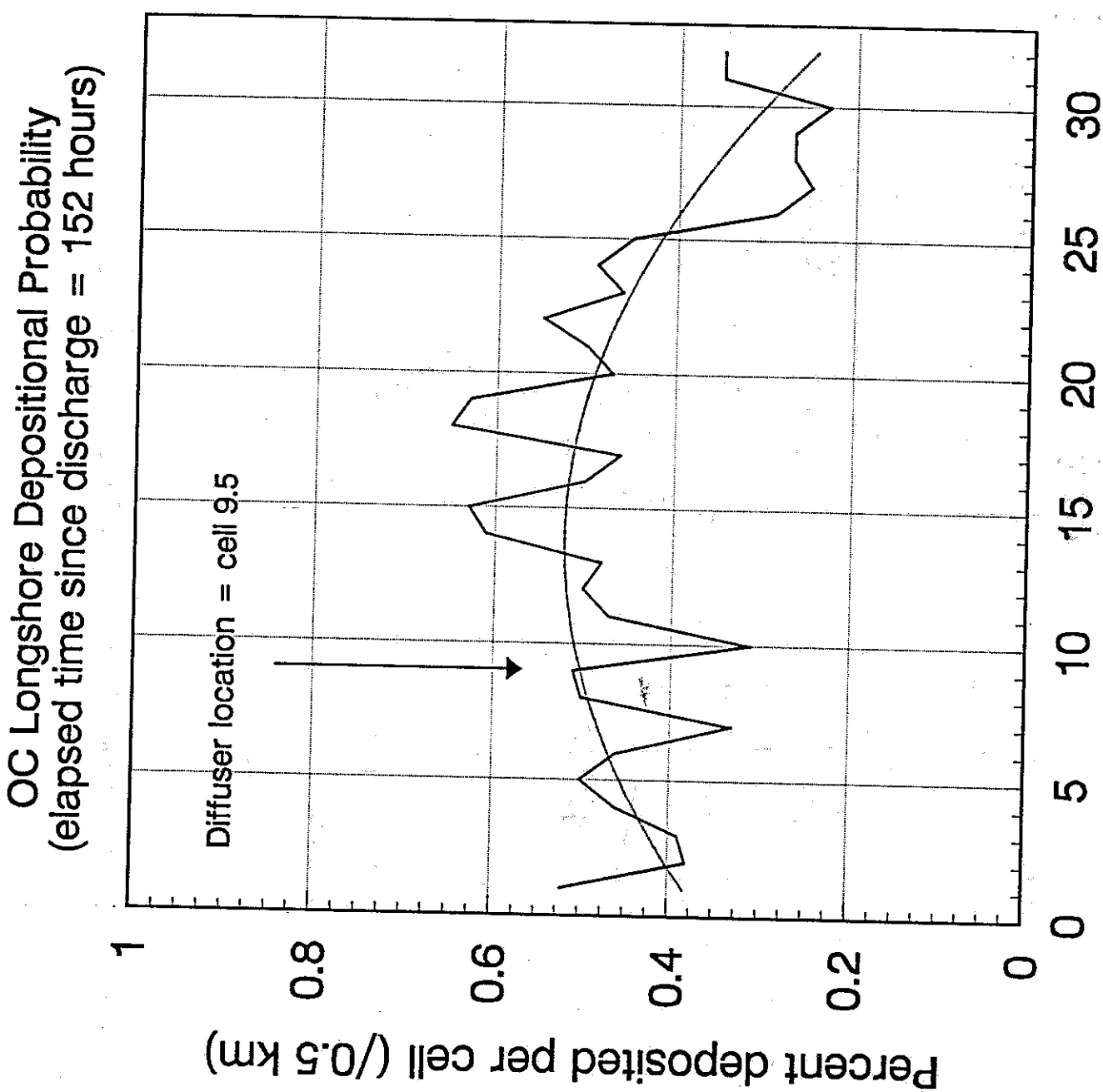

Figure 4.8 - Orange County longshore depositional probability after an elapsed time of 152 hours.

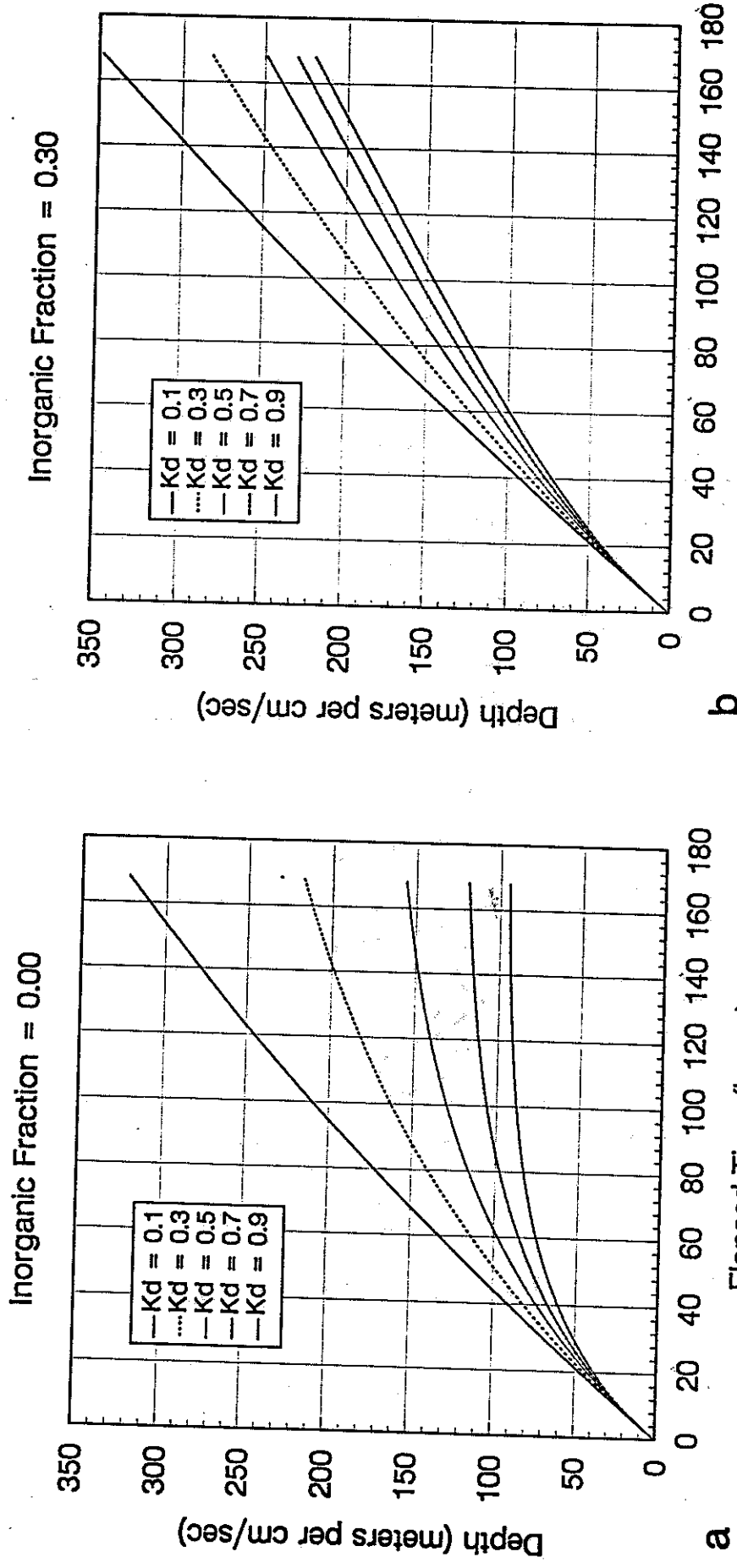

Figure 4.9 - Settling depth for decaying particles. (a) organic particle, (b) 70% organic, 30% inorganic particle.

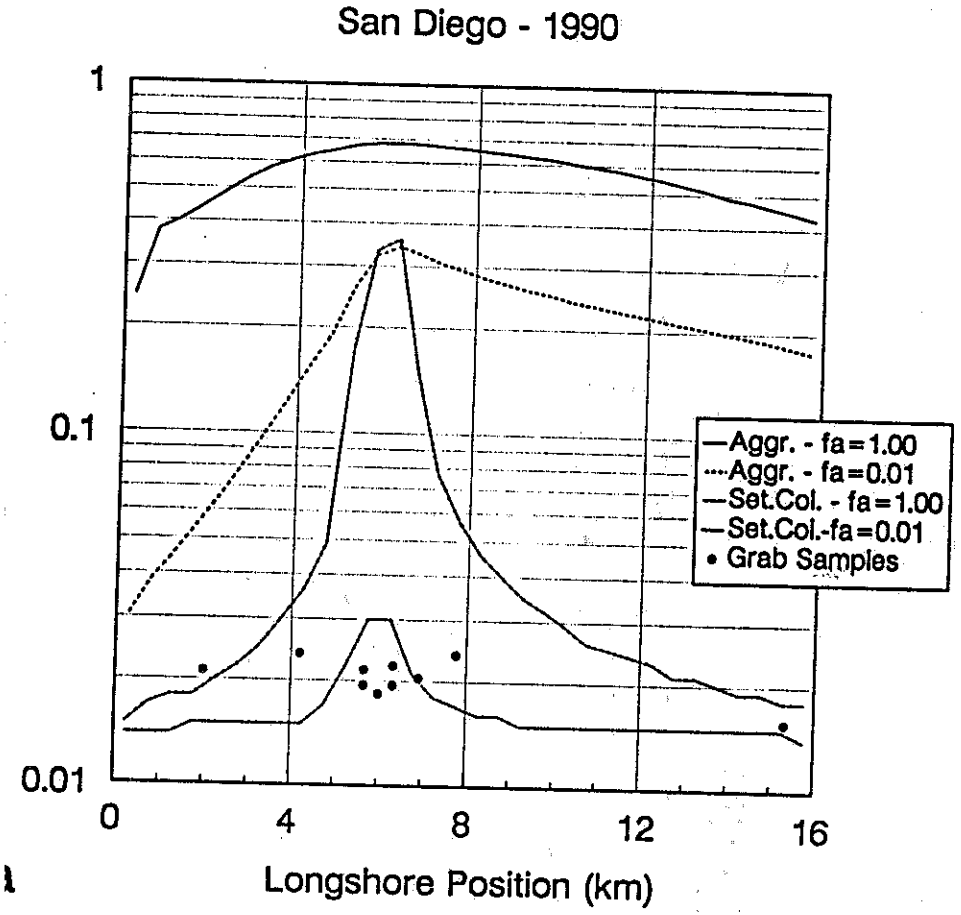

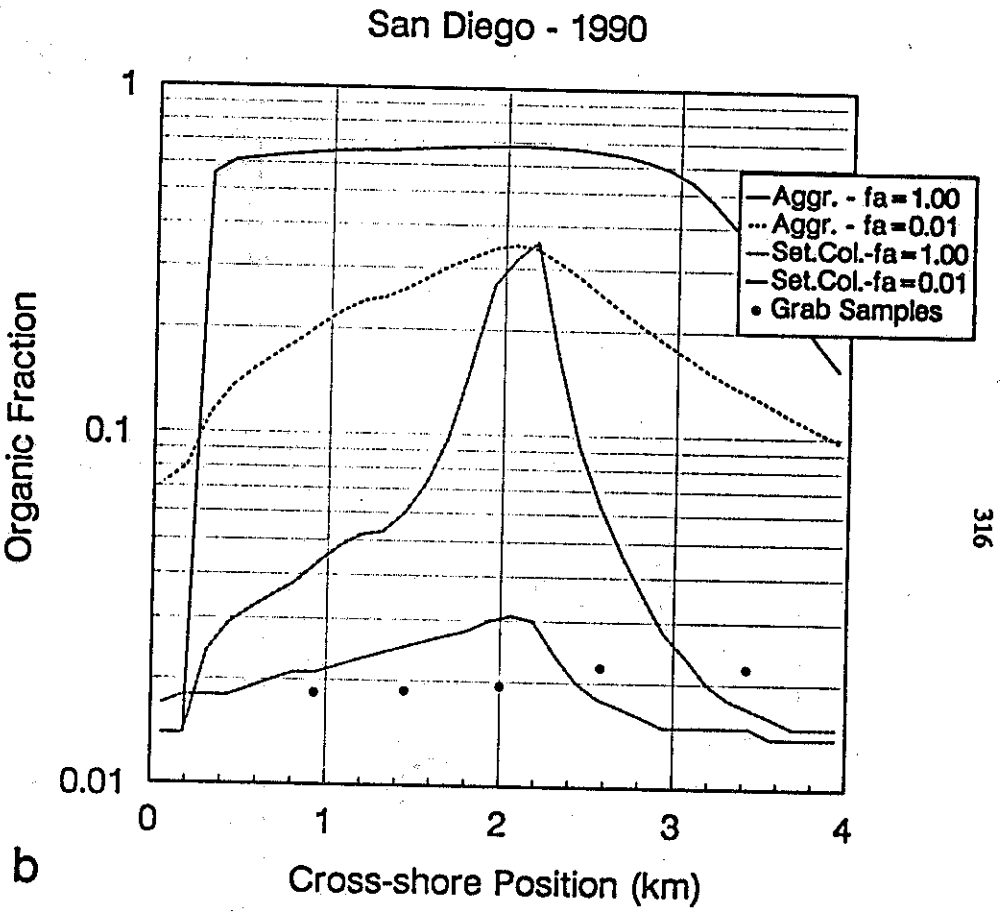

Figure 4.10 - Comparison of predicted and measured organic concentrations - San Diego, SED2D. (a) longshore, (b) cross-shore.

Figure 4.11 - San Diego core profiles. (a) total organic carbon, (b) lead, (c) cadmium.

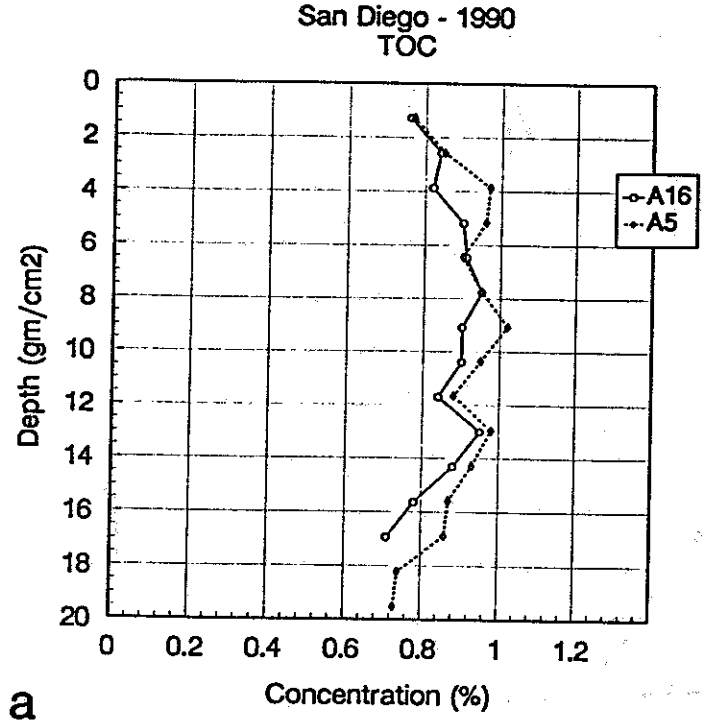

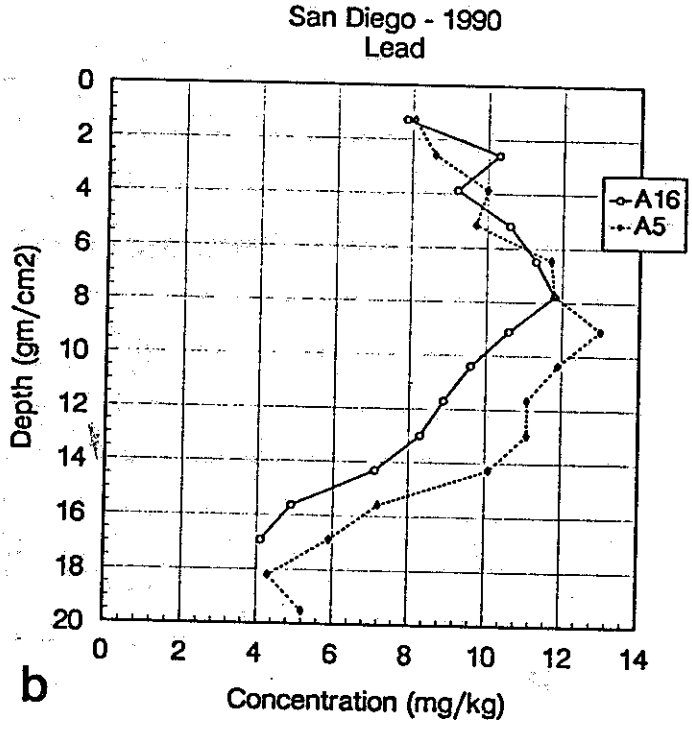

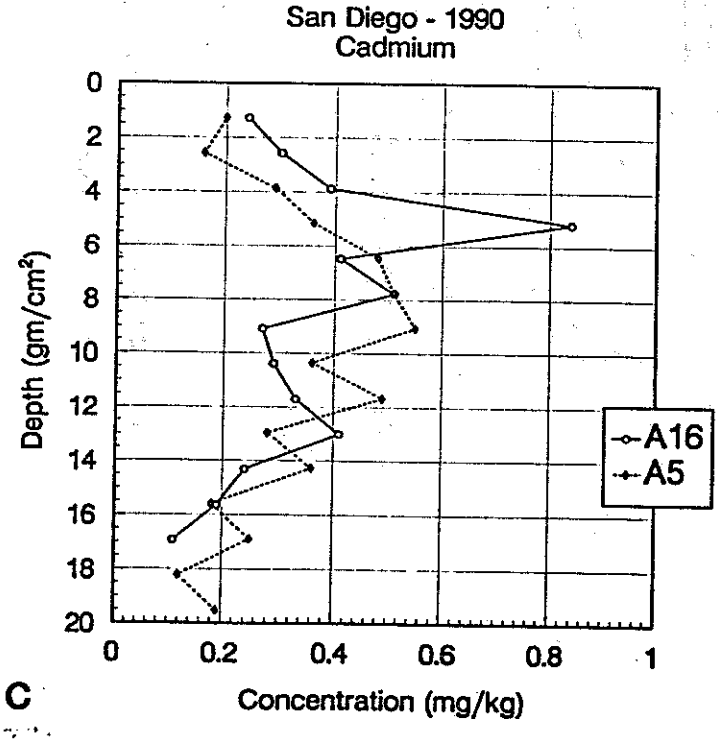

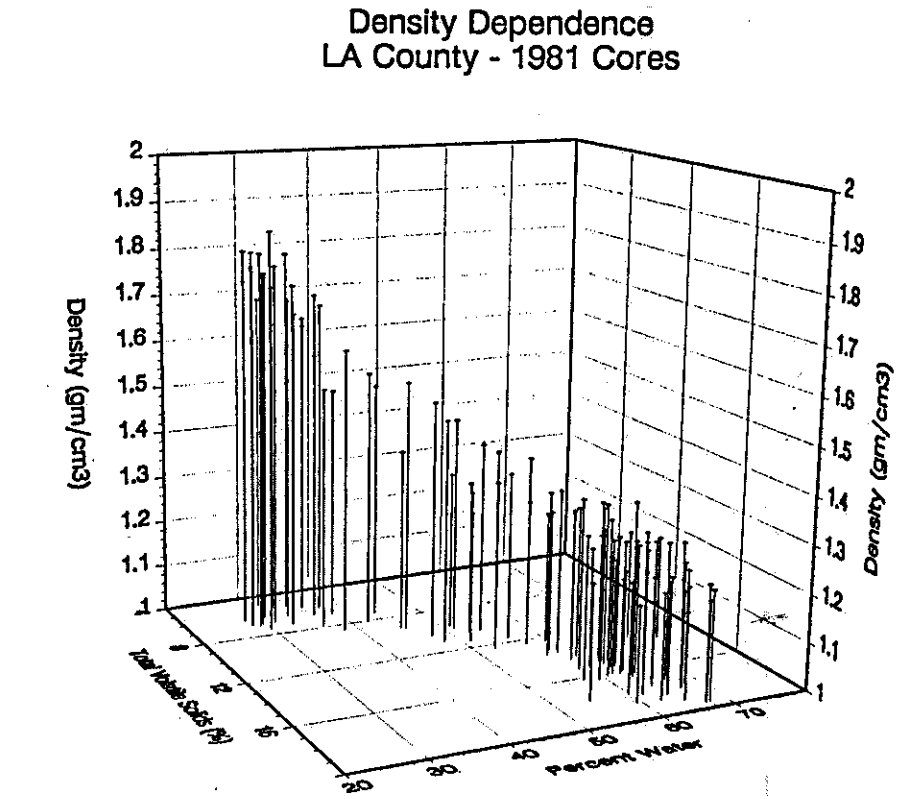

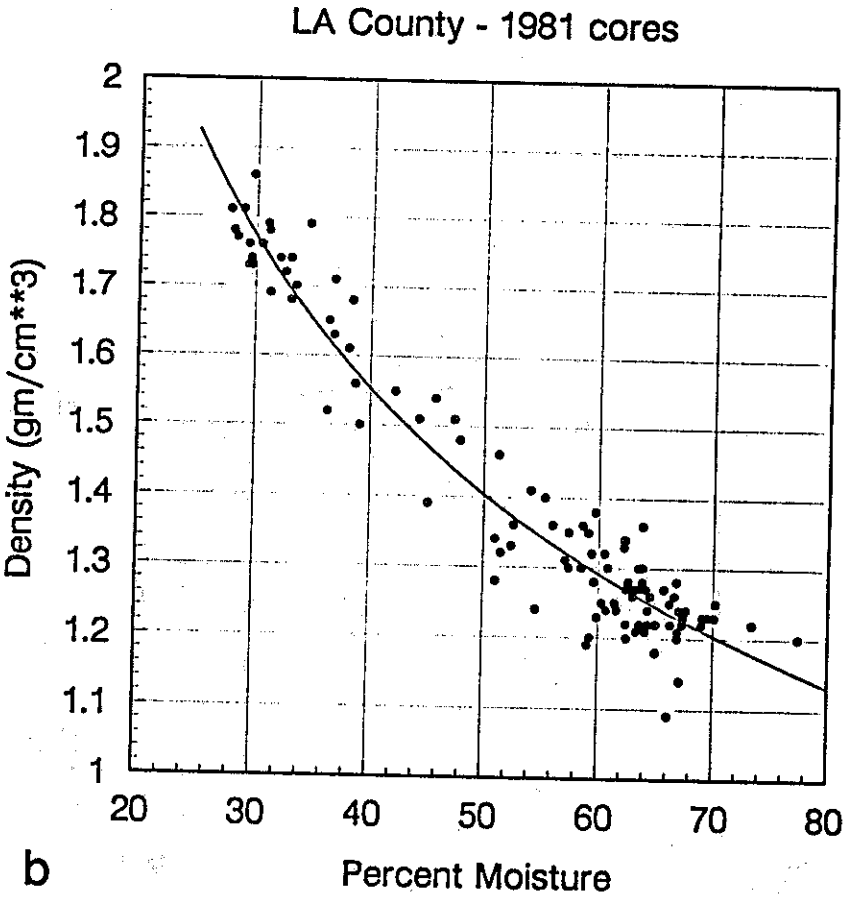

Figure 4.12 - Relationship between sediment density, percent water, and total volatile solids - Palos Verdes. (a) density versus percent water and total volatile solids, (b) density versus percent water.

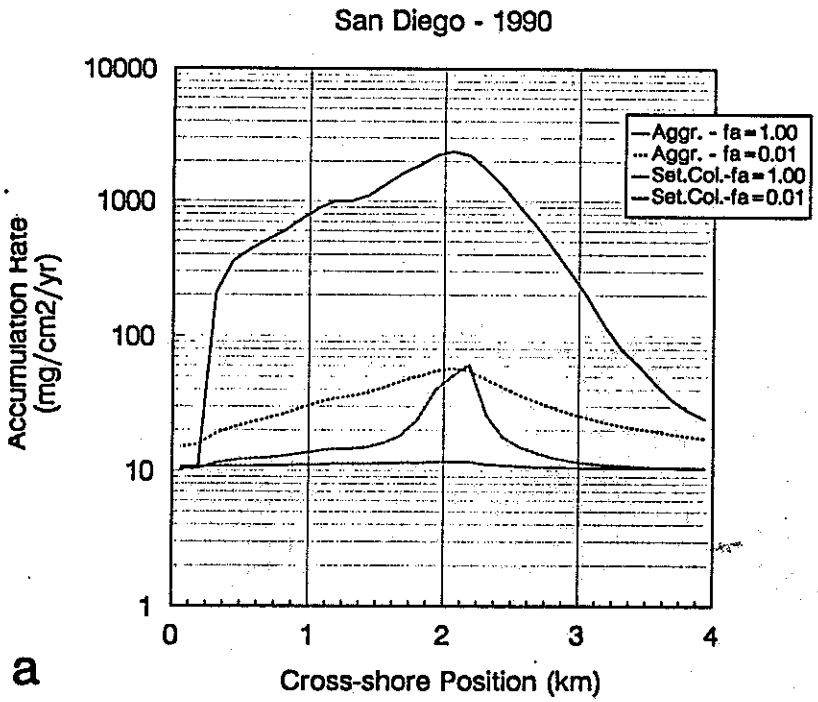

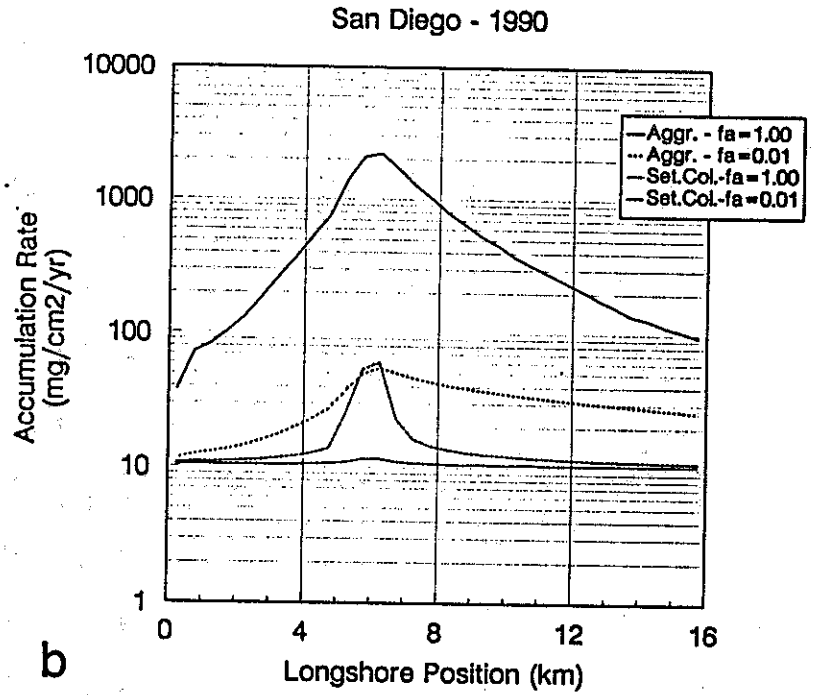

Figure 4.13 - Predicted rates of accumulation of sediment material - San Diego, SED2D. (a) longshore, (b) cross-shore.

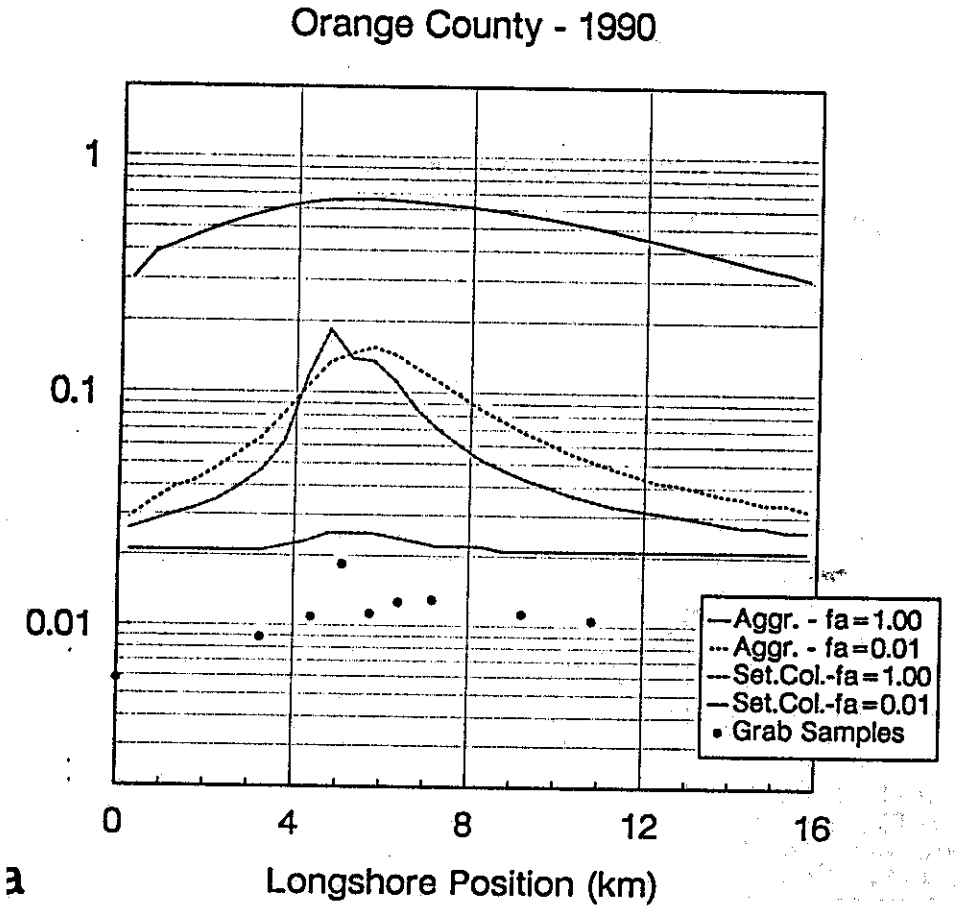

a

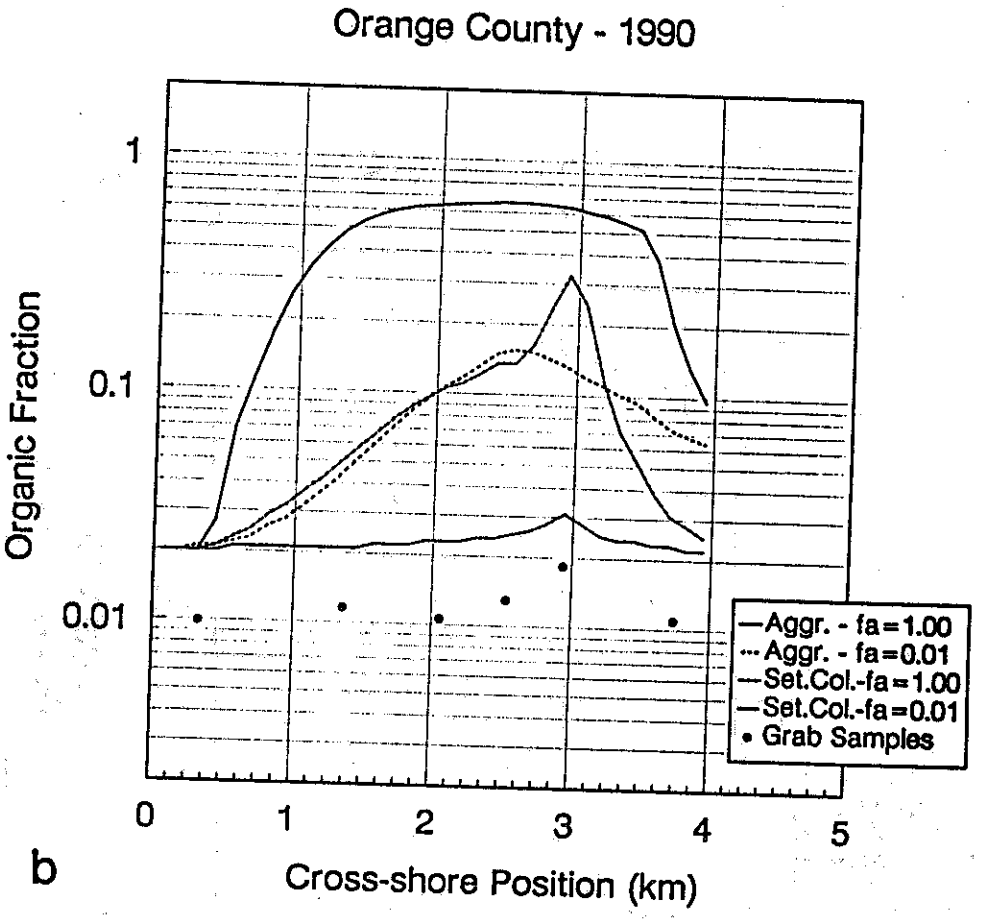

b

Figure 4.14 - Predicted and measured concentrations of surface sediments - SED2D, Orange County.
(a) longshore, (b) cross-shore.

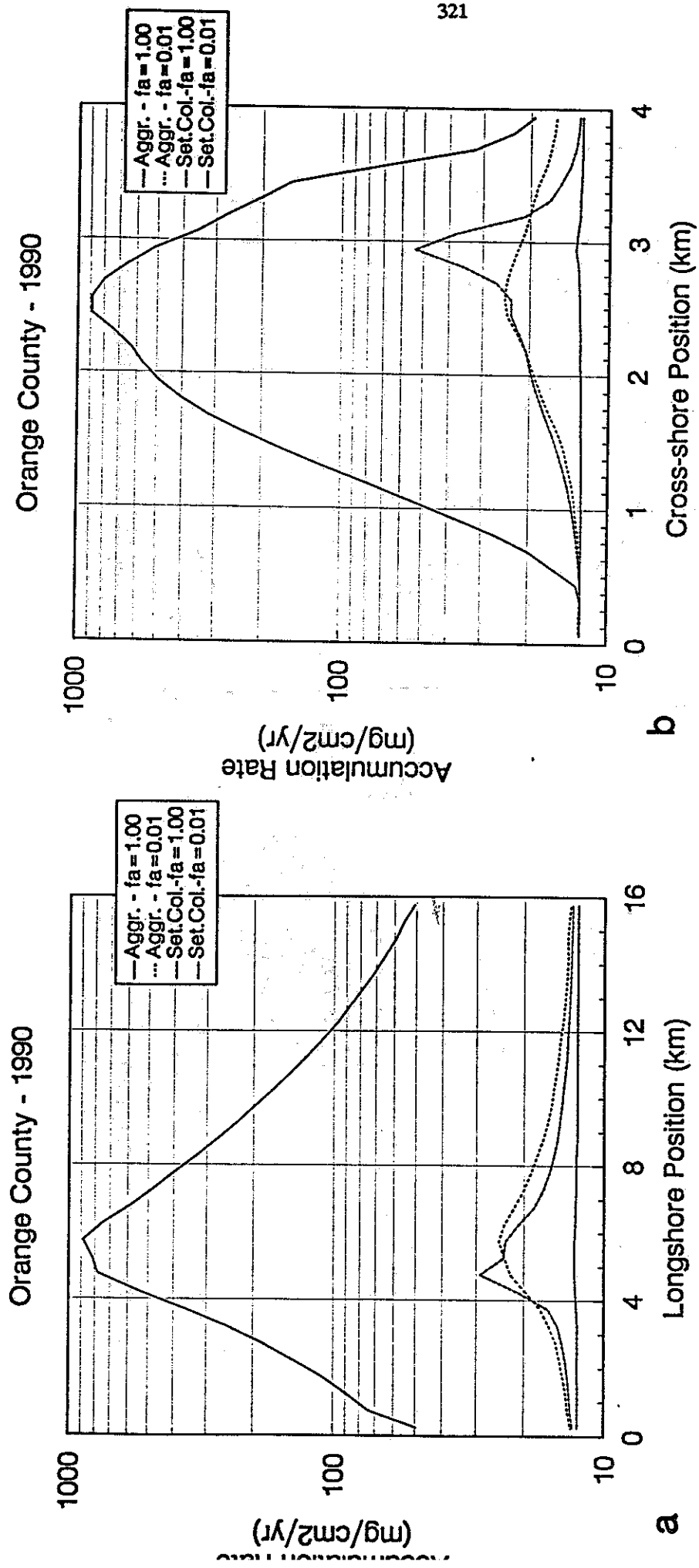

Figure 4.15 - Predicted accumulation fluxes - SED2D, Orange County. (a) longshore, (b) cross-shore.

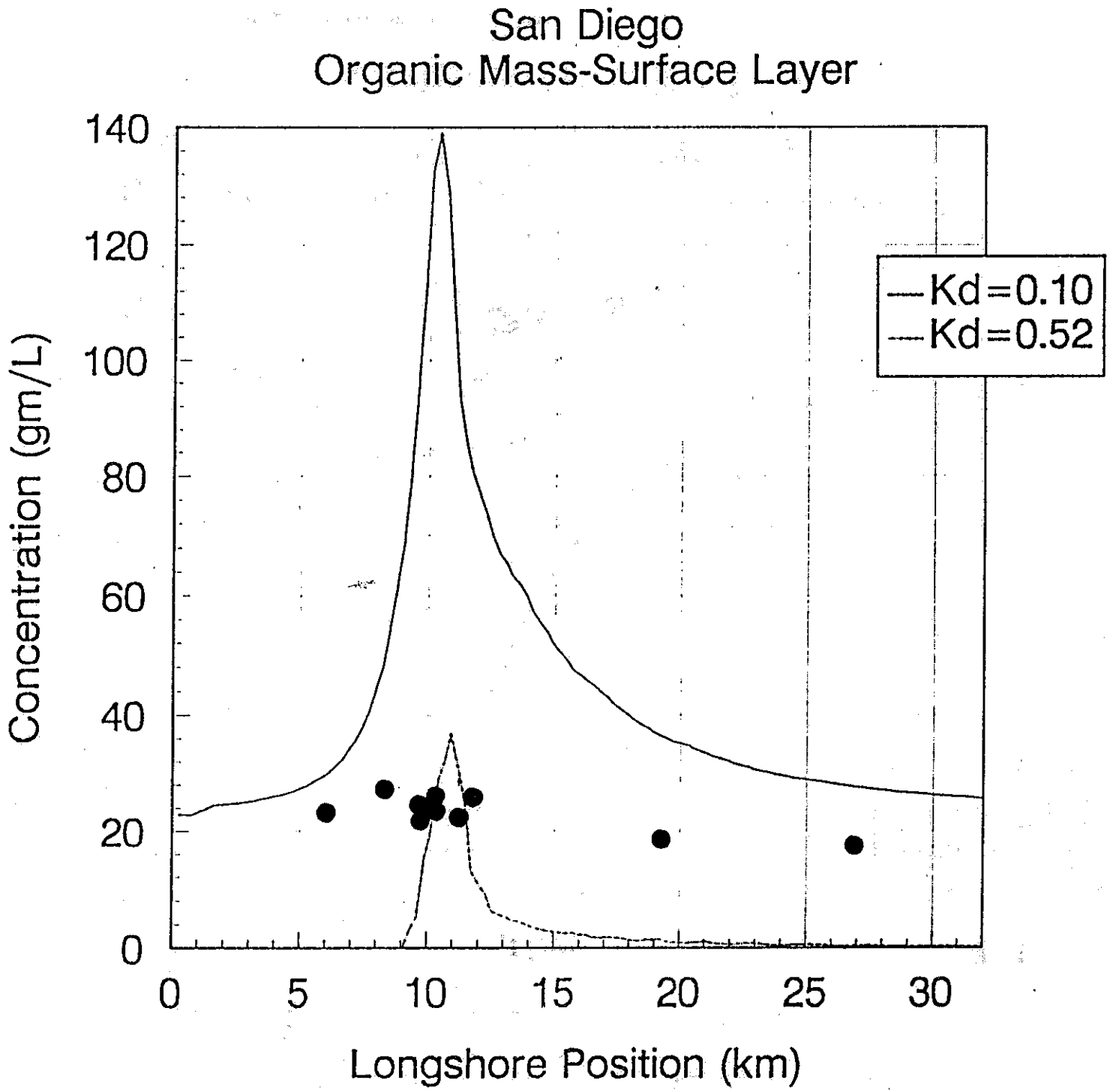

Figure 4.16 - Predicted versus measured concentration of organic material in surface sediments - San Diego, DECAL

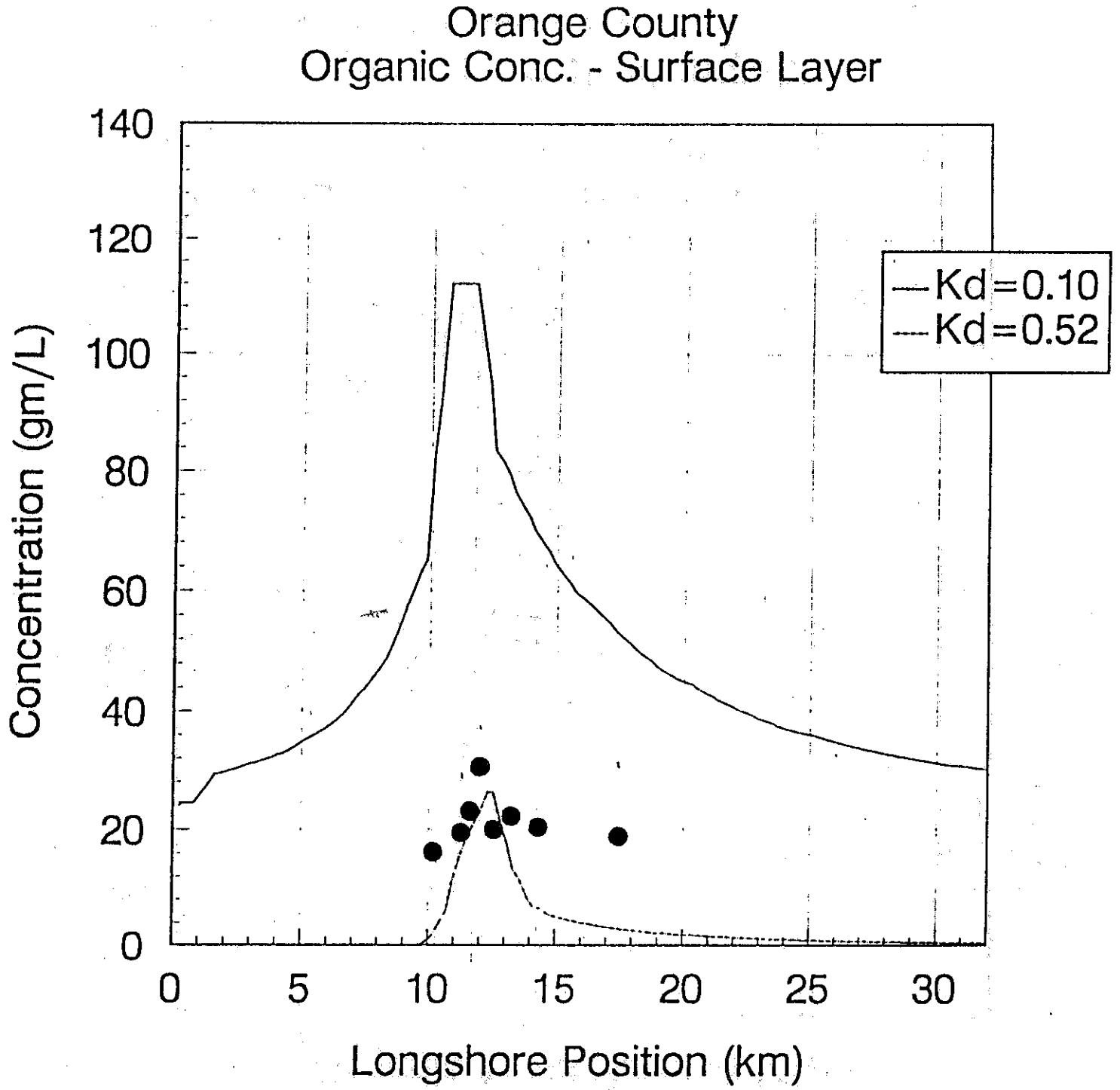

Figure 4.17 - Predicted versus measured concentration of organic material in surface sediments - Orange County, DECAL.

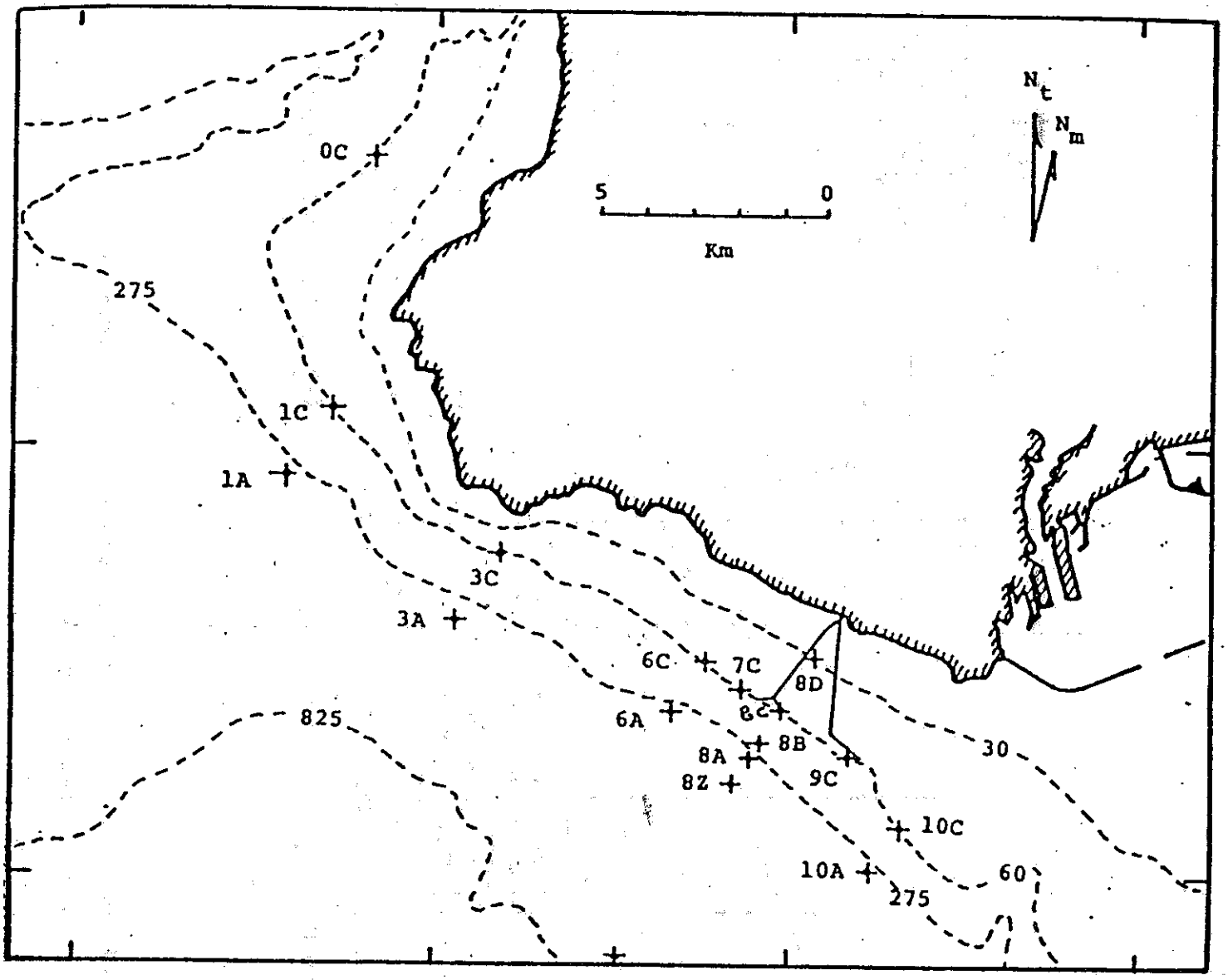

Figure 4.18 - Coring station locations - Palos Verdes.

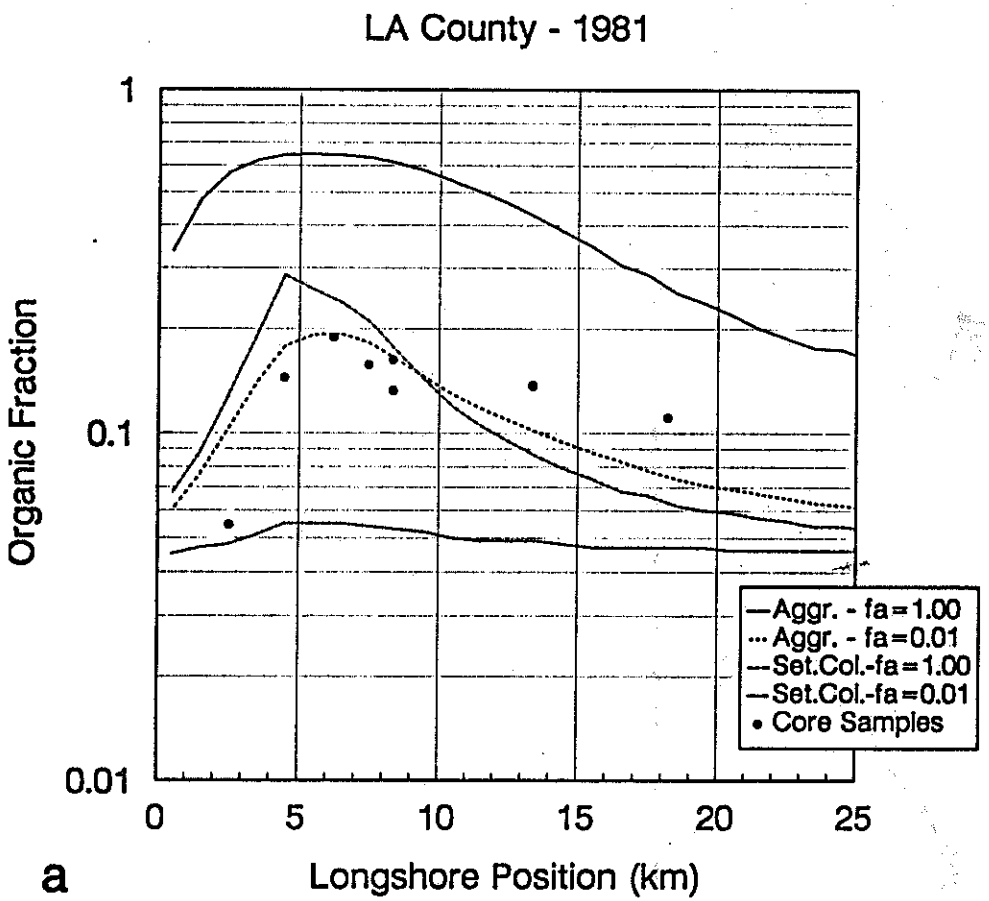

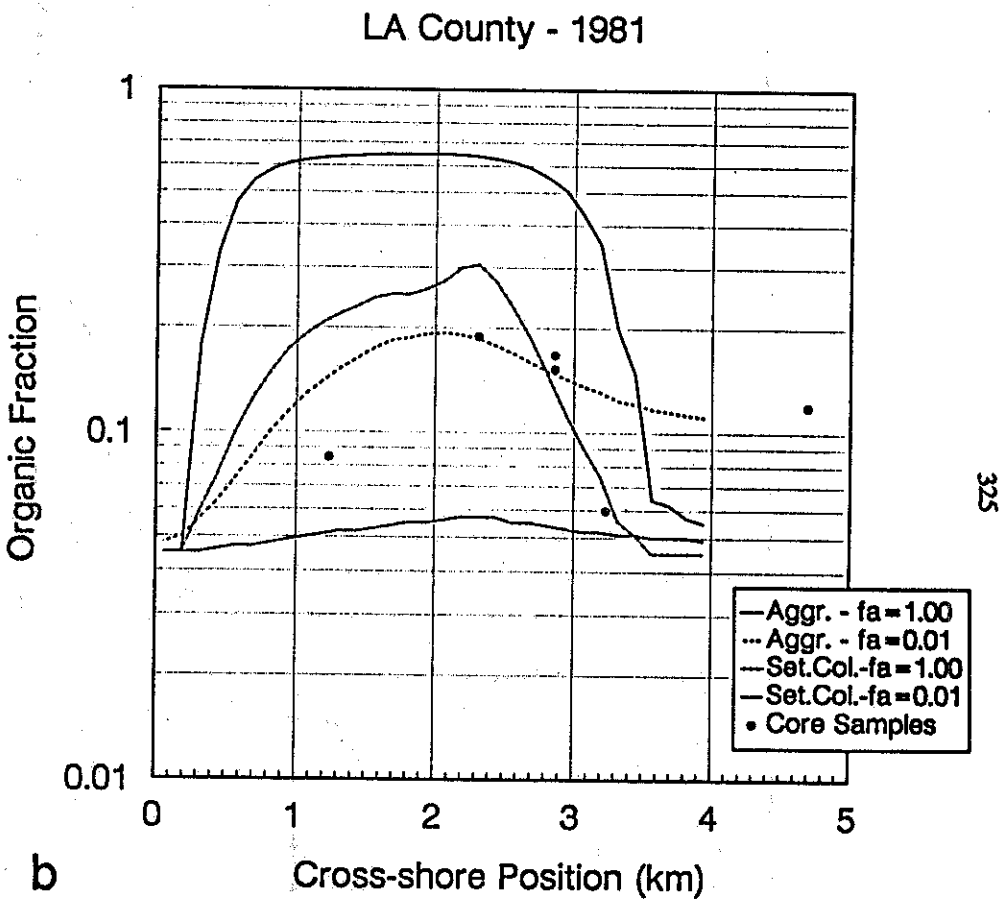

Figure 4.19 - Predicted versus measured concentration of organic material in surface sediments - Palos Verdes, SED2D. (a) longshore, (b) cross-shore (transect 8).

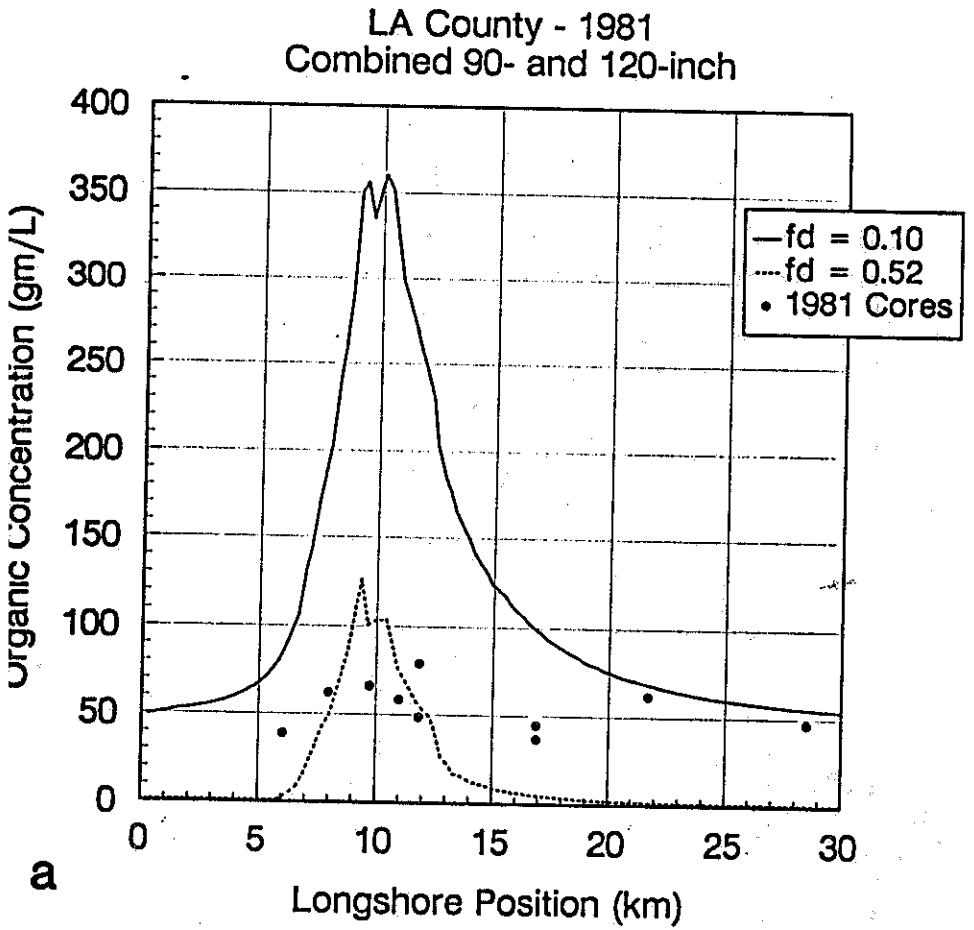

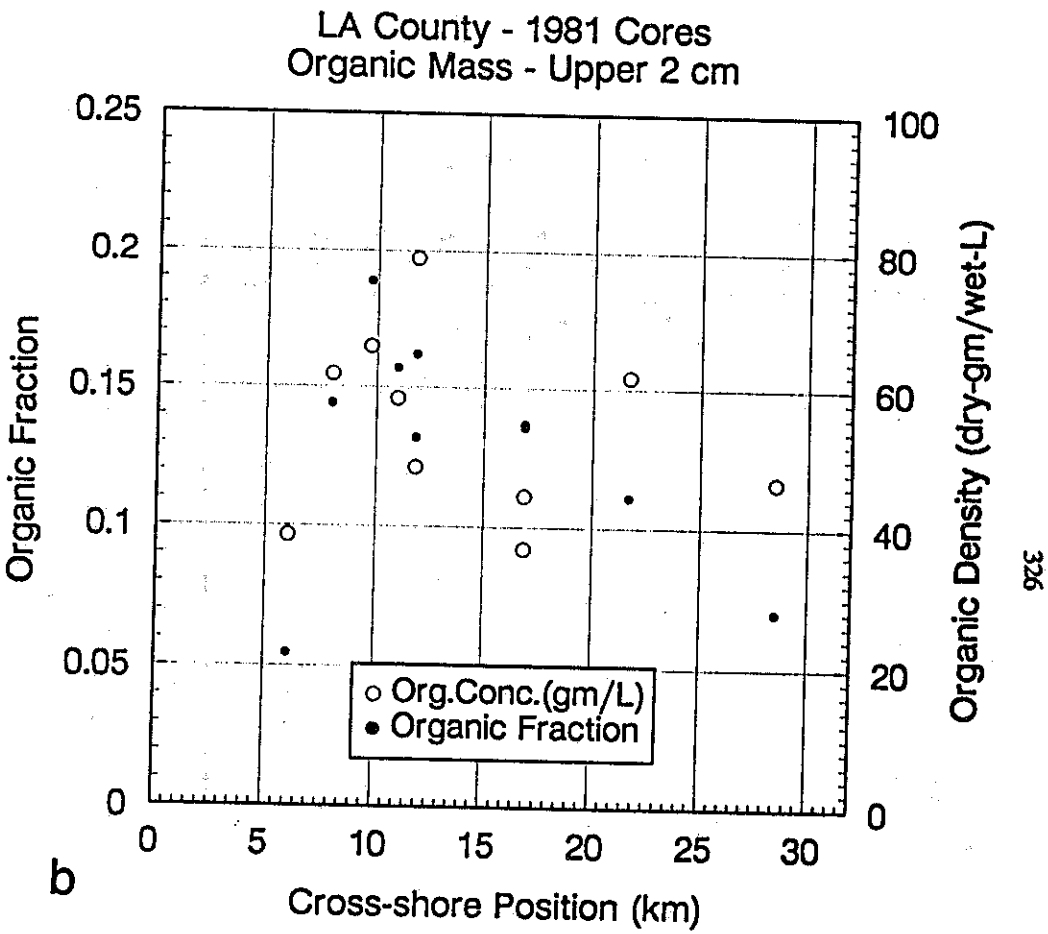

Figure 4.20 - Palos Verdes surface sediments. (a) comparison of DECAL predicted versus measured concentation of organic material in surface sediments - longshore, (b) covariance between organic fraction and organic density/concentration.

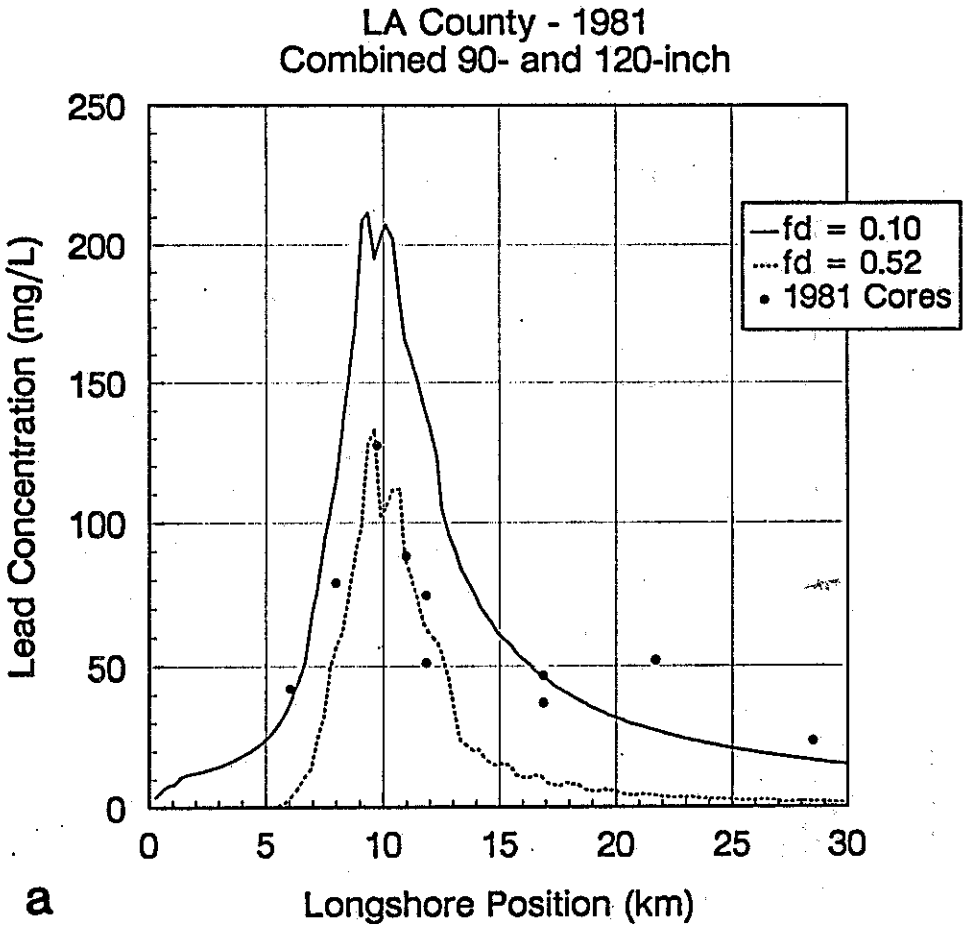

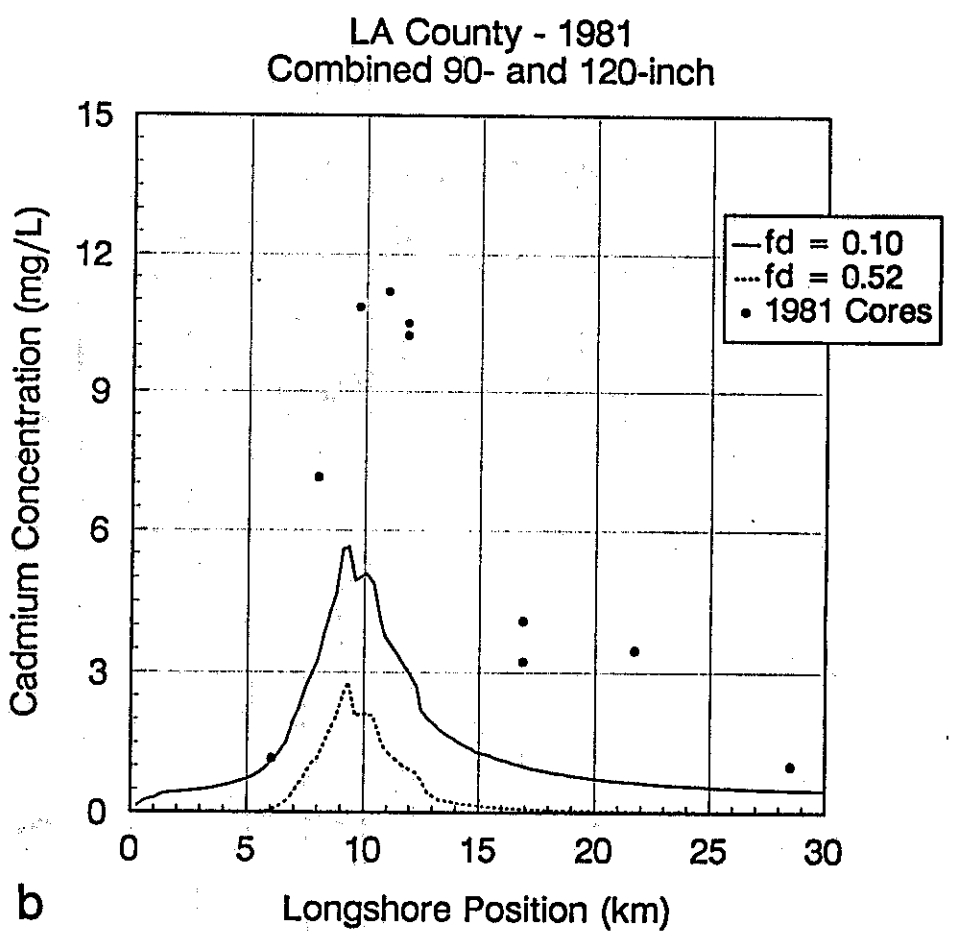

Figure 4.21 - Comparison of predicted and measured trace metal concentrations - Palos Verdes, DECAL, surface sediments. (a) lead, (b) cadmium.

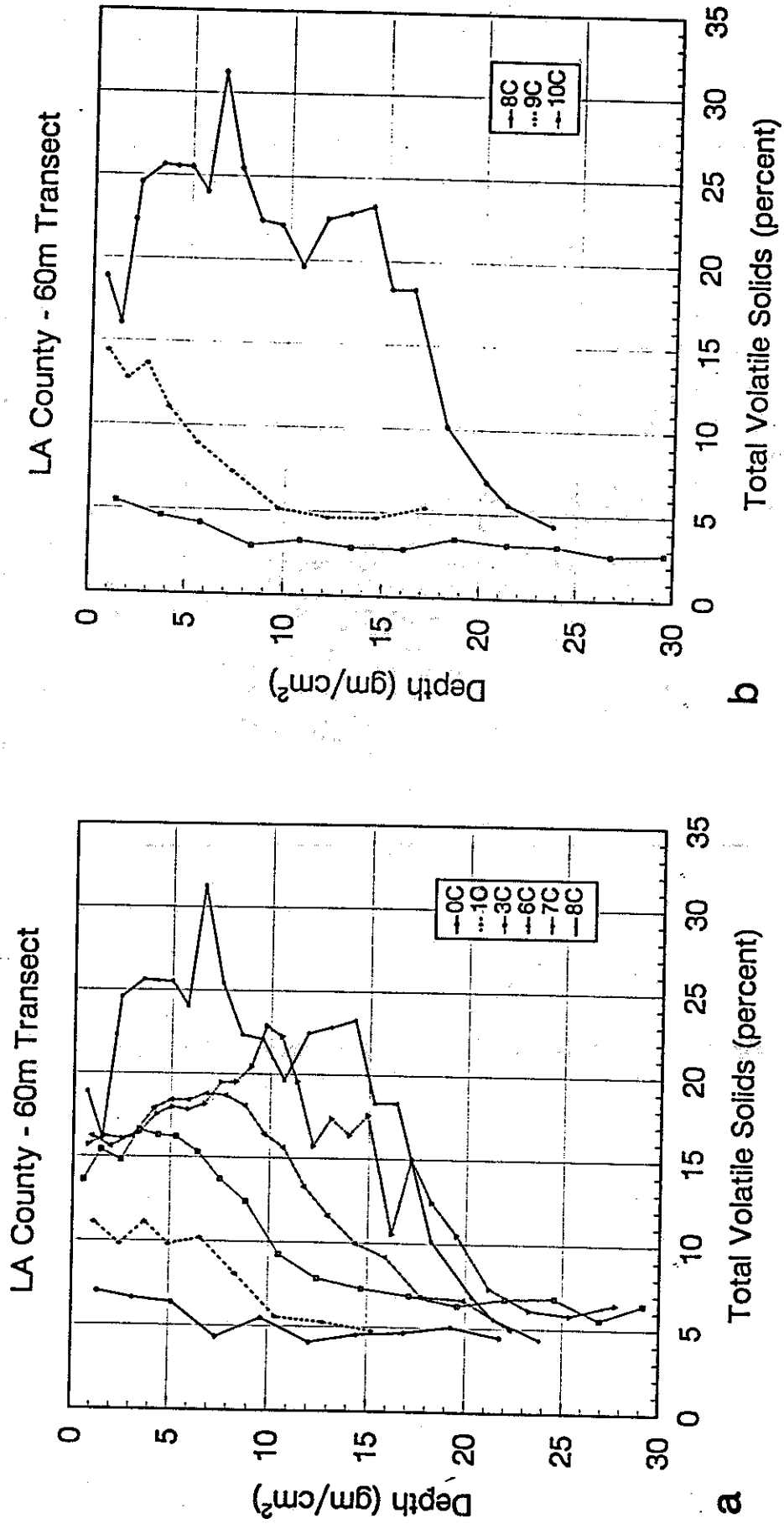

Figure 4.22 - Profiles of sediment organic content - Palos Verdes. (a) upcoast from transect 8, (b) downcoast from transect 8.

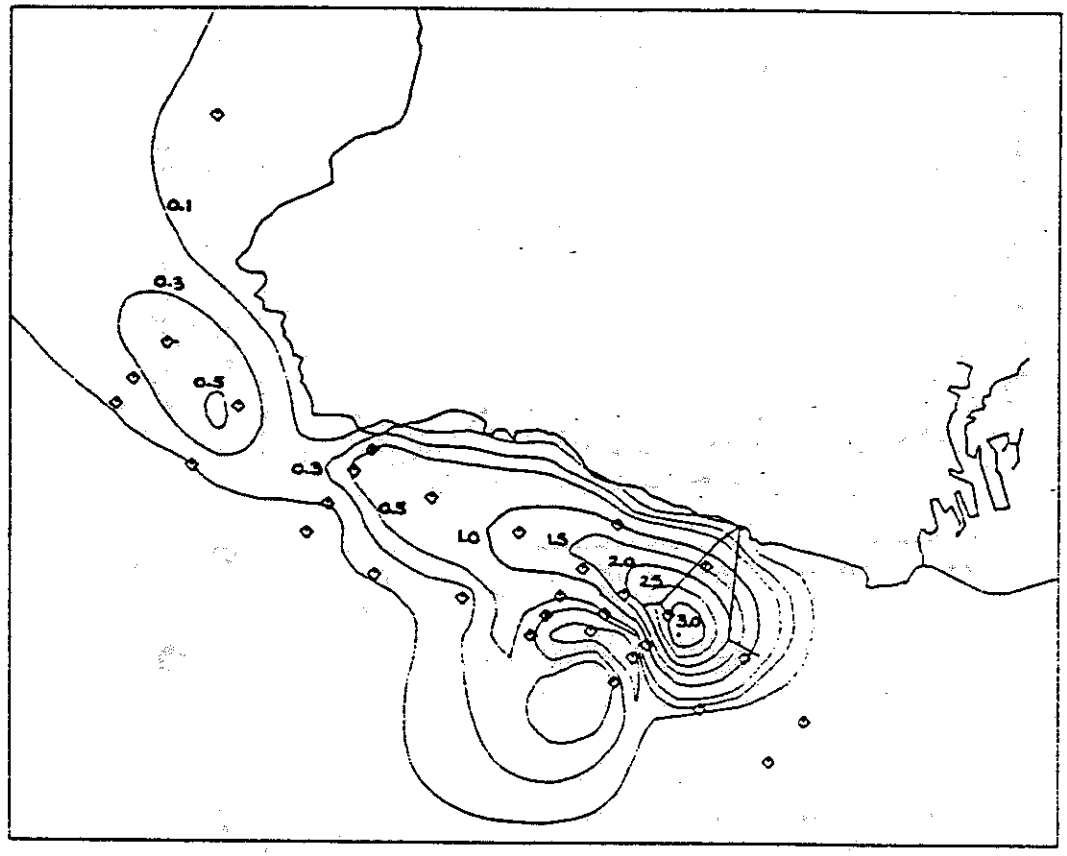

Figure 4.23 - Accumulations of "excess" organic material - Palos Verdes.

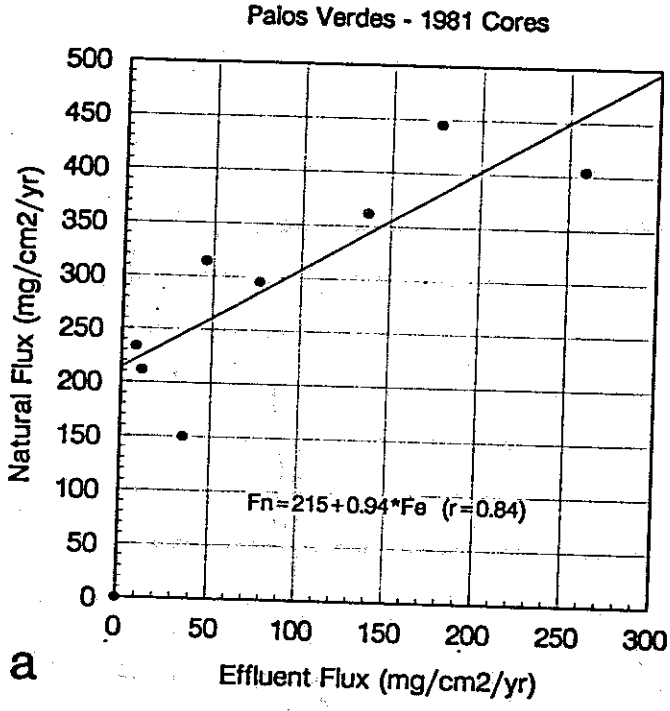

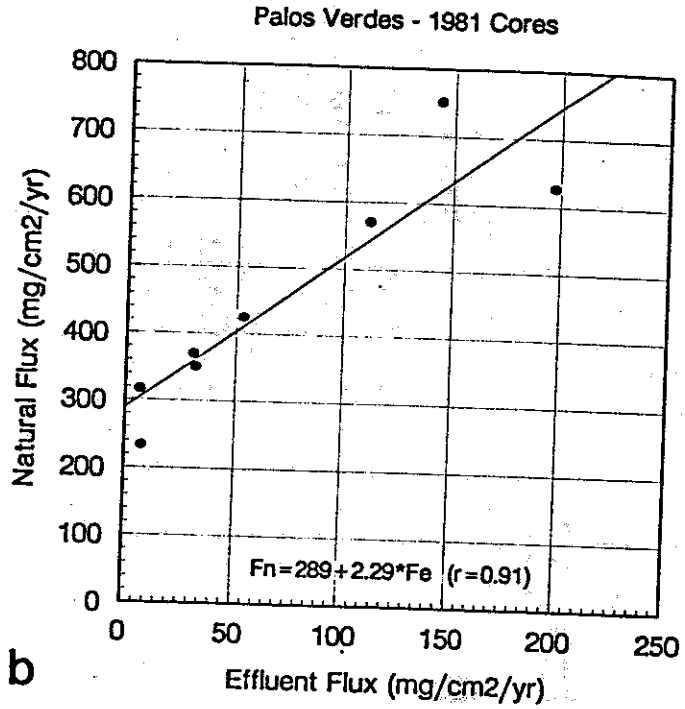

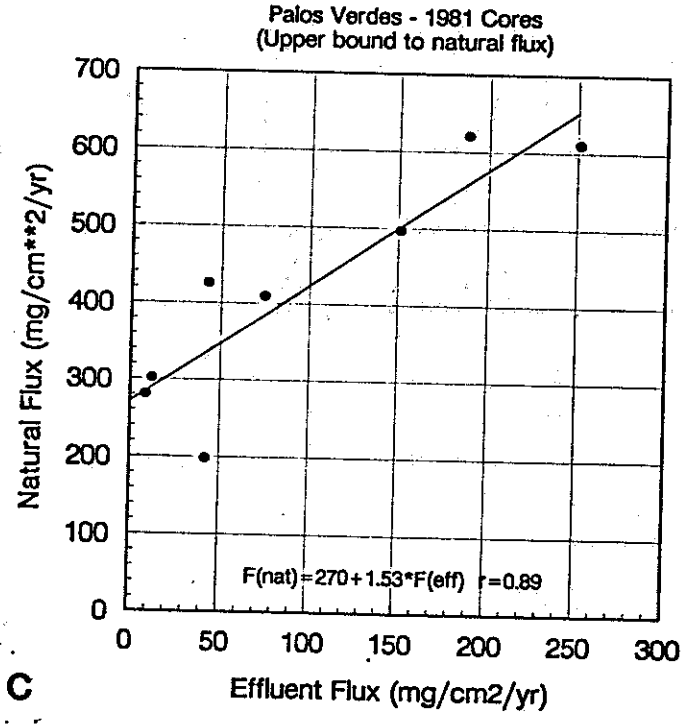

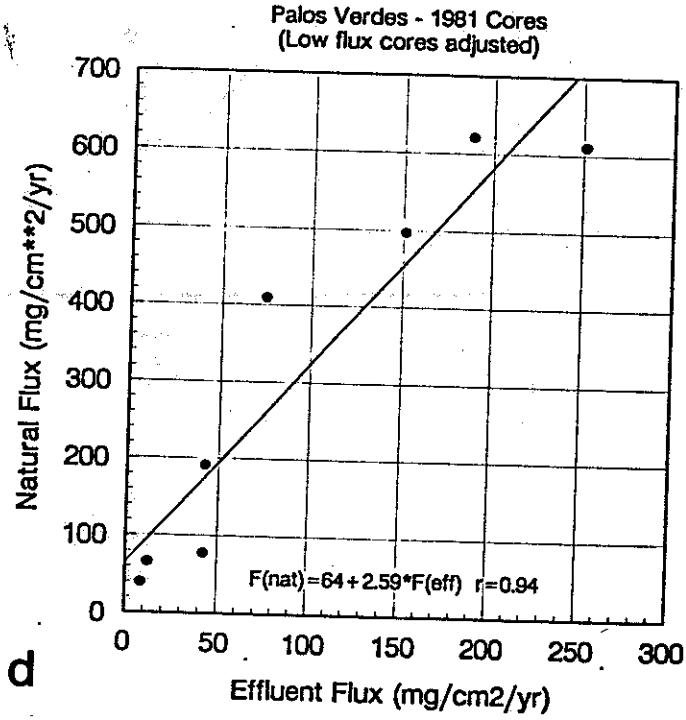

Figure 4.24 - Natural particle versus effluent particle accumulation fluxes - Palos Verdes. (a) ,(b) mid-range estimates of effects of bioturbation, (c) underestimate of bioturbation, (d) overestimate of bioturbation.

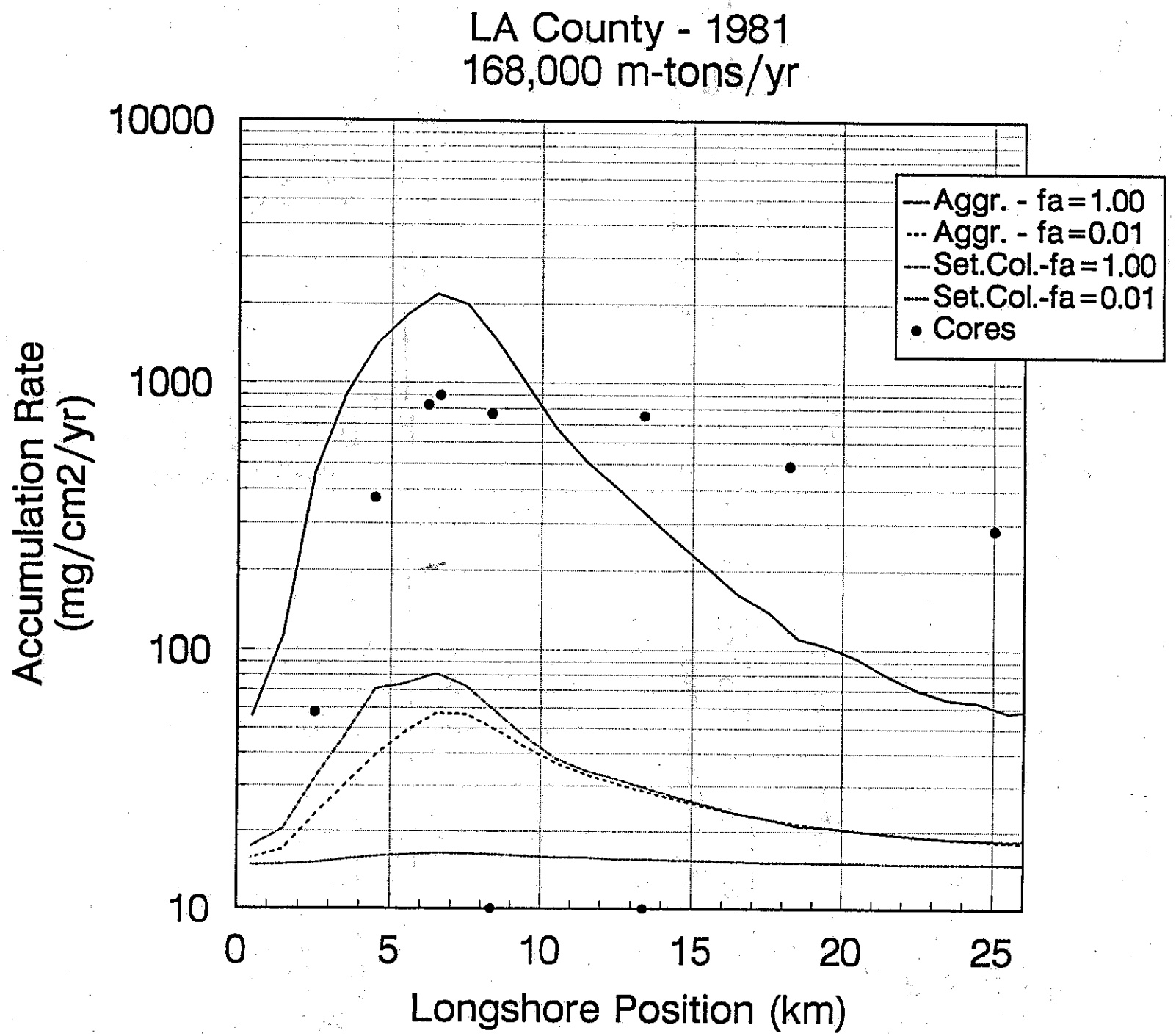

Figure 4.25 - Comparison of predicted and measured accumulations of wastefield-associated particulates - Palos Verdes, SED2D, 60m isobath.